

Joana Rita Antunes Gonçalves Madeira e Góis

# DESIGN AND SYNTHESIS OF RESPONSIVE NANOCARRIERS USING REVERSIBLE DEACTIVATION RADICAL POLYMERIZATION FOR BIOMEDICAL APPLICATIONS

Tese de doutoramento em Engenharia Química, orientada por Professor Doutor Jorge Fernando Jordão Coelho e Professor Doutor Arménio Coimbra Serra e apresentada ao Departamento de Engenharia Química da Faculdade de Ciências e Tecnologia da Universidade de Coimbra

Setembro de 2015



UNIVERSIDADE DE COIMBRA



Joana Rita Antunes Gonçalves Madeira e Góis

# DESIGN AND SYNTHESIS OF RESPONSIVE NANOCARRIERS USING REVERSIBLE DEACTIVATION RADICAL POLYMERIZATION FOR BIOMEDICAL APPLICATIONS

Thesis submitted to the Faculty of Sciences and Technology of the University of Coimbra, to obtain the Degree of  
Doctor in Chemical Engineering

Coimbra

2015



UNIVERSIDADE DE COIMBRA



Joana Rita Antunes Gonçalves Madeira e Góis

# DESIGN AND SYNTHESIS OF RESPONSIVE NANOCARRIERS USING REVERSIBLE DEACTIVATION RADICAL POLYMERIZATION FOR BIOMEDICAL APPLICATIONS

Thesis submitted to the Faculty of Sciences and Technology of the University of Coimbra, to obtain the Degree of  
Doctor in Chemical Engineering

## **Advisors:**

Prof. Dr. Jorge Fernando Jordão Coelho

Prof. Dr. Arménio Coimbra Serra

## **Host institutions:**

University of Coimbra

University of Pennsylvania

Carnegie Mellon University

## **Financing:**

Portuguese Foundation for Science and Technology (FTC)

Doctoral degree grant: SFRH/BD69635/2010

Coimbra

2015



UNIVERSIDADE DE COIMBRA



*À minha família,*





*“The important thing is not to stop questioning.*

*Curiosity has its own reason for existing.”*

Albert Einstein



## Acknowledgments

Como tarefa final deste longo processo cabe-me, neste momento, expressar os meus sinceros agradecimentos a todos aqueles que de modo directo ou indirecto contribuíram para o sucesso deste trabalho.

Ao Professor Jorge Coelho, meu orientador científico, não há palavras que expressem a minha gratidão. Agradeço por ter acreditado e confiado em mim desde o início, me ter motivado e concedido as melhores oportunidades ao longo dos últimos anos. Agradeço também por toda a sua disponibilidade e ajuda prestada ao longo deste processo.

Ao Professor Arménio Serra, meu co-orientador e *mentor* na Química. Obrigada pela confiança demonstrada, pela sua disponibilidade e por todas as discussões, conselhos e sugestões ao longo do trabalho.

Tolya (Anatoliy Popov), thank you for your kindness and for the precious discussions and advices. You always came up with a genial idea and solve the problem! I am also grateful for your gentle welcome and guidance in Philadelphia and at University of Pennsylvania. “Muito obrigada por tudo”.

To Professor Krzysztof Matyjaszewski I want to express my deepest gratitude for welcoming in his laboratory at Carnegie Mellon University and for the helpful discussions, comments and advices. I'm grateful for such wonderful opportunity. I would also like to extend my great appreciation to his wife for having me at home during my stay at Pittsburgh. I've found a home far from home with you both.

To the group members of the Matyjaszewski Polymer Group, it was a pleasure to meet you all and have the chance to work with you. Thank you for the good advices, support, friendship and fun we shared during my stay. A special thanks to the Dominik Konkolewicz for the interest demonstrated in my work and for all the support given, as well as the members from the Architecture Mini-Group Meeting and Dr. James Spanswick for their valuable and constructive suggestions.

To Jim Delikatny, Sean e Mike, for the welcome in their research group at University of Pennsylvania and for keeping a brilliant atmosphere at the lab. Thank you for the good and memorable moments we shared during my stay at UPENN.

## *Acknowledgments*

---

À Professora Helena Gil, que tive o prazer de conhecer durante o Mestrado Integrado em Engenharia Biomédica e que posteriormente me recebeu no grupo de polímeros em 2008. Agradeço por me ter apresentado esta área de polímeros e me ter motivado a seguir para doutoramento. Este primeiro incentivo foi de extrema importância para o que se seguiu.

To Tamaz Guliashvili for his sympathy, critical sense and valuable suggestions during the development of this research work.

Aos membros do Polymer Research Group, especialmente à Ana Fonseca, Nuno Rocha, Filipa Martins e aos colegas do B37, pelos momentos que partilhámos no laboratório e pelo espírito de entreajuda.

À Patrícia Mendonça, minha companheira nas aventuras pelos EUA. Obrigada pelo apoio, amizade, pela partilha e por tudo o que passámos juntas (será sempre: *“jaquinzinhos com arroz de tomate”*).

Ao Dr. Rui Fernandes do Instituto de Biologia Molecular e Celular (IBMC) pela execução das análises de TEM.

Ao Dr. Pedro Cruz, do Laboratório de Ressonância Magnética Nuclear (L-RMN) do Centro de Química de Coimbra, pela execução das análises de NMR.

A todos os funcionários do Departamento de Engenharia Química da Universidade de Coimbra, especialmente à Eng. Maria João Bastos pela realização dos testes de TGA.

À Professora Maria da Graça Rasteiro pela disponibilidade em usar equipamento de DLS.

Ao Professor Jorge Rocha pela disponibilidade em usar o equipamento de espectrofotometria.

À Professora Marta Piñeiro e Dra. Sílvia Maria Gramacho Alexandre pela ajuda e disponibilidade em usar o espectrofotómetro de fluorescência.

À Fundação para a Ciência e Tecnologia pelo financiamento do projecto.

Ao Departamento de Engenharia Química da Faculdade de Ciências e Tecnologia da Universidade de Coimbra, pelas excelentes condições que me proporcionou para o desenvolvimento do trabalho.

Aos Amigos, sempre presentes. Obrigada pelos momentos partilhados, de alegria e de amizade que dão sentido à vida. Obrigada pela “força” especialmente nesta fase final e nos momentos em que estive ausente. Sem vocês não teria sido capaz...

À Família, o pilar da minha formação, obrigada pelo apoio incondicional. Ao meus pais por todo o afecto, paciência e dedicação ao longo destes anos. Obrigada por terem sempre respeitado as minhas escolhas, permitido que tudo fosse possível e por me mostrarem que, com esforço, tudo é alcançável. Um agradecimento especial aos meus avós, pelo carinho e por sempre me fazerem sentir especial. Ao meu irmão Pedro, por estar sempre presente e pelos seus sábios conselhos. À Carla, por ter sempre uma palavra amiga, pela sua preocupação e pelo incentivo ao longo destes anos. Aos meus sobrinhos, Manuel Pedro e João Nuno, por encherem o meu coração e tornarem a minha vida mais feliz.

*“Aqueles que passam por nós, não vão sós, não nos deixam sós. Deixam um pouco de si, levam um pouco de nós.”*

Antoine de Saint-Exupéry



## Abstract

The aim of this work was the development of well-defined co(polymers) based on stimuli-responsive segments to further use as building blocks in the development of nanocarriers for biomedical applications. The synthesis strategy involved the use of reversible deactivation radical polymerization (RDRP) methods, as well as “click” coupling reactions that led to the preparation of well-defined polymers, with controlled molecular weight, narrow molecular weight distributions, and well-defined chain-end functionalities.

The homopolymerization studies of the 2-(diisopropylamino)ethyl methacrylate (DPA) by atom transfer radical polymerization (ATRP) involving an eco-friendly catalytic system that uses sodium dithionite ( $\text{Na}_2\text{S}_2\text{O}_4$ ) as a reducing agent and supplemental activator originated well-defined pH-responsive polymers with controlled properties. The detailed mechanism of such reaction system was investigated and the structure of the initiator, solvent, concentration of the catalyst, and the ratios of  $\text{Na}_2\text{S}_2\text{O}_4$  were adjusted to optimize the polymerization and afford polymers with narrow molecular weight distribution ( $D < 1.15$ ) even at high monomer conversion ( $\sim 90\%$ ). The slow and continuous feed of  $\text{Na}_2\text{S}_2\text{O}_4$  solution to the reaction mixture allowed the polymerization to be carried out in the presence of only 100 ppm of  $\text{CuBr}_2$  when the ligand tris(2-pyridylmethyl)-amine (TPMA) was used. This system was successfully extended to the polymerization of oligo(ethylene oxide) methyl ether methacrylate (OEOMA). The residual metal catalyst concentrations used and non-toxic nature of the  $\text{Na}_2\text{S}_2\text{O}_4$  make this SARA ATRP method very attractive for the well-controlled synthesis of water soluble polymers for biomedical applications. The high conversion and preservation of the chain-end functionality allowed the direct synthesis of POEOMA-*b*-PDPA block copolymers through one-pot polymerization approach. The pH-dependent self-assembly behavior of these brush-like copolymers in aqueous solutions was studied and the preliminary results suggested that the preparation method plays an important role on the final morphology of the nanoaggregates. Due to the pH critical value of the DPA block, these block copolymers form stable nanostructures at physiological pH, but disassemble at  $\text{pH} < 6.2$ . Copolymers composed by longer PDPA segments were found to originate larger self-assembled particles with critical micelle concentration (CMC) in the range of  $1.0 \times 10^{-3} \text{ mg.mL}^{-1}$ .

Despite the high versatility of the ATRP method, it is not very efficient in the polymerization of the so called non-activated monomers, namely vinyl acetate (VAc) and *N*-vinyl caprolactam (NVCL). The reversible addition fragmentation chain transfer (RAFT) was proposed as an alternative RDRP method for the polymerization of such monomers and two new xanthates with alkyne functionalities were designed and synthesized. The kinetic studies revealed that the protected alkyne-terminated RAFT agent (PAT-X<sub>1</sub>) was able to conduct the RAFT polymerization of both VAc and NVCL in 1,4-dioxane at 60 °C, with a good control over the molecular weight and relatively narrow MW distributions ( $\mathcal{D} < 1.4$ ) up to high monomer conversions. The linear evolution of  $M_{n, \text{GPC}}$  with conversion as well as the close agreement between  $M_{n, \text{th}}$  and  $M_{n, \text{GPC}}$  values confirmed the controlled feature of the RAFT system. The poly(*N*-vinyl caprolactam) (PNVCL) is a temperature-responsive polymer and its solution behaviour was fully investigated under different conditions. The stringent control over the polymer molecular weight allows the development of PNVCL with tunable phase transition temperatures around 37 °C. The deprotection of the alkyne functionality of the polymers synthesized by RAFT, allowed a further copper catalyzed azide–alkyne [3+2] dipolar cycloaddition (CuAAC) to obtain new linear block copolymers. This “click” coupling reaction allowed the conjugation of the alkyne-terminated PNVCL synthesized by RAFT with and azide-terminated POEOMA synthesized by ATRP, originating POEOMA-*b*-PNVCL copolymers. Such block copolymers are hydrophilic but, due to the temperature responsive nature of the PNVCL segment, they become amphiphilic at temperatures above its low critical solution temperature (LCST) and self-assemble into spherical vesicular aggregates with narrow size distributions. A small drop in the solution temperature caused the disruption of the nanostructures and induced the fast release of Nile red (NR), an hydrophobic small molecule used as a model drug. Moreover, the sharp and reversible solution properties of the PNVCL block turn those copolymers interesting candidates for the development of temperature-triggered drug delivery systems (DDS). The CuAAC coupling reaction was extended for the development of responsive polymers with linear-dendritic architectures. The synthesized linear pH-responsive and temperature-responsive polymers were conjugated to polyester dendritic structures based on the monomer 2,2-bis(hydroxymethyl) propionic acid (bis-MPA), functionalized with poly(ethylene glycol) (PEG) segments, to obtain linear dendritic block copolymers (LDBC).



This thesis contributed to the development of methods that allow the synthesis of new block copolymers having stimuli-responsive segments, and intended to extend the application of these structures to the development of tailor made nanocarriers to be used as DDS for cancer therapy.



## Resumo

Este trabalho teve como principal objectivo o desenvolvimento de (co)polímeros com estrutura controlada, compostos por segmentos que respondem a estímulos, para posteriormente serem usados como blocos constituintes de nanotransportadores desenvolvidos para aplicações biomédicas. A estratégia de síntese envolveu o uso de métodos de polimerização radicalar por desactivação reversível (RDRP), bem como reacções de conjugação ‘click’, levando à preparação de polímeros bem definidos, com peso molecular controlado, distribuição de pesos moleculares apertada e terminais de cadeia com funcionalidades bem definidas.

Os estudos da homopolimerização do metacrilato de 2-(diisopropil amino)etilo (DPA), por polimerização radicalar por transferência de átomo (ATRP), envolvendo um sistema catalítico mais ecológico, que usa ditonito de sódio ( $\text{Na}_2\text{S}_2\text{O}_4$ ) como activador suplementar e agente redutor (SARA), deu origem a polímeros, bem definidos e com propriedades controladas, capazes de responder a variações pH. O mecanismo detalhado desse sistema de reacção foi investigado e a estrutura do iniciador, solvente, concentração do catalisador, bem como as razões molares de  $\text{Na}_2\text{S}_2\text{O}_4$ , foram ajustadas de modo a otimizar a polimerização e obter polímeros com distribuições de peso molecular apertadas ( $D < 1.15$ ) mesmo para elevadas conversões de monómero (~ 90 %). A adição lenta e contínua de uma solução de  $\text{Na}_2\text{S}_2\text{O}_4$  à mistura de reacção, permitiu que, quando se usa a tris(2-piridilmetil)amina (TPMA) como ligante, a polimerização seja controlada na presença de apenas 100 ppm de  $\text{CuBr}_2$ . Este sistema foi estendido com sucesso à polimerização do metacrilato de eter oligo(etileno óxido) metilo (OEOMA). A concentração residual de catalizador metálico usada, e a natureza não-tóxica do  $\text{Na}_2\text{S}_2\text{O}_4$ , torna este método de SARA ATRP muito atractivo para a síntese controlada de polímeros solúveis em água para aplicações biomédicas. A elevada conversão e a preservação da funcionalidade terminal de cadeia permitem a síntese directa de copolímeros de bloco POEOMA-*b*-PDPA através de uma estratégia ‘one-pot’. O comportamento de ‘self-assembly’ dependente do pH em soluções aquosas deste tipo de copolímeros com estrutura em pente, foi estudado e os resultados preliminares sugerem que o método de preparação tem um papel importante na morfologia final dos nanoagregados. Devido ao valor de pH crítico do bloco DPA, estes copolímeros formam nanoestruturas estáveis a pH fisiológico, mas desagregam-se para  $\text{pH} < 6.2$ .

Copolímeros compostos por segmentos de PDPA mais longos dão origem a partículas maiores, com uma concentração micelar crítica (CMC) na gama dos  $1.0 \times 10^{-3} \text{ mg.mL}^{-1}$ .

Apesar da elevada versatilidade do método de ATRP, verifica-se que não é muito eficaz na polimerização dos denominados monómeros não-activados, nomeadamente o acetato de vinilo (VAc) e a *N*-vinil caprolactama (NVCL). A polimerização radicalar por transferência de cadeia reversível por adição-fragmentação (RAFT) foi estudada como método alternativo de RDRP para a polimerização dos monómeros referidos. Dois novos xantatos com funcionalidades alcino foram desenhados e sintetizados. Os estudos cinéticos revelaram que o agente RAFT com o terminal alcino protegido (PAT- $X_1$ ) era capaz de controlar a polimerização por RAFT de ambos os monómeros, VAc e NVCL, em 1,4-dioxano a 60 °C, com um bom controlo sobre o peso molecular e distribuições de peso moleculares relativamente apertadas ( $D < 1.4$ ) mesmo para conversões elevadas. A evolução linear do  $M_{n,GPC}$  com a conversão, bem como a proximidade dos valores de  $M_{n,th}$  e  $M_{n,GPC}$  confirmaram as características controladas do sistema RAFT. A poli(*N*-vinil caprolactama) (PNVCL) é um polímero que responde à temperatura pelo que o seu comportamento em solução foi investigado detalhadamente em diferentes condições. O controlo apertado sobre o peso molecular do polímero permite o desenvolvimento de PNVCL cujas temperaturas de transição de fase são ajustáveis em torno dos 37 °C. A desprotecção da funcionalidade alcino nos polímeros sintetizados por RAFT permitiu a síntese de novos copolímeros de bloco através da reacção de cicloadição azido-alcino catalizada por cobre (CuAAC). Esta reacção de conjugação ‘click’ tornou possível combinar os segmentos PNVCL com um terminal alcino, sintetizados por RAFT, com os de POEOMA que possuíam terminais azida, sintetizados por ATRP, originando copolímeros POEOMA-*b*-PNVCL. Estes copolímeros de bloco são hidrofílicos mas, devido à capacidade de resposta à temperatura do segmento PNVCL, tornam-se anfifílicos para temperaturas superiores à temperatura crítica de solução inferior (LCST) e organizam-se em estruturas vesiculares esféricas, com distribuições de tamanho estreitas. Uma ligeira redução na temperatura da solução causa a ruptura das nanoestruturas e induz a rápida libertação do vermelho do Nilo (NR), uma pequena molécula hidrofóbica usada como composto modelo. Para além disso, o facto do segmento PNVCL possuir uma solubilidade reversível, com transição rápida, faz com que os copolímeros sintetizados sejam candidatos interessantes para o desenvolvimento de sistemas de libertação que respondem a transições de temperatura.

A reacção de conjugação CuAAC foi alargada ao desenvolvimento de arquitecturas lineares-dendriticas, compostas por polímeros que respondem a estímulos. Ambos os polímeros lineares sintetizados, o polímero que responde ao pH, e o polímero que responde à temperatura, foram conjugados com estruturas dendríticas sintetizadas a partir do monómero ácido 2,2-bis(hidroximetil) propiónico e funcionalizadas na periferia com segmentos de polietileno glicol (PEG), de modo a obter copolímeros de bloco lineares-dendríticos (LDBC).

Este trabalho contribuiu para o desenvolvimento de metodologias que permitem a sínteses de novos copolímeros de bloco, compostos por segmentos que respondem a estímulos. Pretendeu-se com este estudo alargar a aplicações destas estruturas ao desenvolvimento de nanotransportadores específicos para serem usados como DDS em novas terapias contra o cancro.



## List of publications

### Papers published from the research work presented in this thesis:

**Góis, J. R.;** Rocha, N.; Popov, A. V.; Guliashvili, T.; Matyjaszewski, K.; Serra, A. C.; Coelho, J. F. J. (2014). “Synthesis of well-defined functionalized poly(2-(diisopropylamino)ethyl methacrylate) using ATRP with sodium dithionite as a SARA agent”. *Polymer Chemistry*, 5, 3919-3928. (Chapter 2)

**Góis, J. R.;** Konkolewicz, D.; Popov, A. V.; Guliashvili, T.; Matyjaszewski, K.; Serra, A. C.; Coelho, J. F. J. (2014). “Improvement of the control over SARA ATRP of 2-(diisopropylamino) ethyl methacrylate by slow and continuous addition of sodium dithionite”. *Polymer Chemistry*, 5, 4617-4626. (Chapter 3)

**Góis, J. R.,** Popov, A. V., Guliashvili T., Serra, A. C. and Coelho, J. F. J. (2015). “Synthesis of functionalized poly(vinyl acetate) mediated by alkyne-terminated RAFT agents”, *RSC Advances*, 2015, *in press*. (Chapter 5)

### Papers in preparation from the research work presented in this thesis:

**Góis, J. R.,** Rocha, N., Serra, A. C. and Coelho, J. F. J., “Brush-type pH-responsive block copolymers as nanocarriers for smart drug delivery applications”. (Chapter 4)

**Góis, J. R.,** Popov, A. V., Serra, A. C. and Coelho J. F. J., “RAFT polymerization of alkyne terminated *N*-vinyl caprolactam: kinetic studies and polymer characterization”. (Chapter 6)

**Góis, J. R.,** Serra, A. C. and Coelho J. F. J., “Synthesis of new thermo-responsive nanocarriers based on POEOMA-*b*-PDPA prepared using a combination of ATRP, RAFT and CuAAC”. (Chapter 7)

**Papers published from the collaboration in other projects during the PhD program:**

Coelho, J. F.; Ferreira, P. C.; Alves, P.; Cordeiro, R.; Fonseca, A. C.; **Góis, J. R.**; Gil, M. H. (2010). "Drug delivery systems: Advanced technologies potentially applicable in personalized treatments". *The EPMA Journal*, 1 (1), 164-209.

A.C. Fonseca, P. Ferreira, R.A. Cordeiro, P.V. Mendonça, **J.R. Góis**, M.H. Gil, and Jorge F.J. Coelho (2013). "Drug delivery systems for predictive medicine: polymers as tools for advanced applications", in "New Strategies to Advance Pre/Diabetes Care: Integrative Approach by PPPM", *Advances in Predictive, Preventive and Personalised Medicine*, Vol. 3, Springer.

Nuno Rocha, Patrícia Mendonça, **Joana Góis**, Rosemeyre Cordeiro, Ana Fonseca, Tamaz Guliashvili, Krzysztof Matyjaszewski, Arménio Serra, and Jorge Coelho (2013). "The Importance of Controlled/Living Radical Polymerization Techniques in the Design of Tailor Made Nanoparticles for Drug Delivery Systems", in "Drug Delivery Systems: Advanced Technologies Potentially Applicable in Personalised Treatment, Advances" in *Predictive, Preventive and Personalised Medicine*, Volume 4, pp 315-357, Springer.

Rocha, N.; Coelho, J. F. J.; **Góis, J. R.**; Gil, M. H.; Gonçalves, P. M. O. F.; Guthrie, J. T. (2013). "Poly(vinyl chloride)-b-poly(hydroxypropyl acrylate)-b-Poly(vinyl chloride): Understanding the synthesis of an amphiphilic PVC block copolymer on a pilot scale". *Journal of Vinyl and Additive Technology*, 19 (2), 94-104.

Marques, J.; Oliveira, L. F.; Pinto, R. T.; Coutinho, P. J. G.; Parpot, P.; **Góis, J. R.**; Coelho, J. F. J.; Magalhães, F. D.; Tavares, C. J. (2013). "Release of Volatile Compounds from Polymeric Microcapsules Mediated by Photocatalytic Nanoparticles". *International Journal of Photoenergy*, 2013, 9.

Konkolewicz, D.; Krys, P.; **Góis, J. R.**; Mendonça, P. V.; Zhong, M.; Wang, Y.; Gennaro, A.; Isse, A. A.; Fantin, M.; Matyjaszewski, K. (2014). "Aqueous RDRP in the Presence of Cu<sub>0</sub>: The Exceptional Activity of CuI Confirms the SARA ATRP Mechanism". *Macromolecules*, 47(2), 560-570.



Rosa, N.; Martins, G. V.; Bastos, M. M. S. M.; **Góis, J. R.**; Coelho, J. F. J.; Marques, J.; Tavares, C. J.; Magalhães, F. D. (2015). "Preparation of robust polyamide microcapsules by interfacial polycondensation of p-phenylenediamine and sebacoyl chloride and plasticization with oleic acid". *Journal of Microencapsulation*, 32 (4), 349-357.

Catalão, F.; **Góis, J.**; Trino, A.; Serra, A. C.; Coelho, J.(2015). "Facile Synthesis of Well-controlled Poly(glycidyl methacrylate) and its Block Copolymers via SARA ATRP at Room Temperature". *Polymer Chemistry* ,6, 1875-1882.



## Thesis outline

The main goal of this PhD research work was the development of well-defined stimuli-responsive polymers to use as nanocarriers for biomedical applications. The present document is organized in nine chapters:

- Chapter 1 provides a literature review covering the reversible deactivation radical polymerization (RDRP) methods as well as other macromolecular engineering tools to synthesise tailor made macromolecules. Special focus is given to the self-assembly of block copolymers and the importance of using responsive segments to develop nanoparticles with potential applications in cancer therapeutics.

- Chapter 2 describes the synthesis of well-defined poly(2-diisopropylamino)ethyl methacrylate (PDPA), a pH-responsive polymer, using an atom transfer radical polymerization (ATRP) eco-friendly catalytic system based on of sodium dithionite as supplemental activator and reducing agent (SARA).

- Chapter 3 deepens the kinetic studies presented in the aforementioned SARA ATRP method with the objective to enhance the reaction conditions by reducing the concentration of the metal catalyst and to improve the control over the polymers. This chapter also extends the method to the polymerization of another hydrophilic monomer with potential application in the biomedical field, oligo(ethylene oxide) methyl ether methacrylate (OEOMA)

- Chapter 4 reports the use of the reported SARA ATRP system for the straightforward synthesis of POEOMA-*b*-PDPA copolymers via sequential monomer addition. The pH-dependence solution self-assembly of the PDPA based copolymers is studied in an attempt to develop pH-responsive nanocarriers.

- Chapter 5 deals with the design and synthesis of two new reversible addition-fragmentation chain transfer radical polymerization (RAFT) agents functionalized with alkyne moieties for the polymerization of less-activated monomers. The polymerization of vinyl acetate (VAc) is studied as a proof-of-concept.

- Chapter 6 reports the polymerization of *N*-vinyl caprolactam (NVCL) mediated by the RAFT agents presented in Chapter 5. This temperature-responsive polymer is fully characterized and its solutions properties are studied.

- Chapter 7 expands the range of applications of PNVCL through the synthesis of different block copolymers. From a simple “click” coupling conjugation reaction the PNVCL synthesized by RAFT is conjugated to a poly(ethylene glycol) (PEG) based polymer synthesized by ATRP. The ability of this responsive copolymer to form self-assembled aggregates in function of the solution temperature is studied in detail.

- Chapter 8 reports the synthesis of linear dendritic block copolymers, as a different copolymer architecture for the development of nanoparticles. The initial part of the chapter is devoted to the preparation of functionalized dendritic segments based on the 2,2-bis(hydroxymethyl) propionic acid (bis-MPA) and the subsequent part deals with the conjugation of the responsive linear polymers reported in the previous chapters, namely, the PDPA and the PNVCL by a “click” coupling conjugation reaction.

- Chapter 9 presents the most relevant conclusions from this work along with some recommendations for future work.

---

**List of acronyms**

4f-BiB	Pentaerythritol tetrakis(2-bromoisobutyrate)
AAS	Atomic absorption spectroscopy
ABC	Amphiphilic block copolymers
AIBN	2,2'-Azobis(2-methylpropionitrile)
ARGET	Activators regenerated by electron transfer
AT-PDP	Alkyne-terminated poly(2-(diisopropylamino)ethyl methacrylate)
AT-PNVCL	Alkyne-terminated poly( <i>N</i> -vinylcaprolactam)
AT-PVAc	Alkyne-terminated poly(vinyl acetate)
AT-X <sub>1</sub>	<i>O</i> -ethyl- <i>S</i> -(1-propargoxycarbonyl) ethyl- dithiocarbonate (alkyne-terminated RAFT agent)
ATRP	Atom transfer radical polymerization
bis-MPA	2,2-Bis(hydroxymethyl) propionic acid
Bpy	2,2'-Bipyridine
CAC	Critical aggregation concentration
CMC	Critical micelle concentration
CST	Critical solution temperature
CTA	Chain transfer agent
CuAAc	Copper-catalyzed azide-alkyne cycloaddition
DCC	<i>N,N'</i> -dicyclohexylcarbodiimide
DCM	Dichloromethane
DDS	Drug delivery systems
DIC	<i>N,N'</i> -diisopropylcarbodiimide
DLC	Drug loading capacity
DLE	Drug loading efficiency
DLS	Dynamic light scattering
DMAEMA	2-(Dimethylamino)ethyl methacrylate
DMAP	4-(Dimethylamino)pyridine
DMF	Dimethylformamide
<i>dn/dc</i>	Refractive index increment
DPA	2-(Diisopropylamino)ethyl methacrylate
DPTS	4-(Dimethylamino)pyridinium p-toluenesulfonate
DT	Degenerative transfer
DV	Differential viscometer
eATRP	Electrochemically mediated ATRP

## List of acronyms

---

EBiB	2-Bromoisobutyrate
EBPA	Ethyl $\alpha$ -bromophenyl acetate
Et3N	Triethylamine
FDA	Food and Drug Administration
FRP	Free radical polymerization
FTIR	Fourier-transform infrared spectroscopy
GPC	Gel permeation chromatography
HMTETA	1,1,4,7,10,10-Hexamethyltri-ethylenetetramine
HPLC	High performance liquid chromatography
ICAR	Initiators for continuous activator regeneration
IPA	Isopropanol
LCST	Lower critical solution temperature
LDBC	Linear dendritic block copolymers
MA	Methyl acrylate
MALDI-TOF	Matrix-assisted laser desorption ionization time-of-flight
Me <sub>6</sub> TREN	Tris(2-(dimethylamino)ethyl)amine
mPEG	Poly(ethylene glycol) monomethyl ether
MTT	3-(4,5-Dimethylthiazol-2-yl)-2,5-diphenyltetrazolium bromide
N <sub>3</sub> E <sup>i</sup> BBr	(2-Azidoethoxy)ethyl bromoisobutyrate
N <sub>3</sub> -Cum	3-Azido-7-diethylaminocoumarin
NaAsc	Sodium ascorbate
NR	Nile red
NMP	Nitroxide mediated polymerization
NMR	Nuclear magnetic resonance
NPN	<i>N</i> -phenyl-1-naphthylamine
NVCL	<i>N</i> -vinylcaprolactam
NVP	<i>N</i> -vinylpyrrolidone
OEOMA	Oligo(ethylene oxide) methyl ether methacrylate
P4VP	Poly(4-vinylpyridine)
PA	Propargyl alcohol
PAA	Poly(acrylic acid)
PAAm	Poly(acrylamide)
PAT-PNVCL	Protected alkyne-terminated poly( <i>N</i> -vinylcaprolactam)
PAT-PVAc	Protected alkyne-terminated poly(vinyl acetate)
PAT-X1	Protected alkyne-terminated RAFT agent
PBS	Phosphate buffered saline

---

PCL	poly( $\epsilon$ -caprolactone)
PDEAEMA	Poly((2-diethylamino) ethyl methacrylate)
PDI	Polydispersity index
PDMAEMA	Poly(2-(dimethylamino)ethyl methacrylate)
PDPA	Poly(2-(diisopropylamino)ethyl methacrylate)
PEG	Poly(ethylene glycol)
PgBiB	Propargyl 2-bromoisobutyrate
PgEBPA	Propargyl bromophenyl acetate
PMDETA	<i>N,N,N',N'',N'''</i> -penta-methyldiethylenetriamine
PMAA	Poly(methacrylic acid)
PMMA	Poly(methyl methacrylate)
PMPC	Poly(2-(methacryloyloxy)ethyl phosphorylcholine)
PNIPAAm	Poly( <i>N</i> -isopropylacrylamide)
PNVCL	Poly( <i>N</i> -vinylcaprolactam)
POEOMA	Poly(oligo(ethylene oxide) methyl ether methacrylate)
Ppm	Parts per million
PRE	Persistent radical effect
PS	Poly(styrene)
PSD	Particle size distribution
PTFE	Polytetrafluoroethylene
PVAc	Poly(vinyl acetate)
RAFT	Reversible addition fragmentation transfer
RALLS	Right-angle laser-light scattering
RI	Refractive index
RDRP	Reversible deactivation radical polymerization
ROP	Ring opening polymerization
SARA	Supplemental activator and reducing agent
SDS	Sodium dodecyl sulfate
SEC	Size exclusion chromatography
SET-LRP	Single electron transfer living radical polymerization
SFRP	Stable free radical polymerization
SPIONs	Superparamagnetic iron oxide nanoparticles
TBAF	Tetrabutylammonium fluoride
T <sub>CP</sub>	Cloud point temperatures
TEM	Transmission electron microscopy
TEMPO	2,2,6,6-Tetramethylpiperidiny-1-oxyl

*List of acronyms*

---

TGA	Thermogravimetric analysis
THF	Tetrahydrofuran
TMS	Tetramethylsilane
TPMA	Tris(pyridin-2-ylmethyl)amine
TsOH	p-Toluenesulfonic acid
UCST	Upper critical solution temperature
UV-vis	Ultraviolet-visible65
VAc	Vinyl acetate
X <sub>1</sub>	<i>O</i> -ethyl- <i>S</i> -(1-methoxy carbonyl) ethyl dithiocarbonate



**Nomenclature**

$D$	Dispersity
$D_h$	Hydrodynamic diameter
DP	Polymerization degree
$M_{n,GPC}$	Number-average molecular mass determined by GPC
$M_{n,th}$	Theoretical number-average molecular mass
$M_{n,NMR}$	Number-average molecular mass determined by NMR spectroscopy
$k_p^{app}$	Apparent rate constant of propagation
$k_{act}$	Activation rate constant
$k_{deact}$	Deactivation rate constant
MW	Molecular weight
T	Temperature
$\xi$	Zeta potential



## **Contents**

Acknowledgments .....	IX
Abstract .....	XIII
Resumo .....	XVII
List of publications .....	XXI
Thesis outline .....	XXV
List of acronyms .....	XXVII
Nomenclature .....	XXXI
Contents .....	XXXIII
List of figures.....	XLI
List of schemes.....	LI
List of tables.....	LIII
Motivation, targets and research significance .....	LV
<b>Chapter 1. Literature review</b> .....	<b>1</b>
1.1. Macromolecular Engineering .....	3
1.2. Reversible deactivation radical polymerization.....	4
1.2.1. Atom transfer radical polymerization - ATRP .....	7
1.2.2. Reversible addition fragmentation transfer – RAFT .....	9
1.2.3. RDRP – Synthesis of tailor made polymers .....	11
1.4. Responsive polymers .....	15
1.4.1. pH-responsive polymers .....	16
1.4.2. Temperature responsive polymers.....	18
1.5. Self-assembly of block copolymers .....	20
1.6. Polymeric drug delivery systems .....	25
1.7. References.....	29

## Chapter 2.

<b>Synthesis of well-defined functionalized poly(2-(diisopropylamino) ethyl methacrylate) .....</b>	<b>43</b>
2.1. Abstract .....	45
2.2. Introduction.....	45
2.3. Experimental Section.....	47
2.3.1. Materials.....	47
2.3.2. Characterization .....	47
2.3.3. Procedures .....	49
2.4. Results and Discussion .....	51
2.4.1. Influence of water content on the rate of polymerization and control over molar mass of DPA in IPA/water mixtures.....	51
2.4.2. Study of variable degrees of polymerization.....	53
2.4.3. Influence of different ATRP initiators on the rate of polymerization and control over molar mass of DPA in IPA/water mixtures .....	55
2.4.4. <sup>1</sup> H NMR and MALDI-TOF-MS analyses .....	60
2.4.5. Chain extension experiment .....	64
2.4.6. N <sub>3</sub> -Coumarin reaction with alkyne terminated PDPA .....	65
2.5. Conclusions.....	67
2.6. References.....	68

## Chapter 3.

<b>Improvement of the control over SARA ATRP of 2-(diisopropylamino)ethyl methacrylate by slow and continuous addition of sodium dithionite .....</b>	<b>73</b>
3.1. Abstract.....	77
3.2. Introduction.....	77
3.3. Experimental Section.....	79

3.3.1. Materials.....	79
3.3.2. Characterization .....	80
3.3.3. Procedures .....	80
3.4. Results and Discussion .....	81
3.4.1. Influence of the initiator structure and concentration.....	81
3.4.2. Effect of the solvent mixture .....	83
3.4.3. Effect of the initial concentration of Na <sub>2</sub> S <sub>2</sub> O <sub>4</sub> .....	84
3.4.4. Feeding of Na <sub>2</sub> S <sub>2</sub> O <sub>4</sub> .....	85
3.4.5. Variation of copper concentration.....	89
3.4.6. Effect of the ligand.....	90
3.4.7. Polymerization of OEOMA .....	94
3.5. Conclusions.....	95
3.6. References.....	96

## **Chapter 4.**

<b>Brush-Type pH-responsive block copolymers and its self-assembly properties .....</b>	<b>101</b>
4.1. Abstract.....	103
4.2. Introduction.....	103
4.3. Experimental Section.....	107
4.3.1. Materials .....	107
4.3.1. Characterization.....	107
4.3.2. Procedures .....	109
4.4. Results and Discussion .....	111
4.4.1. Synthesis and characterization of POEOMA- <i>b</i> -PDPA block copolymers .....	111
4.4.2. Solution behavior of POEOMA- <i>b</i> -PDPA copolymers – pH titration ....	115
4.4.3. Preparation of particles by solvent exchange method .....	119

4.4.4. TEM analysis of POEOMA- <i>b</i> -PDPA solution aggregates.....	121
4.4.5. Critical micelle concentration.....	122
4.5. Conclusions.....	124
4.6. References.....	125

## **Chapter 5.**

### **Synthesis of alkyne-terminated xanthates for the efficient RAFT polymerization of less-activated monomers ..... 133**

5.1. Abstract.....	135
5.2. Introduction.....	135
5.3. Experimental Section.....	137
5.3.1 Materials.....	137
5.3.2 Characterization.....	138
5.3.3 Procedures.....	139
5.4. Results and Discussion.....	143
5.4.1 Synthesis of the RAFT agents.....	143
5.4.2 Polymerization of VAc using the synthesized RAFT agents.....	147
5.4.3 Thermogravimetric analysis of the RAFT agents.....	151
5.4.4 PVAc chain-end functionality.....	152
5.4.5 Chain extension reaction.....	154
5.4.6 Deprotection of PVAc and coupling reaction with N <sub>3</sub> -PEG.....	155
5.5. Conclusions.....	156
5.6. References.....	157

## **Chapter 6.**

### **RAFT polymerization of alkyne terminated *N*-vinyl caprolactam: kinetic studies and polymer characterization..... 165**

6.1. Abstract.....	167
--------------------	-----

6.2. Introduction.....	167
6.3. Experimental Section.....	170
6.3.1. Materials.....	170
6.3.2. Characterization .....	171
6.3.3. Procedures .....	173
6.4. Results and Discussion .....	175
6.4.1. NVCL handling and purification .....	175
6.4.2. Polymerization of NVCL .....	177
6.4.3. Chemical structure and retention of chain end functionality .....	183
6.4.4. Thermal Analysis .....	189
6.4.5. Temperature-responsive behavior of the PNVCL.....	190
6.4.6. PNVCL based copolymers via a “click” coupling approach .....	196
6.5. Conclusions.....	198
6.6. References.....	199

## **Chapter 7.**

### **Synthesis of new thermo-responsive nanocarriers based on POEOMA-*b*-PNVCL prepared using a combination of ATRP, RAFT and CuAAC..... 205**

7.1. Abstract.....	207
7.3. Experimental section.....	209
7.3.1. Materials .....	209
7.3.2. Characterization.....	210
7.3.3. Procedures .....	212
7.4. Results and Discussion .....	215
7.4.1. Synthesis of N <sub>3</sub> -POEOMA .....	216
7.4.2. Synthesis of alkyne-terminated PNVCL .....	217
7.4.3. Synthesis of POEOMA- <i>b</i> -PNVCL copolymers via CuAAC reaction ...	218

7.4.4. Turbidimetry analysis .....	222
7.4.5. Self-assembly of block copolymers.....	225
7.4.6. Fluorescence assays - studies of guest loading and triggered release ....	234
7.6. References.....	237

## **Chapter 8.**

### **Synthesis of stimuli-responsive linear dendritic block copolymers**

#### **via “click” chemistry ..... 245**

8.1. Abstract.....	247
8.2. Introduction.....	247
8.3. Experimental Section.....	248
8.3.1. Materials .....	248
8.3.2. Characterization.....	249
8.3.3. Procedures .....	251
8.4. Results and Discussion .....	257
8.4.1. Dendron synthesis .....	257
8.4.2. Dendron functionalization .....	263
8.4.3. Synthesis of alkyne terminated linear polymers.....	267
8.4.4. Synthesis of linear-dendritic block copolymers .....	270
8.5. Conclusions.....	276
8.6. References.....	276

## **Chapter 9.**

#### **Final remarks..... 281**

9.1. Overall conclusions.....	283
9.2. Recommendations for future work .....	285
9.3. References.....	287



<b>Annexes .....</b>	<b>289</b>
Annex A. Supporting information for Chapter 2 .....	A1
Annex B. Supporting information for Chapter 3 .....	B1
Annex C. Supporting information for Chapter 4 .....	C1
Annex D. Supporting information for Chapter 5 .....	D1
Annex E. Supporting information for Chapter 6 .....	E1
Annex F. Supporting information for Chapter 7.....	F1
Annex G. Supporting information for Chapter 8.....	G1



## List of figures

<b>Figure 1.1:</b> Macromolecular engineering, the tool to create functional nanostructures: from RDRP methods to self-assembly. ....	3
<b>Figure 1.2:</b> Reversible deactivation radical polymerization (RDRP) methods. ....	5
<b>Figure 1.3:</b> Schematic representation of the normal ATRP and ATRP variations.....	8
<b>Figure 1.4:</b> Mechanism of RAFT polymerization. ....	10
<b>Figure 1.5:</b> Examples of polymers with controlled composition and topology prepared by RDRP. ....	12
<b>Figure 1.6:</b> Schematic representation of the 1,3-dipolar cycloaddition between azides and alkynes and examples of functionalized polymers or possible architectures obtained. ....	14
<b>Figure 1.7:</b> Poly(acrylic acid) chain conformations in water solution. ....	17
<b>Figure 1.8:</b> Polymer conformation according to the solution temperature.....	18
<b>Figure 1.9:</b> Schematic representation of different self-assembly architectures from the same amphiphilic diblock copolymer. ....	20
<b>Figure 1.10:</b> Schematic representation of the dependence of the resultant self-assembly morphology with Israelachvili's packing parameter, $p$ .....	21
<b>Figure 1.11:</b> Schematic representation of the linear dendritic block copolymer architecture and the possibility of dendron multi-surface functionalization. ....	22
<b>Figure 1.12:</b> Schematic representation of the self-assembly of amphiphilic block copolymers and the encapsulation of guest molecules.....	23
<b>Figure 1.13:</b> Schematic representation of the self-assembly of one responsive AB-diblock copolymer.....	24
<b>Figure 1.14:</b> Schematic representation of tumour targeting of long circulating micelle by the EPR effect. ....	27
<b>Figure 2.1:</b> Effect of solvent mixture in the SARA ATRP of DPA, IPA/H <sub>2</sub> O = 95/5 (v/v) (black circle symbols) and IPA/H <sub>2</sub> O = 90/10 (v/v) (grey triangle symbols) at 40 °C: (a) First-order kinetic plot, (b) evolution of MW and $\bar{D}$ with conversion (the dashed line represents theoretical MW at a given conversion). Reaction conditions: [DPA] <sub>0</sub> /solvent = 1/2 (v/v), [DPA] <sub>0</sub> /[EBiB] <sub>0</sub> /[Na <sub>2</sub> S <sub>2</sub> O <sub>4</sub> ] <sub>0</sub> /[CuBr <sub>2</sub> ] <sub>0</sub> /[Me <sub>6</sub> TREN] <sub>0</sub> = 50/1/1/0.1/0.1 (molar).....	52
<b>Figure 2.2:</b> GPC traces of PEG standard ( $M_p = 12\ 000\ \text{g}\cdot\text{mol}^{-1}$ ; $\bar{D} = 1.04$ ) and PDPA samples. Conditions: (a) [DPA] <sub>0</sub> /solvent = 1/2 (v/v), [IPA]/[H <sub>2</sub> O] = 0.95/0.05 (v/v); [DPA] <sub>0</sub> /[EBiB] <sub>0</sub> /[Na <sub>2</sub> S <sub>2</sub> O <sub>4</sub> ] <sub>0</sub> /[CuBr <sub>2</sub> ] <sub>0</sub> /[Me <sub>6</sub> TREN] <sub>0</sub> = 50/1/1/0.1/0.1 (molar); T= 40 °C;	

(b)  $[DPA]_0/\text{solvent} = 1/2$  (v/v),  $[IPA]/[H_2O]=0.90/0.10$  (v/v),  $[DPA]_0/[EBiB]_0/[Na_2S_2O_4]_0/[CuBr_2]_0/[Me_6TREN]_0 = 50/1/1/0.1/0.1$  (molar);  $T= 40$  °C..... 53

**Figure 2.3:** Effect of the target degree of polymerization (DP) in the SARA ATRP of DPA in IPA/H<sub>2</sub>O = 95/5 (v/v) at 40 °C. (a) First-order kinetic plot, (b) evolution of MW and  $\bar{D}$  with conversion (the dashed line represents theoretical MW at a given conversion), Reaction conditions:  $[DPA]_0/\text{solvent} = 1/2$  (v/v),  $[DPA]_0/[EBiB]_0/[Na_2S_2O_4]_0/[CuBr_2]_0/[Me_6TREN]_0 = 100/1/1/0.1/0.1$  (molar) (black circle symbols) or  $[DPA]_0/[EBiB]_0/[Na_2S_2O_4]_0/[CuBr_2]_0/[Me_6TREN]_0 = 50/1/1/0.1/0.1$  (molar) (grey triangle symbols)..... 54

**Figure 2.4:** GPC traces of PEG standard ( $M_p = 12.00 \times 10^3$  g.mol<sup>-1</sup>;  $\bar{D} = 1.04$ ) and PDPA samples for two different target MW (DP 100 (a) and DP 20 (b)). Conditions:  $[DPA]_0/\text{solvent} = 1/2$ (v/v),  $[IPA]/[H_2O] = 0.95/0.05$ (v/v); (a):  $[DPA]_0/[EBiB]_0/[Na_2S_2O_4]_0/[CuBr_2]_0/[Me_6TREN]_0 = 100/1/1/0.1/0.1$  (molar); (b):  $[DPA]_0/[EBiB]_0/[Na_2S_2O_4]_0/[CuBr_2]_0/[Me_6TREN]_0 = 20/1/1/0.1/0.1$  (molar);  $T= 40$  °C. .... 55

**Figure 2.5:** P<sub>g</sub>BiB mediated SARA ATRP of DPA in IPA/H<sub>2</sub>O = 95/5 (v/v) at 40 °C. (a) First-order kinetic plot, (b) evolution of MW and  $\bar{D}$  with conversion (the dashed line represents theoretical MW at a given conversion), and (c) GPC traces of PEG standard ( $M_p = 12.00 \times 10^3$  g.mol<sup>-1</sup>;  $\bar{D}= 1.04$ ) and PDPA samples. Reaction conditions:  $[DPA]_0/\text{solvent} = 1/2$  (v/v),  $[IPA]/[H_2O] = 0.95/0.05$  (v/v);  $[DPA]_0/[PgBiB]_0/[Na_2S_2O_4]_0/[CuBr_2]_0/[Me_6TREN]_0 = 40/1/1/0.1/0.1$  (molar);  $T= 40$  °C..... 56

**Figure 2.6:** GPC traces of linear PDPA and 4-arms star PDPA samples. Conditions:  $[DPA]_0/[IPA]/[H_2O]=1/0.95/0.05$ (v/v); $[DPA]_0/[EBiB]_0/[Na_2S_2O_4]_0/[CuBr_2]_0/[Me_6TREN]_0 = 100/1/1/0.1/0.11$  (molar) (linear);  $[DPA]_0/[4f-BiB]_0/[Na_2S_2O_4]_0/[CuBr_2]_0/[Me_6TREN]_0 = 100/1/4/0.4/0.41$  (star),  $T= 40$  °C. .... 57

**Figure 2.7:** Log-log plot of intrinsic viscosities against MW for linear and 4-arms star PDPA..... 58

**Figure 2.8:** The <sup>1</sup>H NMR spectrum of PDPA-Br ( $M_{n,GPC} = 14.9 \times 10^3$ ;  $M_{n,NMR} = 15.1 \times 10^3$ ,  $\bar{D} = 1.20$ ) in CDCl<sub>3</sub>..... 60

**Figure 2.9:** The <sup>1</sup>H NMR spectra in CDCl<sub>3</sub> of a) P<sub>g</sub>Bib – initiator; b) PDPA-Br obtained at high conversion ( $M_{n,GPC} = 27.9 \times 10^3$ ;  $\bar{D} = 1.09$ ;  $M_{n,NMR} = 25.8 \times 10^3$ ). .... 61

**Figure 2.10:** MALDI-TOF-MS in the linear mode (using DHB as matrix) of PDPA-Br ( $M_{n,GPC} = 14.3 \times 10^3$ ,  $\bar{D} = 1.21$ ) from m/z 1400 to 3000. Conditions:  $[DPA]_0/\text{solvent} = 1/2$  (v/v),  $[IPA]/[H_2O] = 0.95/0.05$  (v/v);  $[DPA]_0/[EBiB]_0/[Na_2S_2O_4]_0/[CuBr_2]_0/[Me_6TREN]_0 = 20/1/1/0.1/0.1$  (molar);  $T= 40$  °C. .... 62

**Figure 2.11:** MALDI-TOF-MS (a) in the linear mode (using DHB as matrix) from m/z 1200 to 9500 and (b) enlargement of the MALDI-TOF-MS from m/z 2000 to 3220 of PDPA-Br ( $M_{n,GPC} = 14.3 \times 10^3$ ,  $\bar{D} = 1.21$ ). Conditions:  $[DPA]_0/H_2O = 1/2$  (v/v),  $[IPA]/[H_2O] = 0.95/0.05$  (v/v);  $[DPA]_0/[EBiB]_0/[Na_2S_2O_4]_0/[CuBr_2]_0/[Me_6TREN]_0 = 20/1/1/0.1/0.1$  (molar);  $T= 40$  °C..... 64

**Figure 2.12:** GPC traces of the PDPA before (black line) and after the chain extension (blue line) experiment. .... 65

- Figure 2.13:** “Click” reaction between alkyne functionalized PDPA and 3-azido-7-diethylaminocoumarin. (i)  $\text{CuSO}_4 \cdot 5\text{H}_2\text{O}$ ; THF/ $\text{H}_2\text{O}$ . ..... 65
- Figure 2.14:** Image of the reaction mixture after the “click” reaction between the alkyne functionalized PDPA and  $\text{N}_3\text{-Cum}$ . The formation of the fluorescent linkage could be easily seen upon irradiation at 365 nm with a hand-held UV lamp. .... 66
- Figure 2.15:**  $^1\text{H}$  NMR spectrum, in  $\text{CDCl}_3$ , of the PDPA-Cu obtained by the “click” reaction between the alkyne-PDPA and the  $\text{N}_3\text{-Cum}$ . ..... 67
- Figure 3.1:** Effect of the ATRP initiator on the SARA ATRP of DPA in IPA/ $\text{H}_2\text{O}$  = 95/5 (v/v) at 40 °C. (a) First-order kinetic plot, (b) evolution of MW and  $\bar{D}$  with conversion (the dashed line represents theoretical MW at a given conversion, and (c) GPC traces with conversion for the reaction with EBPA. Reaction conditions:  $[\text{DPA}]_0/[\text{initiator}]_0/[\text{Na}_2\text{S}_2\text{O}_4]_0/[\text{CuBr}_2]_0/[\text{Me}_6\text{TREN}]_0=100/1/0.5/0.1/0.1$  (molar). ..... 82
- Figure 3.2:** Effect of solvent mixture in the SARA ATRP of DPA, IPA/water = 95/5 (v/v), ethanol/ $\text{H}_2\text{O}$  = 95/5 (v/v) and *tert*-butanol/ $\text{H}_2\text{O}$  = 95/5 (v/v) at 40 °C. (a,c) First-order kinetic plot, (b,d) evolution of MW and  $\bar{D}$  with conversion (the dashed line represents theoretical MW at a given conversion). Reaction conditions:  $[\text{DPA}]_0/[\text{EBiB}]_0/[\text{Na}_2\text{S}_2\text{O}_4]_0/[\text{CuBr}_2]_0/[\text{Me}_6\text{TREN}]_0 = 100/1/0.5/0.1/0.1$  (molar) (a,b);  $[\text{DPA}]_0/[\text{EBPA}]_0/[\text{Na}_2\text{S}_2\text{O}_4]_0/[\text{CuBr}_2]_0/[\text{Me}_6\text{TREN}]_0= 100/1/0.5/0.1/0.1$  (molar) (c,d). ..... 83
- Figure 2.3:** Effect of the ratio of  $\text{Na}_2\text{S}_2\text{O}_4$  on the SARA ATRP of DPA in IPA/water = 95/5 (v/v) at 40 °C. (A) First-order kinetic plot, (B) evolution of MW and  $\bar{D}$  with conversion (the dashed line represents theoretical MW at a given conversion). Reaction conditions:  $[\text{DPA}]_0/[\text{EBiB}]_0/[\text{Na}_2\text{S}_2\text{O}_4]_0/[\text{CuBr}_2]_0/[\text{Me}_6\text{TREN}]_0=100/1/\text{Na}_2\text{S}_2\text{O}_4/0.1/0.1$  (molar). ..... 85
- Figure 3.4:** Effect of the different feeding rates of  $\text{Na}_2\text{S}_2\text{O}_4$  solution in SARA ATRP of DPA, starting with 50% of  $\text{Na}_2\text{S}_2\text{O}_4$  in the solvent mixture, IPA/ $\text{H}_2\text{O}$  = 95/5 (v/v) at 40 °C. (a) First-order kinetic plot, (b) evolution of MW and  $\bar{D}$  with conversion (the dashed line represents theoretical MW at a given conversion). Reaction conditions:  $[\text{DPA}]_0/[\text{EBPA}]_0/[\text{Na}_2\text{S}_2\text{O}_4]_0/[\text{CuBr}_2]_0/[\text{Me}_6\text{TREN}]_0=100/1/\text{feeding}/0.1/0.2$  (molar). ..... 87
- Figure 3.5:** Effect of the feeding rates of  $\text{Na}_2\text{S}_2\text{O}_4$  solution in SARA ATRP of DPA, starting with 40% of  $\text{Na}_2\text{S}_2\text{O}_4$  in the solvent mixture, IPA/ $\text{H}_2\text{O}$  = 95/5 (v/v) at 40 °C. (a) First-order kinetic plot, (b) evolution of MW and  $\bar{D}$  with conversion (the dashed line represents theoretical MW at a given conversion) and, (c) GPC traces with conversion for reaction  $\text{IR}_{\text{Na}_2\text{S}_2\text{O}_4}= 40\%$  and  $\text{FR}_{\text{Na}_2\text{S}_2\text{O}_4}= 19 \text{ nmol} \cdot \text{min}^{-1}$ . Reaction conditions:  $[\text{DPA}]_0/[\text{EBPA}]_0/[\text{Na}_2\text{S}_2\text{O}_4]_0/[\text{CuBr}_2]_0/[\text{Me}_6\text{TREN}]_0=100/1/\text{feeding}/0.1/0.2$  (molar). ..... 89
- Figure 3.6:** Effect of the copper concentration in the SARA ATRP of DPA with feeding rate of aqueous solution of  $\text{Na}_2\text{S}_2\text{O}_4$ ,  $19.4 \text{ nmol} \cdot \text{min}^{-1}$ , starting with 40% of  $\text{Na}_2\text{S}_2\text{O}_4$  in the solvent mixture, IPA/ $\text{H}_2\text{O}$  = 95/5 (v/v) at 40 °C. (a) First-order kinetic plots, (b) evolution of MW and  $\bar{D}$  with conversion (the dashed line represents theoretical MW at a given conversion). Reaction conditions:  $[\text{DPA}]_0/[\text{EBPA}]_0/[\text{Na}_2\text{S}_2\text{O}_4]_0/[\text{CuBr}_2]_0/[\text{Me}_6\text{TREN}]_0=100/1/0.2/\text{CuBr}_2/\text{Me}_6\text{TREN}$  (molar). ..... 90

- Figure 3.7:** Influence of ligand and the copper concentration in the SARA ATRP of DPA with feeding rate of aqueous solution of  $\text{Na}_2\text{S}_2\text{O}_4$ ,  $16\text{nmol}\cdot\text{min}^{-1}$ , starting with 40% of  $\text{Na}_2\text{S}_2\text{O}_4$  in the solvent mixture, IPA/ $\text{H}_2\text{O}$  = 95/5 (v/v) at 40 °C. (a) First-order kinetic plots, (b) evolution of MW and  $\bar{D}$  with conversion (the dashed line represents theoretical MW at a given conversion), (c) GPC traces with conversion for reaction with  $\text{Me}_6\text{TREN}$  and 250ppm of Cu and (d) TPMA with 100ppm of copper. Reaction conditions:  $[\text{DPA}]_0/[\text{EBPA}]_0/[\text{Na}_2\text{S}_2\text{O}_4]_0/[\text{CuBr}_2]_0/[\text{ligand}]_0=100/1/0.2/1/2l$  (molar) ( $l=0.1$  or  $0.025$  for  $\text{Me}_6\text{TREN}$  and  $l=0.01$  for TPMA). ..... 91
- Figure 3.8:** SARA ATRP of OEOMA with feeding rate of aqueous solution of  $\text{Na}_2\text{S}_2\text{O}_4$ ,  $16\text{nmol}/\text{min}$ , starting with 40% of  $\text{Na}_2\text{S}_2\text{O}_4$  in the solvent mixture, 18wt%, IPA/water = 95/5 (v/v) at 25 °C. (a) First-order kinetic plot, (b) evolution of MW and  $\bar{D}$  with conversion (the dashed line represents theoretical MW at a given conversion). Reaction conditions:  $[\text{OEOMA}]_0/[\text{EBPA}]_0/[\text{Na}_2\text{S}_2\text{O}_4]_0/[\text{CuBr}_2]_0/[\text{Me}_6\text{TREN}]_0=30/1/0.2/0.1/0.2$  (molar)..... 94
- Figure 3.9:** GPC traces with conversion for the SARA ATRP of OEOMA with feeding rate of aqueous solution of  $\text{Na}_2\text{S}_2\text{O}_4$ ,  $16\text{nmol}\cdot\text{min}^{-1}$ , starting with 40% of  $\text{Na}_2\text{S}_2\text{O}_4$  in the solvent mixture, 18 wt%, IPA/ $\text{H}_2\text{O}$  = 95/5 (v/v) at 25 °C. Reaction conditions:  $[\text{OEOMA}]_0/[\text{EBPA}]_0/[\text{Na}_2\text{S}_2\text{O}_4]_0/[\text{CuBr}_2]_0/[\text{Me}_6\text{TREN}]_0=30/1/0.2/0.1/0.2$  (molar). ..... 95
- Figure 4.1:** GPC chromatographs of the POEOMA before (dash line) and after the chain extension with DPA, POEOMA-*b*-PDPA (solid line). Reaction conditions:  $[\text{OEOMA}]_0/[\text{EBPA}]_0/[\text{Na}_2\text{S}_2\text{O}_4]_0/[\text{CuBr}_2]_0/[\text{Me}_6\text{TREN}]_0=30/1/0.2/0.1/0.2$  (molar),  $[\text{OEOMA}] = 18$  wt %, in 6 mL of IPA/ $\text{H}_2\text{O}$  = 95/5 (v/v) and slow feeding of  $\text{Na}_2\text{S}_2\text{O}_4$  solution ( $16\text{nmol}\cdot\text{min}^{-1}$ ), 25 °C;  $[\text{DPA}]_0/[\text{POEOMA}]_0=100/1$  (molar). ..... 112
- Figure 4.2:**  $^1\text{H}$  NMR spectrum of POEOMA-*b*-PDPA copolymer in  $\text{CDCl}_3$ ,  $M_{n,\text{GPC}} = 23.2 \times 10^3$ ;  $\bar{D} = 1.29$  ..... 114
- Figure 4.3:** Titration curve of PEOMA<sub>18</sub>-*b*-PDPA<sub>91</sub> copolymer with NaOH 0.02M at 25°C. .... 115
- Figure 4.4:** Degree of copolymer ionization as a function of solution pH, determined from equation 4.1. .... 116
- Figure 4.5:** Variation of hydrodynamic diameter ( $D_h$ ) of POEOMA-*b*-PDPA copolymer in aqueous solutions as a function of solution pH, at 25 °C (the initial copolymer concentration at pH 2 was  $2.0\text{mg}\cdot\text{mL}^{-1}$ ). ..... 117
- Figure 4.6:** Size distribution profile of aqueous block copolymer dispersions, as determined by DLS at 25 °C. Nanostructures formed at pH 7.4 (solid line) and the block copolymer unimers at acidic conditions (dashed line) (copolymer concentration  $\sim 1\text{mg}\cdot\text{mL}^{-1}$ ). ..... 118
- Figure 4.7:** Hydrodynamic diameter ( $D_h$ ) of aqueous block copolymer dispersions at pH 8 after storage at room temperature for several weeks, as determined by DLS at 25°C. The error bars represent the standard deviation, according to the formula,  $\text{PDI} = (\sigma/D_h)^2$ . ..... 119

<b>Figure 4.8:</b> TEM micrographs, negatively stained with uranyl acetate, of self-assembled block copolymers of POEOMA- <i>b</i> -PDPA in water prepared by the solvent exchange method (1.0 mg.mL <sup>-1</sup> ) of: a) POEOMA <sub>17</sub> - <i>b</i> -PDPA <sub>45</sub> and b) POEOMA <sub>18</sub> - <i>b</i> -PDPA <sub>91</sub> taken at a Mag. x 100 000.....	121
<b>Figure 4.9:</b> Chemical structure of <i>N</i> -phenyl-1-naphthylamine (NPN).....	122
<b>Figure 4.10:</b> Fluorescence emission spectra of NPN in the presence of two different concentrations of copolymer solutions (a) and relative fluorescence intensity as a function of copolymer concentration for both POEOMA- <i>b</i> -PDPA copolymers (mg.mL <sup>-1</sup> ) (b).....	123
<b>Figure 5.1:</b> Schematic representation of the most reported xanthates for the RAFT polymerization of PVAc.....	136
<b>Figure 5.2:</b> Structures of RAFT agents synthesized: O-ethyl-S-(1-methoxycarbonyl) ethyl- dithiocarbonate (X <sub>1</sub> ), alkyne-terminated RAFT agent (AT-X <sub>1</sub> ) and protected alkyne-terminated RAFT agent (PAT-X <sub>1</sub> ). .....	144
<b>Figure 5.3:</b> Schematic representation of the synthesis strategy of the alkyne-terminated RAFT agent (AT-X <sub>1</sub> ). .....	145
<b>Figure 5.4:</b> <sup>1</sup> H NMR spectra in CDCl <sub>3</sub> of alkyne-terminated RAFT agent (AT-X <sub>1</sub> ). .....	145
<b>Figure 5.5:</b> Schematic representation of the synthesis strategy of the protected alkyne-terminated RAFT agent (PAT-X <sub>1</sub> ). .....	146
<b>Figure 5.6:</b> <sup>1</sup> H NMR spectra in CDCl <sub>3</sub> of protected alkyne-terminated RAFT agent (PAT-X <sub>1</sub> ). .....	146
<b>Figure 5.7:</b> (a) Kinetic plots of conversion and ln[M] <sub>0</sub> /[M] vs. time and (b) plot of number-average molecular weights ( <i>M</i> <sub>n,GPC</sub> ) and <i>D</i> vs. conversion (%) (the dashed line represents the theoretical molecular weight at a given conversion) for RAFT of VAc at 60 °C in 1,4-dioxane using X <sub>1</sub> . Reaction conditions: [VAc] <sub>0</sub> /[1,4-dioxane] <sub>0</sub> = 1/1 (w/w); [VAc] <sub>0</sub> /[X <sub>1</sub> ] <sub>0</sub> /[AIBN] <sub>0</sub> = 100/1/0.2 (molar). .....	148
<b>Figure 5.8:</b> (a) Kinetic plots of conversion and ln[M] <sub>0</sub> /[M] vs. time and (b) plot of number-average molecular weights ( <i>M</i> <sub>n,GPC</sub> ) and <i>D</i> vs. conversion (%) (the dashed line represents the theoretical molecular weight at a given conversion) for RAFT of VAc at 60 °C in 1,4-dioxane using AT-X <sub>1</sub> . Reaction conditions: [VAc] <sub>0</sub> /[1,4-dioxane] <sub>0</sub> = 1/1 (w/w); [VAc] <sub>0</sub> /[AT-X <sub>1</sub> ] <sub>0</sub> / [AIBN] <sub>0</sub> = 100/1/0.2 (molar). .....	149
<b>Figure 5.9:</b> (a) Kinetic plots of conversion and ln[M] <sub>0</sub> /[M] vs. time, (b) plot of number-average molecular weights ( <i>M</i> <sub>n,GPC</sub> ) and <i>D</i> vs. conversion (%) (the dashed line represents the theoretical molecular weight at a given conversion) and (c) evolution of the GPC traces with conversion for the RAFT polymerization of VAc in 1,4-dioxane at 60 °C using PAT-X <sub>1</sub> . Reaction conditions: [VAc] <sub>0</sub> /[1,4-dioxane] <sub>0</sub> = 1/1 (w/w); [VAc] <sub>0</sub> /[PAT-X <sub>1</sub> ] <sub>0</sub> /[AIBN] <sub>0</sub> = 100/1/0.2 (molar). .....	150
<b>Figure 5.10:</b> TGA weight loss curves of X <sub>1</sub> , AT-X <sub>1</sub> and PAT- X <sub>1</sub> , obtained at a heating rate of 10 °C.min <sup>-1</sup> . .....	152

<b>Figure 5.11:</b> The $^1\text{H}$ NMR spectrum of PVAc synthesized by RAFT polymerization using PAT- $X_1$ ( $M_{n,\text{GPC}} = 6.0 \times 10^3$ ; $M_{n,\text{NMR}} = 7.56 \times 10^3$ , $D = 1.36$ ) in $\text{CDCl}_3$ .	153
<b>Figure 5.12:</b> FTIR-ATR spectra of PAT- $X_1$ and PAT-PVAc.	153
<b>Figure 5.13:</b> UV-vis spectra of free-PVAc and PVAc synthesized through RAFT polymerization using the different RAFT agents, $X_1$ , AT- $X_1$ and PAT- $X_1$ respectively. Samples with $1.5 \text{ mg}\cdot\text{mL}^{-1}$ concentration in chloroform.	154
<b>Figure 5.14:</b> The GPC traces of PAT-PVAc samples before (on the right, grey line) and after chain extension (on the left, black line) experiment.	155
<b>Figure 5.15:</b> Schematic representation of the RAFT polymerization of VAc (1.1), PVAc deprotection (1.2) and synthesis of PEG- <i>b</i> -PVAc block copolymers by the CuAAC reaction (1.3).	155
<b>Figure 5.16:</b> GPC traces of the RALS signal of the PVAc and PVAc- <i>b</i> -PEG copolymer, after the coupling reaction.	156
<b>Figure 6.1:</b> RAFT polymerization of NVCL mediated by <i>O</i> -ethyl- <i>S</i> -(1-methoxycarbonyl)ethyl dithiocarbonate ( $X_1$ ), alkyne-terminated RAFT agent (AT- $X_1$ ) or protected alkyne terminated RAFT agent (PAT- $X_1$ ).	170
<b>Figure 6.2:</b> $^1\text{H}$ NMR spectrum of NVCL in $\text{CDCl}_3$ .	175
<b>Figure 6.3:</b> Schematic representation of NVCL hydrolysis, giving $\epsilon$ -caprolactam and acetaldehyde. <sup>45</sup>	176
<b>Figure 6.4:</b> $^1\text{H}$ NMR spectra of NVCL and 1,4-dioxane before and after 1h at 60 °C, in $\text{CDCl}_3$ .	177
<b>Figure 6.5:</b> Schematic representation and examples of the different classes of CTAs.	178
<b>Figure 6.6:</b> RAFT polymerization of NVCL mediated by $X_1$ , in 1,4-dioxane at 60 °C. (a) First-order kinetic plot, (b) evolution of MW and $D$ with conversion (the dashed line represents theoretical MW at a given conversion). Reaction conditions: $[\text{NVCL}]_0/[\text{X}_1]_0/[\text{AIBN}]_0 = 140/1/0.2$ (molar), $[\text{NVCL}]_0/[1,4\text{-dioxane}]_0 = 1/2$ (w/w).	179
<b>Figure 6.7:</b> RAFT polymerization of NVCL mediated by AT- $X_1$ (circle symbols) or PAT- $X_1$ (triangle symbols), in 1,4-dioxane at 60 °C. (a) First-order kinetic plot, (b) evolution of MW and $D$ with conversion (the dashed line represents theoretical MW at a given conversion). Reaction conditions: $[\text{NVCL}]_0/[\text{RAFT agent}]_0/[\text{AIBN}]_0 = 600/1/0.5$ (molar), $[\text{NVCL}]_0 = 2.47 \text{ M}$ .	180
<b>Figure 6.8:</b> GPC traces with retention time for the RAFT of NVCL at 60°C in 1,4-dioxane using PAT- $X_1$ . Reaction conditions: $[\text{NVCL}]_0/[\text{PAT-}X_1]_0/[\text{AIBN}]_0 = 600/1/0.5$ (molar); $[\text{NVCL}]_0 = 2.47 \text{ M}$ .	181
<b>Figure 6.9:</b> RAFT polymerization of NVCL mediated by PAT- $X_1$ in 1,4-dioxane at 60 °C. (a) First-order kinetic plot, (b) evolution of MW and $D$ with conversion (the dashed	



- line represents theoretical MW at a given conversion) and (c) GPC traces with retention time. Reaction conditions:  $[\text{NVCL}]_0/[\text{PAT-X}_1]_0/[\text{AIBN}]_0 = 600/1/0.5$  (molar),  $[\text{NVCL}]_0 = 3.70 \text{ M}$ ..... 182
- Figure 6.10:**  $^1\text{H}$  NMR spectra in  $\text{CDCl}_3$  of (a) the protected alkyne-terminated PNVCL obtained by RAFT polymerization mediated by PAT- $\text{X}_1$  and (b) alkyne-terminated PNVCL after the deprotection reaction. Reaction conditions:  $[\text{NVCL}]_0/[\text{PAT-X}_1]_0/[\text{AIBN}]_0 = 600/1/0.5$  (molar) in 1,4-dioxane at  $60^\circ\text{C}$ ,  $[\text{NVCL}]_0 = 3.71 \text{ M}$  ( $M_{n,\text{NMR}} = 36.63 \times 10^3$ ,  $M_{n,\text{GPC}} = 38.40 \times 10^3$ ,  $\mathcal{D} = 1.28$ )..... 184
- Figure 6.11:** FTIR spectra of protected alkyne terminated PNVCL (PAT-PNVCL) and alkyne terminated PNVCL obtained after the deprotection reaction (AT-PNVCL) ( $M_{n,\text{GPC}} = 38.40 \times 10^3$ ;  $\mathcal{D} = 1.28$ )..... 185
- Figure 6.12:** MALDI-TOF-MS (a) in the linear mode (using DT as a matrix) from  $m/z$  5000 to 18000 and (b) enlargement of the spectrum from  $m/z$  6200 to 7000 of protected alkyne-terminated PNVCL ( $M_{n,\text{GPC}} = 16.13 \times 10^3$ , and  $\mathcal{D} = 1.38$ ). Reaction conditions:  $[\text{NVCL}]_0/[\text{CTA}]_0/[\text{AIBN}]_0 = 600/1/0.5$  (molar);  $[\text{NVCL}]_0 = 3.71 \text{ M}$ , 1,4-dioxane,  $T = 60^\circ\text{C}$ . ... 187
- Figure 6.13:** MALDI-TOF-MS (a) in the linear mode (using DT as a matrix) from  $m/z$  5000 to 18000 and (b) enlargement of the spectrum from  $m/z$  6200 to 7200 of alkyne-terminated PNVCL after the deprotection reaction ( $M_{n,\text{GPC}} = 18.92 \times 10^3$ , and  $\mathcal{D} = 1.33$ )..... 189
- Figure 6.14:** TGA weight loss curves of the synthesized PNVCL and respective monomer, obtained at a heating rate of  $10^\circ\text{C}\cdot\text{min}^{-1}$ ..... 190
- Figure 6.15:** Schematic representation of the PNVCL conformation according to the aqueous solution temperature..... 191
- Figure 6.16:** Transmittance measurements as a function of temperature for  $1.0 \text{ mg}\cdot\text{mL}^{-1}$  aqueous solution of different kinetic points of the RAFT polymerization of NVCL mediated by PAT- $\text{X}_1$ . Reaction conditions:  $[\text{NVCL}]_0/\text{solvent} = 1/2$  (v/v),  $[\text{NVCL}]_0/[\text{PAT-X}_1]_0/[\text{AIBN}]_0 = 600/1/0.5$  (molar) in 1,4-dioxane,  $T = 60^\circ\text{C}$ ..... 192
- Figure 6.17:** Dependence of LCST with polymer MW. a) Plots of percentage transmittance vs temperature for various PNVCL samples in an aqueous solution ( $1.0 \text{ mg}\cdot\text{mL}^{-1}$ ) (the solid black lines represent the heating cycle and the dashed grey lines represent the cooling cycle). b) Variation of the cloud point temperature ( $T_{\text{CP}}$ ) with the PNVCL molecular weight in the heating cycle (closed symbols) and in the cooling cycles (open symbols). ..... 193
- Figure 6.18:** Percentage transmittance versus temperature plots (right) or number of cycles (left) for the aqueous solutions of the same PNVCL sample ( $1.0 \text{ mg}\cdot\text{mL}^{-1}$ ) synthesized through RAFT polymerization, for three heating and cooling consecutive cycles..... 194
- Figure 6.19:** Percentage transmittance vs temperature plots for the same PNVCL aqueous solution sample ( $1.0 \text{ mg}\cdot\text{mL}^{-1}$ ) synthesized through FRP, for two heating and cooling consecutive cycles ( $1.0^\circ\text{C}\cdot\text{min}^{-1}$ )..... 195

<b>Figure 6.20:</b> Dependence of the heating rate (a) and the presence of salts (b) in the LCST of PNVCCL samples. Percentage transmittance <i>vs</i> temperature plots for the same PNVCCL sample for (a) different heating rates (1.0, 0.5 and 0.1 °C.min <sup>-1</sup> ), in aqueous solution and (b) PBS solution (pH 7.4) and physiological saline solution (1.0 mg.mL <sup>-1</sup> ) (heating rate 1.0 °C.min <sup>-1</sup> ).....	195
<b>Figure 6.21:</b> Schematic representation of the (i) deprotection reaction of PNVCCL synthesized by RAFT mediated by PAT-X <sub>1</sub> and (ii) CuAAC reaction between mPEG-N <sub>3</sub> and AT-PNVCCL to afford PEG- <i>b</i> -PDPA copolymers. ....	197
<b>Figure 6.22:</b> GPC traces of the alkyne terminated PNVCCL (AT-PNVCCL), azide terminated PEG (mPEG-N <sub>3</sub> ) and the PEG- <i>b</i> -PNVCCL copolymer obtained after the CuAAC reaction.....	198
<b>Figure 7.1:</b> Schematic representation of the synthesis of POEOMA- <i>b</i> -PDPA copolymers.....	216
<b>Figure 7.2:</b> <sup>1</sup> H NMR spectrum of N <sub>3</sub> -POEOMA in CDCl <sub>3</sub> , M <sub>n,GPC</sub> = 11.93 x 10 <sup>3</sup> ; Đ = 1.11.....	217
<b>Figure 7.3:</b> The GPC traces of alkyne-terminated PNVCCL before (dashed line) and after the “click” coupling reaction with N <sub>3</sub> -POEOMA, resulting in POEOMA- <i>b</i> -PNVCCL (solid line). ....	218
<b>Figure 7.4:</b> <sup>1</sup> H NMR spectrum of POEOMA- <i>b</i> -PNVCCL block copolymer in CDCl <sub>3</sub> , M <sub>n,GPC</sub> = 44.75 x 10 <sup>3</sup> ; Đ = 1.20. ....	221
<b>Figure 7.5:</b> Transmittance measurements as a function of temperature for 1.0 mg.mL <sup>-1</sup> aqueous solutions of the POEOMA- <i>b</i> -PNVCCL copolymers (heating rate 1.0 °C.min <sup>-1</sup> ), and the precursor homopolymers. ....	222
<b>Figure 7.6:</b> Transmittance measurements as a function of temperature for 1.0 mg.mL <sup>-1</sup> PBS solution (pH 7.4) of the POEOMA- <i>b</i> -PNVCCL copolymers (heating rate 1.0 °C.min <sup>-1</sup> ).....	224
<b>Figure 7.7:</b> Evolution of the cloud point temperature (T <sub>CP</sub> ) of the POEOMA- <i>b</i> -PNVCCL block copolymers 1.0 mg.mL <sup>-1</sup> aqueous solutions (water, PBS solution or physiological saline solution) with the volume fraction of NVCL (Φ <sub>NVCL</sub> ). ....	224
<b>Figure 7.8:</b> Transmittance measurements as a function of temperature for 1.0 mg.mL <sup>-1</sup> PBS solution (pH 7.4) of the POEOMA <sub>16</sub> - <i>b</i> -PNVCCL <sub>126</sub> copolymer (heating/cooling rate 1.0 °C.min <sup>-1</sup> ).....	225
<b>Figure 7.9:</b> Size distribution (by intensity) of POEOMA- <i>b</i> -PNVCCL copolymers in water (0.5 mg.mL <sup>-1</sup> ), T= 45 °C. ....	226
<b>Figure 7.10:</b> Hydrodynamic diameter (D <sub>h</sub> ) of POEOMA <sub>16</sub> - <i>b</i> -PNVCCL <sub>390</sub> at 25 °C (dotted line) and 45 °C (solid line) (0.5 mg.mL <sup>-1</sup> ).....	228
<b>Figure 7.11:</b> Hydrodynamic diameter (D <sub>h</sub> ) of aqueous solution of PNVCCL homopolymer (M <sub>n,GPC</sub> = 41.35 x 10 <sup>3</sup> , Đ = 1.27) at 40 °C (0.5 mg.mL <sup>-1</sup> ). ....	229

<b>Figure 7.12:</b> TEM micrographs of self-assembled block copolymers of (a) POEOMA <sub>16</sub> - <i>b</i> -PNVCL <sub>126</sub> , (b) POEOMA <sub>16</sub> - <i>b</i> -PNVCL <sub>198</sub> , (c) POEOMA <sub>16</sub> - <i>b</i> -PNVCL <sub>240</sub> and (d) POEOMA <sub>16</sub> - <i>b</i> -PNVCL <sub>390</sub> , taken at a Mag. x 100 000 (0.5 mg.mL <sup>-1</sup> ).....	230
<b>Figure 7.13:</b> Dependence of the hydrodynamic diameter (D <sub>h</sub> ) of aqueous solution of POEOMA <sub>16</sub> - <i>b</i> -PNVCL <sub>390</sub> in water (0.5 mg.mL <sup>-1</sup> ) with temperature. ....	231
<b>Figure 7.14:</b> Transmittance measurements as a function of temperature for 0.5 mg.mL <sup>-1</sup> aqueous solution of the POEOMA <sub>16</sub> - <i>b</i> -PNVCL <sub>390</sub> copolymer at two different heating rates, 1.0 °C.min <sup>-1</sup> (triangle grey symbol) and 0.1 °C.min <sup>-1</sup> (square black symbol) with pictures of the sample taken at 30 °C and 45 °C.....	232
<b>Figure 7.15:</b> Fluorescence spectra of Nile red in water at different concentrations of the POEOMA <sub>16</sub> - <i>b</i> -PNVCL <sub>390</sub> copolymer (left) and plot of intensity vs logarithm of concentration of POEOMA <sub>16</sub> - <i>b</i> -PNVCL <sub>390</sub> copolymer (right).....	235
<b>Figure 8.1:</b> Schematic representation of the synthesis of the 4 <sup>th</sup> generation polyester dendron by the double stage convergent approach <sup>23</sup> . (i) TsOH, acetone, r.t.; (ii) KOH, DMF, 100 °C; (iii) DCC, DPTS, DCM; r.t. (iv) Pd/C, H <sub>2</sub> , EtOAc, r.t.; (v) Dowex <sup>®</sup> , H <sup>+</sup> , EtOAc, r.t.; (vi) DCC, DPTS, DCM, r.t.; (vii) Pd/C, H <sub>2</sub> , EtOAc.....	258
<b>Figure 8.2:</b> Schematic representation of the anhydride synthesis from the acetonide protected monomer.....	259
<b>Figure 8.3:</b> Schematic representation of the synthesis of different generation dendrons, by the divergent grow based on anhydride coupling from bis-MPA, with an azide group at the focal point. (i) H <sub>2</sub> O, reflux; (ii) DMAP, DPTS, DCC, DCM, r.t.; (iii) Dowex <sup>®</sup> , H <sup>+</sup> , MeOH, r.t.; (iv) DMAP, pyridine, DCM.....	259
<b>Figure 8.4:</b> Schematic representation of the synthesis of different generation dendrons, by the divergent grow based on anhydride coupling from bis-MPA, with an alkyne group at the focal point. (i) DMAP, DPTS, DCC, DCM, r.t.; (ii) Dowex <sup>®</sup> , H <sup>+</sup> , MeOH, r.t.; (iii) DMAP, pyridine, DCM.....	260
<b>Figure 8.5:</b> <sup>1</sup> H NMR spectra of N <sub>3</sub> -G#1-Ac ((9), N <sub>3</sub> -G#2-Ac (11), N <sub>3</sub> -G#1-(OH) <sub>4</sub> (12), in CDCl <sub>3</sub> . ....	261
<b>Figure 8.6:</b> FTIR-ATR spectra of the azido functionalized dendrons.....	262
<b>Figure 8.7:</b> Schematic representation of the synthesis of mPEG-COOH (a) and the conjugation to the N <sub>3</sub> -G#1-(OH) <sub>2</sub> dendron. (i) and (ii) DCM, r.t.....	263
<b>Figure 8.8:</b> FTIR-ATR spectra of the mPEG and mPEG-COOH. ....	264
<b>Figure 8.9:</b> <sup>1</sup> H NMR spectra of N <sub>3</sub> -G#1-(OH) <sub>2</sub> (10), mPEG <sub>44</sub> -COOH and N <sub>3</sub> -G#1-(mPEG <sub>44</sub> ) <sub>2</sub> , in CDCl <sub>3</sub> . ....	264
<b>Figure 8.10:</b> FTIR-ATR spectra of the initial 1 <sup>st</sup> generation azide dendron (N <sub>3</sub> -G#1-(OH) <sub>2</sub> ) and after functionalization with mPEG-COOH (N <sub>3</sub> -G#1-(mPEG <sub>44</sub> ) <sub>2</sub> ).....	265

<b>Figure 8.11:</b> GPC traces of the mPEG <sub>113</sub> -COOH (dashed line) and the 2 <sup>nd</sup> generation azide dendron functionalized with mPEG <sub>113</sub> (N <sub>3</sub> -G#2-(mPEG <sub>113</sub> ) <sub>4</sub> ) (solid line).....	266
<b>Figure 8.12:</b> two-step synthesis of PgEBPA. ....	267
<b>Figure 8.13:</b> The <sup>1</sup> H NMR spectra of PgEBPA initiator and AT-PDPA in CDCl <sub>3</sub> (M <sub>n,GPC</sub> = 11.31 x10 <sup>3</sup> , Đ = 1.18, M <sub>n,NMR</sub> = 5.90 x10 <sup>3</sup> ). ....	269
<b>Figure 8.14:</b> Schematic representation of (a) (PNVCL) <sub>n</sub> -G#0-mPEG <sub>y</sub> , (b) (PNVCL) <sub>n</sub> -G#1-(mPEG <sub>y</sub> ) <sub>2</sub> and (c) (PNVCL) <sub>n</sub> -G#2-(mPEG <sub>y</sub> ) <sub>4</sub> . ....	271
<b>Figure 8.15:</b> Schematic representation of (a) (PDPA) <sub>n</sub> -G#0-mPEG <sub>y</sub> , (b) (PDPA) <sub>n</sub> -G#1-(mPEG <sub>y</sub> ) <sub>2</sub> and (c) (PDPA) <sub>n</sub> -G#2-(mPEG <sub>y</sub> ) <sub>4</sub> . ....	272
<b>Figure 8.16:</b> <sup>1</sup> H NMR spectrum of the PDPA <sub>49</sub> -G#1-(mPEG <sub>44</sub> ) <sub>2</sub> obtained after the “click” reaction between the N <sub>3</sub> -G#1-(mPEG <sub>44</sub> ) <sub>2</sub> and AT-PDPA <sub>49</sub> , in CDCl <sub>3</sub> .....	273
<b>Figure 8.17:</b> <sup>1</sup> H NMR spectrum of the PNVCL <sub>106</sub> -G#2-(mPEG <sub>44</sub> ) <sub>4</sub> obtained after the “click” reaction between the N <sub>3</sub> -G#2-(mPEG <sub>44</sub> ) <sub>4</sub> and AT-PNVCL <sub>106</sub> , in CDCl <sub>3</sub> .....	273
<b>Figure 8.18:</b> GPC traces of the RALS signal of the PDPA <sub>102</sub> and the LDBC, PDPA <sub>102</sub> -G#1-(mPEG <sub>44</sub> ) <sub>2</sub> copolymer, after the “click” coupling reaction. ....	274
<b>Figure 8.19:</b> GPC traces of the RALS signal of the PNVCL <sub>131</sub> and the LDBC, PNVCL <sub>131</sub> -G#2-(mPEG <sub>44</sub> ) <sub>4</sub> copolymer, after the “click” coupling reaction. ....	274

---

**List of schemes**

<b>Scheme 1.1:</b> Schematic representation of the general equilibrium between dormant and active species in RDRP. ....	4
<b>Scheme 1.2:</b> General schemes of the three main RDRP methods: (1) SFRP, (2) RAFT/DT and (3) Metal Catalyzed. $\bullet Y$ - nitroxide or metal complex; $P_n^\bullet$ - propagation radicals; $P_n-Y$ , $P_n-Z$ , $P_n-X$ – dormant species; Z- iodine, dithioester, organometalic species, etc; $Mt^m/L$ – transition metal complex. ....	6
<b>Scheme 3.1:</b> General mechanism of copper catalyzed ATRP. ....	78
<b>Scheme 3.2:</b> Scheme of the sodium dithionite decomposition. ....	85
<b>Scheme 4.1:</b> a) Chemical structure of the POEOMA- <i>b</i> -PDPA copolymer synthesized by SARA ATRP and b) illustration of the proposed self-assembly mechanism of the POEOMA- <i>b</i> -PDPA copolymers in aqueous media, for $pH > pK_a$ . ....	106



---

**List of tables**

<b>Table 1.1:</b> Examples of temperature responsive polymers and its critical solution temperatures in water. ....	19
<b>Table 2.1:</b> SARA-ATRP of PDA in the presence of CuBr <sub>2</sub> /Me <sub>6</sub> TREN and Na <sub>2</sub> S <sub>2</sub> O <sub>4</sub> at 40 °C in IPA/H <sub>2</sub> O (monomer/solvent ratio: 1/2 (v/v)). ....	59
<b>Table 2.2:</b> MALDI-TOF MS peaks assignment. ....	63
<b>Table 3.1.</b> SARA ATRP of PDA with Na <sub>2</sub> S <sub>2</sub> O <sub>4</sub> , in IPA/H <sub>2</sub> O = 95/5 (v/v) at 40 °C. Reaction conditions: [DPA] <sub>0</sub> /[EBPA] <sub>0</sub> /[Na <sub>2</sub> S <sub>2</sub> O <sub>4</sub> ] <sub>0</sub> /[CuBr <sub>2</sub> ] <sub>0</sub> /[Me <sub>6</sub> TREN] <sub>0</sub> = 100/1/IR <sub>Na<sub>2</sub>S<sub>2</sub>O<sub>4</sub></sub> /0.1/0.2 (molar). ....	93
<b>Table 4.1:</b> List of copolymers prepared by SARA ATRP with Na <sub>2</sub> S <sub>2</sub> O <sub>4</sub> by one-pot polymerization reaction. Reaction conditions: [OEOMA] <sub>0</sub> /[EBPA] <sub>0</sub> /[Na <sub>2</sub> S <sub>2</sub> O <sub>4</sub> ] <sub>0</sub> /[CuBr <sub>2</sub> ] <sub>0</sub> /[Me <sub>6</sub> TREN] <sub>0</sub> =DP/1/0.2/0.1/0.2 (molar), OEOMA 18wt%, IPA/H <sub>2</sub> O= 95/5 (v/v) and slow feeding of Na <sub>2</sub> S <sub>2</sub> O <sub>4</sub> solution (16 nmol.min <sup>-1</sup> ), 40 °C. ....	113
<b>Table 4.2:</b> Characteristics of the self-assembled structures formed in water at 25 °C, from the POEOMA- <i>b</i> -PDPA copolymers using two different self-assembly procedures (1.0 mg.mL <sup>-1</sup> ). ....	120
<b>Table 5.1:</b> Kinetic parameters for the RAFT polymerization of VAc using the X <sub>1</sub> , AT-X <sub>1</sub> or PAT-X <sub>1</sub> in 1,4-dioxane. Reaction conditions: [VAc] <sub>0</sub> /[1,4-dioxane] = 1/1 (w/w); [VAc] <sub>0</sub> /[RAFT agent] <sub>0</sub> /[initiator] <sub>0</sub> = 100/1/0.2. ....	151
<b>Table 6.1:</b> RAFT polymerization of NVCL with PAT-X <sub>1</sub> , in 1,4-dioxane at 60 °C. Reaction conditions: (monomer/solvent ratio: 1/1 (w/w)), [NVCL] <sub>0</sub> /[PAT-X <sub>1</sub> ] <sub>0</sub> /[AIBN] <sub>0</sub> = 600/1/0.5. ....	183
<b>Table 6.2:</b> Elemental analysis of the PNVCL samples synthesized by RAFT polymerization mediated by PAT-X <sub>1</sub> . ....	186
<b>Table 6.3:</b> MALDI-TOF-MS peak assignment for protected alkyne-terminated PNVCL (Figure 6.12). ....	188
<b>Table 6.4:</b> TGA of PNVCL (T <sub>x%</sub> : temperature at x% mass loss; T <sub>on</sub> : extrapolated onset temperature). ....	189
<b>Table 7.1:</b> Characteristics of POEOMA- <i>b</i> -PNVCL block copolymers. ....	220
<b>Table 7.2:</b> Cloud point temperatures (T <sub>CP</sub> ) of the POEOMA- <i>b</i> -PNVCL block copolymers 1.0 mg.mL <sup>-1</sup> in water, PBS solution (pH 7.4) and physiological saline solution (NaCl 0.9% ) (heating rate 1.0 °C.min <sup>-1</sup> ). ....	223
<b>Table 7.3:</b> Characteristics of the self-assembled structures formed in water at 45 °C, from the POEOMA- <i>b</i> -PNVCL copolymers. ....	227

<b>Table 7.4:</b> Characteristics of the self-assembled structures formed at 45 °C from the POEOMA- <i>b</i> -PNVCL copolymers in PBS (pH 7.4) or physiological saline (NaCl 0.9 %) solutions. ....	233
<b>Table 7.5:</b> Results from the encapsulation assays with Nile red. ....	236
<b>Table 8.1:</b> N <sub>3</sub> -dendron-(OH) <sub>x</sub> functionalization with PEG segments.....	266
<b>Table 8.2:</b> Characteristics of the AT-PDPA synthesized by SARA ATRP with Na <sub>2</sub> S <sub>2</sub> O <sub>4</sub> , in IPA/water = 95/5 (v/v) at 40 °C. Reaction conditions: [DPA] <sub>0</sub> /[PgEBPA] <sub>0</sub> /[Na <sub>2</sub> S <sub>2</sub> O <sub>4</sub> ] <sub>0</sub> /[CuBr <sub>2</sub> ] <sub>0</sub> /[Me <sub>6</sub> TREN] <sub>0</sub> =DP/1/0.2/0.1/0.2 + feeding Na <sub>2</sub> S <sub>2</sub> O <sub>4</sub> .....	268
<b>Table 8.3:</b> Characteristics of the PNVCL synthesized by RAFT polymerization with PAT-X <sub>1</sub> , in 1,4-dioxane at 60 °C. Reaction conditions: [NVCL] <sub>0</sub> /[PAT-X <sub>1</sub> ] <sub>0</sub> /[AIBN] <sub>0</sub> = 600/1/0.5, (NVCL/solvent ratio: 1/1 (w/w)). ....	270
<b>Table 8.4:</b> Characteristics of the temperature-responsive LDBC synthesized by CuAAC. ....	271
<b>Table 8.5:</b> Characteristics of the pH-responsive LDBC synthesized by CuAAC. ....	272



## **Motivation, targets and research significance**

Over the last decade, engineered nanomaterials have emerged as a promising route to produce well-defined nanostructures for a broad range of advanced applications. The remarkable developments in reversible deactivation radical polymerization (RDRP) methods allow the synthesis of tailor made (co)polymers, with predicted structure, composition and molecular weight. The possibility to tune the properties of each polymer segment is of extremely importance to afford the preparation of tailor made nanoparticles for biomedical applications. However, most of the reported polymerization methods deal with harmful organic solvents or require the use of high concentrations of metal catalysts which can contaminate the resultant polymer and induce cytotoxicity.

The nanoparticles based on the supramolecular self-assembly of amphiphilic block copolymers have been proposed as an interesting approach for the development of advanced drug delivery systems (DDS). Furthermore, the use of stimuli-responsive polymers allow the adjustment of the solution behavior of the block copolymers according to the surrounding environmental conditions and therefore control the self-assembly process. Therefore, the polymeric nanocarrier becomes an active participant in the transport and release of the drug and its properties can be customized depending on the target application.

This project aimed to improve some polymerization methodologies in order to obtain well-defined polymers with high chain-end functionality. In this sense, the main goal was to synthesize biomedical relevant polymers using RDRP methods under mild reactions conditions (e.g, reduced amounts of metal catalysts and less toxic solvents). At the same time, it was also intended to extend the use of the RDRP methods to some challenging monomers that possess equally interesting properties to be applied in the biomedical field but have not been completely explored due to its less-activated nature. The conjugation of the RDRP methods with the concept of “click” chemistry has increased the scope of macromolecular engineering, allowing the easy and efficient synthesis and modification of (co)polymers. On this matter, the different RDRP methods applied throughout the project were designed to incorporate “clickable” functionalities that allow the functionalization of the resultant polymers or its

conjugation for the development of novel block copolymers and consequently expand the range of possible block copolymer architectures.

It is expected that this work can contribute to the improvement of the synthetic tools for the development of well-defined (co)polymers to be applied in the biomedical field. The use of the RDRP methods and the consequent stringent control over the polymeric structures allows the preparation of nanocarriers with similar size and solution characteristics, resulting in systems that have enhanced pharmacokinetic behavior. The responsive nature of the polymers prepared in the project, and their ability to trigger the DDS fast response, upon a small change in the surrounding environment, turns such materials interesting candidates to be applied in cancer therapies, which is known to be a worldwide disease that affects millions of people. This work will contribute to the development of the next generation of (co)polymers and/or nanoparticles to be applied in cancer therapeutics.

# **Chapter1**

---

---

## **Literature review**



## 1.1. Macromolecular Engineering

The number of nanostructures with different morphologies and architectures that are prepared using amphiphilic block copolymers is growing exponentially. This reality is clearly associated to the recent advances in polymer synthesis, namely the developments in reversible deactivation radical polymerization (RDRP) methods and its conjugation with other organic chemistry strategies (e.g. “click” chemistry).<sup>1, 2</sup> Macromolecular engineering is a discipline that enables the preparation of polymers with controlled size, structure, topology and ultimately the polymer properties. It comprises the design and the development of well-defined polymers with tailored features that fulfil specific applications.<sup>3</sup>

The synthesis of linear, branched, or cross-linked polymers with controlled structure is now well-known and easily accessible for a vast range of polymer functionalities. Individual polymeric architectures can now be tailored for specific applications in a wide range of fields.<sup>4</sup> Nowadays nanotechnology is particularly focused in “nano” architectures constructed by “bottom-up” approaches, through self-assembly methods.<sup>5</sup> The design and synthesis of molecules or macromolecules that can further organize themselves, in solution, by self-assembly into a desired pattern is the key to develop new nanostructures with the specific features (Figure 1.1).

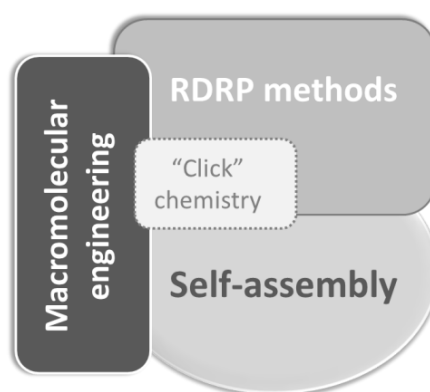


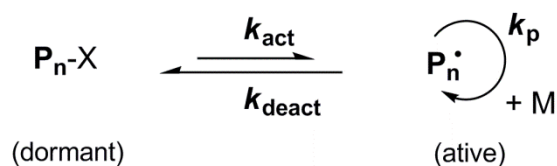
**Figure 1.1:** Macromolecular engineering, the tool to create functional nanostructures: from RDRP methods to self-assembly.

Indeed, the control over the synthesis of macromolecules by changing their chemistry or architecture enables the complete adjustment of their final properties in order to fit specific requirements. Polymer post-functionalization is also an important route to afford new materials with controlled structure. Highly functional and monodisperse macromolecules with tailored architecture constitute the key to prepare efficient and smart nanomaterials, which can be useful for a myriad of advanced applications.<sup>4, 6, 7</sup>

## 1.2. Reversible deactivation radical polymerization

RDRP emerged in the last two decades to overcome the limitations of conventional free radical polymerization (FRP).<sup>8</sup> RDRP methods present several advantages over FRP, such as: compatibility with a wide range of monomers with different functionalities, tolerance to aqueous media, and mild reaction conditions. But at the same time, these methods allow the synthesis of well-defined polymers, due to a stringent control over the macromolecular properties, including molecular weight (MW), molecular weight distribution ( $\mathcal{D}$ ), topology, composition, chain architecture and site-specific functionality.<sup>7, 9, 10</sup> The living character of the polymer chains allows further reinitiation by adding fresh monomers (or post-polymerization modifications) aiming the synthesis of controlled block copolymers. Since 1995, the number of publications on RDRP has been increasing exponentially.<sup>11</sup>

RDRP strategies involve the establishment of an dynamic equilibrium between active (propagating radicals) and dormant species<sup>8, 12-16</sup> that is responsible to maintain a very low concentration of radicals during the polymerization (Scheme 1.1).



**Scheme 1.1:** Schematic representation of the general equilibrium between dormant and active species in RDRP.

The RDRP relies on the extending the life time of the propagation reactions from around 1s (as it is in FRP) to more than 1 day (in some cases). This phenomenon is possible due to the formation of dormant species of ~1 minutes after each ~1 ms of activity. The extension of lifetime of propagating radicals is guaranteed by the dynamic equilibrium between a low concentration of active radicals and a predominant amount of dormant species, which are unable to propagate or terminate. The chains that are not active at a certain moment (they are in their dormant state) are fully capable of being reinitiated or functionalized.<sup>12, 17, 18</sup>

Among several RDRP methods available in the literature, the most studied are either based on a reversible activation/deactivation mechanism: stable free radical polymerization (SFRP), most commonly the nitroxide mediated polymerization (NMP)<sup>19</sup> or metal catalysed RDRP<sup>20, 21</sup>: atom transfer radical polymerization (ATRP)<sup>20</sup> and single electron transfer living radical polymerization (SET-LRP)<sup>22</sup>); or based on reversible chain transfer: the reversible addition fragmentation transfer (RAFT)<sup>10</sup> and the degenerative transfer (DT) (Figure 1.2).

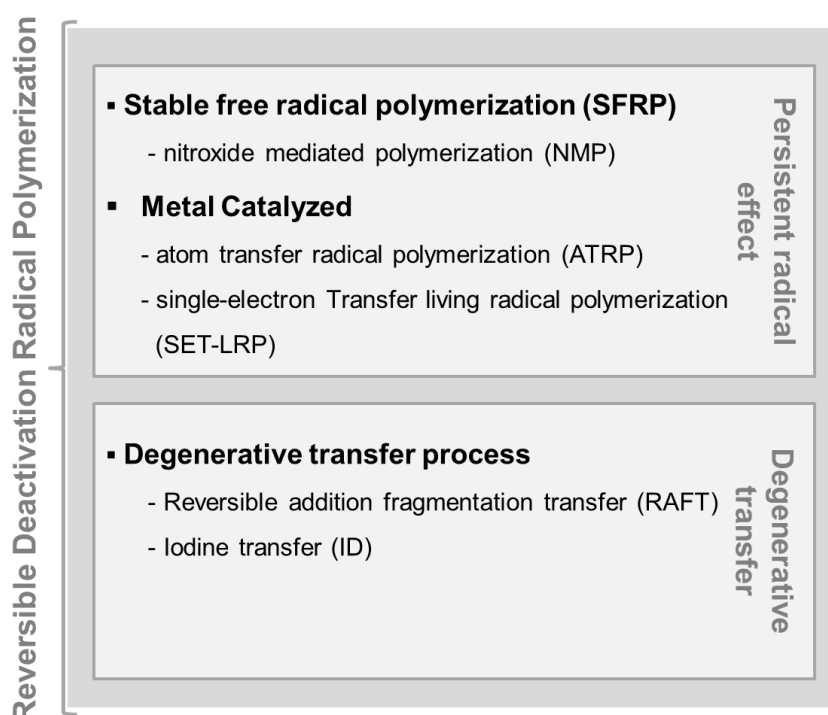
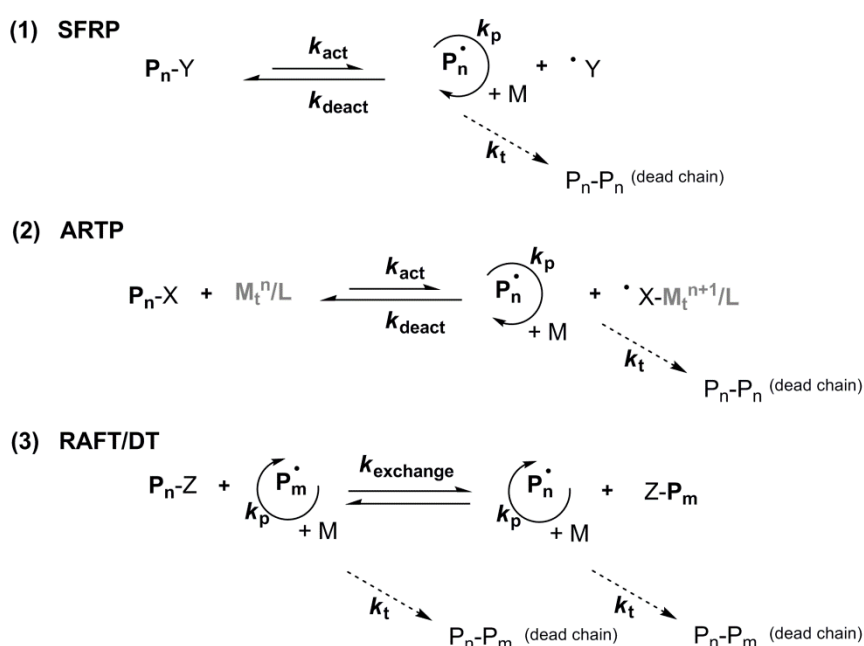


**Figure 1.2:** Reversible deactivation radical polymerization (RDRP) methods.

Both mechanisms involve the equilibrium between active (propagating radicals) and dormant species.<sup>12, 15</sup> The different RDRP methods have a low concentration of propagation chains achieved by a fast transition between active and dormant species. This feature is essential for the control over MW, dispersity ( $\bar{D}$ ) and chain-end functionality. During propagation steps, the growing species should add only a small number of monomer units (in milliseconds) and then be deactivated back to the dormant state (and remain for several seconds).<sup>12</sup> Scheme 1.2 represents the three main RDRP methods.



**Scheme 1.2:** General schemes of the three main RDRP methods: (1) SFRP, (2) RAFT/DT and (3) Metal Catalyzed.  $\bullet Y$ - nitroxide or metal complex;  $P_n^{\bullet}$  - propagation radicals;  $P_n-Y$ ,  $P_n-Z$ ,  $P_n-X$  – dormant species; Z- iodine, dithioester, organometallic species, etc;  $Mt^m/L$  – transition metal complex.

The RDRP dynamic equilibrium can be accomplished in two distinct ways. In the case of SFRP and ATRP (Scheme 1.2, (1) and (2)) the propagating radicals are reversible deactivated to form dormant species as a result of the so-called persistent radical effect (PRE).<sup>23</sup> Generally in NMP the control is achieved with dynamic equilibrium between dormant alkoxyamines and active propagating radicals<sup>16</sup>, being the 2,2,6,6-tetramethylpiperidinyl-1-oxyl (TEMPO) the most used cyclic nitroxide stable



radical to control the polymerization<sup>12</sup> (Scheme 1.2, (1)). Metal catalyzed RDRP is based in the formation of active radicals through a redox process mediated by a transition metal complex<sup>11</sup> (Scheme 1.2, (2)). Regarding the RAFT polymerization (Scheme 1.2, (3)), the mechanism involves the reversible reaction of a RAFT agent between the dormant species and the propagation radicals resulting in the transfer of the end group from the transfer-agent to the radical.<sup>24</sup> In the case of the DT process, this transfer reaction involves, for example an iodine atom (iodine transfer). Both RAFT and ATRP methods will be discussed in more detail in the following sections.

### 1.2.1. Atom transfer radical polymerization - ATRP

Metal catalyzed ATRP is the most studied strategy among RDRP methods due to several reasons: easy procedures compared to the other methods, high efficiency, high tolerance to a wide range of monomer functionalities and the commercial availability of most compounds.<sup>14, 21, 25, 26</sup> In ATRP, the dynamic equilibrium between the growing radicals and the dormant species is mediated by a metal catalyst/ligand complex and an alkyl halide initiator. The general equilibrium of ATRP was presented previously in Scheme 1.1 and is shown again in Figure 1.3, (a). Herein, a transition-metal complex ( $M_t^n/L$ ) composed by a transition metal species and a complexing ligand (L) is responsible for the homolytic cleavage of an alkyl halogen bond  $P_n-X$  (dormant species), which generates the corresponding higher oxidation state metal halide complex  $X-M_t^{n+1}/L$  and the propagation radical  $P_n^\bullet$ .<sup>12</sup> The metal transition between a lower oxidation state and a higher oxidation state controls the ATRP dynamic equilibrium. Different transition metals have been reported in the literature, such as: ruthenium, copper, iron and nickel.<sup>27, 28</sup> The ligand is typically a nitrogen-based compound that promotes the solubilisation of the transition metal in the reaction medium, and also adjusts the redox potential of the metal centre, which controls the reactivity and the dynamics of the atom transfer process.<sup>25</sup> The nature of the metal complex catalyst/ligand should be adjusted depending on the monomer to be polymerized.<sup>12</sup> Besides the structure of the catalysts,<sup>29</sup> other factors such as the reaction medium and the choice of the initiator<sup>30</sup> have an important impact on ATRP equilibrium.<sup>11</sup>

The main drawbacks of the ATRP method are associated with some toxicity of the transition-metal complexes, and possible contamination of the polymer at the end of the polymerization.

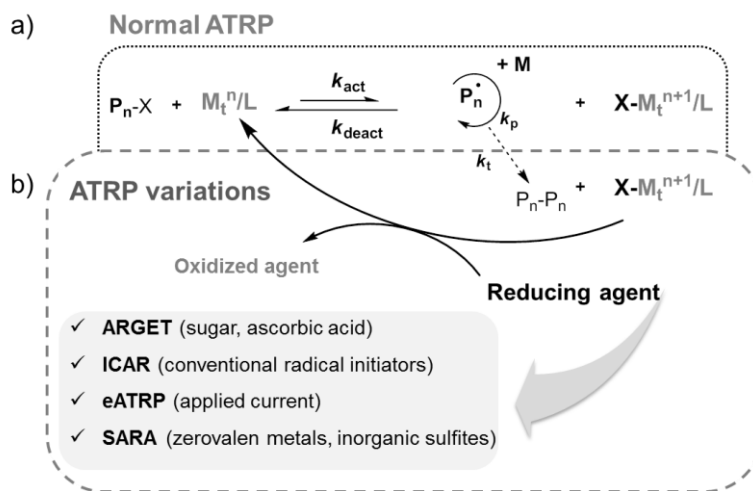


**Figure 1.3:** Schematic representation of the normal ATRP and ATRP variations.

During the last decade, the ATRP process have been evolved significantly from the “original” (or “normal”) ATRP, to some variations that enable the use of only very low concentrations of the metal catalyst and mild reaction conditions. These ATRP variations allow the polymerization to start with the stable  $\text{Cu}^{\text{II}}$  species being the  $\text{Cu}^{\text{I}}$  activator species continuously regenerated in the presence of reducing agents (Figure 1.3, (b)).<sup>11</sup>

In activators regenerated by electron transfer (ARGET), the polymerization occurs in the presence of low amounts of catalyst and reducing agents such as tin(II) 2-ethylhexanoate ( $\text{Sn}(\text{EH}_2)$ ), glucose, ascorbic acid, among others, that continuously regenerate the ATRP activator.<sup>31</sup> In another process, called initiators for continuous activator regeneration (ICAR), a source of organic free radicals (such as azo compounds) is employed to continuous regeneration of the  $\text{Cu}^{\text{I}}$  activator.<sup>32</sup> The use of chemical reducing agents can be replaced by the application of electric current to the system in method called electrochemically mediated ATRP (eATRP). Another important ATRP variation is the supplemental activators and reducing agent (SARA) ATRP, that uses either zero valent metals such as  $\text{Cu}(0)$ ,  $\text{Fe}(0)$ ,  $\text{Zn}(0)$ ,  $\text{Mg}(0)$  or  $\text{Ag}(0)$ , or organic sulfites to act not only as reducing agents but also as supplemental activators

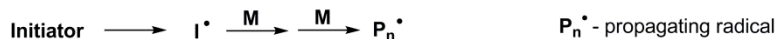
of the dormant species.<sup>33-36</sup> These ATRP variations allow the significant reduction of the required concentrations of the metal catalyst, the use of non-toxic solvents, mild reaction conditions without the need of completely deoxygenated solutions and low reaction temperatures. New trends in such ARTP variation methods involve the design of biologically compatible reaction conditions. On this matter, the use of water, very low copper concentration and a biologically compatible reducing agent allows the direct synthesis of protein-polymer hybrid materials.<sup>37</sup>

### 1.2.2. Reversible addition fragmentation transfer – RAFT

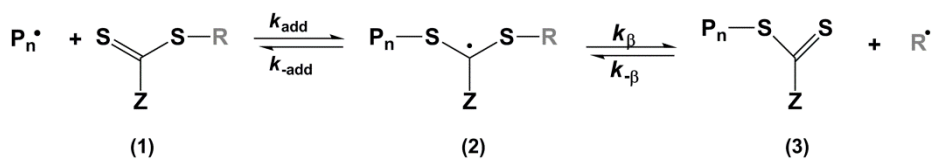
The RAFT polymerization is driven by a degenerative chain transfer process. The polymerization is mediated by RAFT agents that possess a thiocarbonylthio moiety and an R and Z groups (compound 1, Figure 1.4) and involve the use of conventional initiators as a radical source.<sup>38</sup>

The generally accepted mechanism for a RAFT polymerization is composed by a sequence of addition fragmentation equilibria and is presented in Figure 1.4. In the first step, initiation, a conventional radical initiator is decomposed and reacts with the monomer units to generate the first propagating radicals ( $P_n^\bullet$ ). Those oligomeric radicals (1) will react with the RAFT agent (Figure 1.4, step (ii)) forming a polymeric thiocarbonylthio compound (3) and a new radical ( $R^\bullet$ ). All of the RAFT agent should be consumed in this initial equilibrium step. The monomer units will then react with  $R^\bullet$  and a new propagating radical is formed ( $P_m^\bullet$ ) (Figure 1.4, step (iii)). Then, the main equilibrium (Figure 1.4, step (iv)) is established between the active propagating radicals ( $P_n^\bullet$  and  $P_m^\bullet$ ) and the dormant polymeric thiocarbonylthio compounds (3). The polymer chains grow by the addition of new monomer units to the active propagating radicals. In this process, the rapid equilibrium between the propagation step and the formation of the intermediate specie (4) limits the termination reactions and allows the polymer to grow in a controlled manner. However, inherent to the nature of a radical process, some termination reactions will occur (Figure 1.4, step (v)).<sup>38, 39</sup> At the end of the polymerization, the polymeric chain retains the thiocarbonyl group which is responsible for the “living” character of the polymers.

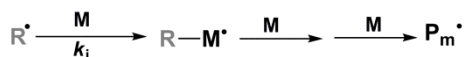
(i) Initiation



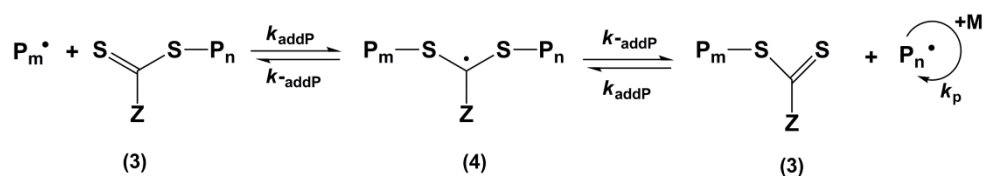
(ii) Initial equilibrium



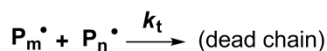
(iii) Reinitiation



(iv) Main equilibrium



(v) Termination

**Figure 1.4:** Mechanism of RAFT polymerization.

The success of the RAFT process is strongly related with the appropriate selection of a RAFT agent for the specific monomer.<sup>10, 12</sup> In the thiocarbonylthio compound, both substituents R and Z highly influence the success of the RAFT polymerization. The leaving group, R, should be a good homolytic leaving group in comparison to the propagating radical and in its radical form should be capable of efficiently reinitiate the polymerization. Z group controls the reactivity of the C=S bond and it influences the rate of radical addition and fragmentation.<sup>12, 40, 41</sup> The mostly reported RAFT agents are the dithioesters (Z = alkyl or aryl), trithiocarbonates (Z = SR'), dithiocarbamates (Z = NR'R'') or xanthates (R = OR').<sup>12</sup> While the first two can efficiently control the polymerization of more activated monomers, such as methacrylates or styrene, they are not suitable for the controlled polymerization of non-activated vinyl monomers such as vinyl acetate (VAc) or N-vinyl lactams.<sup>12, 42, 43</sup>

The RAFT polymerization is a very versatile process that is tolerant to a large range of monomers and to a variety of reaction conditions. In fact, by choosing the correct RAFT

agent is possible to conduct the controlled polymerization of some non-activated monomers, otherwise more difficult to access through other RDRP methods.<sup>44</sup> The main drawback of this polymerization concerns the synthetic methods to obtain the RAFT agents that are extremely laborious. Other limitations involve the scarce number of commercial RAFT agents (or their high price when available) and the color that contaminates the resultant polymer.<sup>38</sup>

### **1.2.3. RDRP – Synthesis of tailor made polymers**

The polymers obtained from RDRP methods possess active chain-ends that can be reinitiated to allow the further polymerization of other monomers, aiming to synthesize block copolymers. Linear copolymers with different compositions and segments are now easily achieved using those methods (Figure 1.5). Complex architectures and the introduction of site-specific functionalities that were unattainable via FRP are now easily achieved through RDRP methods. In this line, the introduction of specific functional groups into the polymeric structures by using functionalized monomers or using multifunctional initiators (or RAFT agents) enlarges the range of possible architectures and complex macromolecules such as stars, comb-like or branched polymers (Figure 1.5).<sup>11, 12, 25</sup>

The active chain ends resulting from the RDRP process can be easily functionalized using different post-polymerization strategies, in order to conjugate the polymeric chains with specific molecules or combine polymeric segments that are difficult to be polymerized together in a controlled manner.<sup>12, 45</sup> Moreover the use of functionalized initiators (or RAFT agents) allows the synthesis of telechelic polymers, i.e., polymers with different functionalities in each chain-end. Through a simple “coupling to” strategy with other molecules or polymers, novel polymeric structures could be obtained. This feature is of particular interest for biomedical applications, because it allows the functionalization of the polymer chain-end groups and incorporates targeting or therapeutic molecules (e.g., antibodies, proteins, etc.).

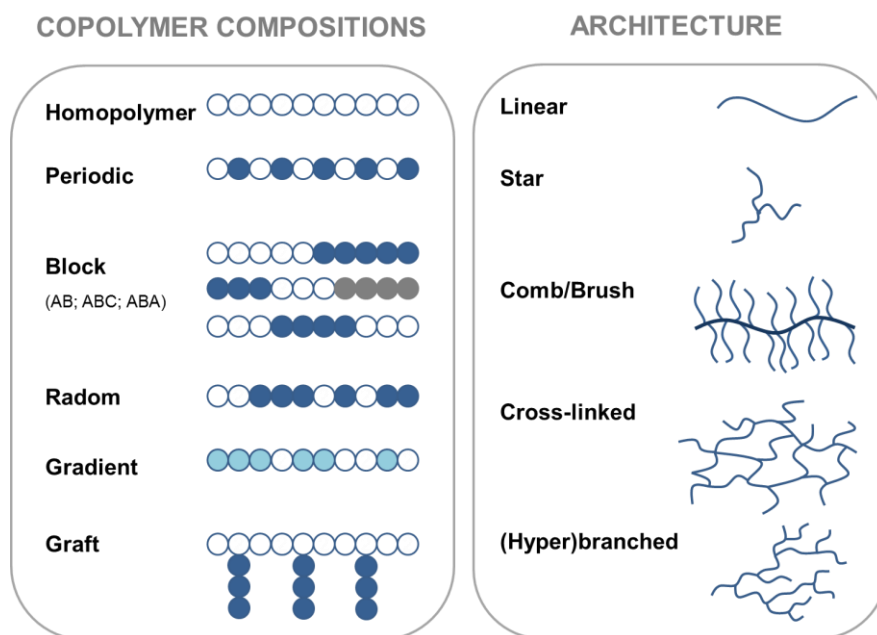


**Figure 1.5:** Examples of polymers with controlled composition and topology prepared by RDRP.

### 1.3. “Click Chemistry”

The concept of “click” chemistry was introduced in 2001 by Sharpless and co-workers<sup>46</sup> and comprises a class of reactions that are mainly characterized by high selectivity, efficiency using simple reaction conditions and little side products that are easily removed by non-chromatographic methods. In polymer chemistry the “click” inspired type of reactions have been in the spotlight over the last years since they are tolerant to a variety of functional groups, which facilitates the synthesis of precise molecular architectures.<sup>46, 47</sup> Several “click” chemistry reactions have been reported in the literature, including the copper-catalyzed azide-alkyne cycloaddition (CuAAC),<sup>48-51</sup> the Diels-Alder cycloaddition,<sup>52, 53</sup> the thiol-ene reaction<sup>54-56</sup> and azide-nitrile cycloaddition.<sup>57, 58</sup> In most cases, the synthetic methodologies applied do not fulfil all the “click” requirements but this concept served as a major inspiration for the modification or conjugation of polymers.<sup>59</sup>

The CuAAC route is the one most reported methods involving “click” inspired conjugation methods, due to the ease of incorporation of “click” functionalities into polymer structures that has been prepared by ATRP and the use of similar catalytic systems.<sup>1, 47, 60</sup> The CuAAC reaction occurs between azide and alkyne functionalities catalysed by Cu(I) to form a 1,4 disubstituted 1,2,3 triazole (Figure 1.6). The incorporation of “clickable” groups into a polymeric chain can be achieved by a polymer post-modification or through a more straightforward strategy that involve the use of functional monomers or functionalized initiators (such as “click” modified ATRP initiators or RAFT agents).<sup>1</sup>

The conjugation of the “click” chemistry concept with RDRP methods has been the basis of a remarkable expansion in the range of (co)polymeric structures that can be prepared through macromolecular engineering (Figure 1.6).<sup>61-63</sup>

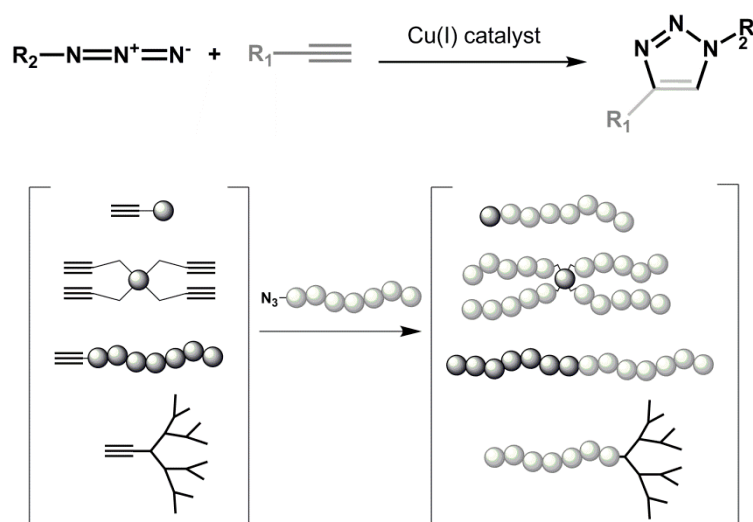


**Figure 1.6:** Schematic representation of the 1,3-dipolar cycloaddition between azides and alkynes<sup>64</sup> and examples of functionalized polymers or possible architectures obtained.

The conjugation of the “click” chemistry with RDRP methods is of major interest when developing advanced macromolecular architectures and has been covered in several reviews.<sup>63, 65-68</sup> Complex polymeric architectures such as linear-dendritic block copolymer<sup>69, 70</sup>, stars<sup>71, 72</sup> or graft copolymers<sup>73, 74</sup> can now be easily achieved. Other example of advanced structures that involve the combination of “click” coupling strategies and RDRP methods are: the modification of inorganic particles,<sup>75-77</sup> the development of ultrathin polymer films,<sup>78</sup> functionalization of block copolymers with cellular targeting ligands (e.g. folic acid),<sup>79, 80</sup> bioconjugation such as polymer-protein<sup>81-84</sup> or even DNA-protein conjugates.<sup>85</sup> The impact of “click” chemistry strategies in the macromolecular engineering field, the alternative reactions and the latest developments has been recently reviewed.<sup>65</sup>



## 1.4. Responsive polymers

Responsive polymers are materials that can undergo reversible changes in their physico-chemical properties in result of small variations in environmental conditions, such as temperature, pH, ionic strength, light irradiation, ionic or metallic interactions, mechanical forces, electric and magnetic fields, or even resulting from a combination of them.<sup>86, 87</sup> This type of polymers is also commonly termed as stimuli-responsive, smart, intelligent, stimuli-sensitive or even environmental sensitive polymers.<sup>87, 88</sup> The polymer response is inherent to their chemical and topological features.<sup>86</sup> Recent developments in polymerization techniques turned possible the preparation of stimuli-responsive polymers with controlled MW, narrow molecular weight distribution, and tailored properties.<sup>7, 87</sup> Among the different type of responses, the most commonly are the polymer dissolution/precipitation, degradation, or swelling/collapsing.<sup>7</sup>

Over the last decade, a massive number of reports have been published dealing with the potential applications of these unique classes of materials in biomedical applications.<sup>86, 87, 89-94</sup> The use of stimuli-responsive nanocarriers in biomedical applications offers an interesting opportunity for drug and gene delivery where the delivery carrier becomes an active participant, rather than passive vehicle. This feature is particularly relevant when the stimulus is intrinsically correlated with pathological environment. The stimuli-responsive nanocarriers are usually stable under physiological conditions but are capable to respond to pathological triggers, such as pH, temperature, the presence of specific enzymes or protein over-expression. Polymeric responsive systems can also be designed to respond to external triggers such as light, ultrasounds or magnetic field.<sup>95-97</sup>

For drug delivery in biological systems, in particular, the release of the encapsulated molecules should occur as a result of a weak external signal. pH and temperature responsive polymers are the most studied among responsive polymers for biomedical applications and drug delivery systems (DDS), since pH and temperature are important physiological triggers. As result, pH- or temperature- sensitive nanocarriers are an interesting therapeutic approach, since they make possible the effective site specific release of therapeutic agents, reducing undesired side-effects. Taking into account the scope of the present work, only the pH and temperature responsive will be discussed in detail in the following sections. Comprehensive information regarding other responsive polymers and its applications can be found in some recent reviews.<sup>97-101</sup>

### 1.4.1. pH-responsive polymers

The extracellular and intracellular pH profile of the biological systems is greatly affected in pathological conditions. In comparison to the normal physiological pH, the pH levels of pathological tissues, such as inflammation, infection and cancer can be significantly lower. In the case of the extracellular pH in solid tumours, the value tends to be lower (6.2 - 6.8) when compared to the normal physiological extracellular pH and blood (7.35 - 7.45).<sup>95, 102, 103</sup> Also, the pH of the inflammatory tissues are in the range of 6.8 while the pH values of some intracellular compartments is significantly lower than cytosolic pH (4.5 - 6.0), specifically the early endosome (pH 6-6.5), late endosome (pH 5 - 6) and lysosomes (pH 4.5-5).<sup>104</sup> Therefore, the pH differences between the healthy and infected tissue can act as an external trigger in responsive DDS and enhance the therapeutic efficacy of the treatment involving the use of stimuli-responsive polymers.

pH-responsive polymers are polymers that contain ionisable pendant functional groups (anionic or cationic polymers), which undergo a conformational change as a response of variations in the surrounding pH values.<sup>93</sup> Usually, the structures that confer the pH-responsive character are pendant weak acid functional groups such as carboxylic acid or phosphoric acid and weak basic functional groups based on amine moieties. The variation of the pH of the environment medium induces the protonation/deprotonation of those side groups leading to a change of the hydrodynamic volume of the polymer chain. Therefore, the aqueous solubility of a pH-responsive polymer is highly correlated with the pH of the solution, since variations above or below the pKa of the responsive groups lead to either protonation or deprotonation of polymer chains.<sup>86</sup> Considering, for example an anionic polymer, the poly(acrylic acid) (PAA), in aqueous solutions it is water soluble for pH values higher than its pKa (4.28), but precipitates when pH decreases due to protonation of the carboxylic pendant groups. Therefore, the polymer chains go from an expanded state (soluble) to a collapsed conformation with the decrease of pH of the solution (Figure 1.7).

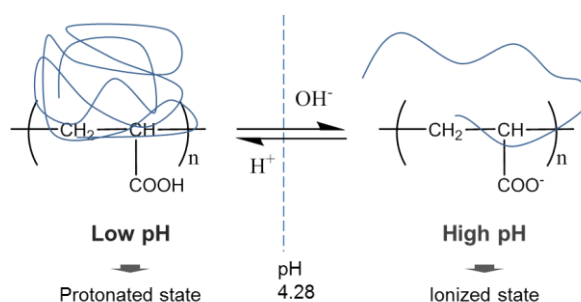


**Figure 1.7:** Poly(acrylic acid) chain conformations in aqueous solution.

Ionisable polymers with a pKa value in the range 3 to 10 are suitable candidates for pH-responsive systems in biomedical applications. Typically the phase transition of these polymers is very sharp, within 0.2-0.3 units of pH.<sup>105</sup> DDS containing pH sensitive polymers have a potential application for localized release of its contents. For instance, polymers with a low pKa can be used for the preparation of DDS for oral drug delivery, since they preserve its structure along with the gastrointestinal tract, and only release its content due to the pH increase in the small intestine. Moreover, polymers with pKa close to 6.2-7.0 are an interesting approach for the development of DDS for cancer therapies. The most popular responsive systems for DDS applications are the ones based on the PAA (pKa ~ 4.28) and the systems containing tertiary amine-based methacrylate polymers, such as poly(2-(dimethylamino)ethyl methacrylate) (PDMAEMA), poly((2-diethylamino) ethyl methacrylate) (PDEAEMA) or poly(2-diisopropylamino)ethyl methacrylate (PDPA) with pKa close to the physiological pH.<sup>104, 106</sup> The responsive behavior of these polymers can be adjusted, by manipulating the composition of the polymer chain, in order to tailor specific pKa values that fulfill a desired application.<sup>107</sup>

### 1.4.2. Temperature responsive polymers

Temperature is a very important physiological indicator. Fever, diseases or local infections are the main causes of the variations in regular body temperature. Temperature responsive (or thermo-responsive) polymers are macromolecular structures whose solubility depends on temperature. The temperature deviation from normal values can act as a trigger in DDSs based on such responsive polymers.<sup>93, 104</sup> Due to a small temperature variation around their critical solution temperature (CST) the temperature responsive polymers undergo a reversible volume phase transition, leading to conformational changes and the formation of hydrophobic domains.<sup>7, 86</sup> Depending on the type of phase transitions that the polymers undertake at the CST, these structures can be characterized by a lower critical solution temperature (LCST) or a upper critical solution temperature (UCST).<sup>104</sup> In water, a polymer with a LCST is soluble in aqueous solution below their LCST due to hydrogen bonding with water molecules. Above the LCST polymers become dehydrated and insoluble, resulting in abrupt phase separation (Figure 1.8).<sup>108</sup> For temperatures higher than LCST the intra- and intermolecular attractions between the hydrophobic parts of the polymer molecules are favoured compared to the water molecules and the polymer undergoes an abrupt change in the macromolecule specific volume.<sup>109</sup> Contrarily, a polymer that exhibits a UCST have their chains collapsed for temperatures below the UCST and upon heating, the chains become completely expanded. The most common of the temperature responsive polymers reported in the literature are listed in Table 1.1.

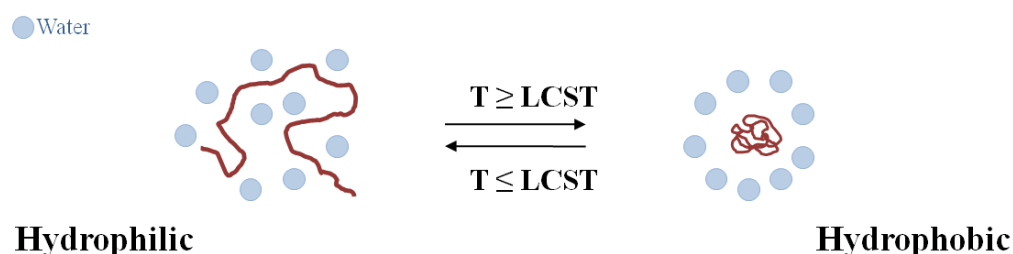


**Figure 1.8:** Polymer conformation according to the solution temperature (adapted from<sup>87</sup>).

**Table 1.1:** Examples of temperature responsive polymers and its critical solution temperatures in water.

	Polymer	CST	Ref.
<b>LCST</b>	Poly( <i>N</i> -isopropylacrylamide) (PNIPAAm)	(~ 32 °C)	110
	Poly(oligoethylene glycol) methacrylates <sup>(*)</sup>	[26-90 °C]	111
	Poly( <i>N</i> -vinylcaprolactam) (PNVCL)	[34-37 °C]	109, 112
	Poly(2-(dimethylamino)ethyl methacrylate) (PDMAEMA) <sup>(**)</sup>	[25-80 °C]	113
<b>UCPT</b>	Poly(acrylamide) (PAAm)	(< 0 °C)	114
	Poly( <i>N</i> -acryloylasparaginamide)	[5-26 °C]	115

<sup>(\*)</sup> dependent on the chain length of the ethylene glycol side group, polymer molecular weight, and concentration. <sup>(\*\*)</sup> dependent on solution pH, polymer molecular weight, architecture and concentration.

PNIPAAm is the most extensive studied temperature responsive polymer for bioengineering applications because its LCST is close to physiological temperature.<sup>116</sup> However, the cytotoxicity associated with PNIPAAm degradation products limits significantly its practical application in DDS.<sup>117-119</sup> Another important drawback of this polymer is the fact that the LCST does not depend on the polymer MW,<sup>120</sup> being classified as class II of LCST polymers. Because of that, PNIPAAm has to be copolymerized with biocompatible segments to improve its cellular tolerance and with other monomers to adjust the LCST value.<sup>121</sup> However, depending on the polymer used, the LCST can be adjusted by varying the polymer MW or polymer concentration. The polymer PNVCL, contrarily to PNIPAAm, presents a LCST that can be tuned by simply varying the polymer MW. This feature associated to its high biocompatibility turns this polymer a very attractive candidate for biomedical applications.<sup>122</sup> However, the non-activated nature of NCVL hinders its controlled polymerization and only a few reports are available in the literature.<sup>123-125</sup>

## 1.5. Self-assembly of block copolymers

The solution self-assembly of amphiphilic block copolymers (ABC) to afford the preparation of nanocarriers for drug delivery is inspired by Nature.<sup>126, 127</sup> ABC are composed by two blocks, with different composition, MW or architecture, that interact differently with their surrounding environment and behaves distinctively in solution.<sup>128</sup> In a selective solvent, and equilibrium conditions, the polymer chains tend to associate and organize themselves (self-assembly) into stable structures.<sup>5</sup> The resultant self-assembled structures are well-defined and ordered aggregates are formed by non-covalent interactions, such as spherical micelles, cylindrical micelles and closed bi- or multilayer structures (Figure 1.9).<sup>89</sup>

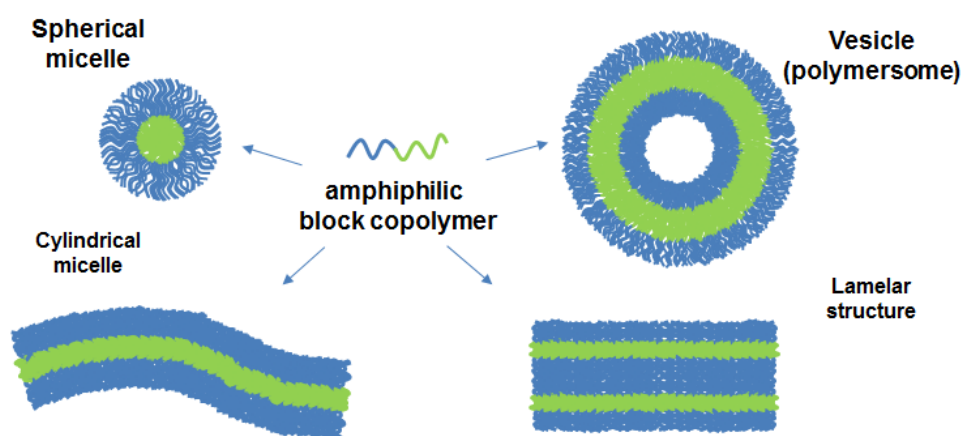


**Figure 1.9:** Schematic representation of different self-assembly architectures from the same amphiphilic diblock copolymer.

The key aspect to afford efficient self-assembly processes lies in the proper design and synthesis of tailor-made molecules or macromolecules that will self-assemble in a controlled manner.<sup>5</sup> Through the RDRP methods discussed in the sections above, it is possible to synthesise well-defined block copolymers composed by segments with different chemical and physical properties. The differences in the block copolymer compositions are responsible for the phase separation of the polymer segments when exposed to a selective solvent. Consequently, the final properties of the solution aggregates could be controlled at the molecular level.

In most cases of self-assembled nanocarriers, the ABC is mainly composed by one hydrophilic and one hydrophobic segments. In aqueous solution, taking into account the nature and architecture of the hydrophilic group of the ABC, the size and composition of the hydrophobic segments as well as physical variables (temperature, pH or others), it is possible to achieve some control of the self-assembly process and obtain self-assembled structures with a pre-determined structures. This feature is of remarkable importance in order to achieve the control over the final characteristics of the nanocarriers (size, morphology and functionality). The ensuing self-assembled morphology is mainly influenced by the nature and macromolecular architecture of each block.<sup>129</sup>

According to the Israelachvili's theory<sup>130</sup> for ABC, the mechanism of the self-assembly in solution relies in the contribution forces of the interfacial hydrophobic attraction and head-group hydrophilic repulsion (Figure 1.10). The resultant morphology of the self-assembled structure is determined by the so called critical packing parameter ( $p$ ) (also named shape factor). This parameter is determined by the equation,  $p = v/(a_0 l_c)$ , that correlates three parameters of the ABC in solution: the volume  $v$  occupied by the hydrophobic chain, the optimal surface area  $a_0$ , and the maximum length  $l_c$  of these chains (Figure 1.10). Generally, when  $p \leq 1/3$  spherical micelles are obtained, while for  $1/2 \leq p \leq 1$ , polymer vesicles are preferred.

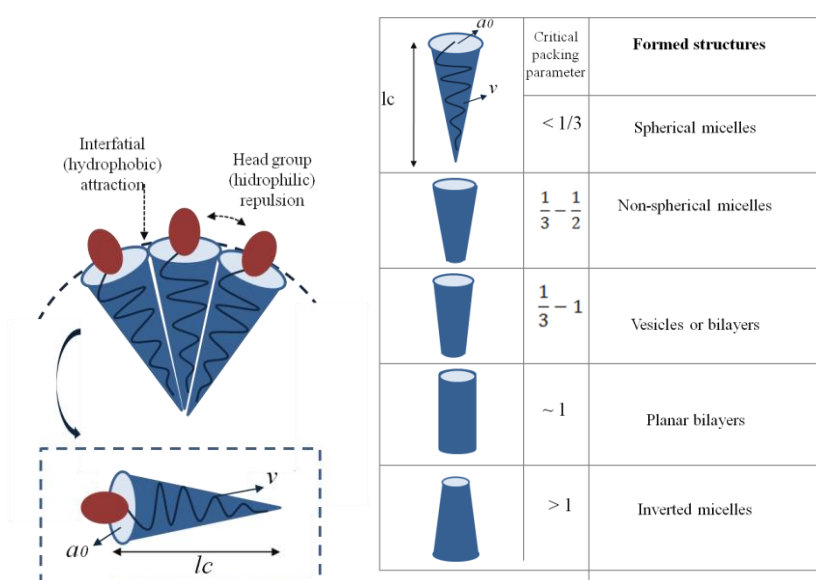


**Figure 1.10:** Schematic representation of the dependence of the resultant self-assembly morphology with Israelachvili's packing parameter,  $p$  (adapted from<sup>130, 131</sup>).

In dilute aqueous solutions of ABC, the unimer to micelle transition occurs when the critical micelle concentration (CMC) and/or over the critical micelle temperature (CMT) are achieved<sup>1</sup>. The block copolymer composition and architecture affect the key parameters of the self-assembly process, such as: CMC, stability, morphology, hydrodynamic size, chemical functionalities in the micelle corona and the core<sup>128</sup>. The CMC value is most commonly employed parameter to evaluate the thermodynamic stability of the self-assembled structures in aqueous solutions.<sup>128, 131</sup> This parameter is very important to understand the stability of the DDS to withstand the dilution in bloodstream or in other delivery conditions. Indeed, compared to common low MW surfactants, amphiphilic polymers generally have much lower CMC values (usually  $10^{-6}$  to  $10^{-4}$  M).<sup>131, 132</sup>

ABC composed by one dendritic segment attached to a hydrophobic linear segment, the so called linear dendritic block copolymers, is a feasible route to generate very compact self-assembly structures (Figure 1.11). Due to the cone-shape morphology, such copolymers are able to form very stable micelles with CMC in the range of  $10^{-8}$  M. Other important advantage of such architectures is the possibility to functionalize the highly branched polar head derived from the dendron segment aiming to improve the nanoparticle performance.<sup>128, 131</sup>

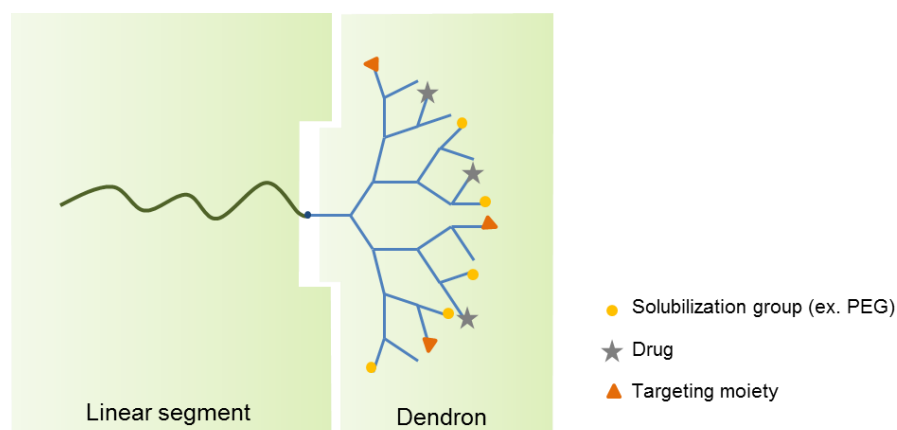


**Figure 1.11:** Schematic representation of the linear dendritic block copolymer architecture and the possibility of dendron multi-surface functionalization.

<sup>1</sup> Those terminologies are derived from the surfactants nomenclature corresponding to the threshold concentration (or temperature) for the formation of micelles. In fact, in the case of self-assembled structures, the correct denomination should be critical aggregation concentration (CMA), although, the CMC nomenclature was adopted in the majority of the literature reports.



Polymer vesicles (also named polymersomes) together with spherical and cylindrical micelles are the three most common self-assembly morphologies of amphiphilic block copolymers in water. The ability of ABC to self-assemble in aqueous environment into highly organized nanostructures as well as the easiness to encapsulate or integrate hydrophobic and/or hydrophilic in the resulting nanoaggregates, makes these strategies very promising for advanced DDS.<sup>129, 133</sup> Due to their hydrophobic inner core, micelles are able to accommodate hydrophobic molecules, while polymersomes can entrap both hydrophilic molecules within the vesicle lumen and also hydrophobic molecules within the membrane core (Figure 1.12). The shell of these self-assembled structures is composed by the hydrophilic segments tuning the particle very stable and water dispersible. Special attention has been paid to polymeric vesicles and micelles as nanocarriers due to their enhanced stability, the possibility to fine control the molecular structure and the surface chemistry to enhance the therapeutic efficiency.<sup>89</sup> In fact, in comparison to lipid-based vesicles (e.g liposomes), the polymersomes are more versatile structures due to the possibility of tuning their final properties through a simple manipulation of the block copolymer chemistry (copolymer composition and MW).<sup>91</sup> Parameters such as the membrane thickness that influences the elasticity, permeability and mechanical stability of the polymersomes or the DDS performance can be easily adjusted.<sup>134</sup>

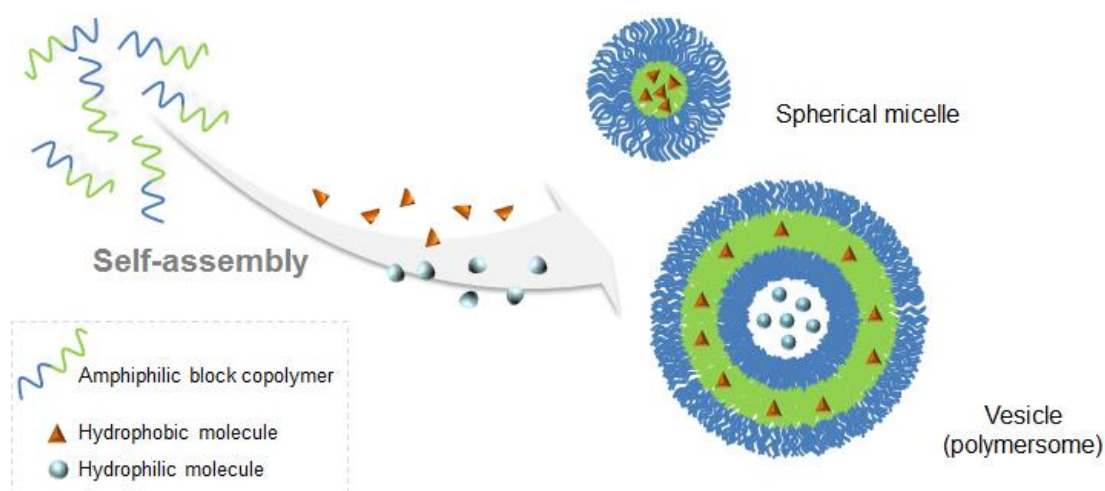


**Figure 1.12:** Schematic representation of the self-assembly of amphiphilic block copolymers and the encapsulation of guest molecules.

As mentioned before the RDRP methods allow a stringent control over the polymer properties, namely the molecular weight distribution. This feature is of particular important to attain ABC blocks with the same characteristics and by that means obtain reproducible self-assembled structures with similar size and performance.<sup>96</sup> Under these conditions, the nanocarriers obtained via self-assembly would have reproducible pharmacokinetic behavior. Furthermore, the possibility of preparing polymeric DDS based on self-assembly of block copolymers composed by pH- or temperature responsive segments with tailored release profiles is extremely relevant. In this sense, the nanocarriers that respond to pH or temperature changes from the normal physiological to abnormal pathological ones, will be able to release their cargo depending on the external environmental conditions. Block copolymers composed by one permanently hydrophilic block and a stimuli-responsive segment allows the self-assembly to be driven according to the external conditions (Figure 1.13). Depending on the stimuli sensitivity of the segment in the block copolymer, by changing the surrounding environment conditions (e.g. pH or temperature), the hydrophilicity of the segment will change, turning the block copolymer amphiphilic, leading to the self-assembly. These stimuli-responsive nanocarriers are particularly interesting in the case of DDS that require a target and fast rate of release of the guest molecules, such as in cancer therapies. In the case of responsive block copolymers, the solution self-assembly process is reversible, depending on the duration of the application of the external stimuli.<sup>108</sup>

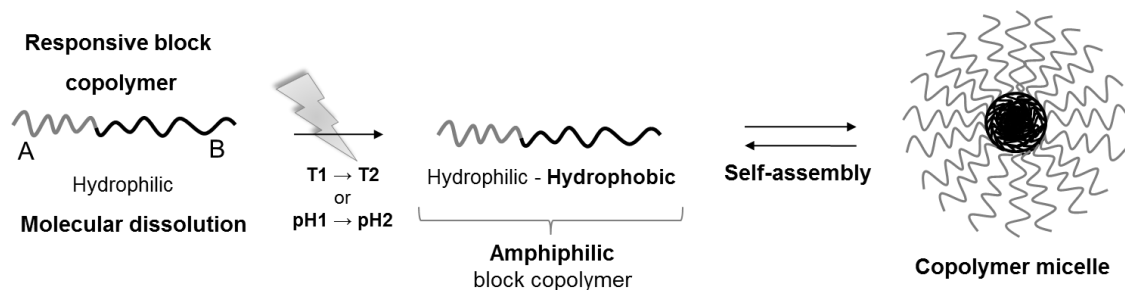


**Figure 1.13:** Schematic representation of the self-assembly of one responsive AB-diblock copolymer.

## 1.6. Polymeric drug delivery systems

Polymeric DDS are essentially synthetic drug carriers capable to transport and deliver a biologically active compound in a controlled manner, i.e., with pre-defined time period and releasing rate.<sup>7</sup>

Designing a polymeric DDS requires a previous knowledge of the specific chemical and biological characteristics of the therapeutic molecule and the polymers. It is possible to tailor the polymeric DDS behaviour adapting their structural characteristics, i.e. the copolymer composition, molecular weight, geometry and chemical functionality of the polymers and ultimately control the self-assembly process.

The incorporation of the drug into the polymeric DDS is usually driven by hydrophobic/hydrophilic interactions, electrostatic attractions, hydrogen bonding and/or covalent bonds.<sup>89, 96</sup> The development of molecular nanostructures with well-defined particle shapes and sizes is of eminent interest in biomedical applications for the delivery of the active pharmaceuticals or imaging agents.<sup>95</sup> Such nanocarriers would avoid the direct use of drugs and prevent the undesired systemic side effects and premature drug degradation.<sup>135</sup>

DDS based on the self-assembly of block copolymers are versatile drug carriers, with increased stability, site specificity and blood circulation resistance.<sup>89</sup>

The properties of the polymeric segments play an important role in the final properties of the self-assembled materials.<sup>136</sup> Therefore, the selection of the block copolymer composition should be driven by the target application for the final self-assembled structure. Primarily, the polymeric carriers for drug delivery applications should fulfil the biological safety requirements, namely: be nontoxic, nonimmunogenic, biocompatible, as well as the products resulting from its degradation.<sup>95, 137</sup> Ideally, DDS should have a high drug loading capacity, adequate stability in the bloodstream, long time circulation properties, and selective accumulation at the site of action together with a suitable drug release profile.<sup>89, 137</sup>

The size of the copolymer particle is a very important factor when considering biomedical applications. For biological purpose, the size of the polymer carrier should be less than 100 nm (ideally), to avoid clearance by the liver and spleen, while at the same time facilitating uptake by non-phagocytic cells such as tumour cells.<sup>138</sup> These

nanocarriers can easily be achieved through the “bottom-up” strategies like the self-assembly method.<sup>139</sup> Using RDRP methods is possible to control the size of the block segments, allowing the preparation of precise nanocarriers via self-assembly. Therefore, the polymeric drug delivery carrier can be carefully designed to fit the aforementioned specificities and consequently maximize drug bioavailability, improve therapeutic efficacy and at the same time minimise side effects.<sup>140</sup> Several polymeric self-assembled nanocarriers for drug and gene delivery using polymer synthesised by RDRP methods have been proposed.<sup>141-143</sup>

One of the major challenges of the DDS is the site-specific drug delivery, i.e., the delivery to a preselected target tissue.<sup>87</sup> Strategies for localized target drug delivery can be a promising alternative to the applied nonspecific methods and may significantly improve the effectiveness of drugs and minimizing untoward side effects.<sup>131, 144, 145</sup> Synthetic modifications, such as particle surface functionalization for cellular targeting is a commonly used approach to promote active cellular targeting, increase cellular uptake and overcome the lack of efficiency of the polymeric DDS.<sup>95</sup> The surface functionalization can also improve the drug entrapment, enhance drug protection or even promote drug delivery.<sup>146</sup>

In the specific case of cancer, after injection, the nanoparticles have to travel in the bloodstream and should accumulate in solid tumour tissue due to the enhanced permeability and retention effect (EPR).<sup>147</sup> In contrast to healthy blood vessels, endothelial cells constituents of tumour vasculature are leaky, essentially due to rapid development of the tumour vasculature and the resultant vessels have pores with approximately 400 nm diameter. These intercellular gaps enable the access of nanocarriers to the extravascular tumour tissue. Also, the lack of effective tumour lymphatic drainage leads to macromolecular accommodation on the extracellular medium of the tumour tissues (Figure 1.14).<sup>148-150</sup>

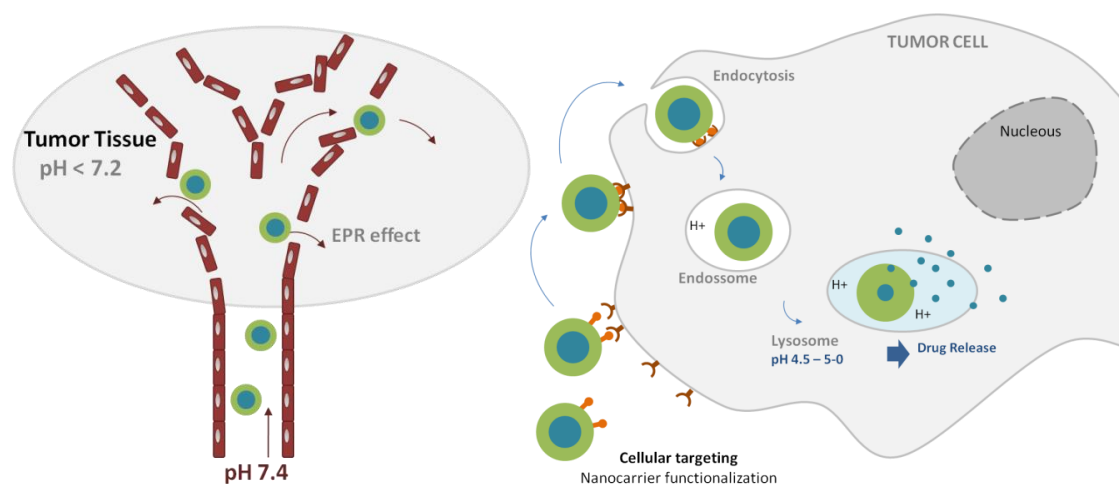


**Figure 1.14:** Schematic representation of tumour targeting of long circulating micelle by the EPR effect.

Ideally, the drug release should occur some minutes after the nanocarrier enter the tumour tissue/cell. The decreasing of pH in extracellular tumour environment should be sufficient to trigger the DDS response and release the drug in the extracellular tumour medium and destroy tumour cells. Otherwise, after cell recognition, the nanoparticle should enter the cell by endocytosis. At this moment, the acidic media of the endosome/lysosome intracellular organelles should trigger the nanoparticle dissociation and consequent drug release (Figure 1.14).

In the case of DDS for cancer therapy, the nanoparticles should possess a long-term structural stability in the blood stream (for systemic administration), but also a target, effective and rapid drug release rate, affecting only the tumour cells, i.e., the system should be stable in physiological conditions but highly reactive in the tumour zone. Such properties can be possibly achieved using a polymeric nanocarrier composed by stimuli-responsive segments that triggers the drug release.<sup>97, 151</sup> The incorporation of biorecognition molecules can be achieved using a simple post-polymerization reaction. The inclusion of folic acid in the nanocarriers surface is one of the main reported strategies for nanoparticle functionalization in DDS for cancer.<sup>145, 152, 153</sup> Beyond the cell recognition molecules, polyethylene glycol (PEG) is one interesting polymer for coating the nanoparticles.<sup>154</sup> PEG has a well-known biological compatibility and stealth properties. PEG functionalization reduces the polymeric carrier cytotoxicity effects, prevents protein complexation, and can also reduce immunogenicity and antigenicity by

shielding the system from being recognized by the immune system.<sup>155</sup> PEG also creates a hydrodynamic barrier that prevents recognition, uptake and removal by the reticuloendothelial system (RES), allowing the DDS to stay longer in the bloodstream.<sup>145, 156, 157</sup> Other strategies of nanocarriers functionalization involve the conjugation with fluorescent dyes allowing the tracing of the DDS biodistribution.<sup>158-160</sup>

Responsible polymeric self-assembled materials are an expanding field with high potential application in chemotherapeutic approaches. Detailed information concerning the recent developments can be found in the literature.<sup>97, 161</sup>

The present PhD work was envisaged to take advantage of the most recent RDRP methods for the synthesis of well-defined responsive block copolymers that are able to self-assemble in supramolecular nanostructures for drug delivery. RDRP methods have been explored and developed for the polymerization of different monomers with high relevance in the biomedical applications. Features such as the development of more efficient and eco-friendly ATRP catalytic systems with reduced concentrations of catalysts, as well as the development of methods that allow the polymerization of non-activated monomers were exhaustively studied. The development of chain-end “click” functionalized polymers was also used to synthesize new block copolymer architectures based on responsive block copolymers. These macrostructures were used to afford innovative self-assembled structures with potential application as responsive DDS for biomedical applications, specifically, chemotherapeutic approaches.

## 1.7. References

1. Golas, P.L. and K. Matyjaszewski (2007). Click chemistry and ATRP: A beneficial union for the preparation of functional materials. *Qsar & Combinatorial Science*, 26(11-12): 1116-1134.
2. Pyun, J., X.Z. Zhou, E. Drockenmuller, and C.J. Hawker (2003). Macromolecules of controlled architecture. *Journal of Materials Chemistry*, 13(11): 2653-2660.
3. Matyjaszewski, K. and N.V. Tsarevsky (2014). Macromolecular Engineering by Atom Transfer Radical Polymerization. *Journal of the American Chemical Society*, 136(18): 6513-6533.
4. Hourani, R. and A. Kakkar (2010). Advances in the Elegance of Chemistry in Designing Dendrimers. *Macromolecular Rapid Communications*, 31(11): 947-974.
5. Whitesides, G.M. and B. Grzybowski (2002). Self-Assembly at All Scales. *Science*, 295(5564): 2418-2421.
6. Sumerlin, B.S. and A.P. Vogt (2010). Macromolecular Engineering through Click Chemistry and Other Efficient Transformations. *Macromolecules*, 43(1): 1-13.
7. Coelho, J.F., P.C. Ferreira, P. Alves, R. Cordeiro, A.C. Fonseca, J.R. Góis, and M.H. Gil (2010). Drug delivery systems: Advanced technologies potentially applicable in personalized treatments. *The EPMA Journal*, 1(1): 164-209.
8. Matyjaszewski, K., S. Gaynor, and J.-S. Wang (1995). Controlled Radical Polymerizations: The Use of Alkyl Iodides in Degenerative Transfer. *Macromolecules*, 28(6): 2093-2095.
9. Qiu, J., B. Charleux, and K. Matyjaszewski (2001). Controlled/living radical polymerization in aqueous media: homogeneous and heterogeneous systems. *Progress in Polymer Science*, 26(10): 2083-2134.
10. Boyer, C., V. Bulmus, T.P. Davis, V. Ladmiral, J.Q. Liu, and S. Perrier (2009). Bioapplications of RAFT Polymerization. *Chemical Reviews*, 109(11): 5402-5436.
11. Matyjaszewski, K. (2012). Atom Transfer Radical Polymerization (ATRP): Current Status and Future Perspectives. *Macromolecules*, 45(10): 4015-4039.
12. Braunecker, W.A. and K. Matyjaszewski (2007). Controlled/living radical polymerization: Features, developments, and perspectives. *Progress in Polymer Science*, 32(1): 93-146.

13. Greszta, D., D. Mardare, and K. Matyjaszewski (1994). Living Radical Polymerization. 1. Possibilities and Limitations *Macromolecules*, 27(3): 638-644.
14. Wang, J.S. and K. Matyjaszewski (1995). Controlled Living Radical Polymerization - Atom-Transfer Radical Polymerization in the Presence of Transition-metal Complexes *Journal of the American Chemical Society*, 117(20): 5614-5615.
15. Zetterlund, P.B., Y. Kagawa, and M. Okubo (2008). Controlled/living radical polymerization in dispersed systems. *Chemical Reviews*, 108(9): 3747-3794.
16. Matyjaszewski, K. (2009). Controlled Radical Polymerization: State of the Art in 2008. *Controlled/Living Radical Polymerization: Progress in Atrp*, 1023: 3-13.
17. Matyjaszewski, K. and J. Spanswick (2005). Controlled/living radical polymerization. *Materials Today*, 8(3): 26-33.
18. Matyjaszewski, K. and N.V. Tsarevsky (2009). Nanostructured functional materials prepared by atom transfer radical polymerization. *Nature Chemistry*, 1(4): 276-288.
19. Kazmaier, P.M., K. Daimon, M.K. Georges, G.K. Hamer, and R.P.N. Veregin (1997). Nitroxide-mediated "living" free radical polymerization: A rapid polymerization of (chloromethyl)styrene for the preparation of random, block, and segmental arborescent polymers. *Macromolecules*, 30(8): 2228-2231.
20. Ayres, N. (2011). Atom Transfer Radical Polymerization: A Robust and Versatile Route for Polymer Synthesis. *Polymer Reviews*, 51(2): 138-162.
21. Kamigaito, M., T. Ando, and M. Sawamoto (2001). Metal-catalyzed living radical polymerization. *Chemical Reviews*, 101(12): 3689-3745.
22. Percec, V., T. Guliashvili, J.S. Ladislaw, A. Wistrand, A. Stjerndahl, M.J. Sienkowska, M.J. Monteiro, and S. Sahoo (2006). Ultrafast synthesis of ultrahigh molar mass polymers by metal-catalyzed living radical polymerization of acrylates, methacrylates, and vinyl chloride mediated by SET at 25 degrees C. *Journal of the American Chemical Society*, 128(43): 14156-14165.
23. Fischer, H. (2001). The Persistent Radical Effect: A Principle for Selective Radical Reactions and Living Radical Polymerizations. *Chemical Reviews*, 101(12): 3581-3610.
24. Chiefari, J., Y.K. Chong, F. Ercole, J. Krstina, J. Jeffery, T.P.T. Le, R.T.A. Mayadunne, G.F. Meijs, C.L. Moad, G. Moad, E. Rizzardo, and S.H. Thang (1998). Living Free-Radical Polymerization by Reversible Addition-Fragmentation Chain Transfer: The RAFT Process. *Macromolecules*, 31(16): 5559-5562.



25. Matyjaszewski, K. and J.H. Xia (2001). Atom transfer radical polymerization. *Chemical Reviews*, 101(9): 2921-2990.
26. Tsarevsky, N.V. and K. Matyjaszewski (2007). "Green" Atom Transfer Radical Polymerization: From Process Design to Preparation of Well-Defined Environmentally Friendly Polymeric Materials. *Chemical Reviews*, 107(6): 2270-2299.
27. Ouchi, M., T. Terashima, and M. Sawamoto (2009). Transition Metal-Catalyzed Living Radical Polymerization: Toward Perfection in Catalysis and Precision Polymer Synthesis. *Chemical Reviews*, 109(11): 4963-5050.
28. di Lena, F. and K. Matyjaszewski (2010). Transition metal catalysts for controlled radical polymerization. *Progress in Polymer Science*, 35(8): 959-1021.
29. Tang, W. and K. Matyjaszewski (2006). Effect of Ligand Structure on Activation Rate Constants in ATRP. *Macromolecules*, 39(15): 4953-4959.
30. Tang, W. and K. Matyjaszewski (2007). Effects of Initiator Structure on Activation Rate Constants in ATRP. *Macromolecules*, 40(6): 1858-1863.
31. Jakubowski, W. and K. Matyjaszewski (2006). Activators Regenerated by Electron Transfer for Atom-Transfer Radical Polymerization of (Meth)acrylates and Related Block Copolymers. *Angewandte Chemie International Edition*, 45(27): 4482-4486.
32. Matyjaszewski, K., W. Jakubowski, K. Min, W. Tang, J. Huang, W.A. Braunecker, and N.V. Tsarevsky (2006). Diminishing catalyst concentration in atom transfer radical polymerization with reducing agents. *Proceedings of the National Academy of Sciences*, 103(42): 15309-15314.
33. Williams, V.A. and K. Matyjaszewski (2015). Expanding the ATRP Toolbox: Methacrylate Polymerization with an Elemental Silver Reducing Agent. *Macromolecules*.
34. Konkolewicz, D., P. Krys, J.R. Góis, P.V. Mendonça, M. Zhong, Y. Wang, A. Gennaro, A.A. Isse, M. Fantin, and K. Matyjaszewski (2014). Aqueous RDRP in the Presence of Cu<sup>0</sup>: The Exceptional Activity of CuI Confirms the SARA ATRP Mechanism. *Macromolecules*, 47(2): 560-570.
35. Zhang, Y., Y. Wang, and K. Matyjaszewski (2011). ATRP of Methyl Acrylate with Metallic Zinc, Magnesium, and Iron as Reducing Agents and Supplemental Activators. *Macromolecules*, 44(4): 683-685.
36. Abreu, C.M.R., A.C. Serra, A.V. Popov, K. Matyjaszewski, T. Gulashvili, and J.F.J. Coelho (2013). Ambient temperature rapid SARA ATRP of acrylates and methacrylates in alcohol-water solutions mediated by a mixed sulfite/Cu(II)Br<sub>2</sub> catalytic system. *Polymer Chemistry*, 4(23): 5629-5636.

37. Simakova, A., S.E. Averick, D. Konkolewicz, and K. Matyjaszewski (2012). Aqueous ARGET ATRP. *Macromolecules*, 45(16): 6371-6379.
38. Moad, G., E. Rizzardo, and S.H. Thang (2012). Living Radical Polymerization by the RAFT Process - A Third Update. *Australian Journal of Chemistry*, 65(8): 985-1076.
39. Semsarilar, M. and S. Perrier (2010). 'Green' reversible addition-fragmentation chain-transfer (RAFT) polymerization. *Nature Chemistry*, 2(10): 811-820.
40. Keddie, D.J., G. Moad, E. Rizzardo, and S.H. Thang (2012). RAFT Agent Design and Synthesis. *Macromolecules*, 45(13): 5321-5342.
41. Moad, G., E. Rizzardo, and S.H. Thang (2008). Toward Living Radical Polymerization. *Accounts of Chemical Research*, 41(9): 1133-1142.
42. Jeong, N.S., M. Redhead, C. Bosquillon, C. Alexander, M. Kelland, and R.K. O'Reilly (2011). The Missing Lactam-Thermoresponsive and Biocompatible Poly(N-vinylpiperidone) Polymers by Xanthate-Mediated RAFT Polymerization. *Macromolecules*, 44(4): 886-893.
43. Perrier, S. and P. Takolpuckdee (2005). Macromolecular design via reversible addition-fragmentation chain transfer (RAFT)/xanthates (MADIX) polymerization. *Journal of Polymer Science Part A: Polymer Chemistry*, 43(22): 5347-5393.
44. Matyjaszewski, K. (2003). General Concepts and History of Living Radical Polymerization, in *Handbook of Radical Polymerization*. John Wiley & Sons, Inc. 361-406.
45. Willcock, H. and R.K. O'Reilly (2010). End group removal and modification of RAFT polymers. *Polymer Chemistry*, 1(2): 149-157.
46. Kolb, H.C., M.G. Finn, and K.B. Sharpless (2001). Click chemistry: Diverse chemical function from a few good reactions. *Angewandte Chemie-International Edition*, 40(11): 2004-+.
47. Binder, W.H. and R. Sachsenhofer (2008). 'Click' chemistry in polymer and material science: An update. *Macromolecular Rapid Communications*, 29(12-13): 952-981.
48. Meldal, M. and C.W. Tornøe (2008). Cu-catalyzed azide-alkyne cycloaddition. *Chemical Reviews*, 108(8): 2952-3015.
49. Rostovtsev, V.V., L.G. Green, V.V. Fokin, and K.B. Sharpless (2002). A Stepwise Huisgen Cycloaddition Process: Copper(I)-Catalyzed Regioselective "Ligation" of Azides and Terminal Alkynes. *Angewandte Chemie International Edition*, 41(14): 2596-2599.

50. Lutz, J.-F. (2007). 1,3-Dipolar Cycloadditions of Azides and Alkynes: A Universal Ligation Tool in Polymer and Materials Science. *Angewandte Chemie International Edition*, 46(7): 1018-1025.
51. Lutz, J.F. (2007). 1,3-dipolar cycloadditions of azides and alkynes: A universal ligation tool in polymer and materials science. *Angewandte Chemie-International Edition*, 46(7): 1018-1025.
52. Kim, T.-D., J. Luo, Y. Tian, J.-W. Ka, N.M. Tucker, M. Haller, J.-W. Kang, and A.K.Y. Jen (2006). Diels–Alder “Click Chemistry” for Highly Efficient Electrooptic Polymers. *Macromolecules*, 39(5): 1676-1680.
53. Durmaz, H., A. Dag, O. Altintas, T. Erdogan, G. Hizal, and U. Tunca (2007). One-Pot Synthesis of ABC Type Triblock Copolymers via in situ Click [3 + 2] and Diels–Alder [4 + 2] Reactions. *Macromolecules*, 40(2): 191-198.
54. Killops, K.L., L.M. Campos, and C.J. Hawker (2008). Robust, Efficient, and Orthogonal Synthesis of Dendrimers via Thiol-ene “Click” Chemistry. *Journal of the American Chemical Society*, 130(15): 5062-5064.
55. Dondoni, A. (2008). The Emergence of Thiol–Ene Coupling as a Click Process for Materials and Bioorganic Chemistry. *Angewandte Chemie International Edition*, 47(47): 8995-8997.
56. Becer, C.R., R. Hoogenboom, and U.S. Schubert (2009). Click Chemistry beyond Metal-Catalyzed Cycloaddition. *Angewandte Chemie International Edition*, 48(27): 4900-4908.
57. Tsarevsky, N.V., K.V. Bernaerts, B. Dufour, F.E. Du Prez, and K. Matyjaszewski (2004). Well-Defined (Co)polymers with 5-Vinyltetrazole Units via Combination of Atom Transfer Radical (Co)polymerization of Acrylonitrile and “Click Chemistry”-Type Postpolymerization Modification. *Macromolecules*, 37(25): 9308-9313.
58. Demko, Z.P. and K.B. Sharpless (2001). Preparation of 5-Substituted 1H-Tetrazoles from Nitriles in Water†. *The Journal of Organic Chemistry*, 66(24): 7945-7950.
59. Barner-Kowollik, C., F.E. Du Prez, P. Espeel, C.J. Hawker, T. Junkers, H. Schlaad, and W. Van Camp (2011). “Clicking” Polymers or Just Efficient Linking: What Is the Difference? *Angewandte Chemie International Edition*, 50(1): 60-62.
60. Lutz, J.F., H.G. Börner, and K. Weichenhan (2006). Combining ATRP and “click” chemistry: a promising platform toward functional biocompatible polymers and polymer bioconjugates. *Macromolecules*, 39(19): 6376-6383.

61. Golas, P.L. and K. Matyjaszewski (2010). Marrying click chemistry with polymerization: expanding the scope of polymeric materials. *Chemical Society Reviews*, 39(4): 1338-1354.
62. Lutz, J.-F., H.G. Börner, and K. Weichenhan (2005). Combining Atom Transfer Radical Polymerization and Click Chemistry: A Versatile Method for the Preparation of End-Functional Polymers. *Macromolecular Rapid Communications*, 26(7): 514-518.
63. Akeroyd, N. and B. Klumperman (2011). The combination of living radical polymerization and click chemistry for the synthesis of advanced macromolecular architectures. *European Polymer Journal*, 47(6): 1207-1231.
64. Rostovtsev, V.V., L.G. Green, V.V. Fokin, and K.B. Sharpless (2002). A stepwise Huisgen cycloaddition process: Copper(I)-catalyzed regioselective "ligation" of azides and terminal alkynes. *Angewandte Chemie-International Edition*, 41(14): 2596-+.
65. Espeel, P. and F.E. Du Prez (2015). "Click"-Inspired Chemistry in Macromolecular Science: Matching Recent Progress and User Expectations. *Macromolecules*, 48(1): 2-14.
66. Such, G.K., A.P.R. Johnston, K. Liang, and F. Caruso (2012). Synthesis and functionalization of nanoengineered materials using click chemistry. *Progress in Polymer Science*, 37(7): 985-1003.
67. Gregory, A. and M.H. Stenzel (2012). Complex polymer architectures via RAFT polymerization: From fundamental process to extending the scope using click chemistry and nature's building blocks. *Progress in Polymer Science*, 37(1): 38-105.
68. Meng, X. and K.J. Edgar. "Click" reactions in polysaccharide modification. *Progress in Polymer Science*.
69. Carlmark, A., C.J. Hawker, A. Hult, and M. Malkoch (2009). New methodologies in the construction of dendritic materials. *Chemical Society Reviews*, 38(2): 352-362.
70. Dong, C.-M. and G. Liu (2013). Linear-dendritic biodegradable block copolymers: from synthesis to application in bionanotechnology. *Polymer Chemistry*, 4(1): 46-52.
71. Zhang, Y., H. Liu, J. Hu, C. Li, and S. Liu (2009). Synthesis and Aggregation Behavior of Multi-Responsive Double Hydrophilic ABC Miktoarm Star Terpolymer. *Macromolecular Rapid Communications*, 30(11): 941-947.

- 
72. Gao, H. and K. Matyjaszewski (2006). Synthesis of Star Polymers by a Combination of ATRP and the “Click” Coupling Method. *Macromolecules*, 39(15): 4960-4965.
  73. Jiang, X., M.C. Lok, and W.E. Hennink (2007). Degradable-brushed pHEMA-pDMAEMA synthesized via ATRP and click chemistry for gene delivery. *Bioconjugate Chemistry*, 18(6): 2077-2084.
  74. Tsarevsky, N.V., S.A. Bencherif, and K. Matyjaszewski (2007). Graft Copolymers by a Combination of ATRP and Two Different Consecutive Click Reactions. *Macromolecules*, 40(13): 4439-4445.
  75. Ranjan, R. and W.J. Brittain (2007). Combination of Living Radical Polymerization and Click Chemistry for Surface Modification. *Macromolecules*, 40(17): 6217-6223.
  76. Wang, Y., J. Chen, J. Xiang, H. Li, Y. Shen, X. Gao, and Y. Liang (2009). Synthesis and characterization of end-functional polymers on silica nanoparticles via a combination of atom transfer radical polymerization and click chemistry. *Reactive and Functional Polymers*, 69(6): 393-399.
  77. Zhang, T., Y. Wu, X. Pan, Z. Zheng, X. Ding, and Y. Peng (2009). An approach for the surface functionalized gold nanoparticles with pH-responsive polymer by combination of RAFT and click chemistry. *European Polymer Journal*, 45(6): 1625-1633.
  78. Such, G.K., J.F. Quinn, A. Quinn, E. Tjipto, and F. Caruso (2006). Assembly of Ultrathin Polymer Multilayer Films by Click Chemistry. *Journal of the American Chemical Society*, 128(29): 9318-9319.
  79. Lee, S.-M., H. Chen, T.V. O’Halloran, and S.T. Nguyen (2009). “Clickable” Polymer-Caged Nanobins as a Modular Drug Delivery Platform. *Journal of the American Chemical Society*, 131(26): 9311-9320.
  80. De, P., S.R. Gondi, and B.S. Sumerlin (2008). Folate-Conjugated Thermoresponsive Block Copolymers: Highly Efficient Conjugation and Solution Self-Assembly. *Biomacromolecules*, 9(3): 1064-1070.
  81. Dirks, A.J., S.S. van Berkel, N.S. Hatzakis, J.A. Opsteen, F.L. van Delft, J.J.L.M. Cornelissen, A.E. Rowan, J.C.M. van Hest, F.P.J.T. Rutjes, and R.J.M. Nolte (2005). Preparation of biohybrid amphiphiles via the copper catalysed Huisgen [3 + 2] dipolar cycloaddition reaction. *Chemical Communications*, (33): 4172-4174.
  82. Lee, B.S., J.K. Lee, W.-J. Kim, Y.H. Jung, S.J. Sim, J. Lee, and I.S. Choi (2007). Surface-Initiated, Atom Transfer Radical Polymerization of Oligo(ethylene

- glycol) Methyl Ether Methacrylate and Subsequent Click Chemistry for Bioconjugation. *Biomacromolecules*, 8(2): 744-749.
83. Shi, W., S. Dolai, S. Averick, S.S. Fernando, J.A. Saltos, W. L'Amoreaux, P. Banerjee, and K. Raja (2009). A General Methodology Toward Drug/Dye Incorporated Living Copolymer–Protein Hybrids: (NIRF Dye-Glucose) Copolymer–Avidin/BSA Conjugates as Prototypes. *Bioconjugate Chemistry*, 20(8): 1595-1601.
84. Li, M., P. De, S.R. Gondi, and B.S. Sumerlin (2008). Responsive Polymer-Protein Bioconjugates Prepared by RAFT Polymerization and Copper-Catalyzed Azide-Alkyne Click Chemistry. *Macromolecular Rapid Communications*, 29(12-13): 1172-1176.
85. Averick, S.E., E. Paredes, D. Grahacharya, B.F. Woodman, S.J. Miyake-Stoner, R.A. Mehl, K. Matyjaszewski, and S.R. Das (2012). A Protein–Polymer Hybrid Mediated By DNA. *Langmuir*, 28(4): 1954-1958.
86. Hu, J. and S. Liu (2010). Responsive Polymers for Detection and Sensing Applications: Current Status and Future Developments. *Macromolecules*, 43(20): 8315-8330.
87. Bajpai, A.K., J. Bajpai, R. Saini, and R. Gupta (2011). Responsive Polymers in Biology and Technology. *Polymer Reviews*, 51(1): 53-97.
88. Carreira, A.S., F. Goncalves, P.V. Mendonca, M.H. Gil, and J.F.J. Coelho (2010). Temperature and pH responsive polymers based on chitosan: Applications and new graft copolymerization strategies based on living radical polymerization. *Carbohydrate Polymers*, 80(3): 618-630.
89. Onaca, O., R. Enea, D.W. Hughes, and W. Meier (2009). Stimuli-Responsive Polymersomes as Nanocarriers for Drug and Gene Delivery. *Macromolecular Bioscience*, 9(2): 129-139.
90. de Las Heras Alarcon, C., S. Pennadam, and C. Alexander (2005). Stimuli responsive polymers for biomedical applications. *Chem Soc Rev*, 34(3): 276-85.
91. Meng, F.H., Z.Y. Zhong, and J. Feijen (2009). Stimuli-Responsive Polymersomes for Programmed Drug Delivery. *Biomacromolecules*, 10(2): 197-209.
92. Motornov, M., Y. Roiter, I. Tokarev, and S. Minko (2010). Stimuli-responsive nanoparticles, nanogels and capsules for integrated multifunctional intelligent systems. *Progress in Polymer Science*, 35(1-2): 174-211.
93. Bajpai, A.K., S.K. Shukla, S. Bhanu, and S. Kankane (2008). Responsive polymers in controlled drug delivery. *Progress in Polymer Science*, 33(11): 1088-1118.

94. Motornov, M., Y. Roiter, I. Tokarev, and S. Minko (2010). Stimuli-responsive nanoparticles, nanogels and capsules for integrated multifunctional intelligent systems. *Progress in Polymer Science*, 35(1–2): 174-211.
95. Calderon, M., M.A. Quadir, M. Strumia, and R. Haag (2010). Functional dendritic polymer architectures as stimuli-responsive nanocarriers. *Biochimie*, 92(9): 1242-1251.
96. Rocha, N., P. Mendonça, J. Góis, R. Cordeiro, A. Fonseca, P. Ferreira, T. Gulashvili, K. Matyjaszewski, A. Serra, and J. Coelho (2013). The Importance of Controlled/Living Radical Polymerization Techniques in the Design of Tailor Made Nanoparticles for Drug Delivery Systems, in *Drug Delivery Systems: Advanced Technologies Potentially Applicable in Personalised Treatment*, J. Coelho, Editor. Springer Netherlands. 315-357.
97. Kaur, S., C. Prasad, B. Balakrishnan, and R. Banerjee (2015). Trigger responsive polymeric nanocarriers for cancer therapy. *Biomaterials Science*, 3(7): 955-987.
98. Roy, D., J.N. Cambre, and B.S. Sumerlin (2010). Future perspectives and recent advances in stimuli-responsive materials. *Progress in Polymer Science*, 35(1–2): 278-301.
99. Stuart, M.A.C., W.T.S. Huck, J. Genzer, M. Mueller, C. Ober, M. Stamm, G.B. Sukhorukov, I. Szleifer, V.V. Tsukruk, M. Urban, F. Winnik, S. Zauscher, I. Luzinov, and S. Minko (2010). Emerging applications of stimuli-responsive polymer materials. *Nature Materials*, 9(2): 101-113.
100. Liu, F. and M.W. Urban (2010). Recent advances and challenges in designing stimuli-responsive polymers. *Progress in Polymer Science*, 35(1-2): 3-23.
101. Yan, X., F. Wang, B. Zheng, and F. Huang (2012). Stimuli-responsive supramolecular polymeric materials. *Chemical Society Reviews*, 41(18): 6042-6065.
102. Engin, K., D.B. Leeper, J.R. Cater, A.J. Thistlethwaite, L. Tupchong, and J.D. McFarlane (1995). Extracellular pH Distribution in Human Tumors *International Journal of Hyperthermia*, 11(2): 211-216.
103. Lee, E.S., K. Na, and Y.H. Bae (2003). Polymeric micelle for tumor pH and folate-mediated targeting. *Journal of Controlled Release*, 91(1-2): 103-113.
104. Schmaljohann, D. (2006). Thermo- and pH-responsive polymers in drug delivery. *Advanced Drug Delivery Reviews*, 58(15): 1655-1670.
105. Cabane, E., X. Zhang, K. Langowska, C. Palivan, and W. Meier (2012). Stimuli-Responsive Polymers and Their Applications in Nanomedicine. *Biointerphases*, 7(1-4): 1-27.

106. Hu, J., G. Zhang, Z. Ge, and S. Liu (2014). Stimuli-responsive tertiary amine methacrylate-based block copolymers: Synthesis, supramolecular self-assembly and functional applications. *Progress in Polymer Science*, 39(6): 1096-1143.
107. Sousa-Herves, A., R. Riguera, and E. Fernandez-Megia (2012). PEG-dendritic block copolymers for biomedical applications. *New Journal of Chemistry*, 36(2): 205-210.
108. Lee, H.I., J.A. Lee, Z.Y. Poon, and P.T. Hammond (2008). Temperature-triggered reversible micellar self-assembly of linear-dendritic block copolymers. *Chemical Communications*, (32): 3726-3728.
109. Vihola, H., A. Laukkanen, H. Tenhu, and J. Hirvonen (2008). Drug Release Characteristics of Physically Cross-Linked Thermosensitive Poly(N-vinylcaprolactam) Hydrogel Particles. *Journal of Pharmaceutical Sciences*, 97(11): 4783-4793.
110. Schild, H.G. (1992). Poly(N-isopropylacrylamide): experiment, theory and application. *Progress in Polymer Science*, 17(2): 163-249.
111. Lutz, J.-F. (2008). Polymerization of oligo(ethylene glycol) (meth)acrylates: Toward new generations of smart biocompatible materials. *Journal of Polymer Science Part A: Polymer Chemistry*, 46(11): 3459-3470.
112. Maeda, Y., T. Nakamura, and I. Ikeda (2002). Hydration and phase behavior of poly(N-vinylcaprolactam) and poly(N-vinylpyrrolidone) in water. *Macromolecules*, 35(1): 217-222.
113. Plamper, F.A., M. Ruppel, A. Schmalz, O. Borisov, M. Ballauff, and A.H.E. Müller (2007). Tuning the Thermoresponsive Properties of Weak Polyelectrolytes: Aqueous Solutions of Star-Shaped and Linear Poly(N,N-dimethylaminoethyl Methacrylate). *Macromolecules*, 40(23): 8361-8366.
114. Seuring, J. and S. Agarwal (2012). First Example of a Universal and Cost-Effective Approach: Polymers with Tunable Upper Critical Solution Temperature in Water and Electrolyte Solution. *Macromolecules*, 45(9): 3910-3918.
115. Glatzel, S., A. Laschewsky, and J.-F. Lutz (2011). Well-Defined Uncharged Polymers with a Sharp UCST in Water and in Physiological Milieu. *Macromolecules*, 44(2): 413-415.
116. Rzaev, Z.M.O., S. Dinçer, and E. Pişkin (2007). Functional copolymers of N-isopropylacrylamide for bioengineering applications. *Progress in Polymer Science*, 32(5): 534-595.
117. Çakal, E.i. and S. Çavuş (2010). Novel Poly(N-vinylcaprolactam-co-2-(diethylamino)ethyl methacrylate) Gels: Characterization and Detailed



- Investigation on Their Stimuli-Sensitive Behaviors and Network Structure. *Industrial & Engineering Chemistry Research*, 49(22): 11741-11751.
118. Vihola, H., A. Laukkanen, L. Valtola, H. Tenhu, and J. Hirvonen (2005). Cytotoxicity of thermosensitive polymers poly(N-isopropylacrylamide), poly(N-vinylcaprolactam) and amphiphilically modified poly(N-vinylcaprolactam). *Biomaterials*, 26(16): 3055-3064.
  119. Vihola, H., A.K. Marttila, J.S. Pakkanen, M. Andersson, A. Laukkanen, A.M. Kaukonen, H. Tenhu, and J. Hirvonen (2007). Cell-polymer interactions of fluorescent polystyrene latex particles coated with thermosensitive poly (N-isopropylacrylamide) and poly (N-vinylcaprolactam) or grafted with poly(ethylene oxide)-macromonomer. *International Journal of Pharmaceutics*, 343: 238-246.
  120. Shtanko, N.I., W. Lequeieu, E.J. Goethals, and F.E. Du Prez (2003). pH- and thermo-responsive properties of poly(N-vinylcaprolactam-co-acrylic acid) copolymers. *Polymer International*, 52(10): 1605-1610.
  121. Hodorog, A., C. Ibanescu, M. Danu, B. Simionescu, L. Rocha, and N. Hurduc (2012). Thermo-sensitive polymers based on graft polysiloxanes. *Polymer Bulletin*, 69(5): 579-595.
  122. Medeiros, S.F., J.C.S. Barboza, M.I. Re, R. Giudici, and A.M. Santos (2010). Solution Polymerization of N-vinylcaprolactam in 1,4-dioxane. Kinetic Dependence on Temperature, Monomer, and Initiator Concentrations. *Journal of Applied Polymer Science*, 118(1): 229-240.
  123. Shao, L., M. Hu, L. Chen, L. Xu, and Y. Bi (2012). RAFT polymerization of N-vinylcaprolactam and effects of the end group on the thermal response of poly(N-vinylcaprolactam). *Reactive and Functional Polymers*, 72(6): 407-413.
  124. Wan, D., Q. Zhou, H. Pu, and G. Yang (2008). Controlled radical polymerization of N-vinylcaprolactam mediated by xanthate or dithiocarbamate. *Journal of Polymer Science Part A: Polymer Chemistry*, 46(11): 3756-3765.
  125. Hurtgen, M., J. Liu, A. Debuigne, C. Jerome, and C. Detrembleur (2012). Synthesis of thermo-responsive poly(N-vinylcaprolactam)-containing block copolymers by cobalt-mediated radical polymerization. *Journal of Polymer Science Part A: Polymer Chemistry*, 50(2): 400-408.
  126. Tyrrell, Z.L., Y.Q. Shen, and M. Radosz (2010). Fabrication of micellar nanoparticles for drug delivery through the self-assembly of block copolymers. *Progress in Polymer Science*, 35(9): 1128-1143.

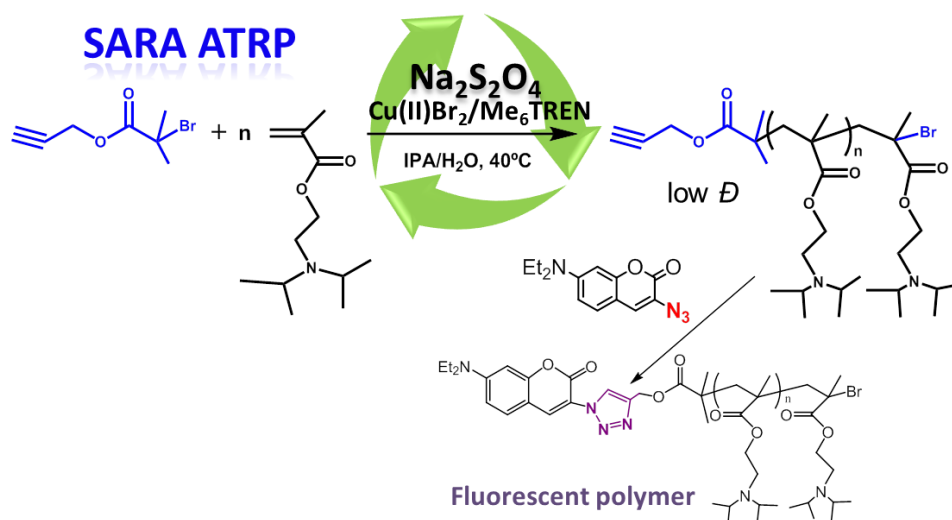
127. Guo, B., X.Y. Sun, Y.F. Zhou, and D.Y. Yan (2010). Supramolecular self-assembly and controllable drug release of thermosensitive hyperbranched multiarm copolymers. *Science China-Chemistry*, 53(3): 487-494.
128. Rodriguez-Hernandez, J., F. Checot, Y. Gnanou, and S. Lecommandoux (2005). Toward 'smart' nano-objects by self-assembly of block copolymers in solution. *Progress in Polymer Science*, 30: 691-724.
129. Rodríguez-Hernández, J., F. Chécot, Y. Gnanou, and S. Lecommandoux (2005). Toward 'smart' nano-objects by self-assembly of block copolymers in solution. *Progress in Polymer Science*, 30(7): 691-724.
130. Israelachvili, J.N. (1992). Intermolecular and surface forces: London:Harcourt Brace and Company.
131. Tian, L. and P.T. Hammond (2006). Comb-dendritic block copolymers as tree-shaped macromolecular amphiphiles for nanoparticle self-assembly. *Chemistry of Materials*, 18(17): 3976-3984.
132. Lavasanifar, A., J. Samuel, and G.S. Kwon (2001). The effect of alkyl core structure on micellar properties of poly(ethylene oxide)-block-poly(-aspartamide) derivatives. *Colloids and Surfaces B: Biointerfaces*, 22(2): 115-126.
133. Mai, Y. and A. Eisenberg (2012). Self-assembly of block copolymers. *Chemical Society Reviews*, 41(18): 5969-5985.
134. BM, D., D.S. Won Yy Fau - Ege, J.C. Ege Ds Fau - Lee, F.S. Lee Jc Fau - Bates, D.E. Bates Fs Fau - Discher, D.A. Discher De Fau - Hammer, and H. DA (1999). - Polymersomes: tough vesicles made from diblock copolymers. *Science*, 284(5417): 1143-6.
135. Freichels, H., R. Jérôme, and C. Jérôme (2011). Sugar-labeled and PEGylated (bio)degradable polymers intended for targeted drug delivery systems. *Carbohydrate Polymers*, 86(3): 1093-1106.
136. Petros, R.A. and J.M. DeSimone (2010). Strategies in the design of nanoparticles for therapeutic applications. *Nat Rev Drug Discov*, 9(8): 615-627.
137. Wood, K.C., S.R. Little, R. Langer, and P.T. Hammond (2005). A family of hierarchically self-assembling linear-dendritic hybrid polymers for highly efficient targeted gene delivery. *Angewandte Chemie-International Edition*, 44(41): 6704-6708.
138. Gillies, E.R., T.B. Jonsson, and J.M.J. Frechet (2004). Stimuli-responsive supramolecular assemblies of linear-dendritic copolymers. *Journal of the American Chemical Society*, 126(38): 11936-11943.

139. Kwon, G.S. and T. Okano (1996). Polymeric micelles as new drug carriers. *Advanced Drug Delivery Reviews*, 21(2): 107-116.
140. Siegwart, D.J., J.K. Oh, and K. Matyjaszewski (2012). ATRP in the design of functional materials for biomedical applications. *Progress in Polymer Science*, 37(1): 18-37.
141. Xu, F.J. and W.T. Yang (2011). Polymer vectors via controlled/living radical polymerization for gene delivery. *Progress in Polymer Science*, 36(9): 1099-1131.
142. Wei, H., R.-X. Zhuo, and X.-Z. Zhang (2013). Design and development of polymeric micelles with cleavable links for intracellular drug delivery. *Progress in Polymer Science*, 38(3-4): 503-535.
143. Tyrrell, Z.L., Y. Shen, and M. Radosz (2010). Fabrication of micellar nanoparticles for drug delivery through the self-assembly of block copolymers. *Progress in Polymer Science*, 35(9): 1128-1143.
144. Wang, S.H., X.Y. Shi, M. Van Antwerp, Z.Y. Cao, S.D. Swanson, X.D. Bi, and J.R. Baker (2007). Dendrimer-functionalized iron oxide nanoparticles for specific targeting and imaging of cancer cells. *Advanced Functional Materials*, 17: 3043-3050.
145. Wang, M. and M. Thanou (2010). Targeting nanoparticles to cancer. *Pharmacological Research*, 62(2): 90-99.
146. Gillies, E.R. and J.M.J. Frechet (2005). pH-responsive copolymer assemblies for controlled release of doxorubicin. *Bioconjugate Chemistry*, 16(2): 361-368.
147. Duncan, R. (2003). The dawning era of polymer therapeutics. *Nature Reviews Drug Discovery*, 2(5): 347-360.
148. Maeda, H., G.Y. Bharate, and J. Daruwalla (2009). Polymeric drugs for efficient tumor-targeted drug delivery based on EPR-effect. *European Journal of Pharmaceutics and Biopharmaceutics*, 71(3): 409-419.
149. MacEwan, S.R., D.J. Callahan, and A. Chilkoti (2010). Stimulus-responsive macromolecules and nanoparticles for cancer drug delivery. *Nanomedicine*, 5(5): 793-806.
150. Davis, M.E., Z. Chen, and D.M. Shin (2008). Nanoparticle therapeutics: an emerging treatment modality for cancer. *Nature Reviews Drug Discovery*, 7(9): 771-782.
151. Oh, K.T., H. Yin, E.S. Lee, and Y.H. Bae (2007). Polymeric nanovehicles for anticancer drugs with triggering release mechanisms. *Journal of Materials Chemistry*, 17(38): 3987-4001.

152. Poly, J., D.J. Wilson, M. Destarac, and D. Taton (2008). Synthesis of Poly(vinyl acetate) Nanogels by Xanthate-Mediated Radical Crosslinking Copolymerization. *Macromolecular Rapid Communications*, 29(24): 1965-1972.
153. Licciardi, M., G. Giammona, J.Z. Du, S.P. Armes, Y.Q. Tang, and A.L. Lewis (2006). New folate-functionalized biocompatible block copolymer micelles as potential anti-cancer drug delivery systems. *Polymer*, 47(9): 2946-2955.
154. Knop, K., R. Hoogenboom, D. Fischer, and U.S. Schubert (2010). Poly(ethylene glycol) in Drug Delivery: Pros and Cons as Well as Potential Alternatives. *Angewandte Chemie International Edition*, 49(36): 6288-6308.
155. Jang, W.D., K.M.K. Selim, C.H. Lee, and I.K. Kang (2009). Bioinspired application of dendrimers: From bio-mimicry to biomedical applications. *Progress in Polymer Science*, 34(1): 1-23.
156. Allen, T.M., C. Hansen, F. Martin, C. Redemann, and A. Yauyoung (1991). Liposomes Containing Synthetic Lipid Derivatives of Poly(ethylene Glycol) Show Prolonged Circulation Half-lives In Vivo. *Biochimica Et Biophysica Acta*, 1066(1): 29-36.
157. Brewer, E., J. Coleman, and A. Lowman (2011). Emerging Technologies of Polymeric Nanoparticles in Cancer Drug Delivery. *Journal of Nanomaterials*.
158. Haag, R. (2004). Supramolecular drug-delivery systems based on polymeric core-shell architectures. *Angewandte Chemie-International Edition*, 43(3): 278-282.
159. Sharma, A., K. Neibert, R. Sharma, D. Maysinger, and A. Kakkar (2011). Facile Construction of Multifunctional Nanocarriers Using Sequential Click Chemistry for Applications in Biology. *Macromolecules*: null-null.
160. Naeini, A.T., M. Adeli, and M. Vossoughi (2010). Poly(citric acid)-block-poly(ethylene glycol) copolymers-new biocompatible hybrid materials for nanomedicine. *Nanomedicine-Nanotechnology Biology and Medicine*, 6(4): 556-562.
161. Frisch, H. and P. Besenius (2015). pH-Switchable Self-Assembled Materials. *Macromolecular Rapid Communications*, 36(4): 346-363.

## Chapter 2

### Synthesis of well-defined functionalized poly(2-(diisopropylamino)ethyl methacrylate)



The contents of this chapter are published in: **Gois, J. R., Rocha, N.; Popov, A. V., Guliashvili, T., Matyjaszewski, K., Serra, A. C., Coelho, J. F. J.**; “Synthesis of well-defined functionalized poly(2-(diisopropylamino)ethyl methacrylate) using ATRP with sodium dithionite as a SARA agent”. *Polymer Chemistry*, 2014, 5 (12), 3919-3928.



## 2.1. Abstract

2-(Diisopropylamino)ethyl methacrylate (DPA) was polymerized by atom transfer radical polymerization (ATRP) using sodium dithionite ( $\text{Na}_2\text{S}_2\text{O}_4$ ) as a reducing agent and supplemental activator with  $\text{Cu(II)Br}_2/\text{Me}_6\text{TREN}$  catalytic system at 40 °C in a mixture isopropanol-water. The effects of the solvent mixture and the initiator structure on the polymerization kinetics were studied. The eco-friendly catalytic system described is suitable for the synthesis poly(2-(diisopropylamino)ethyl methacrylate) (PDPA) with controlled molecular weight (MW), low dispersity ( $\mathcal{D}$ ), and well-defined chain-end functionality. Both linear and 4-arms star polymers with various target MW were synthesised. The  $^1\text{H}$  NMR and MALDI-TOF analysis confirmed the molecular structure and high chain-end functionality of the obtained polymers. The use of an alkyne functionalized initiator allowed further copper catalyzed azide-alkyne [3+2] dipolar cycloaddition reaction (CuAAC) with 3-azido-7-diethylamino-coumarin ( $\text{N}_3\text{-cum}$ ), a fluorescent biocompatible molecule.

## 2.2. Introduction

The discovery of reversible deactivation radical polymerization (RDRP) methods has brought an unprecedented interest over this technology during the last two decades.<sup>1</sup> The possibility of synthesizing tailor made polymers with controlled composition, architecture, molecular weight (MW) and active chain-end functionalities by radical reactions opened a myriad of opportunities for macromolecular engineering. Among several RDRP methods reported in the literature, ATRP is the most often used due to several intrinsic advantages, such as simplicity, high tolerance to different monomer functionalities, and the commercial availability of most compounds. In order to reduce the catalyst levels, several variations of the initial ATRP concept have been reported in the literature, such as: activators regenerated by electron transfer (ARGET) ATRP,<sup>2</sup> initiator for continuous activator regeneration (ICAR) ATRP,<sup>3</sup> supplemental activator and reducing agent (SARA) ATRP,<sup>4, 5</sup> and polymerization in the presence of  $\text{Cu}^0$ .<sup>6-9</sup> These methods require ppm amounts of the catalyst to afford fast and controlled polymerization at room temperature. Organic sulphites have recently been reported by our research group as very efficient SARA agents).<sup>10, 11</sup> Amongst the organic sulphites

that were studied, sodium dithionite (Na<sub>2</sub>S<sub>2</sub>O<sub>4</sub>)<sup>12</sup> is the most efficient reducing agent that can convert the Cu(II) species into Cu(I).<sup>10, 11</sup> The reactions proceeded in a very controlled manner in alcohol/water solvent mixtures, with faster polymerization at higher contents of water in the system.<sup>11</sup>

Poly(2-(diisopropylamino)ethyl methacrylate) (PDPA) is a tertiary amine methacrylate with a hydrophilic/hydrophobic transition at pH around 6.2,<sup>13, 14</sup> making it a very attractive polymer for biomedical applications. Several studies have been reported using DPA-based copolymers for the preparation of smart vesicles<sup>15, 16</sup> and micelles<sup>17</sup> for gene and drug delivery applications.<sup>14, 18</sup> The first report concerning the ATRP of DPA was carried out in methanol with a Cu(I)Br/2,2'-bipyridine (Bpy) complex using an water soluble poly(2-methacryloyloxyethyl phosphorylcholine) macroinitiator.<sup>19</sup> Thereafter, several DPA based copolymers were synthesized using the same approach with slightly variations in the solvent used and the copper based catalytic complexes: Cu(I)Br/1,1,4,7,10,10-hexamethyltri-ethylenetetramine (HMTETA);<sup>20</sup> Cu(I)Br/*N,N,N',N'',N'''*-penta-methyldiethylenetriamine (PMDETA);<sup>18</sup> or Cu(I)Cl/PMDETA,<sup>21</sup> and Cu(I)Cl/Bpy.<sup>22</sup> The aforementioned systems required a considerable amount of catalyst to control the polymerization and to afford polymers of low dispersity (*D*). This fact is a serious issue if one intends to prepare well-controlled PDPA molecular structures for biomedical applications, requiring, for instance, highly demanding purification procedures.<sup>23</sup> Concerning the potential of PDPA-based polymeric structures for biomedical applications,<sup>18, 21</sup> hereafter it is proposed the ATRP of DPA using a more biocompatible and eco-friendly catalyst system that involves the use of Food and Drug Administration (FDA) approved additives in the presence of only trace amounts of copper. The influence of the solvent and the ATRP initiator were evaluated in the SARA ATRP of DPA using Na<sub>2</sub>S<sub>2</sub>O<sub>4</sub> as a reducing agent (and supplemental activator). The use of alkyne-terminated initiators allowed a further conjugation of the products with other molecules or polymers by a “click” reaction with no need of any post-modification reactions. The 3-azido-7-diethylamino-coumarin (N<sub>3</sub>-cum) molecule was used as a model azido-compound, since the formation of a fluorescent product can confirm the success of the “click” reaction.<sup>24</sup> The living character of the synthesised PDPA also allowed the polymeric chain-growth to obtain copolymeric structures or any post-polymerization modification. Moreover, the combination with the coumarin dye can be used to provide fluorescent molecular probing to these materials.<sup>24, 25</sup>



## 2.3. Experimental Section

### 2.3.1. Materials

2-(Diisopropylamino)ethyl methacrylate (DPA) (97% stabilized, Aldrich), was passed over a sand/alumina column before use in order to remove the hydroquinone inhibitors. Sodium dithionite ( $\text{Na}_2\text{S}_2\text{O}_4$ ) (>87%, Merck), copper(II) bromide ( $\text{CuBr}_2$ ) (99+%+ extra pure, anhydrous, Acros), copper(II) sulphate ( $\text{CuSO}_4$ ) ( $\geq 99\%$ , Sigma), sodium ascorbate (NaAsc) ( $\geq 98\%$ , Sigma), ethyl 2-bromoisobutyrate (EBiB) (98%; Aldrich), pentaerythritol tetrakis(2-bromoisobutyrate) (4f-BiB) (97%; Aldrich), sodium azide ( $\text{NaN}_3$ ) ( $\geq 99.5\%$ , Sigma-Aldrich), deuterated chloroform ( $\text{CDCl}_3$ ) (+1% TMS, Eurisotop), 2-propanol (IPA) (Fisher Chemical), tetrahydrofuran (THF) (Fisher Chemical), poly(ethylene glycol) (PEG) standards (analytical standards for GPC, Fluka), poly(styrene) (PS) standards (Sigma) were used as received. Purified water (Milli-Q<sup>®</sup>) (Millipore, resistivity >18 M $\Omega$  cm) was obtained by reverse osmosis. Tris(2-(dimethylamino)ethyl)amine ( $\text{Me}_6\text{TREN}$ )<sup>26</sup> and propargyl 2-bromoisobutyrate (PgBiB)<sup>27</sup> were synthesized according the procedures described in the literature (PgBiB: <sup>1</sup>H NMR (400 MHz,  $\text{CDCl}_3$ ,  $\delta$  (ppm)): 4.90 (d, 2H,  $\text{COOCH}_2$ ); 2.50 (t, 1H,  $\text{COOCH}_2\equiv\text{CH}$ ); 1.80 (s, 6H,  $\text{C}(\text{CH}_3)_2$ ). 3-azido-7-diethylaminocoumarin ( $\text{N}_3\text{-Cum}$ ) was synthesized according to the procedures described in the literature<sup>24</sup> (<sup>1</sup>H NMR (400 MHz,  $\text{CDCl}_3$ ,  $\delta$  (ppm)): 7.21 (d, 2H,  $-\text{CH}-$ ); 7.11 (s, 1H,  $-\text{CH}-$ ); 6.66 (d, 1H,  $-\text{CH}-$ ), 6.57 (s, 1H,  $-\text{CH}-$ ); 3.46 (q, 4H,  $-\text{N}-(\text{CH}_2)_2$ ); 1.21 (t, 6H,  $-\text{C}-(\text{CH}_3)_2$ )).

### 2.3.2. Characterization

Size exclusion chromatography (SEC) analysis was performed using a system equipped with an online degasser, a refractive index (RI) detector and a set of columns: Shodex OHpak SB-G guard column, OHpak SB-802.5HQ and OHpak SB-804HQ columns. The polymers were eluted at a flow rate of 0.5 mL.min<sup>-1</sup> with 0.1 M  $\text{Na}_2\text{SO}_4$  (aq) /1 wt% acetic acid/0.02%  $\text{NaN}_3$  at 40 °C. Before the injection (50  $\mu\text{L}$ ) the samples were filtered through a polyester membrane with 0.45  $\mu\text{m}$  pore. The system was calibrated with narrow  $D$  PEG standards. The number-average molecular weight ( $M_{n,\text{GPC}}$ ) and  $D$  of the synthesized polymers were determined by conventional calibration using Clarity software version 2.8.2.648.

For the 4-armed polymers, high performance gel permeation chromatography (HPSEC) was performed using a Viscotek (ViscotekTDAmx) with a differential viscometer (DV), right-angle laser-light scattering (RALLS, Viscotek), and refractive index (RI) detectors, using column set of a PL 10  $\mu\text{m}$  guard column followed by one MIXED-E PLgel column and one MIXED-C PLgel column. Previously filtered THF was used as an eluent at a flow rate of  $1 \text{ mL}\cdot\text{min}^{-1}$  at  $30 \text{ }^\circ\text{C}$ . The samples were filtered through a polytetrafluoroethylene membrane with  $0.2 \text{ }\mu\text{m}$  pore before injection and the system was calibrated with narrow PS standards. The  $dn/dc$  of PDPA in THF at  $30 \text{ }^\circ\text{C}$  was determined as 0.077 (for  $\lambda = 670 \text{ nm}$ ) using a RUDOLPH RESEARCH J357 Automatic Refractometer (J357-NDS-670-CC). The  $M_{n,\text{GPC}}$  and  $\bar{D}$  of synthesized polymers were determined by using a multidetectors calibration (OmniSEC software version: 4.6.1.354).

$^1\text{H}$  nuclear magnetic resonance (NMR) spectra were recorded on a Bruker Avance III 400 MHz spectrometer, with a 5 mm TXI triple resonance detection probe, in  $\text{CDCl}_3$  with tetramethylsilane (TMS) as an internal standard. Conversion of monomers was determined by integration of monomer and polymer peaks using MestReNova software version: 6.0.2-5475.

For matrix-assisted laser desorption ionization time-of-flight mass spectroscopy (MALDI-TOF-MS) analysis, the PDPA samples were dissolved in THF at a concentration of  $20 \text{ mg}\cdot\text{mL}^{-1}$  and 2,5-dihydroxybenzoic acid (DHB) ( $20 \text{ mg}\cdot\text{mL}^{-1}$  in THF) was used as a matrix. The dried-droplet sample preparation technique was used to obtain a 1:1 ratio (sample/matrix); an aliquot of  $1 \text{ }\mu\text{L}$  of each sample was directly spotted on the MTP AnchorChip TM 600/384 TF MALDI target, BrukerDaltonik (Bremen Germany) and, before the sample dried,  $1 \text{ }\mu\text{L}$  of matrix solution in THF was added and the mixture allowed to dry at room temperature, to allow matrix crystallization. External mass calibration was performed with a peptide calibration standard (PSCII) for the range 700-3000 (9 mass calibration points),  $0.5 \text{ }\mu\text{L}$  of the calibration solution and matrix previously mixed in an Eppendorf tube (1:2, v/v) were applied directly on the target and allowed to dry at room temperature. Mass spectra were recorded using an Autoflex III smartbeam1 MALDITOF-MS mass spectrometer Bruker Daltonik (Bremen, Germany) operating in the linear and reflection positive ion mode. Ions were formed upon irradiation by a smart beam laser using a frequency of 200 Hz. Each mass spectrum was produced by averaging 2500 laser shots collected

across the whole sample spot surface by screening in the range  $m/z$  500-7500. The laser irradiance was set to 35-40 % (relative scale 0-100) arbitrary units according to the corresponding threshold required for the applied matrix systems.

### 2.3.3. Procedures

#### **Typical procedure for the SARA ATRP of DPA (DP = 50) catalyzed by $[\text{Na}_2\text{S}_2\text{O}_4]/[\text{CuBr}_2]/[\text{Me}_6\text{TREN}] = 1/0.1/0.1$ in isopropanol/water mixture.**

A mixture of  $\text{CuBr}_2$  (3.67 mg, 0.016 mmol),  $\text{Me}_6\text{TREN}$  (4.16 mg, 0.018 mmol) and water (195  $\mu\text{L}$ ) was placed in a Schlenk tube reactor that was sealed by using a rubber septa.  $\text{Na}_2\text{S}_2\text{O}_4$  (32.86 mg, 0.164 mmol) and a mixture of DPA (1.75 g, 8.21 mmol) and EBiB (32.02 mg, 0.164 mmol) in IPA (3.697 mL) (previously bubbled with nitrogen for about 15 minutes) was added to the reactor and frozen in liquid nitrogen. The Schlenk tube reactor containing the reaction mixture was deoxygenated with three freeze-vacuum-thaw cycles and purged with nitrogen. The Schlenk tube reactor was placed in a water bath at 40 °C with stirring (600 rpm). Aliquots of the reaction mixture were collected periodically during the polymerization by using an airtight syringe and purging the side arm of the Schlenk tube reactor with nitrogen. The samples were analysed by  $^1\text{H}$  NMR spectroscopy in order to determine the monomer conversion, and by GPC to determine MW and  $D$  of the PDPA.

#### **Chain extension experiment.**

A mixture of  $\text{CuBr}_2$  (4.84mg, 0.02 mmol),  $\text{Me}_6\text{TREN}$  (5.48 mg, 0.02 mmol) and water (152  $\mu\text{L}$ ) was placed in a Schlenk tube reactor that was sealed by using rubber septa.  $\text{Na}_2\text{S}_2\text{O}_4$  (47.5 mg, 0.024 mmol) and a mixture of DPA (1.37 g, 6.42 mmol) and EBiB (41.7 mg, 0.21 mmol) in IPA (2.892 mL) (previously bubbled with nitrogen for about 15 minutes) was added to the reactor and frozen in liquid nitrogen. The Schlenk tube reactor containing the reaction mixture was deoxygenated with five freeze-vacuum thaw cycles and purged with nitrogen. The Schlenk tube reactor was placed in a water bath at 40 °C with stirring (600 rpm) and the reaction proceeded for 4 hours (75% conversion,  $M_{n,\text{th}} = 4.94 \times 10^3$ ,  $M_{n,\text{GPC}} = 15.30 \times 10^3$ ,  $D = 1.20$ ). After that, a degassed solution of DPA (1.61g, 7.56 mmol) in IPA/ $\text{H}_2\text{O}$  (2.76 mL/145  $\mu\text{L}$ ) was added and the reaction proceeded for 24h.

**“Click” reaction between the alkyne terminated-PDPA (AT-PDPA) and 3-azido-7-diethylamino coumarin (N<sub>3</sub>-Cum).**

AT-PDPA (341.16 mg, 0.012 mmol,  $M_{n, GPC} = 27.6 \times 10^3$ ,  $\mathcal{D} = 1.11$ ) synthesized by SARA ATRP and N<sub>3</sub>-Cum (4.81 mg, 0.018 mmol) were dissolved in 6 mL of THF. NaAsc (1.96 mg, 0.010 mmol dissolved in water (0.4 mL) were added to the previous mixture, the vessel were sealed with a rubber septum and the mixture bubbled with nitrogen for about 10 min. A fresh solution of CuSO<sub>4</sub> (0.54 mL, 0.003 mmol) in water were added under nitrogen and the reaction proceed at room temperature overnight. The reaction was observed by UV fluorescence at 366 nm. To remove the excess of N<sub>3</sub>-Cum and the catalysts, the product was dialysed against a THF-water mixture (50:50) for 2 days. The product was analysed by <sup>1</sup>H NMR spectroscopy and by fluorescence restoration ( $\lambda_{ex} = 365$  nm) in order to confirm the success of the “click” reaction.

## 2.4. Results and Discussion

The reports available in the literature concerning the ATRP of DPA based polymers involve the use of high concentration of copper catalysts and, in some cases toxic solvents, such as THF or methanol. The control over the polymerization is achieved by Cu(I)Br (or Cu(I)Cl) chelated with various nitrogen based ligands such as Bpy,<sup>13, 19, 22, 28</sup> PMDETA<sup>21</sup> or HMTETA<sup>20</sup> at high concentrations. However, polymers intended to be applied in the biomedical field requires the use of safer solvent mixtures and an accurate removal of the catalyst from the final product.

The use of inorganic sulfites, such as Na<sub>2</sub>S<sub>2</sub>O<sub>4</sub>, sodium bisulfite (NaHSO<sub>3</sub>) and sodium metabisulfite (Na<sub>2</sub>S<sub>2</sub>O<sub>5</sub>), as reducing agents and supplemental activators in ATRP of methyl acrylate (MA) has recently been reported.<sup>10, 11</sup> The ability to control the polymerization with small amounts of copper/ligand system in alcohol/water mixture makes these systems very promising for polymer synthesis for biomedical applications.

As the amount of water has a strong impact on the kinetics of ATRP, initially, the experiments were conducted to determine influence of water content in the SARA ATRP of DPA using Na<sub>2</sub>S<sub>2</sub>O<sub>4</sub> as a reducing agent.<sup>11</sup> Subsequently, the method was applied for the polymerization of DPA with various target molecular weights and different ATRP initiators (alkyne terminated initiator (PgBiB) and a 4-arms star initiator (4f-BiB)). All reactions were performed using a ratio [DPA]<sub>0</sub>/solvent = 1/2 (v/v) and a molar ratio [Na<sub>2</sub>S<sub>2</sub>O<sub>4</sub>]<sub>0</sub>/[CuBr<sub>2</sub>]<sub>0</sub>/[Me<sub>6</sub>TREN]<sub>0</sub> = 1/0.1/0.1.

### 2.4.1. Influence of water content on the rate of polymerization and control over molar mass of DPA in IPA/water mixtures

In SARA ATRP mediated by a mixed sulfite-Cu(II)Br<sub>2</sub>/ligand catalytic system the use of small amounts of water in the reaction mixture can enhance the solubilization of the inorganic salts leading to faster reactions.<sup>11</sup> Abreu and co-authors have found that for the polymerization of methyl acrylate in a mixture ethanol/water, using the system [MA]<sub>0</sub>/[EBiB]<sub>0</sub>/[Na<sub>2</sub>S<sub>2</sub>O<sub>4</sub>]<sub>0</sub>/[CuBr<sub>2</sub>]<sub>0</sub>/[Me<sub>6</sub>TREN]<sub>0</sub>, the optimum content of water was 35%. Up to this value, the polymerization rate increased with the water content maintaining the control over the MW and *D*.<sup>11</sup>

In order to find the optimal ratio of IPA/ $\text{H}_2\text{O}$  to afford a controlled ATRP of DPA, two different ratios IPA/ $\text{H}_2\text{O}$  have been studied. Figure 2.1 presents the kinetic plots of SARA ATRP of DPA conducted at 40 °C in IPA/ $\text{H}_2\text{O}$  mixtures using 5 or 10% (v/v) of water in the solvent mixture.

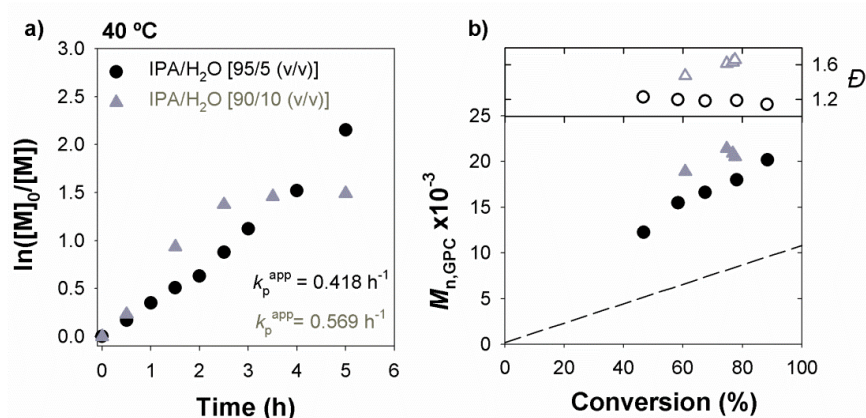


**Figure 2.1:** Effect of solvent mixture in the SARA ATRP of DPA, IPA/ $\text{H}_2\text{O}$  = 95/5 (v/v) (black circle symbols) and IPA/ $\text{H}_2\text{O}$  = 90/10 (v/v) (grey triangle symbols) at 40 °C: (a) First-order kinetic plot, (b) evolution of MW and  $\bar{D}$  with conversion (the dashed line represents theoretical MW at a given conversion). Reaction conditions:  $[\text{DPA}]_0/\text{solvent} = 1/2$  (v/v),  $[\text{DPA}]_0 / [\text{EBiB}]_0 / [\text{Na}_2\text{S}_2\text{O}_4]_0 / [\text{CuBr}_2]_0 / [\text{Me}_6\text{TREN}]_0 = 50/1/1/0.1/0.1$  (molar).

It should be mentioned that to poor solubility of sodium dithionite in isopropanol, the polymerizations should always be carried out in the presence of small amount of water. The presence of 5% (v/v) of water in the reaction solvent mixture allows the polymerization to proceed with a first order kinetic relative to the monomer, reaching 80% conversion in 5 hours, with low  $\bar{D}$  ( $\bar{D} = 1.14$ ). The GPC traces (Figure 2.2 (a)) of the samples that were taken at different reaction times show that, for the polymerization carried out at 5% (v/v) of water, a unimodal distribution and a gradual shift towards higher MW with time was obtained. When the ATRP was conducted with a high water content, (10%, v/v) in the solvent mixture, a lower monomer conversion and an uncontrolled polymerization was observed. This fact is supported by the deviations of the ATRP kinetics from a “living” behavior<sup>29</sup> in Figure 2.1 and by broad GPC traces that are shown in Figure 2.2(b).

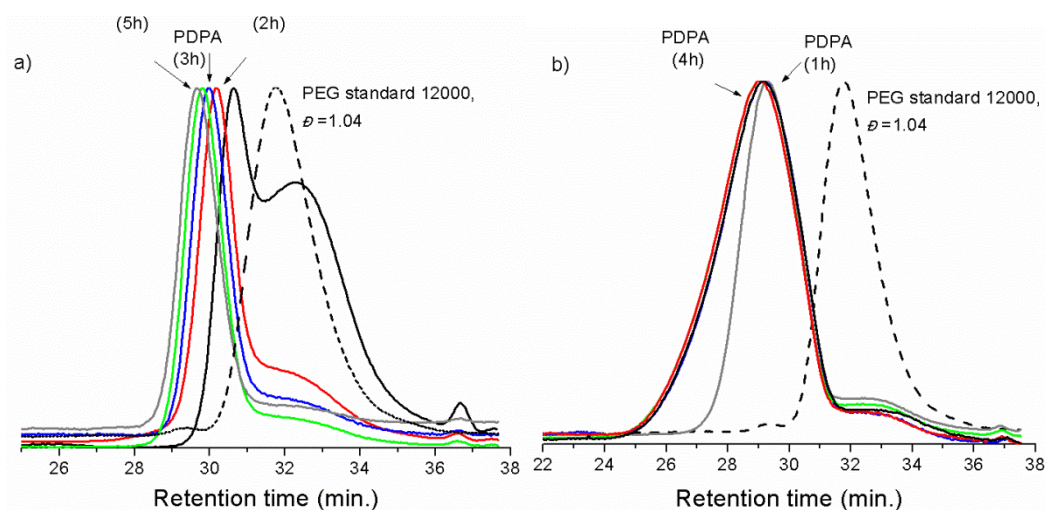


**Figure 2.2:** GPC traces of PEG standard ( $M_p = 12\,000\text{ g}\cdot\text{mol}^{-1}$ ;  $D = 1.04$ ) and PDPA samples. Conditions: (a)  $[\text{DPA}]_0/\text{solvent} = 1/2$  (v/v),  $[\text{IPA}]/[\text{H}_2\text{O}] = 0.95/0.05$  (v/v);  $[\text{DPA}]_0 / [\text{EBiB}]_0 / [\text{Na}_2\text{S}_2\text{O}_4]_0 / [\text{CuBr}_2]_0 / [\text{Me}_6\text{TREN}]_0 = 50/1/1/0.1/0.1$  (molar);  $T = 40\text{ }^\circ\text{C}$ ; (b)  $[\text{DPA}]_0/\text{solvent} = 1/2$  (v/v),  $[\text{IPA}]/[\text{H}_2\text{O}] = 0.90/0.10$  (v/v),  $[\text{DPA}]_0 / [\text{EBiB}]_0 / [\text{Na}_2\text{S}_2\text{O}_4]_0 / [\text{CuBr}_2]_0 / [\text{Me}_6\text{TREN}]_0 = 50/1/1 / 0.1/0.1$  (molar);  $T = 40\text{ }^\circ\text{C}$ .

The high  $D$  may result from the reduced solubility of PDPA in this solvent mixture (IPA/H<sub>2</sub>O = 90/10 (v/v)). In fact, it has been experimentally observed that for 10% (v/v) of water, the synthesized PDPA samples of higher MW presented significantly lower solubility in the solvent mixture when compared to those with 5% (v/v) of water. Although most of the critical characteristics of a "living" polymerization are achieved, such as the linear growth of MW with conversion and low  $D$  values throughout the reaction, when ATRP was carried with 5% (v/v) of water, the GPC traces present a tailing in the curve. This deviation become less predominant for higher DPA monomer conversion, suggesting the occurrence of termination reactions at the early stages of the polymerization due to the high concentration of radicals caused by the presence of the dithionite.<sup>12, 30, 31</sup>

#### 2.4.2. Study of variable degrees of polymerization

The influence of the target degree of polymerization (DP) on the SARA ATRP of DPA is presented in Figure 2.3. As expected, the polymerization rate decreases for a higher targeted DP. This decrease can be attributed to a lower concentration of radicals in the

polymerization mixture. Although the kinetics of polymerization at DP 100 shows a typical profile of a “living” polymerization, with a linear increase of the MW with the conversion, there is a tendency towards higher  $\bar{D}$  when compared to those obtained at the DP of 50. Figure 2.4 compares the GPC traces obtained for DP=100 and 20.

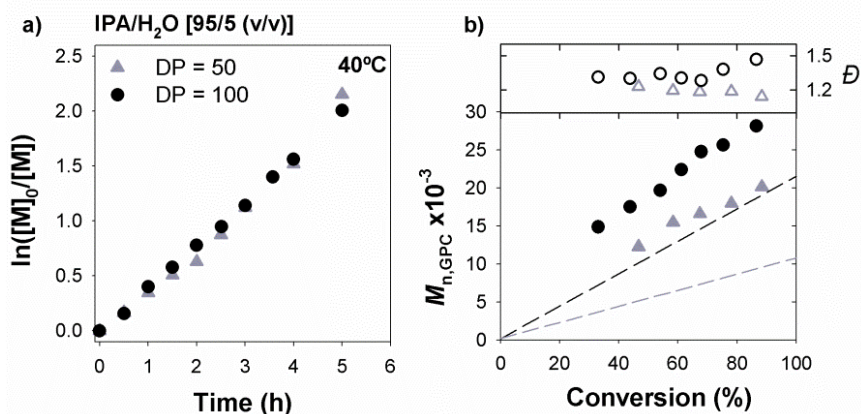


**Figure 2.3:** Effect of the target degree of polymerization (DP) in the SARA ATRP of DPA in IPA/H<sub>2</sub>O = 95/5 (v/v) at 40 °C. (a) First-order kinetic plot, (b) evolution of MW and  $\bar{D}$  with conversion (the dashed line represents theoretical MW at a given conversion), Reaction conditions:  $[\text{DPA}]_0/\text{solvent} = 1/2$  (v/v),  $[\text{DPA}]_0/[\text{EBiB}]_0/[\text{Na}_2\text{S}_2\text{O}_4]_0/[\text{CuBr}_2]_0/[\text{Me}_6\text{TREN}]_0 = 100/1/1/0.1/0.1$  (molar) (black circle symbols) or  $[\text{DPA}]_0/[\text{EBiB}]_0/[\text{Na}_2\text{S}_2\text{O}_4]_0/[\text{CuBr}_2]_0/[\text{Me}_6\text{TREN}]_0 = 50/1/1/0.1/0.1$  (molar) (grey triangle symbols).

The GPC traces obtained for DP of 100 shows a shift towards higher MW values with time, but, in this case, the tailing for lower MW segments is not as evident as for lower DP. This observation may be attributed to a lower concentration of dead chain ends, likely due to the reduced concentration of radicals. In fact, polymerizations with a much lower DP (DP = 20) (Figure 2.4 (b)) show GPC curves with more evident low MW tail. For the other polymerizations carried out with higher DP, the main peak remains with a narrow MW distribution, still suggesting a controlled PDPA chain growth. The formation of lower MW fraction which decreases with the monomer conversion, suggests that there is a loss of active chain end functionality at the beginning of the polymerization. This effect may be attributed to the high concentration of sodium dithionite and possible inefficient deactivation by the Cu(II)Br<sub>2</sub> complex, leading to termination reactions and becoming more pronounced when the catalyst is at a higher concentration.



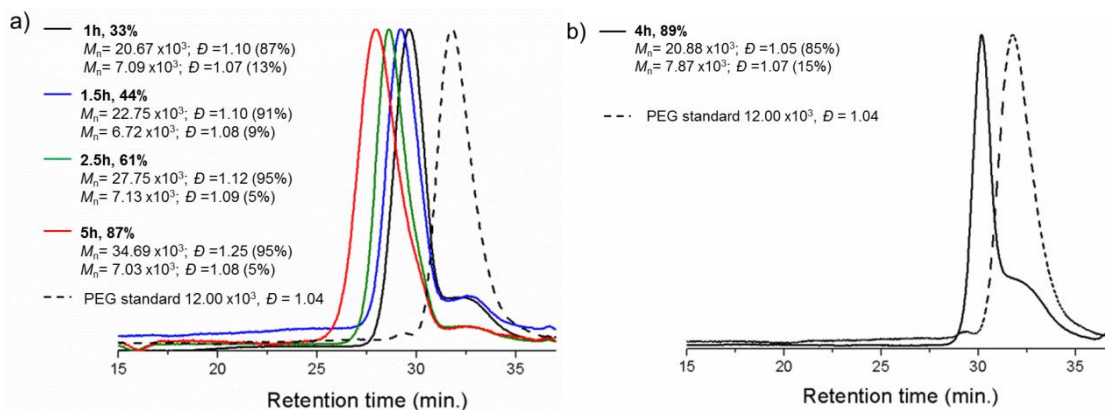


**Figure 2.4:** GPC traces of PEG standard ( $M_p = 12.00 \times 10^3 \text{ g.mol}^{-1}$ ;  $D = 1.04$ ) and PDPA samples for two different target MW (DP 100 (a) and DP 20 (b)). Conditions:  $[DPA]_0/\text{solvent} = 1/2$  (v/v),  $[IPA]/[H_2O] = 0.95/0.05$  (v/v); (a):  $[DPA]_0/[EBiB]_0/[Na_2S_2O_4]_0/[CuBr_2]_0/[Me_6TREN]_0 = 100/1/1/0.1/0.1$  (molar); (b):  $[DPA]_0/[EBiB]_0/[Na_2S_2O_4]_0/[CuBr_2]_0/[Me_6TREN]_0 = 20/1/1/0.1/0.1$  (molar);  $T = 40 \text{ }^\circ\text{C}$ .

To further evaluate the effect of the  $Cu(II)Br_2/Me_6TREN$  complex concentration in the formation of these low MW PDPA fractions, two similar reactions were performed using different ratios of the  $Cu(II)Br_2/Me_6TREN$  complex to the initiator (0.1 and 0.2). No significant changes were observed in the MW control, since both PDPA present similar low MW tailing (Figure A.3 in Annex A).

### 2.4.3. Influence of different ATRP initiators on the rate of polymerization and control over molar mass of DPA in IPA/water mixtures

In order to evaluate the possibility of preparing telechelic PDPA with different chain-end functionalities, an alkyne terminated initiator (PgBib) was used in the SARA ATRP reactions of DPA. Figure 2.5 presents the kinetic plots of DPA polymerization for a target DP of 40. When PgBiB was used as ATRP initiator (Figure 2.5) the kinetic plot showed similar behavior compared to EBiB. The polymerization reaches high monomer conversion (92%) in less than 4 hours with relatively low  $D$  ( $D = 1.22$ ). The kinetic data obtained under the same reaction conditions for normal ATRP revealed a much slower polymerization (Figure A.4, Annex A).

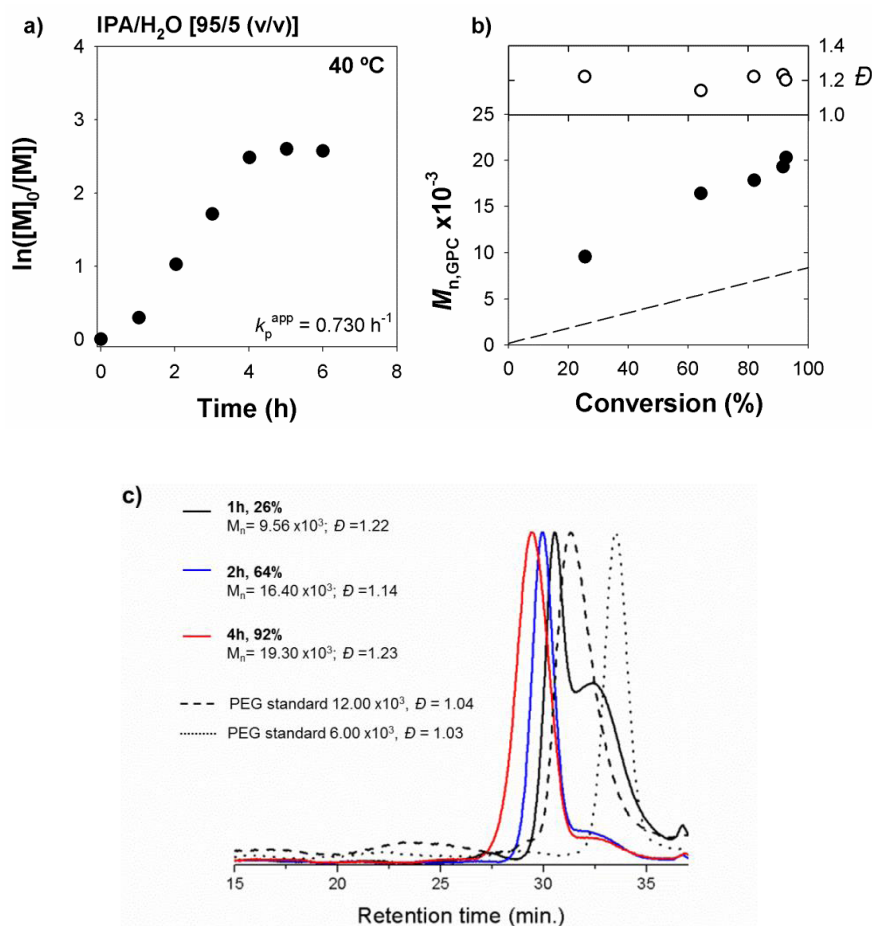


**Figure 2.5:** PgBiB mediated SARA ATRP of DPA in IPA/ $\text{H}_2\text{O}$  = 95/5 (v/v) at 40 °C. (a) First-order kinetic plot, (b) evolution of MW and  $\bar{D}$  with conversion (the dashed line represents theoretical MW at a given conversion), and (c) GPC traces of PEG standard ( $M_p = 12.00 \times 10^3$  g.mol $^{-1}$ ;  $\bar{D} = 1.04$ ) and PDPA samples. Reaction conditions:  $[\text{DPA}]_0/\text{solvent} = 1/2$  (v/v),  $[\text{IPA}]/[\text{H}_2\text{O}] = 0.95/0.05$  (v/v);  $[\text{DPA}]_0 / [\text{PgBiB}]_0 / [\text{Na}_2\text{S}_2\text{O}_4]_0 / [\text{CuBr}_2]_0 / [\text{Me}_6\text{TREN}]_0 = 40/1/1/0.1/0.1$  (molar);  $T = 40$  °C.

Additionally, a 4-armed ATRP initiator (4f-BiB) was further evaluated with this SARA ATRP catalytic system. Star-shaped initiators can generate complex polymeric architectures, which may provide unique functionalities in biomedical applications.<sup>32</sup> The use of 4f-BiB for the  $\text{Na}_2\text{S}_2\text{O}_4/\text{Cu(II)Br}_2/\text{Me}_6\text{TREN}$  catalytic system in IPA/ $\text{H}_2\text{O}$  [95/5 (v/v)] was evaluated to prepare four-armed star PDPA and compare with the linear counterpart. Two polymers with the same total target MW were synthesized using a 4f-BiB and EBiB. The comparison of both GPC traces, from the linear polymer (DP 100) with the 4 arms star polymer with DP 25 (Figure 2.6), shows that the trace

from the star polymer is eluted at a volume greater than its linear counterpart. In fact, this observation may be explained by the lower hydrodynamic volume that a star polymer occupies when compared to its linear analogue.

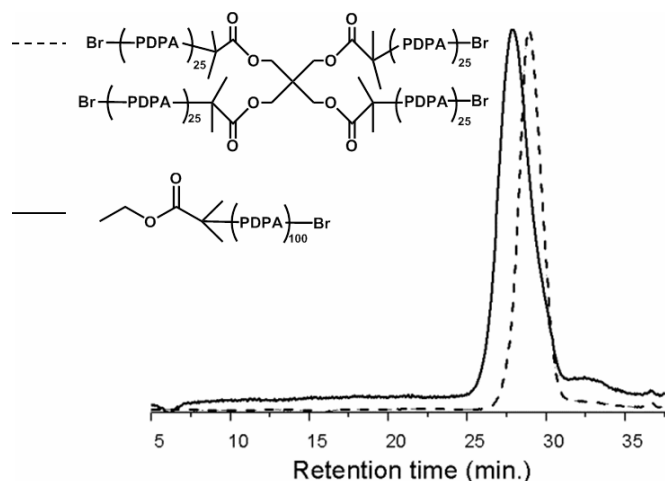


**Figure 2.6:** GPC traces of linear PDPA and 4-arms star PDPA samples. Conditions:  $[DPA]_0/[IPA]/[H_2O] = 1/0.95/0.05$  (v/v);  $[DPA]_0/[EBiB]_0/[Na_2S_2O_4]_0/[CuBr_2]_0/[Me_6TREN]_0 = 100/1/1/0.1/0.11$  (molar) (linear);  $[DPA]_0/[4f-BiB]_0/[Na_2S_2O_4]_0/[CuBr_2]_0/[Me_6TREN]_0 = 100/1/4/0.4/0.41$  (star),  $T = 40$  °C.

For an accurate characterization of the 4-arms star PDPA, the GPC analysis was performed using a multi-detectors systems, including differential viscometer (DV) and a right-angle laser-light scattering (RALLS) detector in addition to the refractive index (RI) detector. Mark-Houwink plots of log intrinsic viscosity as a function of log MW were calculated for the 4-arms star PDPA and the linear analog in order to explore the conformation of the polymer in solution and are presented in Figure 2.7. The resulting plot of the 4-arms star polymer consists in a parallel line to the linear one indicating that a star polymer has a lower intrinsic viscosity at any given molecular weight when compared to the linear one. The relationship between the MW and the intrinsic viscosity is given by the equation,  $[\eta] = k M^a$ , being  $[\eta]$  the intrinsic viscosity,  $M$  the molecular weight and  $k$ ,  $a$  the Mark-Houwink constants. The Mark-Houwink exponent (slope of the curves), which depends on the polymer configuration in solution, is considerably lower for the 4-arms PDPA polymer ( $a = 0.59$ ), indicating a more compact and dense

structure, than the linear one ( $a=0.65$ ). The  $k$  value observed for star and linear polymer was  $9.38 \times 10^{-4}$  and  $5.37 \times 10^{-4}$ , respectively.

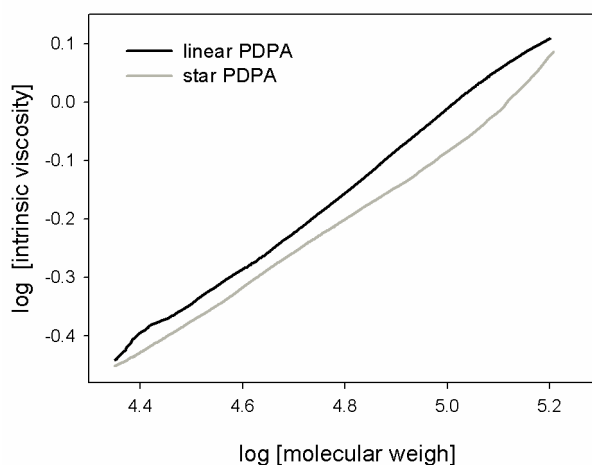


**Figure 2.7:** Log-log plot of intrinsic viscosities against MW for linear and 4-arms star PDPA.

The kinetic data obtained for the different reaction conditions used for the SARA ATRP of DPA are summarized in Table 2.1. The results indicate that when EBiB was used, as expected, the faster polymerizations were observed for higher contents of water (entries 2 and 4). This observation suggests that high water amount in the system allows faster reduction of  $\text{Cu(II)Br}_2$  species to  $\text{Cu(I)Br}$ , which should be related to the higher solubility of the dithionite salt. However, the  $D$  obtained is also higher, limiting the content water that can be used in this system to 10% (v/v). It is also interesting to notice that for PgBiB initiator (entries 9 and 10) the PDI remains low even using 10% (v/v) of water in the polymerization mixture.

**Table 2.1:** SARA-ATRP of PDA in the presence of CuBr<sub>2</sub>/Me<sub>6</sub>TREN and Na<sub>2</sub>S<sub>2</sub>O<sub>4</sub> at 40 °C in IPA/H<sub>2</sub>O (monomer/solvent ratio: 1/2 (v/v)).

Entry	[DPA] <sub>0</sub> /[initiator] <sub>0</sub> /[Na <sub>2</sub> S <sub>2</sub> O <sub>4</sub> ] <sub>0</sub> / [CuBr <sub>2</sub> ] <sub>0</sub> / [Me <sub>6</sub> TREN] <sub>0</sub>	Initiator	[IPA]/[H <sub>2</sub> O] (v/v)	$k_p^{app}$ (h <sup>-1</sup> )	Time (h) <sup>a</sup>	Conv. (%) <sup>a</sup>	$M_{n,th}^a$ x10 <sup>3</sup>	$M_{n,GPC}^a$ x10 <sup>3</sup>	$\mathcal{D}^a$
<b>1</b>	50/1/1/0.1/0.1	EBiB	0.95/0.05	0.418	5	88	9.55	20.15	1.14
<b>2</b>	50/1/1/0.1/0.1	EBiB	0.90/0.10	0.569	5	83	8.81	20.51	1.66
<b>3</b>	100/1/1/0.1/0.1	EBiB	0.95/0.05	0.416	5	87	18.79	28.14	1.47
<b>4</b>	100/1/1/0.1/0.1	EBiB	0.90/0.10	0.678	5	62	13.35	23.85	1.54
<b>5</b>	20/1/1/0.1/0.1	EBiB	0.95/0.05	---	4	98	4.53	14.32	1.20
<b>6</b>	20/1/1/0.2/0.2	EBiB	0.95/0.05	---	4	92	4.10	15.20	1.20
<b>7</b>	40/1/1/0.1/0.1	PgBiB	0.95/0.05	0.730	5	96	8.01	20.28	1.20
<b>8</b>	100/1/1/0.1/0.1	PgBiB	0.95/0.05	---	14	95	28.76	28.76	1.40
<b>9</b>	90/1/1/0.1/0.1	PgBiB	0.90/0.10	---	2	64	12.42	30.62	1.24
<b>10</b>	100/1/4/0.4/0.4	4f-BiB	0.95/0.05	---	5	99	21.69	29.68 <sup>(*)</sup>	1.17

<sup>(\*)</sup> Values obtained from the last sample from the kinetic studies. <sup>(\*)</sup> Data from THF GPC.

#### 2.4.4. $^1\text{H}$ NMR and MALDI-TOF-MS analyses

The chemical structure of the PDPA synthesized by SARA ATRP was determined with  $^1\text{H}$  NMR and MALDI-TOF-MS techniques.

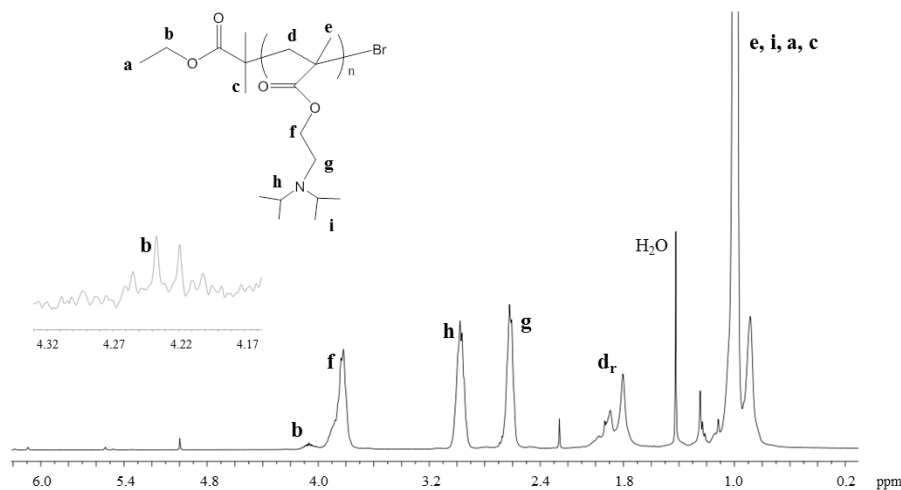


**Figure 2.8:** The  $^1\text{H}$  NMR spectrum of PDPA-Br ( $M_{n,\text{GPC}} = 14.9 \times 10^3$ ;  $M_{n,\text{NMR}} = 15.1 \times 10^3$ ,  $D = 1.20$ ) in  $\text{CDCl}_3$ .

In the  $^1\text{H}$  NMR spectrum of a PDPA shown in Figure 2.8, the peaks observed at 3.82 ppm (**f**,  $-\text{OCH}_2\text{CH}_2-$ ), 2.98 ppm (**h**,  $-(\text{CH}-\text{N})_2-$ ), 2.62 ppm (**g**,  $-\text{CH}_2\text{CH}_2\text{N}-$ ), 1.7-2.1 ppm (**d**,  $-\text{CH}_2-$  of the polymer backbone), resonances at 1 ppm (**i**,  $-(\text{CH}(\text{CH}_3)_2-$ ; **e**, “methacrylic”  $\text{CH}_3$ ) are in agreement with the expected PDPA chemical structure.<sup>33-36</sup> The peak of the methylene group (**b**) of the initiator fragment ( $\text{CH}_2$ ) can be found at 4.1 ppm and its three methyl resonances (**a**, **c**) are overlapped with other methyl group signals at the region around 1.0 ppm. Although the calculation of  $M_{n,\text{NMR}}$  for methacrylates is not simple, due to signals overlapping and low intensity of the resonances of the initiator moieties, the degree of polymerization was calculated comparing integrals of **h**, methylene protons at 2.98 ppm and of the sum of **a**, **c**, **e**, and **i** methyl protons at 0.9-1.1 ppm. From the ratio  $2n/(9+15n) = I_{\text{h}}/I_{\text{a,c,e,i}}$ ,  $n = 70$  was obtained, the calculated the  $M_{n,\text{NMR}} = M_{\text{initiator}} + n(M_{\text{monomer}}) = 15.1 \times 10^3$  which is close to the MW determined by GPC. Comparison of the  $^1\text{H}$  NMR PDPA spectrum of the PDPA with the  $^1\text{H}$  NMR spectra of predominantly syndiotactic poly(methyl methacrylate) (PMMA) (resonances of *racemo* **d<sub>r</sub>** methylenes at 1.8 ppm) and predominantly isotactic PMMA (two groups of *meso* **d<sub>m</sub>** methylene signals of the same intensity at 2.4 and 1.4 ppm)<sup>33</sup>) led to conclusion that the PDPA have a very high

syndiotactic content due to steric hindrance of the diisopropylaminoethyl moiety. The calculated syndiotactic content is 98% - the ratio of integral values of  $d_r$  (1.7-2.1 ppm) and  $h$ , methylene protons. This value is in a good agreement with our previous observations of different syndiotacticity for poly(alkyl acrylates) with alkyl groups of different bulkiness (Me, Et, Bu, iBu, tBu, lauryl, 2-Methoxyethyl) obtained by  $\text{Na}_2\text{S}_2\text{O}_4$ -catalyzed Single Electron Transfer – Degenerative Chain Transfer Living Radical Polymerization (SET-DT LRP).<sup>11, 37-42</sup> The percentage of the bromo-chain-end functionality cannot be determined since the PDPA signals of the protons near the terminal bromo-chain-end are overlapped with the proton signals of the main polymeric chain ( $d$ ,  $e$ ).

The presence of chain end functionality for the PDPA synthesized using the PgBiB as ATRP initiator could also be identified by  $^1\text{H}$  NMR spectroscopy (Figure 2.9). In the NMR spectrum of the pure polymer the characteristic peaks of the  $\text{CH}_3$ - and  $-\text{CH}_2$ -groups that are adjacent to the terminal Br chains ends are overlapped with those of the methylene protons of the polymeric chain ( $d$ ,  $e$ ) and, thus, the degree of active bromo-chain ends could not be calculated. The methylene protons resulting originally from the PgBiB initiator ( $k$ ), which can be observed at 4.62 ppm, allows estimating of the number-average MW,  $M_{n,\text{NMR}} = 25.8 \times 10^3$ .

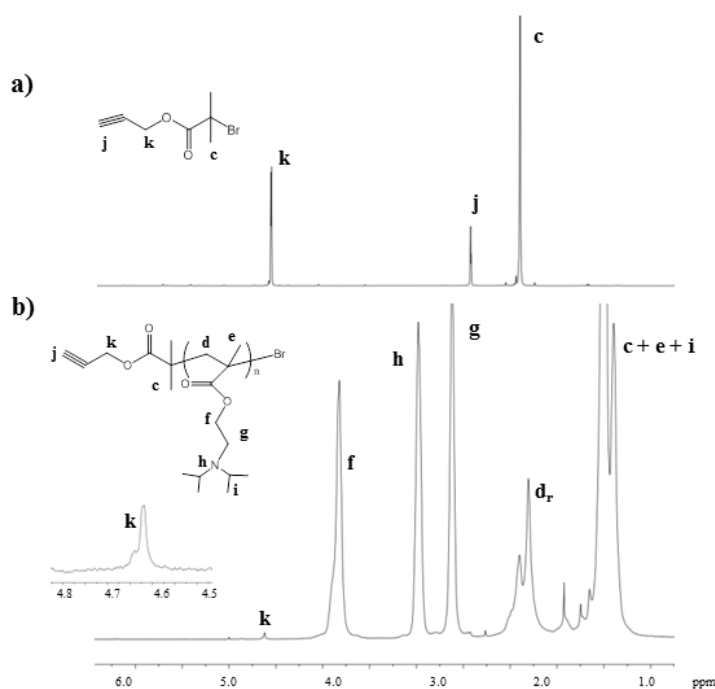


**Figure 2.9:** The  $^1\text{H}$  NMR spectra in  $\text{CDCl}_3$  of a) PgBiB – initiator; b) PDPA-Br obtained at high conversion ( $M_{n,\text{GPC}} = 27.9 \times 10^3$ ;  $D = 1.09$ ;  $M_{n,\text{NMR}} = 25.8 \times 10^3$ ).

The MALDI-TOF-MS spectrum of PDPA in the linear mode with  $m/z$  ranging from 1400 to 3000 and 1200 to 9500 is shown in Figure 2.10 and Figure 2.11(a). Enlargement of the latter in  $m/z$  2000-3220 range is shown in Figure 2.11(b). One or two series of main peaks are separated by an interval corresponding to a DPA repeating unit ( $211 = 213 - 2 = M_{\text{DPA}} - M_{\text{H}_2}$  mass units), that can be explained by the loss of hydrogen from diisopropylaminoethyl fragment. Tertiary amines are strong photoreducers.<sup>37, 43, 44</sup> Ethyl diisopropyl amine loses hydrogen under photolysis in the presence of a photosensitizer with quantum yield  $> 90\%$ .<sup>43</sup> Under MALDI conditions (excited matrix molecules, laser irradiation) ethyl diisopropyl amine moieties can lose hydrogen quantitatively. It is important to notice that no MALDI-TOF results for PDPA were reported so far.

The assignment of the peaks is presented in Table 2.2. The general formula for peaks in Figure 2.9 and for the bigger set of signals in Figure 2.11 (Table 2.2<sup>a</sup>) is  $\text{MW}_{\text{MALDI peak } n} = \text{MW}_{\text{exp}} = \text{MW}_{\text{ca}} + m\text{H} = (\text{EBIB} + (\text{DPA}-2\text{H})_n - \text{Br} + \text{K}^+ + m\text{H})$ , where  $n$  – the number of repeat units (DPA-2H),  $m = (-5) - 5$ , can depend on MW and MALDI conditions, for example the laser power. Odd values of  $m$  can indicate that hydrogen abstraction occurs through a radical mechanism that corresponds to literature data.<sup>37, 43, 44</sup> Values of  $m$  increase with molecular weight. The loss of Br functionality in the polymer structure has been reported in MALDI-TOF-MS of acrylate-based polymers produced by ATRP.<sup>45, 46</sup> Thus, the loss of halides could be attributed to the polymerization reactions or a result of fragmentation in the MALDI mass spectroscopy.

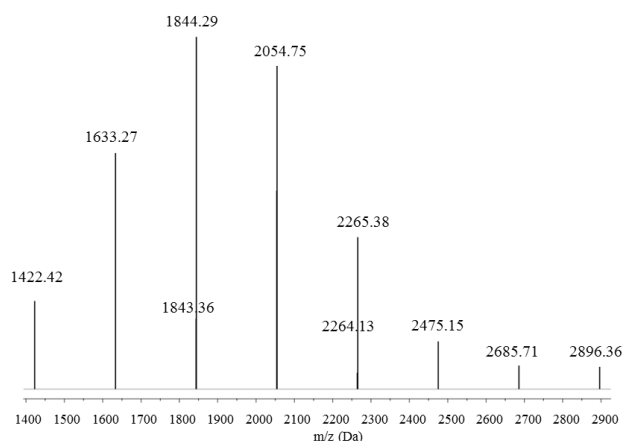


**Figure 2.10:** MALDI-TOF-MS in the linear mode (using DHB as matrix) of PDPA-Br ( $M_{n,\text{GPC}} = 14.3 \times 10^3$ ,  $D = 1.21$ ) from  $m/z$  1400 to 3000. Conditions:  $[\text{DPA}]_0/\text{solvent} = 1/2$  (v/v),  $[\text{IPA}]/[\text{H}_2\text{O}] = 0.95/0.05$  (v/v);  $[\text{DPA}]_0/[\text{EBiB}]_0/[\text{Na}_2\text{S}_2\text{O}_4]_0/[\text{CuBr}_2]_0/[\text{Me}_6\text{TREN}]_0 = 20/1/1/0.1/0.1$  (molar);  $T = 40$  °C.



The minor peak set in Figure 2.12 and Table 2.2 can be attributed to adduct of the above fragments with 4-hydroxybutanal,  $\text{HO}(\text{CH}_2)_3\text{CHO}$ , HBA MW 88.11, which in an impurity in THF solvent.<sup>47</sup> Table 2.2<sup>b</sup> demonstrates an excellent agreement for this suggestion ( $m = 0; 1$ ).

**Table 2.2:** MALDI-TOF MS peaks assignment.

<sup>a,b</sup> n	<sup>a</sup> MWca Figure 2.10, 2.12 (major set)	MWexp Figure 2.10	<sup>a</sup> m	<sup>a</sup> MWexp Figure 2.12 (major set)	<sup>a</sup> m	<sup>b</sup> MWca Figure 2.12 (minor set)	MWexp Figure 2.12 (minor set)	<sup>b</sup> m
6	1422.06	1422.42	0					
7	1633.36	1633.27	0					
8	1844.66	1844.29	0					
9	2055.96	2054.75	-1	2060.87	5	2144.07	2144.96	1
10	2267.26	2265.38	-2	2271.87	5	2355.37	2355.97	1
11	2478.56	2475.15	-3	2482.89	4	2566.67	2566.86	0
12	2689.86	2685.71	-4	2693.73	4	2777.97	2777.84	0
13	2901.16	2896.36	-5	2904.81	4	2989.27	2989.01	0
14	3112.46			3115.82	3	3200.57	3200.16	0

<sup>a</sup> MW = MWca + mH = EBiB + (DPA - 2H) - Br + K + mH;

<sup>b</sup> MWmin = MWca min + mH = EBiB + (DPA - 2H) - Br + HBA + K + mH; where EBiB = 195.06, DPA = 213.32, H = 1.01, Br = 79.9, K = 39.1, HBA = 88.11, n – the number of repeat units (DPA - 2H), m – number of additional H atoms left in PDPA.

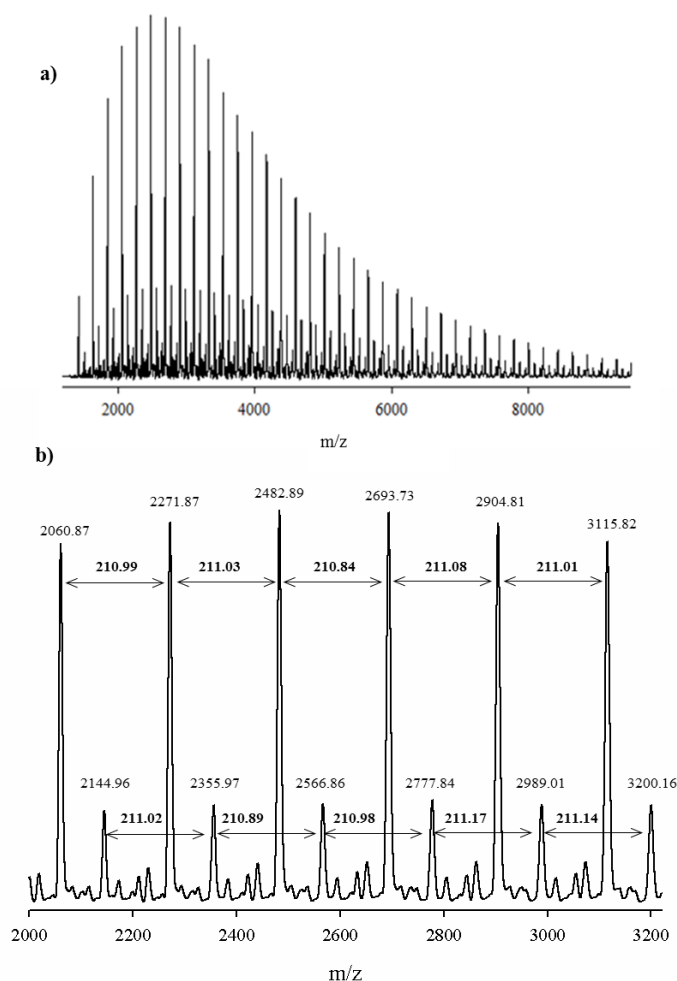


**Figure 2.11:** MALDI-TOF-MS (a) in the linear mode (using DHB as matrix) from m/z 1200 to 9500 and (b) enlargement of the MALDI-TOF-MS from m/z 2000 to 3220 of PDPA-Br ( $M_{n,\text{GPC}} = 14.3 \times 10^3$ ,  $D = 1.21$ ). Conditions:  $[\text{DPA}]_0/\text{H}_2\text{O} = 1/2$  (v/v),  $[\text{IPA}]/[\text{H}_2\text{O}] = 0.95/0.05$  (v/v);  $[\text{DPA}]_0/[\text{EBiB}]_0/[\text{Na}_2\text{S}_2\text{O}_4]_0/[\text{CuBr}_2]_0/[\text{Me}_6\text{TREN}]_0 = 20/1/1/0.1/0.1$  (molar);  $T = 40^\circ\text{C}$ .

#### 2.4.5. Chain extension experiment

To prove the presence of the terminal Br chain ends in the growing polymer chains and the “living” nature of the PDPA obtained by SARA ATRP, a chain extension experiment was carried out. As shown in Figure 2.12, a shift towards lower retention volumes of the GPC trace of the PDPA sample was observed when new monomer was supplied. The MW of the PDPA macroinitiator obtained at 75% conversion ( $M_{n,\text{th}} = 4.94 \times 10^3$ ,  $M_{n,\text{GPC}} = 15.3 \times 10^3$ ,  $D = 1.20$ ) nearly doubled, while maintaining a narrow MW distribution, with the addition of fresh monomer ( $M_{n,\text{th}} = 14.4 \times 10^3$ ,  $M_{n,\text{GPC}} = 27.3 \times 10^3$ ,  $D = 1.15$ ).

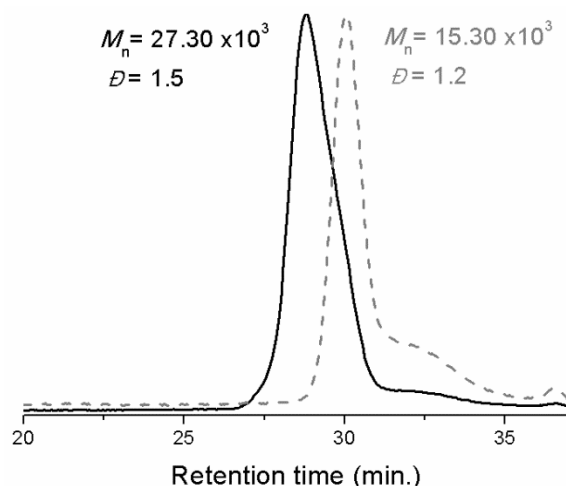


**Figure 2.12:** GPC traces of the PDPA before (black line) and after the chain extension (blue line) experiment.

This result indicates that the “living” character of the synthesized PDPA can be obtained through the application of the  $\text{Na}_2\text{S}_2\text{O}_4$ -mediated SARA ATRP catalytic system, thus, suggesting that this catalytic system can be applied in the synthesis of block copolymers, with no need of further addition of catalysts to the reaction mixture. Also, the movement toward high MW suggests that the absence of Br functionality observed in the MALDI-TOF part is due fragmentation during the analysis.

#### 2.4.6. $\text{N}_3$ -Coumarin reaction with alkyne terminated PDPA

In order to provide further evidence for the presence of the alkyne moiety in the polymer chain end, the AT-PDPA was reacted with an azidocoumarin compound, 3-azido-7-diethylaminocoumarin (Figure 2.13).

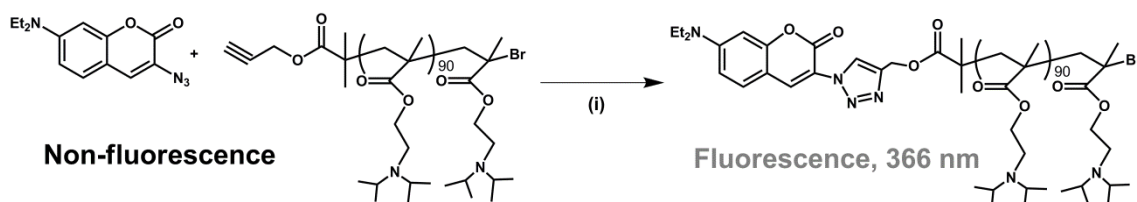


**Figure 2.13:** “Click” reaction between alkyne functionalized PDPA and 3-azido-7-diethylaminocoumarin. (i)  $\text{CuSO}_4 \cdot 5\text{H}_2\text{O}$ ; THF/ $\text{H}_2\text{O}$ .

The coumarin dye molecules are biocompatible and have been used as fluorescent molecular probes.<sup>48</sup> Both compounds alone are not fluorescent, but after the azide-alkyne cycloaddition, the formation of the triazole compound provides final structure with fluorescence (highly fluorescent linkage at 366 nm) (Figure 2.14).



**Figure 2.14:** Image of the reaction mixture after the “click” reaction between the alkyne functionalized PDPA and N<sub>3</sub>-Cum. The formation of the fluorescent linkage could be easily seen upon irradiation at 365 nm with a hand-held UV lamp.

Figure 2.15 presents the <sup>1</sup>H NMR spectrum of the “click” reaction product. The characteristic peak of the triazole ring appears at 8.53 ppm (**s**) and the signal from the methylene protons from the azide chain end functionalized PDPA, which becomes adjacent to the triazol group formed in the “click” reaction, is present at 5.25 ppm (**k**). Moreover, it can be observed that the characteristic peak of the two protons near the alkyne moiety in the AT-PDPA at 4.62 ppm had disappeared, which indicates the complete reaction of the polymer.

These results confirms the telechelic structure of the PDPA structures that can be obtained with more environmentally attractive sulphite-base SARA ATRP catalytic system presented in this Chapter.

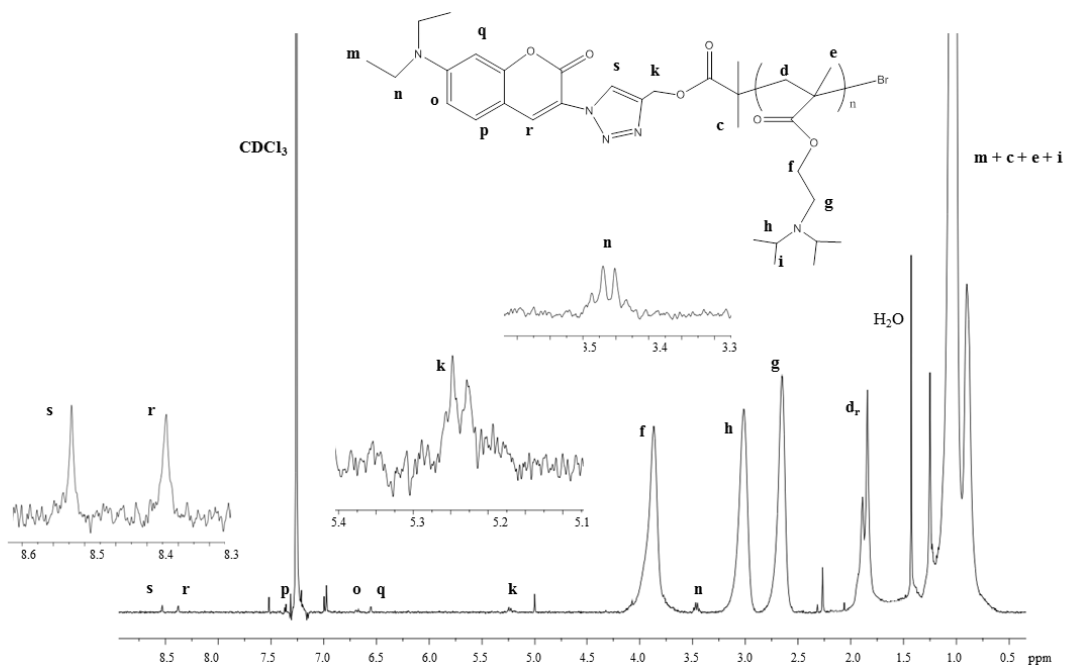


**Figure 2.15:**  $^1\text{H}$  NMR spectrum, in  $\text{CDCl}_3$ , of the PDPA-Cu obtained by the "click" reaction between the alkyne-PDPA and the  $\text{N}_3$ -Cum.

## 2.5. Conclusions

The pH-responsive PDPA was successfully synthesized using an eco-friendly, inexpensive and less toxic SARA ATRP system at  $40\text{ }^\circ\text{C}$ , in the presence of inorganic sulfites ( $\text{Na}_2\text{S}_2\text{O}_4$ ) and a  $\text{Cu(II)Br}_2/\text{Me}_6\text{TREN}$  complex in a mixture of isopropanol and water. The catalytic system was able to control the polymerization of DPA with a low amount of water, 5% (v/v), in the solvent mixture. The controlled/"living" character of this system was supported by kinetic data and chain extension experiments. The controlled molecular structure of the obtained polymers was confirmed by  $^1\text{H}$  NMR and MALDI-TOF analysis. Moreover, the inclusion of an alkyne chain end functionality was shown to be able to allow post-polymerization functionalization PDPA prepare with this catalytic system through CuAAC reaction.

## 2.6. References

1. Matyjaszewski, K. (2012). Atom Transfer Radical Polymerization (ATRP): Current Status and Future Perspectives. *Macromolecules*, 45(10): 4015-4039..
2. Jakubowski, W. and K. Matyjaszewski (2006). Activators Regenerated by Electron Transfer for Atom-Transfer Radical Polymerization of (Meth)acrylates and Related Block Copolymers. *Angewandte Chemie International Edition*, 45(27): 4482-4486..
3. Matyjaszewski, K., W. Jakubowski, K. Min, W. Tang, J.Y. Huang, W.A. Braunecker, and N.V. Tsarevsky (2006). Diminishing catalyst concentration in atom transfer radical polymerization with reducing agents. *Proceedings of the National Academy of Sciences of the United States of America*, 103(42): 15309-15314..
4. Mendonça, P.V., A.C. Serra, J.F.J. Coelho, A.V. Popov, and T. Guliashvili (2011). Ambient temperature rapid ATRP of methyl acrylate, methyl methacrylate and styrene in polar solvents with mixed transition metal catalyst system. *European Polymer Journal*, 47(7): 1460-1466..
5. Zhang, Y., Y. Wang, and K. Matyjaszewski (2011). ATRP of Methyl Acrylate with Metallic Zinc, Magnesium, and Iron as Reducing Agents and Supplemental Activators. *Macromolecules*, 44(4): 683-685..
6. Konkolewicz, D., Y. Wang, M. Zhong, P. Krys, A.A. Isse, A. Gennaro, and K. Matyjaszewski (2013). Reversible-Deactivation Radical Polymerization in the Presence of Metallic Copper. A Critical Assessment of the SARA ATRP and SET-LRP Mechanisms. *Macromolecules*, 46(22): 8749-8772..
7. Peng, C.-H., M. Zhong, Y. Wang, Y. Kwak, Y. Zhang, W. Zhu, M. Tonge, J. Buback, S. Park, P. Krys, D. Konkolewicz, A. Gennaro, and K. Matyjaszewski (2013). Reversible-Deactivation Radical Polymerization in the Presence of Metallic Copper. Activation of Alkyl Halides by Cu-0. *Macromolecules*, 46(10): 3803-3815..
8. Wang, Y., M. Zhong, W. Zhu, C.-H. Peng, Y. Zhang, D. Konkolewicz, N. Bortolamei, A.A. Isse, A. Gennaro, and K. Matyjaszewski (2013). Reversible-Deactivation Radical Polymerization in the Presence of Metallic Copper. Comproportionation-Disproportionation Equilibria and Kinetics. *Macromolecules*, 46(10): 3793-3802..
9. Zhong, M., Y. Wang, P. Krys, D. Konkolewicz, and K. Matyjaszewski (2013). Reversible-Deactivation Radical Polymerization in the Presence of Metallic Copper. Kinetic Simulation. *Macromolecules*, 46(10): 3816-3827..

10. Abreu, C.M.R., P.V. Mendonca, A.C. Serra, A.V. Popov, K. Matyjaszewski, T. Guliashvili, and J.F.J. Coelho (2012). Inorganic Sulfites: Efficient Reducing Agents and Supplemental Activators for Atom Transfer Radical Polymerization. *Acs Macro Letters*, 1(11): 1308-1311..
11. Abreu, C.M.R., A.C. Serra, A.V. Popov, K. Matyjaszewski, T. Guliashvili, and J.F.J. Coelho (2013). Ambient temperature rapid SARA ATRP of acrylates and methacrylates in alcohol-water solutions mediated by a mixed sulfite/Cu(ii)Br<sub>2</sub> catalytic system. *Polymer Chemistry*, 4(23): 5629-5636..
12. Percec, V., A.V. Popov, E. Ramirez-Castillo, J.F.J. Coelho, and L.A. Hinojosa-Falcon (2004). Non-transition metal-catalyzed living radical polymerization of vinyl chloride initiated with iodoform in water at 25 °C. *Journal of Polymer Science Part A: Polymer Chemistry*, 42(24): 6267-6282..
13. Stenzel, M.H., L. Cummins, G.E. Roberts, T.P. Davis, P. Vana, and C. Barner-Kowollik (2003). Xanthate Mediated Living Polymerization of Vinyl Acetate: A Systematic Variation in MADIX/RAFT Agent Structure. *Macromolecular Chemistry and Physics*, 204(9): 1160-1168..
14. Licciardi, M., Y. Tang, N.C. Billingham, and S.P. Armes (2005). Synthesis of novel folic acid-functionalized biocompatible block copolymers by atom transfer radical polymerization for gene delivery and encapsulation of hydrophobic drugs. *Biomacromolecules*, 6(2): 1085-1096..
15. Du, J., L. Fan, and Q. Liu (2012). pH-Sensitive Block Copolymer Vesicles with Variable Trigger Points for Drug Delivery. *Macromolecules*, 45(20): 8275-8283..
16. Massignani, M., I. Canton, N. Patikarnmonthon, N.J. Warren, S.P. Armes, A.L. Lewis, and G. Battaglia (2010). Cellular delivery of antibodies: effective targeted subcellular imaging and new therapeutic tool. *Nature Precedings*: 4427..
17. Giacomelli, F.C., P. Stepanek, C. Giacomelli, V. Schmidt, E. Jager, A. Jager, and K. Ulbrich (2011). pH-triggered block copolymer micelles based on a pH-responsive PDPA (poly[2-(diisopropylamino)ethyl methacrylate]) inner core and a PEO (poly(ethylene oxide)) outer shell as a potential tool for the cancer therapy. *Soft Matter*, 7(19): 9316-9325..
18. Zhou, K., Y. Wang, X. Huang, K. Luby-Phelps, B.D. Sumer, and J. Gao (2011). Tunable, Ultrasensitive pH-Responsive Nanoparticles Targeting Specific Endocytic Organelles in Living Cells. *Angewandte Chemie-International Edition*, 50(27): 6109-6114..
19. Lobb, E.J., I. Ma, N.C. Billingham, S.P. Armes, and A.L. Lewis (2001). Facile synthesis of well-defined, biocompatible phosphorylcholine-based methacrylate

- copolymers via atom transfer radical polymerization at 20 degrees C. *Journal of the American Chemical Society*, 123(32): 7913-7914..
20. Giacomelli, C., V. Schmidt, and R. Borsali (2007). Specific Interactions Improve the Loading Capacity of Block Copolymer Micelles in Aqueous Media. *Langmuir*, 23(13): 6947-6955..
  21. Liang, K., G.K. Such, Z. Zhu, Y. Yan, H. Lomas, and F. Caruso (2011). Charge-Shifting Click Capsules with Dual-Responsive Cargo Release Mechanisms. *Advanced Materials*, 23(36): H273-+..
  22. Blanz, A., M. Massignani, G. Battaglia, S.P. Armes, and A.J. Ryan (2009). Tailoring Macromolecular Expression at Polymersome Surfaces. *Advanced Functional Materials*, 19(18): 2906-2914..
  23. Mueller, L. and K. Matyjaszewski (2010). Reducing Copper Concentration in Polymers Prepared via Atom Transfer Radical Polymerization. *Macromolecular Reaction Engineering*, 4(3-4): 180-185..
  24. Sivakumar, K., F. Xie, B.M. Cash, S. Long, H.N. Barnhill, and Q. Wang (2004). A Fluorogenic 1,3-Dipolar Cycloaddition Reaction of 3-Azidocoumarins and Acetylenes†. *Organic Letters*, 6(24): 4603-4606..
  25. Nadler, A. and C. Schultz (2013). The Power of Fluorogenic Probes. *Angewandte Chemie-International Edition*, 52(9): 2408-2410..
  26. Ciampolini, M. and N. Nardi (1966). Five-Coordinated High-Spin Complexes of Bivalent Cobalt, Nickel, and Copper with Tris(2-dimethylaminoethyl)amine. *Inorganic Chemistry*, 5(1): 41-44..
  27. Rocha, N., P.V. Mendonça, J.P. Mendes, P.N. Simões, A.V. Popov, T. Guliasvili, A.C. Serra, and J.F.J. Coelho (2013). Facile Synthesis of Well-Defined Telechelic Alkyne-Terminated Polystyrene in Polar Media Using ATRP With Mixed Fe/Cu Transition Metal Catalyst. *Macromolecular Chemistry and Physics*, 214(1): 76-84..
  28. Du, J.Z., Y.P. Tang, A.L. Lewis, and S.P. Armes (2005). pH-sensitive vesicles based on a biocompatible zwitterionic diblock copolymer. *Journal of the American Chemical Society*, 127(51): 17982-17983..
  29. Braunecker, W.A. and K. Matyjaszewski (2007). Controlled/living radical polymerization: Features, developments, and perspectives. *Progress in Polymer Science*, 32(1): 93-146..
  30. Percec, V., A.V. Popov, E. Ramirez-Castillo, J.F.J. Coelho, and L.A. Hinojosa-Falcon (2005). Phase transfer catalyzed single electron transfer–degenerative chain transfer mediated living radical polymerization (PTC-SET–DTLRP) of vinyl chloride catalyzed by sodium dithionite and initiated with iodoform in



- water at 43 °C. *Journal of Polymer Science Part A: Polymer Chemistry*, 43(4): 779-788..
31. Lough, S.M. and J.W. McDonald (1987). Synthesis of tetraethylammonium dithionite and its dissociation to the sulfur dioxide radical anion in organic solvents. *Inorganic Chemistry*, 26(13): 2024-2027..
  32. Zhou, Y., W. Huang, J. Liu, X. Zhu, and D. Yan (2010). Self-Assembly of Hyperbranched Polymers and Its Biomedical Applications. *Advanced Materials*, 22(41): 4567-4590..
  33. Bovey, F.A. (1972). *High Resolution NMR of Macromolecules* Academic Press..
  34. Dayananda, K., M. Kim, B. Kim, and D. Lee (2007). Synthesis and characterization of MPEG-b-PDPA amphiphilic block copolymer via atom transfer radical polymerization and its pH-dependent micellar behavior. *Macromolecular Research*, 15(4): 385-391..
  35. Peng, C.-L., L.-Y. Yang, T.-Y. Luo, P.-S. Lai, S.-J. Yang, W.-J. Lin, and M.-J. Shieh (2010). Development of pH sensitive 2-(diisopropylamino)ethyl methacrylate based nanoparticles for photodynamic therapy. *Nanotechnology*, 21(15)..
  36. Taktak, F.F. and V. Butun (2010). Synthesis and physical gels of pH- and thermo-responsive tertiary amine methacrylate based ABA triblock copolymers and drug release studies. *Polymer*, 51(16): 3618-3626..
  37. Miyake, Y., K. Nakajima, and Y. Nishibayashi (2012). Visible-Light-Mediated Utilization of  $\alpha$ -Aminoalkyl Radicals: Addition to Electron-Deficient Alkenes Using Photoredox Catalysts. *Journal of the American Chemical Society*, 134(7): 3338-3341..
  38. Coelho, J.F.J., E.Y. Carvalho, D.S. Marques, A.V. Popov, P.M. Goncalves, and M.H. Gil (2007). Synthesis of Poly(lauryl acrylate) by Single-Electron Transfer/Degenerative Chain Transfer Living Radical Polymerization Catalyzed by Na<sub>2</sub>S<sub>2</sub>O<sub>4</sub> in Water. *Macromolecular Chemistry and Physics*, 208(11): 1218-1227..
  39. Coelho, J.F.J., E.Y. Carvalho, D.S. Marques, A.V. Popov, V. Percec, and M.H. Gil (2008). Influence of the isomeric structures of butyl acrylate on its single-electron transfer-degenerative chain transfer living radical polymerization in water Catalyzed by Na<sub>2</sub>S<sub>2</sub>O<sub>4</sub>. *Journal of Polymer Science Part A: Polymer Chemistry*, 46(19): 6542-6551..
  40. Coelho, J.F.J., E.Y. Carvalho, D.S. Marques, A.V. Popov, V. Percec, P.M.F.O. Gonçalves, and M.H. Gil (2008). Synthesis of poly(ethyl acrylate) by single electron transfer-degenerative chain transfer living radical polymerization in

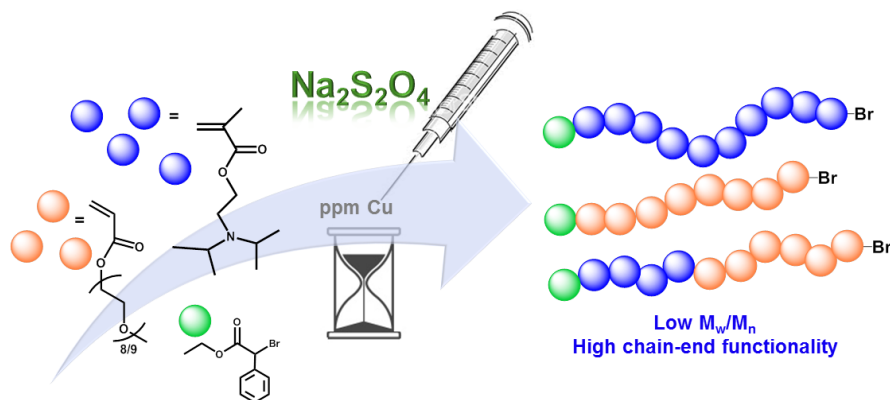
- water catalyzed by Na<sub>2</sub>S<sub>2</sub>O<sub>4</sub>. *Journal of Polymer Science Part A: Polymer Chemistry*, 46(2): 421-432..
41. Coelho, J.F.J., J. Gois, A.C. Fonseca, R.A. Carvalho, A.V. Popov, V. Percec, and M.H. Gil (2009). Synthesis of poly(2-methoxyethyl acrylate) by single electron transfer—Degenerative transfer living radical polymerization catalyzed by Na<sub>2</sub>S<sub>2</sub>O<sub>4</sub> in water. *Journal of Polymer Science Part A: Polymer Chemistry*, 47(17): 4454-4463..
  42. Coelho, J.F.J., A.M.F.P. Silva, A.V. Popov, V. Percec, M.V. Abreu, P.M.O.F. Gonçalves, and M.H. Gil (2006). Single electron transfer—degenerative chain transfer living radical polymerization of N-butyl acrylate catalyzed by Na<sub>2</sub>S<sub>2</sub>O<sub>4</sub> in water media. *Journal of Polymer Science Part A: Polymer Chemistry*, 44(9): 2809-2825..
  43. Lewis, F.D. and T.-I. Ho (1980). Selectivity of tertiary amine oxidations. *Journal of the American Chemical Society*, 102(5): 1751-1752..
  44. Cohen, S.G., A. Parola, and G.H. Parsons (1973). Photoreduction by amines. *Chemical Reviews*, 73(2): 141-161..
  45. Coca, S., C.B. Jasieczek, K.L. Beers, and K. Matyjaszewski (1998). Polymerization of acrylates by atom transfer radical polymerization. Homopolymerization of 2-hydroxyethyl acrylate. *Journal of Polymer Science Part A: Polymer Chemistry*, 36(9): 1417-1424..
  46. Haddleton, D.M., C. Waterson, P.J. Derrick, C.B. Jasieczek, and A.J. Shooter (1997). Monohydroxy terminally functionalized poly(methyl methacrylate) from atom transfer radical polymerization. *Chem. Commun.*, (7): 683-684..
  47. Lou, X., C.A. Leenders, A.A.M. Onzen, R.A. Bovee, J.J. Dongen, J.J.M. Vekemans, and E.W. Meijer (2013). False Results Caused by Solvent Impurity in Tetrahydrofuran for MALDI TOF MS Analysis of Amines. *Journal of The American Society for Mass Spectrometry*: 1-4..
  48. Schiedel, M.-S., C.A. Briehn, and P. Bäuerle (2001). Single-Compound Libraries of Organic Materials: Parallel Synthesis and Screening of Fluorescent Dyes. *Angewandte Chemie International Edition*, 40(24): 4677-4680..

## Chapter 3

---

---

### Improvement of the control over SARA ATRP of 2-(diisopropylamino)ethyl methacrylate by slow and continuous addition of sodium dithionite



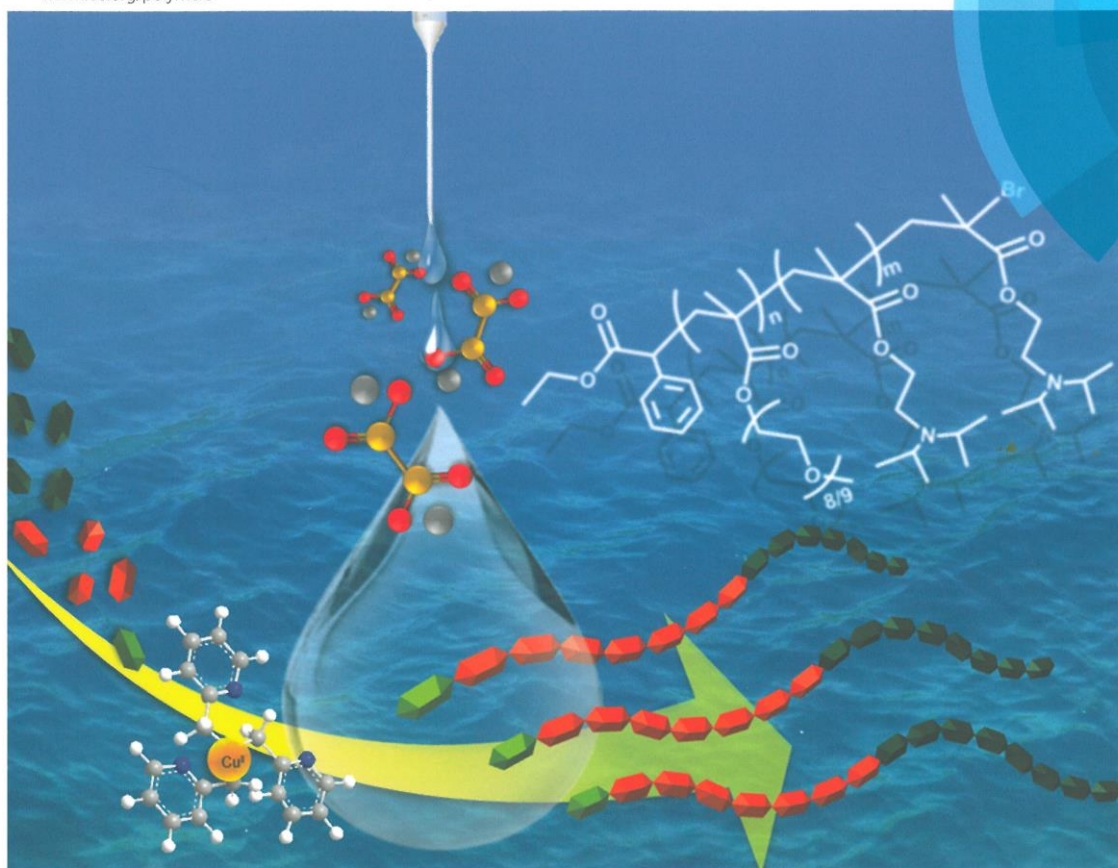
The contents of this chapter are published in: **Gois, J. R.**, Konkolewicz, D., Popov, A. V., Guliashvili, T., Matyjaszewski, K., Serra, A. C., Coelho, J. F. J.; "Improvement of the control over SARA ATRP of 2-(diisopropylamino)ethyl methacrylate by slow and continuous addition of sodium dithionite". *Polymer Chemistry* 2014, 5 (16), 4617-4626.

(This work was selected for the journal cover pager)



# Polymer Chemistry

www.rsc.org/polymers



ISSN 1759-9954



**PAPER**

Jorge F. J. Coelho *et al.*  
Improvement of the control over SARA ATRP of 2-(diisopropylamino)ethyl methacrylate by slow and continuous addition of sodium dithionite

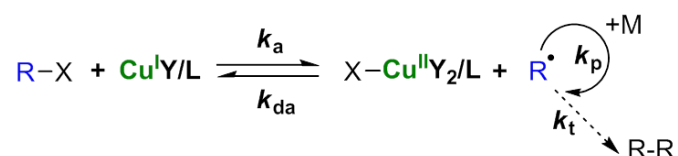


### 3.1. Abstract

The kinetics and detailed mechanism of supplemental activator and reducing agent (SARA) atom transfer radical polymerization (ATRP) of 2-(diisopropylamino) ethyl methacrylate (DPA) using sodium dithionite ( $\text{Na}_2\text{S}_2\text{O}_4$ ) were investigated. The influence of the initiator, solvent, structure concentration of the catalyst, and the ratios of  $\text{Na}_2\text{S}_2\text{O}_4$  were adjusted to optimize the polymerization. Well controlled polymers required  $\text{Na}_2\text{S}_2\text{O}_4$  to be slowly and continuously feed to the reaction mixture, with 500 parts per million (ppm) of  $\text{CuBr}_2$  with tris(2-dimethylamino)amine ( $\text{Me}_6\text{TREN}$ ) as a ligand. The initial content of  $\text{Na}_2\text{S}_2\text{O}_4$  in the reaction mixture, the feeding rate and copper catalyst concentration were optimized to provide polymers with narrow molecular weight distribution ( $D < 1.15$ ) at high monomer conversion ( $\sim 90\%$ ). Interestingly, the results revealed that when tris(2-pyridylmethyl)-amine (TPMA) was used as a ligand, the amount of copper required to achieve similar control of the polymerization could be decreased 5 times. This system was successfully extended to the polymerization of oligo(ethylene oxide) methyl ether methacrylate (OEOMA). The low catalyst concentrations and non-toxic nature of the  $\text{Na}_2\text{S}_2\text{O}_4$  make this SARA ATRP method attractive for the synthesis of well controlled water soluble polymers for biomedical applications.

### 3.2. Introduction

The synthesis of well-defined polymers, with predefined molecular weights (MW), narrow MW distributions, controlled composition and complex architectures is possible through reversible deactivation radical polymerization (RDRP) methods.<sup>1, 2</sup> Among the RDRP techniques reported in the literature, atom transfer radical polymerization (ATRP) is one of the most robust and versatile methods to polymerize a wide range of monomers under mild reaction conditions.<sup>3-6</sup> In ATRP an alkyl halide is activated by a transition metal catalyst in a low oxidation state, typically  $\text{Cu}^{\text{I}}/\text{L}$ , to generate the corresponding radical and transition metal complex in its higher oxidation state, typically  $\text{X-Cu}^{\text{II}}/\text{L}$  (Scheme 3.1).<sup>7</sup>



**Scheme 3.1:** General mechanism of copper catalyzed ATRP.

The radical propagates by adding monomer units until it is deactivated to the corresponding dormant alkyl halide by the transition metal complex in its higher oxidation state.<sup>2</sup> This dynamic equilibrium between propagating radicals and alkyl halides as dormant species ensures that the majority of chains grow at the same rate.<sup>3, 8</sup>

One limitation of traditional ATRP methods is that they require catalyst concentrations greater than 1000 parts per million (ppm) to maintain an acceptable rate of polymerization.<sup>3</sup>

The high catalyst loading leads to a significant contamination of the resulting polymer with often highly colored and toxic transition metal complexes. The high catalyst concentrations combined with the use of organic solvents makes traditional ATRP environmentally challenging. Over the last decade, several strategies have been developed to make ATRP more eco-friendly.<sup>9</sup> These strategies aim to decrease the amount of catalyst required, and to use green solvents such as water or alcohols. Several variations of the initial ATRP concept have been proposed to diminish the concentration of Cu needed in the reaction. In all cases the activator complex, namely  $\text{Cu}^{\text{I}}$ , is regenerated through a relatively slow reaction which compensates for termination events. Activator regeneration can be achieved by directly reducing the excess  $\text{Cu}^{\text{II}}$  as in activators regenerated by electron transfer (ARGET) ATRP,<sup>10</sup> using a continuous supply of radicals from the decomposition of a radical initiator as in initiator for continuous activator regeneration (ICAR) ATRP.<sup>11</sup> Other methods for ATRP with low catalyst concentrations include electrochemical reduction of  $\text{Cu}(\text{II})$ , photochemical activator regeneration, and an interesting system called supplemental activator and reducing agent (SARA) ATRP.<sup>12-14</sup> SARA ATRP uses either sulfites or zerovalent transition metals (e.g  $\text{Cu}(0)$ ,  $\text{Fe}(0)$ ,  $\text{Zn}(0)$  or  $\text{Mg}(0)$ ) to activate alkyl halides directly and to reduce excess  $\text{Cu}^{\text{II}}$  to  $\text{Cu}^{\text{I}}$  to compensate for radical termination.<sup>15-18</sup>



Inorganic sulfites, especially sodium dithionite ( $\text{Na}_2\text{S}_2\text{O}_4$ ) have been reported as particularly effective additives in SARA ATRP<sup>19, 20</sup> and single electron transfer-degenerative chain transfer mediated living radical polymerization SET-DTLRP.<sup>21-27</sup> Sulfites are very efficient reducing agents for  $\text{Cu}^{\text{II}}$  species. In our previous work<sup>28</sup> SARA ATRP was described for the first time for the homopolymerization of the pH-responsive poly(2-(diisopropylamino)ethyl methacrylate) (PDPA). Although the average MW in the original system was controlled, narrow MW distributions were not achieved, with  $D$  exceeding 1.2.

PDPA is a pH-responsive polymer with a pKa around 6.2,<sup>29, 30</sup> typically used in biomedical applications.<sup>31-36</sup> PDPA-based copolymers have been widely used in the preparation of smart nanostructures for the controlled release of small molecules<sup>33, 36, 37</sup> complexation and delivery of genetic material,<sup>38</sup> specific targeting,<sup>32, 34</sup> or magnetic resonance imaging (MRI) contrast agents.<sup>39</sup>

These specific applications require narrow MW distributions, and the polymers should be synthesized with the lowest possible copper catalyst concentration, to facilitate purification after polymerization. In this paper, SARA ATRP with  $\text{Na}_2\text{S}_2\text{O}_4$  was used to polymerize DPA in a mixture of isopropanol (IPA)/water at 40 °C. Several reaction parameters were optimized to give well-defined polymers with low copper concentrations. The method was extended to the polymerize oligo(ethylene oxide) methyl ether methacrylate (OEOMA).

### 3.3. Experimental Section

#### 3.3.1. Materials

2-(Diisopropylamino)ethyl methacrylate (DPA) (97%, Scientific Polymer Products Inc.), oligo(ethylene oxide) methyl ether methacrylate (OEOMA) (99%, average molecular weight 475, Aldrich) and 2-(dimethylamino)ethyl methacrylate (DMAEMA) (98%, Aldrich) were passed over a column of basic alumina to remove inhibitor prior to use. Sodium dithionite ( $\text{Na}_2\text{S}_2\text{O}_4$ ) (85%, ACROS Organics), copper(II) bromide ( $\text{CuBr}_2$ ) (99.999%, Aldrich), ethyl  $\alpha$ -bromophenyl acetate (EBPA) (97%, Alfa Aesar), water (HPLC grade, Fisher Scientific), isopropanol (IPA) (ACS grade, Fisher Scientific), tetrahydrofuran (THF) (ACS grade, Fisher Scientific), *tert*-butanol ( $\geq 99.5\%$ , Sigma-

aldrich), ethanol (95%, Pharmco-AAPER), diphenyl ether ( $\geq 99\%$ , Aldrich), deuterated chloroform ( $\text{CDCl}_3$ ) (99.8%, Cambridge Isotope Laboratories), anhydrous magnesium sulphate (99%, Aldrich) were used as received. Tris(2-(dimethylamino)ethyl)amine ( $\text{Me}_6\text{TREN}$ )<sup>40</sup> and tris(pyridin-2-ylmethyl)amine (TPMA) were synthesized as reported in the literature.<sup>41,42</sup>

### 3.3.2. Characterization

A KDS Scientific, Legato 101 syringe pump was used for continuous feeding polymerizations. Monomer conversion was measured using  $^1\text{H}$  NMR spectroscopy in  $\text{CDCl}_3$  using a Bruker Avance 500 MHz spectrometer at room temperature. The number-average MW ( $M_{n, \text{GPC}}$ ) and dispersity, ( $D$ ) of the synthesized polymers were determined by gel permeation chromatography (GPC). The GPC system used a Waters 515 HPLC pump and a Waters 2414 refractive index detector using PSS columns (Styrogel  $10^2$ ,  $10^3$ ,  $10^5$  Å) with tetrahydrofuran (THF) containing 10 mM  $\text{LiTf}_2\text{N}$  and 10 mM 1-butylimidazole as the eluent, at a flow rate of 1 mL/min at 35 °C.<sup>43</sup> The GPC samples were prepared in THF with diphenyl ether as the internal standard.

### 3.3.3. Procedures

#### Typical procedure for the SARA ATRP of DPA.

A mixture of  $\text{CuBr}_2$  (1.05 mg, 4.70  $\mu\text{mol}$ ),  $\text{Me}_6\text{TREN}$  (2.16 mg, 9.40  $\mu\text{mol}$ ) and water (83  $\mu\text{L}$ ) was placed in a Schlenk tube reactor that was sealed by using a rubber septa.  $\text{Na}_2\text{S}_2\text{O}_4$  (1.92 mg, 9.40  $\mu\text{mol}$ ) and a mixture of DPA (1.00 g, 4.70 mmol) and EBPA (11.40 mg, 47.00  $\mu\text{mol}$ ) in IPA (3.17 mL) (previously bubbled with nitrogen for about 15 minutes) was added to the reactor and frozen in liquid nitrogen. The reaction mixture was deoxygenated by three freeze-pump-thaw cycles and purged with nitrogen. The Schlenk tube was placed in an oil bath at 40 °C with stirring (600 rpm). An aqueous solution of  $\text{Na}_2\text{S}_2\text{O}_4$  (34.3  $\text{mg}\cdot\text{mL}^{-1}$ ) (previous purged with nitrogen) was continuously injected into the reaction medium using a syringe pump at a rate of 116  $\text{nL}\cdot\text{min}^{-1}$  (19.4  $\text{nmol}\cdot\text{min}^{-1}$ ). Samples were periodically withdrawn from the reaction mixture and analyzed by GPC and  $^1\text{H}$  NMR.

### Typical procedure for the SARA ATRP of OEOMA.

The procedures for the SARA ATRP of OEOMA using  $\text{Na}_2\text{S}_2\text{O}_4$  were similar to the DPA, but the monomer concentration was adjusted to 18% (w/w). A mixture of  $\text{CuBr}_2$  (1.7 mg, 7.7  $\mu\text{mol}$ ),  $\text{Me}_6\text{TREN}$  (3.5 mg, 15.4  $\mu\text{mol}$ ) and water (125  $\mu\text{L}$ ) was placed in a Schlenk tube that was sealed by using a rubber septa.  $\text{Na}_2\text{S}_2\text{O}_4$  (3.1 mg, 15.4  $\mu\text{mol}$ ) and a mixture of OEOMA<sub>475</sub> (1.01 g, 2.31 mmol) and EBPA (18.69 mg, 76.9  $\mu\text{mol}$ ) in IPA (4.74 mL) (previously bubbled with nitrogen for about 15 minutes) was added to the reactor and frozen in liquid nitrogen. The reaction mixture was deoxygenated by three freeze-pump-thaw cycles and purged with nitrogen. The additional  $\text{Na}_2\text{S}_2\text{O}_4$  aqueous solution (125  $\mu\text{L}$ , 37.8  $\text{mg}\cdot\text{mL}^{-1}$ ) was slowly feed into the reaction mixture using a syringe pump at a feed rate 87  $\text{nL}\cdot\text{min}^{-1}$  (16.1  $\text{nmol}\cdot\text{min}^{-1}$ ). Samples were periodically withdrawn from the reaction mixture and analyzed by GPC and  $^1\text{H}$  NMR.

## 3.4. Results and Discussion

The use of  $\text{Na}_2\text{S}_2\text{O}_4$  in SARA ATRP of DPA was recently reported.<sup>28</sup>  $\text{Na}_2\text{S}_2\text{O}_4$  acts as a powerful reducing agent for  $\text{X-Cu}^{\text{II}}/\text{L}$  species allowing efficient regeneration of  $\text{Cu}^{\text{I}}/\text{L}$  species, as well as generating radicals by its role as a supplemental activator. For the homopolymerization of DPA, unless otherwise specified, all the reactions were performed at 40 °C, using a monomer to solvent ratio 1/3 (v/v) and a solvent mixture of IPA/water of [95/5 (v/v)]. In the following sections, the effects of various reaction parameters are investigated to determine the most suitable conditions for the polymerization.

### 3.4.1. Influence of the initiator structure and concentration

One of the most important factors to consider in ATRP is matching the initiator and monomer structures. Two different ATRP initiators were evaluated for the SARA ATRP of DPA using  $\text{Na}_2\text{S}_2\text{O}_4$ , with  $\alpha$ -bromophenyl acetate (EBPA) being more active than ethyl 2-bromoisobutyrate (EBiB)<sup>44</sup> (Figure 3.1). Therefore, the initiation was expected to be more efficient with EBPA than with EBiB. The reaction conditions used for kinetics in Figure 3.1 (a) are the same for both EBPA and EBiB, because  $\text{Na}_2\text{S}_2\text{O}_4$  most probably generates carbon centered radicals rapidly from the initiator species (as a

supplemental activator to Cu(I) species). As a result, the rate of polymerization is controlled by the rate of activator regeneration<sup>15</sup>. Although EBPA is a more active initiator than EBiB, both systems showed good agreement with the theoretical MW with  $\bar{D}$  values between 1.25 and 1.3. The evolution of well controlled MW distributions for the EBPA initiated polymerization is confirmed in Figure 3.1 (c). As expected, by decreasing the initiator concentration, the  $M_n$  measured by GPC increases (Figure B.1, Annex B, effect of target DP on the SARA ATRP of DPA). At lower alkyl halide concentration, radical concentration is also lower and hence polymerization slows down.

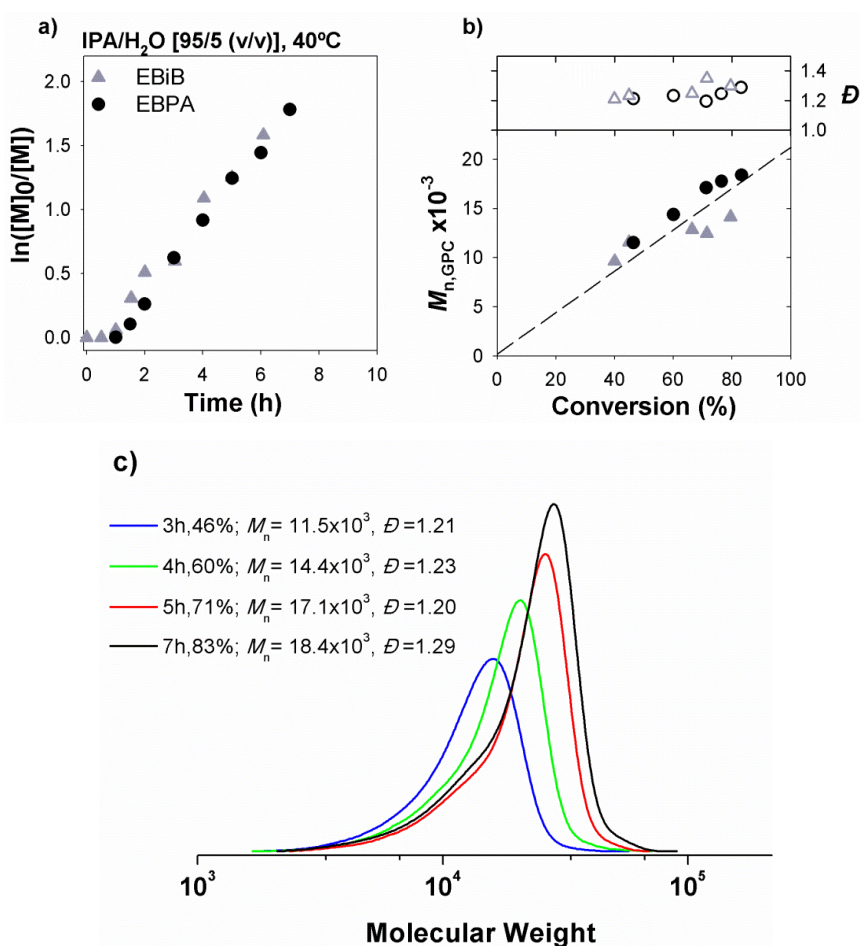


**Figure 3.1:** Effect of the ATRP initiator on the SARA ATRP of DPA in IPA/H<sub>2</sub>O = 95/5 (v/v) at 40 °C. (a) First-order kinetic plot, (b) evolution of MW and  $\bar{D}$  with conversion (the dashed line represents theoretical MW at a given conversion, and (c) GPC traces with conversion for the reaction with EBPA. Reaction conditions:  $[DPA]_0/[initiator]_0/[Na_2S_2O_4]_0/[CuBr_2]_0/[Me_6TREN]_0 = 100/1/0.5/0.1/0.1$  (molar).

### 3.4.2. Effect of the solvent mixture

Previously, it was shown that for SARA ATRP of DPA with  $\text{Na}_2\text{S}_2\text{O}_4$ , the water content in the solvent mixture should be kept at 5% (v/v).<sup>28</sup> Here, IPA, ethanol and *tert*-butanol were examined as solvents for the polymerization of DPA with 5 % water mixtures. As seen in Figure 3.2 (a) and Figure 3.2 (c), the rate of polymerization is the same in all three solvents. Figure 3.2 (b) and Figure 3.2 (d) indicate that the evolution of  $M_n$  is similar in all three cases, regardless of the initiator used.

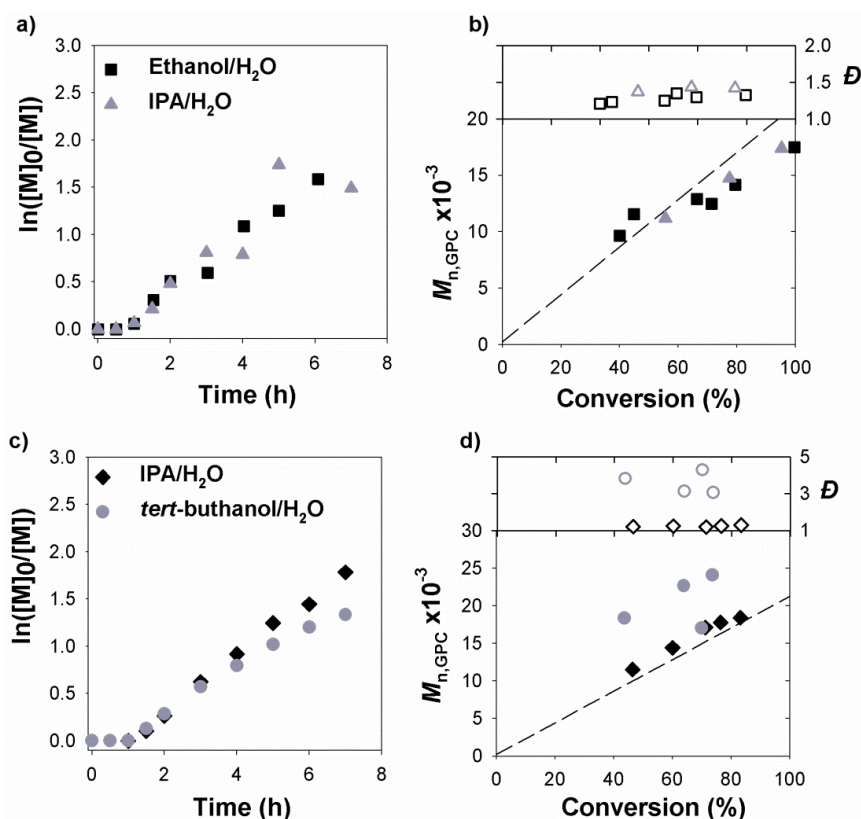


**Figure 3.2:** Effect of solvent mixture in the SARA ATRP of DPA, IPA/water = 95/5 (v/v), ethanol/H<sub>2</sub>O = 95/5 (v/v) and *tert*-butanol/H<sub>2</sub>O = 95/5 (v/v) at 40 °C. (a,c) First-order kinetic plot, (b,d) evolution of MW and  $\bar{D}$  with conversion (the dashed line represents theoretical MW at a given conversion). Reaction conditions:  $[\text{DPA}]_0/[\text{EBiB}]_0/[\text{Na}_2\text{S}_2\text{O}_4]_0/[\text{CuBr}_2]_0/[\text{Me}_6\text{TREN}]_0 = 100/1/0.5/0.1/0.1$  (molar) (a,b);  $[\text{DPA}]_0/[\text{EBPA}]_0/[\text{Na}_2\text{S}_2\text{O}_4]_0/[\text{CuBr}_2]_0/[\text{Me}_6\text{TREN}]_0 = 100/1/0.5/0.1/0.1$  (molar) (c,d).

While ethanol and IPA gave similar control over the polymer's MW, and  $\bar{D}$  values in the order of 1.3-1.4 (Figure 3.2 (b)), *tert*-butanol gave MW above the theoretical line and  $\bar{D}$  values greater than 2 (Figure 3.2 (d)). This fact could be related with the decrease

of solubility of the resultant PDPA in the polymerization mixture for *tert*-butanol, since the polymer partially precipitates at high monomer conversions. In the remainder part of this work, IPA was used as the solvent.

### 3.4.3. Effect of the initial concentration of Na<sub>2</sub>S<sub>2</sub>O<sub>4</sub>

In the literature, the reported SARA reactions were performed by adding the total amount of the Na<sub>2</sub>S<sub>2</sub>O<sub>4</sub> at the beginning of the reaction, with the molar ratio initiator/Na<sub>2</sub>S<sub>2</sub>O<sub>4</sub> = 1/1.<sup>19, 20, 28</sup> However, such higher concentrations of the Na<sub>2</sub>S<sub>2</sub>O<sub>4</sub> salt can lead to very high rate of activator (re)generation and to accelerated termination reactions, leading to a significant decrease in the end-group functionality. Therefore it is essential to choose a Na<sub>2</sub>S<sub>2</sub>O<sub>4</sub> concentration in the reaction system that provides a sufficiently fast rate of activator (re)generation that the polymerization occurs in a reasonable time frame, without being too fast, as the high radical concentration could lead to a significant loss of end group functionality. Several reactions were performed in which the concentration of reducing agent in the polymerization mixture was varied from 0.3 to 1 equivalents to the alkyl halide (Figure 2.3). The decrease of concentration of Na<sub>2</sub>S<sub>2</sub>O<sub>4</sub> from 1 to 0.5, led to similar polymerization rate, MW and *D*. This observation suggests that above a certain concentration, adding more of the dithionite salt does not contribute to increase the polymerization rate. One possibility is that the Na<sub>2</sub>S<sub>2</sub>O<sub>4</sub> salt is only partially soluble in the reaction mixture, and therefore increasing the amount added above the saturation concentration leads to minimal improvement in the rate of reaction. A possible explanation for the very slow rate of reaction with 0.3 equivalents of Na<sub>2</sub>S<sub>2</sub>O<sub>4</sub> to alkyl halide is that a large fraction of the Na<sub>2</sub>S<sub>2</sub>O<sub>4</sub> is consumed reducing Cu<sup>II</sup> to Cu<sup>I</sup>, implying that there is only a small amount left to maintain the SARA ATRP reaction. In fact, the polymerization only starts after 6 hours and the monomer reaches 50% of conversion after 24h ( $M_{n,GPC} = 8.3 \times 10^3$ ; *D* = 1.4) (Figure B.2, Annex B). However, using 0.3 to 1 equivalent of Na<sub>2</sub>S<sub>2</sub>O<sub>4</sub> leads to similar control over the MW and *D*.

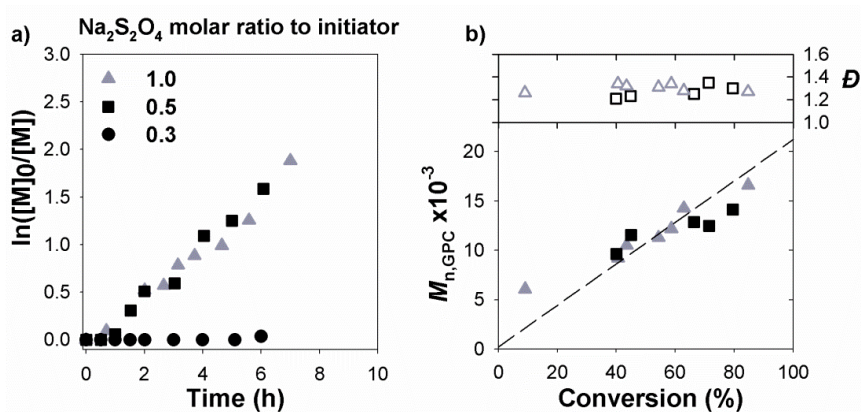
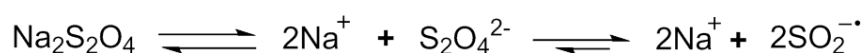


**Figure 2.3:** Effect of the ratio of  $\text{Na}_2\text{S}_2\text{O}_4$  on the SARA ATRP of DPA in IPA/water = 95/5 (v/v) at 40 °C. (A) First-order kinetic plot, (B) evolution of MW and  $\bar{D}$  with conversion (the dashed line represents theoretical MW at a given conversion). Reaction conditions:  $[\text{DPA}]_0/[\text{EBiB}]_0/[\text{Na}_2\text{S}_2\text{O}_4]_0/[\text{CuBr}_2]_0/[\text{Me}_6\text{TREN}]_0=100/1/\text{Na}_2\text{S}_2\text{O}_4/0.1/0.1$  (molar).

#### 3.4.4. Feeding of $\text{Na}_2\text{S}_2\text{O}_4$

$\text{Na}_2\text{S}_2\text{O}_4$  is a powerful reducing agent that quickly converts  $\text{Cu}^{\text{II}}$  to  $\text{Cu}^{\text{I}}$  species.<sup>19</sup> However, due to the poor solubility of  $\text{Na}_2\text{S}_2\text{O}_4$  in alcohols, the water content in the system could be a key factor when considering the SARA ATRP of DPA using  $\text{Na}_2\text{S}_2\text{O}_4$ . In water, the  $\text{Na}_2\text{S}_2\text{O}_4$  forms  $\text{Na}^+$  and  $\text{S}_2\text{O}_4^{2-}$  and the dissociation of the  $\text{S}_2\text{O}_4^{2-}$  will form two molecules of the  $\text{SO}_2^{\bullet-}$  radical anion (Scheme 3.2).<sup>45</sup> A higher fraction of water in the system promotes the efficient dissolution of the dithionite salt and consequently its dissociation into  $\text{SO}_2^{\bullet-}$ .<sup>20, 28</sup> It is important to note that the dissociation constant of  $\text{S}_2\text{O}_4^{2-}$  in water is very small,  $K_d \sim 10^{-6}$  mM<sup>45, 46</sup> but it increases with the decreasing of polarity of the solvent.<sup>47</sup> Nevertheless, the data in Figure 2.3 suggest that the limited solubility of  $\text{Na}_2\text{S}_2\text{O}_4$  in the reaction mixture has a great influence on the polymerization rate perhaps greater than the dissociation of the  $\text{S}_2\text{O}_4^{2-}$ . The data in Figure 3.2 suggest that the formation of  $\text{SO}_2^{\bullet-}$  is very rapidly followed by the radical anion acting as a supplemental activator and reducing agent.



**Scheme 3.2:** Scheme of the sodium dithionite decomposition.

Even though the preliminary results showed that a SARA ATRP of DPA proceeded in a controlled manner, adding all of  $\text{Na}_2\text{S}_2\text{O}_4$  at the beginning of the reaction could produce high radical concentrations in the early phase of the reaction, possible leading to undesired termination reactions. This effect is mostly visible in the polymer GPC traces, with a prominent low MW tail (Figure 3.1 (c)). We envisaged a solution for this issue by adding small amounts of reducing agent over an extended period of time to maintain its relatively low concentration over the whole polymerization.

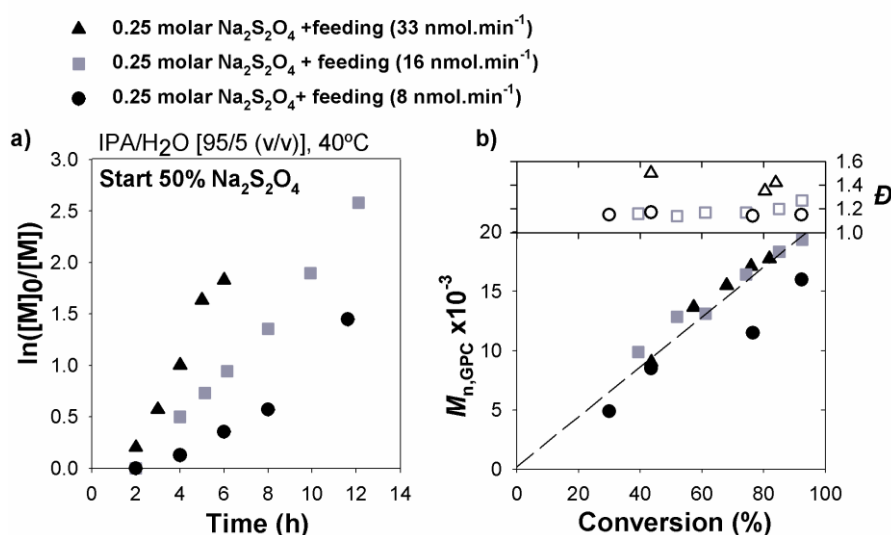
In an attempt to understand the significance of the feeding on the control over SARA ATRP of DPA using  $\text{Na}_2\text{S}_2\text{O}_4$ , the reactions were performed with different feeding rates at which an aqueous solution of  $\text{Na}_2\text{S}_2\text{O}_4$  was fed into the system. Several feeding rates of the  $\text{Na}_2\text{S}_2\text{O}_4$  aqueous solution ( $\text{FR}_{\text{Na}_2\text{S}_2\text{O}_4}$ ) and initial concentrations of the salt in the solvent mixture ( $\text{IR}_{\text{Na}_2\text{S}_2\text{O}_4}$ ) were tested. In all experiments the reaction started with 2.5% (v/v) of water in the polymerization mixture and the feeding was conducted so that the final water content in the polymerization mixture was 5% (v/v). The feeding was stopped when the total molar ratio of  $\text{Na}_2\text{S}_2\text{O}_4$  added in the solution reached 0.5 molar (molar ratio to initiator), which is the same ratio as in well-controlled experiments without feeding, using one single  $\text{Na}_2\text{S}_2\text{O}_4$  addition.

The reaction was very slow in experiments where the initial concentration of  $\text{Na}_2\text{S}_2\text{O}_4$  was zero, and  $\text{Na}_2\text{S}_2\text{O}_4$  fed at a rate of  $\text{FR}_{\text{Na}_2\text{S}_2\text{O}_4} = 39.1 \text{ nmol}\cdot\text{min}^{-1}$  ( $139 \text{ nL}\cdot\text{min}^{-1}$ ) was the only source of dithionite salts, with an induction period of 5 hours (Figure B.3, Annex B). The reaction only started when the concentration of the  $\text{Na}_2\text{S}_2\text{O}_4$  in the solution mixture reached a 0.25 molar ratio to initiator, which corresponds to 50% of the total amount of  $\text{Na}_2\text{S}_2\text{O}_4$  added. After this point the polymerization proceeded rapidly, reaching within 5 hours 60% conversion. The GPC data also show that this polymerization with feeding of  $\text{Na}_2\text{S}_2\text{O}_4$  gives similar control over the  $M_n$  and  $D$  values as experiments without feeding, with good agreement between theoretical and experimental MW and  $D = 1.2 - 1.25$ .

To further investigate the effect of feeding  $\text{Na}_2\text{S}_2\text{O}_4$  the initial concentration of  $\text{Na}_2\text{S}_2\text{O}_4$  in the polymerization mixture was established 50% of the total  $\text{Na}_2\text{S}_2\text{O}_4$  (0.25 molar ratio to initiator) and the feeding rate of the  $\text{Na}_2\text{S}_2\text{O}_4$  solution was varied from 8 to  $33 \text{ nmol}\cdot\text{min}^{-1}$ . To ensure that the same amount of  $\text{Na}_2\text{S}_2\text{O}_4$  was added to the reaction mixture these feeding rates correspond to 6 to 24h reactions times (Figure 3.4).

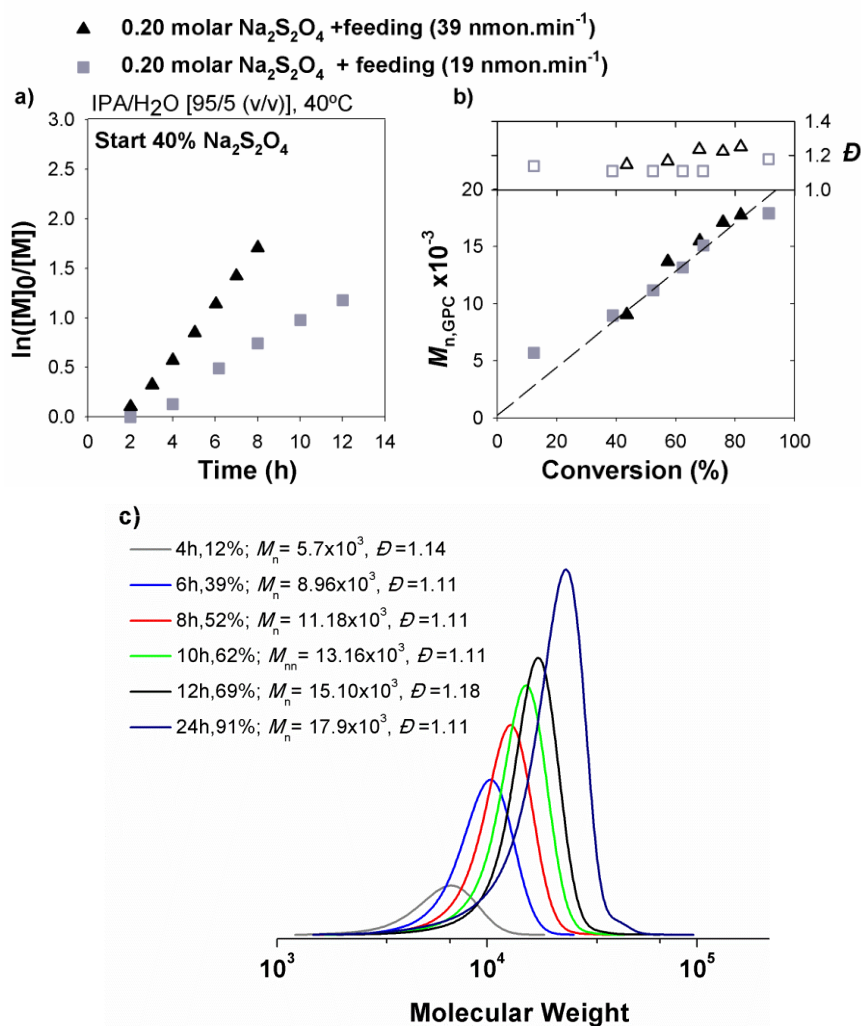


Figure 3.4(a) indicates that the lower feeding rates led to a decrease in the polymerization rate. The reaction with  $FR_{Na_2S_2O_4} = 33 \text{ nmol}\cdot\text{min}^{-1}$  has one hour of induction period and reached a conversion of 80% after 5 hours. Slowing the  $FR_{Na_2S_2O_4}$  to  $16 \text{ nmol}\cdot\text{min}^{-1}$  and  $8 \text{ nmol}\cdot\text{min}^{-1}$  increased the induction period to 3 h. After 12h reaction, the reaction with  $FR_{Na_2S_2O_4} = 16 \text{ nmol}\cdot\text{min}^{-1}$  reached 92% conversion. For the reaction with  $FR_{Na_2S_2O_4} = 8 \text{ nmol}\cdot\text{min}^{-1}$  after 12h reaction, the monomer conversion was 77%. This is expected based on the fact that the SARA reactions of the dithionite species control the rate of reaction. In all cases, Figure 3.4(b) shows good agreement between the theoretical MW ( $M_{n,th}$ ) and the  $M_{n,GPC}$ , and  $\bar{D}$  values in between 1.15 and 1.4. Although reducing the rate at which  $Na_2S_2O_4$  is fed into the system decreased the polymerization rate, the control over the polymerization improved, as measured the  $\bar{D}$  values. In particular, going from a  $FR_{Na_2S_2O_4} = 33 \text{ nmol}\cdot\text{min}^{-1}$  to  $FR_{Na_2S_2O_4} = 16 \text{ nmol}\cdot\text{min}^{-1}$  the  $\bar{D}$  dropped from approximately 1.4 for the system with  $FR_{Na_2S_2O_4} = 33 \text{ nmol}\cdot\text{min}^{-1}$  to 1.2-1.3 for the system with  $FR_{Na_2S_2O_4} = 16 \text{ nmol}\cdot\text{min}^{-1}$ . Interestingly, Figure 3.4(b), shows that the reaction with  $FR_{Na_2S_2O_4} = 8 \text{ nmol}\cdot\text{min}^{-1}$  demonstrated no increase in the  $\bar{D}$  values at higher monomer conversions which could be due to the smaller influence of termination reactions in this system, although the  $M_{n,GPC}$  values are slightly below the theoretical ones.



**Figure 3.4:** Effect of the different feeding rates of  $Na_2S_2O_4$  solution in SARA ATRP of DPA, starting with 50% of  $Na_2S_2O_4$  in the solvent mixture, IPA/H<sub>2</sub>O = 95/5 (v/v) at 40 °C. (a) First-order kinetic plot, (b) evolution of MW and  $\bar{D}$  with conversion (the dashed line represents theoretical MW at a given conversion). Reaction conditions:  $[DPA]_0/[EBPA]_0/[Na_2S_2O_4]_0/[CuBr_2]_0/[Me_6TREN]_0 = 100/1/feeding/0.1/0.2$  (molar).

In subsequent studies, the initial concentration of  $\text{Na}_2\text{S}_2\text{O}_4$  in the polymerization mixture was then reduced to 40% of the total  $\text{Na}_2\text{S}_2\text{O}_4$  added (0.2 molar ratio to initiator) and two feeding rates were evaluated (39.0 and 19.4  $\text{nmol}\cdot\text{min}^{-1}$ ) that corresponds to 6 and 12 hour feeding times. The kinetics is presented in Figure 3.5(a). Both reactions had a 2 hour induction period, and as expected, the polymerization rate decreased with the slower feeding rate. Figure 3.5 (b) presents the GPC traces of the reaction that starts with 0.2 molar ratio of  $\text{Na}_2\text{S}_2\text{O}_4$  to initiator, and  $\text{FR}_{\text{Na}_2\text{S}_2\text{O}_4} = 19$  and 39  $\text{nmol}\cdot\text{min}^{-1}$ . The GPC data indicate that the reaction with  $\text{FR}_{\text{Na}_2\text{S}_2\text{O}_4}=19$   $\text{nmol}\cdot\text{min}^{-1}$  had very narrow MW distributions throughout the whole polymerization ( $\bar{D} = 1.1 - 1.2$ ) and the  $M_{n,\text{GPC}}$  values were in excellent agreement with the theoretical ones. The GPC traces in Figure 3.5(c) show the evolution of the  $\bar{D}$  for the polymerization starting with 40% of the total  $\text{Na}_2\text{S}_2\text{O}_4$  added with a remainder fed at 19  $\text{nmol}\cdot\text{min}^{-1}$ . The absence of low MW tailing is evident in the traces in Figure 3.5 (c), which is not the case for the polymerizations without feeding of  $\text{Na}_2\text{S}_2\text{O}_4$  (Figure 3.1(b)). The effect of the feeding rate on the polymerization rate is given in Figure B.4 (Annex B). The data in Figure B.4 shows that the rate of the polymerization, measured by the slope of the semi-logarithmic plot, is proportional to the square-root of the feeding rate. This is consistent with the 0.5 order observed for ICAR ATRP, or other processes where activator regeneration, combined with radical termination, is the rate determining step.<sup>9, 15, 48, 49</sup>



**Figure 3.5:** Effect of the feeding rates of  $\text{Na}_2\text{S}_2\text{O}_4$  solution in SARA ATRP of DPA, starting with 40% of  $\text{Na}_2\text{S}_2\text{O}_4$  in the solvent mixture, IPA/ $\text{H}_2\text{O}$  = 95/5 (v/v) at 40 °C. (a) First-order kinetic plot, (b) evolution of MW and  $\bar{D}$  with conversion (the dashed line represents theoretical MW at a given conversion) and, (c) GPC traces with conversion for reaction  $\text{IR}_{\text{Na}_2\text{S}_2\text{O}_4} = 40\%$  and  $\text{FR}_{\text{Na}_2\text{S}_2\text{O}_4} = 19 \text{ nmol}\cdot\text{min}^{-1}$ . Reaction conditions:  $[\text{DPA}]_0/[\text{EBPA}]_0/[\text{Na}_2\text{S}_2\text{O}_4]_0/[\text{CuBr}_2]_0/[\text{Me}_6\text{TREN}]_0 = 100/1/\text{feeding}/0.1/0.2$  (molar).

### 3.4.5. Variation of copper concentration

Whenever a polymer is to be applied in the biomedical field, it is important to remove contaminants and toxic compounds, including the residual copper catalysts. Therefore, it is advantageous to synthesize polymers with lowest possible catalyst concentrations to simplify the polymer purification. Figure 3.6 shows the effect of lowering the catalyst concentration on the polymerization, the copper concentration was varied from 1000 to

250 ppm with 40% of the total  $\text{Na}_2\text{S}_2\text{O}_4$  added initially and  $\text{FR}_{\text{Na}_2\text{S}_2\text{O}_4} = 19 \text{ nmol}\cdot\text{min}^{-1}$ . Figure 3.6 suggests that it is possible to reduce the amount of copper to 250 ppm while maintaining a similar rate of polymerization and control over the MW and  $\mathcal{D}$ . There is a slight increase in  $\mathcal{D}$  at 250 ppm of copper, compared to the higher catalyst loadings.

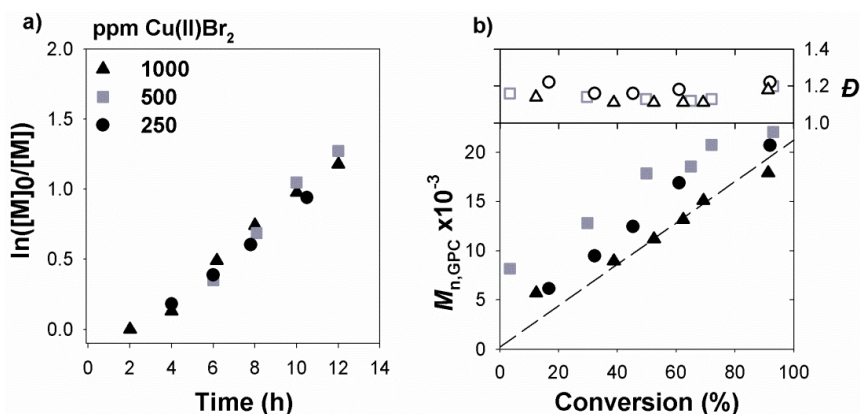


**Figure 3.6:** Effect of the copper concentration in the SARA ATRP of DPA with feeding rate of aqueous solution of  $\text{Na}_2\text{S}_2\text{O}_4$ ,  $19.4 \text{ nmol}\cdot\text{min}^{-1}$ , starting with 40% of  $\text{Na}_2\text{S}_2\text{O}_4$  in the solvent mixture, IPA/ $\text{H}_2\text{O}$  = 95/5 (v/v) at 40 °C. (a) First-order kinetic plots, (b) evolution of MW and  $\mathcal{D}$  with conversion (the dashed line represents theoretical MW at a given conversion). Reaction conditions:  $[\text{DPA}]_0/[\text{EBPA}]_0/[\text{Na}_2\text{S}_2\text{O}_4]_0/[\text{CuBr}_2]_0/[\text{Me}_6\text{TREN}]_0 = 100/1/0.2/\text{CuBr}_2/\text{Me}_6\text{TREN}$  (molar).

### 3.4.6. Effect of the ligand

Another parameter that can be varied in copper-mediated polymerizations is the nature, activity and stability of the catalyst, by varying the ligand structure. Interestingly, substituting  $\text{Me}_6\text{TREN}$  for a stronger binding ligand, tris(2-pyridylmethyl)-amine (TPMA),<sup>44, 50</sup> allowed for similar control over the polymerization with only 100 ppm of copper (Figure 3.7), compared to the 500 ppm needed to achieve similar control using  $\text{Me}_6\text{TREN}$  as the ligand.

The polymerization rate with 100 ppm of Cu/TPMA catalyst was slightly faster than the reaction with  $\text{Me}_6\text{TREN}$  and 250 ppm of Cu, and the control over the MWs was similar, with lower  $\mathcal{D}$ . Furthermore,  $\mathcal{D}$  were similar for 250 ppm of Cu/ $\text{Me}_6\text{TREN}$  catalyst and

100 ppm of Cu/TPMA catalyst, typically in the range 1.1 - 1.2, with the TPMA system leading to slightly narrower MW distributions.

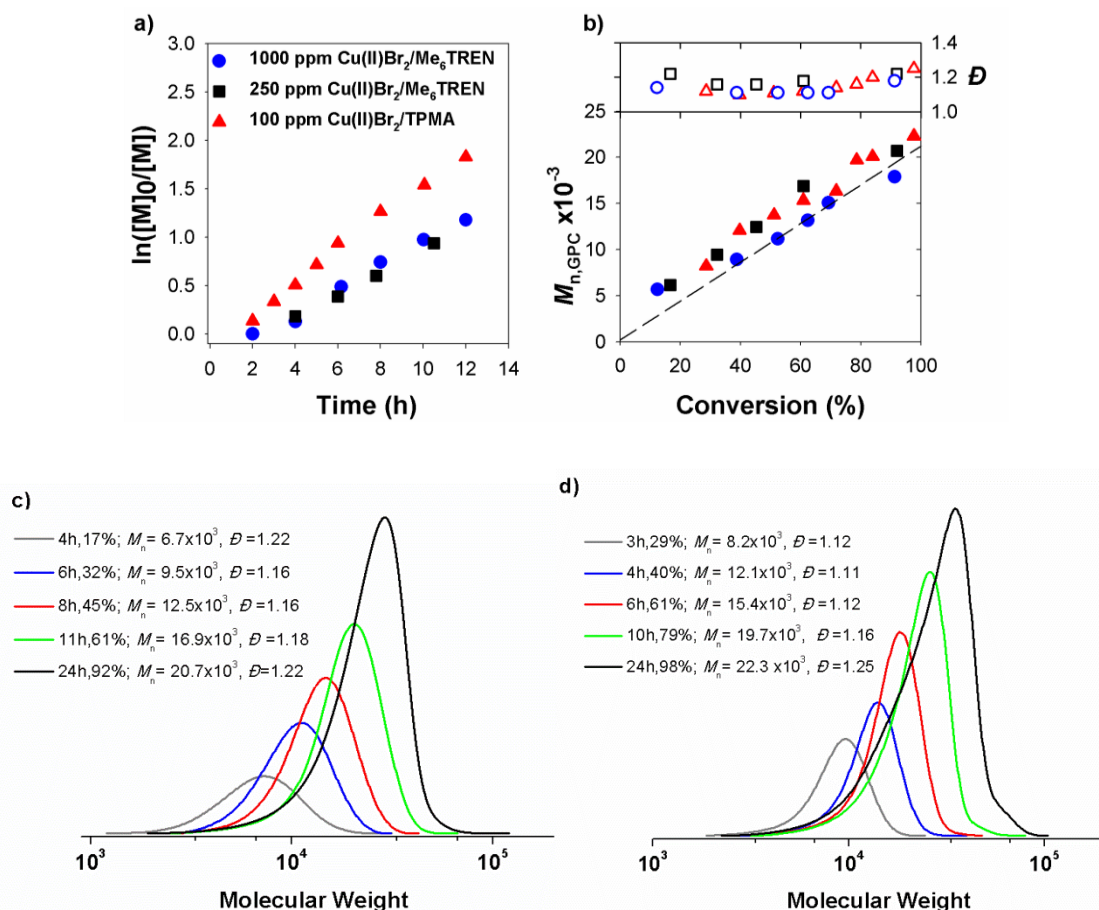


**Figure 3.7:** Influence of ligand and the copper concentration in the SARA ATRP of DPA with feeding rate of aqueous solution of Na<sub>2</sub>S<sub>2</sub>O<sub>4</sub>, 16nmol.min<sup>-1</sup>, starting with 40% of Na<sub>2</sub>S<sub>2</sub>O<sub>4</sub> in the solvent mixture, IPA/H<sub>2</sub>O = 95/5 (v/v) at 40 °C. (a) First-order kinetic plots, (b) evolution of MW and  $\bar{D}$  with conversion (the dashed line represents theoretical MW at a given conversion), (c) GPC traces with conversion for reaction with Me<sub>6</sub>TREN and 250ppm of Cu and (d) TPMA with 100ppm of copper. Reaction conditions: [DPA]<sub>0</sub>/[EBPA]<sub>0</sub>/[Na<sub>2</sub>S<sub>2</sub>O<sub>4</sub>]<sub>0</sub>/[CuBr<sub>2</sub>]<sub>0</sub>/[ligand]<sub>0</sub>=100/1/0.2/1/2l (molar) (l=0.1 or 0.025 for Me<sub>6</sub>TREN and l=0.01 for TPMA).

A summary of all experiments performed to optimize the polymerization is shown in Table 3.1. The main conclusion of the data in Table 3.1 is that SARA ATRP of DPA can yield well controlled polymers if the  $\text{Na}_2\text{S}_2\text{O}_4$  solution is slowly and continuously fed into the reaction mixture. As expected, higher feeding rates led to faster polymerizations with inferior control. Another key conclusion from these experiments is that the initial concentration of  $\text{Na}_2\text{S}_2\text{O}_4$  should not be too high, since this will cause a large amount of termination early in the reaction, as evidenced by low MW tailing in the GPC traces and higher  $D$ . The results in Table 3.1 also indicate that very well-controlled polymers can be synthesized using just 100 ppm of the  $\text{Cu}^{\text{II}}\text{Br}_2/\text{TPMA}$  complex, and that  $\text{Cu}^{\text{II}}\text{Br}_2/\text{Me}_6\text{TREN}$  at 250 ppm gives similar results to those at 100 ppm of  $\text{Cu}^{\text{II}}\text{Br}_2/\text{TPMA}$ .

**Table 3.1.** SARA ATRP of PDA with Na<sub>2</sub>S<sub>2</sub>O<sub>4</sub> in IPA/H<sub>2</sub>O = 95/5 (v/v) at 40 °C. Reaction conditions: [DPA]<sub>0</sub>/[EBPA]<sub>0</sub>/ [Na<sub>2</sub>S<sub>2</sub>O<sub>4</sub>]<sub>0</sub>/[CuBr<sub>2</sub>]<sub>0</sub>/[Me<sub>6</sub>TREN]<sub>0</sub> = 100/1/IR<sub>Na<sub>2</sub>S<sub>2</sub>O<sub>4</sub></sub>/0.1/0.2 (molar).

Entry	IR <sub>Na<sub>2</sub>S<sub>2</sub>O<sub>4</sub></sub> , % <sup>a</sup>	FR <sub>Na<sub>2</sub>S<sub>2</sub>O<sub>4</sub></sub> , nmol.min <sup>-1</sup>	Feeding time, h	Time <sup>b</sup>	Conv, % <sup>b</sup>	k <sub>p</sub> <sup>app</sup> , h <sup>-1</sup>	M <sub>n,th</sub> x10 <sup>3b</sup>	M <sub>n,GPC</sub> x10 <sup>3b</sup>	D <sup>a</sup>	Cu, ppm <sup>c</sup>
1 <sup>d</sup>	100	-	-	7	85	0.254	18.4	16.6	1.27	1000
2 <sup>d</sup>	50	-	-	24	99	0.289	20.92	17.50	1.32	1000
3 <sup>d</sup>	30	-	-	48	88	0.044	17.40	18.57	1.43	1000
4	50	-	-	7	83	0.301	17.71	18.4	1.28	1000
5	0	39.1	10	22	93	0.141	20.3	17.30	1.23	1000
6	50	32.6	6	6	84	0.472	18.59	18.57	1.42	1000
7	50	16.3	12	12	92	0.235	20.31	19.34	1.27	1000
8	50	8.15	24	24	92	0.149	20.17	15.98	1.15	1000
9	40	39.0	6	8	82	0.272	17.78	17.76	1.25	1000
10	40	19.4	12	24	91	0.124	19.9	17.9	1.18	1000
11 <sup>e</sup>	40	19.4	12	24	93	0.157	20.41	22.08	1.20	500
12 <sup>f</sup>	40	19.4	12	24	92	0.117	20.05	20.70	1.22	250
13 <sup>g</sup>	40	19.4	12	24	98	0.170	21.20	22.3	1.25	100

IR<sub>Na<sub>2</sub>S<sub>2</sub>O<sub>4</sub></sub>: Initial ratio of Na<sub>2</sub>S<sub>2</sub>O<sub>4</sub> to the initiator (0.5 molar max); FR<sub>Na<sub>2</sub>S<sub>2</sub>O<sub>4</sub></sub>: Feeding rate of Na<sub>2</sub>S<sub>2</sub>O<sub>4</sub>; <sup>a</sup> molar ratio to initiator; <sup>b</sup> values obtained from the last sample from the kinetic study; <sup>c</sup> calculated by the initial molar ration of CuBr<sub>2</sub> to the monomer; <sup>d</sup>EBiB was used as initiator; [CuBr<sub>2</sub>]<sub>0</sub>/[Me<sub>6</sub>TREN]<sub>0</sub> = 0.05/0.1; [CuBr<sub>2</sub>]<sub>0</sub>/[Me<sub>6</sub>TREN]<sub>0</sub> = 0.025/0.1; <sup>e</sup>TPMA was used as ligand, [CuBr<sub>2</sub>]<sub>0</sub>/[TPMA]<sub>0</sub> = 0.01/0.02.

### 3.4.7. Polymerization of OEOMA

Although DPA is an important monomer for biomedical applications, it is also important to investigate other water soluble functional methacrylates, and determine whether the conditions developed can be used to control the polymerization of a wide range of functional monomers. Therefore, the present catalytic system was applied to OEOMA, as a representative methacrylic monomer. The reactions were performed using the conditions: IPA/water = 95/5 (v/v),  $[\text{EBPA}]_0/[\text{Na}_2\text{S}_2\text{O}_4]_0/[\text{CuBr}_2]_0/[\text{Me}_6\text{TREN}]_0 = 1/0.2/0.1/0.2$  (molar) and slow feed of  $\text{Na}_2\text{S}_2\text{O}_4$ , but the monomer concentration was adjusted to 18% (w/w). In the case of OEOMA, more diluted solutions were used, since the literature shows that higher concentrations of oligo(ethylene oxide) based monomers can lead to broader MW distributions.<sup>51</sup> The kinetic plots for the homopolymerization of OEOMA are presented in Figure 3.8, and they show linear first order kinetics. Additionally, the evolution of MW is linear with conversion, and  $\bar{D}$  was close to 1.1 throughout the polymerization. The GPC traces, Figure 3.9, show a shift to higher MW with conversion.

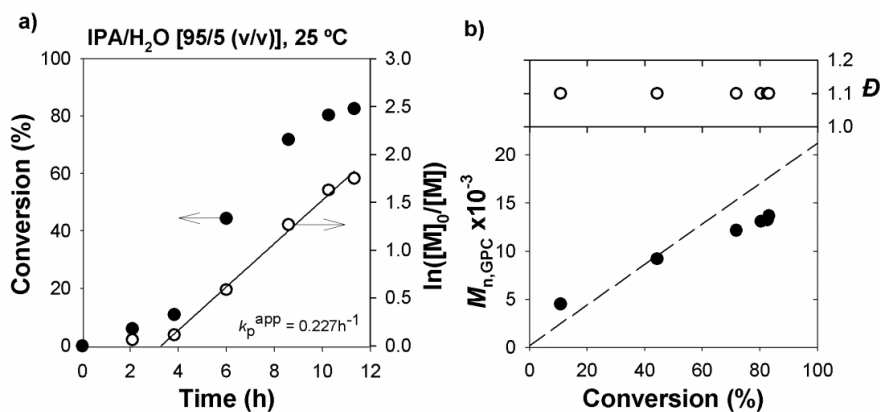


**Figure 3.8:** SARA ATRP of OEOMA with feeding rate of aqueous solution of  $\text{Na}_2\text{S}_2\text{O}_4$ , 16nmol/min, starting with 40% of  $\text{Na}_2\text{S}_2\text{O}_4$  in the solvent mixture, 18wt%, IPA/water = 95/5 (v/v) at 25 °C. (a) First-order kinetic plot, (b) evolution of MW and  $\bar{D}$  with conversion (the dashed line represents theoretical MW at a given conversion). Reaction conditions:  $[\text{OEOMA}]_0/[\text{EBPA}]_0/[\text{Na}_2\text{S}_2\text{O}_4]_0/[\text{CuBr}_2]_0/[\text{Me}_6\text{TREN}]_0=30/1/0.2/0.1/0.2$  (molar).



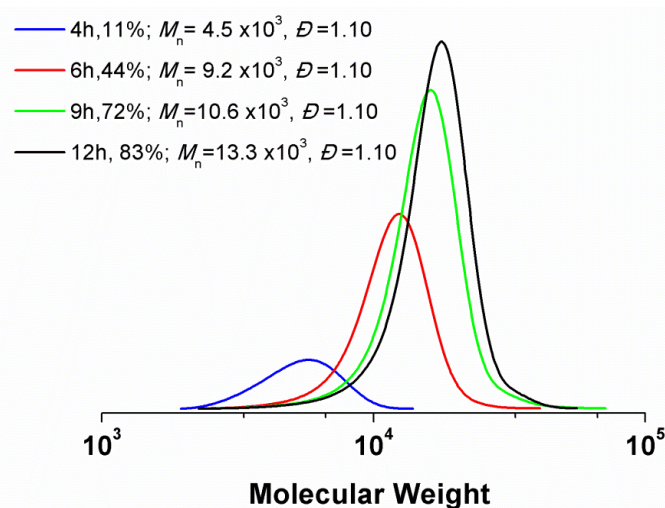


**Figure 3.9:** GPC traces with conversion for the SARA ATRP of OEOMA with feeding rate of aqueous solution of  $\text{Na}_2\text{S}_2\text{O}_4$ ,  $16\text{nmol}\cdot\text{min}^{-1}$ , starting with 40% of  $\text{Na}_2\text{S}_2\text{O}_4$  in the solvent mixture, 18 wt%, IPA/ $\text{H}_2\text{O}$  = 95/5 (v/v) at 25 °C. Reaction conditions:  $[\text{OEOMA}]_0/[\text{EBPA}]_0/[\text{Na}_2\text{S}_2\text{O}_4]_0/[\text{CuBr}_2]_0/[\text{Me}_6\text{TREN}]_0=30/1/0.2/0.1/0.2$  (molar).

### 3.5. Conclusions

Well-defined polymers of a pH responsive monomer, DPA, were synthesized through SARA ATRP in the presence of  $\text{Na}_2\text{S}_2\text{O}_4$  and  $\text{CuBr}_2$ /ligand complex. The preferred reaction medium was a mixture of isopropanol and water (95/5 (v/v)). The polymerization conditions of this eco-friendly and inexpensive SARA ATRP system were enhanced to prepare well-controlled polymers using relatively low copper catalyst concentrations. The slow and continuous feeding of  $\text{Na}_2\text{S}_2\text{O}_4$  solution into the reaction mixture improves the control over the polymerization. Slower feeding rates reduced the polymerization rate, but the control over the polymerization was enhanced. Furthermore, the use of TPMA as ligand allowed polymerization to be carried out in the presence of only 100 ppm of copper, reaching 80% of monomer conversion after 10 h ( $M_{n,\text{GPC}} = 19.7 \times 10^3$ ;  $D = 1.16$ ). Due to the reduced catalyst concentration this is a promising method for the synthesis of pH responsive polymers that could be used in the biomedical field.

### 3.6. References

1. Braunecker, W.A. and K. Matyjaszewski (2007). Controlled/living radical polymerization: Features, developments, and perspectives. *Progress in Polymer Science*, 32(1): 93-146.
2. Goto, A. and T. Fukuda (2004). Kinetics of living radical polymerization. *Progress in Polymer Science*, 29(4): 329-385.
3. Matyjaszewski, K. and J. Xia (2001). Atom Transfer Radical Polymerization. *Chemical Reviews*, 101(9): 2921-2990.
4. Matyjaszewski, K. (2012). Atom Transfer Radical Polymerization (ATRP): Current Status and Future Perspectives. *Macromolecules*, 45(10): 4015-4039.
5. Coessens, V., T. Pintauer, and K. Matyjaszewski (2001). Functional polymers by atom transfer radical polymerization. *Progress in Polymer Science*, 26(3): 337-377.
6. Wang, J.S. and K. Matyjaszewski (1995). CONTROLLED LIVING RADICAL POLYMERIZATION - ATOM-TRANSFER RADICAL POLYMERIZATION IN THE PRESENCE OF TRANSITION-METAL COMPLEXES. *Journal of the American Chemical Society*, 117(20): 5614-5615.
7. Guliashvili, T., P.V. Mendonça, A.C. Serra, A.V. Popov, and J.F.J. Coelho (2012). Copper-Mediated Controlled/"Living" Radical Polymerization in Polar Solvents: Insights into Some Relevant Mechanistic Aspects. *Chemistry – A European Journal*, 18(15): 4607-4612.
8. Matyjaszewski, K. and N.V. Tsarevsky (2009). Nanostructured functional materials prepared by atom transfer radical polymerization. *Nature Chemistry*, 1(4): 276-288.
9. Tsarevsky, N.V. and K. Matyjaszewski (2007). "Green" Atom Transfer Radical Polymerization: From Process Design to Preparation of Well-Defined Environmentally Friendly Polymeric Materials. *Chemical Reviews*, 107(6): 2270-2299.
10. Jakubowski, W. and K. Matyjaszewski (2006). Activators Regenerated by Electron Transfer for Atom-Transfer Radical Polymerization of (Meth)acrylates and Related Block Copolymers. *Angewandte Chemie International Edition*, 45(27): 4482-4486.
11. Matyjaszewski, K., W. Jakubowski, K. Min, W. Tang, J.Y. Huang, W.A. Braunecker, and N.V. Tsarevsky (2006). Diminishing catalyst concentration in atom transfer radical polymerization with reducing agents. *Proceedings of the National Academy of Sciences of the United States of America*, 103(42): 15309-15314.
12. Mendonça, P.V., A.C. Serra, J.F.J. Coelho, A.V. Popov, and T. Guliashvili (2011). Ambient temperature rapid ATRP of methyl acrylate, methyl methacrylate and styrene in polar solvents with mixed transition metal catalyst system. *European Polymer Journal*, 47(7): 1460-1466.

13. Zhang, Y., Y. Wang, and K. Matyjaszewski (2011). ATRP of Methyl Acrylate with Metallic Zinc, Magnesium, and Iron as Reducing Agents and Supplemental Activators. *Macromolecules*, 44(4): 683-685.
14. Abreu, C.M.R., P.V. Mendonça, A.C. Serra, J.F.J. Coelho, A.V. Popov, and T. Guliashvili (2012). Accelerated Ambient-Temperature ATRP of Methyl Acrylate in Alcohol–Water Solutions with a Mixed Transition-Metal Catalyst System. *Macromolecular Chemistry and Physics*, 213(16): 1677-1687.
15. Konkolewicz, D., Y. Wang, M. Zhong, P. Krys, A.A. Isse, A. Gennaro, and K. Matyjaszewski (2013). Reversible-Deactivation Radical Polymerization in the Presence of Metallic Copper. A Critical Assessment of the SARA ATRP and SET-LRP Mechanisms. *Macromolecules*, 46(22): 8749-8772.
16. Peng, C.-H., M. Zhong, Y. Wang, Y. Kwak, Y. Zhang, W. Zhu, M. Tonge, J. Buback, S. Park, P. Krys, D. Konkolewicz, A. Gennaro, and K. Matyjaszewski (2013). Reversible-Deactivation Radical Polymerization in the Presence of Metallic Copper. Activation of Alkyl Halides by Cu-0. *Macromolecules*, 46(10): 3803-3815.
17. Wang, Y., M. Zhong, W. Zhu, C.-H. Peng, Y. Zhang, D. Konkolewicz, N. Bortolamei, A.A. Isse, A. Gennaro, and K. Matyjaszewski (2013). Reversible-Deactivation Radical Polymerization in the Presence of Metallic Copper. Comproportionation-Disproportionation Equilibria and Kinetics. *Macromolecules*, 46(10): 3793-3802.
18. Zhong, M., Y. Wang, P. Krys, D. Konkolewicz, and K. Matyjaszewski (2013). Reversible-Deactivation Radical Polymerization in the Presence of Metallic Copper. Kinetic Simulation. *Macromolecules*, 46(10): 3816-3827.
19. Abreu, C.M.R., P.V. Mendonca, A.C. Serra, A.V. Popov, K. Matyjaszewski, T. Guliashvili, and J.F.J. Coelho (2012). Inorganic Sulfites: Efficient Reducing Agents and Supplemental Activators for Atom Transfer Radical Polymerization. *Acs Macro Letters*, 1(11): 1308-1311.
20. Abreu, C.M.R., A.C. Serra, A.V. Popov, K. Matyjaszewski, T. Guliashvili, and J.F.J. Coelho (2013). Ambient temperature rapid SARA ATRP of acrylates and methacrylates in alcohol-water solutions mediated by a mixed sulfite/Cu(II)Br-2 catalytic system. *Polymer Chemistry*, 4(23): 5629-5636.
21. Coelho, J.F.J., E.Y. Carvalho, D.S. Marques, A.V. Popov, P.M. Goncalves, and M.H. Gil (2007). Synthesis of Poly(lauryl acrylate) by Single-Electron Transfer/Degenerative Chain Transfer Living Radical Polymerization Catalyzed by Na<sub>2</sub>S<sub>2</sub>O<sub>4</sub> in Water. *Macromolecular Chemistry and Physics*, 208(11): 1218-1227.
22. Coelho, J.F.J., E.Y. Carvalho, D.S. Marques, A.V. Popov, V. Percec, and M.H. Gil (2008). Influence of the isomeric structures of butyl acrylate on its single-electron

transfer-degenerative chain transfer living radical polymerization in water Catalyzed by Na<sub>2</sub>S<sub>2</sub>O<sub>4</sub>. *Journal of Polymer Science Part A: Polymer Chemistry*, 46(19): 6542-6551.

23. Coelho, J.F.J., E.Y. Carvalho, D.S. Marques, A.V. Popov, V. Percec, P.M.F.O. Gonçalves, and M.H. Gil (2008). Synthesis of poly(ethyl acrylate) by single electron transfer-degenerative chain transfer living radical polymerization in water catalyzed by Na<sub>2</sub>S<sub>2</sub>O<sub>4</sub>. *Journal of Polymer Science Part A: Polymer Chemistry*, 46(2): 421-432.

24. Coelho, J.F.J., J. Gois, A.C. Fonseca, R.A. Carvalho, A.V. Popov, V. Percec, and M.H. Gil (2009). Synthesis of poly(2-methoxyethyl acrylate) by single electron transfer—Degenerative transfer living radical polymerization catalyzed by Na<sub>2</sub>S<sub>2</sub>O<sub>4</sub> in water. *Journal of Polymer Science Part A: Polymer Chemistry*, 47(17): 4454-4463.

25. Coelho, J.F.J., A.M.F.P. Silva, A.V. Popov, V. Percec, M.V. Abreu, P.M.O.F. Gonçalves, and M.H. Gil (2006). Single electron transfer–degenerative chain transfer living radical polymerization of N-butyl acrylate catalyzed by Na<sub>2</sub>S<sub>2</sub>O<sub>4</sub> in water media. *Journal of Polymer Science Part A: Polymer Chemistry*, 44(9): 2809-2825.

26. Percec, V., A.V. Popov, E. Ramirez-Castillo, J.F.J. Coelho, and L.A. Hinojosa-Falcon (2004). Non-transition metal-catalyzed living radical polymerization of vinyl chloride initiated with iodoform in water at 25 °C. *Journal of Polymer Science Part A: Polymer Chemistry*, 42(24): 6267-6282.

27. Percec, V., A.V. Popov, E. Ramirez-Castillo, J.F.J. Coelho, and L.A. Hinojosa-Falcon (2005). Phase transfer catalyzed single electron transfer–degenerative chain transfer mediated living radical polymerization (PTC-SET–DTLRP) of vinyl chloride catalyzed by sodium dithionite and initiated with iodoform in water at 43 °C. *Journal of Polymer Science Part A: Polymer Chemistry*, 43(4): 779-788.

28. Gois, J.R., N. Rocha, A.V. Popov, T. Guliashvili, K. Matyjaszewski, A.C. Serra, and J.F.J. Coelho (2014). Synthesis of well-defined functionalized poly(2-(diisopropylamino)ethyl methacrylate) using ATRP with sodium dithionite as a SARA agent. *Polymer Chemistry*.

29. Licciardi, M., Y. Tang, N.C. Billingham, and S.P. Armes (2005). Synthesis of novel folic acid-functionalized biocompatible block copolymers by atom transfer radical polymerization for gene delivery and encapsulation of hydrophobic drugs. *Biomacromolecules*, 6(2): 1085-1096.

30. Ma, Y.H., Y.Q. Tang, N.C. Billingham, S.P. Armes, A.L. Lewis, A.W. Lloyd, and J.P. Salvage (2003). Well-defined biocompatible block copolymers via atom transfer radical polymerization of 2-methacryloyloxyethyl phosphorylcholine in protic media. *Macromolecules*, 36(10): 3475-3484.

31. Faccia, P.A. and J.I. Amalvy (2013). Synthesis, characterization, and swelling behavior of new pH-sensitive hydrogels derived from copolymers of 2-hydroxyethyl

methacrylate and 2-(diisopropylamino)ethylmethacrylate. *Journal of Applied Polymer Science*, 127(3): 1974-1980.

32. Zhou, K., H. Liu, S. Zhang, X. Huang, Y. Wang, G. Huang, B.D. Sumer, and J. Gao (2012). Multicolored pH-Tunable and Activatable Fluorescence Nanoplatfrom Responsive to Physiologic pH Stimuli. *Journal of the American Chemical Society*, 134(18): 7803-7811.

33. Du, J., L. Fan, and Q. Liu (2012). pH-Sensitive Block Copolymer Vesicles with Variable Trigger Points for Drug Delivery. *Macromolecules*, 45(20): 8275-8283.

34. Zhou, K., Y. Wang, X. Huang, K. Luby-Phelps, B.D. Sumer, and J. Gao (2011). Tunable, Ultrasensitive pH-Responsive Nanoparticles Targeting Specific Endocytic Organelles in Living Cells. *Angewandte Chemie-International Edition*, 50(27): 6109-6114.

35. Yu, H., Y. Zou, Y. Wang, X. Huang, G. Huang, B.D. Sumer, D.A. Boothman, and J. Gao (2011). Overcoming Endosomal Barrier by Amphotericin B-Loaded Dual pH-Responsive PDMA-b-PDPA Micelleplexes for siRNA Delivery. *Acs Nano*, 5(11): 9246-9255.

36. Giacomelli, F.C., P. Stepanek, C. Giacomelli, V. Schmidt, E. Jager, A. Jager, and K. Ulbrich (2011). pH-triggered block copolymer micelles based on a pH-responsive PDPA (poly[2-(diisopropylamino)ethyl methacrylate]) inner core and a PEO (poly(ethylene oxide)) outer shell as a potential tool for the cancer therapy. *Soft Matter*, 7(19): 9316-9325.

37. Taktak, F.F. and V. Butun (2010). Synthesis and physical gels of pH- and thermo-responsive tertiary amine methacrylate based ABA triblock copolymers and drug release studies. *Polymer*, 51(16): 3618-3626.

38. Lomas, H., I. Canton, S. MacNeil, J. Du, S.P. Armes, A.J. Ryan, A.L. Lewis, and G. Battaglia (2007). Biomimetic pH Sensitive Polymersomes for Efficient DNA Encapsulation and Delivery. *Advanced Materials*, 19(23): 4238-4243.

39. Zhang, S., K. Zhou, G. Huang, M. Takahashi, A. Dean Sherry, and J. Gao (2013). A novel class of polymeric pH-responsive MRI CEST agents. *Chemical Communications*, 49(57): 6418-6420.

40. Xia, J., S.G. Gaynor, and K. Matyjaszewski (1998). Controlled/"Living" Radical Polymerization. Atom Transfer Radical Polymerization of Acrylates at Ambient Temperature. *Macromolecules*, 31(17): 5958-5959.

41. Tyeklar, Z., R.R. Jacobson, N. Wei, N.N. Murthy, J. Zubieta, and K.D. Karlin (1993). Reversible reaction of dioxygen (and carbon monoxide) with a copper(I) complex. X-ray structures of relevant mononuclear Cu(I) precursor adducts and the

trans-( $\mu$ -1,2-peroxo)dicopper(II) product. *Journal of the American Chemical Society*, 115(7): 2677-2689.

42. Xia, J. and K. Matyjaszewski (1999). Controlled/"Living" Radical Polymerization. Atom Transfer Radical Polymerization Catalyzed by Copper(I) and Picolyamine Complexes. *Macromolecules*, 32(8): 2434-2437.

43. He, H., M. Zhong, B. Adzima, D. Luebke, H. Nulwala, and K. Matyjaszewski (2013). A Simple and Universal Gel Permeation Chromatography Technique for Precise Molecular Weight Characterization of Well-Defined Poly(ionic liquid)s. *Journal of the American Chemical Society*, 135(11): 4227-4230.

44. Tang, W., Y. Kwak, W. Braunecker, N.V. Tsarevsky, M.L. Coote, and K. Matyjaszewski (2008). Understanding Atom Transfer Radical Polymerization: Effect of Ligand and Initiator Structures on the Equilibrium Constants. *Journal of the American Chemical Society*, 130(32): 10702-10713.

45. Lyons, D. and G. Nickless (1968). *Inorganic Sulfur Chemistry*, ed. G. Nickless. New York: Elsevier.

46. Lambeth, D.O. and G. Palmer (1973). The kinetics and mechanism of reduction of electron transfer proteins and other compounds of biological interest by dithionite. *J Biol Chem*, 248(17): 6095-103.

47. Lough, S.M. and J.W. McDonald (1987). Synthesis of tetraethylammonium dithionite and its dissociation to the sulfur dioxide radical anion in organic solvents. *Inorganic Chemistry*, 26(13): 2024-2027.

48. Rosen, B.M. and V. Percec (2009). Single-Electron Transfer and Single-Electron Transfer Degenerative Chain Transfer Living Radical Polymerization. *Chemical Reviews*, 109(11): 5069-5119.

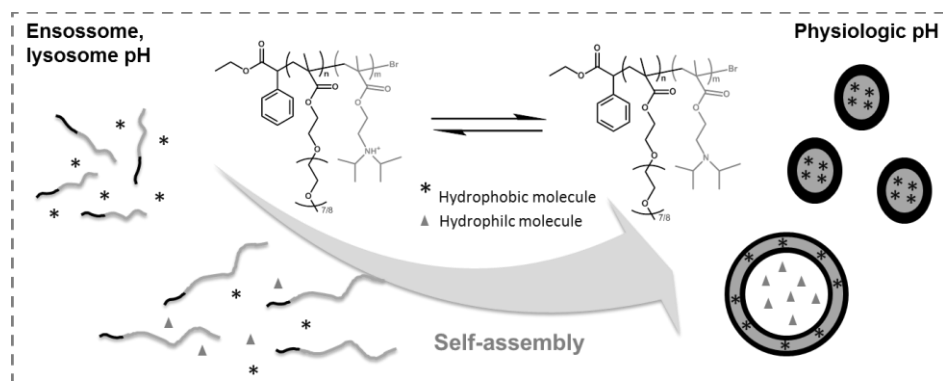
49. Matyjaszewski, K., W. Jakubowski, K. Min, W. Tang, J. Huang, W.A. Braunecker, and N.V. Tsarevsky (2006). Diminishing catalyst concentration in atom transfer radical polymerization with reducing agents. *Proceedings of the National Academy of Sciences*, 103(42): 15309-15314.

50. Tsarevsky, N.V., W.A. Braunecker, and K. Matyjaszewski (2007). Electron transfer reactions relevant to atom transfer radical polymerization. *Journal of Organometallic Chemistry*, 692(15): 3212-3222.

51. Konkolewicz, D., P. Kryszewski, J.R. Góis, P.V. Mendonça, M. Zhong, Y. Wang, A. Gennaro, A.A. Isse, M. Fantin, and K. Matyjaszewski (2014). Aqueous RDRP in the Presence of Cu<sub>0</sub>: The Exceptional Activity of CuI Confirms the SARA ATRP Mechanism. *Macromolecules*.

## Chapter 4

### Brush-Type pH-responsive block copolymers and its self-assembly properties



*The contents of this chapter will be submitted for publication: Góis, J. R., Rocha, N., Serra, A. C. and Coelho, J. F. J., “Brush-type pH-responsive block copolymers as nanocarriers for smart drug delivery applications”.*





## 4.1. Abstract

Well-defined stimuli-responsive diblock copolymers of poly(oligo(ethylene oxide) methyl ether methacrylate)-*b*-poly(2-(diisopropylamino)ethyl methacrylate) (POEOMA-*b*-PDPA) were successfully synthesized via supplemental activator and reducing agent (SARA) atom transfer radical polymerization (ATRP), using a slow and continuous feed of sodium dithionite (Na<sub>2</sub>S<sub>2</sub>O<sub>4</sub>). The high monomer conversion and the preservation of the polymer chain-end functionality allowed the direct synthesis of POEOMA-*b*-PDPA copolymers by one-pot polymerization reaction using an eco-friendly solvent mixture, very low copper catalyst concentrations and mild reaction conditions. The success of the synthesis was accessed by gel permeation chromatography (GPC) and the molecular structures were confirmed by <sup>1</sup>H nuclear magnetic resonance (<sup>1</sup>H NMR) spectroscopy. The pH-dependent self-assembly behavior of these brush-like copolymers in aqueous solutions was studied using potentiometric titration and dynamic light scattering (DLS) analysis. The self-assembly method was found to play an important role on the final morphology of the nanoaggregates. The influence of the volume fraction of DPA in the final self-assembled structure was investigated. Longer pH-responsive segments were found to originate larger self-assembled particles. The CMC of POEOMA-*b*-PDPA estimated by fluorescence spectroscopy, in aqueous medium was determined to be 1.0 x 10<sup>-3</sup> mg.mL<sup>-1</sup>. Due to the pH critical value of the DPA block, these block copolymers form stable nanostructures at physiological pH, but disassemble at pH < 6.2. This feature is particularly relevant for development of well-defined nanocarriers for cancer therapy that could take advantage of the well-known pH drop of the tumor tissues.

## 4.2. Introduction

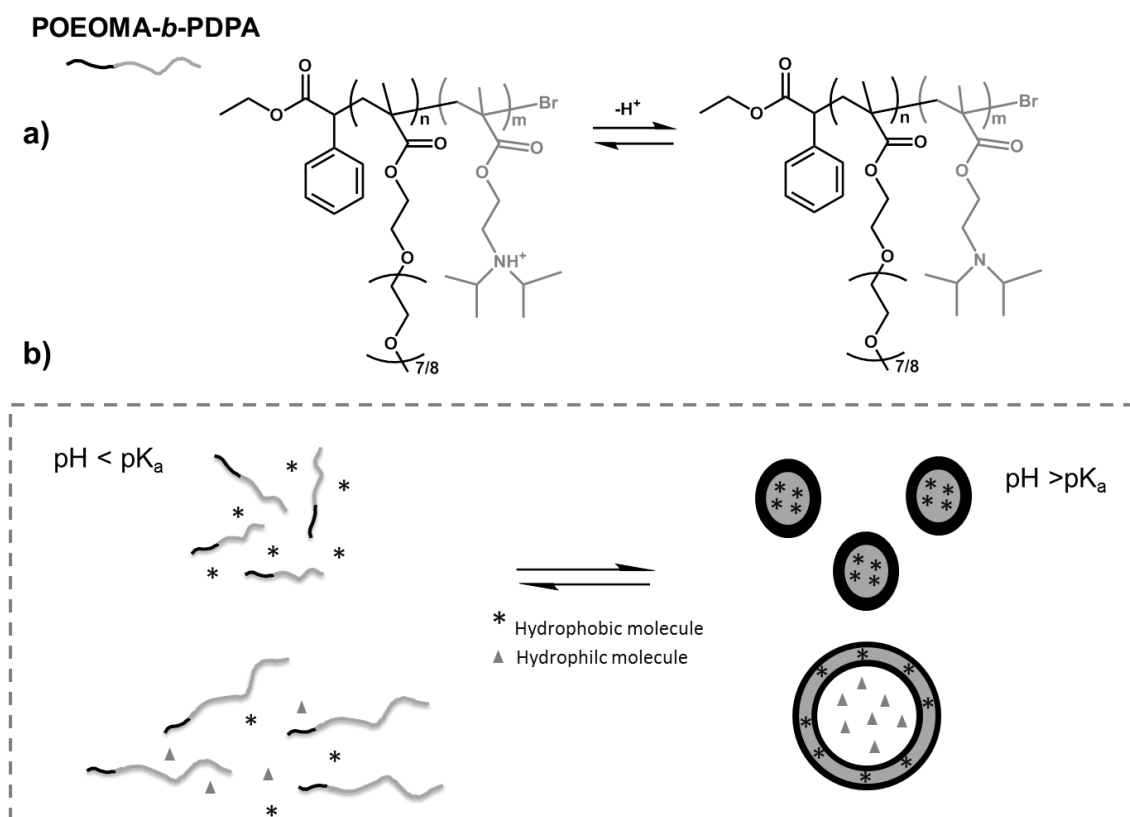
pH-responsive nanocarriers based on the self-assembly of block copolymers have been extensively reported as a potential approach for localized trigger release in drug delivery systems (DDS).<sup>1</sup> Such block copolymers are commonly composed by a pH-responsive segment and a permanent hydrophilic segment. Those structures are amphiphilic for pH values above the pK<sub>a</sub> of the pH-responsive segment and self-assemble into organized nanostructures, but become water soluble for lower pH values. This feature is of

particular interest in nanocarriers for biomedical applications, due to the pH drop inside some cellular compartments, such as endosomes or lysosomes (pH  $\approx$  5.6), in comparison to the physiological pH (pH  $\approx$  7.4). In the case of pH-responsive block copolymers, this slight pH variation could be enough to disassemble the nanostructure promoting the release of the encapsulated active compounds. Polyethylene glycol (PEG) is a highly hydrophilic polymer that confers biocompatibility and provides the nanocarriers with a shielding effect, avoiding its recognition by the immune system, which extends its systemic circulation.<sup>2</sup> Advances in reversible deactivation radical polymerization (RDRP) methods have turned possible the synthesis of a wide range of well-defined polymers, with controlled molecular weight (MW), narrow MW distributions, controlled composition, complex architectures and high chain-end functionality<sup>3, 4</sup> In RDRP methods, different strategies can be followed to incorporate PEG moieties into block copolymers: the use of linear PEG macroinitiators;<sup>5, 6</sup> or PEG reversible addition fragmentation transfer (RAFT) agents;<sup>7</sup> or through the use of PEG based monomers such as oligo(ethylene oxide) methyl ether methacrylates (OEOMA).<sup>8</sup> <sup>9</sup> Poly((oligo(ethylene oxide) methyl ether methacrylate)<sub>475</sub>) (POEOMA<sub>475</sub>) is a non-linear PEG, composed by methacrylate monomer units with a pendent short polyethylene glycol chains ( $\sim$  9 ethylene oxide units average). These structures are composed by PEG segments disposed perpendicularly to the polymer chain (brush-type PEG polymer) and present similar biological characteristics to the linear counterparts.<sup>10</sup> POEOMA<sub>475</sub> is water soluble (for temperatures below 90 °C<sup>11</sup>), non-cytotoxic and biocompatible polymer.<sup>12</sup> Due to their characteristics, POEOMA based copolymers have attracted great interest in several biomedical applications, including: surface modifications;<sup>13, 14</sup> coatings for superparamagnetic iron oxide nanoparticles;<sup>15</sup> biodegradable nanogels;<sup>16</sup> bioconjugates;<sup>17, 18</sup> and DDS.<sup>19, 20</sup> Rudolph and co-workers have found that the increase in OEOMA molar fraction in *N,N*-dimethylaminoethyl methacrylate (DMAEMA) copolymers (POEOMA-*co*-PDMAEMA) used as gene vector agents, stabilizes the nanocarriers, promotes its biocompatibility and prevents the gene vector aggregation.<sup>21</sup> In fact, the POEOMA block sequence plays an important role in the polymeric gene vector design. The nanoplexes composed by the complexation of genetic material with triblock copolymers of PDMAEMA-*b*-POEOMA-*b*-PDMAEMA exhibit very low cytotoxicity, but exhibit relatively lower gene expression.<sup>22</sup> A detailed RAFT polymerization of several pH- and temperature-responsive copolymers composed by poly(4-vinylpyridine)-*b*-POEOMA (P4VP-*b*-POEOMA) was reported by Dincer and

co-workers,<sup>23</sup> which studied its ability to form different micellar structures depending on the block copolymer composition and solution characteristics.

The tertiary amine methacrylate-based block copolymers are one of the most promising pH-responsive polymers for biomedical applications, due to the possibility of tuning their solution hydrophilic/hydrophobic transition (pK<sub>a</sub>) around the physiological pH.<sup>24</sup> Poly(2-(diisopropylamino)ethyl methacrylate) (PDPA) is a pH-responsive polymer with a pK<sub>a</sub> value around 6.2.<sup>25, 26</sup> Several PEG-*b*-PDPA copolymers have been proposed for different biomedical applications such as nanocarriers for cancer therapy,<sup>27-29</sup> non-viral gene delivery systems,<sup>30, 31</sup> or tunable pH-responsive fluorescent nanoparticles for both *in vitro*<sup>32, 33</sup> and *in vivo*<sup>34</sup> studies. The entrapment of superparamagnetic iron oxide nanoparticles (SPIONs) extended the range of applications of PEG-DPA based micelles to diagnosis imaging systems.<sup>35</sup>

Despite the enormous potential of the PDPA for biomedical applications, the scarce literature available dealing with the controlled synthesis of this polymer involve the use of unattractive reaction conditions, such as: toxic organic solvents, multi-step and laborious reaction procedures<sup>36, 37</sup> and high concentrations of copper catalyst.<sup>25, 26, 38</sup> In Chapter 3 and Chapter 4, an eco-friendly and inexpensive system based on SARA ATRP was developed, that allows the controlled polymerization of DPA using mixtures of isopropanol (IPA)/water, residual amounts of soluble copper at 40 °C.<sup>39, 40</sup> In this Chapter, it is proposed the use of the SARA ATRP system using the slow and continuous feed of Na<sub>2</sub>S<sub>2</sub>O<sub>4</sub> for the development of block copolymers composed by POEOMA and PDPA (Scheme 4.1). The block copolymers POEOMA-*b*-PDPA were synthesized through a one-pot polymerization from POEOMA macroinitiators in the presence of trace amounts of copper. Due to the pH-responsiveness of DPA segments, it is expected that POEOMA-*b*-PDPA copolymers self-assemble into organized nanostructures for application as pH-responsive DDS (Scheme 4.1).



**Scheme 4.1:** a) Chemical structure of the POEOMA-*b*-PDPA copolymer synthesized by SARA ATRP and b) illustration of the proposed self-assembly mechanism of the POEOMA-*b*-PDPA copolymers in aqueous media, for  $\text{pH} > \text{pK}_a$ .

## 4.3. Experimental Section

### 4.3.1. Materials

2-(Diisopropylamino)ethyl methacrylate (DPA) (97%, Scientific Polymer Products Inc.), oligo(ethylene oxide) methyl ether methacrylate (OEOMA<sub>475</sub>) (99%, average molecular weight 475, Aldrich) was purified by passing over a column filled with basic alumina to remove inhibitor. Sodium dithionite (Na<sub>2</sub>S<sub>2</sub>O<sub>4</sub>) (85%, ACROS Organics), copper(II) bromide (Cu<sup>II</sup>Br<sub>2</sub>) (99.999%, Aldrich), ethyl  $\alpha$ -bromophenyl acetate (EBPA) (97%, Alfa Aesar), *N*-phenyl-1-naphthylamine (NPN) (98%, Sigma-Aldrich), water (HPLC grade, Fisher Scientific), isopropanol (IPA) (ACS grade, Fisher Scientific), tetrahydrofuran (THF) (ACS grade, Fisher Scientific), deuterated chloroform (CDCl<sub>3</sub>) (99.8%, Cambridge Isotope Laboratories) were used as received. Tris(2-(dimethylamino)ethyl)amine (Me<sub>6</sub>TREN) was synthesized as reported in the literature<sup>41, 42</sup>. Purified water (Milli-Q<sup>®</sup>, Millipore, resistivity 18M $\Omega$ .cm) was obtained by reverse osmosis.

### 4.3.1. Characterization

A KDS Scientific, Legato 101 syringe pump was used for continuous feeding polymerizations.

The number-average MW ( $M_{n,GPC}$ ) and dispersity ( $D$ ) of the synthesized polymers were determined by gel permeation chromatography (GPC). The GPC system used a Waters 515 HPLC pump and a Waters 2414 refractive index detector using PSS columns (Styrogel 10<sup>2</sup>, 10<sup>3</sup>, 10<sup>5</sup> Å) with tetrahydrofuran (THF) containing 10 mM LiTf<sub>2</sub>N and 10 mM 1-butylimidazole as the eluent, at a flow rate of 1 mL.min<sup>-1</sup> at 35 °C.<sup>43</sup> The GPC samples were prepared in THF with diphenyl ether as the internal standard and filtered through a polytetrafluoroethylene (PTFE) membrane with 0.2  $\mu$ m pores before injection.

The <sup>1</sup>H nuclear magnetic resonance (NMR) spectra were recorded on a Bruker Avance III 400 MHz spectrometer, with a 5 mm TXI triple resonance detection probe, in CDCl<sub>3</sub> with tetramethylsilane (TMS) as an internal standard. The conversion was determined

by integration of monomer and polymer peaks using MestReNova software version: 6.0.2-5475.

Dynamic light scattering (DLS) measurements were performed on a Malvern Instrument Zetasizer Nano-ZS (Malvern Instruments Ltd., UK). The particle size distribution (PSD) (in intensity), average hydrodynamic particle size average (z-average) and polydispersity index (PDI) were determined with Zetasizer 7.03 software. Measurements were made at 25 °C and using a backward scattering angle of 173°. The samples were filtered before measurements through a 0.45 µm pore size PET filter (Chromafil® PET, Macherey-Nagel). At least three measurements were taken for each sample. Zeta-potential measurements were performed using a Zetasizer Nano-ZS (Malvern Instruments Ltd.), coupled to laser Doppler electrophoresis and determined using a Smoluchovski model.

The residual copper content in the block copolymers was evaluated by atomic absorption spectroscopy (AAS). AAS was performed on a Perkin Elmer (model 3300, USA). The block copolymers were dissolved in a 0.1 M HCl solution (5.0 mg.mL<sup>-1</sup>) and the pH of the solution was adjusted to 5. At least five measurements were taken for each sample.

Transmission electron microscopy (TEM) was used to observe the size and morphology of the nanoaggregates prepared with the different copolymers. The aqueous dispersion was deposited onto a formvar-carbon-coated copper grid and negatively stained with uranyl acetate aqueous solution (1% wt). The samples were examined using a Jeol JEM 1400 transmission electron microscope (Germany). Images were digitally recorded using a Gatan SC 1000 ORIUS CCD Camera (Warrendale, USA).

Fluorescence studies were performed using a Perkin Elmer (LS 45) fluorescence spectrophotometer. For the measurements, 2.0 mL of solution was placed in a 10 mm<sup>2</sup> quartz cell. An excitation wavelength of 550 nm was used and the emission spectra were recorded in the 575-750 nm wavelength range at a scan rate of 500 nm.min<sup>-1</sup>.

### 4.3.2. Procedures

#### Synthesis of a POEOMA-*b*-PDPA block copolymer.

A mixture of CuBr<sub>2</sub> (2.58 mg, 11.5 μmol), Me<sub>6</sub>TREN (5.31 mg, 23.1 μmol) and water (125 μL) was placed in a Schlenk tube reactor that was sealed by using a rubber septa. Na<sub>2</sub>S<sub>2</sub>O<sub>4</sub> (4.72 mg, 23.1 μmol) and a mixture of OEOMA (1.01 g, 2.31 mmol) and EBPA (28.03 mg, 0.12 mmol) in IPA (4.74 mL) (previously bubbled with nitrogen for about 15 minutes) was added to the reactor and frozen in liquid nitrogen. The reaction mixture was deoxygenated by three freeze-pump-thaw cycles and purged with nitrogen. The additional Na<sub>2</sub>S<sub>2</sub>O<sub>4</sub> aqueous solution (125 μL, 185 mM) was slow feed into the reaction mixture using a syringe pump at a feed rate 87 nL.min<sup>-1</sup> (16.1 nmol.min<sup>-1</sup>). The polymerization proceeded for 12h at 25 °C (87% conversion,  $M_{n,th} = 8.570 \times 10^3$ ,  $M_{n,GPC} = 11.75 \times 10^3$ ,  $\mathcal{D} = 1.18$ ). After that, the DPA (1.23 g, 5.76 mmol), previously bubbled with nitrogen for about 15 minutes, was added and allowed to polymerize for 12h (89% conversion,  $M_{n,th} = 18.06 \times 10^3$ ,  $M_{n,GPC} = 23.20 \times 10^3$ ,  $\mathcal{D} = 1.29$ ). The final POEOMA-*b*-PDPA copolymer was purified by dialysis and obtained as a transparent viscous solid.

#### Self-assembly of POEOMA-*b*-PDPA copolymers.

The self-assembled nanostructures were carried out following two different methods: the titration method<sup>25</sup> or the solvent exchange method.<sup>27</sup> For titration method, the self-assembly was induced by the pH change. The block copolymer was completely dissolved into 0.1 M HCl solution and then the pH of the solution was slowly increased by adding aliquots of 0.1 M NaOH solution. The final block copolymer concentration was adjusted to 1.0 mg.mL<sup>-1</sup> with water. For the solvent exchange method, the block copolymer was firstly dissolved in THF at a concentration of 10 mg.mL<sup>-1</sup>. 500 μL of the block copolymer solution were then added drop-wise to 5 mL of Milli-Q water at basic pH (~8), under vigorous stirring. The sample was left overnight at room temperature, under stirring to evaporate the organic solvent and stabilize the nanostructures. This stock polymer solution with concentration 1.0 mg.mL<sup>-1</sup> was used in the subsequent studies for nanoparticles size and morphology, DLS and TEM.

#### Potentiometric titration of POEOMA-*b*-PDPA copolymers.

The POEOMA-*b*-PDPA copolymer (50 mg) was dissolved in 5 mL 0.1 M HCl solution and diluted to a concentration of 2 mg.mL<sup>-1</sup> with Milli-Q water. The pH titration was

carried out at 25 °C, by adding small volumes (50-200  $\mu\text{L}$ ) of 0.02 M NaOH solution under stirring. The pH increase, in the range of 2 to 11, was monitored as a function of the total added volume of NaOH ( $V_{\text{NaOH}}$ ). The pH values were measured using a Crison Basic 20 pH meter (Crison, Allela, Spain). For the measurements of the hydrodynamic diameter ( $D_h$ ) by DLS along the titration experiment, 1 mL of solution in a specific pH point was taken and filtered through a 0.45  $\mu\text{m}$  PET filter (Chromafil<sup>®</sup> PET, Macherey-Nagel).

#### **Determination of the critical micelle concentration.**

Critical micelle concentration (CMC) of POEOMA-*b*-PDPA copolymers was measured in water at pH 7.4 using the fluorescent probe *N*-phenyl-1-naphthylamine (NPN).<sup>44</sup> POEOMA-*b*-PDPA stock solutions (2.0  $\text{mg}\cdot\text{mL}^{-1}$ ) were prepared by dissolving the copolymer into 0.1M HCl solutions and then slowly adjust the solution pH to 7.4 by adding aliquots of 0.1 M NaOH solution. Several polymer solutions (4 mL) with concentrations in the range  $1.0 \times 10^{-2}$  to  $5.0 \times 10^{-5}$   $\text{mg}\cdot\text{mL}^{-1}$  were prepared from the stock solutions, adjusting the final volume with water. 10  $\mu\text{L}$  of NPN stock solution ( $2.0 \times 10^{-4}$  M) in ethanol were added to the copolymer solutions. The solutions were left to stabilize at room temperature overnight, under magnetic stirring, to allow the evaporation of ethanol and to reach the solubilization equilibrium between NPN and the copolymer. Aqueous solutions without copolymer were used as control. The final concentration of NPN in the sample was  $5.0 \times 10^{-7}$  M. The NPN fluorescence emission after the excitation at  $\lambda = 356$  nm was recorded using a fluorimeter. The maximum fluorescence intensity of NPN was measured as a function of polymer concentration.



## 4.4. Results and Discussion

### 4.4.1. Synthesis and characterization of POEOMA-*b*-PDPA block copolymers

The literature reports concerning the synthesis of copolymers of POEOMA and PDPA is very scarce. Random copolymers of PEOMA<sub>360</sub> and PDPA were synthesized by conventional free radical polymerization (FRP) ( $M_n \sim 22.0 \times 10^3$ ,  $1.35 < D < 1.78$ ).<sup>45</sup> The synthesis of the POEOMA-*b*-PDPA block copolymers was reported for the first time by Hu *et al.* using RAFT polymerization.<sup>7</sup> The authors started by the synthesis of a macro-RAFT agents of PDPA that was further used for the polymerization of the POEOMA block. This multi-step approach and the need of purifying the first block possess several difficulties that compromise the stringent control over the block copolymers. This fact was evidenced by the  $D$  of the block copolymer above 1.4. A similar strategy was reported by Lomas and co-authors<sup>31</sup> but in this case using a POEOMA macro-RAFT agent. The polymerization rate was low even at 70 °C, and the block copolymers were obtained as red viscous solid due to the use of 2-cyanoprop-2-yl dithiobenzoate as initial RAFT agent. In this case, post-modification procedures are required to avoid the toxicity associated with the dithiobenzoate moiety presented in the polymer chain-end.

Amongst RDRP methods, SARA ATRP stands out as an efficient method for the preparation of well-defined (co)polymers under mild reaction conditions and reduced concentrations of copper catalyst.<sup>46, 47</sup> Na<sub>2</sub>S<sub>2</sub>O<sub>4</sub> have been reported as particularly effective SARA agent for acrylates and methacrylates.<sup>39, 48, 49</sup>

In this work, well controlled POEOMA-*b*-PDPA block copolymers with different compositions and molecular weights were synthesized through a one-pot polymerization reaction, using Na<sub>2</sub>S<sub>2</sub>O<sub>4</sub> as SARA agent. The first monomer, OEOMA was polymerized through SARA ATRP using a slow feeding of Na<sub>2</sub>S<sub>2</sub>O<sub>4</sub> (16.1 nmol.min<sup>-1</sup>), in a mixture IPA/water [95/5 (v/v)]. The living features of the synthesized polymer, allowed the further chain extension using DPA as the second monomer via one-pot procedure. DPA was injected into the reaction mixture when the first polymerization reached high monomer conversion (~ 90 %). The feeding conditions were kept during both steps of the synthesis and no additional CuBr<sub>2</sub> catalyst was added. The success of the block copolymer synthesis was confirmed by a clear shift of the GPC traces of the POEOMA

macroinitiator towards high MWs (Figure 4.1).

The robustness of the catalytic system enabled the synthesis of different block copolymers that are summarized in Table 4.1.

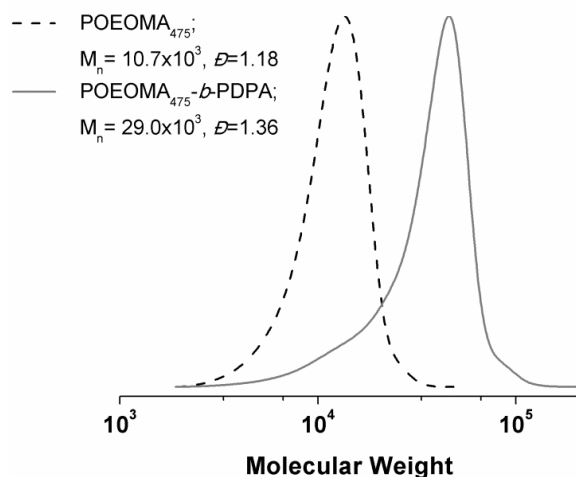


**Figure 4.1:** GPC chromatographs of the POEOMA before (dash line) and after the chain extension with DPA, POEOMA-*b*-PDPA (solid line). Reaction conditions:  $[OEOMA]_0/[EBPA]_0/[Na_2S_2O_4]_0/[CuBr_2]_0/[Me_6TREN]_0=30/1/0.2/0.1/0.2$  (molar),  $[OEOMA] = 18$  wt %, in 6 mL of IPA/H<sub>2</sub>O = 95/5 (v/v) and slow feeding of Na<sub>2</sub>S<sub>2</sub>O<sub>4</sub> solution (16 nmol.min<sup>-1</sup>), 25 °C;  $[DPA]_0/[POEOMA]=100/1$  (molar).

**Table 4.1:** List of copolymers prepared by SARA ATRP with Na<sub>2</sub>S<sub>2</sub>O<sub>4</sub> by one-pot polymerization reaction. Reaction conditions: [OEOMA]<sub>0</sub>/[EBPA]<sub>0</sub>/[Na<sub>2</sub>S<sub>2</sub>O<sub>4</sub>]<sub>0</sub>/[CuBr<sub>2</sub>]<sub>0</sub>/[Me<sub>6</sub>TREN]<sub>0</sub> = DP/1/0.2/0.1/0.2 (molar), OEOMA 18wt%, IPA/H<sub>2</sub>O =95/5 (v/v) and slow feeding of Na<sub>2</sub>S<sub>2</sub>O<sub>4</sub> solution (16 nmol.min<sup>-1</sup>), 40 °C.

Copolymer <sup>f</sup>	1 <sup>st</sup> block (POEOMA)			POEOMA- <i>b</i> -PDPA				
	<i>M</i> <sub>n,th</sub>	<i>M</i> <sub>n,GPC</sub>	<i>D</i> <sup>b</sup>	<i>M</i> <sub>n,th</sub>	<i>M</i> <sub>n,GPC</sub>	<i>D</i> <sup>b</sup>	Cu <sub>res</sub> (wt%) <sup>c</sup>	ΦPDPA <sup>e</sup>
	x10 <sup>3a</sup>	x10 <sup>3b</sup>		x10 <sup>3a</sup>	x10 <sup>3b</sup>			
POEOMA <sub>25</sub> - <i>b</i> -PDPA <sub>48</sub>	14.60	13.24	1.18	22.46	27.00	1.33	0.00072	0.44
POEOMA <sub>17</sub> - <i>b</i> -PDPA <sub>45</sub>	8.57	11.75	1.18	18.06	23.20	1.29	0.00214	0.46
POEOMA <sub>18</sub> - <i>b</i> -PDPA <sub>91</sub>	8.60	10.70	1.18	25.35	28.95	1.36	0.00228	0.69
POEOMA <sub>10</sub> - <i>b</i> -PDPA <sub>48</sub>	8.50	9.72	1.17	14.36	22.17	1.5	0.005	0.66

<sup>a</sup> Determined by <sup>1</sup>H NMR; <sup>b</sup> determined by GPC measurement using THF as eluent. <sup>c</sup> residual copper content determined by AAS; <sup>d</sup> determined by pH titration experiments in water at 25°C; <sup>e</sup> volume fraction of DPA, <sup>f</sup> the subscripts indicate the mean degrees of polymerization (DP) of each block determined from the monomer conversion by <sup>1</sup>H NMR.

The slow and continuous fed of Na<sub>2</sub>S<sub>2</sub>O<sub>4</sub> to the reaction mixture allows the polymerization to be carried out in the presence of low copper catalyst concentration and therefore simplifies significantly enormously the further purification procedures.<sup>39</sup> The residual copper content in the final block copolymers, determined by elemental analysis, was in range of 7.2 x 10<sup>-4</sup> to 5.0 x 10<sup>-3</sup> wt %. Such differences were related to the different target degree of polymerization (DP) of the first segment (POEOMA), where higher DP values lead to lower amounts of soluble copper in the reaction mixture.

The chemical structure of the POEOMA-*b*-PDPA block copolymer was confirmed by <sup>1</sup>H NMR spectroscopy (Figure 4.2). The peaks observed at 4.07 ppm (**g**, -OCH<sub>2</sub>CH<sub>2</sub>-), 3.64 ppm (**h**, **i** and **j**, -CH<sub>2</sub>-(CH<sub>2</sub>CH<sub>2</sub>O)<sub>n</sub>-) and 3.37 ppm (**k**, -OCH<sub>3</sub>) correspond to the characteristic proton signals of POEOMA,<sup>50</sup> while the peaks observed at 3.87 ppm (**n**, -OCH<sub>2</sub>CH<sub>2</sub>-), 3.01 ppm (**p**, -(CH-N)<sub>2</sub>-), 2.66 ppm (**o**, -CH<sub>2</sub>CH<sub>2</sub>N-) are in agreement with the expected PDPA chemical structure.<sup>39</sup> The characteristic peaks of the methylene protons belonging to copolymer backbone were identified at 1.8-1.9 ppm (**e**, **l**, -CH<sub>2</sub>- of the polymer backbone) and the resonances at 1.0 ppm correspond to both methacrylic groups in the polymer backbone (**f** and **m**) and the characteristic methyl groups of

PDPA (**q**,  $-\text{CH}(\text{CH}_3)_2$ ). It is also possible to identify the signal from the proton (**c**) of the initiator fragment ( $-\text{CH}$ ) at 5.00 ppm as well as the protons from the aromatic group (**d** and **d'**) at 6.97 and 7.21 ppm, respectively. The remaining signals from the initiator, the signals from the methylene group (**b**) ( $-\text{CH}_2$ ) and the terminal methyl group (**a**) ( $-\text{CH}_3$ ), are overlapped with other signals from the polymer.

Despite the identification of the signal from the proton (**c**) of the initiator fragment ( $-\text{CH}$ ) at 5.00 ppm, in the  $^1\text{H}$  NMR spectrum of the final block copolymers, the poor signal to noise ratio hampered the accurate calculation of  $M_{n,\text{NMR}}$ . The  $^1\text{H}$  NMR of the pure block copolymer allowed the determination of the DPA volume fraction ( $\Phi_{\text{DPA}}$ ), from the ratio  $(I_{\text{o}}/2)M_{\text{DPA}} / [(I_{\text{o}}/2)M_{\text{DPA}} + (I_{\text{k}}/3)M_{\text{OEOMA}}]$ , with  $M_{\text{DPA}}$  and  $M_{\text{OEOMA}}$  the molecular mass of DPA and OEOMA monomers respectively, assuming that the polymer density is equal to  $1.0 \text{ g mL}^{-1}$  (Table 4.1).<sup>51</sup> For that purpose, the characteristics peaks from PDPA at 2.66 ppm (**o**,  $-\text{CH}_2\text{CH}_2\text{N}-$ ) and from POEOMA at 3.37 ppm (**k**,  $-\text{OCH}_3$ ) were used. The  $\Phi_{\text{DPA}}$  value is close to the volume fraction determined from each monomer conversion,  $\text{DP}_{\text{DPA}}M_{\text{DPA}} / (\text{DP}_{\text{DPA}}M_{\text{DPA}} + \text{DP}_{\text{OEOMA}}M_{\text{OEOMA}})$ .

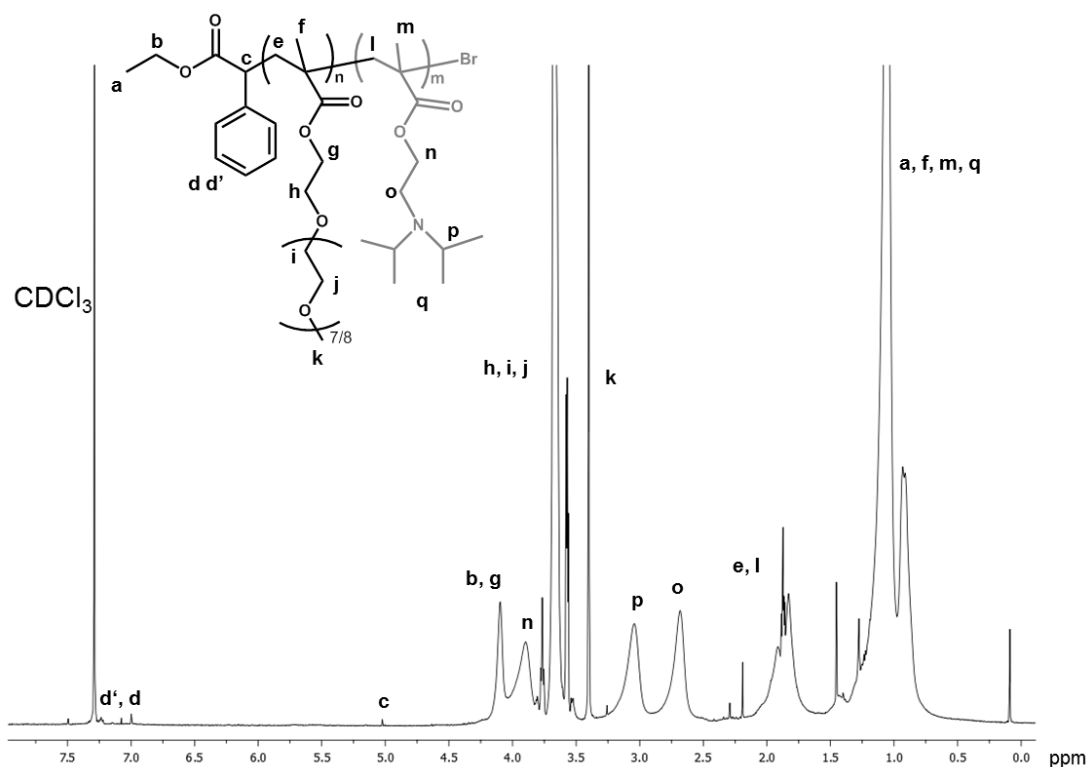


**Figure 4.2:**  $^1\text{H}$  NMR spectrum of POEOMA-*b*-PDPA copolymer in  $\text{CDCl}_3$ ,  $M_{n,\text{GPC}} = 23.2 \times 10^3$ ;  $\mathcal{D} = 1.29$

#### 4.4.2. Solution behavior of POEOMA-*b*-PDPA copolymers – pH titration

In this work, two block copolymers, POEOMA<sub>17</sub>-*b*-PDPA<sub>45</sub> and POEOMA<sub>18</sub>-*b*-PDPA<sub>91</sub> were studied in detail. Both copolymers present a brush type hydrophilic segment of POEOMA with the same length and two distinct sizes of DPA block. The length of the hydrophilic segment was chosen taking in consideration the MW of similar block copolymers described in the literature.<sup>51</sup>

The acid-base behavior of the block copolymers was evaluated by titration using as starting conditions a 0.1 M HCl solution. The structural changes of the block copolymers dependent of the pH were evaluated by DLS analysis.

Potentiometric titration curves of the block copolymers in water and at room temperature were obtained for both copolymers, by plotting the solution pH against the volume of added NaOH ( $V_{\text{NaOH}}$ ). The acidic dissociation constants ( $K_a$ ) were measured from the midpoint of the plateau region of each curve.<sup>52</sup> The pKa values for the block copolymers for POEOMA<sub>17</sub>-*b*-PDPA<sub>45</sub> and POEOMA<sub>18</sub>-*b*-PDPA<sub>91</sub> (Figure 4.3) were found to be 6.28 and 6.25, respectively. At acidic pH the tertiary amine groups of the DPA block are totally protonated. The close values of pKa obtained between the two block copolymers suggests that in the range of PDPA block length used, this segment has no major effect on the final value of pKa. Both polymers cause a buffer effect in the medium around the pKa. These results are in agreement with the pKa values from similar block copolymers described in the literature.<sup>7, 53</sup> Nevertheless, it is important to notice that the value of the pKa of the PDPA based copolymers slightly increases with an increase of the ionic strength of the solution (e.g., physiological saline solutions).<sup>7</sup>

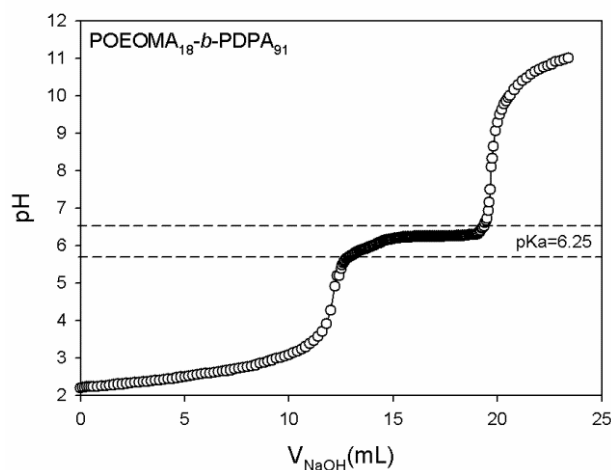


**Figure 4.3:** Titration curve of POEOMA<sub>18</sub>-*b*-PDPA<sub>91</sub> copolymer with NaOH 0.02M at 25°C.

The degree of copolymer ionization ( $\alpha$ ) as a function of solution pH was estimated using the Henderson-Hasselbach equation (Equation 4.1) and the pKa values obtained from potentiometric titrations. The results are plotted in Figure 4.4. At pH 6.2 the comparison of the ratio of protonated to deprotonated tertiary amine groups in both copolymers was negligible.

$$\alpha = \frac{1}{1+10^{(pH-pKa)}} \quad (\text{Equation 4.1})$$

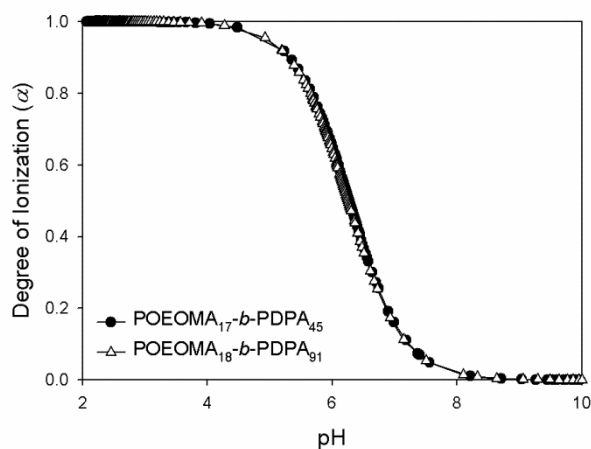


**Figure 4.4:** Degree of copolymer ionization as a function of solution pH, determined from equation 4.1.

Due to the pH dependent solubility of the PDPA segment, nanoaggregates of POEOMA-*b*-PDPA can be easily prepared directly in water by adjusting the solution pH, avoiding the use of any co-solvent.<sup>25</sup> For acidic pH values, the PDPA segment is fully protonated turning the block copolymer completely soluble. The tertiary amines in the PDPA segment are acting as an ionizable hydrophobic blocks. By increasing the solution pH, those amine groups become gradually deprotonated and the hydrophilicity of the PDPA block decreases progressively. For solution pH above the pKa, the DPA block is completely water insoluble and shrinks, leading to the self-assembly of the copolymer. In order to avoid the polymer precipitation, the increase of the solution pH should be gradual. The pH-induced self-assembly was monitored by DLS analysis. The variation of average hydrodynamic diameter ( $D_h$ ) of POEOMA-*b*-PDPA copolymers in aqueous solutions as a function of the pH is presented in Figure 4.5 (see Annex C, Table

C.1, for detailed information) and the solution behavior of the POEOMA-*b*-PDPA diblock copolymer, determined by DLS studies at 25 °C, is plotted in Figure 4.6.

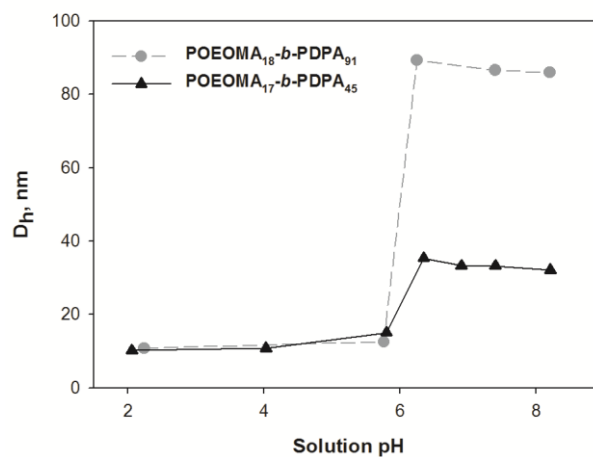


**Figure 4.5:** Variation of hydrodynamic diameter ( $D_h$ ) of POEOMA-*b*-PDPA copolymer in aqueous solutions as a function of solution pH, at 25 °C (the initial copolymer concentration at pH 2 was 2.0 mg.mL<sup>-1</sup>).

Below pH = 6, the copolymer chains were completely dissolved (unimers), as indicated by the small hydrodynamic size (~ 11 nm). The DLS scattering intensity was very low and almost no signal was detected. From Figure 4.5, it is possible to observe the sharp transition in the  $D_h$  for pHs values above the polymer pKa, revealing the formation of the self-assembly aggregates. At these pH values, the DLS results show a single size distribution (Figure 4.6) with a high scattering intensity. The results show that longer PDPA segments lead to larger self-assembled aggregates. POEOMA<sub>17</sub>-*b*-PDPA<sub>45</sub> form nanostructures with an  $D_H$ , of  $33 \pm 20$  nm, whereas the  $D_H$  increases up to  $86 \pm 34$  nm, for a longer PDPA segment. The DLS results also suggest that the pH-responsive behavior of the POEOMA-*b*-PDPA copolymers was reversible. By reducing the solution pH to 5.8 (below the pKa), the block copolymer becomes soluble and no particles were observed (Figure 4.6). It is known that the balance between the hydrophobic and hydrophilic segments in the block copolymers dictates the nanoparticles formation and its thermodynamic stability.<sup>54</sup>

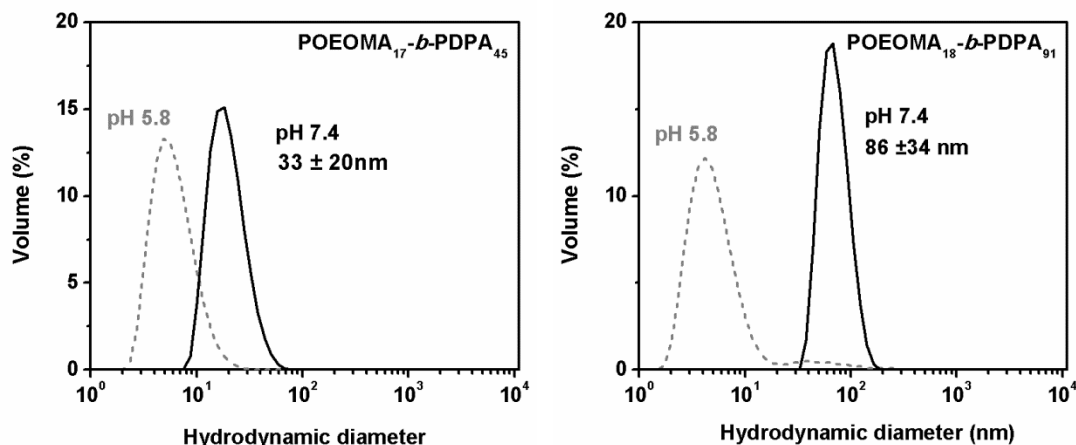


**Figure 4.6:** Size distribution profile of aqueous block copolymer dispersions, as determined by DLS at 25 °C. Nanostructures formed at pH 7.4 (solid line) and the block copolymer unimers at acidic conditions (dashed line) (copolymer concentration ~ 1 mg.mL<sup>-1</sup>).

As expected, these results corroborate the fact that the resultant morphology of the self-assemblies from amphiphilic linear diblock copolymers is mainly defined by the volume fraction ( $\Phi$ ) of the hydrophobic segment. Other factors such as the architecture of the blocks and the chemical nature of the repeating units have also an important role in the morphology of the resultant self-assembly aggregates.<sup>55</sup> In general, for  $0.3 < \Phi_{\text{hydrophobic segment}} < 0.70$ , the formation of spherical micelles are favorable, while for  $\Phi_{\text{hydrophobic segment}} > 0.70$  vesicles are preferable.<sup>54, 56</sup> The effect of the length of the PDPA block in the block copolymer of poly(2-(methacryloyloxy)ethyl phosphorylcholine)-*b*-PDPA (PMPC-*b*-PDPA) have been extensively studied. By varying the copolymer ratio between the hydrophilic and the hydrophobic segments, spherical micelles<sup>25, 51</sup> or vesicles<sup>57, 58</sup> were formed. Furthermore, recent studies suggest that the temperature of the solution, along with the length of the PDPA segment, have a major role in the morphology of the PDPA based self-assemblies.<sup>52</sup> Other factors such as the presence of salts or other solution additives can also affect the size and shape of polymer based nanoparticles.<sup>54</sup>

The stability of the colloidal aggregates of the POEOMA<sub>18</sub>-*b*-PDPA<sub>91</sub> was assessed by DLS in solution during several weeks (Figure 4.7). The results indicate that the nanostructures are stable for the time period considered. This observation could be



ascribed to the dense PEG based brushes that cover the surface of the nanostructures avoiding aggregation.

The DLS results of the self-assembled structures formed by the titration method, from similar block copolymers reported in the literature<sup>31</sup>, POEOMA<sub>26</sub>-*b*-PDPA<sub>50</sub> ( $M_{n,GPC} = 21.2 \times 10^3$ ,  $D = 1.18$ ) reveal a particle size distribution (PSD) in the range of 50 to 300 nm, but no details about the analysis (i.e.,  $D_h$  and PDI) were provided.

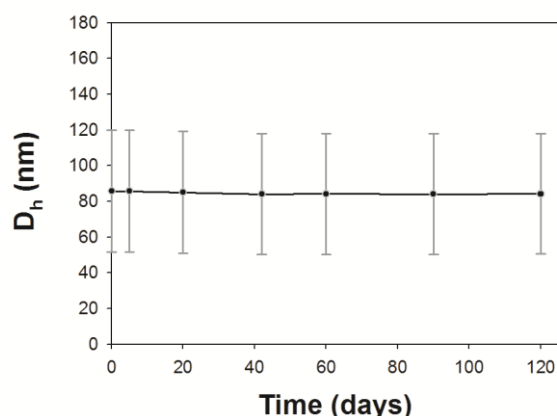


**Figure 4.7:** Hydrodynamic diameter ( $D_h$ ) of aqueous block copolymer dispersions at pH 8 after storage at room temperature for several weeks, as determined by DLS at 25°C. The error bars represent the standard deviation, according to the formula,  $PDI = (\sigma/D_h)^2$ .

The  $\zeta$  potential of polymers was determined to evaluate the charge of the PDPA based copolymers. As expected, the acidic solutions of block copolymers (pH = 3) present a positive  $\zeta$  potential value, around 26 mV due to the complete protonation of the PDPA block, while for pH > pKa, the  $\zeta$  potential of the block copolymer solution is close to zero (-1 mV). Similar  $\zeta$  potential values are reported in the literature.<sup>53</sup>

#### 4.4.3. Preparation of particles by solvent exchange method

The method used in the solution self-assembly of amphiphilic block copolymer may interfere with the particle size, PDI and morphology of the final aggregates.<sup>59</sup> Besides titration, another route to prepare self-assemble nanoparticles via self-assembly is the

so-called solvent exchange method (also named nanoprecipitation). In this method, the pure block copolymer was firstly dissolved in one organic solvent (THF) that is a thermodynamically good solvent for both blocks and is also miscible with water (non-solvent). A small volume of the organic solution is added to water (pH ~ 8), under stirring and the organic solvent is left to evaporate slowly to allow the formation of the nanoaggregates.

The particle size distributions of the obtained structures were determined by DLS, and the  $D_h$  and PDI are listed Table 4.2. Once again, the results suggest that the micelle size is mainly dictated by the length of the hydrophobic block. However, in this case, the copolymer with shorter DPA segment presents larger  $D_h$  in comparison to the results obtained for the self-assembly induced by titration. In fact, the slow increase of the pH of the solution promotes a continuous protonation of the tertiary amine groups of DPA, allowing the gradual organization of the block copolymer chains resulting in more compact self-assembled structures.

**Table 4.2:** Characteristics of the self-assembled structures formed in water at 25 °C, from the POEOMA-*b*-PDPA copolymers using two different self-assembly procedures (1.0 mg.mL<sup>-1</sup>).

Copolymer	pH chance method			Solvent exchange method		
	$D_h$ (nm) <sup>a</sup>	PDI	$\sigma$ (nm) <sup>b</sup>	$D_h$ (nm) <sup>a</sup>	PDI	$\sigma$ (nm) <sup>b</sup>
POEOMA <sub>17</sub> - <i>b</i> -PDPA <sub>45</sub>	33	0.36	20	71	0.29	38
POEOMA <sub>18</sub> - <i>b</i> -PDPA <sub>91</sub>	86	0.16	34	216	0.37	42

<sup>a</sup> mean value of the hydrodynamic diameter of the particle; <sup>b</sup> PDI width ( $\sigma$ ) determined using the equation:  $PDI=(\sigma/D_h)^2$ ;

Previous studies on the self-assembly induced by nanoprecipitation revealed that the polymer concentration as well as the nature of both solvents play an important role in the nanoparticle size and size distribution.<sup>60-62</sup> For these reasons, additional studies to optimize the self-assembly of the POEOMA-*b*-PDPA copolymers should be performed in order to obtain reproducible and monodisperse systems. This issue is of particular importance in the development of nanocarriers to entrap hydrophobic drugs. In this case, the drug is dissolved in the organic solution along with the polymer. The self-

assembly of the block copolymer is induced by the solvent exchange method and the drug is entrapped in the hydrophobic domains of the block copolymer.<sup>27</sup> On this matter, it is known that the loading capacity of the polymeric nanostructures is significantly affected by the specific interactions between the hydrophobic polymeric domain and the hydrophobic guest molecule.<sup>63</sup> For hydrophilic drugs, in which the drug is inside the inner aqueous compartment of the vesicular structures, the self-assembly of the block copolymer can be done by the titration method, since the drug is always soluble in water.

#### 4.4.4. TEM analysis of POEOMA-*b*-PDPA solution aggregates

The morphology of the self-assembled nanoparticles, obtained by the solvent exchange method, was evaluated by TEM. Figure 4.8 presents the TEM micrographs for the aggregates resulting from the self-assembly of the two POEOMA-*b*-PDPA copolymers. The results reveal that both block copolymers form spherical aggregates in water, for  $\text{pH} > \text{pKa}$  with diameter around 31 nm and in the range 160 to 180 nm for POEOMA<sub>17</sub>-*b*-PDPA<sub>45</sub> and POEOMA<sub>18</sub>-*b*-PDPA<sub>91</sub> respectively. The diameter of the nanoparticles estimated by TEM was in close agreement to the  $D_h$  values obtained by DLS for the POEOMA<sub>17</sub>-*b*-PDPA<sub>45</sub>, although larger aggregates were observed for the POEOMA<sub>18</sub>-*b*-PDPA<sub>91</sub>.

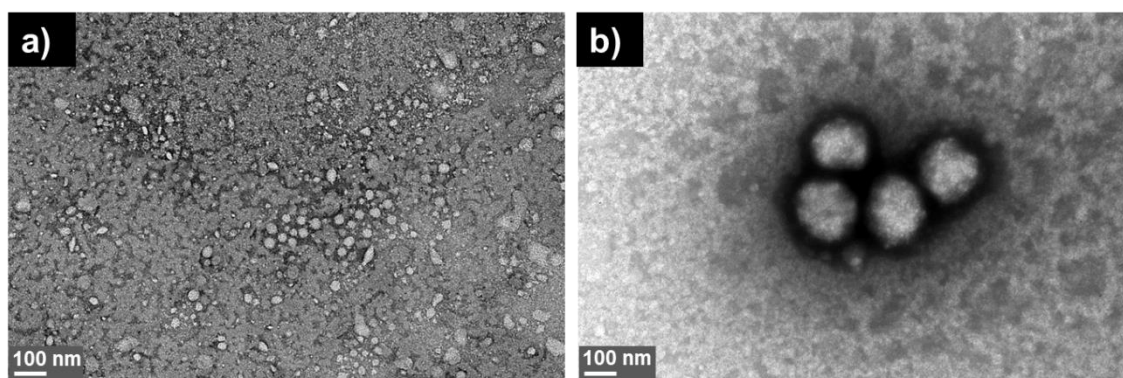


**Figure 4.8:** TEM micrographs, negatively stained with uranyl acetate, of self-assembled block copolymers of POEOMA-*b*-PDPA in water prepared by the solvent exchange method ( $1.0 \text{ mg}\cdot\text{mL}^{-1}$ ) of: a) POEOMA<sub>17</sub>-*b*-PDPA<sub>45</sub> and b) POEOMA<sub>18</sub>-*b*-PDPA<sub>91</sub> taken at a Mag. x 100 000.

#### 4.4.5. Critical micelle concentration

When designing block copolymers to be used as building blocks in a DDS, the critical micelle concentration (CMC) is one important parameter to ensure that the nanocarriers do not disassemble into unimers upon dilution in the blood stream, and to prevent the premature release of its content before reaching the target tissue. Fluorescence spectroscopy is a very sensitive technique to determine the CMC of amphiphilic block copolymers and in general, pyrene is the standard hydrophobic probe for the determination of the CMC.<sup>64, 65</sup> However, the resolution from the available UV-vis spectrometer was not enough to separate the intensity characteristic peaks of pyrene probe at 371 nm and 383 nm and thereby the fluorescence intensity ratio ( $I_3/I_1$ ) from which the CMC is determined, was not possible to calculate.<sup>66</sup> Therefore, the CMC value of the solution self-assembled nanostructures formed from POEOMA-*b*-PDPA samples was determined using an alternative fluorescence probe, the *N*-phenyl-1-naphthylamine (NPN) (Figure 4.9).<sup>67</sup>

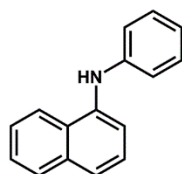


**Figure 4.9:** Chemical structure of *N*-phenyl-1-naphthylamine (NPN).

NPN molecule is uncharged at  $\text{pH} \geq 6$ , with reduced solubility in water. The fluorescence emission of the NPN in water is almost negligible, whereas it increases in apolar media, namely in the hydrophobic domains of the self-assembled structures. As shown in Figure 4.10(a), the fluorescence intensity of NPN varies depending in the surrounding environment, being almost negligible for very diluted block copolymer solutions, and well defined in the presence of the nanoparticles, when NPN is surrounded by an hydrophobic environment.

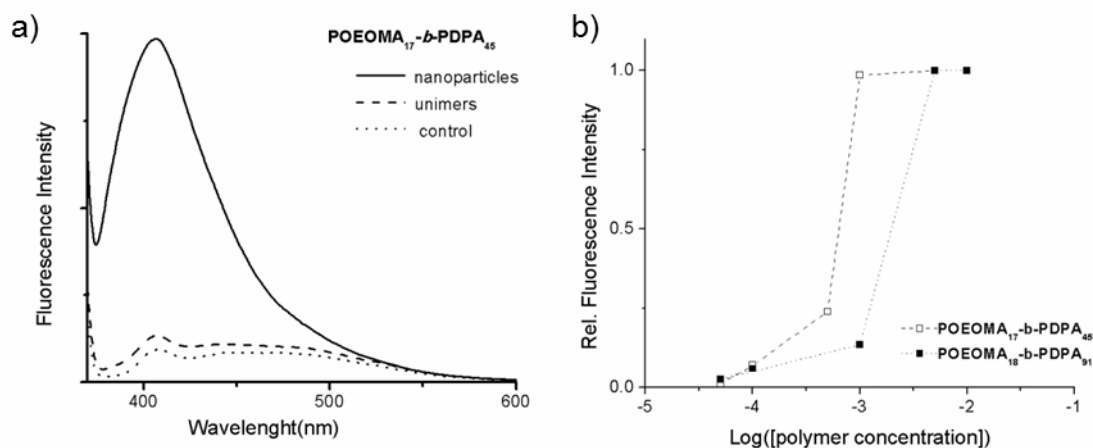


**Figure 4.10:** Fluorescence emission spectra of NPN in the presence of two different concentrations of copolymer solutions (a) and relative fluorescence intensity as a function of copolymer concentration for both POEOMA-*b*-PDPA copolymers ( $\text{mg}\cdot\text{mL}^{-1}$ ) (b).

Figure 4.10 (b) shows the NPN emission intensity versus the logarithm of the concentration of the block polymers. The NPN emission intensity increases rapidly with a slight increase of the block copolymer solution concentration, from  $0.5 \times 10^{-3}$  to  $1.0 \times 10^{-3} \text{ mg}\cdot\text{mL}^{-1}$ . The CMC is determined from the interception of the two straight lines that correspond to the free NPN in the aqueous environment (unimers) and the entrapped NPN within the hydrophobic domains of the nanoparticles (non-polar environment). The CMC of POEOMA<sub>17</sub>-*b*-PDPA<sub>45</sub> and POEOMA<sub>18</sub>-*b*-PDPA<sub>91</sub> was determined to be  $4.0 \times 10^{-4}$  and  $1.0 \times 10^{-3} \text{ mg}\cdot\text{mL}^{-1}$ , respectively. In comparison to low molecular weight surfactants, such as the sodium dodecyl sulfate (SDS) (CMC  $\sim 2.0 \text{ mg}\cdot\text{mL}^{-1}$ ) or even high molecular weight surfactants such as Tween 80<sup>®</sup> (CMC  $\sim 15.7 \times 10^{-3} \text{ mg}\cdot\text{mL}^{-1}$ ), the block copolymers CMC values are much lower which suggest that the presented macromolecules could be interesting candidates to prepare stable nanoaggregates for DDS applications.<sup>68</sup>

Analogous block copolymers reported by Hu and co-workers<sup>7</sup>, PDPA<sub>31</sub>-*b*-POEOMA<sub>29</sub> ( $M_{n,\text{GPC}} = 21.45 \times 10^3$ ,  $D = 1.4$ ), presented CMC values in the range of  $2.6 \times 10^{-3} \text{ mg}\cdot\text{mL}^{-1}$  for micelles with  $D_h = 27 \text{ nm}$ . Giacomelli and co-authors determined the CMC of PMPC<sub>30</sub>-*b*-PDPA<sub>30</sub> and PMPC<sub>30</sub>-*b*-PDPA<sub>60</sub> copolymers (determined by fluorescence spectroscopy using pyrene as a probe) to be  $25 \times 10^{-3}$  and  $14 \times 10^{-3} \text{ mg}\cdot\text{mL}^{-1}$ , respectively.<sup>51</sup> The copolymer with longer DPA segments have lower CMC value, that

could be related with the earlier segregation of the DPA units from the aqueous medium. However, a similar PMPC<sub>30</sub>-*b*-PDPA<sub>50</sub> copolymer functionalized with folic acid<sup>26</sup> presented a lower CMC of  $4.0 \times 10^{-3} \text{ mg.mL}^{-1}$ . In our case, the preliminary results reveal much lower CMC values. Even so, the probe used for the determination of the CMC was not the same as the one reported for similar copolymers, therefore a direct comparison may not be entirely valid. Furthermore, in our case, the copolymer with longer DPA block has slightly higher CMC values.

#### **4.5. Conclusions**

The SARA ATRP with the slow and continuous feed of Na<sub>2</sub>S<sub>2</sub>O<sub>4</sub> allowed the straightforward synthesis of POEOMA-*b*-PDPA copolymers via sequential monomer addition. The attractive reaction conditions of the system, such as the reduced amount of copper catalyst, the use of less toxic solvents, the high monomer conversions obtained and reasonably narrow MW turns it very convenient for the preparation of copolymers to be applied in the biomedical field. The presence of the pH-responsive PDPA block, enables the possibility to trigger the solution assembly/disassembly of the nanostructures, by changing the pH of the solution. Those pH-responsive POEOMA-*b*-PDPA copolymers form very stable nanoparticles at physiological pH. The size of the nanoaggregates can be controlled in the range 33 nm to 86 nm by an easy adjustment of the size of the PDPA segment. Also, by tuning the molecular weight of the DPA block, it is possible to control the size and morphology of the self-assembled structure. Those pH-responsive block copolymers could be a prospective candidate as smart nanocarriers for tumor targeting drug delivery since they present similar characteristics to the ones reported in the literature. Further studies to explore the physicochemical parameters associated with the POEOMA-*b*-PDPA self-assemblies and concerning the drug encapsulation efficiency and the drug release profiles should be performed. The results reported here open the possibility of using alkyne terminated initiators for SARA ATRP (following the strategy presented in Chapter 2), which will allow the further surface functionalization of the nanoparticles prepared with POEOMA-*b*-PDPA copolymers. Specific moieties can be used to promote the active targeting and enhance the efficiency of the therapeutics.

## 4.6. References

1. Onaca, O., R. Enea, D.W. Hughes, and W. Meier (2009). Stimuli-Responsive Polymersomes as Nanocarriers for Drug and Gene Delivery. *Macromolecular Bioscience*, 9(2): 129-139.
2. Brewer, E., J. Coleman, and A. Lowman (2011). Emerging Technologies of Polymeric Nanoparticles in Cancer Drug Delivery. *Journal of Nanomaterials*.
3. Kamigaito, M. (2011). Recent developments in metal-catalyzed living radical polymerization. *Polym J*, 43(2): 105-120.
4. Braunecker, W.A. and K. Matyjaszewski (2007). Controlled/living radical polymerization: Features, developments, and perspectives. *Progress in Polymer Science*, 32(1): 93-146.
5. Sant, V.P., D. Smith, and J.-C. Leroux (2004). Novel pH-sensitive supramolecular assemblies for oral delivery of poorly water soluble drugs: preparation and characterization. *Journal of Controlled Release*, 97(2): 301-312.
6. Yusa, S., M. Sugahara, T. Endo, and Y. Morishima). Preparation and characterization of a pH-responsive nanogel based on a photo-cross-linked micelle formed from block copolymers with controlled structure. *Langmuir* 2009, 25(9): 5258-65. doi: 10.1021/la803878s.
7. Hu, Y.Q., M.S. Kim, B.S. Kim, and D.S. Lee (2007). Synthesis and pH-dependent micellization of 2-(diisopropylamino)ethyl methacrylate based amphiphilic diblock copolymers via RAFT polymerization. *Polymer*, 48(12): 3437-3443.
8. Wang, Z.-K., D. Wang, H. Wang, J.-J. Yan, Y.-Z. You, and Z.-G. Wang (2011). Preparation of biocompatible nanocapsules with temperature-responsive and bioreducible properties. *Journal of Materials Chemistry*, 21(40): 15950-15956.
9. Chan, N., H.W. Jung, S.M. Noh, and J.K. Oh (2014). Functional amphiphilic oligo(ethylene oxide) methacrylate-based block copolymers: synthesis by an activator regenerated by electron transfer process for atom transfer radical polymerization and aqueous micellization. *Polymer International*, 63(5): 858-867.
10. Knop, K., R. Hoogenboom, D. Fischer, and U.S. Schubert (2010). Poly(ethylene glycol) in Drug Delivery: Pros and Cons as Well as Potential Alternatives. *Angewandte Chemie International Edition*, 49(36): 6288-6308.
11. Lutz, J.-F. (2008). Polymerization of oligo(ethylene glycol) (meth)acrylates: Toward new generations of smart biocompatible materials. *Journal of Polymer Science Part A: Polymer Chemistry*, 46(11): 3459-3470.

12. Lutz, J.-F., J. Andrieu, S. Üzgün, C. Rudolph, and S. Agarwal (2007). Biocompatible, Thermoresponsive, and Biodegradable: Simple Preparation of “All-in-One” Biorelevant Polymers. *Macromolecules*, 40(24): 8540-8543.
13. Hyun, J., H. Ma, Z. Zhang, T.P. Beebe Jr, and A. Chilkoti (2003). Universal Route to Cell Micropatterning Using an Amphiphilic Comb Polymer. *Advanced Materials*, 15(7-8): 576-579.
14. Chen, Y., D. Liu, Q. Deng, X. He, and X. Wang (2006). Atom transfer radical polymerization directly from poly(vinylidene fluoride): Surface and antifouling properties. *Journal of Polymer Science Part A: Polymer Chemistry*, 44(11): 3434-3443.
15. Lutz, J.-F., S. Stiller, A. Hoth, L. Kaufner, U. Pison, and R. Cartier (2006). One-Pot Synthesis of PEGylated Ultrasmall Iron-Oxide Nanoparticles and Their in Vivo Evaluation as Magnetic Resonance Imaging Contrast Agents. *Biomacromolecules*, 7(11): 3132-3138.
16. Oh, J.K., D.J. Siegwart, H.-i. Lee, G. Sherwood, L. Peteanu, J.O. Hollinger, K. Kataoka, and K. Matyjaszewski (2007). Biodegradable Nanogels Prepared by Atom Transfer Radical Polymerization as Potential Drug Delivery Carriers: Synthesis, Biodegradation, in Vitro Release, and Bioconjugation. *Journal of the American Chemical Society*, 129(18): 5939-5945.
17. Tao, L., G. Mantovani, F. Lecolley, and D.M. Haddleton (2004).  $\alpha$ -Aldehyde Terminally Functional Methacrylic Polymers from Living Radical Polymerization: Application in Protein Conjugation “Pegylation”. *Journal of the American Chemical Society*, 126(41): 13220-13221.
18. Reyes-Ortega, F., F.J. Parra-Ruiz, S.E. Averick, G. Rodriguez, M.R. Aguilar, K. Matyjaszewski, and J. San Roman (2013). Smart heparin-based bioconjugates synthesized by a combination of ATRP and click chemistry. *Polymer Chemistry*, 4(9): 2800-2814.
19. Yang, Y.Q., W.J. Lin, B. Zhao, X.F. Wen, X.D. Guo, and L.J. Zhang (2012). Synthesis and Physicochemical Characterization of Amphiphilic Triblock Copolymer Brush Containing pH-Sensitive Linkage for Oral Drug Delivery. *Langmuir*, 28(21): 8251-8259.
20. Yang, Y.Q., L.S. Zheng, X.D. Guo, Y. Qian, and L.J. Zhang (2011). pH-Sensitive Micelles Self-Assembled from Amphiphilic Copolymer Brush for Delivery of Poorly Water-Soluble Drugs. *Biomacromolecules*, 12(1): 116-122.
21. Üzgün, S., Ö. Akdemir, G. Hasenpusch, C. Maucksch, M.M. Golas, B. Sander, H. Stark, R. Imker, J.-F. Lutz, and C. Rudolph (2010). Characterization of Tailor-Made Copolymers of Oligo(ethylene glycol) Methyl Ether Methacrylate and N,N-Dimethylaminoethyl Methacrylate as Nonviral Gene Transfer Agents:



- Influence of Macromolecular Structure on Gene Vector Particle Properties and Transfection Efficiency. *Biomacromolecules*, 11(1): 39-50.
22. Yao, Y., D.-F. Feng, Y.-P. Wu, Q.-J. Ye, L. Liu, X.-X. Li, S. Hou, Y.-L. Yang, C. Wang, L. Li, and X.-Z. Feng (2011). Influence of block sequences in polymer vectors for gene transfection in vitro and toxicity assessment of zebrafish embryos in vivo. *Journal of Materials Chemistry*, 21(12): 4538-4545.
  23. Topuzogullari, M., V. Bulmus, E. Dalgakiran, and S. Dincer (2014). pH- and temperature-responsive amphiphilic diblock copolymers of 4-vinylpyridine and oligoethyleneglycol methacrylate synthesized by RAFT polymerization. *Polymer*, 55(2): 525-534.
  24. Hu, J., G. Zhang, Z. Ge, and S. Liu (2014). Stimuli-responsive tertiary amine methacrylate-based block copolymers: Synthesis, supramolecular self-assembly and functional applications. *Progress in Polymer Science*, 39(6): 1096-1143.
  25. Ma, Y.H., Y.Q. Tang, N.C. Billingham, S.P. Armes, A.L. Lewis, A.W. Lloyd, and J.P. Salvage (2003). Well-defined biocompatible block copolymers via atom transfer radical polymerization of 2-methacryloyloxyethyl phosphorylcholine in protic media. *Macromolecules*, 36(10): 3475-3484.
  26. Licciardi, M., Y. Tang, N.C. Billingham, and S.P. Armes (2005). Synthesis of novel folic acid-functionalized biocompatible block copolymers by atom transfer radical polymerization for gene delivery and encapsulation of hydrophobic drugs. *Biomacromolecules*, 6(2): 1085-1096.
  27. Giacomelli, F.C., P. Stepanek, C. Giacomelli, V. Schmidt, E. Jager, A. Jager, and K. Ulbrich (2011). pH-triggered block copolymer micelles based on a pH-responsive PDPA (poly[2-(diisopropylamino)ethyl methacrylate]) inner core and a PEO (poly(ethylene oxide)) outer shell as a potential tool for the cancer therapy. *Soft Matter*, 7(19): 9316-9325.
  28. Yu, P., H. Yu, C. Guo, Z. Cui, X. Chen, Q. Yin, P. Zhang, X. Yang, H. Cui, and Y. Li (2015). Reversal of doxorubicin resistance in breast cancer by mitochondria-targeted pH-responsive micelles. *Acta Biomaterialia*, 14: 115-124.
  29. Yu, H., Z. Xu, D. Wang, X. Chen, Z. Zhang, Q. Yin, and Y. Li (2013). Intracellular pH-activated PEG-b-PDPA wormlike micelles for hydrophobic drug delivery. *Polymer Chemistry*, 4(19): 5052-5055.
  30. Yu, H., Y. Zou, Y. Wang, X. Huang, G. Huang, B.D. Sumer, D.A. Boothman, and J. Gao (2011). Overcoming Endosomal Barrier by Amphotericin B-Loaded Dual pH-Responsive PDMA-b-PDPA Micelleplexes for siRNA Delivery. *Acs Nano*, 5(11): 9246-9255.

31. Lomas, H., A.P.R. Johnston, G.K. Such, Z. Zhu, K. Liang, M.P. van Koeverden, S. Alongkornchotikul, and F. Caruso (2011). Polymersome-Loaded Capsules for Controlled Release of DNA. *Small*, 7(14): 2109-2119.
32. Zhou, K., Y. Wang, X. Huang, K. Luby-Phelps, B.D. Sumer, and J. Gao (2011). Tunable, Ultrasensitive pH-Responsive Nanoparticles Targeting Specific Endocytic Organelles in Living Cells. *Angewandte Chemie-International Edition*, 50(27): 6109-6114.
33. Zhou, K., H. Liu, S. Zhang, X. Huang, Y. Wang, G. Huang, B.D. Sumer, and J. Gao (2012). Multicolored pH-Tunable and Activatable Fluorescence Nanoplatfrom Responsive to Physiologic pH Stimuli. *Journal of the American Chemical Society*, 134(18): 7803-7811.
34. Wang, Y., K. Zhou, G. Huang, C. Hensley, X. Huang, X. Ma, T. Zhao, B.D. Sumer, R.J. DeBerardinis, and J. Gao (2014). A nanoparticle-based strategy for the imaging of a broad range of tumours by nonlinear amplification of microenvironment signals. *Nat Mater*, 13(2): 204-212.
35. Zhang, Z., Q. Sun, J. Zhong, Q. Yang, H. Li, C. Du, B. Liang, and X. Shuai (2014). Magnetic resonance imaging-visible and pH-sensitive polymeric micelles for tumor targeted drug delivery. *J Biomed Nanotechnol*, 10(2): 216-26.
36. Jager, A., E. Jager, F. Surman, A. Hocherl, B. Angelov, K. Ulbrich, M. Drechsler, V.M. Garamus, C. Rodriguez-Emmenegger, F. Nallet, and P. Stepanek (2015). Nanoparticles of the poly([N-(2-hydroxypropyl)]methacrylamide)-*b*-poly[2-(diisopropylamino)ethyl methacrylate] diblock copolymer for pH-triggered release of paclitaxel. *Polymer Chemistry*, 6(27): 4946-4954.
37. Xu, X., A.E. Smith, S.E. Kirkland, and C.L. McCormick (2008). Aqueous RAFT Synthesis of pH-Responsive Triblock Copolymer mPEO-PAPMA-PDPAEMA and Formation of Shell Cross-Linked Micelles†. *Macromolecules*, 41(22): 8429-8435.
38. He, L.H., E.S. Read, S.P. Armes, and D.J. Adams (2007). Direct synthesis of controlled-structure primary amine-based methacrylic polymers by living radical polymerization. *Macromolecules*, 40(13): 4429-4438.
39. Gois, J.R., D. Konkolewicz, A.V. Popov, T. Guliashvili, K. Matyjaszewski, A.C. Serra, and J.F.J. Coelho (2014). Improvement of the control over SARA ATRP of 2-(diisopropylamino)ethyl methacrylate by slow and continuous addition of sodium dithionite. *Polymer Chemistry*, 5(16): 4617-4626.
40. Gois, J.R., N. Rocha, A.V. Popov, T. Guliashvili, K. Matyjaszewski, A.C. Serra, and J.F.J. Coelho (2014). Synthesis of well-defined functionalized poly(2-(diisopropylamino)ethyl methacrylate) using ATRP with sodium dithionite as a SARA agent. *Polymer Chemistry*, 5(12): 3919-3928.

41. Britovsek, G.J.P., J. England, and A.J.P. White (2005). Non-heme Iron(II) Complexes Containing Tripodal Tetradentate Nitrogen Ligands and Their Application in Alkane Oxidation Catalysis. *Inorganic Chemistry*, 44(22): 8125-8134.
42. Ciampolini, M. and N. Nardi (1966). Five-Coordinated High-Spin Complexes of Bivalent Cobalt, Nickel, and Copper with Tris(2-dimethylaminoethyl)amine. *Inorganic Chemistry*, 5(1): 41-44.
43. He, H., M. Zhong, B. Adzima, D. Luebke, H. Nulwala, and K. Matyjaszewski (2013). A Simple and Universal Gel Permeation Chromatography Technique for Precise Molecular Weight Characterization of Well-Defined Poly(ionic liquid)s. *Journal of the American Chemical Society*, 135(11): 4227-4230.
44. Brito, R.M. and W.L. Vaz (1986). Determination of the critical micelle concentration of surfactants using the fluorescent probe N-phenyl-1-naphthylamine. *Anal Biochem*, 152(2): 250-5.
45. Peng, C.-L., L.-Y. Yang, T.-Y. Luo, P.-S. Lai, S.-J. Yang, W.-J. Lin, and M.-J. Shieh (2010). Development of pH sensitive 2-(diisopropylamino)ethyl methacrylate based nanoparticles for photodynamic therapy. *Nanotechnology*, 21(15).
46. Zhang, Y., Y. Wang, and K. Matyjaszewski (2011). ATRP of Methyl Acrylate with Metallic Zinc, Magnesium, and Iron as Reducing Agents and Supplemental Activators. *Macromolecules*, 44(4): 683-685.
47. Mendonça, P.V., A.C. Serra, J.F.J. Coelho, A.V. Popov, and T. Guliashvili (2011). Ambient temperature rapid ATRP of methyl acrylate, methyl methacrylate and styrene in polar solvents with mixed transition metal catalyst system. *European Polymer Journal*, 47(7): 1460-1466.
48. Abreu, C.M.R., P.V. Mendonca, A.C. Serra, A.V. Popov, K. Matyjaszewski, T. Guliashvili, and J.F.J. Coelho (2012). Inorganic Sulfites: Efficient Reducing Agents and Supplemental Activators for Atom Transfer Radical Polymerization. *Acs Macro Letters*, 1(11): 1308-1311.
49. Gois, J.R., N. Rocha, A.V. Popov, T. Guliashvili, K. Matyjaszewski, A.C. Serra, and J.F.J. Coelho (2014). Synthesis of well-defined functionalized poly(2-(diisopropylamino)ethyl methacrylate) using ATRP with sodium dithionite as a SARA agent. *Polymer Chemistry*.
50. Bes, L., S. Angot, A. Limer, and D.M. Haddleton (2003). Sugar-Coated Amphiphilic Block Copolymer Micelles from Living Radical Polymerization: Recognition by Immobilized Lectins. *Macromolecules*, 36(7): 2493-2499.

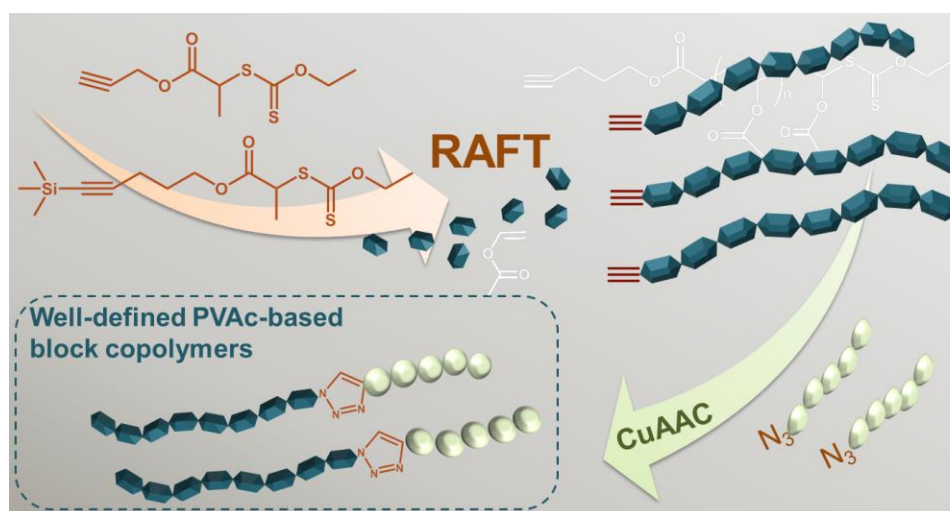
51. Giacomelli, C., L. Le Men, R. Borsali, J. Lai-Kee-Him, A. Brisson, S.P. Armes, and A.L. Lewis (2006). Phosphorylcholine-Based pH-Responsive Diblock Copolymer Micelles as Drug Delivery Vehicles: Light Scattering, Electron Microscopy, and Fluorescence Experiments. *Biomacromolecules*, 7(3): 817-828.
52. Pearson, R.T., N.J. Warren, A.L. Lewis, S.P. Armes, and G. Battaglia (2013). Effect of pH and Temperature on PMPC–PDPA Copolymer Self-Assembly. *Macromolecules*, 46(4): 1400-1407.
53. Zhu, L., S. Powell, and S.G. Boyes (2015). Synthesis of tertiary amine-based pH-responsive polymers by RAFT Polymerization. *Journal of Polymer Science Part A: Polymer Chemistry*, 53(8): 1010-1022.
54. Bates, F.S. and G.H. Fredrickson (1990). Block Copolymer Thermodynamics: Theory and Experiment. *Annual Review of Physical Chemistry*, 41(1): 525-557.
55. Choucair, A. and A. Eisenberg (2003). Control of amphiphilic block copolymer morphologies using solution conditions. *Eur. Phys. J. E*, 10(1): 37-44.
56. Jain, S. and F.S. Bates (2003). On the Origins of Morphological Complexity in Block Copolymer Surfactants. *Science*, 300(5618): 460-464.
57. Du, J.Z., Y.P. Tang, A.L. Lewis, and S.P. Armes (2005). pH-sensitive vesicles based on a biocompatible zwitterionic diblock copolymer. *Journal of the American Chemical Society*, 127(51): 17982-17983.
58. Du, J., L. Fan, and Q. Liu (2012). pH-Sensitive Block Copolymer Vesicles with Variable Trigger Points for Drug Delivery. *Macromolecules*, 45(20): 8275-8283.
59. Rocha, N., J. Mendes, L. Duraes, H. Maleki, A. Portugal, C.F.G.C. Geraldes, A. Serra, and J. Coelho (2014). Poly(ethylene glycol)-block-poly(4-vinyl pyridine) as a versatile block copolymer to prepare nanoaggregates of superparamagnetic iron oxide nanoparticles. *Journal of Materials Chemistry B*, 2(11): 1565-1575.
60. Lepeltier, E., C. Bourgaux, and P. Couvreur (2014). Nanoprecipitation and the “Ouzo effect”: Application to drug delivery devices. *Advanced Drug Delivery Reviews*, 71: 86-97.
61. Salvage, J., C. Thom, A. Lewis, G. Phillips, and A. Lloyd (2015). Nanoprecipitation of polymeric nanoparticle micelles based on 2-methacryloyloxyethyl phosphorylcholine (MPC) with 2-(diisopropylamino)ethyl methacrylate (DPA), for intracellular delivery applications. *Journal of Materials Science: Materials in Medicine*, 26(3): 1-14.
62. Perevyazko, I.Y., J.T. Delaney, A. Vollrath, G.M. Pavlov, S. Schubert, and U.S. Schubert (2011). Examination and optimization of the self-assembly of biocompatible, polymeric nanoparticles by high-throughput nanoprecipitation. *Soft Matter*, 7(10): 5030-5035.

- 
63. Giacomelli, C., V. Schmidt, and R. Borsali (2007). Specific Interactions Improve the Loading Capacity of Block Copolymer Micelles in Aqueous Media. *Langmuir*, 23(13): 6947-6955.
  64. Winnik, F.M. (1993). Photophysics of preassociated pyrenes in aqueous polymer solutions and in other organized media. *Chemical Reviews*, 93(2): 587-614.
  65. Kalyanasundaram, K. and J.K. Thomas (1977). Environmental effects on vibronic band intensities in pyrene monomer fluorescence and their application in studies of micellar systems. *Journal of the American Chemical Society*, 99(7): 2039-2044.
  66. Lee, A.S., A.P. Gast, V. Bütün, and S.P. Armes (1999). Characterizing the Structure of pH Dependent Polyelectrolyte Block Copolymer Micelles. *Macromolecules*, 32(13): 4302-4310.
  67. Brito, R.M.M. and W.L.C. Vaz (1986). Determination of the critical micelle concentration of surfactants using the fluorescent probe N-phenyl-1-naphthylamine. *Analytical Biochemistry*, 152(2): 250-255.
  68. Torchilin, V.P. (2007). Micellar Nanocarriers: Pharmaceutical Perspectives. *Pharmaceutical Research*, 24(1): 1-16.



## Chapter 5

### Synthesis of alkyne-terminated xanthates for the efficient RAFT polymerization of less-activated monomers



The contents of this chapter were published in RSC Advances: **Gois, J. R., Popov, A. V., Guliashvili, T., Serra, A. C., Coelho, J. F. J.**, "Synthesis of functionalized poly(vinyl acetate) mediated by alkyne-terminated RAFT agents", 2015, in press





## 5.1. Abstract

Two new xanthates with alkyne functionalities were synthesized for the reversible addition fragmentation chain transfer (RAFT) polymerization of vinyl acetate (VAc). The new RAFT agents were fully characterized by  $^1\text{H}$  and  $^{13}\text{C}$  NMR spectroscopy. Unlike the alkyne terminated RAFT agent (AT- $X_1$ ) the protected alkyne-terminated RAFT agent (PAT- $X_1$ ) was able to conduct the RAFT polymerization of VAc with a good control over the molecular weight (MW) and relatively narrow MW distributions ( $D < 1.4$ ). The linear evolution of  $M_{n,\text{GPC}}$  with conversion as well as the close agreement between  $M_{n,\text{th}}$  and  $M_{n,\text{GPC}}$  values confirmed the controlled feature of the RAFT system. It is worth to mention that the polymer dispersity remain very low ( $D < 1.20$ ) until relatively high monomer conversions (60%) knowing the non-activated nature of VAc. The chain end-functionality of the obtained polymers was evaluated by  $^1\text{H}$  NMR, FTIR-ATR and UV-vis absorption analysis. The “livingness” of the obtained polymer was confirmed by a successful chain extension experiment. The deprotection of the alkyne functionality in the PVAc, allowed a further copper catalyzed azide–alkyne [3+2] dipolar cycloaddition (CuAAC) reaction with an azido terminated-poly(ethylene glycol) (PEG- $\text{N}_3$ ), to afford PVAc-PEG block copolymers as proof-of-concept.

## 5.2. Introduction

The reversible deactivation radical polymerization (RDRP) has witnessed enormous improvements during two decades.<sup>1-5</sup> For RDRP of activated monomers such as acrylates, methacrylates or styrene different modifications of atom transfer radical polymerization (ATRP) are successfully applied.<sup>6-10</sup> However, the development of new RDRP systems that are able to polymerize such non-activated monomers, as vinyl chloride<sup>11-13</sup>, *N*-vinyl pyrrolidone<sup>14</sup> or vinyl acetate (VAc)<sup>15, 16</sup> remains an important challenge. The reversible addition–fragmentation chain transfer (RAFT) polymerization is considered a very effective RDRP method for the polymerization of less activated monomers.<sup>12, 17</sup> Other RDRP methods mediated by transition metal catalysts<sup>18, 19</sup>, iodine transfer<sup>11, 20</sup> or nitroxides<sup>21</sup> have been studied for vinyl chloride and VAc. Recently, some authors reported the use of cobalt complex as organic metallic complexes for the controlled synthesis of poly(vinyl acetate) (PVAc).<sup>22-25</sup> VAc stands out as one of the

most studied non-activated vinyl monomers.<sup>26</sup> PVAc has a wide range of industrial applications, from paints to coatings as well as its hydrolyzed derivative, poly(vinyl alcohol) (PVA), that extends its applications to the biomedical field.<sup>27</sup>

The choice of the RAFT agent is of utmost importance for the success of this RDRP method.<sup>28, 29</sup> For non-activated monomers, xanthate mediated RAFT polymerization, also known as macromolecular design via interchange of xanthate (MADIX/RAFT)<sup>30</sup> is one of the most straightforward RDRP strategies to afford optimal control over the polymerization. Due to the high reactivity of the VAc propagating radical, the RAFT agent should have an efficient leaving group, with similar reactivity to the growing macroradical towards the monomer addition. Most of the literature reports, concerning the xanthate mediated RAFT polymerization of VAc, refer the use of methyl(ethoxy carbonyl sulfanyl acetate) (Figure 5.1, Y<sub>1</sub>)<sup>31-33</sup>, *O*-ethyl-*S*-(1-methoxy carbonyl) ethyl dithiocarbonate (also known as methyl 2-((ethoxycarbonothio)thio) propanoate), with 2-propionyl moiety as the leaving group (Figure 5.1, X<sub>1</sub>), for either bulk<sup>34</sup>, solution<sup>35, 36</sup> or miniemulsion polymerizations<sup>33</sup>, or very similar RAFT agents.<sup>37, 38</sup> Nevertheless, other RAFT agents such as dithiocarbamates have also been reported for the well-defined polymerization of VAc.<sup>39, 40</sup>

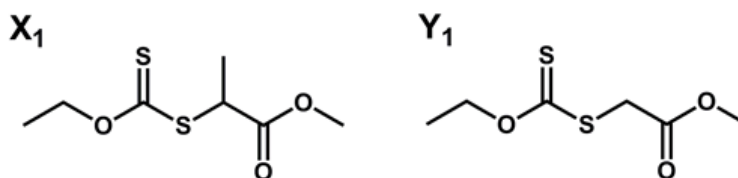


**Figure 5.1:** Schematic representation of the most reported xanthates for the RAFT polymerization of PVAc.

The conjugation of polymers through a post polymerization coupling strategy is a powerful tool in macromolecular engineering to afford new block copolymers with segments that are impossible to link by direct copolymerization. In fact, the single step synthesis of block copolymers is limited to few monomers functionalities, usually with similar chemical and physical properties, or require the use of specific RAFT agents based on a switchable dithiocarbamate moiety that are able to mediate the

polymerization of both activated and non-activated monomers.<sup>41</sup> In the case of non-activated monomers, where controlled copolymerization is more difficult, the reactions inspired by the “click” coupling approach are a convenient strategy to achieve new polymer architectures, otherwise difficult to access.<sup>42-44</sup> The direct polymerization using a “clickable” functionalized RAFT agent is a common strategy to afford polymers with a specific chain-end functionality, without the need of post-modification procedures.<sup>45</sup> CuAAC reaction between azide and alkyne chain-end functionalities is one of the most explored “click” reaction.<sup>46</sup> Stenzel and co-workers reported the facile synthesis of poly(styrene)-*b*-PVAc block copolymers through a “click” coupling approach from a PVAc synthesized using an azido-xanthate RAFT agent and poly(styrene) synthesized using one alkyne-dithiobenzoate agent.<sup>45</sup> A similar strategy was proposed, by the same group, for the synthesis of comb-like copolymers, from the reaction of an azido functionalized linear PVAc with one alkyne modified methacrylate monomer.<sup>47</sup> The literature involving the use of xanthates with alkyne functionality is very scarce. To the best of our knowledge, only one reference is available describing the synthesis of (*S*)-2-(propynyl propionate)-*O*-ethyl xanthate, an alkyne terminated RAFT agent, for the controlled synthesis of *N*-vinylpyrrolidone.<sup>48</sup> The aim of the present study was to synthesize new efficient alkyne functionalized xanthate RAFT agents, able to conduct controlled polymerization of vinyl acetate. The present strategy enabled the straightforward preparation of PVAc block copolymers through a simple post polymerization coupling method.

### 5.3. Experimental Section

#### 5.3.1 Materials

Vinyl acetate (VAc) ( $\geq 99\%$ , Aldrich) was purified by passing the monomer through a basic alumina column and then distilled under vacuum (bp 72 - 73 °C). 2,2'-Azobis(2-methylpropionitrile) (AIBN) (98%, Fluka,) was purified by recrystallization from methanol before use. 1,4-Dioxane (99.8%, Acros Organics) was passed through alumina column to remove peroxides and distilled under reduced pressure prior to use. Poly(ethylene glycol) methyl ether (mPEG<sub>113</sub>, MW = 5000 Da) (Aldrich) was dried by azeotropic distillation with toluene. Trigonox 187-W40 (40% water and methanol

emulsion of diisobutryl peroxide, AkzoNobel), sodium ascorbate (NaAsc) ( $\geq 98\%$ , Sigma), copper(II) sulfate pentahydrate ( $\text{CuSO}_4 \cdot 5\text{H}_2\text{O}$ ) ( $\geq 98\%$ , Aldrich), sodium azide ( $\text{NaN}_3$ ) ( $\geq 99.5\%$ , Sigma-Aldrich), methyl 2-bromopropionate (98%, Aldrich), methanol (99.9%, Fisher Scientific), dichloromethane (DCM) (99.99%, Fisher Scientific), potassium ethyl xanthogenate (96%; Aldrich) anhydrous sodium sulfate ( $\geq 98\%$ , Fisher Chemical), ethyl acetate ( $\geq 99.5\%$ , Fisher Scientific), diethyl ether (99.85%, Fisher Scientific), hexane (99.05%, Fisher Scientific), thionyl chloride ( $\geq 99\%$ , Sigma-Aldrich), propargyl alcohol (PA) (99%, Aldrich), triethylamine ( $\text{Et}_3\text{N}$ ) ( $\geq 99\%$ , Sigma-Aldrich), 2-bromopropionic acid ( $\geq 99\%$ , Aldrich), 5-trimethylsilyl-4-pentyn-1-ol (96%; Aldrich), *N*-(3-dimethylaminopropyl)-*N'*-ethylcarbodiimide hydrochloride ( $\geq 99.0\%$ , Sigma), 4-(dimethylamino)pyridine (DMAP) ( $\geq 99\%$ , Aldrich), tetrabutylammonium fluoride trihydrate ( $\text{TBAF} \cdot 3\text{H}_2\text{O}$ ) (99%, Acros Organics), sodium azide (99%; Aldrich), tetrahydrofuran (THF) ( $\geq 99.9\%$ , Sigma-Aldrich), dimethylformamide (DMF) ( $\geq 99.8\%$ ; Sigma-Aldrich), deuterated chloroform ( $\text{CDCl}_3$ ) ( $\geq 99.8\%$ , Euriso-top, +1% TMS) and deuterated DCM ( $\text{CD}_2\text{Cl}_2$ ) ( $\geq 99.6\%$ , Euriso-top) were used as received. Azido terminated-poly(ethylene glycol) ( $\text{mPEG}_{113}\text{-N}_3$ ) was synthesized by a nucleophilic substitution of poly(ethylene glycol) methyl ether bromoisobutyrate ( $\text{mPEG}_{113}\text{-BiB}$ ) (previously synthesized according to the literature procedures<sup>49</sup>) using  $\text{NaN}_3$  in DMF (procedure adapted from literature<sup>50</sup>) (see Annexe D for detailed synthesis).

### **5.3.2 Characterization**

The  $^1\text{H}$  and  $^{13}\text{C}$  NMR spectra were recorded on a Bruker DMX-360 (360 MHz for  $^1\text{H}$  NMR and 90 MHz for  $^{13}\text{C}$  NMR, with a 5-mm manual switching QNP) and a Bruker Avance III spectrometer (400 MHz, with a 5-mm TIX triple resonance detection probe), in a deuterated solvent. Monomer conversions were determined by integration of monomer and polymer peaks using MestRenova software version: 6.0.2-5475. Fourier-transform infrared spectroscopy (FTIR) was performed at 64 scans and with a  $4\text{ cm}^{-1}$  resolution between  $500$  and  $3500\text{ cm}^{-1}$ , using a JASCO 4200 FTIR spectrometer, operating in the ATR mode (MKII GoldenGate™ Single Reflexion ATR System). The thermogravimetric analysis (TGA) was carried out on a TGA Q 500 machine (TA Instruments) with a heating ramp set at a constant  $10\text{ }^\circ\text{C}\cdot\text{min}^{-1}$ , and covering a

temperature range from 25 to 300 °C. High performance gel permeation chromatography (HPSEC) was performed using a Viscotek (ViscotekTDMax) with a differential viscometer (DV), right-angle laser-light scattering (RALLS, Viscotek), and refractive index (RI) detectors, using column set of a PL 10 µm guard column followed by one MIXED-E PLgel column and one MIXED-C PLgel column. Filtered THF was used as an eluent at a flow rate of 1 mL.min<sup>-1</sup> at 30 °C. The samples were filtered through a polytetrafluoroethylene (PTFE) membrane with 0.2 µm pore before injection and the system was calibrated with narrow PS standards. The  $dn/dc$  of PVAc in THF at 30 °C was determined as 0.0581 (for  $\lambda = 670$  nm) using a RUDOLPH RESEARCH J357 Automatic Refractometer (J357-NDS-670-CC). Molecular weight ( $M_{n,GPC}$ ) and dispersity ( $D$ ) of synthesized polymers were determined by using either a universal calibration or multidetector analysis (OmniSEC software version: 4.6.1.354). Ultraviolet-visible (UV-Vis) spectroscopy was carried out using a Jasco V-530 spectrophotometer. The analyses were carried out in chloroform in the 250 – 400 nm range at 25 °C. Absorption spectra were measured from 250 to 400 nm with a resolution of 2.0 nm in a 10 mm UV-cuvette.

### 5.3.3 Procedures

#### Synthesis of (*RS*)-*O*-ethyl-*S*-(1-methoxycarbonyl) ethyl- dithiocarbonate (**X<sub>1</sub>**).

Methyl 2- bromopropionate (5.13 g, 30.73 mmol) was dissolved in 100 mL of methanol and the solution was cooled down in an ice bath. Potassium ethyl xanthogenate (5.74 g, 34.38 mmol) was then slowly added over a period of 30 minutes. After the complete dissolution of the salt, the reaction mixture was stirred at room temperature during 24 h. The KBr formed was filtered under vacuum, the product was extracted with an ether/hexane mixture (2:1 vol.%), washed three times with water and dried over anhydrous sodium sulfate. The solvent was evaporated at reduced pressure to give a yellow liquid that was further purified by column chromatography on silica with hexane/ethyl acetate (10:1 vol.%) as the eluent to give **X<sub>1</sub>** (4.30g, 67 %). <sup>1</sup>H NMR (360 MHz, CDCl<sub>3</sub>,  $\delta$  (ppm)): 4.6232 (q, 1H, <sup>3</sup>J<sub>HH</sub>= 7.14 Hz, diastereotopic -OCHHCH<sub>3</sub>), 4.6199 (q, 1H, <sup>3</sup>J<sub>HH</sub>= 7.1 Hz, diastereotopic -OCHHCH<sub>3</sub>), 4.36 (q, 1H, <sup>3</sup>J<sub>HH</sub>= 7.4 Hz, -CH), 3.73 (s, 3H, -CH<sub>3</sub>), 1.56 (d, 3H, <sup>3</sup>J<sub>HH</sub>= 7.4 Hz, -CHCH<sub>3</sub>), 1.40 (t, 3H, J<sub>HH</sub>= 7.14 Hz, -CH<sub>2</sub>CH<sub>3</sub>).

**Synthesis of alkyne-terminated RAFT agent, *O*-ethyl-*S*-(1-propargoxycarbonyl) ethyl- dithiocarbonate (AT- X<sub>1</sub>).**

**2-Bromopropionyl chloride:** 4.00 mL of thionyl chloride (5.14 mmol) was slowly added to 4.50 mL of 2-bromopropionic acid (50.00 mmol). A small amount of DMF (10 $\mu$ L) was used to catalyze the reaction. The mixture was heated to 80 °C and stirred until the complete release of gaseous by-products of the reaction. The product was used without any further purification steps.

**(*RS*)-Propargyl 2-bromopropionate:** A solution of PA (2.80 g, 50.00 mmol) and Et<sub>3</sub>N (5.06 g, 50.00 mmol) in DCM was cooled down to ~ -20 °C with liquid nitrogen. The 2-bromopropionyl chloride was added in portions to the solution. The solution was left off from the cold and kept under stirring until reach the room temperature. The product was washed three times with water and the organic phase was dried under anhydrous sodium sulfate. After solvent evaporation the product was obtained as a light yellow oil (6.98g, 73%). <sup>1</sup>H NMR (360 MHz, CDCl<sub>3</sub>,  $\delta$  (ppm)): 4.7599 (d, 1H, <sup>4</sup>J<sub>HH</sub>= 2.5 Hz, diastereotopic HC $\equiv$ C-CHHO-), 4.7524 (d, 1H, <sup>4</sup>J<sub>HH</sub>= 2.5 Hz, diastereotopic HC $\equiv$ C-CHHO-), 4.39 (q, 1H, <sup>3</sup>J<sub>HH</sub> = 6.9 Hz, -CH-Br), 2.5 (t, 1H, J<sub>HH</sub>= 2.5 Hz, HC $\equiv$ C-), 1.82 (d, 3H, <sup>3</sup>J<sub>HH</sub>= 6.9 Hz, -CH<sub>3</sub>). <sup>13</sup>C NMR (90 MHz, CDCl<sub>3</sub>):  $\delta$  (ppm) 169.48 (C=O), 76.86 ( $\equiv$ C-), 75.74 (HC $\equiv$ ), 53.40 (CH<sub>2</sub>-O), 39.30 (CH-Br), 21.58 (Br-CH<sub>3</sub>).

**AT- X<sub>1</sub>:** Propargyl 2-bromopropionate (4.04 g, 21.13 mmol) was dissolved in 25 mL of PA and the solution was cooled down in an ice bath. Potassium ethyl xanthogenate (3.84 g, 23.92 mmol) was then added to the solution in portions over a period of 30 minutes. After the complete dissolution of the salt, the reaction mixture was stirred at room temperature overnight. The solid KBr was filtered off, the filtrate was extracted with ether/hexane (2:1 vol.%) and the extract was washed three times with water (500 mL) and dried over anhydrous sodium sulfate. The solvent was evaporated at reduced pressure to give a yellow liquid that was further purified by column chromatography on silica starting with hexane and then hexane/ethyl acetate (10:1 vol.%) as the eluent to give AT-X<sub>1</sub> as a yellow liquid (2.64 g, 54%). <sup>1</sup>H NMR (360 MHz, CDCl<sub>3</sub>,  $\delta$  (ppm)): 4.7335 (d, 1H, <sup>4</sup>J<sub>HH</sub>= 2.4 Hz, diastereotopic  $\equiv$ C-CHH-O), 4.7321 (d, 1H, <sup>4</sup>J<sub>HH</sub>= 2.4 Hz, diastereotopic  $\equiv$ C-CHH-O), 4.6310 (q, 1H, <sup>3</sup>J<sub>HH</sub>= 7.1 Hz, diastereotopic CHH-CH<sub>3</sub>), 4.6302 (q, 1H, <sup>3</sup>J<sub>HH</sub>= 7.1 Hz, diastereotopic CHH-CH<sub>3</sub>), 4.41 (q, 1H, <sup>3</sup>J<sub>HH</sub> = 7.4 Hz, CH-CH<sub>3</sub>), 2.49 (t, 1H, <sup>4</sup>J<sub>HH</sub> = 2.4 Hz, CH $\equiv$ C), 1.58 (d, 3H,

$^3J_{\text{HH}} = 7.4$  Hz,  $\text{CH}_3\text{-CH}$ ), 1.41 (t, 3H,  $^3J_{\text{HH}} = 7.1$  Hz,  $\text{CH}_3\text{-CH}_2$ ).  $^{13}\text{C}$  NMR (90 MHz,  $\text{CDCl}_3$ ,  $\delta$  (ppm)): 211.69 (C=S), 170.79 (C=O), 77.16 ( $\equiv\text{C-}$ ), 75.46 (H C $\equiv$ ), 70.44 ( $\text{CH}_2\text{-CH}_3$ ), 53.13 ( $\text{CH}_2\text{-O}$ ), 46.83 ( $\text{CH-CH}_3$ ), 16.68 ( $\text{CH}_3\text{-CH}$ ), 13.73 ( $\text{CH}_3\text{-CH}_2$ ) (the peak at 77.16 ppm is overlapped with the solvent peak).  $^{13}\text{C}$  NMR (90 MHz,  $\text{CD}_2\text{Cl}_2$ , (ppm)): 212.14 (C=S), 171.12 (C=O), 77.74 ( $\equiv\text{C-}$ ), 75.64 (HC $\equiv$ ), 71.14 ( $\text{CH}_2\text{-CH}_3$ ), 53.54 ( $\text{CH}_2\text{-O}$ ), 47.14 ( $\text{CH-CH}_3$ ), 16.96 ( $\text{CH}_3\text{-CH}$ ), 13.97 ( $\text{CH}_3\text{-CH}_2$ ).

### Synthesis of protected alkyne terminated RAFT agents (PAT- $\text{X}_1$ ).

**2-(Ethoxycarbonothioylthio)propanoic acid:** 4.18 g (27.30 mmol) of 2-bromopropionic acid was dissolved in 40 mL of dry methanol. The solution was cooled down in an ice bath. Potassium ethyl xanthogenate 5.126 g (31.98 mmol) was slowly added to the methanol solution, in portions, over a period of 30 min. After the complete dissolution of potassium ethyl xanthogenate, the ice bath was removed and the reaction proceeded at room temperature for 24h. The reaction by-product, KBr, was filtered under reduced pressure and the product extracted with an ether/hexane mixture (2:1 vol.%), washed three times with water and dried over anhydrous sodium sulfate. The product was obtained after the solvent evaporation at reduced pressure.  $^1\text{H}$  NMR (400 MHz,  $\text{CDCl}_3$ ,  $\delta$  (ppm)): 10.00 (s, 1H, -OH), 4.6419 (q, 1H,  $^3J_{\text{HH}} = 7.1$  Hz, diastereotopic  $\text{CHH-CH}_3$ ), 4.6399 (q, 1H,  $^3J_{\text{HH}} = 7.1$  Hz, diastereotopic  $\text{CHH-CH}_3$ ), 4.41 (q, 1H,  $^3J_{\text{HH}} = 7.47$  Hz, -CH-  $\text{CH}_3$ ), 1.60 (d, 3H,  $^3J_{\text{HH}} = 7.4$  Hz, - $\text{CH}_3\text{-CH}$ ), 1.41 (t, 3H,  $^3J_{\text{HH}} = 7.1$  Hz, - $\text{CH}_3\text{-CH}_2$ ).

**PAT-  $\text{X}_1$ :** In a 200 mL flask, the 2-(ethoxycarbonothioylthio) propanoic acid (0.60g, 3,10 mmol) was dissolved in 60 mL of dry DCM. 5-Trimethylsilyl-4-pentyn-1-ol (0.68 mL, 3.74 mmol) was added and the mixture was cooled down to 0°C and bubbled with argon. *N*-(3-dimethylaminopropyl)-*N'*-ethylcarbodiimide hydrochloride (0.78 g, 4.09 mmol) and DMAP (5.76 mg, 0.05 mmol) were then added to the solution and the mixture was stirred in the ice bath for more 30 min. The reaction was left at room temperature for 24h. The RAFT agent was purified by column chromatography on silica with hexane/ethyl acetate (10:1 vol.%) as the eluent. The PAT- $\text{X}_1$  was obtained as a yellow oil (0.89g, 86.6 %).  $^1\text{H}$  NMR (400 MHz,  $\text{CDCl}_3$ ):  $\delta$  (ppm) 4.64 (q, 2H,  $^3J_{\text{HH}} = 7.12$  Hz;  $\text{CH}_2\text{-CH}_3$ ), 4.38 (q, 1H,  $^3J_{\text{HH}} = 7.30$  Hz, -CH-  $\text{CH}_3$ ), 4.23 (t, 2H,  $^3J_{\text{HH}} = 6.28$  Hz;  $\text{CH}_2\text{-O}$ ), 2.33 (t, 2H,  $^3J_{\text{HH}} = 7.05$ Hz; C $\equiv$ C- $\text{CH}_2\text{-}$ ), 1.87 (m, 2H,  $^3J_{\text{HH}} = 6.66$  Hz; - $\text{CH}_2\text{-}$ ), 1.57 (d, 3H,  $^3J_{\text{HH}} = 7.14$  Hz, - $\text{CH}_3\text{-CH}$ ), 1.42 (t, 3H,  $^3J_{\text{HH}} = 7.13$  Hz, - $\text{CH}_3\text{-CH}_2$ ),

0.14 (s, 9H,  $(\text{CH}_3)_3\text{-Si}$ ).  $^{13}\text{C}$  NMR (90 MHz,  $\text{CDCl}_3$ )  $\delta$  (ppm) 212.22 (C=S), 171.48 (C=O), 105.60 ( $\equiv\text{C-O}$ ), 85.63 (Si-C $\equiv$ ), 70.41 ( $\text{CH}_2\text{-CH}_3$ ), 64.45 ( $\text{CH}_2\text{-O}$ ), 47.33 ( $\text{CH-CH}_3$ ), 27.71 ( $\text{CH}_2\text{-CH}_2\text{-CH}_2$ ), 17.01 ( $\equiv\text{C-CH}_2\text{-}$ ), 16.65 ( $\text{CH}_3\text{-CH}$ ), 13.83 ( $\text{CH}_3\text{-CH}_2$ ), 0.22 ( $(\text{CH}_3)_3$ ).

**Typical procedure for the RAFT polymerization of VAc with [VAc/X<sub>1</sub>/AIBN] = 100:1:0.2 in 1,4-dioxane.**

VAc (2.02 g, 23.49 mmol), X<sub>1</sub> (48.47 mg, 0.23 mmol), AIBN (7.82 mg, 0.05 mg) and 1,4-dioxane (1.93 mL; previously bubbled with nitrogen for about 10 min) were placed into a 25 mL Schlenk reactor. The reactor was sealed, frozen in liquid nitrogen, and the mixture was deoxygenated with four freeze-vacuum-thaw cycles and purged with nitrogen. The Schlenk reactor was placed in an oil bath at 60 °C with stirring (500 rpm). Different reaction mixture samples were collected during the polymerization through an airtight syringe, purging the side arm of the Schlenk reactor with nitrogen. The collected samples were analyzed by  $^1\text{H}$  NMR spectroscopy to calculate the monomer conversion and theoretical molecular weight ( $M_{n,\text{th}}$ ), and by GPC to determine  $M_{n,\text{GPC}}$  and  $\mathcal{D}$  of the polymers. The other RAFT polymerizations were carried out employing the same procedure described but using AT-X<sub>1</sub> or PAT-X<sub>1</sub> as the RAFT agents.

**Typical procedure for the chain extension of PVAc.**

A sample of protected alkyne-terminated PVAc (PAT-PVAc) ( $M_{n,\text{GPC}} = 3.01 \times 10^3$ ,  $\mathcal{D} = 1.20$ ) synthesized through a typical RAFT polymerization using the PAT-X<sub>1</sub>, and purified by precipitation in cold hexane, was used as macro-RAFT agent in a new RAFT polymerization. Briefly, the PAT-PVAc (31.8 mg, 13.4  $\mu\text{mol}$ ) was dissolved in 1,4-dioxane (7 mL) and placed into a Schlenk reactor. 360  $\mu\text{L}$  of a stock solution of AIBN (1.1 mg, 6.64  $\mu\text{mol}$ ) in 1,4-dioxane was added to the reactor followed by the addition of VAc (4 mL, 46.46 mmol). The reactor was sealed, frozen in liquid nitrogen, and the mixture was deoxygenated with four freeze-vacuum-thaw cycles and purged with nitrogen. The Schlenk reactor was placed in an oil bath at 60 °C with stirring (500 rpm). After 72h of reaction, a sample was collected and analyzed by GPC.

**Typical procedure for PVAc deprotection.**

A solution of pure PAT-PVAc ( $M_{n,\text{GPC}} = 6.0 \times 10^3$ ,  $\mathcal{D} = 1.36$ ) (0.25 g,  $4.20 \times 10^{-2}$  mmol) in THF (10 mL) was bubbled with nitrogen for about 10 minutes and cooled down to -20 °C. Then, 2.14 mL of a 0.2 M solution of TBAF $\cdot$ 3H<sub>2</sub>O (0.43 mmol) was slowly



added to the polymer solution. After stirring for 30 minutes at low temperature, the reaction proceeded over night at ambient temperature. The reaction mixture was passed through a silica column to remove the excess of TBAF and the alkyne-terminated PVAc (AT-PVAc) was recovered by precipitation in cold hexane, dried under vacuum and analyzed by  $^1\text{H}$  NMR.

#### **Coupling reaction between AT-PVAc and N<sub>3</sub>-PEG.**

The AT-PVAc obtained after the deprotection of the PAT-PVAc (50 mg, 8.33  $\mu\text{mol}$ ) and N<sub>3</sub>-PEG (55 mg, 10.8  $\mu\text{mol}$ ) were dissolved into 5 mL of THF. The mixture was placed in a round-bottom flask equipped with a magnetic stir bar and sealed with a rubber septum. A stock solution of sodium ascorbate (40 mM; 250  $\mu\text{L}$ ) in deionized water was added to the solution and the mixture was bubbled with nitrogen for 20 min to remove oxygen. Lastly, a degassed stock solution of CuSO<sub>4</sub>·5H<sub>2</sub>O (13 mM; 250  $\mu\text{L}$ ) in deionized water was injected into the flask under nitrogen atmosphere. The reaction was allowed to proceed under stirring at 40 °C for 48 h. The final mixture was passed through an alumina column to remove the copper catalyst and the product precipitated into cold hexanes. The product was analyzed by GPC and FTIR-ATR spectroscopy in order to confirm the success of the coupling reaction.

## **5.4. Results and Discussion**

### **5.4.1 Synthesis of the RAFT agents**

The use of functionalized RAFT agents allows the direct synthesis of polymeric structures with a pre-determined chain-end functionality, which avoids further steps involving the modification of the terminals in the polymeric chain structures with specific chemical groups. Such groups are suitable for further conjugation reactions, namely reactions inspired by the “click” coupling strategies. Herein, two different RAFT agents for the polymerization of non-activated monomers were synthesized (AT-X<sub>1</sub> and PAT-X<sub>1</sub>), based on *O*-ethyl-*S*-(1-methoxycarbonyl) ethyl- dithiocarbonate xanthate (X<sub>1</sub>).<sup>34-36</sup> The structures of the RAFT agents are present in Figure 5.2.

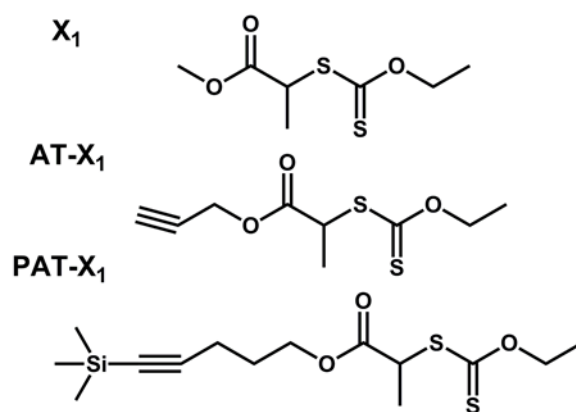


**Figure 5.2:** Structures of RAFT agents synthesized: O-ethyl-S-(1-methoxycarbonyl) ethyl-dithiocarbonate (X<sub>1</sub>), alkyne-terminated RAFT agent (AT-X<sub>1</sub>) and protected alkyne-terminated RAFT agent (PAT-X<sub>1</sub>).

The xanthate X<sub>1</sub> was synthesized through the reaction of potassium ethyl xanthogenate with methyl 2-bromopropionate in methanol according to similar procedures reported in literature for analogous RAFT agents.<sup>51, 52</sup> The success of the reactions was confirmed by <sup>1</sup>H NMR (Figure D.1, Annex D). Although the impurities after the synthesis are very small, the purification procedures are crucial to avoid RAFT agent contaminations that could interfere with the success of the polymerization.

The synthesis of the AT-X<sub>1</sub> was already been reported by Patel and co-authors for the polymerization of *N*-vinylpyrrolidone.<sup>48</sup> However, the method reported here is easier, cleaner and more efficient than the aforementioned method that involves the carbodiimide activation. The synthesis of AT-X<sub>1</sub> was carried out into two steps; firstly, the synthesis of the alkyne terminated bromide through the reaction of 2-bromopropionyl chloride and propargyl alcohol (PA), followed by the bromine substitution with the potassium ethyl xanthogenate (Figure 5.3).

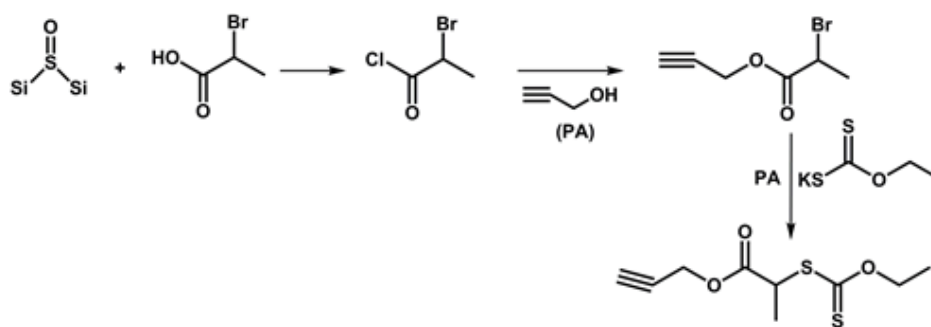


**Figure 5.3:** Schematic representation of the synthesis strategy of the alkyne-terminated RAFT agent (AT-X<sub>1</sub>).

The success of the reaction was confirmed by <sup>1</sup>H and <sup>13</sup>C spectroscopy (Figure 5.4 and Figure D.2 and Figure D.3 (Annex D)). The FTIR-ATR spectra of the AT- X<sub>1</sub> (Figure D.4, Annex D) shows the presence of the characteristic alkyne C≡H stretch vibration at 3300 cm<sup>-1</sup><sup>47</sup>, and also the -C=S and C-S stretching vibrations at 1044 cm<sup>-1</sup> and 633 cm<sup>-1</sup>, respectively.

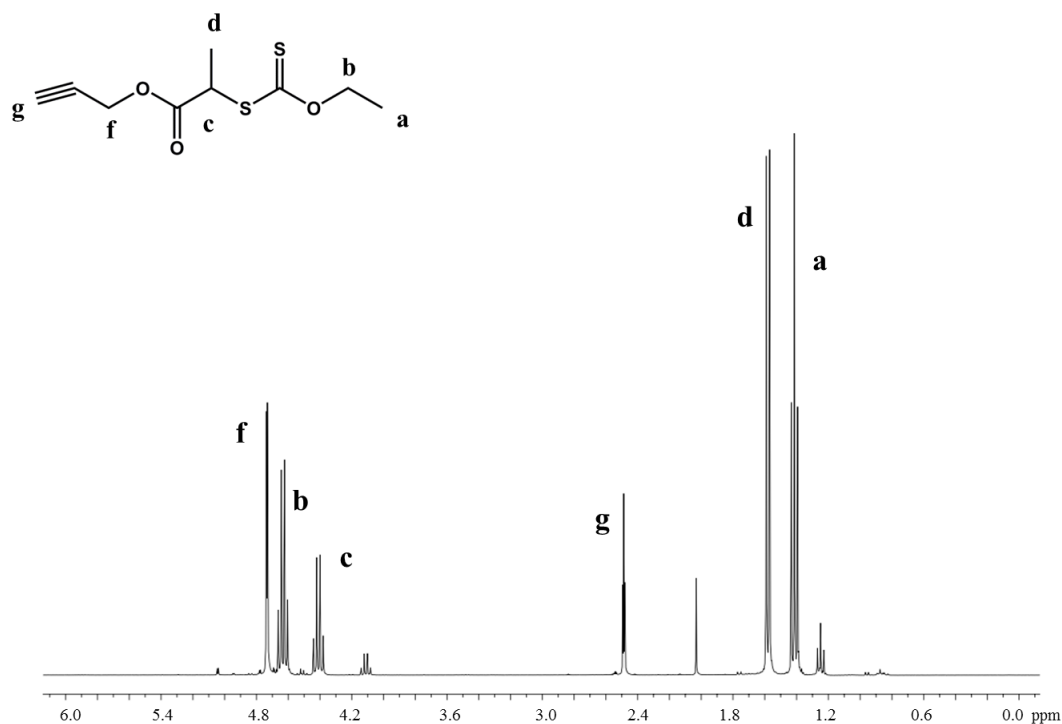


**Figure 5.4:** <sup>1</sup>H NMR spectra in CDCl<sub>3</sub> of alkyne-terminated RAFT agent (AT-X<sub>1</sub>).

It is known that the alkyne group in the RAFT agent may interfere with the radical polymerization process.<sup>45</sup> In order to evaluate this possibility, the synthesis of new protected RAFT agent (protected alkyne-terminated RAFT agent (PAT-X<sub>1</sub>)) using a trimethyl silyl group was envisaged. For the synthesis of the PAT-X<sub>1</sub>, 2-(ethoxycarbonothioylthio) propanoic acid, was firstly synthesized through the reaction of potassium ethyl xantogenate and 2-bromopropionic acid in methanol. The further coupling reaction with 5-trimethylsilyl-4-pentyn-1-ol originates PAT- X<sub>1</sub> (Figure 5.5).

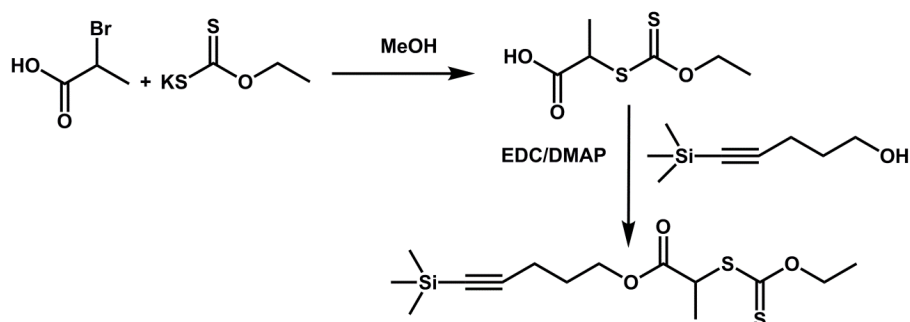


**Figure 5.5:** Schematic representation of the synthesis strategy of the protected alkyne-terminated RAFT agent (PAT-X<sub>1</sub>).

The success of the reaction was confirmed by <sup>1</sup>H NMR (Figure 5.6) and <sup>13</sup>C NMR spectroscopy (Figure D.5, Annex D).

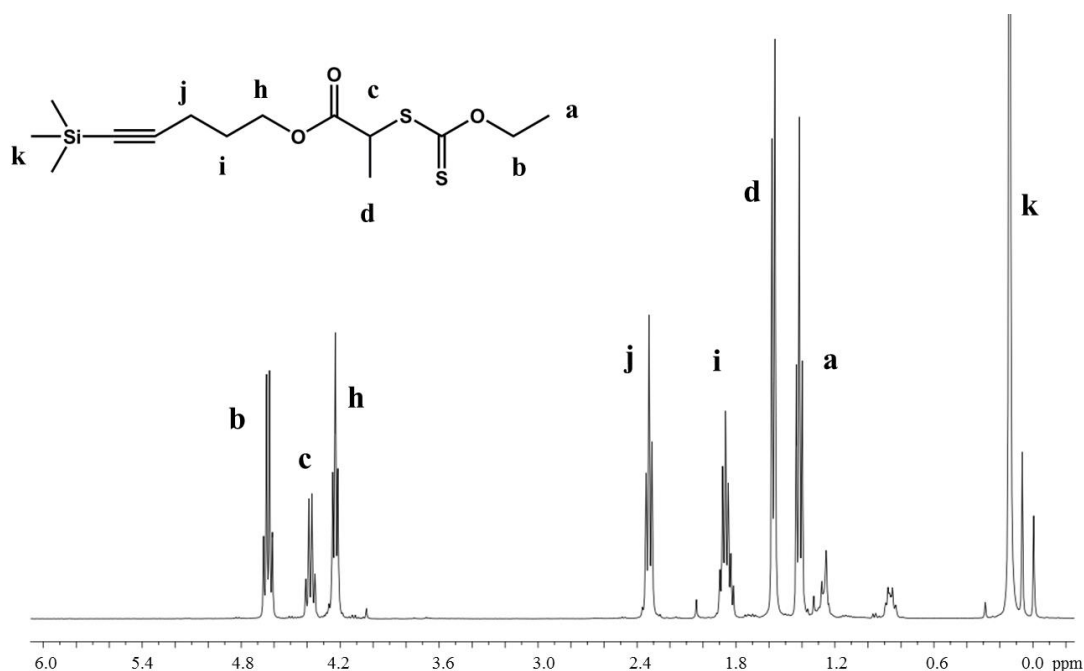


**Figure 5.6:** <sup>1</sup>H NMR spectra in CDCl<sub>3</sub> of protected alkyne-terminated RAFT agent (PAT-X<sub>1</sub>).

It should be noted that all three target molecules contain a chiral center C\*HMeS(CO). It makes geminal methylene protons CHH diastereotopic and causes anisochrony due to unequal magnetic field sensed by these nuclei.<sup>53-55</sup> The resonance signals of these protons are overlapped in the spectrum of PAT-X<sub>1</sub>, whereas the <sup>1</sup>H NMR spectra of X<sub>1</sub> and AT- X<sub>1</sub> revealed resolved peaks of each such proton. Therefore, the difference in chemical shifts for these anisochronic protons is 0.0135 ppm for -OCHHCH<sub>3</sub> in X<sub>1</sub>, 0.0014 ppm for CH≡C-CHHO- and 0.0009 ppm for -OCHHCH<sub>3</sub> in AT- X<sub>1</sub>. Interestingly, the chemical shift difference of 0.0075 ppm for CH≡C-CHHO- diastereotopic protons in propargyl 2-bromopropionate is almost equal to <sup>4</sup>J<sub>HH</sub> coupling constant, thus making a quasitriplet from the two doublets (Annex D).

#### 5.4.2 Polymerization of VAc using the synthesized RAFT agents

To investigate the ability of the RAFT agents to control the polymerization of non-activated monomers, VAc was used as a model monomer. The polymerization of VAc was carried out using the different xantathes in 1,4-dioxane ([1,4-dioxane]<sub>0</sub>/[VAc]<sub>0</sub> = 1/1 (w/w)) at 60 °C and initiated by the AIBN. The ratio of RAFT agent:AIBN was kept at 1:0.2. Monomer conversions were calculated using <sup>1</sup>H NMR spectroscopy by comparing the integrations of the -CH signals on the VAc (δ = 4.50 ppm) with the corresponding signals of the polymer backbone (δ = 4.80 ppm). X<sub>1</sub> was used for comparison purposes, since it was already reported for the synthesis of well-defined PVAc.<sup>34-36</sup> Despite the good results obtained when X<sub>1</sub> was used (Figure 5.7), the polymer does not have the necessary functionality that would allow further coupling reactions with other molecules or polymers. In the case of X<sub>1</sub>, polymer post-modification reactions would be required in order to achieve a specific functionality in the polymer chain-end. In this context, the concept of the direct introduction of the desired functionality in the RAFT agent is preferable.

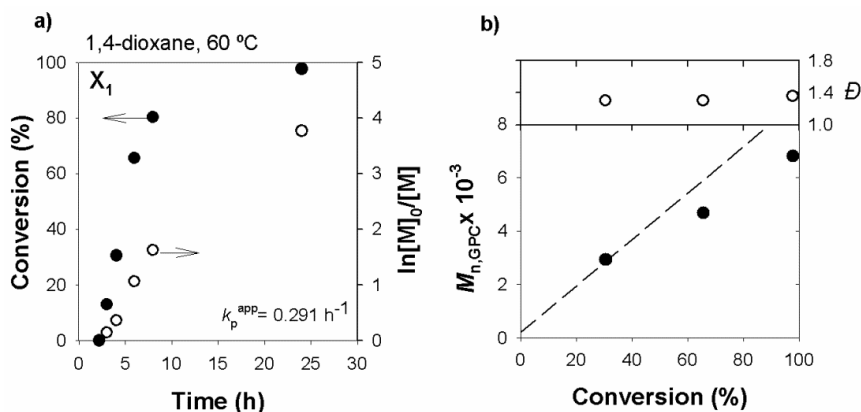


**Figure 5.7:** (a) Kinetic plots of conversion and  $\ln[M]_0/[M]$  vs. time and (b) plot of number-average molecular weights ( $M_{n, GPC}$ ) and  $\bar{D}$  vs. conversion (%) (the dashed line represents the theoretical molecular weight at a given conversion) for RAFT of VAc at 60 °C in 1,4-dioxane using  $X_1$ . Reaction conditions:  $[VAc]_0/[1,4\text{-dioxane}]_0 = 1/1$  (w/w);  $[VAc]_0/[X_1]_0/[AIBN]_0 = 100/1/0.2$  (molar).

The kinetic data presented in Figure 5.7 for  $X_1$  reveals that the polymer  $M_n$  increases linearly with monomer conversion and  $\bar{D}$  remain below 1.4 throughout the polymerization. The obtained values are in accordance with similar literature reports for xanthate mediated RAFT polymerizations of VAc in bulk<sup>32</sup> or in ethyl acetate.<sup>35, 36</sup>

The AT- $X_1$  and PAT-  $X_1$  are xanthate molecules with similar structure to  $X_1$  but with a slight variation of the end-group functionality of the leaving group (R group). The protection of the alkyne moiety (PAT-  $X_1$ ) was performed in order to observe the role of the terminal alkyne in the polymerization course. It is known that the alkyne hydrogen in the end of the leaving group of the RAFT agent may interfere with the radical polymerization<sup>45</sup>. In fact, when  $X_1$  was replaced by AT-  $X_1$ , using similar reaction conditions, the homopolymerization of VAc was slower, and larger  $\bar{D}$  were observed, as shown in the kinetic data presented in Figure 5.8 and GPC traces in Figure D.6 (Annex D).

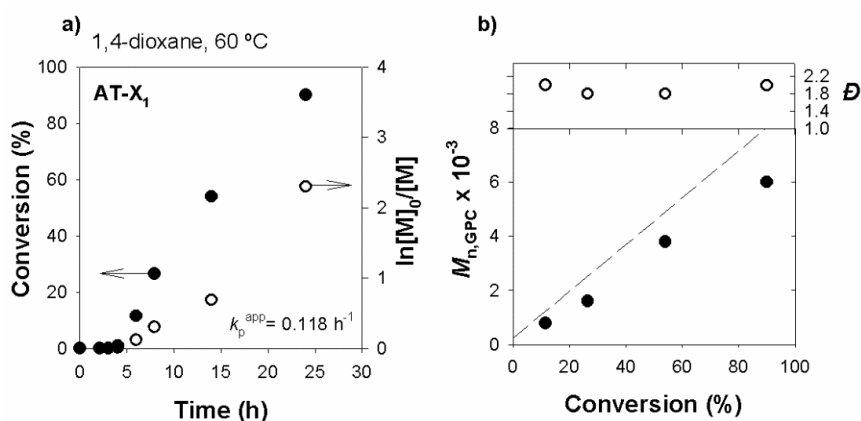


**Figure 5.8:** (a) Kinetic plots of conversion and  $\ln[M]_0/[M]$  vs. time and (b) plot of number-average molecular weights ( $M_{n,\text{GPC}}$ ) and  $\bar{D}$  vs. conversion (%) (the dashed line represents the theoretical molecular weight at a given conversion) for RAFT of VAc at 60 °C in 1,4-dioxane using AT-X<sub>1</sub>. Reaction conditions:  $[\text{VAc}]_0/[\text{1,4-dioxane}]_0 = 1/1$  (w/w);  $[\text{VAc}]_0/[\text{AT-X}_1]_0/[\text{AIBN}]_0 = 100/1/0.2$  (molar).

Figure 5.9 presents the kinetic data obtained for the homopolymerization of VAc using the protected alkyne-terminated RAFT agents (PAT-X<sub>1</sub>). The first-order kinetic and the linear evolution of the MW with the conversion indicate a controlled polymerization. It is interesting to notice that below 70% conversion, the  $\bar{D}$  values are very low for a non-activated monomer such as VAc ( $\bar{D} < 1.2$ ), but tend to increase for high monomer conversions. For conversions above 80%, the  $M_{n,\text{GPC}}$  values become smaller than  $M_{n,\text{th}}$ . This observation may be ascribed to irreversible transfer reactions, chain transfer reactions to monomer and polymer, due to the very reactive nature of the VAc propagating radical.<sup>56</sup> This effect is mostly detected in the polymer GPC traces by the presence of a prominent low MW tail (high retention volume) (Figure 5.9 (c)) and consequent broad molecular weight distributions from moderate to higher monomer conversions. Similar results were already reported for similar RAFT polymerization of VAc (bulk, 60 °C).<sup>57,58</sup>

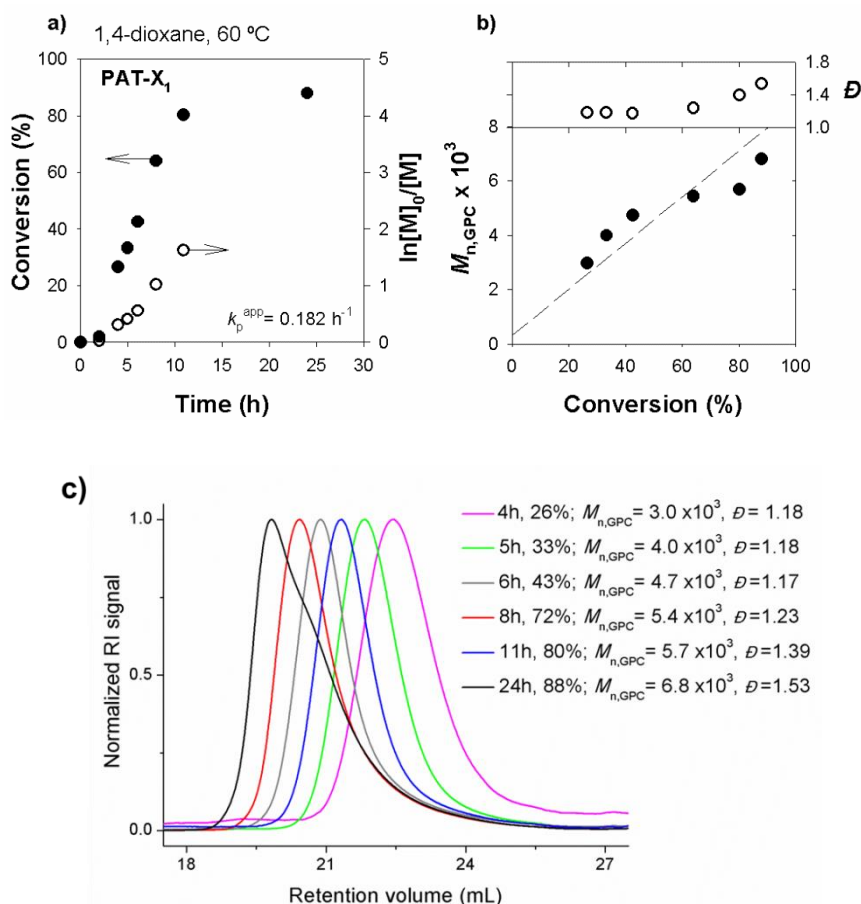


**Figure 5.9:** (a) Kinetic plots of conversion and  $\ln[M]_0/[M]$  vs. time, (b) plot of number-average molecular weights ( $M_{n,GPC}$ ) and  $\bar{D}$  vs. conversion (%) (the dashed line represents the theoretical molecular weight at a given conversion) and (c) evolution of the GPC traces with conversion for the RAFT polymerization of VAc in 1,4-dioxane at 60 °C using PAT-X<sub>1</sub>. Reaction conditions:  $[VAc]_0/[1,4\text{-dioxane}]_0 = 1/1$  (w/w);  $[VAc]_0/[PAT-X_1]_0/[AIBN]_0 = 100/1/0.2$  (molar).

It should be noted the presence of an induction period for the different RAFT agents studied, which could be related with slower fragmentation of the initial RAFT agent and release of the R group. Moreover, several literature reports dealing with the xanthate mediated RAFT polymerization of PVAc reported a similar observation.<sup>59, 60</sup> Even so, for our novel PAT-X<sub>1</sub>, the observed induction period is much smaller. The summary of all experiments performed using the three different RAFT agents is shown in Table 5.1. The results suggest that only the RAFT agents xanthates X<sub>1</sub> and PAT-X<sub>1</sub> were able to control a controlled polymerization of VAc with relatively narrow MW distributions, up to high conversions. Despite the high  $\bar{D}$  value obtained for the last kinetic point using



PAT- $X_1$ , in comparison with the  $X_1$ , the kinetic results present in Figure 5.9, indicate that the  $\bar{D}$  values tend to increase with reaction conversion. The broad MW distribution observed for the reactions with the alkyne functionalized RAFT agent (AT- $X_1$ ) prove the inefficiency of such compound to conduct a controlled polymerization of VAc. On this matter, the  $\bar{D}$  values of the PVAc synthesized through RAFT using AT- $X_1$  or using FRP conditions are similar ( $\bar{D} = 2.2$ ). Furthermore, for the RAFT polymerization of VAc two different free radical initiators were used; the AIBN, and a very fast peroxide initiator, diisobutyl peroxide (Trigonox 187-W40).<sup>12</sup> No polymerization reaction occur in the presence of Trigonox 187-W40 at 42 °C, using the same reaction conditions as for AIBN (Table 5.1, entries 1,5).

**Table 5.1:** Kinetic parameters for the RAFT polymerization of VAc using the  $X_1$ , AT- $X_1$  or PAT- $X_1$  in 1,4-dioxane. Reaction conditions:  $[VAc]_0/[1,4\text{-dioxane}] = 1/1$  (w/w);  $[VAc]_0/[RAFT\text{ agent}]_0/[initiator]_0 = 100/1/0.2$ .

Entry	RAFT agent	Initiator	Temp., °C	Time (h) <sup>a</sup>	Conv. <sup>a</sup> , %	$K_p^{app}$ , h <sup>-1</sup>	$M_{n,th}^a$ x 10 <sup>-3</sup>	$M_{n,GPC}^a$ x 10 <sup>-3</sup>	$\bar{D}^a$
1	$X_1$	AIBN	60	24	98	0.291	8.7	6.80	1.4
2	AT- $X_1$	AIBN	60	24	90	0.118	8.0	6.0	2.0
3	PAT- $X_1$	AIBN	60	32	96	0.182	8.52	6.69	1.6
4	---	AIBN	60	16	--	--	--	6.06	2.2
5	$X_1$	Trigonox	42	48	no polymerization				

<sup>a</sup>values obtained from the last sample from the kinetic study.

### 5.4.3 Thermogravimetric analysis of the RAFT agents

The thermal behavior of RAFT agents was analyzed by TGA (Figure 5.10). The results reveal a single step of mass loss, at relatively low temperatures, for the different RAFT agents synthesized. In order to evaluate the nature of this event, a preparative experiment in a sealed flask under nitrogen was carried out, at 130 °C during 2h. The comparison of <sup>1</sup>H-NMR spectra of the RAFT agent before and after the thermal treatment has shown no differences on the peak integrations, which indicates that the mass loss observed in TGA traces are related to volatilization. No significant mass loss

was observed after the experiment. Regarding the effect of the structure of R group, the results suggest that the volatilization temperature increases with the following order: PAT- $X_1$  > AT- $X_1$  >  $X_1$ .

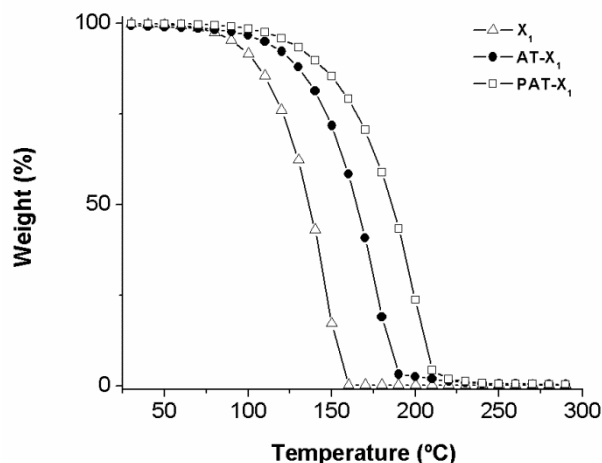


**Figure 5.10:** TGA weight loss curves of  $X_1$ , AT- $X_1$  and PAT-  $X_1$ , obtained at a heating rate of  $10\text{ }^\circ\text{C}\cdot\text{min}^{-1}$ .

#### 5.4.4 PVAc chain-end functionality

The chemical structure of the PVAc synthesized by RAFT polymerization was determined with  $^1\text{H}$  NMR, FTIR-ATR and UV-vis analysis. Figure 5.11 shows the  $^1\text{H}$  NMR spectrum of a PVAc sample synthesized using the PAT- $X_1$ . The characteristic peaks of the PVAc structure at 1.75 ppm (**o**, **o'**,  $-\text{CH}_2-\text{CH}-$ ), 2.02 ppm (**n**, **n'**,  $-\text{CH}_3$ ), 4.86 ppm (**m**,  $-\text{CH}_2-\text{CH}-$ ) and 6.62 ppm (**m'**,  $-\text{CH}_2-\text{CH}-\text{S}$ ) are in agreement with the data reported in the literature.<sup>37</sup> The retention of RAFT functionality is evidenced by the peaks from the PAT- $X_1$  at 0.14 ppm (**k**,  $-\text{Si}(\text{CH}_3)_3-$ ), 0.88 ppm (**a**,  $-\text{CH}_2-\text{CH}_3$ ), 1.17 ppm (**d**,  $-\text{CH}-\text{CH}_3$ ), 2.31 ppm (**j**,  $\text{C}\equiv\text{C}-\text{CH}_2$ ), 3.74 ppm (**b**,  $-\text{CH}_2-\text{CH}_3$ ), 4.07 ppm (**c**,  $-\text{CH}-\text{CH}_3$ ) and 4.15 ppm (**h**,  $-\text{CH}_2-\text{O}-$ ).

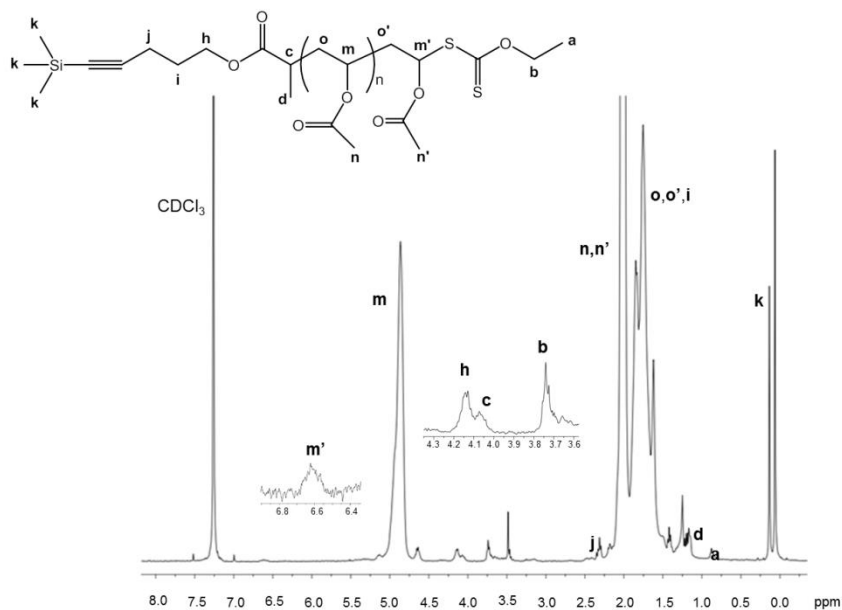


**Figure 5.11:** The  $^1\text{H}$  NMR spectrum of PVAc synthesized by RAFT polymerization using PAT-  $X_1$  ( $M_{n,\text{GPC}} = 6.0 \times 10^3$ ;  $M_{n,\text{NMR}} = 7.56 \times 10^3$ ,  $D = 1.36$ ) in  $\text{CDCl}_3$ .

The preservation of the terminal chain-end during the RAFT reaction can also be accessed by FTIR-ATR analysis. The FTIR-ATR spectra of the PAT-  $X_1$  and the PVAc synthesized using the PAT-  $X_1$  is shown in Figure 5.12. The bands at  $2850\text{--}2940\text{ cm}^{-1}$  are associated to both symmetric and asymmetric C- H stretching vibrations. A strong absorption band at  $1740\text{ cm}^{-1}$  is related with the  $\text{--C=O}$  stretching vibration (carbonyl bond of the ester). The characteristic bands of the xanthate group,  $\text{--C=S}$  and  $\text{C-S}$ , at  $1044\text{ cm}^{-1}$  and  $633\text{ cm}^{-1}$  respectively and the characteristic bands of the trimethylsilyl group ( $\text{--Si--(CH}_3\text{)}_3$ ), at  $755\text{ cm}^{-1}$  and  $840\text{ cm}^{-1}$  are present in both FTIR-ATR spectra.

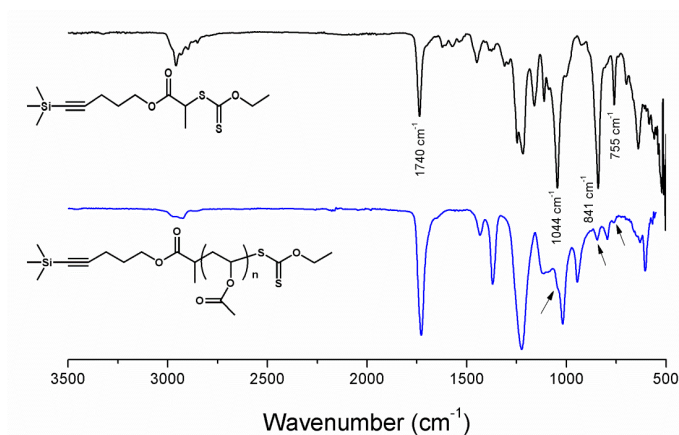


**Figure 5.12:** FTIR-ATR spectra of PAT- $X_1$  and PAT-PVAc.

Ultraviolet-visible (UV-Vis) spectroscopy has been used as an efficient tool to identify the presence of the characteristic -C=S end-group of polymers prepared by RAFT polymerization. The polymer Z-group can be lost during the polymerization process due to side reactions of the thiocarbonyl groups or due to the inherent termination reactions that occurs during the polymerization.<sup>61</sup> The UV-Vis spectra in chloroform of all synthesized PVAc are presented in Figure 5.13. All samples show an absorption band below 300 nm ascribed to the thiocarbonyl bound, indicating the presence of such groups in the final polymer backbone. This thiocarbonyl group can be further removed or transformed in order to achieve a desired functionality and easily conjugate the polymer with other molecules or polymer segments.<sup>62, 63</sup>

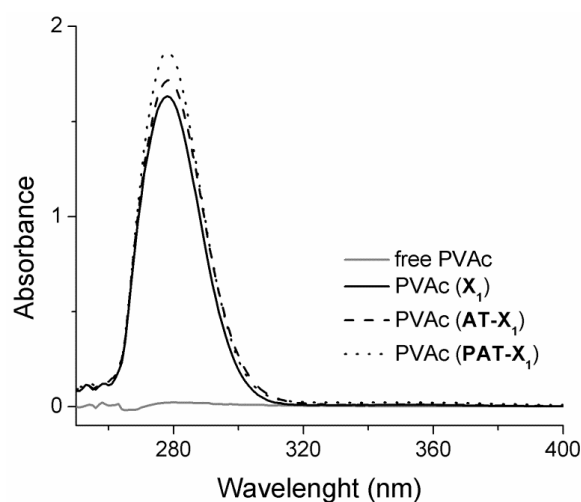


**Figure 5.13:** UV-vis spectra of free-PVAc and PVAc synthesized through RAFT polymerization using the different RAFT agents, X<sub>1</sub>, AT-X<sub>1</sub> and PAT-X<sub>1</sub> respectively. Samples with 1.5 mg.mL<sup>-1</sup> concentration in chloroform.

#### 5.4.5 Chain extension reaction

The PVAc synthesized through RAFT polymerization ( $M_{n, GPC} = 3.01 \times 10^3$ ,  $D = 1.20$ ) was purified and used as macro-RAFT agent. Figure 5.14 shows the complete shift of the MW distribution from a PVAc macroinitiator (macro PAT-PVAc) to a higher MW values (extended PVAc,  $M_{n, GPC} = 10.64 \times 10^3$ ,  $D = 1.88$ ) confirming the “living” nature of the polymer.

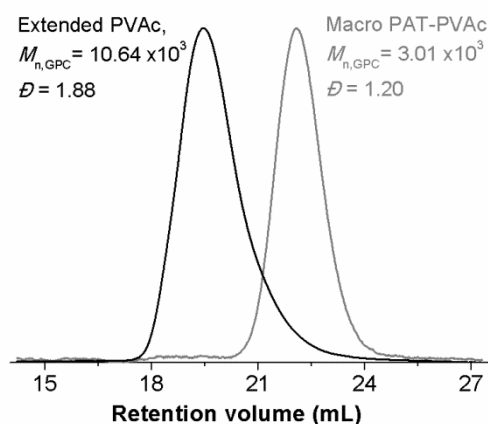


**Figure 5.14:** The GPC traces of PAT-PVAc samples before (on the right, grey line) and after chain extension (on the left, black line) experiment.

#### 5.4.6 Deprotection of PVAc and coupling reaction with N<sub>3</sub>-PEG

After the RAFT polymerization of VAc using the PAT-X<sub>1</sub> (Figure 5.15 (1.1)), the protective trimethyl silyl group was removed using TBAF (Figure 5.15 (1.2)). The success of the reaction was confirmed by the disappearance of the characteristic trimethyl silyl signal (k) at 0.14 ppm by the <sup>1</sup>H NMR spectrum of the unprotected PVAc (Figure 5.11 (k)) and Figure D.7, Annex D). As a proof of concept an azide terminated PEG (N<sub>3</sub>-PEG) was used for the post-polymerization coupling reaction with an alkyne-terminated PVAc (AT-PVAc) (Figure 5.15 (1.3)).

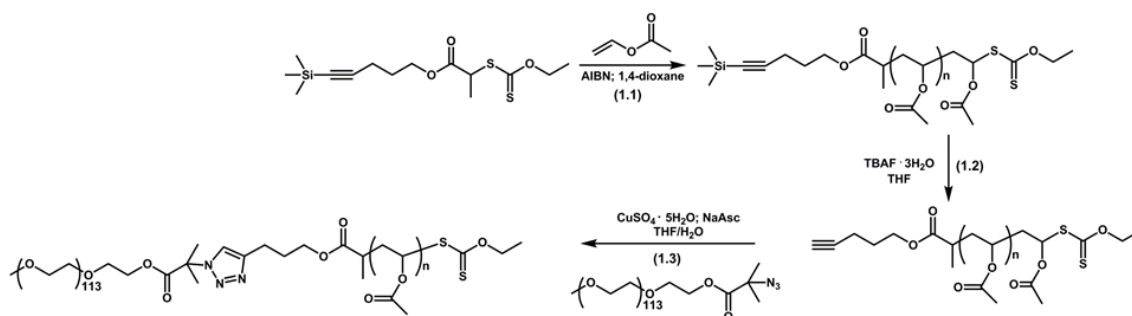


**Figure 5.15:** Schematic representation of the RAFT polymerization of VAc (1.1), PVAc deprotection (1.2) and synthesis of PEG-*b*-PVAc block copolymers by the CuAAC reaction (1.3).

The success of the synthesis of the PEG-*b*-PVAc copolymer was evaluated by GPC and FTIR-ATR spectroscopy. Figure 5.16 shows the clear shift of the MW distribution of the PVAc block towards higher MW values. Moreover, the comparison of FTIR-ATR spectra of the homopolymer precursors, N<sub>3</sub>-PEG and AT-PVAc with the copolymer PEG-*b*-PVAc (Figure D.8, Annex D), confirms the presence of the characteristic bands from each homopolymer segment in the spectrum of the copolymer and reveals the disappearance of the characteristic azide signal at 2100 cm<sup>-1</sup>, confirming the success of the coupling reaction.

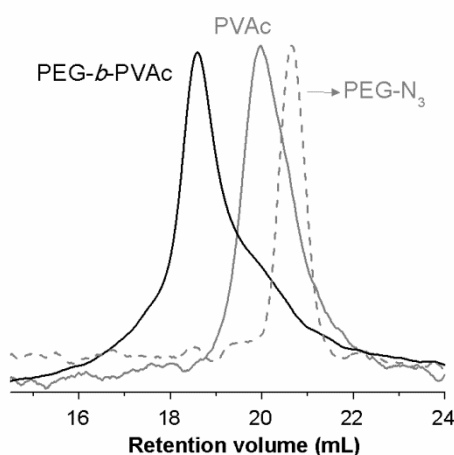


**Figure 5.16:** GPC traces of the RALS signal of the PVAc and PVAc-*b*-PEG copolymer, after the coupling reaction.

## 5.5. Conclusions

We reported the synthesis of one protected alkyne containing xanthate RAFT agent, able to efficiently control the polymerization of VAc. The protection of the alkyne moiety in the RAFT agent is crucial to afford a polymerization with a good control over the MW and with low *D*. The structural analysis of the PVAc, performed by <sup>1</sup>H NMR, FTIR-ATR and UV-vis experiments reveal the retention of the chain-end functionality. The “living” nature of the PVAc synthesized through RAFT was confirmed by a successful chain extension experiment. After the deprotection of the alkyne end group, the well-defined alkyne-terminated PVAc can be easily conjugated with azido-terminated structures through a CuAAC reaction.

## 5.6. References

1. Roth, P.J., C. Boyer, A.B. Lowe, and T.P. Davis (2011). RAFT polymerization and thiol chemistry: a complementary pairing for implementing modern macromolecular design. *Macromol Rapid Commun*, 32(15): 1123-43.
2. Ghadban, A. and L. Albertin (2013). Synthesis of glycopolymer architectures by reversible-deactivation radical polymerization. *Polymers (Basel, Switz.)*, 5(2): 431-526, 96 pp.
3. Konkolewicz, D., Y. Wang, M. Zhong, P. Kryszewski, A.A. Isse, A. Gennaro, and K. Matyjaszewski (2013). Reversible-Deactivation Radical Polymerization in the Presence of Metallic Copper. A Critical Assessment of the SARA ATRP and SET-LRP Mechanisms. *Macromolecules (Washington, DC, U. S.)*, 46(22): 8749-8772.
4. Peng, C.-H., T.-Y. Yang, Y. Zhao, and X. Fu (2014). Reversible deactivation radical polymerization mediated by cobalt complexes: recent progress and perspectives. *Org. Biomol. Chem.*, 12(43): 8580-8587.
5. Wang, W., J. Zhao, N. Zhou, J. Zhu, W. Zhang, X. Pan, Z. Zhang, and X. Zhu (2014). Reversible deactivation radical polymerization in the presence of zero-valent metals: from components to precise polymerization. *Polym. Chem.*, 5(11): 3533-3546.
6. Abreu, C.M.R., A.C. Serra, A.V. Popov, K. Matyjaszewski, T. Guliashvili, and J.F.J. Coelho (2013). Ambient temperature rapid SARA ATRP of acrylates and methacrylates in alcohol-water solutions mediated by a mixed sulfite/Cu(II)Br<sub>2</sub> catalytic system. *Polym. Chem.*, 4(23): 5629-5636.
7. Gois, J.R., D. Konkolewicz, A.V. Popov, T. Guliashvili, K. Matyjaszewski, A.C. Serra, and J.F.J. Coelho (2014). Improvement of the control over SARA ATRP of 2-(diisopropylamino)ethyl methacrylate by slow and continuous addition of sodium dithionite. *Polym. Chem.*, 5(16): 4617-4626.
8. Guliashvili, T., P.V. Mendonca, A.C. Serra, A.V. Popov, and J.F.J. Coelho (2012). Copper-Mediated Controlled/"Living" Radical Polymerization in Polar Solvents: Insights into Some Relevant Mechanistic Aspects. *Chem. - Eur. J.*, 18(15): 4607-4612.
9. Mendonca, P.V., A.C. Serra, J.F.J. Coelho, A.V. Popov, and T. Guliashvili (2011). Ambient temperature rapid ATRP of methyl acrylate, methyl methacrylate and styrene in polar solvents with mixed transition metal catalyst system. *Eur. Polym. J.*, 47(7): 1460-1466.
10. Mendes, J.P., F. Branco, C.M.R. Abreu, P.V. Mendonca, A.V. Popov, T.

- Guliashvili, A.C. Serra, and J.F.J. Coelho (2014). Synergistic Effect of 1-Butyl-3-methylimidazolium Hexafluorophosphate and DMSO in the SARA ATRP at Room Temperature Affording Very Fast Reactions and Polymers with Very Low Dispersity. *ACS Macro Lett.*, 3(6): 544-547.
11. Percec, V., A.V. Popov, E. Ramirez-Castillo, J.F.J. Coelho, and L.A. Hinojosa-Falcon (2004). Non-transition metal-catalyzed living radical polymerization of vinyl chloride initiated with iodoform in water at 25 °C. *Journal of Polymer Science Part A: Polymer Chemistry*, 42(24): 6267-6282.
  12. Abreu, C.M.R., P.V. Mendonça, A.C. Serra, J.F.J. Coelho, A.V. Popov, G. Gryn'ova, M.L. Coote, and T. Guliashvili (2012). Reversible Addition–Fragmentation Chain Transfer Polymerization of Vinyl Chloride. *Macromolecules*, 45(5): 2200-2208.
  13. Piette, Y., A. Debuigne, C. Jerome, V. Bodart, R. Poli, and C. Detrembleur (2012). Cobalt-mediated radical (co)polymerization of vinyl chloride and vinyl acetate. *Polymer Chemistry*, 3(10): 2880-2891.
  14. Johnson, I.J., E. Khosravi, O.M. Musa, R.E. Simnett, and A.M. Eissa (2015). Xanthates designed for the preparation of N-Vinyl pyrrolidone-based linear and star architectures via RAFT polymerization. *J. Polym. Sci., Part A: Polym. Chem.*, 53(6): 775-786.
  15. Iovu, M.C. and K. Matyjaszewski (2003). Controlled/living radical polymerization of vinyl acetate by degenerative transfer with alkyl iodides. *Macromolecules*, 36(25): 9346-9354.
  16. Percec, V., T. Guliashvili, J.S. Ladislaw, A. Wistrand, A. Stjerndahl, M.J. Sienkowska, M.J. Monteiro, and S. Sahoo (2006). Ultrafast Synthesis of Ultrahigh Molar Mass Polymers by Metal-Catalyzed Living Radical Polymerization of Acrylates, Methacrylates, and Vinyl Chloride Mediated by SET at 25 °C. *Journal of the American Chemical Society*, 128(43): 14156-14165.
  17. Harrison, S., X. Liu, J.-N. Ollagnier, O. Coutelier, J.-D. Marty, and M. Destarac (2014). RAFT Polymerization of Vinyl Esters: Synthesis and Applications. *Polymers*, 6(5): 1437.
  18. Mendes, J.P., F. Branco, C.M.R. Abreu, P.V. Mendonça, A.C. Serra, A.V. Popov, T. Guliashvili, and J.F.J. Coelho (2014). Sulfolane: an Efficient and Universal Solvent for Copper-Mediated Atom Transfer Radical (co)Polymerization of Acrylates, Methacrylates, Styrene, and Vinyl Chloride. *ACS Macro Letters*, 3(9): 858-861.
  19. Huadong, T., R. Maciej, and S. Youqing (2009). Controlled/"Living" Radical



- Polymerization of Vinyl Acetate, in *Controlled/Living Radical Polymerization: Progress in ATRP*. American Chemical Society. 139-157.
20. Percec, V., A.V. Popov, E. Ramirez-Castillo, and J.F.J. Coelho (2005). Single electron transfer-degenerative chain transfer mediated living radical polymerization (SET-DTLRP) of vinyl chloride initiated with methylene iodide and catalyzed by sodium dithionite. *J. Polym. Sci., Part A: Polym. Chem.*, 43(4): 773-778.
  21. Braun, D. (2005). Controlled free-radical polymerization of vinyl chloride. *Journal of Vinyl and Additive Technology*, 11(3): 86-90.
  22. Peng, C.-H., J. Scricco, S. Li, M. Fryd, and B.B. Wayland (2008). Organo-Cobalt Mediated Living Radical Polymerization of Vinyl Acetate. *Macromolecules*, 41(7): 2368-2373.
  23. Lin, Y.-C., Y.-L. Hsieh, Y.-D. Lin, and C.-H. Peng (2014). Cobalt Bipyridine Bisphenolate Complex in Controlled/Living Radical Polymerization of Vinyl Monomers. *Macromolecules*, 47(21): 7362-7369.
  24. Kermagoret, A., Y. Nakamura, M. Bourguignon, C. Detrembleur, C. Jérôme, S. Yamago, and A. Debuigne (2014). Expanding the Scope of Controlled Radical Polymerization via Cobalt–Tellurium Radical Exchange Reaction. *ACS Macro Letters*, 3(1): 114-118.
  25. Morin, A.N., C. Detrembleur, C. Jérôme, P. De Tullio, R. Poli, and A. Debuigne (2013). Effect of Head-to-Head Addition in Vinyl Acetate Controlled Radical Polymerization: Why Is Co(acac)<sub>2</sub>-Mediated Polymerization so Much Better? *Macromolecules*, 46(11): 4303-4312.
  26. Moad, G., E. Rizzardo, and S.H. Thang (2005). Living Radical Polymerization by the RAFT Process. *Australian Journal of Chemistry*, 58(6): 379-410.
  27. Paradossi, G., F. Cavalieri, E. Chiessi, C. Spagnoli, and M. Cowman (2003). Poly(vinyl alcohol) as versatile biomaterial for potential biomedical applications. *Journal of Materials Science: Materials in Medicine*, 14(8): 687-691.
  28. Destarac, M. (2011). On the Critical Role of RAFT Agent Design in Reversible Addition-Fragmentation Chain Transfer (RAFT) Polymerization. *Polymer Reviews*, 51(2): 163-187.
  29. Moad, G., E. Rizzardo, and S.H. Thang (2012). Living Radical Polymerization by the RAFT Process - A Third Update. *Australian Journal of Chemistry*, 65(8): 985-1076.

30. Boyer, C., V. Bulmus, T.P. Davis, V. Ladmiral, J.Q. Liu, and S. Perrier (2009). Bioapplications of RAFT Polymerization. *Chemical Reviews*, 109(11): 5402-5436.
31. Dufils, P.E., G. David, B. Boutevin, G. Woodward, G. Otter, A. Guinaudeau, S. Mazières, and M. Destarac (2012). Phosphonate-terminated poly(vinyl acetate) synthesized by RAFT/MADIX polymerization. *Journal of Polymer Science Part A: Polymer Chemistry*, 50(10): 1997-2007.
32. Stenzel, M.H., L. Cummins, G.E. Roberts, T.P. Davis, P. Vana, and C. Barner-Kowollik (2003). Xanthate Mediated Living Polymerization of Vinyl Acetate: A Systematic Variation in MADIX/RAFT Agent Structure. *Macromolecular Chemistry and Physics*, 204(9): 1160-1168.
33. Simms, R.W., T.P. Davis, and M.F. Cunningham (2005). Xanthate-Mediated Living Radical Polymerization of Vinyl Acetate in Miniemulsion. *Macromolecular Rapid Communications*, 26(8): 592-596.
34. Theis, A., T.P. Davis, M.H. Stenzel, and C. Barner-Kowollik (2006). Probing the reaction kinetics of vinyl acetate free radical polymerization via living free radical polymerization (MADIX). *Polymer*, 47(4): 999-1010.
35. Schmitt, J., N. Blanchard, and J. Poly (2011). Controlled synthesis of branched poly(vinyl acetate)s by xanthate-mediated RAFT self-condensing vinyl (co)polymerization. *Polymer Chemistry*, 2(10): 2231-2238.
36. Girard, E., T. Tassaing, J.-D. Marty, and M. Destarac (2011). Influence of macromolecular characteristics of RAFT/MADIX poly(vinyl acetate)-based (co)polymers on their solubility in supercritical carbon dioxide. *Polymer Chemistry*, 2(10): 2222-2230.
37. Patel, V.K., N.K. Vishwakarma, A.K. Mishra, C.S. Biswas, and B. Ray (2012). (S)-2-(ethyl propionate)-(O-ethyl xanthate)- and (S)-2-(Ethyl isobutyrate)-(O-ethyl xanthate)-mediated RAFT polymerization of vinyl acetate. *Journal of Applied Polymer Science*, 125(4): 2946-2955.
38. Charmot, D., P. Corpart, H. Adam, S.Z. Zard, T. Biadatti, and G. Bouhadir (2000). Controlled radical polymerization in dispersed media. *Macromolecular Symposia*, 150(1): 23-32.
39. Keddie, D.J., C. Guerrero-Sanchez, G. Moad, R.J. Mulder, E. Rizzardo, and S.H. Thang (2012). Chain Transfer Kinetics of Acid/Base Switchable N-Aryl-N-Pyridyl Dithiocarbamate RAFT Agents in Methyl Acrylate, N-Vinylcarbazole and Vinyl Acetate Polymerization. *Macromolecules*, 45(10): 4205-4215.
40. Destarac, M., D. Charmot, X. Franck, and S.Z. Zard (2000). Dithiocarbamates as

- universal reversible addition-fragmentation chain transfer agents. *Macromolecular Rapid Communications*, 21(15): 1035-1039.
41. Keddie, D.J. (2014). A guide to the synthesis of block copolymers using reversible-addition fragmentation chain transfer (RAFT) polymerization. *Chemical Society Reviews*, 43(2): 496-505.
  42. Fournier, D., R. Hoogenboom, and U.S. Schubert (2007). Clicking polymers: a straightforward approach to novel macromolecular architectures. *Chemical Society Reviews*, 36(8): 1369-1380.
  43. Benaglia, M., J. Chiefari, Y.K. Chong, G. Moad, E. Rizzardo, and S.H. Thang (2009). Universal (Switchable) RAFT Agents. *Journal of the American Chemical Society*, 131(20): 6914-6915.
  44. Gregory, A. and M.H. Stenzel (2012). Complex polymer architectures via RAFT polymerization: From fundamental process to extending the scope using click chemistry and nature's building blocks. *Progress in Polymer Science*, 37(1): 38-105.
  45. Quemener, D., T.P. Davis, C. Barner-Kowollik, and M.H. Stenzel (2006). RAFT and click chemistry: A versatile approach to well-defined block copolymers. *Chemical Communications*, (48): 5051-5053.
  46. Kolb, H.C., M.G. Finn, and K.B. Sharpless (2001). Click chemistry: Diverse chemical function from a few good reactions. *Angewandte Chemie-International Edition*, 40(11): 2004-+.
  47. Quémener, D., M.L. Hellayé, C. Bissett, T.P. Davis, C. Barner-Kowollik, and M.H. Stenzel (2008). Graft block copolymers of propargyl methacrylate and vinyl acetate via a combination of RAFT/MADIX and click chemistry: Reaction analysis. *Journal of Polymer Science Part A: Polymer Chemistry*, 46(1): 155-173.
  48. Patel, V.K., N.K. Vishwakarma, A.K. Mishra, C.S. Biswas, P. Maiti, and B. Ray (2013). Synthesis of alkyne-terminated xanthate RAFT agents and their uses for the controlled radical polymerization of N-vinylpyrrolidone and the synthesis of its block copolymer using click chemistry. *Journal of Applied Polymer Science*, 127(6): 4305-4317.
  49. Sun, X., H. Zhang, X. Huang, X. Wang, and Q.-F. Zhou (2005). Synthesis of poly(ethylene oxide)-block-poly(methyl methacrylate)-block-polystyrene triblock copolymers by two-step atom transfer radical polymerization. *Polymer*, 46(14): 5251-5257.
  50. Rocha, N., P.V. Mendonca, J.P. Mendes, P.N. Simoes, A.V. Popov, T. Guliashvili,

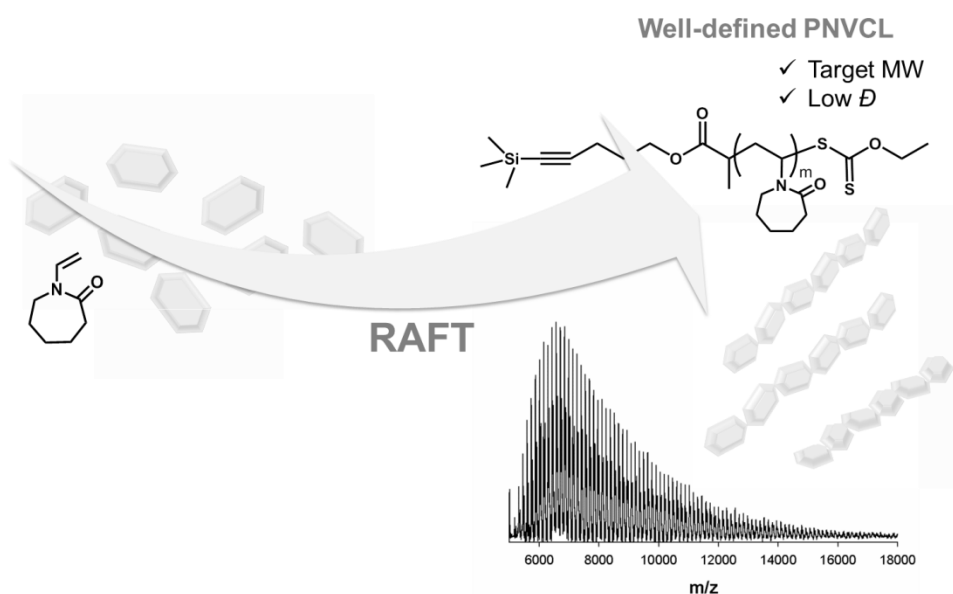
- A.C. Serra, and J.F.J. Coelho (2013). Facile Synthesis of Well-Defined Telechelic Alkyne-Terminated Polystyrene in Polar Media Using ATRP With Mixed Fe/Cu Transition Metal Catalyst. *Macromol. Chem. Phys.*, 214(1): 76-84.
51. Destarac, M., C. Brochon, J.-M. Catala, A. Wilczewska, and S.Z. Zard (2002). Macromolecular design via the interchange of xanthates (MADIX): polymerization of styrene with O-ethyl xanthates as controlling agents. *Macromol. Chem. Phys.*, 203(16): 2281-2289.
52. Mori, H., E. Kudo, Y. Saito, A. Onuma, and M. Morishima (2010). RAFT Polymerization of Vinyl Sulfonate Esters for the Controlled Synthesis of Poly(lithium vinyl sulfonate) and Sulfonated Block Copolymers. *Macromolecules (Washington, DC, U. S.)*, 43(17): 7021-7032.
53. Eliel, E.L. (1982). Prostereoisomerism (prochirality). *Top. Curr. Chem.*, 105(1): 1-76.
54. Fujita, S. (2006). Complete settlement of long-standing confusion on the term 'prochirality' in stereochemistry. Proposal of pro-RS-stereogenicity and integrated treatment with prochirality. *Tetrahedron*, 62(4): 691-705.
55. Bentley, R. (2007). A reflection prochirality. *Chem. Educ.*, 12(5): 316-321.
56. Britton, D., F. Heatley, and P.A. Lovell (1998). Chain Transfer to Polymer in Free-Radical Bulk and Emulsion Polymerization of Vinyl Acetate Studied by NMR Spectroscopy. *Macromolecules*, 31(9): 2828-2837.
57. Bernard, J., A. Favier, L. Zhang, A. Nilasaroya, T.P. Davis, C. Barner-Kowollik, and M.H. Stenzel (2005). Poly(vinyl ester) Star Polymers via Xanthate-Mediated Living Radical Polymerization: From Poly(vinyl alcohol) to Glycopolymer Stars. *Macromolecules*, 38(13): 5475-5484.
58. Favier, A., C. Barner-Kowollik, T.P. Davis, and M.H. Stenzel (2004). A Detailed On-Line FT/NIR and <sup>1</sup>H NMR Spectroscopic Investigation into Factors Causing Inhibition in Xanthate-Mediated Vinyl Acetate Polymerization. *Macromolecular Chemistry and Physics*, 205(7): 925-936.
59. Yan, Y., W. Zhang, Y. Qiu, Z. Zhang, J. Zhu, Z. Cheng, W. Zhang, and X. Zhu (2010). Universal xanthate-mediated controlled free radical polymerizations of the "less activated" vinyl monomers. *Journal of Polymer Science Part A: Polymer Chemistry*, 48(22): 5206-5214.
60. Fleet, R., J.B. McLeary, V. Grumel, W.G. Weber, H. Matahwa, and R.D. Sanderson (2007). Preparation of New Multiarmed RAFT Agents for the Mediation of Vinyl Acetate Polymerization. *Macromolecular Symposia*, 255(1): 8-19.

61. Skrabania, K., A. Miasnikova, A.M. Bivigou-Koumba, D. Zehm, and A. Laschewsky (2011). Examining the UV-vis absorption of RAFT chain transfer agents and their use for polymer analysis. *Polymer Chemistry*, 2(9): 2074-2083.
62. Willcock, H. and R.K. O'Reilly (2010). End group removal and modification of RAFT polymers. *Polymer Chemistry*, 1(2): 149-157.
63. Keddie, D.J., G. Moad, E. Rizzardo, and S.H. Thang (2012). RAFT Agent Design and Synthesis. *Macromolecules*, 45(13): 5321-5342.



## Chapter 6

# RAFT polymerization of alkyne terminated *N*-vinyl caprolactam: kinetic studies and polymer characterization



The contents of this chapter will be submitted for publication: **Góis, J. R., Popov, A. V., Serra, A. C. and Coelho J. F. J.,** “RAFT polymerization of alkyne terminated *N*-vinyl caprolactam: kinetic studies and polymer characterization”.





## 6.1. Abstract

The synthesis of alkyne-functionalized poly (*N*-vinyl caprolactam) (PNVCL) by reversible addition fragmentation chain transfer (RAFT) using two new xanthates is reported. The kinetic data obtained for the RAFT polymerization of NVCL in 1,4-dioxane at 60 °C revealed a linear increase of the polymer molecular weight with the monomer conversion as well as low dispersity ( $D$ ) during the entire course of the polymerization. Despite the non-activated nature of the monomer, which difficult the control over the polymerization, the results showed that the use of a protected alkyne-terminated RAFT agent (PAT- $X_1$ ) allowed the synthesis of well-defined PNVCL with low  $D$  ( $D < 1.4$ ), and good conversion rates (70%) in 12h. The resulting PNVCL was fully characterized using  $^1\text{H}$  nuclear magnetic resonance ( $^1\text{H}$  NMR), matrix-assisted laser desorption ionization time-of-flight mass spectrometry (MALDI-TOF-MS), Fourier-transform infrared spectroscopy (FTIR) and gel permeation chromatography (GPC) techniques. The temperature-responsive features of PNVCL in aqueous solutions were fully investigated under different conditions using turbidimetry. The presented strategy allows the synthesis of well-defined PNVCL with sharp and reversible phase transition temperatures around 37 °C. By manipulating the polymer molecular weight, or the solution properties, it is possible to tune the PNVCL phase transition. As a proof-of concept, the alkyne functionalized PNVCL was used to afford new linear block copolymers, by reacting with an azide terminated poly(ethylene glycol) ( $\text{N}_3$ -PEG) through the copper catalyzed azide-alkyne [3+2] dipolar cycloaddition (CuAAC) reaction.

## 6.2. Introduction

Temperature-responsive polymers (also known as thermo-responsive polymers), whose solubility depends on solution temperature have been widely investigated for biomedical applications.<sup>1-3</sup> Poly(*N*-vinylcaprolactam) (PNVCL) is a nonionic, water soluble, temperature responsive polymer derived from an inexpensive monomer, *N*-vinylcaprolactam (NVCL). PNVCL exhibits a lower critical solution temperature (LCST) close to the physiological temperature (34 - 37°C).<sup>4-7</sup> Furthermore, PNVCL is biocompatible<sup>8,9</sup> and has low cytotoxic<sup>7, 10, 11</sup>, which makes it a very attractive polymer

to be applied in the biomedical field.<sup>5, 6, 9, 10, 12, 13</sup> In comparison to other polymers with LCST close to physiological temperature, i.e. poly(*N*-isopropylacrylamide) (PNIPAM), the PNVCL stands out as temperature-responsive material for biomedical applications since the hydrolysis of the amide group of the NVCL units does not form harmful small compounds.<sup>10, 11</sup> Recent *in vitro* studies suggest that PNVCL is well tolerated at concentrations below 10 mg.ml<sup>-1</sup> and presents a low cytotoxicity for polymers with lower molecular weight (MW).<sup>11, 13, 14</sup> Through 3-(4,5-dimethylthiazol-2-yl)-2,5-diphenyltetrazolium bromide (MTT) tests, Zhang et al<sup>15</sup> demonstrate that PNVCL homopolymers and NVCL copolymers with *N*-vinylpyrrolidone (NVP), and hydrophobic *N*-t-boc-tryptophanamido-*N*-methacryl thioureas are non-cytotoxic. For concentrations ranging from 0.1 to 100 µg mL<sup>-1</sup> the cell viability of the polymer was almost 100 % at 37 °C, compared to negative controls. Recently, Jayakumar and co-workers<sup>8</sup> developed biodegradable and thermo-responsive polymeric nanoparticles based on chitosan and PNVCL for cancer drug delivery, confirming the low-toxicity and the efficient cell uptake of the nanocarriers.

PNVCL exhibits a “classical” Flory-Huggins miscibility behaviour (Type I) in water.<sup>4</sup> It is known that the decrease of the MW of PNVCL increases the LCST value, mainly due to increase of hydrophilicity of the polymer.<sup>16</sup> Indeed, the LCST value of the PNVCL is very sensitive to changes in the polymer MW, concentration and composition of the solution, which makes the transition hydrophilic/hydrophobic very tuneable without the need of others structural changes involving, for example, the addition of hydrophobic segments (e.g. poly(vinyl acetate) (PVAc)).<sup>17</sup> Due to the attractive properties of PNVCL for biomedical applications, several reports have been published using nanoparticles based on PNVCL for drug delivery systems (DDS),<sup>8, 14, 15, 18</sup> nanoparticles for photodynamic therapy,<sup>19</sup> radiotherapy of solid tumours,<sup>20</sup> hydrogels,<sup>21</sup> films<sup>22</sup> or other applications such as dental restorative cements.<sup>9</sup>

The non-activated nature of NVCL turns its controlled polymer synthesis extremely challenging. Indeed, most of the available references involving the use of PNVCL deal with free radical polymerization (FRP) using 2,2'-azobis(2-methylpropionitrile) (AIBN) as conventional initiator.<sup>4, 9-11, 15, 23</sup> The FRP hampers any stringent control over the structure, morphology or composition. This critical limitation is even more relevant in polymers as PNVCL that present strong structure-performance dependence. The available literature dealing with the synthesis of well-defined PNVCL by reversible

deactivation radical polymerization (RDRP) methods is very scarce, with only a few reports about reversible addition fragmentation chain transfer (RAFT) polymerization,<sup>16, 24-26</sup> cobalt-mediated radical polymerization,<sup>17, 27, 28</sup> and atom transfer radical polymerization.<sup>29-31</sup> For the RAFT polymerization of NVCL, the choice of the RAFT agent is of extremely importance to attain PNVCL with controlled features. Being the RAFT polymerization mediated by xanthates, generally designated as macromolecular design via interchange of xanthates (MADIX)/RAFT polymerization, the most suitable strategy. *O*-Ethyl xanthates have been reported as efficient RAFT agents for the synthesis of non-activated monomers.<sup>24, 26</sup> Beija and co-authors used the *O*-ethyl-*S*-(1-methoxycarbonyl)ethyl dithiocarbonate ( $X_1$ ) as a RAFT agent for the synthesis of PNVCL in 1,4-dioxane. PNVCL, with a range of MW from 18000 to 150000 g.mol<sup>-1</sup> with narrow MW distribution ( $D \sim 1.1$ ).<sup>25</sup>

The concept of “click” chemistry, introduced by Sharpless and co-workers<sup>32</sup> is a very convenient synthetic tool in polymer chemistry to afford polymers with diverse compositions, topologies or functionalities. Among several ‘click’ chemistry reactions reported in the literature, the copper-catalyzed azide-alkyne [3+2] dipolar cycloaddition (CuAAC) reaction is the most popular.<sup>33-35</sup> It is a high selective reaction with almost complete conversion obtained under mild reaction conditions.<sup>33, 34, 36</sup> The conjugation of different molecules is possible by using initiators, monomers or polymers functionalized with “click” moieties.<sup>37</sup> The primary goal of this work was the development of suitable polymerization conditions to afford well-controlled PNVCL via RAFT polymerization with a specific polymer chain end-functionality. The use of a functionalized RAFT agents presents several advantages: eliminates the need of post-polymerization reactions to functionalize the polymer and facilitates the synthesis of complex structures and expands the range of applications of this temperature-responsive polymer.

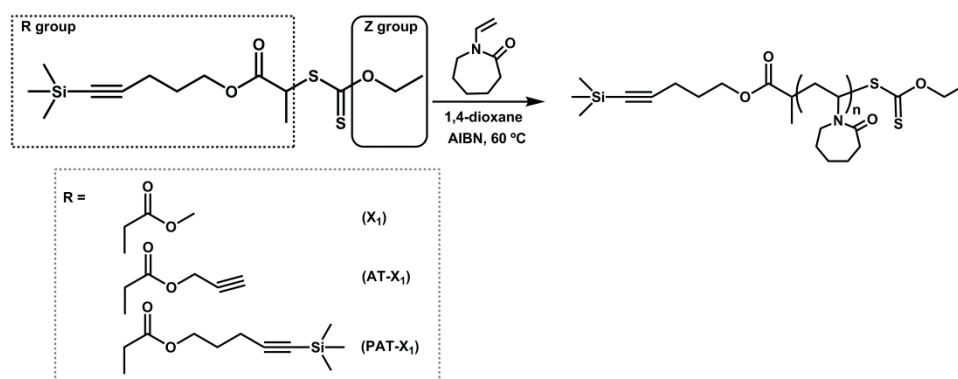


**Figure 6.1:** RAFT polymerization of NVCL mediated by *O*-ethyl-*S*-(1-methoxycarbonyl)ethyl dithiocarbonate (X<sub>1</sub>), alkyne-terminated RAFT agent (AT-X<sub>1</sub>) or protected alkyne terminated RAFT agent (PAT-X<sub>1</sub>).

## 6.3. Experimental Section

### 6.3.1. Materials

*N*-vinylcaprolactam (98%, Sigma-Aldrich) was dissolved in hexane and purified by passing through a short alumina column and then recrystallized. 2,2'-Azobis(2-methylpropanitrile) (AIBN) (98%, Fluka) was purified by recrystallization from methanol before use. The 1,4-dioxane (99.8%, Acros Organics) was dried over calcium hydride and distilled under reduced pressure prior to use. Poly(ethylene glycol) methyl ether (mPEG<sub>113</sub>, MW = 5000 Da) (Aldrich) was dried by azeotropic distillation with toluene ( $M_{n,GPC} = 5.06 \times 10^3$ ;  $D = 1.03$ ). Tetrabutylammonium fluoride trihydrate (TBAF·3H<sub>2</sub>O) (99%, Acros Organics), 2-(2-chloroethoxy)ethanol (99%, Sigma-Aldrich), sodium azide (NaN<sub>3</sub>) (≥ 99.5%, Sigma-Aldrich), hexadecyltrimethyl ammonium bromide (≥ 99%, Sigma-Aldrich), succinic anhydride (≥ 99%, Sigma-Aldrich), 4-(dimethylamino)pyridine (DMAP) (≥ 99 %, TCI Europe), *N,N'*-diisopropylcarbodiimide (DIC) (99%, Sigma-Aldrich), sodium ascorbate (NaAsc) (≥ 98%, Sigma), copper(II) sulfate pentahydrate (CuSO<sub>4</sub>·5H<sub>2</sub>O) (≥ 98%, Aldrich), anhydrous sodium sulfate (≥ 98 %, Fisher Chemical), dithranol (DT) (98%, Sigma-Aldrich), phosphate buffered Saline (PBS) tablets (Sigma), deuterated chloroform (CDCl<sub>3</sub>) (Euriso-top, +1% TMS), hexane (≥ 98.5%, Fisher Scientific), ethyl acetate (Fisher Chemical), dichloromethane (DCM) (99.99%, Fisher Scientific), diethyl ether (> 99%, Fisher Scientific), petroleum ether (Fisher Scientific), and tetrahydrofuran

(THF) (Fisher Scientific), were used as received. Purified water (MilliQ<sup>®</sup>, Millipore, resistivity >18 M $\Omega$ ·cm) was obtained by reverse osmosis. For gel permeation chromatography (GPC), poly(methyl methacrylate) (PMMA) standards (Polymer Laboratories) (99%, ~70 mesh, Acros) and high performance liquid chromatography (HPLC) dimethylformamide (DMF) (HPLC grade, Panreac) were used as received.

The RAFT agents used in the RAFT polymerization of NVCL, *O*-ethyl-*S*-(1-methoxycarbonyl) ethyl- dithiocarbonate ( $X_1$ ), alkyne-terminated RAFT agent (AT- $X_1$ ) and protected alkyne-terminated RAFT agent (PAT-  $X_1$ ) were synthesized according to the methods previously described in Chapter 5.

The azido ethoxy ethanol,<sup>38</sup> carboxylic acid-terminated poly(ethylene glycol) methyl ether (mPEG-COOH) and azide terminated poly(ethylene glycol) methyl ether (mPEG-N<sub>3</sub>)<sup>39</sup> were synthesized based on the procedures described in the literature. The detailed synthesis is presented in Annexe E.

### 6.3.2. Characterization

The chromatographic parameters of the samples were determined by gel permeation chromatography (GPC), with refractive index (RI) (Knauer K-2301), differential viscometer (DV) and right angle light scattering (Viscotek 270 Dual Detector) detectors. The column set consisted of a PL 10- $\mu$ L guard column (50 x 7.5 mm<sup>2</sup>), followed by two MIXED-B PL columns (300 x 7.5 mm<sup>2</sup>, 10  $\mu$ L). The HPLC pump was set with a flow rate of 1 mL·min<sup>-1</sup> and the analyses were carried out at 60 °C using an Elder CH-150 heater. The eluent was DMF, containing 0.3% of LiBr. The samples were filtered through a polytetrafluoroethylene (PTFE) membrane with 0.2  $\mu$ m pore size before injection (100  $\mu$ L). The system was calibrated with narrow PMMA standards. The  $M_{n,GPC}$  and  $D$  of the synthesized polymers were determined by using a multidetector calibration system (OmniSEC software version: 4.6.1.354). The refractive index increment ( $dn/dc$ ) of the PNVCL in DMF at 60 °C was determined using an automatic refractometer for  $\lambda = 670$  nm (Rudolph Research, J357 NDS-670-CC).

<sup>1</sup>H and <sup>13</sup>C nuclear magnetic resonance (NMR) spectra were recorded on a Bruker Avance III 400 MHz spectrometer, with a 5 mm TXI triple resonance detection probe, in CDCl<sub>3</sub> with tetramethylsilane (TMS) as an internal standard. Conversion of

monomers was determined by integration of monomer and polymer peaks using MestReNova software version: 6.0.2-5475.

For matrix-assisted laser desorption ionization time-of-flight mass spectroscopy (MALDI-TOF-MS) analysis, the PNVCL samples were dissolved in THF at a concentration of 10 mg.mL<sup>-1</sup> and dithranol (DT) (25 mg.mL<sup>-1</sup> in THF) was used as a matrix and ionization agent. 10 µL of the PNVCL solution was mixed with 10 µL of the DT solution in a 1 mL Eppendorf tube. The dried-droplet sample preparation technique was used: 2 µL of the mixture was directly spotted on the MTP TF MALDI target, Bruker Daltonik (Bremen, Germany) and allowed to dry at room temperature, to allow matrix crystallization. The analysis was done in triplicate for each sample. External mass calibration was performed with a peptide calibration standard (Bruker Starter Kit) for 250 mass calibration points. Mass spectra were recorded using an Ultraflex III TOF/TOF MALDI-TOF mass spectrometer Bruker Daltonik (Bremen, Germany) operating in the linear positive ion mode, working under flexControl software (version 3.4, Bruker Daltonik, Bremen, Germany). Ions were formed upon irradiation by a smart beam laser using a frequency of 200 Hz. Each mass spectrum was produced by averaging 2000 laser shots collected across the whole sample spot surface by screening in the range m/z 5-20 kDa. The laser irradiance was set to 50 % (relative scale 0-100) arbitrary units according to the corresponding threshold required for the applied matrix systems. Data analysis was done with flexAnalysis software (version 3.4, Bruker Daltonik, Bremen, Germany).

Elemental composition of the PNVCL synthesized by RAFT was determined using an elemental analyzer EA1108 CHNS-O from Fisons Instruments.

Fourier-transform infrared spectroscopy (FTIR) was performed at room temperature, at 128 scans and with a 4 cm<sup>-1</sup> resolution between 500 and 4000 cm<sup>-1</sup>, using a JASCO 4200 FTIR spectrophotometer (MKII GoldenGate™ Single Reflexion ATR System).

The thermogravimetric analysis (TGA) were carried out on a TGA Q 500 machine (TA Instruments), from room temperature up to 600 °C, at a 10 °C.min<sup>-1</sup> heating rate, under a dry nitrogen atmosphere (at 40 mL.min<sup>-1</sup>) using approximately 5mg of the sample.

**Turbidimetry analysis.**

The determination of the cloud point temperatures ( $T_{CP}$ ) was achieved by turbidimetry analysis. The PNVCL polymers were dissolved in MilliQ<sup>®</sup> water at 1.0 mg.ml<sup>-1</sup> concentration. The solutions were maintained at room temperature for at least 6h to reach equilibrium. The optical transmittance at 630 nm of each PNVCL solution was monitored as a function of temperature using a modular UV-vis spectrometer equipped with a UV-Vis light source (DH-2000, Ocean optics) and a temperature controlled cuvette holder (qpod<sup>®</sup>, Quantum Northwest, Inc.) with magnetic stirrer, run by a water circulating temperature controller (TC 125, Quantum Northwest, Inc.). The solution transmittance was assessed with time using SpectraScan software version: 1.0. The heating/cooling rate was 1 °C.min<sup>-1</sup>, 0.5 °C.min<sup>-1</sup> or 0.1 °C.min<sup>-1</sup>. The  $T_{CP}$  was defined as the intercept of the tangents at the onset of turbidity. MilliQ<sup>®</sup> water was used as reference.

**6.3.3. Procedures****Typical procedure for the MADIX/RAFT polymerization of NVCL.**

The NVCL (4.00 g, 28.74 mmol), PAT-X<sub>1</sub> (15.93 mg, 0.05mmol) and AIBN (3.93 mg, 0.02 mmol) were dissolved in 3.87 mL of 1,4-dioxane and placed in a 25 mL Schlenk reactor. The mixture was bubbled with nitrogen for about 40 minutes at ambient temperature. The Schlenk reactor was then sealed, flushed with nitrogen and placed in an oil bath at 60 °C under stirring (500 rpm). For the kinetic studies, different reaction mixture samples were collected during the polymerization by using an airtight syringe and purging the side arm of the Schlenk tube reactor with nitrogen. The samples were analyzed by <sup>1</sup>H NMR spectroscopy in order to calculate the monomer conversion and by GPC to determine de  $M_{n, GPC}$  and  $\bar{D}$ . The final reaction mixture was precipitated in cold petroleum ether, dissolved in THF and precipitated again in cold petroleum ether (2x) and dried over vacuum to obtain PNVCL as white powder.

**Typical procedure for the PNVCL deprotection.**

2.02 g (0.06 mmol) of pure PNVCL obtained from a RAFT polymerization mediated by PAT-X<sub>1</sub> ( $M_{n, th} = 31.33 \times 10^3$ ,  $M_{n, GPC} = 35.35 \times 10^3$ ,  $\bar{D} = 1.25$ ) was dissolved in 20 mL of THF and bubbled with nitrogen for about 10 minutes. The PNVCL solution was cooled down to -20 °C and 700 μL of a 0.2 M solution of TBAF·3H<sub>2</sub>O (0.14 mmol) was slowly

added to the polymer solution. After stirring for 30 minutes at low temperature, the reaction proceeded overnight at ambient temperature. The reaction mixture was passed through a silica column to remove the excess of TBAF and the alkyne-terminated PNVCL (AT-PNVCL) was recovered by precipitation in cold petroleum ether, dried under vacuum and analyzed by  $^1\text{H}$  NMR and GPC ( $M_{n,\text{GPC}} = 38.90 \times 10^3$ ,  $D = 1.26$ ).

**“Click” reaction between AT-PNVCL and  $\text{N}_3$ -PEG.**

60 mg of the AT- PNVCL obtained after the deprotection of the protected alkyne-terminated PNVCL ( $M_{n,\text{GPC}} = 16.13 \times 10^3$ ,  $D = 1.38$ ) (3.72  $\mu\text{mol}$ ) and 29.3 mg of  $\text{N}_3$ -PEG (5.58  $\mu\text{mol}$ ) were dissolved into 3 mL of THF. The mixture was placed in a round-bottom flask equipped with a magnetic stir bar and sealed with a rubber septum. A stock solution of NaAsc (22.3 mM; 500 $\mu\text{L}$ ) in deionized water was added to the solution and the mixture was bubbled with nitrogen for 20 min to remove oxygen. Lastly, a degassed stock solution of  $\text{CuSO}_4 \cdot 5\text{H}_2\text{O}$  (11.1 mM; 500  $\mu\text{L}$ ) in deionized water was injected into the flask under nitrogen atmosphere. The reaction was allowed to proceed under stirring at 30  $^\circ\text{C}$  for 24 h. The final reaction mixture was dialyzed (MW cut-off 12 400 Da) against deionized water and the block copolymer was obtained after freeze drying. The product was analyzed by GPC in order to confirm the success of the “click” coupling reaction.



## 6.4. Results and Discussion

### 6.4.1. NVCL handling and purification

The NVCL monomer is a hygroscopic solid at room temperature ( $T_m \sim 35 - 38^\circ\text{C}$ ), and very sensitive to hydrolysis.<sup>40, 41</sup> The monomer purity was found to vary substantial among suppliers and even among batches from the same supplier ( $^1\text{H}$  NMR spectrum of the PNVCL in Annex E, Figure E.2 (a)). The presence of monomer inhibitors, namely the *N,N'*-di-*sec*-butyl-*p*-phenylenediamine and contaminants, contributes to an yellowish color of the monomer, which requires a careful purification. Several purification procedures reported in the literature were endeavored. In the first attempt, the monomer was distilled under reduced pressure to remove the inhibitors.<sup>16, 24, 42</sup> This procedure was proved to be ineffective since the monomer could easily degrade due to the high temperatures employed in the distillation (above  $90^\circ\text{C}$ ) ( $^1\text{H}$  NMR spectra of the degraded PNVCL in Annex E, Figure E.2 (b)) Other authors reported the recrystallization from hexane,<sup>43, 44</sup> but it was found to be ineffective to remove all the monomer impurities. Therefore, in order to remove the inhibitors without the degradation of monomer, the NVCL was dissolved in hexane, the solution was slightly heat above NVCL melting point ( $35 - 38^\circ\text{C}$ ), and then passed through a basic alumina column to remove the inhibitors. After recrystallization, the pure white crystalline monomer was filtered, vacuum dried and then stored at  $4^\circ\text{C}$ . The presence of impurities was checked by  $^1\text{H}$  NMR spectroscopy (Figure 6.2).

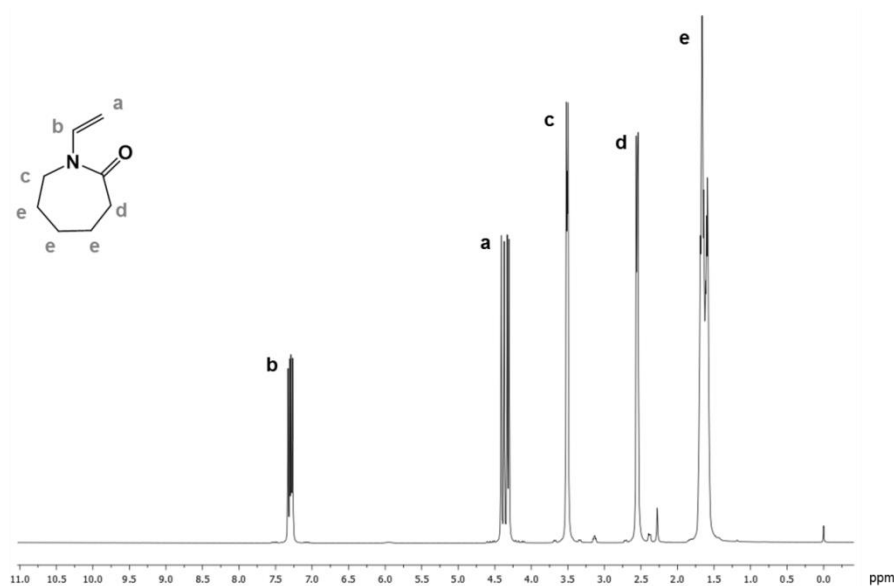


**Figure 6.2:**  $^1\text{H}$  NMR spectrum of NVCL in  $\text{CDCl}_3$ .

The peaks observed at 7.32 ppm (**b**,  $-CH-$ ), 4.37 ppm (**a**,  $-CH_2-$ ), 3.52 ppm (**c**,  $-CH_2-N-$ ), 2.57 ppm (**d**,  $-CH_2-CO-$ ) and 1.64 ppm (**e**,  $-(CH_2)_3-$ ) are in agreement with the expected NVCL chemical structure.

In addition to the purity of monomer, for the RAFT polymerization of NVCL, all of the reagents and solvents should be in an anhydrous form in order to avoid undesired side reactions. It is reported that the presence of water traces in the system could lead to NVCL hydrolysis during the polymerization reaction.<sup>45</sup> As a consequence, the monomer may participate in two distinct and competitive reactions: the monomer addition or the monomer degradation (e.g. hydrolysis). These two distinct mechanisms are responsible for monomer consumption, but only the first generates the NVCL polymer. This issue is particular relevant for the synthesis of well controlled macromolecules, in which the polymer MW should increase linearly with monomer conversion. If the monomer is consumed in side reactions, rather than in polymerization, the final monomer conversion obtained by  $^1H$  NMR spectroscopy, from the comparison of the polymer and monomer signals, will not be consistent with the evolution of the theoretical molecular weight ( $M_{n,th}$ ). The hydrolysis of the NVCL monomer is a topic of discussion in some literature reports.<sup>41, 45</sup> The NVCL acidic hydrolysis leads to the formation of  $\epsilon$ -caprolactam and acetaldehyde molecules (Figure 6.3).<sup>45</sup> In order to prove the existence of the NVCL degradation products in the polymerization reaction media, due to the possible presence of water traces, a simple experiment was carried out by mixing the monomer with the reaction solvent, 1,4-dioxane (99.8 % purity), at 60 °C. Samples from the initial mixture and the mixture after 1h at 60 °C were analyzed by  $^1H$  NMR spectroscopy. The spectrum shown in Figure 6.4 reveal the appearance of the acetaldehyde characteristic peak around 9.7 ppm (from the proton in the  $-CHO-$  aldehyde bound), and  $\epsilon$ -caprolactam around 3.20 ppm, indicating the above supposition. Another direct evidence of the presence of the acetaldehyde in the mixture was the increase of pressure inside the reactor. The acetaldehyde has a boiling point around 20 °C, meaning that at experimental temperature (60 °C), it is gaseous leading to the increase of pressure inside the reactor.

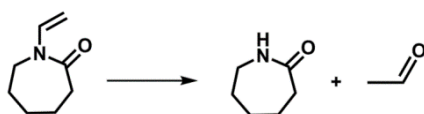


**Figure 6.3:** Schematic representation of NVCL hydrolysis, giving  $\epsilon$ -caprolactam and acetaldehyde.<sup>45</sup>

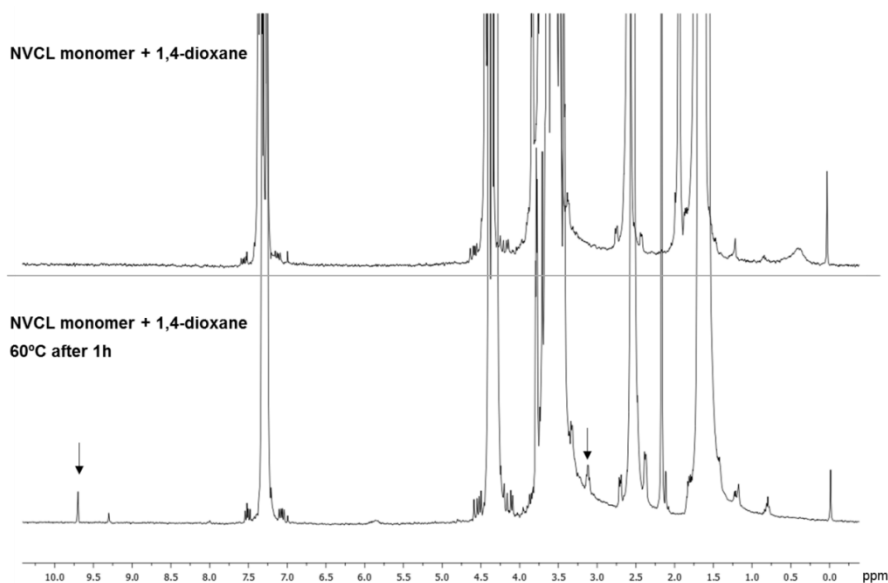


**Figure 6.4:**  $^1\text{H}$  NMR spectra of NVCL and 1,4-dioxane before and after 1h at 60 °C, in  $\text{CDCl}_3$ .

#### 6.4.2. Polymerization of NVCL

NVCL is a classic non-activated monomer, as vinyl acetate (VAc) and *N*-vinylpyrrolidone (NVP)<sup>42</sup> and vinyl chloride<sup>46</sup> since electron density around the double bond is very low. This feature turns radicals very reactive and therefore difficult to control. Some authors reported the use of cobalt mediated radical polymerization of NVCL.<sup>27</sup> However, the protocol proposed is very laborious. The synthesis of low MW NVCL with narrow MW distributions is possible but for higher ratio monomer/initiator, the  $\bar{D}$  increases and the monomer conversions remains low (~30 %). It has been reported that to avoid intermolecular coupling reactions, the monomer to initiator ratio should be high and the polymerization has to be stopped at low monomer conversions (< 20%).<sup>31</sup>

The RAFT polymerization mediated by xanthates has been described as the most suitable approach for the synthesis of well-controlled PNVCL with high yields and chain-end fidelity. RAFT agents such as trithiocarbonates and dithioesters can efficiently control the polymerization of more activated monomers, such as methacrylates or styrene, but are not suitable for the polymerization of non-activated vinyl monomers such as VAc or *N*-vinylactams (Figure 6.5).<sup>47, 48</sup> In the first report of the RAFT homopolymerization of NVCL, in 2005, by Devasia and co-authors,<sup>26</sup> the

2-(ethoxy carbon thioyl thio) propanoate ( $X_1$ ) was used as RAFT agent. The reaction occurs at 80 °C and PNVCL with MW up to 33 000  $\text{g}\cdot\text{mol}^{-1}$  ( $D = 1.65$ ) was obtained but no kinetic data was reported. Kinetic studies of the RAFT polymerization of low MW PNVCL mediated by a xanthate ( $B_1$ , Figure 6.5) or dithiocarbamate ( $D_1$ , Figure 6.5)<sup>24</sup> suggested that xanthates are the most suitable RAFT agents for the polymerization of PNVCL. Similar studies using a trithiocarbonate ( $A_1$ , Figure 6.5) or a dithiocarbamate ( $C_1$ , Figure 6.5) as RAFT agents<sup>16</sup> reveal slow reactions, with MW up to 20 000  $\text{g}\cdot\text{mol}^{-1}$  ( $D = 1.33$ ) after 60h.

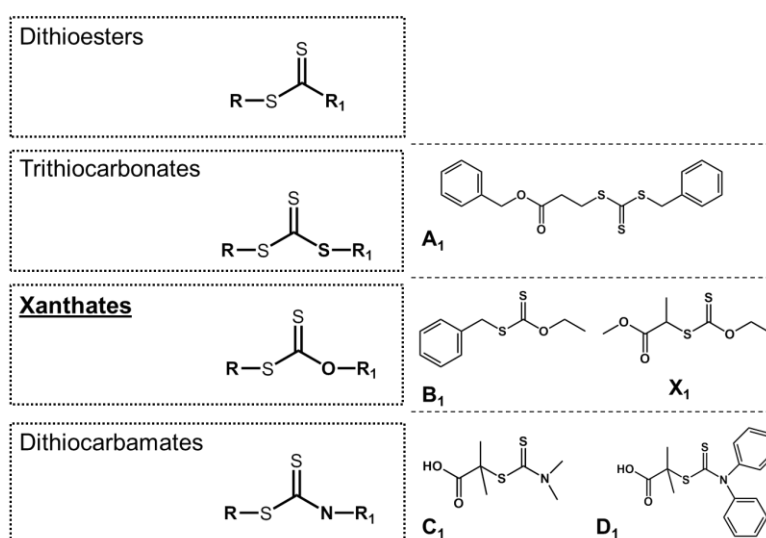


**Figure 6.5:** Schematic representation and examples of the different classes of CTAs.

Initially, in this study, the RAFT agent  $X_1$  (Figure 6.5) was evaluated for the polymerization of NVCL. The polymerization was conducted at 60 °C in 1,4-dioxane, using a monomer/solvent ratio = 1/2 (v/v),  $[\text{NVCL}] = 2.47 \text{ M}$ ,  $[\text{X}_1] = 16.47 \text{ mM}$  and  $[\text{AIBN}] = 3.29 \text{ mM}$ . The kinetic data (Figure 6.6) reveals a first-order kinetic with respect to monomer, in accordance with the literature.<sup>25</sup> The control over the polymer MW was very good taking into account the non-activated nature of monomer ( $D \sim 1.2$ ). Nevertheless, the polymerization was too slow, reaching only 60% of monomer conversion after 24h.

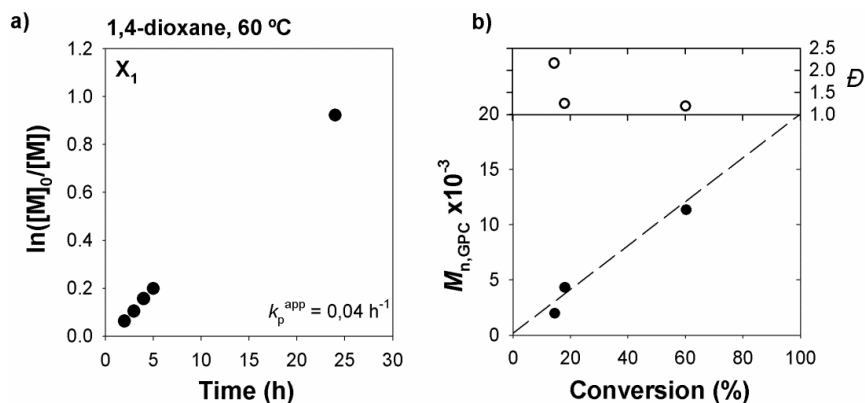


**Figure 6.6:** RAFT polymerization of NVCL mediated by  $X_1$ , in 1,4-dioxane at 60 °C. (a) First-order kinetic plot, (b) evolution of MW and  $\bar{D}$  with conversion (the dashed line represents theoretical MW at a given conversion). Reaction conditions:  $[\text{NVCL}]_0/[\text{X}_1]_0/[\text{AIBN}]_0 = 140/1/0.2$  (molar),  $[\text{NVCL}]_0/[\text{1,4-dioxane}]_0 = 1/2$  (w/w).

Different reports in the literature dealing with the RAFT polymerization of NVCL, show that low concentrations of RAFT agents lead to faster reactions, and reduces the polymerization induction periods.<sup>24, 25</sup> The degree of polymerization (DP), i.e., the ratio monomer to RAFT agent ( $[\text{NVCL}]_0/[\text{RAFT agent}]_0$ ), was increased from 140 to 600 and the xanthates with the alkyne moieties were evaluated for the RAFT polymerization of NVCL. The kinetic studies were carried out under the same reaction conditions, at 60 °C in 1,4-dioxane, using a monomer/solvent ratio = 1/2 (v/v),  $[\text{NVCL}] = 2.47 \text{ M}$ ,  $[\text{RAFT agent}] = 4.12 \text{ mM}$  and  $[\text{AIBN}] = 2.06 \text{ mM}$ . The results presented in Figure 6.7 show that both RAFT agents were able to mediate a successful RAFT polymerization of NVCL because both kinetics show a linear increase of MW with conversion, a good agreement between  $M_{n,\text{th}}$  and  $M_{n,\text{GPC}}$ , while maintaining narrow MW distributions ( $\bar{D} \sim 1.4$ ). An induction period was observed in both cases; nevertheless, the results suggest that the protection of the alkyne functionality of the RAFT agent could lead to a significant reduction of the induction period, from 4h to 1h. This effect has already been reported for the RAFT polymerization of VAc under similar reaction conditions (Chapter 5). Both reactions show a low polymerization rate, but the data reveal also that the protection of the alkyne functionality of RAFT agents leads to a faster and more controlled NVCL polymerization. For PAT- $X_1$  the conversion reached 40% after 24h, while, for the same time, is only 23 % for AT- $X_1$  ( $M_{n,\text{GPC}} = 13.7 \times 10^3$ ;  $\bar{D} = 1.37$ ).

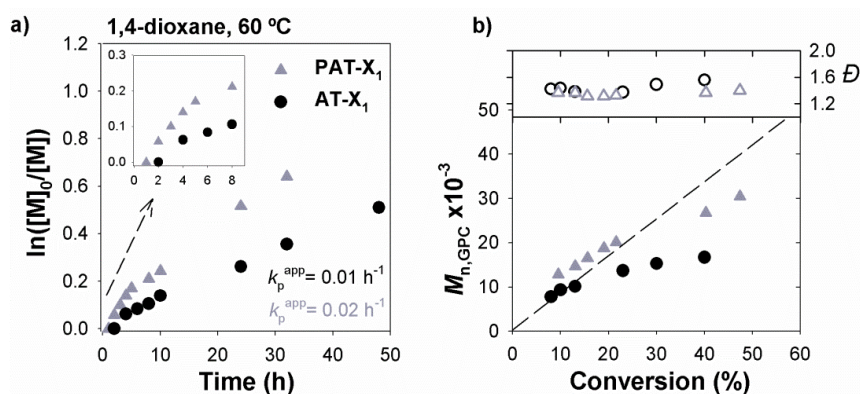


**Figure 6.7:** RAFT polymerization of NVCL mediated by AT-X<sub>1</sub> (circle symbols) or PAT-X<sub>1</sub> (triangle symbols), in 1,4-dioxane at 60 °C. (a) First-order kinetic plot, (b) evolution of MW and  $\bar{D}$  with conversion (the dashed line represents theoretical MW at a given conversion). Reaction conditions:  $[NVCL]_0/[RAFT \text{ agent}]_0/[AIBN]_0 = 600/1/0.5$  (molar),  $[NVCL]_0 = 2.47 \text{ M}$ .

The chromatographic parameters of the PNVCL samples were determined using a GPC equipment coupled with a triple detector system in DMF containing 0.3% of LiBr as elution solvent. From all the solvents reported in the literature, DMF appears to be the most suitable GPC eluent for NVCL based polymers.<sup>30</sup> The polymer GPC traces from the RAFT polymerization of NVCL mediated by PAT-X<sub>1</sub> kinetics points are plotted in Figure 6.8. The GPC curves are unimodal and symmetric. It is possible to observe the movement of the peaks towards low retention volume in the course of the polymerization, indicating the controlled polymer chain growth. The MW increases linearly along the reaction time while the  $\bar{D}$  remains low throughout the polymerization ( $\bar{D} < 1.37$ ).

The refractive index increment ( $dn/dc$ ) of both PNVCL synthesized using AT-X<sub>1</sub> and PAT-X<sub>1</sub> were determined (Annex E, Figure E.3). There is a slight change in the  $dn/dc$  values of the PNVCL that could be related with the presence of different polymer end-groups.

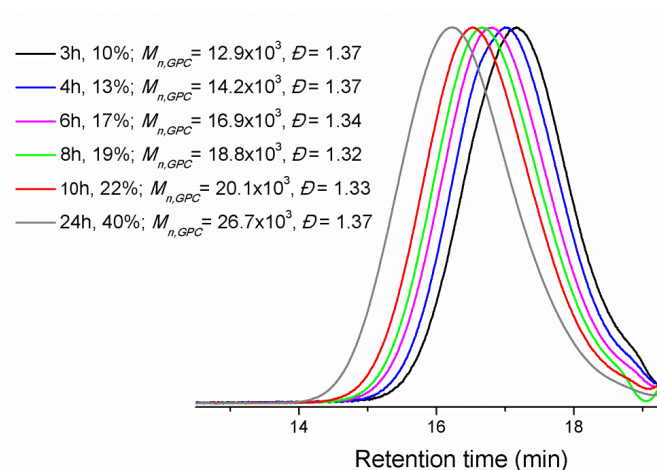


**Figure 6.8:** GPC traces with retention time for the RAFT of NVCL at 60°C in 1,4-dioxane using PAT-X<sub>1</sub>. Reaction conditions: [NVCL]<sub>0</sub>/[PAT-X<sub>1</sub>]<sub>0</sub>/[AIBN]<sub>0</sub> = 600/1/0.5 (molar); [NVCL]<sub>0</sub> = 2.47 M.

Aiming to achieve fast polymerizations, the RAFT of NVCL was carried out at higher monomer/solvent ratio (1/1 (w/w)). The reaction was conducted under the same conditions, at 60 °C, in 1,4-dioxane, with [NVCL] = 3.70 M, [RAFT agent] = 6.16 mM and [AIBN] = 3.06 mM. The kinetic results shown in Figure 6.9 reveal an increase of reaction rate maintaining a similar control over the polymer MW and  $\bar{D}$ . The evolution of MWs is linear with conversion and the  $\bar{D}$  was close to 1.3 throughout the polymerization. However, due to the high target degree of polymerization (DP = 600), above 50% of conversion, the solution viscosity increases considerably, leading to a reduction in radical mobility. This fact precludes the addition of new monomer units to the active chain-ends, and most probably is responsible for the limited monomer conversion around 70% and the increase of  $\bar{D}$  after 12h of reaction.

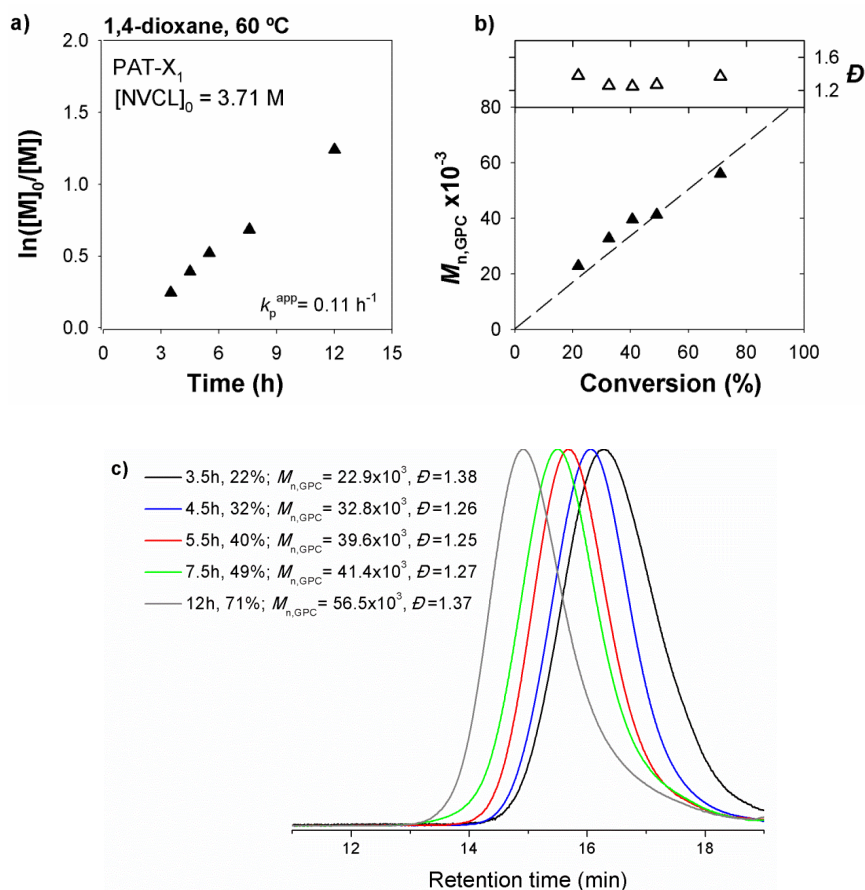


**Figure 6.9:** RAFT polymerization of NVCL mediated by PAT-X<sub>1</sub> in 1,4-dioxane at 60 °C. (a) First-order kinetic plot, (b) evolution of MW and  $\bar{D}$  with conversion (the dashed line represents theoretical MW at a given conversion) and (c) GPC traces with retention time. Reaction conditions:  $[NVCL]_0/[PAT-X_1]_0/[AIBN]_0 = 600/1/0.5$  (molar),  $[NVCL]_0 = 3.70 \text{ M}$ .

A series of well-defined homopolymers were prepared by RAFT polymerization, using the reaction conditions described previously, by stopping the polymerization at different monomer conversions (Table 6.1). The polymer obtained presented fairly low  $\bar{D}$ , concerning the challenging nature of the monomer and the obtained  $M_{n,GPC}$  are in agreement with  $M_{n,th}$ . Using the same reaction conditions, the polymerization of NVCL in the absence of RAFT agent (FRP) (Table 1, entry 6) is faster, leading to high MW polymers with broad MW distribution (Annex E, Figure E.4, comparison of the GPC traces of PNVCL synthesized via FRP and RAFT polymerization). Two different free radical initiators were used; the AIBN, and a very fast peroxide initiator, diisobutyl peroxide (Trigonox 187-W40).<sup>46</sup> Surprisingly, using the same reaction conditions, no polymerization occurs in the presence of the diisobutyl peroxide



**Table 6.1:** RAFT polymerization of NVCL with PAT-X<sub>1</sub>, in 1,4-dioxane at 60 °C. Reaction conditions: (monomer/solvent ratio: 1/1 (w/w)), [NVCL]<sub>0</sub>/[PAT-X<sub>1</sub>]<sub>0</sub>/[AIBN]<sub>0</sub>=600/1/0.5.

Entry	Time	Conv, %	$M_{n,th} \times 10^3$	$M_{n,GPC} \times 10^3$	$\mathcal{D}$	$T_{CP}, ^\circ C^b$
1	3h30	18	15.1	16.13	1.38	37.59
2	4h00	21	17.8	22.88	1.38	37.05
3	4h30	33	27.4	32.82	1.26	36.73
4	8h00	50	41.8	41.35	1.27	36.56
5	14h00	71	59.8	56.05	1.37	35.9
6 <sup>a</sup>	30m	---	---	1650.00	> 2	---

<sup>a</sup> FRP of NVCL, in 1,4-dioxane at 60 °C. Reaction conditions: (monomer/solvent ratio: 1/1 (w/w)), [AIBN]<sub>0</sub> = 0.015 [NVCL]<sub>0</sub>. <sup>b</sup> Determined by turbidimetry analysis.

### 6.4.3. Chemical structure and retention of chain end functionality

The chemical structure of the PNVCL synthesized through RAFT polymerization mediated by the PAT-X<sub>1</sub> was confirmed by <sup>1</sup>H NMR spectroscopy. The spectrum of a purified PNVCL sample is presented in Figure 6.10 and reveals the resonances of the NVCL repeat unit at 4.42 ppm (**m**, -CH<sub>2</sub>-CH-), 3.20 ppm (**r**, -NCO-CH<sub>2</sub>-), 2.49 ppm (**n**, -CH<sub>2</sub>-NCO-) and 1.74-1.44 (**o**, **p,q**, -(CH<sub>2</sub>)<sub>3</sub>- (lactam ring) and **l**, -CH<sub>2</sub>- (polymer backbone)).<sup>24</sup> The presence of the characteristic signal of the trimethyl silyl protons around 0 ppm (**k**, -Si(CH<sub>3</sub>)<sub>3</sub>-) in Figure 6.10 (a) evidences the success of the reaction and the retention of the RAFT functionality in the polymer α-chain end. This characteristic signal disappears after the deprotection reaction with TBAF, resulting in the alkyne-functionalized PNVCL (Figure 6.10 (b)). The ratio between the integrals of **m**, the proton from the polymer backbone at 4.42 ppm with the integrals of the RAFT fragment **k**, the trimethylsilyl protons at 0.13 ppm corresponds to the degree of polymerization (DP) and allows the calculation of the average-number MW ( $M_{n,NMR}$ ) of the PNVCL by <sup>1</sup>H NMR spectroscopy, using the equation:  $M_{n,NMR} = M_{CTA} + DP \times M_{NVCL}$ . The  $M_{n,NMR}$  of the PNVCL was calculated to be  $36.63 \times 10^3$  and it is in good agreement with the value obtained by GPC for the same polymer. The <sup>1</sup>H NMR spectrum of the pure polymer does not allow the assessment of the other characteristic proton peaks of the RAFT agent, i.e., the -CH<sub>2</sub>-CH<sub>3</sub> near the xanthate moiety (**a**, **b**) and the ones near

the alkyne terminal (**c**, **d**, **h**, **i**, **j** and **s**) due to the overlapping with other proton signals from the polymeric chain or due to solvent contamination.

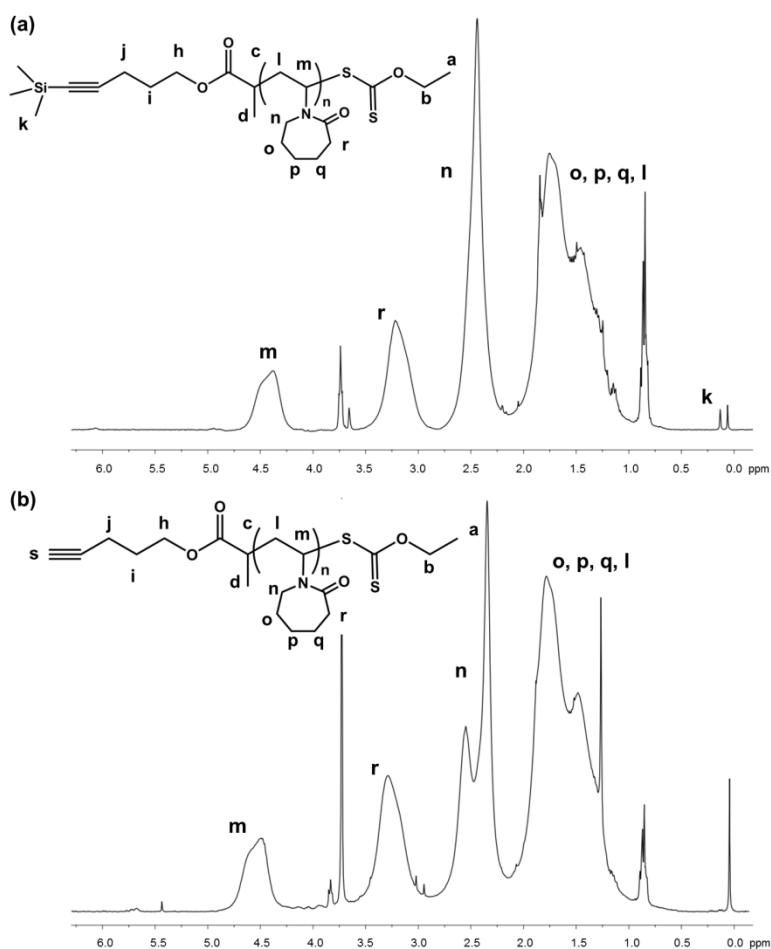


**Figure 6.10:** <sup>1</sup>H NMR spectra in CDCl<sub>3</sub> of (a) the protected alkyne-terminated PNVCCL obtained by RAFT polymerization mediated by PAT-X<sub>1</sub> and (b) alkyne-terminated PNVCCL after the deprotection reaction. Reaction conditions: [NVCL]<sub>0</sub>/[PAT-X<sub>1</sub>]<sub>0</sub>/[AIBN]<sub>0</sub> = 600/1/0.5 (molar) in 1,4-dioxane at 60 °C, [NVCL]<sub>0</sub> = 3.71 M ( $M_{n,NMR} = 36.63 \times 10^3$ ,  $M_{n,GPC} = 38.40 \times 10^3$ ,  $D = 1.28$ ).

The chemical structure of the synthesized PNVCCL was also investigated by FTIR (Figure 6.11). A strong characteristic peak of PNVCCL backbone and caprolactam ring appears at 2924 cm<sup>-1</sup> (aliphatic CH stretching peaks). The peak of C=O stretching vibration the PNVCCL is present at 1625 cm<sup>-1</sup>. The peaks at 1480 cm<sup>-1</sup> and 1441 cm<sup>-1</sup> are ascribed to the C-N and -CH<sub>2</sub>- stretching vibration, respectively. The broad peak at 3500-3300 cm<sup>-1</sup> is ascribed to -OH group resultant from the hygroscopic nature of the

PNVCL<sup>43</sup>. The PNVCL after the deprotection reaction (AT-PNVCL) maintains its structure.

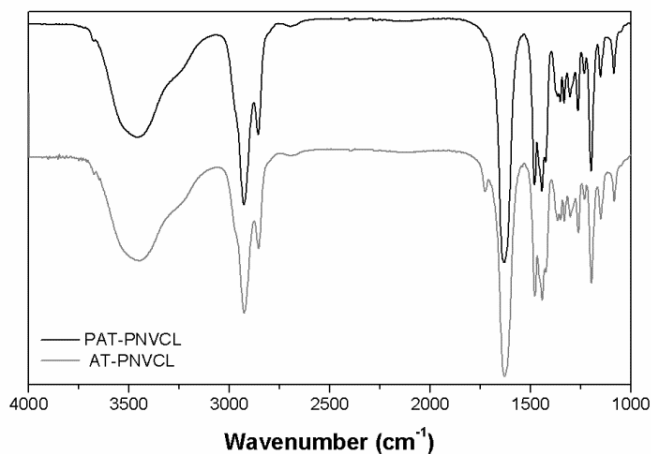


**Figure 6.11:** FTIR spectra of protected alkyne terminated PNVCL (PAT-PNVCL) and alkyne terminated PNVCL obtained after the deprotection reaction (AT-PNVCL) ( $M_{n, GPC} = 38.40 \times 10^3$ ;  $D = 1.28$ ).

In RAFT, just like in other RDRP methods, the resultant polymer can be telechelic, with distinct  $\alpha$  and  $\omega$  chain-end functionalities. The  $\alpha$ -chain end moiety, the protected alkyne functionality, was obtained from the modification of the R group of the RAFT agent. After the polymerization, the characteristic RAFT thiocarbonylthio group remains in the opposing polymer chain-end<sup>49</sup> and it is responsible for its “living” character. The presence of these specific characteristic RAFT end-groups is usually accessed by a chain extension experiment. Characterization techniques such as FTIR and UV-vis analysis<sup>50</sup> have been described for the evaluation of the  $-S-C=S$  chain end functionality. Herein, those techniques were applied unsuccessfully, probably due to the high MW of the polymers. Therefore, the presence of the sulfur moiety in the PNVCL homopolymer, synthesized by RAFT polymerization, was confirmed by elemental analysis (Table 6.2).

**Table 6.2:** Elemental analysis of the PNVCL samples synthesized by RAFT polymerization mediated by PAT-X<sub>1</sub>.

Entry	Sample	$M_{n,GPC}$ $\times 10^3$	$\bar{D}$	%N (w/w)	%C (w/w)	%H (w/w)	%S (w/w)
1	PAT-PNVCL <sup>a</sup>	38.40	1.28	9.158	63.809	9.678	0.244
2	AT-PNVCL <sup>b</sup>			8.715	62.933	9.058	0.301
3	PAT-PNVCL <sup>a</sup>	32.82	1.26	9.168	63.981	9.476	0.621
4	AT-PNVCL <sup>b</sup>			9.275	65.205	9.508	0.622
5	PAT-PNVCL <sup>a</sup>	41.35	1.27	9.056	63.344	9.167	0.405
6	AT-PNVCL <sup>b</sup>			9.339	65.947	9.788	0.583

<sup>a</sup>sample of pure PNVCL synthesized by RAFT polymerization mediated by PAT-CTA; <sup>b</sup>sample of pure PNVCL after the deprotection reaction of the alkyne chain-end functionality.

The chemical structure of the synthesized PNVCL was confirmed by MALDI-TOF analysis. It should be mentioned that there is only one report in the literature concerning the MALDI-TOF analysis of PNVCL synthesized by RAFT mediated by a dithiocarbamate,<sup>24</sup> however the authors suggested that the polymerization did not occur in a strictly living manner. The MALDI-TOF-MS of the protected alkyne-terminated PNVCL synthesized by RAFT polymerization, in the linear mode with *m/z* ranging from 5000 to 18000 is shown in Figure 6.12(a) and the enlargement of the 6200-7100 range is presented in Figure 6.12(b). Five series of peaks are separated by an interval corresponding to a NVCL repeat unit (139.20 mass units). Each group of peaks consists of the molecular ion of the polymer chain of R-PNVCL-Z where R and Z are the groups from the RAFT agent, R= Si(CH<sub>3</sub>)<sub>3</sub>-C≡C-(CH<sub>3</sub>)<sub>2</sub>-O-C-O-C(H)CH<sub>3</sub> and Z= S-C(S)-O-CH<sub>2</sub>CH<sub>3</sub>, plus the matrix (DT) (main series) or impurities in the matrix (series of less intensive peaks).<sup>51</sup> The assignment of all the peaks shown in Figure 6.12 is presented in Table 6.3. The molecular structure, molecular weight of DT and the suggested DT impurities (DT<sub>imp</sub>) reported in the literature<sup>51</sup> and other structures identified by us are presented in Annex E (Figure E.5).

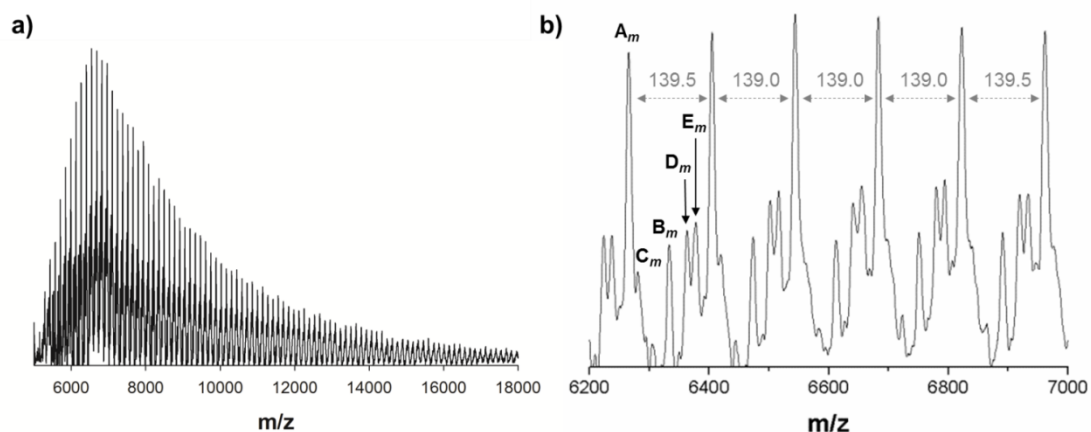


**Figure 6.12:** MALDI-TOF-MS (a) in the linear mode (using DT as a matrix) from  $m/z$  5000 to 18000 and (b) enlargement of the spectrum from  $m/z$  6200 to 7000 of protected alkyne-terminated PNVCCL ( $M_{n, GPC} = 16.13 \times 10^3$ , and  $\mathcal{D} = 1.38$ ). Reaction conditions:  $[NVCL]_0/[CTA]_0/[AIBN]_0 = 600/1/0.5$  (molar);  $[NVCL]_0 = 3.71$  M, 1,4-dioxane,  $T = 60$  °C.

Moreover, one of the series of smaller peaks,  $B_m$ , is attributed to a polymer chain R-PNVCL, resultant from the elimination of the  $S-C(S)-O-CH_2CH_3$  group, from the polymer chain-end under MALDI conditions, as the difference between the  $B_m$  peak and the expected MW is 122 mass units (Annex E, Figure E.6).<sup>52, 53</sup>

The success of the PNVCCL deprotection reaction was also confirmed by the MALDI-TOF technique. The MALDI-TOF-MS spectrum of PNVCCL after the deprotection reaction, in the linear mode, with  $m/z$  ranging from 5000 to 18000 and its enlargement in the  $m/z$  range 6200-7200 are shown in Figure 6.13. As expected, the series of peaks are separated by an interval corresponding to the NVCL repeating unit, revealing the integrity of the monomer units after the deprotection reaction.

**Table 6.3:** MALDI-TOF-MS peak assignment for protected alkyne-terminated PNVCL (Figure 6.12).

<i>n</i>	A set		B set		C set		D set		E set	
	MW <sub>cat</sub> <sup>a</sup>	MW <sub>exp</sub>	MW <sub>cat</sub> <sup>b</sup>	MW <sub>exp</sub>	MW <sub>cat</sub> <sup>c</sup>	MW <sub>exp</sub>	MW <sub>cat</sub> <sup>d</sup>	MW <sub>exp</sub>	MW <sub>cat</sub> <sup>e</sup>	MW <sub>exp</sub>
41	A <sub>1</sub>	6265.9	6265.2		C <sub>1</sub>	6279.7	6280.3			
42	A <sub>2</sub>	6405.1	6404.7		C <sub>2</sub>	6419.1	6419.1	D <sub>1</sub>	6363.1	6362.4
43	A <sub>3</sub>	6544.3	6543.7		C <sub>3</sub>	6558.3	6560.0	D <sub>2</sub>	6502.3	6501.9
44	A <sub>4</sub>	6683.5	6682.8	B <sub>1</sub>	6334.1	6332.6		D <sub>3</sub>	6641.5	6640.6
45				B <sub>2</sub>	6473.2	6473.3				
46				B <sub>3</sub>	6612.4	6612.3				

*n*-the number of repeat units (NVCL), where PAT-X<sub>1</sub> = 332.55 g.mol<sup>-1</sup>, NVCL = 139.20 g.mol<sup>-1</sup>, DT=226.23 g.mol<sup>-1</sup>, SHCSOCH<sub>2</sub>CH<sub>3</sub> = 122.21 g.mol<sup>-1</sup>; DT<sub>imp(D)</sub> = 240.21 g.mol<sup>-1</sup>; DT<sub>imp(D)</sub> = 184.28 g.mol<sup>-1</sup>; DT<sub>imp(D)</sub> = 198.27 g.mol<sup>-1</sup>.  
<sup>a</sup> MW<sub>cat</sub> = PAT-X<sub>1</sub> + *m*PNVCL + DT; <sup>b</sup> MW<sub>cat</sub> = PAT-X<sub>1</sub> + *m*PNVCL - SHCSOCH<sub>2</sub>CH<sub>3</sub> - H; <sup>c</sup> MW<sub>cat</sub> = PAT-X<sub>1</sub> + *n*PNVCL + DT<sub>imp(D)</sub>; <sup>d</sup> MW<sub>cat</sub> = PAT-X<sub>1</sub> + *n*PNVCL + DT<sub>imp(D)</sub>; <sup>e</sup> MW<sub>cat</sub> = PAT-X<sub>1</sub> + *n*PNVCL + DT<sub>imp(D)</sub>.

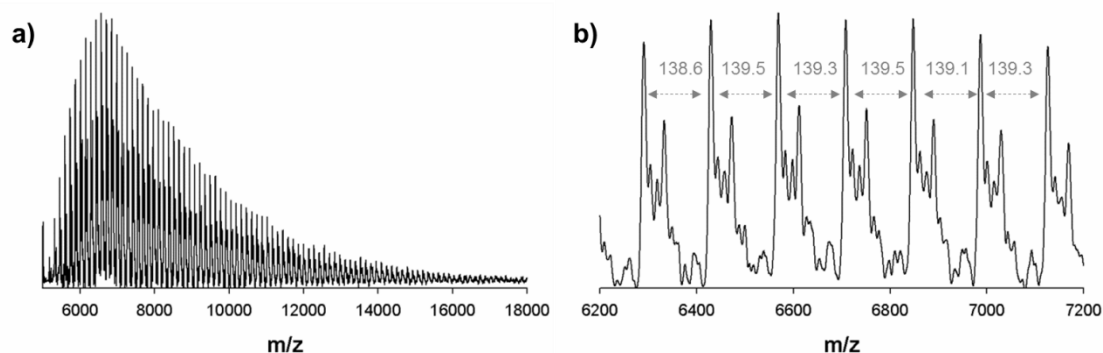


**Figure 6.13:** MALDI-TOF-MS (a) in the linear mode (using DT as a matrix) from  $m/z$  5000 to 18000 and (b) enlargement of the spectrum from  $m/z$  6200 to 7200 of alkyne-terminate PNVCCL after the deprotection reaction ( $M_{n,GPC} = 18.92 \times 10^3$ , and  $D = 1.33$ ).

The peak series is attributed to a polymer chain  $R'-PVC-Z$ , where R group corresponds to the  $HC\equiv C-(CH_3)_2-O-C-O-C(H)CH_3$  moiety in the PNVCCL chain-end, plus the DT or  $DT_{imp}$  in the matrix. The detail information about the assignment of the peaks from the MALDI-TOF analysis of the deprotected PNVCCL is presented in Annex E, Figure E.7 and Table E.1.

#### 6.4.4. Thermal Analysis

The thermogravimetric analysis of the NVCL and the PNVCCL are presented in Table 6.4 and Figure 6.14.

**Table 6.4:** TGA of PNVCCL ( $T_{x\%}$ : temperature at  $x\%$  mass loss;  $T_{on}$ : extrapolated onset temperature).

Entry	$T_{5\%}/^{\circ}C$	$T_{10\%}/^{\circ}C$	$T_{on}/^{\circ}C$
NVCL	77.55	88.22	107.07
PAT-PNVCCL <sup>a</sup>	66.20	353.11	398.85
AT-PNVCCL <sup>b</sup>	58.02	363.43	398.98
FRP-PNVCCL <sup>c</sup>	78.38	330.74	399.70

<sup>a</sup> obtained from RAFT polymerization of NVCL mediated by PAT-CTA ( $M_{n,GPC} = 38.40 \times 10^3 \text{ gmol}^{-1}$ ); <sup>b</sup> obtained after the deprotection reaction of (a); <sup>c</sup> obtained by FRP of NVCL.

The polymer shows a single degradation stage around 400 °C. Comparing the profiles of the PNVCL samples analyzed, it is impossible to establish a relation between the synthesis strategy and the degradation profile. In this line, the differences between the TGA traces of the uncontrolled PNVCL synthesized through FRP and the well-defined PNVCL synthesized by RAFT polymerization were not relevant and are in agreement with the literature<sup>43</sup>. Furthermore, and more importantly, it is shown that the deprotection reactions have no deleterious effects on the polymer thermal stability.

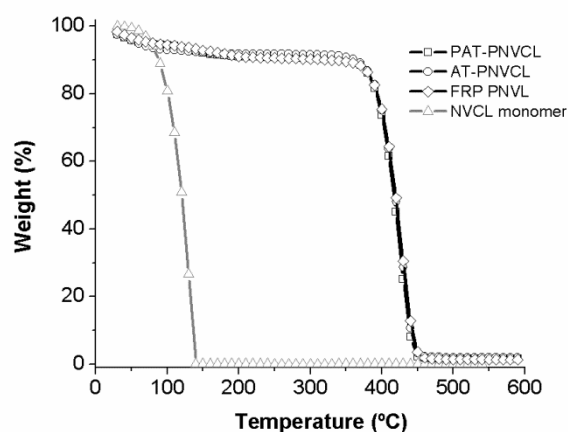


**Figure 6.14:** TGA weight loss curves of the synthesized PNVCL and respective monomer, obtained at a heating rate of 10 °C.min<sup>-1</sup>.

#### 6.4.5. Temperature-responsive behavior of the PNVCL

The NVCL monomer contains a seven-membered lactam ring with one hydrophilic amide group directly connected to the hydrophobic carbon-carbon backbone chain (Figure 6.1). Due to the presence of hydrophilic and hydrophobic groups in its structure, the resulting polymer is soluble in both aqueous and organic media.<sup>54</sup> Temperature-responsive polymers can undergo reversible solvation and desolvation due to a small variation in solution temperature.<sup>55, 56</sup> For solution temperatures above the cloud point temperature ( $T_{CP}$ ), the PNVCL exhibits a phase transition behavior, resulting in conformational changes in the polymer that leads to the formation of hydrophobic domains and consequent change in polymer solubility.<sup>2, 57</sup> Above  $T_{CP}$ , the intra- and intermolecular attractions between the hydrophobic parts of the polymer molecules are



favoured compared to the interactions with water molecules, and the polymer undergoes an abrupt change in the macromolecule specific volume (Figure 6.15).<sup>21</sup>

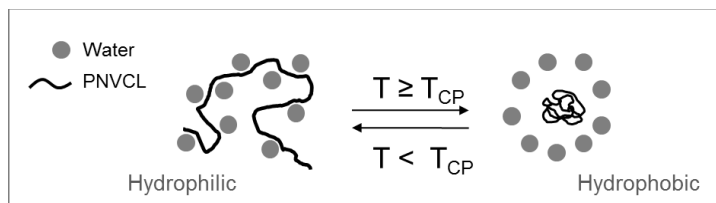


**Figure 6.15:** Schematic representation of the PNVCCL conformation according to the aqueous solution temperature.

The phase transition temperature of PNVCCL in aqueous solutions, decreases with increasing the polymer concentration.<sup>16</sup> Contrarily to other temperature-responsive polymers (e.g. PNIPAM), the PNVCCL solution behavior with temperature is strongly affected by other factors such as the polymer MW and end-groups.<sup>4, 16, 25</sup> The dependence of the LCST of the PNVCCL with MW was evaluated along with the RAFT reaction kinetics by turbidimetry analysis. The transmittance of light through aqueous solutions of the polymer was measured at 630 nm using a UV-vis spectrometer and a heating or cooling rate of 1.0 °C.min<sup>-1</sup>. The  $T_{CP}$  of homopolymer aqueous solutions (1.0 mg.mL<sup>-1</sup>), the temperature at which the polymer becomes insoluble, were determined, from the inflection point of the curve in the transmittance *vs* temperature plots.<sup>58</sup> As expected, the  $T_{CP}$  of PNVCCL decreases along with increasing the MW (Figure 6.16). With the course of the reaction, the  $T_{CP}$  varies from 39.7 °C to 37.3 °C.

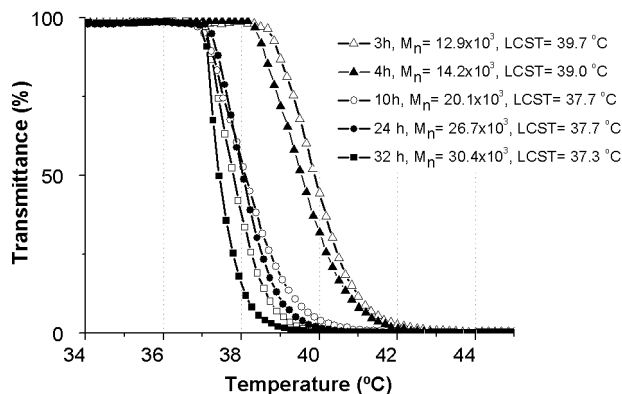


**Figure 6.16:** Transmittance measurements as a function of temperature for  $1.0 \text{ mg.mL}^{-1}$  aqueous solution of different kinetic points of the RAFT polymerization of NVCL mediated by PAT- $X_1$ . Reaction conditions:  $[\text{NVCL}]_0/\text{solvent} = 1/2$  (v/v),  $[\text{NVCL}]_0/[\text{PAT- } X_1]_0/[\text{AIBN}]_0 = 600/1/0.5$  (molar) in 1,4-dioxane,  $T = 60 \text{ }^\circ\text{C}$ .

In an attempt to match the LCST of PNVCL with physiological temperature, some authors reported strategies involving the copolymerization of other monomers such as  $\epsilon$ -caprolactone or *N*-vinylpyrrolidone.<sup>59</sup> Herein, the solution behavior of the pure homopolymers presented in Table 6.1 was also studied in order to create a library of polymers with different LCSTs. The temperature-responsive behavior of PNVCL aqueous solutions was evaluated for both heating and cooling cycles for a fixed polymer concentration of  $1.0 \text{ mg.mL}^{-1}$  and a heating cooling rate of  $1.0 \text{ }^\circ\text{C.min}^{-1}$ . The results are shown in Figure 6.17. All solutions exhibited a very sharp transition in the solution transmittance, close to the human body temperatures, and their temperature-responsive behavior was reversible.

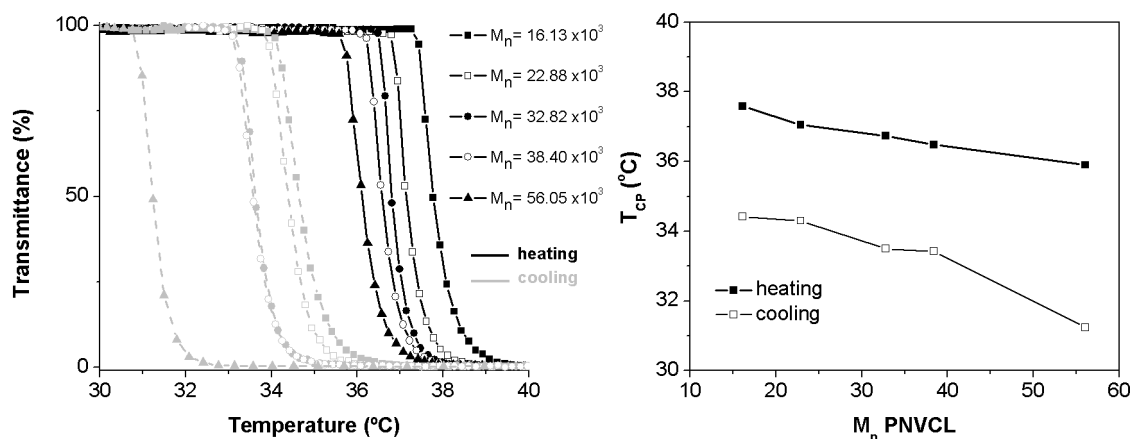


**Figure 6.17:** Dependence of LCST with polymer MW. a) Plots of percentage transmittance vs temperature for various PNVL samples in an aqueous solution ( $1.0 \text{ mg}\cdot\text{mL}^{-1}$ ) (the solid black lines represent the heating cycle and the dashed grey lines represent the cooling cycle). b) Variation of the cloud point temperature ( $T_{CP}$ ) with the PNVL molecular weight in the heating cycle (closed symbols) and in the cooling cycles (open symbols).

Increasing the solution temperature above the  $T_{CP}$ , causes an abrupt change in the polymer conformation, the polymer becomes insoluble and precipitates. As long as the solution temperature is higher than  $T_{CP}$ , the polymer remains insoluble and the solution is cloudy (Annex E, Figure E.8, pictures of PNVL solution at room temperature and above the  $T_{CP}$ ). The effect of the PNVL MW on the LCST had been studied by several authors.<sup>42</sup> Nevertheless, the polymerization method presented here allows a much tighter correlation between the polymer MW and  $T_{CP}$ , especially for high MWs. Contrary to what would be expected, a large hysteresis in the transition temperature between the heating and cooling cycles was observed in the different PNVL samples analyzed. The difference between the transitions temperatures increases along with PNVL MW (Figure 6.17, b)). It should be noted that most of the literature reports concerning the solution behavior of PNVL only present the heating cycle. As a general practice, the authors tend to adjust the solution properties (polymer concentration) or the conditions of the turbidimetry tests, including the heating rates, to fit a desired  $T_{CP}$ . In the case of the PNVL synthesized by RAFT, the temperature-responsive phenomenon of PNVL is reversible and highly reproducible. The aqueous solution of PNVL at  $1.0 \text{ mg}\cdot\text{mL}^{-1}$  shows reversible changes in the transmittance

between 30 and 40 °C with no changes observed in the transmittance transitions for the three consecutive heating/cooling cycles (Figure 6.18).

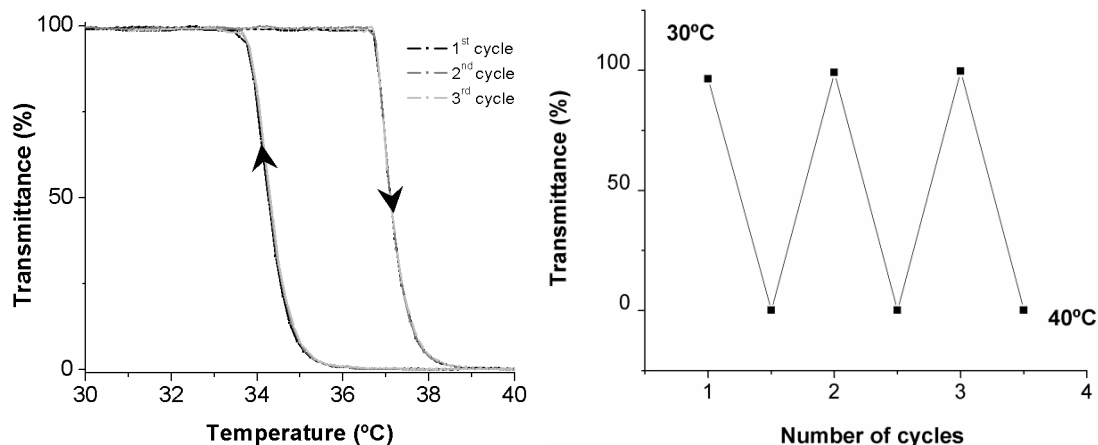


**Figure 6.18:** Percentage transmittance versus temperature plots (right) or number of cycles (left) for the aqueous solutions of the same PNVCL sample ( $1.0 \text{ mg.mL}^{-1}$ ) synthesized through RAFT polymerization, for three heating and cooling consecutive cycles.

Due to the uncontrolled behavior of the FRP polymerization, it is not possible to tailor the PNVCL MW and consequently the  $T_{CP}$ . In the case of PNVCL synthesized via FRP, it exhibits a sharp transition in the solution transmittance during a heating cycle of  $1.0 \text{ }^\circ\text{C.min}^{-1}$ , for two consecutive cycles (Figure 6.19). However, in the cooling cycle, the PNVCL has a different behavior. The transition in solution turbidimetry was soft and gradual, started from the beginning of the cooling cycle ( $45^\circ\text{C}$ ). The recovery in the solution transmittance is inconstant, as evidenced by the differences between the two cooling cycles. Despite the sharp transition in the solution turbidimetry for the PNVCL synthesized by FRP, its solution behavior above the  $T_{CP}$  is unpredictable.

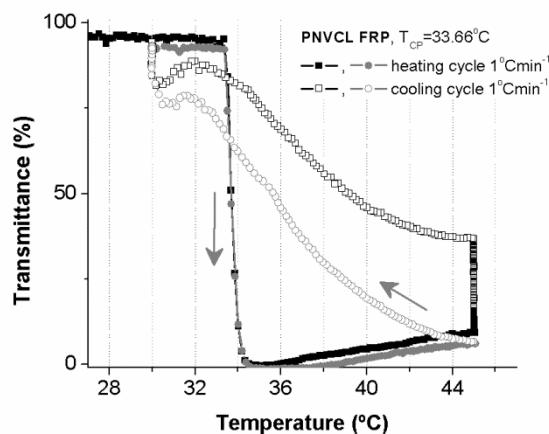


**Figure 6.19:** Percentage transmittance vs temperature plots for the same PNVCL aqueous solution sample ( $1.0 \text{ mg.mL}^{-1}$ ) synthesized through FRP, for two heating and cooling consecutive cycles ( $1.0 \text{ }^{\circ}\text{C.min}^{-1}$ ).

Furthermore, the  $T_{CP}$  is dependent on the solution heating rate, as evidenced in Figure 6.20 (a). Slowing down the heating rate from  $1.0 \text{ }^{\circ}\text{C.min}^{-1}$  to  $0.1 \text{ }^{\circ}\text{C.min}^{-1}$  reduces significantly the  $T_{CP}$  of the sample from  $36.93 \text{ }^{\circ}\text{C}$  to  $35.20 \text{ }^{\circ}\text{C}$ .

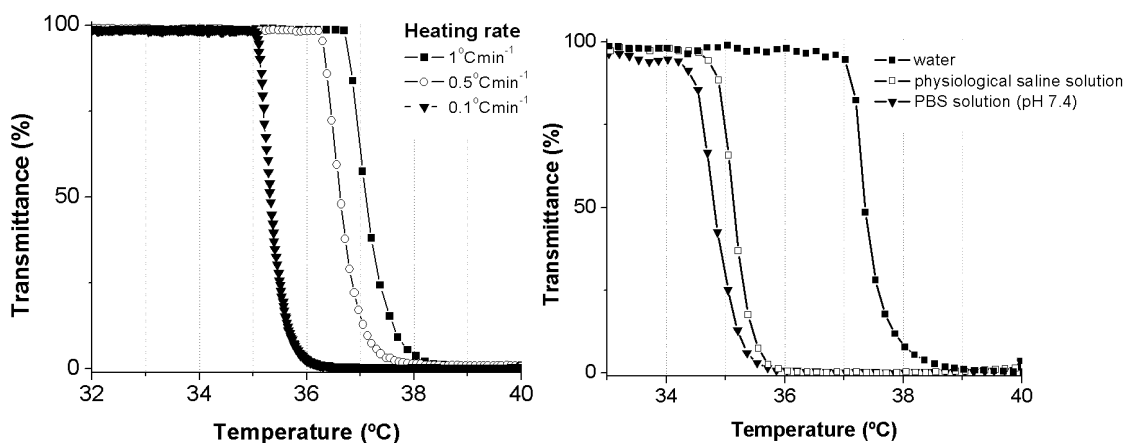


**Figure 6.20:** Dependence of the heating rate (a) and the presence of salts (b) in the LCST of PNVCL samples. Percentage transmittance vs temperature plots for the same PNVCL sample for (a) different heating rates ( $1.0$ ,  $0.5$  and  $0.1 \text{ }^{\circ}\text{C.min}^{-1}$ ), in aqueous solution and (b) PBS solution (pH  $7.4$ ) and physiological saline solution ( $1.0 \text{ mg.mL}^{-1}$ ) (heating rate  $1.0 \text{ }^{\circ}\text{C.min}^{-1}$ ).

Moreover, the hydrophilic/hydrophobic transition of the PNVCL samples was lowered in the presence of salts, i.e. for the same heating rate, the decay in the transmittance percentage for PNVCL in PBS solution or NaCl saline solution occurs earlier than in water solutions (Figure 6.20 b)). For the same PNVCL sample, the  $T_{CP}$  was shifted from 37.36 °C in water to 34.70 °C in PBS solution. These results could be related with the salting-out effect.<sup>20</sup> For solution temperatures below the  $T_{CP}$ , there is strong interaction between the PNVCL and water molecules, causing the complete polymer solvation (Figure 6.15), and at these temperatures the polymer is completely soluble. By introducing the salts into the system, the correspondent ions will preferably interact with the hydrophilic segment of the PNVCL (N-C=O bound), reducing the degree of polymer solvation. Therefore, the interactions between the hydrophobic part of the PNVCL dominates over the interactions between hydrophilic part, promoting an earlier phase separation of the polymer.<sup>11</sup>

#### **6.4.6. PNVCL based copolymers via a “click” coupling approach**

Most of the authors aiming to obtain a specific functionality in the PNVCL chain-end, use a traditional chain transfer agent (CTA), such as 3-mercaptopropanoic acid.<sup>42</sup> and an uncontrolled polymerization of PNVCL occurs in the presence of the conventional initiator AIBN. The final polymer retains the acid functionality but it is obtained in low conversions and low MW. The desired functional group is further introduced in the polymer chain-end via a carbodiimide coupling reaction. This strategy was adopted by Zhang and co-workers to introduce an alkyne functionality in the chain-end of low MW PNVCL for further conjugation with an azide terminated poly( $\epsilon$ -caprolactone).<sup>60</sup> Likewise, this approach was also reported for the preparation of radiolabeled PNVCL.<sup>20</sup>

Herein, the synthesis of alkyne functionalized PNVCL allows the further straightforward synthesis of PNVCL block copolymers by a ‘click’ conjugation approach, using the CuAAC reaction.

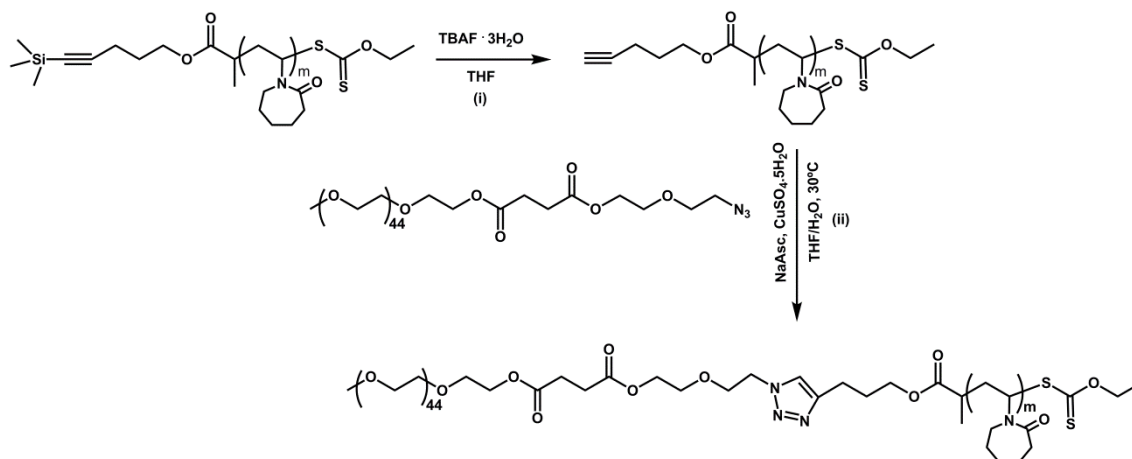


**Figure 6.21:** Schematic representation of the (i) deprotection reaction of PNVCCL synthesized by RAFT mediated by PAT-X<sub>1</sub> and (ii) CuAAC reaction between mPEG-N<sub>3</sub> and AT-PNVCL to afford PEG-*b*-PDPA copolymers.

After the RAFT polymerization of PNVCCL using the PAT-X<sub>1</sub>, the protective trimethyl silyl group was removed using TBAF (Figure 6.21, (i)). The success of the reaction was confirmed by the disappearance of the characteristic trimethyl silyl signal (**k**) at 0.14 ppm in the <sup>1</sup>H NMR spectrum of the unprotected PNVCCL (Figure 6.10). As a proof-of-concept, an azide functionalized PEG molecule, mPEG-N<sub>3</sub>, was conjugated to the alkyne terminated PNVCCL to afford PEG-*b*-PNVCCL copolymers (Figure 6.21, (ii)). The mPEG-N<sub>3</sub> was synthesized from the conjugation of the azido ethoxy ethanol with a carboxylic acid terminated PEG (mPEG-COOH) (the schematic representation of the synthesis of mPEG-N<sub>3</sub> and the correspondent FTIR-ATR spectrum are present in Annex E, Figure E.1 and Figure E.9).

The CuAAC reaction, between the AT-PNVCL and mPEG-N<sub>3</sub>, occurred in a mixture THF/water at 30 °C (Figure 6.21, (ii)). The success of the “click” coupling reaction was evaluated by GPC, with a shift of the PNVCCL precursor towards high MW values (low retention volume) (Figure 6.22). Despite the efforts to purify the resultant PNVCCL-*b*-PEG copolymer, the low MW tail observed in the GPC trace of the precursor mPEG-N<sub>3</sub> (probably resultant from a low MW impurity), was present in the final copolymer GPC trace.

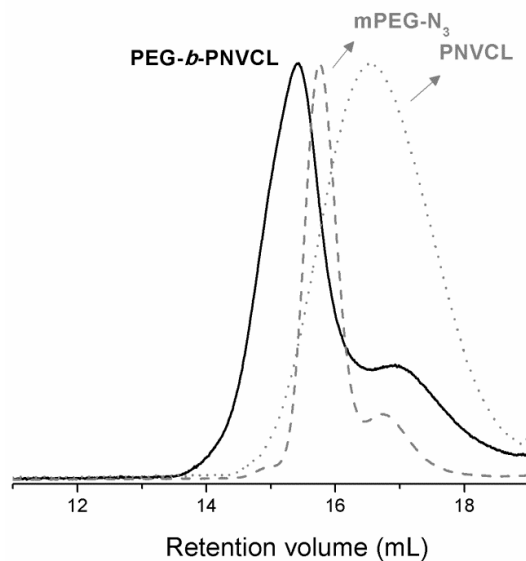


**Figure 6.22:** GPC traces of the alkyne terminated PNVL (AT-PNVL), azide terminated PEG (mPEG-N<sub>3</sub>) and the PEG-*b*-PNVL copolymer obtained after the CuAAC reaction.

## 6.5. Conclusions

Well-defined PNVL, with well controlled MW and narrow MW distributions was synthesized from RAFT polymerization, mediated by an alkyne functionalized RAFT agent. PNVL present a very sharp and reversible response to temperature in a range close to human physiological temperature. The LCST of the PNVL can be tuned by varying the polymer MW, solutions characteristics or the heating rate. The alkyne moiety at the PNVL chain-end allows further conjugation to other molecules or polymers and facilitates the development of new PNVL based block copolymers.



## 6.6. References

1. Ganta, S., H. Devalapally, A. Shahiwala, and M. Amiji (2008). A review of stimuli-responsive nanocarriers for drug and gene delivery. *Journal of Controlled Release*, 126(3): 187-204..
2. Schmaljohann, D. (2006). Thermo- and pH-responsive polymers in drug delivery. *Advanced Drug Delivery Reviews*, 58(15): 1655-1670..
3. Bajpai, A.K., J. Bajpai, R. Saini, and R. Gupta (2011). Responsive Polymers in Biology and Technology. *Polymer Reviews*, 51(1): 53-97..
4. Meeussen, F., E. Nies, H. Berghmans, S. Verbrughe, E. Goethals, and F. Du Prez (2000). Phase behaviour of poly(N-vinyl caprolactam) in water. *Polymer*, 41(24): 8597-8602..
5. Maeda, Y., T. Nakamura, and I. Ikeda (2002). Hydration and phase behavior of poly(N-vinylcaprolactam) and poly(N-vinylpyrrolidone) in water. *Macromolecules*, 35(1): 217-222..
6. Lau, A.C.W. and C. Wu (1999). Thermally sensitive and biocompatible poly(N-vinylcaprolactam): Synthesis and characterization of high molar mass linear chains. *Macromolecules*, 32(3): 581-584..
7. Chee, C.K., S. Rimmer, I. Soutar, and L. Swanson (2006). Fluorescence investigations of the conformational behaviour of poly(N-vinylcaprolactam). *Reactive & Functional Polymers*, 66(1): 1-11..
8. Rejinold, N.S., K.P. Chennazhi, S.V. Nair, H. Tamura, and R. Jayakumar (2011). Biodegradable and thermo-sensitive chitosan-g-poly(N-vinylcaprolactam) nanoparticles as a 5-fluorouracil carrier. *Carbohydrate Polymers*, 83(2): 776-786..
9. Moshaverinia, A., N. Roohpour, J.A. Darr, and I.U. Rehman (2009). Synthesis and characterization of a novel N-vinylcaprolactam-containing acrylic acid terpolymer for applications in glass-ionomer dental cements. *Acta Biomaterialia*, 5(6): 2101-2108..
10. Shtanko, N.I., W. Lequeieu, E.J. Goethals, and F.E. Du Prez (2003). pH- and thermo-responsive properties of poly(N-vinylcaprolactam-co-acrylic acid) copolymers. *Polymer International*, 52(10): 1605-1610..
11. Vihola, H., A. Laukkanen, L. Valtola, H. Tenhu, and J. Hirvonen (2005). Cytotoxicity of thermosensitive polymers poly(N-isopropylacrylamide), poly(N-vinylcaprolactam) and amphiphilically modified poly(N-vinylcaprolactam). *Biomaterials*, 26(16): 3055-3064..

12. Negru, I., M. Teodorescu, P.O. Stanescu, C. Draghici, A. Lungu, and A. Sarbu (2010). Poly(N-vinylcaprolactam)-b-poly(ethylene glycol)-b-poly (N-vinylcaprolactam) Triblock Copolymers Synthesis by ATRP and thermal gelation properties of the aqueous solutions. *Materiale Plastice*, 47(1): 35-41..
13. Vihola, H., A.K. Marttila, J.S. Pakkanen, M. Andersson, A. Laukkanen, A.M. Kaukonen, H. Tenhu, and J. Hirvonen (2007). Cell-polymer interactions of fluorescent polystyrene latex particles coated with thermosensitive poly (N-isopropylacrylamide) and poly (N-vinylcaprolactam) or grafted with poly(ethylene oxide)-macromonomer. *International Journal of Pharmaceutics*, 343: 238-246..
14. Vihola, H., A. Laukkanen, J. Hirvonen, and H. Tenhu (2002). Binding and release of drugs into and from thermosensitive poly(N-vinyl caprolactam) nanoparticles. *European Journal of Pharmaceutical Sciences*, 16(1-2): 69-74..
15. Zhang, L.F., Y. Liang, and L.Z. Meng (2010). Thermo-sensitive amphiphilic poly(N-vinylcaprolactam) copolymers: synthesis and solution properties. *Polymers for Advanced Technologies*, 21(10): 720-725..
16. Shao, L., M. Hu, L. Chen, L. Xu, and Y. Bi (2012). RAFT polymerization of N-vinylcaprolactam and effects of the end group on the thermal response of poly(N-vinylcaprolactam). *Reactive and Functional Polymers*, 72(6): 407-413..
17. Kermagoret, A., C.-A. Fustin, M. Bourguignon, C. Detrembleur, C. Jerome, and A. Debaigne (2013). One-pot controlled synthesis of double thermoresponsive N-vinylcaprolactam-based copolymers with tunable LCSTs. *Polymer Chemistry*, 4(8): 2575-2583..
18. Shah, S., A. Pal, R. Gude, and S. Devi (2010). Synthesis and characterization of thermo-responsive copolymeric nanoparticles of poly(methyl methacrylate-co-N-vinylcaprolactam). *European Polymer Journal*, 46: 958-967..
19. Peng, C.-L., L.-Y. Yang, T.-Y. Luo, P.-S. Lai, S.-J. Yang, W.-J. Lin, and M.-J. Shieh (2010). Development of pH sensitive 2-(diisopropylamino)ethyl methacrylate based nanoparticles for photodynamic therapy. *Nanotechnology*, 21(15): 155103-155115..
20. Černoč, P., Z. Černočová, J. Kučka, M. Hrubý, S. Petrova, and P. Štěpánek (2015). Thermoresponsive polymer system based on poly(N-vinylcaprolactam) intended for local radiotherapy applications. *Applied Radiation and Isotopes*, 98(0): 7-12..
21. Vihola, H., A. Laukkanen, H. Tenhu, and J. Hirvonen (2008). Drug Release

- Characteristics of Physically Cross-Linked Thermosensitive Poly(N-vinylcaprolactam) Hydrogel Particles. *Journal of Pharmaceutical Sciences*, 97(11): 4783-4793..
22. Kharlampieva, E., V. Kozlovskaya, J. Tyutina, and S.A. Sukhishvili (2005). Hydrogen-bonded multilayers of thermoresponsive polymers. *Macromolecules*, 38(25): 10523-10531..
  23. Verbrugge, S., K. Bernaerts, and F.E. Du Prez (2003). Thermo-responsive and emulsifying properties of poly(N-vinylcaprolactam) based graft copolymers. *Macromolecular Chemistry and Physics*, 204(9): 1217-1225..
  24. Wan, D., Q. Zhou, H. Pu, and G. Yang (2008). Controlled radical polymerization of N-vinylcaprolactam mediated by xanthate or dithiocarbamate. *Journal of Polymer Science Part A: Polymer Chemistry*, 46(11): 3756-3765..
  25. Beija, M., J.-D. Marty, and M. Destarac (2011). Thermoresponsive poly(N-vinyl caprolactam)-coated gold nanoparticles: sharp reversible response and easy tunability. *Chemical Communications*, 47(10): 2826-2828..
  26. Devasia, R., R. Borsali, S. Lecommandoux, R.L. Bindu, N. Mougin, and Y. Gnanou (2005). Synthesis of poly(N-vinylcaprolactam)-block-poly(N-vinylpyrrolidone) diblock copolymer by RAFT and the formation of thermosensitive mesoglobules in water. *Abstracts of Papers of the American Chemical Society*, 230: 512-POLY..
  27. Hurtgen, M., J. Liu, A. Debuigne, C. Jerome, and C. Detrembleur (2012). Synthesis of thermo-responsive poly(N-vinylcaprolactam)-containing block copolymers by cobalt-mediated radical polymerization. *Journal of Polymer Science Part A: Polymer Chemistry*, 50(2): 400-408..
  28. Kermagoret, A., K. Mathieu, J.-M. Thomassin, C.-A. Fustin, R. Duchene, C. Jerome, C. Detrembleur, and A. Debuigne (2014). Double thermoresponsive di- and triblock copolymers based on N-vinylcaprolactam and N-vinylpyrrolidone: synthesis and comparative study of solution behaviour. *Polymer Chemistry*..
  29. Yang, Y.Z., J. Li, M.Q. Hu, L. Chen, and Y.M. Bi (2014). Well-defined poly(DL-lactide)-b-poly(N-vinylcaprolactam) copolymers: synthesis, solution properties and in vitro degradation. *Journal of Polymer Research*, 21(9)..
  30. Singh, P., A. Srivastava, and R. Kumar (2012). Synthesis of amphiphilic poly(N-vinylcaprolactam) using ATRP protocol and antibacterial study of its silver nanocomposite. *Journal of Polymer Science Part A: Polymer Chemistry*, 50(8): 1503-1514..
  31. Jiang, X., Y. Li, G. Lu, and X. Huang (2013). A novel poly(N-vinylcaprolactam)-

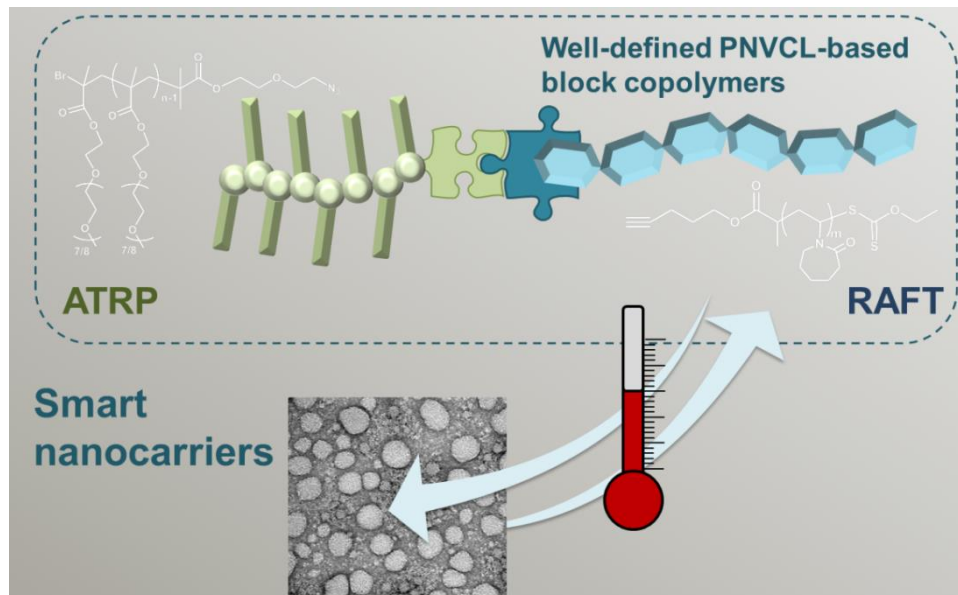
- based well-defined amphiphilic graft copolymer synthesized by successive RAFT and ATRP. *Polymer Chemistry*, 4(5): 1402-1411..
32. Kolb, H.C., M.G. Finn, and K.B. Sharpless (2001). Click chemistry: Diverse chemical function from a few good reactions. *Angewandte Chemie-International Edition*, 40(11): 2004-+..
  33. Lutz, J.F. (2007). 1,3-dipolar cycloadditions of azides and alkynes: A universal ligation tool in polymer and materials science. *Angewandte Chemie-International Edition*, 46(7): 1018-1025..
  34. Meldal, M. and C.W. Tornøe (2008). Cu-catalyzed azide-alkyne cycloaddition. *Chemical Reviews*, 108(8): 2952-3015..
  35. Rostovtsev, V.V., L.G. Green, V.V. Fokin, and K.B. Sharpless (2002). A stepwise Huisgen cycloaddition process: Copper(I)-catalyzed regioselective "ligation" of azides and terminal alkynes. *Angewandte Chemie-International Edition*, 41(14): 2596-+..
  36. Binder, W.H. and R. Sachsenhofer (2008). 'Click' chemistry in polymer and material science: An update. *Macromolecular Rapid Communications*, 29(12-13): 952-981..
  37. Mansfeld, U., C. Pietsch, R. Hoogenboom, C.R. Becer, and U.S. Schubert (2010). Clickable initiators, monomers and polymers in controlled radical polymerizations - a prospective combination in polymer science. *Polymer Chemistry*, 1(10): 1560-1598..
  38. Mespouille, L., M. Vachaudéz, F. Suriano, P. Gerbaux, O. Coulembier, P. Degee, R. Flammang, and P. Dubois (2007). One-pot synthesis of well-defined amphiphilic and adaptative block copolymers via versatile combination of "Click" chemistry and ATRP. *Macromolecular Rapid Communications*, 28: 2151-2158..
  39. Ma, X., Z. Zhou, E. Jin, Q. Sun, B. Zhang, J. Tang, and Y. Shen (2013). Facile Synthesis of Polyester Dendrimers as Drug Delivery Carriers. *Macromolecules*, 46(1): 37-42..
  40. Shostakovskiy, M.F., N.A. Medzykhovskaya, and M.G. Zelenskaya (1952). Synthesis and polymerization of vinylcaprolactam. *Bulletin of the Academy of Sciences of the USSR, Division of chemical science*, 1(4): 627-632..
  41. Shostakovskiy, M.F., F.P. Sidelkovskaya, and M.G. Zelenskaya (1954). The ionic hydrolysis of vinyl lactams in an acid medium. *Bulletin of the Academy of Sciences of the USSR, Division of chemical science*, 3(4): 589-592..

42. Medeiros, S.F., J.C.S. Barboza, M.I. Re, R. Giudici, and A.M. Santos (2010). Solution Polymerization of N-vinylcaprolactam in 1,4-dioxane. Kinetic Dependence on Temperature, Monomer, and Initiator Concentrations. *Journal of Applied Polymer Science*, 118(1): 229-240..
43. Kozanoğlu, S., T. Özdemir, and A. Usanmaz (2011). Polymerization of N-Vinylcaprolactam and Characterization of Poly(N-Vinylcaprolactam). *Journal of Macromolecular Science, Part A*, 48(6): 467-477..
44. Garcia-Olaiz, G.D., K.A. Montoya-Villegas, A. Licea-Claverie, and N.A. Cortez-Lemus (2015). Synthesis and characterization of four- and six-arm star-shaped poly(epsilon-caprolactone)-b-poly(N-vinylcaprolactam): Micellar and core degradation studies. *Reactive & Functional Polymers*, 88: 16-23..
45. Imaz, A., J.I. Miranda, J. Ramos, and J. Forcada (2008). Evidences of a hydrolysis process in the synthesis of N-vinylcaprolactam-based microgels. *European Polymer Journal*, 44(12): 4002-4011..
46. Abreu, C.M.R., P.V. Mendonça, A.C. Serra, J.F.J. Coelho, A.V. Popov, G. Gryn'ova, M.L. Coote, and T. Guliashvili (2012). Reversible Addition-Fragmentation Chain Transfer Polymerization of Vinyl Chloride. *Macromolecules*, 45(5): 2200-2208..
47. Jeong, N.S., M. Redhead, C. Bosquillon, C. Alexander, M. Kelland, and R.K. O'Reilly (2011). The Missing Lactam-Thermoresponsive and Biocompatible Poly(N-vinylpiperidone) Polymers by Xanthate-Mediated RAFT Polymerization. *Macromolecules*, 44(4): 886-893..
48. Perrier, S. and P. Takolpuckdee (2005). Macromolecular design via reversible addition-fragmentation chain transfer (RAFT)/xanthates (MADIX) polymerization. *Journal of Polymer Science Part A: Polymer Chemistry*, 43(22): 5347-5393..
49. Chiefari, J. and E. Rizzardo (2003). Control of Free-Radical Polymerization by Chain Transfer Methods, in *Handbook of Radical Polymerization*. John Wiley & Sons, Inc. 629-690..
50. Chiefari, J., Y.K. Chong, F. Ercole, J. Krstina, J. Jeffery, T.P.T. Le, R.T.A. Mayadunne, G.F. Meijs, C.L. Moad, G. Moad, E. Rizzardo, and S.H. Thang (1998). Living Free-Radical Polymerization by Reversible Addition-Fragmentation Chain Transfer: The RAFT Process. *Macromolecules*, 31(16): 5559-5562..
51. Europe, C. (2004). European Pharmacopoeia 5.0. Council of Europe. 1468..
52. Moad, G., E. Rizzardo, and S.H. Thang (2011). End-functional polymers,

- thiocarbonylthio group removal/transformation and reversible addition–fragmentation–chain transfer (RAFT) polymerization. *Polymer International*, 60(1): 9-25..
53. Willcock, H. and R.K. O'Reilly (2010). End group removal and modification of RAFT polymers. *Polymer Chemistry*, 1(2): 149-157..
54. Nasimova, I.R., E.E. Makhaeva, and A.R. Khokhlov (2001). Poly(N-vinylcaprolactam) gel/organic dye complexes as sensors for metal ions in aqueous salt solutions. *Journal of Applied Polymer Science*, 81(13): 3238-3243..
55. Coelho, J.F., P.C. Ferreira, P. Alves, R. Cordeiro, A.C. Fonseca, J.R. Góis, and M.H. Gil (2010). Drug delivery systems: Advanced technologies potentially applicable in personalized treatments. *The EPMA Journal*, 1(1): 164-209..
56. Hu, J. and S. Liu (2010). Responsive Polymers for Detection and Sensing Applications: Current Status and Future Developments. *Macromolecules*, 43(20): 8315-8330..
57. Sun, S. and P. Wu (2011). Infrared Spectroscopic Insight into Hydration Behavior of Poly(N-vinylcaprolactam) in Water. *The Journal of Physical Chemistry B*, 115(40): 11609-11618..
58. Schmaljohann, D., J. Oswald, B. Jørgensen, M. Nitschke, D. Beyerlein, and C. Werner (2003). Thermo-Responsive PNiPAAm-g-PEG Films for Controlled Cell Detachment. *Biomacromolecules*, 4(6): 1733-1739..
59. Yu, Y.C., G. Li, J. Kim, and J.H. Youk (2013). One-pot synthesis of poly(N-vinylcaprolactam)-based biocompatible block copolymers using a dual initiator for ROP and RAFT polymerization. *Polymer*, 54(22): 6119-6124..
60. Wu, Q.H., J. Yi, Z.L. Yin, S.Y. Wang, Q. Yang, S.Y. Wu, X.M. Song, and G.L. Zhang (2013). Synthesis and self-assembly of new amphiphilic thermosensitive poly(N-vinylcaprolactam)/poly(epsilon-caprolactone) block copolymers via the combination of ring-opening polymerization and click chemistry. *Journal of Polymer Research*, 20(10)..

## Chapter 7

### Synthesis of new thermo-responsive nanocarriers based on POEOMA-*b*-PNVCL prepared using a combination of ATRP, RAFT and CuAAC



The contents of this chapter will be submitted for publication: **Góis, J. R., Serra, A. C. and Coelho J. F. J.**, "Synthesis of new thermo-responsive nanocarriers based on POEOMA-*b*-PDPA prepared using a combination of ATRP, RAFT and CuAAC".





## 7.1. Abstract

Narrowly distributed diblock copolymers comprising a non-linear poly(ethylene glycol) (PEG) analogue and a biocompatible temperature-responsive block were successfully synthesized for the first time using a “click” coupling strategy, the copper catalyzed azide-alkyne [3+2] dipolar cycloaddition (CuAAC) reaction. The alkyne-terminated poly(*N*-vinyl caprolactam) (PNVCL) was obtained by reversible addition fragmentation chain transfer (RAFT) polymerization and the  $\alpha$ -azide terminated poly(oligo(ethylene oxide) methyl ether methacrylate ( $N_3$ -POEOMA) was synthesized by supplemental activator and reducing agent (SARA) atom transfer radical polymerization (ATRP). The resultant POEOMA-*b*-PNVCL copolymers are hydrophilic but became amphiphilic at temperatures above the low critical solution temperature (LCST) of the PNVCL and self-assemble into organized nanostructures. The thermal induced self-assembly behavior of these block copolymers and its dependence on block composition and solution properties, were accessed by turbidimetry and dynamic light scattering (DLS) analysis. Faster heating rates promote the formation of smaller and more stable particles ( $D_h \sim 150$ -180) with narrow size distributions (PDI < 0.1). TEM results show the formation of spherical vesicular aggregates at 45 °C. The encapsulation of Nile red (NR), a model hydrophobic drug, into the hydrophobic domain of the diblock copolymer nanostructures as well as its temperature-triggered release was demonstrated by fluorescence spectroscopy. A small drop in the solution temperature causes the disruption of the nanostructures and induces the fast release of the hydrophobic content.

## 7.2. Introduction

poly(*N*-vinyl caprolactam) (PNVCL) is a water soluble, non-ionic, thermo-responsive polymer that undergoes a phase separation in water for temperature above its cloud point ( $T_{CP}$ ). In the case of the PNVCL, the  $T_{CP}$  is dependent on the polymer molecular weight (MW)<sup>1-3</sup> and solution concentration.<sup>2</sup> Due to its biocompatibility and low cytotoxicity, PNVCL stands out as an ideal polymer for biomedical applications, especially when compared to poly(*N*-isopropylacrylamide) (PNIPAM).<sup>4</sup> The combination of such features turns PNVCL a very interesting hydrophobic segment to be used in experiments with solution temperatures above the  $T_{CP}$ . The conjugation of

PNVCL with permanent hydrophilic segments such as PEG (or derivatives) enables the synthesis of temperature-responsive block copolymers. Such block copolymers are amphiphilic for temperatures above the  $T_{CP}$  of PNVCL and therefore can form well-defined nanoaggregates via self-assembly routes. These stimuli-responsive structures have an enormous potential for advanced drug delivery systems (DDS), mostly because the assembly and disassembly of the block copolymers does not require the use of any additive.<sup>5, 6</sup> Nevertheless, constraints involving the successful use of reversible deactivation radical polymerization (RDRP) methods for the controlled polymerization of NVCL (see Chapter 6) hampered the wide use of this promising polymer in nanodelivery. Indeed, the literature reports on RDRP of PNVCL homo and (co)polymers are very scarce and consequentially its full potential has not been exploited yet. NVCL has been synthesized by reversible addition fragmentation chain transfer (RAFT),<sup>1, 2, 7, 8</sup> cobalt-mediated radical polymerization<sup>9-11</sup> and atom transfer radical polymerization (ATRP).<sup>12-14</sup> The non-activated nature of PNVCL poses several difficulties involving the synthesis of block copolymers with other segments by using a common RDRP method. The use of cobalt as organic metallic complexes allows the synthesis of block copolymers of poly(vinyl acetate)-*b*-PNVCL (PVAc-*b*-PNVCL)<sup>9</sup> as well as poly(vinyl alcohol)-*b*-PNVCL obtained after the hydrolysis of the PVAc segment<sup>6</sup>. Other strategies report the modification of the terminal chain-end groups of a first segment into a macro-RAFT agent for further RAFT polymerization of NVCL.<sup>15</sup> Using this approach, narrowly distributed block copolymers of PEG-*b*-PNVCL were obtained from a poly(ethylene glycol) methyl ether (mPEG)macro-RAFT agent<sup>16</sup> or PNVCL based linear dendritic block copolymers from a dendritic aromatic polyamide macro-RAFT agent.<sup>17</sup> A similar strategy involved the combination of ring opening polymerization (ROP) and RAFT to obtain linear poly( $\epsilon$ -caprolactone)-*b*-PNVCL (PCL-*b*-PNVCL) block copolymers from a macro-PCL RAFT agent,<sup>18</sup> from a bi-functional initiator<sup>19</sup> and also using ramified architectures such as stars with PCL cores.<sup>20</sup>

Poly(oligo(ethylene oxide) methyl ether methacrylate (POEOMA) is a brush-type polymer composed by pendent short PEG monomer units that is easily polymerized by RDRP methods.<sup>21</sup> POEOMA based copolymers have been reported in several different applications in the biomedical field, including inorganic nanocarriers,<sup>22</sup> biodegradable

nanogels,<sup>23</sup> bioconjugates,<sup>24, 25</sup> gene delivery systems,<sup>26, 27</sup> and stimuli-responsive micelles.<sup>28</sup>

The conjugation of different homopolymers through a “click” chemistry approach<sup>29</sup> has been reported as a convenient and straightforward strategy in macromolecular engineering, for the development of block copolymers otherwise difficult to achieve.

In this work, controlled functionalized homopolymers of POEOMA and PNVCL were prepared via a combination of ATRP and RAFT. Well-defined block copolymers of POEOMA-*b*-PNVCL were obtained from the CuAAC reaction between one azide terminated POEOMA (N<sub>3</sub>-POEOMA) and one alkyne terminated PNVCL (AT-PNVCL). The block copolymers were characterized and its temperature induced self-assembly studied. The ability of such block copolymers to encapsulate water-insoluble molecules into its hydrophobic domain was also accessed by fluorescence spectroscopy, using Nile red (NR) as a model hydrophobic drug.

## 7.3. Experimental section

### 7.3.1. Materials

N-vinylcaprolactam (NVCL) (98%, Sigma-Aldrich) was purified by passing through a short alumina column and recrystallized in hexanes. Oligo(ethylene oxide) methyl ether methacrylate (OEOMA<sub>500</sub>, with  $M = 500 \text{ gmol}^{-1}$  and pendent EO units  $DP \approx 8$ ) (99%, Aldrich) was purified by passing through a column filled with basic alumina to remove inhibitor. Sodium dithionite (Na<sub>2</sub>S<sub>2</sub>O<sub>4</sub>) (> 87%, Merck), copper(II) bromide (CuBr<sub>2</sub>) (99+% extra pure, anhydrous, Acros), sodium ascorbate (NaAsc) ( $\geq 98\%$ , Sigma), copper(II) sulfate pentahydrate (CuSO<sub>4</sub>·5H<sub>2</sub>O) ( $\geq 98.0\%$ , Sigma-Aldrich), tetrabutylammonium fluoride trihydrate (TBAF·3H<sub>2</sub>O) (99%, Acros Organics), 2-(2-chloroethoxy)ethanol (99%, Sigma-Aldrich), sodium azide (NaN<sub>3</sub>) ( $\geq 99.5\%$ , Sigma-Aldrich), triethylamine (Et<sub>3</sub>N) ( $\geq 99\%$ , Sigma-Aldrich),  $\alpha$ -bromoisobutyryl bromide (98%, Sigma-Aldrich), Nile red (NR) (TCI Europe), deuterated chloroform (CDCl<sub>3</sub>) (Euriso-top, Euriso-top, +1% TMS), deuterium oxide (D<sub>2</sub>O) (Euriso-top), phosphate buffered saline (PBS) tablets (Sigma), isopropanol (IPA) (Fisher Chemical), ethyl acetate (Fisher Chemical), hexane ( $\geq 98.5\%$ , Fisher Scientific), petroleum ether

(Fisher Scientific), and tetrahydrofuran (THF) (Fisher Scientific) were used as received. 2,2'-Azobis(2-methylpropionitrile) (AIBN) (Fluka, 98%) was purified by recrystallization from methanol before use. The 1,4-dioxane (Acros Organics, 99.8%) was dried over CaH<sub>2</sub> and distilled under reduced pressure prior to use. Purified water (Milli-Q<sup>®</sup>, Millipore, resistivity > 18MΩ.cm) was obtained by reverse osmosis. For gel permeation chromatography (GPC), poly(methyl methacrylate) (PMMA) standards (Polymer Laboratories) (Acros, 99%, ~70 mesh) and high performance liquid chromatography (HPLC) dimethylformamide (DMF) (HPLC grade, Panreac) were used as received.

Protected alkyne-terminated RAFT agent (PAT-X<sub>1</sub>) was synthesized according to the methods described in Chapter 5. Tris(2-dimethylamino)amine (Me<sub>6</sub>TREN)<sup>30</sup> and 2-(2-azidoethoxy)ethyl bromoisobutyrate (N<sub>3</sub>E<sup>i</sup>BBR)<sup>31</sup> were prepared following the procedures described in the literature. Briefly, the 2-(2-azidoethoxy)ethanol was synthesized from 2-(2-chloroethoxy)ethanol and sodium azide and then reacted with 2-bromoisobutyryl bromide to give N<sub>3</sub>E<sup>i</sup>BBR, <sup>1</sup>H NMR (400 MHz, CDCl<sub>3</sub>, δ (ppm)): 1.95 (s, 6H, (CH<sub>3</sub>)<sub>2</sub>C), 3.39 (t, 2H, CH<sub>2</sub>N<sub>3</sub>), 3.70 (t, 2H, N<sub>3</sub>CH<sub>2</sub>CH<sub>2</sub>O), 3.76 (t, 2H, COOCH<sub>2</sub>CH<sub>2</sub>O), 4.35 (t, 2H, CH<sub>2</sub>OCO); <sup>13</sup>C NMR (100 MHz, D<sub>2</sub>O, δ (ppm)): 50.23 (N<sub>3</sub>-CH<sub>2</sub>-), 60.38 (-CH<sub>2</sub>-OH), 69.12 (N<sub>3</sub>-CH<sub>2</sub>-CH<sub>2</sub>-O), 71.64 (O-CH<sub>2</sub>-CH<sub>2</sub>-OH).

### 7.3.2. Characterization

<sup>1</sup>H and <sup>13</sup>C nuclear magnetic resonance (NMR) spectra were recorded on a Bruker Avance III 400 MHz spectrometer, with a 5 mm TXI triple resonance detection probe, in CDCl<sub>3</sub> or D<sub>2</sub>O with tetramethylsilane (TMS) as an internal standard. The conversion was determined by integration of monomer and polymer peaks using MestReNova software version: 6.0.2-5475.

Fourier-transform infrared attenuated total reflection (FTIR-ATR) spectra were acquired in the range of 500 – 4000 cm<sup>-1</sup>, using a JASCO 4200 FTIR spectrophotometer (Jasco, Japan) equipped with a single horizontal Golden Gate ATR cell, at 128 scans and with a 4cm<sup>-1</sup> resolution.

The chromatographic parameters of the samples were determined by gel permeation chromatography (GPC), with refractive index (RI) (Knauer K-2301), differential viscometer (DV) and right angle light scattering (Viscotek 270 Dual Detector) detectors. The column set consisted of a PL 10- $\mu$ L guard column (50 x 7.5 mm<sup>2</sup>), followed by two MIXED-B PL columns (300 x 7.5mm<sup>2</sup>, 10  $\mu$ L). The HPLC pump was set with a flow rate of 1 mL.min<sup>-1</sup> and the analyses were carried out at 60 °C using an Elder CH-150 heater. The eluent was DMF, containing 0.3% of LiBr. The samples were filtered through a polytetrafluoroethylene (PTFE) membrane with 0.2  $\mu$ m pore size before injection (100  $\mu$ L). The system was calibrated with narrow PMMA standards. The  $dn/dc$  of PNVCL and POEOMA in DMF at 60 °C was determined to be 0.088 and 0.049 respectively, for  $\lambda = 670$  nm, using a automatic refractometer (Rudolph Research, J357 NDS-670-CC). The  $M_{n, GPC}$  and dispersity ( $\mathcal{D}$ ) of the synthesized polymers were determined by using a multidetector calibration system (OmniSEC software version: 4.6.1.354).

The determination of the cloud point temperatures ( $T_{CP}$ ) was achieved by turbidimetry analysis. The PNVCL polymers were dissolved in MilliQ water at 1.0 mg.ml<sup>-1</sup> concentration. The solutions were maintained at room temperature for at least 6h to reach equilibrium. The optical transmittance at 630 nm of each PNVCL solution was monitored as a function of temperature using a modular UV-vis spectrometer equipped with a UV-vis light source (DH-2000, Ocean optics) and a temperature controlled cuvette holder (qpod<sup>®</sup>, Quantum Northwest, Inc.) with magnetic stirrer, run by a water circulating temperature controller (TC 125, Quantum Northwest, Inc.). The solution transmittance was assessed with time using SpectraScan software version: 1.0. The heating/cooling rate was 1 °C.min<sup>-1</sup>, 0.5 °C.min<sup>-1</sup> or 0.1 °C.min<sup>-1</sup>. The  $T_{CP}$  was defined as the intercept of the tangents at the onset of turbidity. MilliQ<sup>®</sup> water was used as reference.

Dynamic light scattering (DLS) measurements were performed on a Malvern Instrument Zetasizer Nano-ZS (Malvern Instruments Ltd., UK). The particle size distribution (in intensity), average hydrodynamic particle size average (z-average) and polydispersity index (PDI) were determined with Zetasizer 7.03 software. Measurements were made at 25 °C and using a backward scattering angle of 173°. Zeta-potential measurements were performed using a Zetasizer Nano-ZS (Malvern Instruments Ltd.), coupled to laser Doppler electrophoresis and determined using a Smoluchovski model.

Transmission electron microscopy (TEM) was used to observe the size and morphology of the nanoaggregates prepared with the different copolymers. Due to the temperature dependence of the nanostructures, 8  $\mu\text{L}$  of copolymer solution aqueous dispersion at 45  $^{\circ}\text{C}$  ( $0.2 \text{ mg}\cdot\text{mL}^{-1}$ ) was mounted on 400 mesh copper grid, inside an oven (45  $^{\circ}\text{C}$ ), and the excess of water was gently removed with a paper filter. The sample was cooled down in liquid nitrogen and freeze dried to remove the water traces. The samples were negatively stained with uranyl acetate 1% wt aqueous solution and then examined using a Jeol JEM 1400 transmission electron microscope (Germany). Images were digitally recorded using a Gatan SC 1000 ORIUS CCD Camera (Warrendale, USA).

The thermogravimetric analysis (TGA) were carried out on a TGA Q 500 machine (TA Instruments), from room temperature up to 600  $^{\circ}\text{C}$ , at a 10  $^{\circ}\text{C}\cdot\text{min}^{-1}$  heating rate, under a dry nitrogen atmosphere (at 40  $\text{mL}\cdot\text{min}^{-1}$ ) using approximately 5 mg of the sample.

Fluorescence studies were performed using a Perkin Elmer (LS 45) fluorescence spectrophotometer. For the measurements, 2.0 mL of solution was placed in a 10  $\text{mm}^2$  quartz cell. An excitation wavelength of 550 nm was used and the emission spectra were recorded in the 575-750 nm wavelength range at a scan rate of 500  $\text{nm}\cdot\text{min}^{-1}$ .

### 7.3.3. Procedures

#### **Synthesis of azido terminated POEOMA ( $\text{N}_3$ -POEOMA).**

The synthesis of  $\text{N}_3$ -POEOMA segments via supplemental activator and reducing agent (SARA) ATRP was carried out following a method recently reported that involves the slow and continuous feed of  $\text{Na}_2\text{S}_2\text{O}_4$  (Chapter 3),<sup>32</sup> in a mixture IPA/water with  $[\text{OEOMA}]_0/[\text{N}_3\text{E}^i\text{BBr}]_0/[\text{Na}_2\text{S}_2\text{O}_4]_0/[\text{CuBr}_2]_0/[\text{Me}_6\text{TREN}]_0=20/1/0.2/0.1/0.2$  (molar). Briefly, a mixture of  $\text{CuBr}_2$  (4.08 mg, 18.3  $\mu\text{mol}$ ),  $\text{Me}_6\text{TREN}$  (8.40 mg, 36.5  $\mu\text{mol}$ ) and water (207  $\mu\text{L}$ ) was placed in a Schlenk tube reactor that was sealed by using a rubber septa.  $\text{Na}_2\text{S}_2\text{O}_4$  (7.48 mg, 43.0  $\mu\text{mol}$ ) and a mixture of  $\text{OEOMA}_{500}$  (1.84 g, 2.31 mmol) and  $\text{N}_3\text{E}^i\text{BBr}$  (51.15 mg, 0.18 mmol) in IPA (7.89 mL) (previously bubbled with nitrogen for about 15 minutes) was added to the reactor and frozen in liquid nitrogen. The reaction mixture was deoxygenated by three freeze-pump-thaw cycles and purged with nitrogen. The additional  $\text{Na}_2\text{S}_2\text{O}_4$  aqueous solution (207  $\mu\text{L}$ , 189 mM) was slow feed into the reaction mixture using a syringe pump at a feed rate 144  $\text{nL}\cdot\text{min}^{-1}$

( $27.15 \text{ nmol min}^{-1}$ ). The polymerization proceeded for 15h at  $40 \text{ }^\circ\text{C}$  (79% conversion,  $M_{n,\text{th}} = 8.25 \times 10^3$ ,  $M_{n,\text{GPC}} = 11.93 \times 10^3$ ,  $D = 1.11$ ). The final polymer was purified by dialysis.

#### **Synthesis of alkyne terminated PNVCL (AT-PNVCL).**

A PNVCL with a protected alkyne terminal was obtained from a typical RAFT polymerization reaction mediated by the protected alkyne-terminated RAFT agent (PAT-X<sub>1</sub>) (as described in Chapter 6). The polymerization was carried out in 1,4-dioxane at  $60 \text{ }^\circ\text{C}$  for 210 minutes. PNVCL was obtained with 21% conversion,  $M_{n,\text{th}} = 18.7 \times 10^3$ ,  $M_{n,\text{GPC}} = 22.88 \times 10^3$ ,  $D = 1.38$ ). The polymer was purified by precipitation in cold petroleum ether and dried under vacuum. For the deprotection of the polymer alkyne terminal, a solution of pure PNVCL (1.03 g,  $4.51 \times 10^{-2} \text{ mmol}$ ) in THF (20 mL) was bubbled with nitrogen for about 10 minutes and then cooled down to  $-20^\circ\text{C}$ . A 0.2 M solution of TBAF·3H<sub>2</sub>O (1.13 mL,  $2.26 \times 10^{-1} \text{ mmol}$ ) was slowly added to the polymer solution. After stirring for 30 minutes at low temperature, the reaction proceeded over night at room temperature. The reaction mixture was passed through a silica column to remove the excess of TBAF and the polymer, AT-PNVCL, was recovered by precipitation in petroleum ether.  $M_{n,\text{GPC}} = 25.10 \times 10^3$ ,  $D = 1.35$ .

#### **“Click” reaction between the AT-NVCL and N<sub>3</sub>-POEOMA - synthesis of POEOMA-*b*-PNVCL copolymers.**

The AT- PNVCL ( $M_{n,\text{GPC}} = 32.82 \times 10^3$ ,  $D = 1.26$ ) (100 mg, 3.05  $\mu\text{mol}$ ), N<sub>3</sub>-POEOMA ( $M_{n,\text{GPC}} = 11.93 \times 10^3$ ,  $D = 1.10$ ) (48 mg, 3.96  $\mu\text{mol}$ ) and NaAsc (3.0 mg, 15.23  $\mu\text{mol}$ ) were dissolved in a mixture of THF (4mL) and water (1 mL). The flask equipped with a magnetic stir bar was sealed with a rubber septum and the mixture was bubbled with nitrogen for about 30 minutes. A degassed stock solution of CuSO<sub>4</sub>·5H<sub>2</sub>O in water (500  $\mu\text{L}$ , 12 mM) was injected into the flask under nitrogen atmosphere and the reaction proceeded for 48h at room temperature. The final product was purified by dialysis (MWCO = 25 000 g.mol<sup>-3</sup>) against water for several days to remove the excess of N<sub>3</sub>-POEOMA and the catalysts. The block copolymer was recovered by freeze drying.

#### **Preparation of self-assembled structures.**

The POEOMA-*b*-PNVCL copolymers were dissolved in water, PBS or physiological saline solution (NaCl 0.9 %), to prepare stock solutions with final polymer concentration of  $1 \text{ mg.mL}^{-1}$ . The solutions were allowed to dissolve overnight and

filtered through a 0.45  $\mu\text{m}$  PET filter (Chromafil<sup>®</sup> PET, Macherey-Nagel). When necessary those solutions were diluted to 0.5  $\text{mg}\cdot\text{mL}^{-1}$  and 0.1  $\text{mg}\cdot\text{mL}^{-1}$ . The self-assembled structures were directly obtained by increasing the solution temperature up to 45 °C.

#### **Determination of the critical micelle concentration.**

The critical micelle concentration (CMC) of the POEOMA-*b*-PDPA copolymer was determined by fluorescent spectroscopy using nile red (NR) as a fluorescence probe. A stock solution of the block copolymer (1.0  $\text{mg}\cdot\text{mL}^{-1}$ ) was prepared in water and filtered through a 0.45  $\mu\text{m}$  PET filter (Chromafil<sup>®</sup> PET, Macherey-Nagel). This solution was used to prepare different series of block copolymer solutions, with concentrations ranging from 0.25 to 3.0  $\times 10^{-3}$   $\text{mg}\cdot\text{mL}^{-1}$  in water. 20 $\mu\text{L}$  of NR solution in THF (1.0  $\times 10^{-3}$   $\text{mol}\cdot\text{L}^{-1}$ ) was added to 2.0 mL of each nanoparticle solution in dark. The samples were incubated overnight, under magnetic stirring, at 45 °C to evaporate the THF and equilibrate the NR with the nanostructures. Their fluorescence emission, from 575 to 750nm, was measured using an excitation wavelength of 550 nm. The CMC was determined from a graph of fluorescence intensity vs log(copolymer concentration), as the intersection of the tangents to the two linear portions of the graph.<sup>33</sup>

#### **Encapsulation of nile red as a model for hydrophobic molecules.**

NR was used as a model hydrophobic drug. 100  $\mu\text{L}$  of 4  $\text{mg}\cdot\text{mL}^{-1}$  NR solution in THF (0.4 mg) was added to 2 mL of the copolymer solution, (0.1  $\text{mg}\cdot\text{mL}^{-1}$ ) under magnetic stirring, at ambient temperature. The solution was heated (45 °C) to trigger the formation of the copolymer nanostructures and the evaporation of the organic solvent. The unloaded fraction of NR that precipitated out of the solution, was removed by filtration through a 0.45  $\mu\text{m}$  pore size PET filter (Chromafil<sup>®</sup> PET, Macherey-Nagel). A purple/pink dispersion was obtained. The drug content inside the copolymer nanostructures was determined by UV-vis spectroscopy as described below. A control experiment, with only NR, was performed using the same method.

#### **Determination of the probe loading content in the nanostructures.**

Fluorescence spectroscopy was used to estimate the probe content inside the nanostructures. For calibration experiments several NR solutions in THF were prepared with concentrations ranging from 1.0  $\times 10^{-8}$  to 1.0  $\times 10^{-7}$  M. The maximum absorption at the emission intensity  $\lambda_{\text{max}} = 587$  nm (for excitation  $\lambda = 550$  nm) depended linearly on



the NR concentration (Annex F, Figure F.1 (a)) The analytical curve of NR (Annex F, Figure F.1 (b)) allows the estimation of the probe content inside the block copolymer nanostructures.

The volume of the aqueous NR-loaded block copolymer dispersion obtained after the NR filtration was corrected to 5 mL with THF in order to disrupt the nanostructures and release the NR fraction. The amount of NR was determined by UV-vis spectroscopy. The drug loading capacity (DLC) and the drug loading efficiency (DLE) were estimated using equations 7.1 and 7.2, respectively.<sup>34</sup>

$$DLC (\%) = \frac{\text{mass of probe loaded}}{\text{mass of copolymer}} \times 100 \quad (\text{Equation 7.1})$$

$$DLE (\%) = \frac{\text{mass of probe loaded}}{\text{mass of probe used}} \times 100 \quad (\text{Equation 7.2})$$

## 7.4. Results and Discussion

Reactions based on the “click” chemistry approaches allows the conjugation of polymer segments with distinct characteristics enabling the access to copolymers with different chemical and physical properties that are difficult to attain by other synthetic processes. The use of an azide or alkyne terminated polymer enables further conjugation with the complementary terminated functionality through the CuAAC reaction. It is a very convenient post-polymerization coupling reaction, especially when the homopolymer segments are composed by monomers with different reactivities that would have to be polymerized with different synthetic strategies. As described in the Chapter 6, NVCL is a non-activated monomer and its controlled polymerization is very challenging. From an alkyne functionalized RAFT agent is possible to develop well-defined polymers that can be further conjugated with molecules or polymers that possess the azide complementary functionality. Herein, the alkyne-terminated PNVCL synthesized via RAFT polymerization described in the previous chapter was reacted to an  $\alpha$ -azide terminated POEOMA (N<sub>3</sub>-POEOMA), synthesized by supplemental activator and reducing agent (SARA) atom transfer radical polymerization (ATRP) to afford POEOMA-*b*-PNVCL copolymers (Figure 7.1).

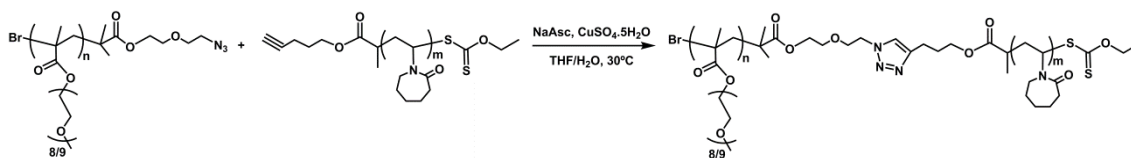


**Figure 7.1:** Schematic representation of the synthesis of POEOMA-*b*-PDPA copolymers.

#### 7.4.1. Synthesis of N<sub>3</sub>-POEOMA

Oligo(ethylene oxide) methyl ether methacrylates (OEOMA) are macromonomers composed by pendent oligo(ethylene glycol) segments that are easily polymerized through ATRP methods<sup>21</sup> affording poly(ethylene glycol) (PEG) based polymers with controlled features.<sup>35</sup> Particularly, poly(oligo(ethylene oxide) methyl ether methacrylate 500) (POEOMA<sub>500</sub>), whose monomeric unit is composed by 8 to 9 ethylene oxide units (average), is hydrophilic (for temperatures below 90 °C<sup>35</sup>), exhibits a high biocompatibility<sup>36</sup> and low cytotoxicity. As they are mainly composed of PEG segments, these brush-type PEG analogues present similar biological characteristics to the linear PEG polymers.<sup>37</sup>

The well-defined synthesis of POEOMA through SARA ATRP was reported in Chapter 3. The slow and continuous feeding of sodium dithionite (Na<sub>2</sub>S<sub>2</sub>O<sub>4</sub>) solution into the reaction mixture allows the use of residual amounts of soluble copper catalyst, while controlling the *D* for high monomer conversions.<sup>32</sup> Due to the versatility of the synthesis, N<sub>3</sub>-POEOMA is easily achieved by using an azide functionalized ATRP initiator, the (2-azidoethoxy)ethyl bromoisobutyrate (N<sub>3</sub>EiBBr).<sup>31</sup> This ATRP initiator was obtained from the reaction of 2-bromoisobutyryl bromide with 2-(azidoethoxy) ethanol (see Annex F for the schematic representation of the N<sub>3</sub>EiBBr synthesis, Figure F.2). The success of the reaction was confirmed by <sup>1</sup>H and <sup>13</sup>C NMR spectroscopy (Annex F, Figure F.3 and Figure F.4) and FTIR-ATR (Annex F, Figure F.5).

OEOMA<sub>500</sub> was polymerized by SARA ATRP using a Cu(II)Br<sub>2</sub>/Me<sub>6</sub>TREN catalytic system at 40 °C in an IPA/water mixture and continuous feeding of Na<sub>2</sub>S<sub>2</sub>O<sub>4</sub> (27.15 nmol.min<sup>-1</sup>). Well-defined low molecular weight N<sub>3</sub>-POEOMA was obtained at high monomer conversion, with controlled MW ( $M_{n, GPC} = 11.93 \times 10^3$ , *D* = 1.11).

The chemical structure of the N<sub>3</sub>-POEOMA was accessed by <sup>1</sup>H NMR spectroscopy (Figure 7.2). The signals in the <sup>1</sup>H NMR spectrum observed at 4.07 ppm (**h**,

$-\text{OCH}_2\text{CH}_2-$ ), 3.82-3.46 ppm (**i**, **l**, **k**,  $-\text{CH}_2-(\text{CH}_2\text{CH}_2\text{O})_n-$ ), 3.37 ppm (**l**,  $-\text{OCH}_3-$ ), 1.84 ppm (**m**, **f**,  $-\text{CH}_2\text{C}-$ ) and 1.00-0.84 ppm (**g**, **g'**,  $-\text{CH}_3-$ ) are in agreement with the expected POEOMA structure.<sup>38, 39</sup> In the  $^1\text{H}$  NMR spectrum of the pure  $\text{N}_3$ -POEOMA the majority of the methylene characteristic peaks of the azide initiator fragment (**a**, **b** and **c**) are overlapped with those from polymer around 3.5 ppm. The polymer  $\alpha$ -end functionality was confirmed by the presence of the methylene protons (**d**) at 4.31 ppm as well as the methyl protons ( $-(\text{CH}_3)_2-$ ) (**e**) at 1.08 and 1.19 ppm. The characteristic FTIR absorption band at  $2100\text{cm}^{-1}$  assigned to the azide group of  $\text{N}_3\text{EiBBr}$  is also present in the FTIR spectra of the polymer (Annex F, Figure F.5).

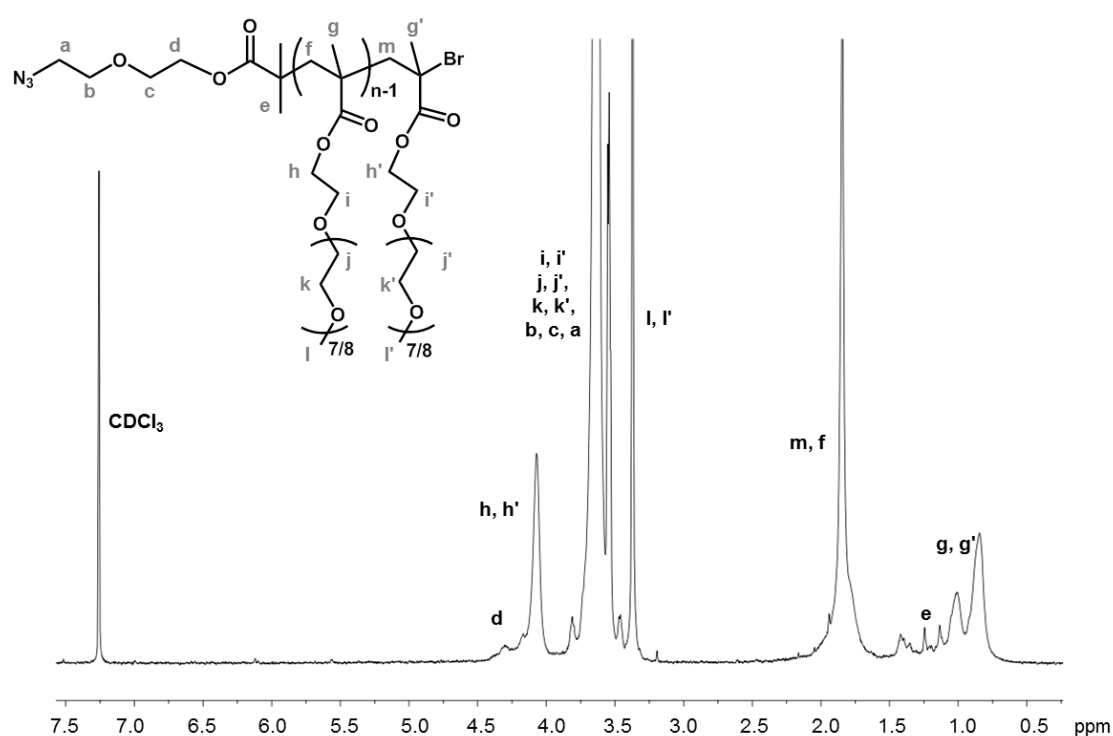


**Figure 7.2:**  $^1\text{H}$  NMR spectrum of  $\text{N}_3$ -POEOMA in  $\text{CDCl}_3$ ,  $M_{n,\text{GPC}} = 11.93 \times 10^3$ ;  $D = 1.11$ .

#### 7.4.2. Synthesis of alkyne-terminated PNVCL

Due to the nature of the NVCL monomer, RAFT polymerization has been described as the simplest strategy to obtain PNVCL with controlled MW, low  $D$ , and pre-determined chain end functionalities. Cai et al introduced the concept of macromolecular design via interchange of xanthates (MADIX)/RAFT polymerization of PNVCL mediated by an azide terminated RAFT agent (*O*-(2-azidoethyl) *S*-benzy dithiocarbonate), for posterior conjugation to an alkyne terminated hyperbranched PCL polymer.<sup>40</sup> Herein, the RAFT

polymerization of NVCL was mediated by the protected alkyne-terminated xanthate introduced in Chapter 6. The RAFT polymerization occurs in 1,4-dioxane, at 60 °C, using a xanthate RAFT agent with an protected alkyne functionality (PAT-X<sub>1</sub>). Well-defined polymers of PNVCL were obtained using the same reaction conditions ( $[NVCL]_0/[PAT-X_1]_0/[AIBN]_0 = 600/1/0.5$ ;  $[NVCL]_0 = 3.71$  M) but stopping the reaction at different monomer conversions (Table 7.1). Alkyne-terminated polymers (AT-PNVCL) were further obtained after a simple deprotection reaction with TBAF and the chemical structure was confirmed by <sup>1</sup>H NMR spectroscopy (annex F, Figure F.6).

#### 7.4.3. Synthesis of POEOMA-*b*-PNVCL copolymers via CuAAC reaction

After the synthesis of the N<sub>3</sub>-POEOMA and the alkyl-terminated PNVCL, the polymers were conjugated via “click” chemistry approach, using the CuAAC reaction. This is a very commonly used coupling strategy for macromolecular engineering due to its tolerance to a wide range of functional groups, high specificity and high yields.<sup>41</sup>

The success of the CuAAC reaction was confirmed by GPC. Figure 7.3 shows a clear shift of the GPC trace of the PNVCL homopolymer towards high MW after the coupling reaction, resulting in the POEOMA-*b*-PNVCL copolymer. The movement of the GPC trace was not complete and both curves were overlapped for low MW values (high retention volume). This observation could be related with the problems associated with the GPC analysis of PNVCL based polymers, mainly the inefficient separation of this polymer and the preference for low retentions volumes<sup>2, 42</sup>.

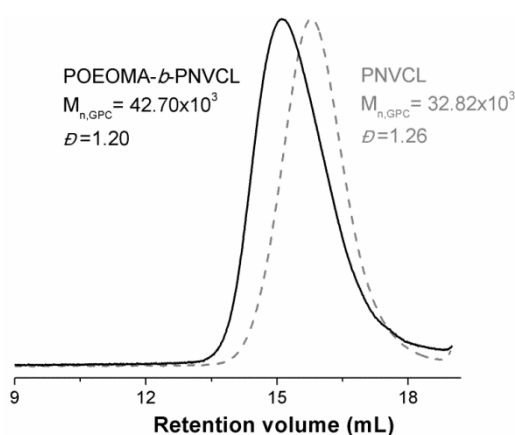


**Figure 7.3:** The GPC traces of alkyne-terminated PNVCL before (dashed line) and after the “click” coupling reaction with N<sub>3</sub>-POEOMA, resulting in POEOMA-*b*-PNVCL (solid line).

Furthermore, the length the N<sub>3</sub>-POEOMA segment is quite small to allow complete shift of the GPC trace. Figure 7.3 also shows a slight tailing in the conjugated product for low MW values, suggesting a possible contamination of unreacted homopolymers. For the coupling reaction, the N<sub>3</sub>-POEOMA block was used in excess (ratio 1.3:1) to ensure the complete reaction of the alkyne terminated PNVCL segments. This strategy was envisaged knowing the low MW and high hydrophilicity of the N<sub>3</sub>-POEOMA that facilitates the elimination of the unreacted homopolymer by dialysis.

The introduction of the “click” functionalities in both homopolymers was achieved from the ATRP initiator and the RAFT agent used. The possible loss of the  $\alpha$ -chain-end functionality has confirmed by the <sup>1</sup>H NMR analysis (Figure 7.2 and Figure 6.10, Chapter 6). The presence of some contamination in final products, involving the existence of residual homopolymers, can be related with the incomplete coupling reaction or to the inefficient purification of the block copolymer by dialysis.

To accurately characterize the POEOMA-*b*-PNVCL copolymer by GPC, the specific refractive index increment ( $dn/dc$ ) of each copolymer in the analysis conditions (solvent and temperature) was calculated from the  $dn/dc$  of each homopolymer segments (Equation 7.3)

$$\frac{1}{\left(\frac{dn}{dc}\right)} = \frac{w_{PNVCL}}{\left(\frac{dn}{dc}\right)_{PNVCL}} + \frac{w_{POEOMA}}{\left(\frac{dn}{dc}\right)_{POEOMA}} \quad (\text{Equation 7.3})$$

, where  $w_{PNVCL}$  and  $w_{POEOMA}$  are the weight fraction of PNVCL and POEOMA, respectively. The  $dn/dc$  values of pure homopolymers POEOMA and PNVCL in DMF at 60 °C, were determined from the slope of the curve from the plots of refractive index vs concentration as 0.05 mL.g<sup>-1</sup> and 0.088 mL.g<sup>-1</sup> respectively (Annex F, Figure F.7 and Annex E, Figure E.3). The theoretical  $dn/dc$  values of each block copolymer were determined and used for the calculation of the final MW of the block copolymer. The results are presented in Table 7.1. Overall, the  $M_{n,GPC}$  of the block copolymers match very well the sum of both  $M_{n,GPC}$  of the two building blocks, POEOMA and PNVCL.

**Table 7.1:** Characteristics of POEOMA-*b*-PNVCL block copolymers.

	Block copolymer								
	POEOMA	PNVCL							
	$M_{n, \text{GPC}} \times 10^3$ <sup>a</sup>	$D$ <sup>a</sup>	$M_{n, \text{GPC}} \times 10^3$ <sup>b</sup>	$D$ <sup>b</sup>	$M_{n, \text{th}} \times 10^3$	$dn/dc$ <sup>c</sup>	$M_{n, \text{GPC}} \times 10^3$	$D$ <sup>c</sup>	$\Phi_{\text{NVCL}}$ <sup>d</sup>
POEOMA <sub>16</sub> - <i>b</i> -PNVCL <sub>126</sub> <sup>e</sup>	11.93	1.11	22.88	1.38	34.81	0.070	37.11	1.15	0.63
POEOMA <sub>16</sub> - <i>b</i> -PNVCL <sub>198</sub> <sup>e</sup>	11.93	1.11	32.82	1.26	44.75	0.073	42.70	1.20	0.70
POEOMA <sub>16</sub> - <i>b</i> -PNVCL <sub>240</sub> <sup>e</sup>	11.93	1.11	36.12	1.29	48.05	0.074	50.93	1.16	0.78
POEOMA <sub>16</sub> - <i>b</i> -PNVCL <sub>390</sub> <sup>e</sup>	11.93	1.11	56.00	1.37	67.93	0.078	74.49	1.23	0.83

<sup>a</sup> $dn/dc$  (POEOMA<sub>500</sub>)<sub>DMF, 60°C</sub> = 0.05 mL·g<sup>-1</sup>; <sup>b</sup> $dn/dc$  (PNVCL)<sub>DMF, 60°C</sub> = 0.088 mL·g<sup>-1</sup>; <sup>c</sup> $dn/dc$  of block copolymers in DMF, at 60°C, determined using the Equation 7.3, <sup>d</sup> volume fraction of NVCL determined from <sup>1</sup>H NMR analysis of the pure block copolymer, <sup>e</sup>the subscripts indicate the mean degrees of polymerization (DP) of each block, determined from monomer conversion by <sup>1</sup>H NMR.

The success of the ‘click’ coupling reaction was also confirmed by the presence of the characteristic peaks of both segments in the  $^1\text{H}$  NMR spectrum of the pure block copolymer, presented in Figure 7.4.

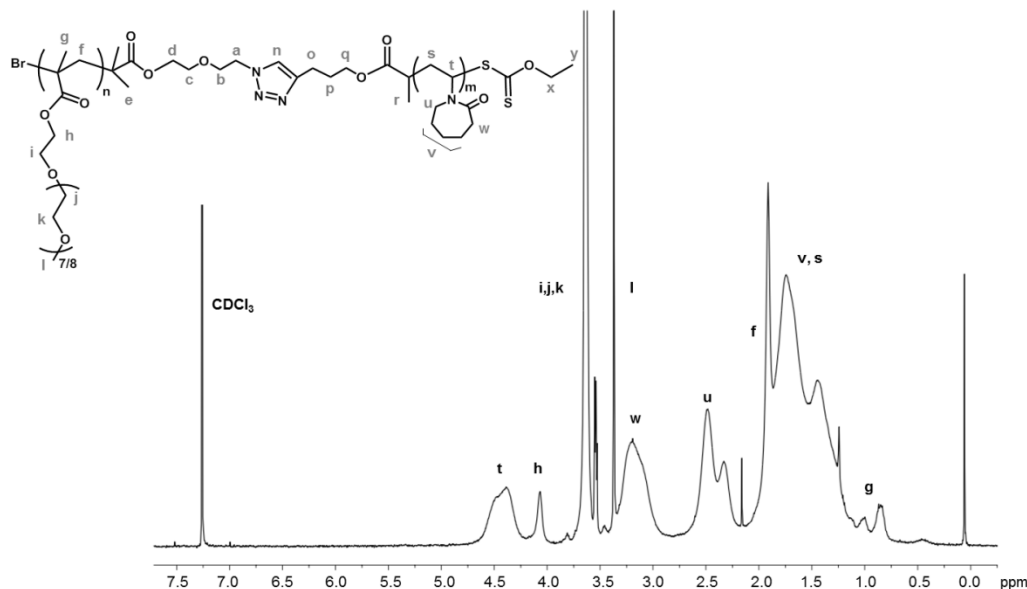


**Figure 7.4:**  $^1\text{H}$  NMR spectrum of POEOMA-*b*-PNVCL block copolymer in  $\text{CDCl}_3$ ,  $M_{n,\text{GPC}} = 44.75 \times 10^3$ ;  $D = 1.20$ .

While the peaks observed at 4.42 ppm (**t**,  $-\text{CH}_2-\text{CH}-$ ), 3.20 ppm (**w**,  $-\text{NCO}-\text{CH}_2-$ ), 2.49 ppm (**u**,  $-\text{CH}_2-\text{NCO}-$ ) and 1.74-1.44 (**v**,  $-(\text{CH}_2)_3-$  (lactam ring) and **s**,  $-\text{CH}_2-$  (polymer backbone)) correspond to the characteristic proton signals of PNVCL presented before (Chapter 6, Figure 6.9). The peaks observed at 4.07 ppm (**h**,  $-\text{OCH}_2\text{CH}_2-$ ), 3.64 ppm (**i**, **j** and **k**,  $-\text{CH}_2-(\text{CH}_2\text{CH}_2\text{O})_n-$ ) and 3.37 ppm (**l**,  $-\text{OCH}_3$ ), 1.91 ppm (**f**,  $-\text{CH}_2-$  (polymer backbone)) and 1.02-0.84 ppm (**g**,  $-\text{C}-\text{CH}_3$ ) correspond to the characteristic proton signals of POEOMA also observed in Figure 7.2. From the  $^1\text{H}$  NMR spectrum of the POEOMA-*b*-PNVCL copolymer it is not possible to observe the signal from the characteristic proton of the triazol ring formed in the click reaction (**n**), as well as the deviation of the adjacent protons (**a** and **o**), due to the high MW of the polymers and the overlapping signals. Although, the  $^1\text{H}$  NMR signal from the protons of the methylene group (**h**) of the POEOMA segment and the protons from the PNVCL repeating unit (**t**) are well resolved. Therefore is possible to calculate the NVCL volume fraction ( $\Phi_{\text{NVCL}}$ ) of each block copolymer, from the ratio of the corresponding signal integrals,  $(I_{\text{t}} \cdot M_{\text{NVCL}} / [I_{\text{t}} \cdot M_{\text{NVCL}} + (I_{\text{h}}/2) \cdot M_{\text{POEOMA}}])$ , with  $M_{\text{NVCL}}$  and  $M_{\text{POEOMA}}$  the

molecular mass of the NVCL and POEOMA monomers, respectively. The results are presented in Table 7.1.

#### 7.4.4. Turbidimetry analysis

A set of well-defined thermo-responsive diblock copolymers, POEOMA-*b*-PNVCL, with  $D < 1.23$  (Figure 7.1) were analyzed by turbidimetry to evaluate its solution behavior and thermal response. The length of the hydrophilic, POEOMA, segment was kept constant for the several diblock copolymers. The MW and consequently, the volume fraction of the PNVCL segment ( $\Phi_{\text{NVCL}}$ ) was varied in order to obtain copolymers with different compositions (Table 7.1). It is well known that the block copolymer characteristics, such as the architecture, the nature of the hydrophilic group, the size and composition of the hydrophobic block are determinant factors in its solution behavior.<sup>43, 44</sup> The volume fractions of each block copolymer were calculated assuming that the polymer density is equal to  $1.0 \text{ g.mL}^{-1}$ .<sup>45</sup>

In order to evaluate the effect of the PNVCL MW in the temperature-response of the block copolymers, polymer solutions of  $1.0 \text{ mg.mL}^{-1}$  were heated at a predetermined rate ( $1.0 \text{ }^\circ\text{C.min}^{-1}$ ) and the transmittance of the sample was measured as a function of temperature (Figure 7.5).

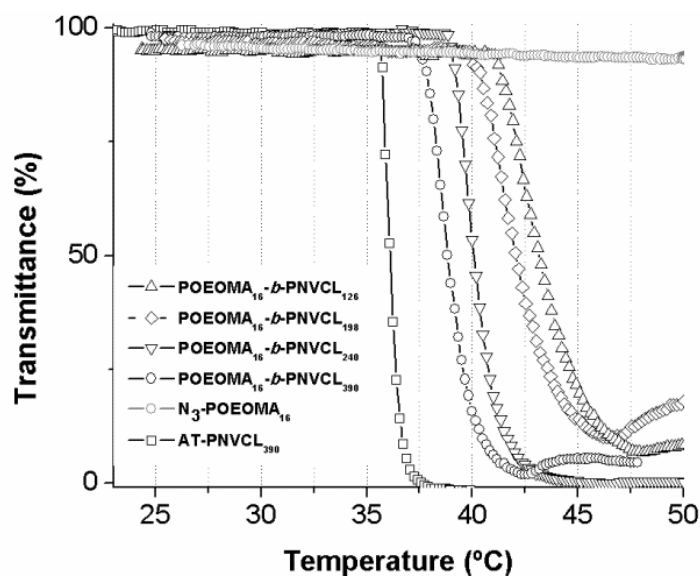


**Figure 7.5:** Transmittance measurements as a function of temperature for  $1.0 \text{ mg.mL}^{-1}$  aqueous solutions of the POEOMA-*b*-PNVCL copolymers (heating rate  $1.0 \text{ }^\circ\text{C.min}^{-1}$ ), and the precursor homopolymers.



The increase in the solution temperature leads to the hydrophilic/hydrophobic transition of the PNVCL segment, turning the solution cloudy. The cloud point temperature ( $T_{CP}$ ) of the block copolymers was found to decrease with the increase of molecular weight of the PNVCL segment. This result follows the same tendency observed for the solution behavior of the PNVCL homopolymers presented in Chapter 6.

The length of the temperature-responsive block was found to have a direct correlation with the  $T_{CP}$  value and the profile of the transmittance transition of block copolymer aqueous solutions. However, the transition in the solution transmittance of the block copolymers is smoother when compared to the correspondent PVCL homopolymer counterpart. Similar observations were reported by Liu and co-authors for PEG-*b*-PNVCL copolymers.<sup>16</sup> The comparison between the turbidimetry results of the POEOMA-*b*-PNVCL copolymers and the PNVCL (Chapter 6) also evidences a high  $T_{CP}$  value for the homopolymer. This result may suggest the reduced contamination of unreacted NVCL chains in the POEOMA-*b*-PNVCL copolymer. If there was an evidenced NVCL homopolymer contamination, the transition in the solution transmittance would occur earlier. As expected, the N<sub>3</sub>-POEOMA segment does not present a phase transition in these ranges of solution temperatures.<sup>35</sup>

As demonstrated in Chapter 6, the  $T_{CP}$  of PNVCL homopolymer aqueous solutions diminish in the presence of salts. Herein, a similar study was performed to evaluate the temperature-response of the block copolymers in the two most common media applied in the biomedical field: PBS solution (pH 7.4) and physiological saline solution respectively (1.0 mg.mL<sup>-1</sup>).

**Table 7.2:** Cloud point temperatures ( $T_{CP}$ ) of the POEOMA-*b*-PNVCL block copolymers 1.0 mg.mL<sup>-1</sup> in water, PBS solution (pH 7.4) and physiological saline solution (NaCl 0.9% ) (heating rate 1.0 °C.min<sup>-1</sup>).

	H <sub>2</sub> O	PBS (pH 7.4)	NaCl 0.9%
POEOMA <sub>16</sub> - <i>b</i> -PNVCL <sub>126</sub>	42.41	39.49	39.48
POEOMA <sub>16</sub> - <i>b</i> -PNVCL <sub>198</sub>	41	37.94	38.91
POEOMA <sub>16</sub> - <i>b</i> -PNVCL <sub>240</sub>	39.6	36.22	37.5
POEOMA <sub>16</sub> - <i>b</i> -PNVCL <sub>390</sub>	38.5	35.5439	36.28
PNVCL <sub>390</sub>	35.9	--	--

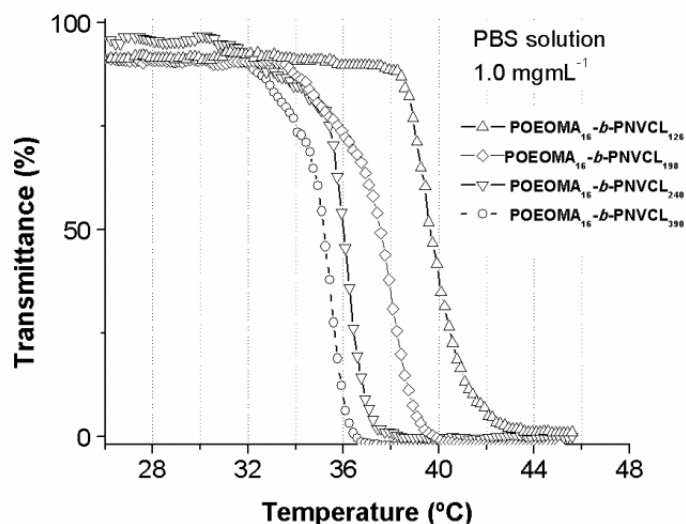


**Figure 7.6:** Transmittance measurements as a function of temperature for 1.0 mg.mL<sup>-1</sup> PBS solution (pH 7.4) of the POEOMA-*b*-PNVCL copolymers (heating rate 1.0 °C.min<sup>-1</sup>).

The  $T_{CP}$  of the block copolymers was found to drop in the presence of salts as evidenced in Figure 7.6 and Table 7.2. Moreover, the results reveal a linear dependence of the solution  $T_{CP}$  with the volume fraction of the NVCL segment in the POEOMA-*b*-PNVCL (Figure 7.7).

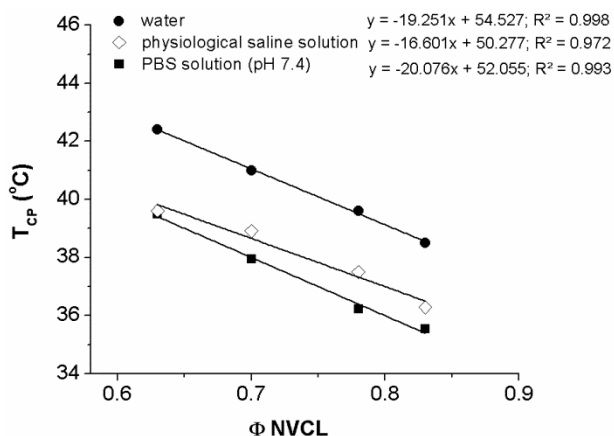


**Figure 7.7:** Evolution of the cloud point temperature ( $T_{CP}$ ) of the POEOMA-*b*-PNVCL block copolymers 1.0 mg.mL<sup>-1</sup> aqueous solutions (water, PBS solution or physiological saline solution) with the volume fraction of NVCL ( $\Phi_{NVCL}$ ).

In all cases, independently of the presence of salts in the solution, the solution transmittance decreases to values close to zero. Nevertheless, and a slight loss of solution turbidimetry above the  $T_{CP}$  was observed for the solutions without salt (Figure 7.5) supporting the theory that salts anticipates the NVCL phase transition. The different copolymers exhibit a single and defined transition in the solution transmittance, indicative of low contamination of the block copolymer with unreacted PNVCL chains. As well as for PNVCL homopolymers, the temperature-induced phase transition in the block copolymers is reversible with hysteresis behavior. As observed in Figure 7.8, for the block copolymer with the short PNVCL block. In the cooling cycle that proceeds the heating cycle ( $1\text{ }^{\circ}\text{C}\cdot\text{min}^{-1}$ ), the transition in the solution transmittance occurs for lower temperatures and the recovery in transparency is almost complete.

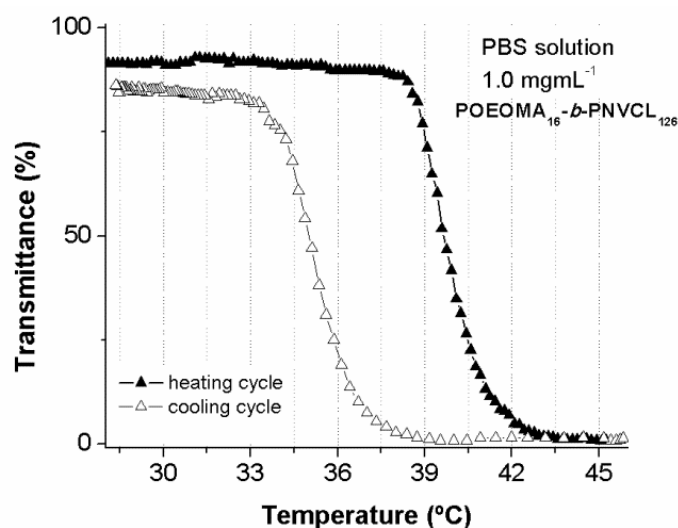


**Figure 7.8:** Transmittance measurements as a function of temperature for  $1.0\text{ mgmL}^{-1}$  PBS solution (pH 7.4) of the  $\text{POEOMA}_{16}\text{-}b\text{-PNVCL}_{126}$  copolymer (heating/cooling rate  $1.0\text{ }^{\circ}\text{C}\cdot\text{min}^{-1}$ ).

#### 7.4.5. Self-assembly of block copolymers

$\text{POEOMA-}b\text{-PNVCL}$  copolymers are expected to be hydrophilic at room temperature, with both segments solvated. The increase of the solution temperature above the low critical solution temperature (LCST) of the thermo-responsive segment ( $T > T_{CP}$ ) will result in an unbalance of the solvation of hydrophilic/hydrophobic parts leading to a phase separation of the PNVCL segment turning the block copolymer amphiphilic. The solution behavior and the thermal response of the block copolymers were also addressed by DLS analysis. The block copolymer was firstly dissolved in water at room

temperature overnight. After the complete dissolution the solution was filtered through a membrane of poly(propylene) (0.45  $\mu\text{m}$  pore size) and placed in a 45  $^{\circ}\text{C}$  water bath to induce the self-assembly. The DLS analysis was performed at 45  $^{\circ}\text{C}$ , temperature at which the PNVCL segment is completely hydrophobic as shown by the turbidimetry analysis. At this temperature the block copolymers formed particles with unimodal distributions with mean diameters in the range of 200 to 260 nm (Table 7.3 and Figure 7.9).

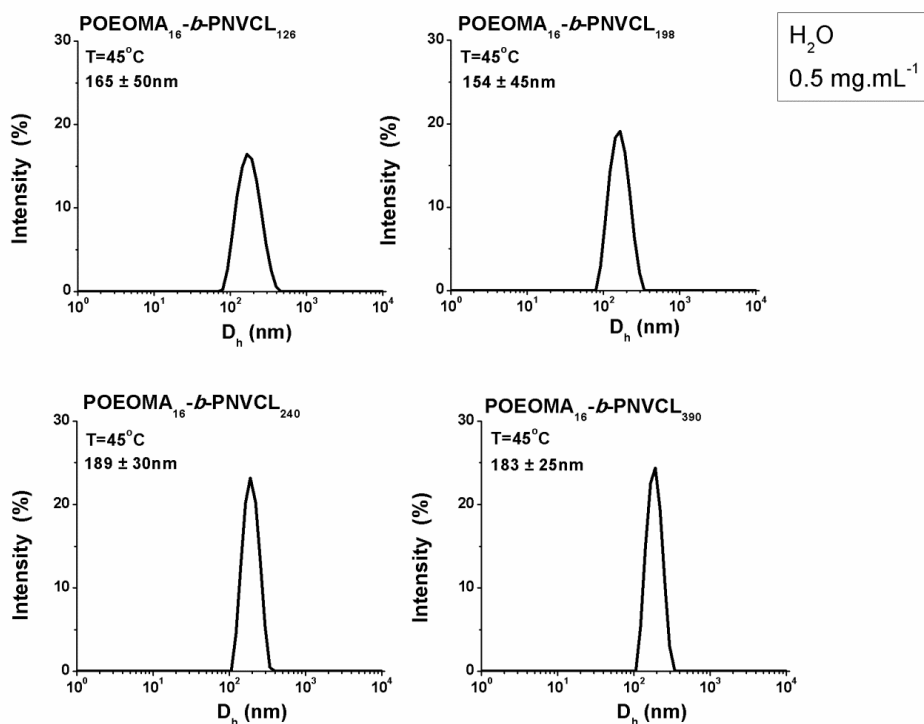


**Figure 7.9:** Size distribution (by intensity) of POEOMA-*b*-PNVCL copolymers in water (0.5 mg.mL<sup>-1</sup>), T= 45  $^{\circ}\text{C}$ .

Furthermore, for a dissolution of the block copolymers of 0.5 mg.mL<sup>-1</sup>, the mean value of the hydrodynamic diameter ( $D_h$ ) of the particle at 45  $^{\circ}\text{C}$  decreases up to 165 nm as well as the broadness of the particle size distribution (PDI) (Table 7.3). The deviation from the  $D_h$  ( $\sigma$ ) was calculated from PDI values, through the using the equation:  $\text{PDI} = (\sigma/D_h)^2$ . For 0.5 mg.mL<sup>-1</sup> aqueous solutions, all the block copolymers present a perfect monodisperse distribution of  $D_h$  ( $\text{PDI} < 0.1$ ). The DLS results suggest that concentrated solutions promote the aggregation between particles resulting in larger  $D_h$ . The brush-type morphology of the POEOMA is responsible for its globular shape in aqueous solutions.<sup>46</sup> The aggregation behavior of POEOMA<sub>475</sub> homopolymers was

studied in detail by He and co-workers.<sup>38</sup> The hydrophilic/hydrophobic balance in the POEOMA<sub>475</sub> molecule, from the linear hydrophobic methacrylate backbone and hydrophilic PEG side chains, leads to the formation of micellar aggregates, for solution concentrations above the critical aggregation concentration (CAC) of 0.7 mg.mL<sup>-1</sup>. For more concentrated solutions of POEOMA-*b*-PNVCL (1.0 mg.mL<sup>-1</sup>), the DLS results reveal larger D<sub>h</sub> in comparison to the diluted solutions (0.5 mg.mL<sup>-1</sup>). This result could be attributed to the aggregation effect of the POEOMA chains. It is expected that the hydrophilic PEG segments that compose the POEOMA block are in the shell of the self-assembled structures, whereas the hydrophobic PNVCL segments are in the core. For higher copolymer concentrations the hydrophobic compartment of the self-assembled structures can also accommodate the hydrophobic domain of the POEOMA segments, resulting in particles with larger hydrodynamic volume. The effect of the POEOMA aggregation was also reported by Sun and co-authors<sup>47</sup> in the solution behavior of polymers composed by an hydrophobic dendritic architecture functionalized with POEOMA segments. Herein, in this study, the content of the PNVCL block is much higher than that of the hydrophilic part and the resultant self-assembled structures (for concentration 0.5 mg.mL<sup>-1</sup>) have a narrow size distributions (PDI < 0.09). Therefore, our results suggest that, for lower concentrations, the hydrophilic POEOMA segment provides a stable interface between the hydrophobic PNVCL and the aqueous medium and stabilizes the self-assemblies.

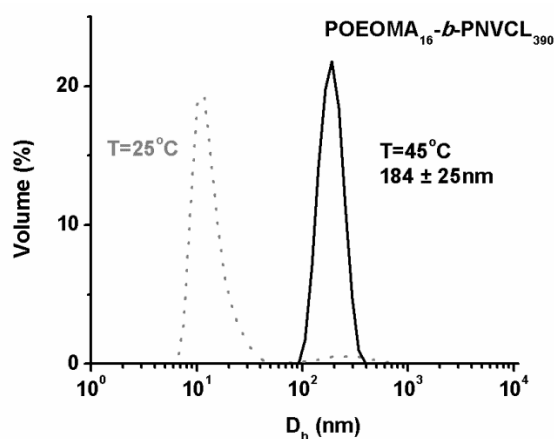
**Table 7.3:** Characteristics of the self-assembled structures formed in water at 45 °C, from the POEOMA-*b*-PNVCL copolymers.

	Conc. (mg.mL <sup>-1</sup> )	D <sub>h</sub> (nm) <sup>a</sup>	PDI	σ (nm) <sup>b</sup>	CMC <sup>c</sup> (mg.L <sup>-1</sup> )
POEOMA <sub>16</sub> - <i>b</i> -PNVCL <sub>126</sub>	1.0	260	0.186	112	83.7
	0.5	165	0.092	50	
POEOMA <sub>16</sub> - <i>b</i> -PNVCL <sub>198</sub>	1.0	201	0.093	61	58.9
	0.5	154	0.084	45	
POEOMA <sub>16</sub> - <i>b</i> -PNVCL <sub>240</sub>	1.0	253	0.180	107	31.3
	0.5	189	0.025	30	
POEOMA <sub>16</sub> - <i>b</i> -PNVCL <sub>390</sub>	1.0	235	0.090	71	20.5
	0.5	182.9	0.019	25	

<sup>a</sup>mean value of the hydrodynamic diameter of the particle; <sup>b</sup>PDI width (σ) determined using the equation: PDI=(σ/D<sub>h</sub>)<sup>2</sup>; <sup>c</sup>critical micelle concentration (CMC) of the block copolymers determined from Nile red fluorescence assays determined at 45 °C.

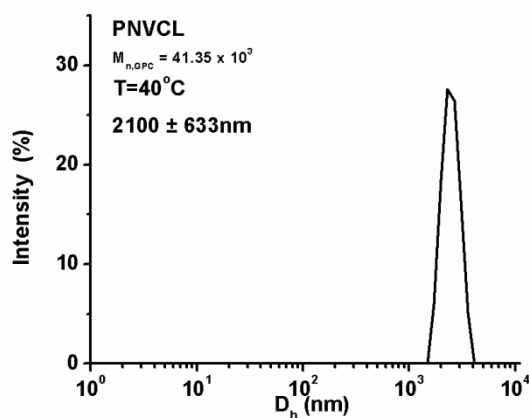
Most of the literature describing the solution behavior of POEOMA block copolymers deals with sheprical micelles<sup>39, 48, 49</sup> or worm-like<sup>50</sup> micelles as preferred self-assemblies morphologies. Yang and co-authors<sup>51</sup> developed very stable pH-sensitive micelles (CMC = 1 - 4 mg.L<sup>-1</sup>) from the self-assembly of amphiphilic copolymer bushes of poly(methyl methacrylate-co-methacrylic acid)-*b*-poly(OEOMA) (PMMA-*co*-PMAA)-*b*-POEOMA). The micelles with hydrodynamic diameter from 120 to 250 nm and low PDI (~ 0.09) were able to entrap poorly water soluble drugs in its hydrophobic core and release them upon increasing the pH solution. Similar results were obtained for the self-assembly of poly(lactide)-*b*-PMAA-*b*-POEOMA (PLA-*b*-PMAA-*b*-POEOMA).<sup>28</sup> It is well known that for amphiphilic diblock copolymers, the volume fraction ( $\Phi$ ) of the hydrophobic segment, along with the architecture of the blocks and the chemical nature of the repeating units, strongly influences the morphology of the self-assembly aggregates.<sup>52</sup> When the  $0.3 < \Phi_{\text{hydrophobic segment}} < 0.70$ , the formation of spherical micelles are favorable, while for  $\Phi_{\text{hydrophobic segment}} > 0.70$  vesicles are preferable.<sup>53, 54</sup> Herein, the series of the PNVCL block copolymers present a  $\Phi_{\text{NVCL}}$  close or higher than 0.7. Therefore, self-assembly into vesicles are expected, which are in agreement with the larger  $D_h$  obtained. No evidences of a direct correlation between the volume fraction of NVCL and the size of the particle were observed.

Figure 7.10 presents the size distribution of POEOMA<sub>16</sub>-*b*-PNVCL<sub>390</sub> in water (0.5 mg.mL<sup>-1</sup>) and the absence of particles at room temperature (25 °C). For all block copolymers, no particles were formed at room temperature, indicating the complete dissolution of the block copolymers. The size distribution of the other block copolymers is presented in Annex F (Figure F.8).



**Figure 7.10:** Hydrodynamic diameter ( $D_h$ ) of POEOMA<sub>16</sub>-*b*-PNVCL<sub>390</sub> at 25 °C (dotted line) and 45 °C (solid line) (0.5 mg.mL<sup>-1</sup>).

The hydrodynamic size of the PNVCL homopolymer in solution, for temperatures above the  $T_{CP}$ , is 10 times higher, when compared to the block copolymers (Figure 7.11), indicating that PNVCL precipitates out of the solution.



**Figure 7.11:** Hydrodynamic diameter ( $D_h$ ) of aqueous solution of PNVCL homopolymer ( $M_{n,GPC} = 41.35 \times 10^3$ ,  $D = 1.27$ ) at 40 °C ( $0.5 \text{ mg}\cdot\text{mL}^{-1}$ ).

The morphology of the self-assembled copolymer was investigated by TEM (Figure 7.12). A micrograph of the TEM grid prepared using the same method, only with water (without polymer), was used as control (Annex F, Figure F.9). The results suggest the formation of vesicular spherical aggregates. Nevertheless, the diameter of the aggregates determined by TEM is smaller than the  $D_h$  obtained by DLS. This discrepancy could be related with the method of sample preparation and the theoretical model used to determine the particle size distribution by DLS.

Additional micrographs of the self-assembled block copolymers, with different magnifications are presented in Annex F (Figure F.10 to Figure F.12).

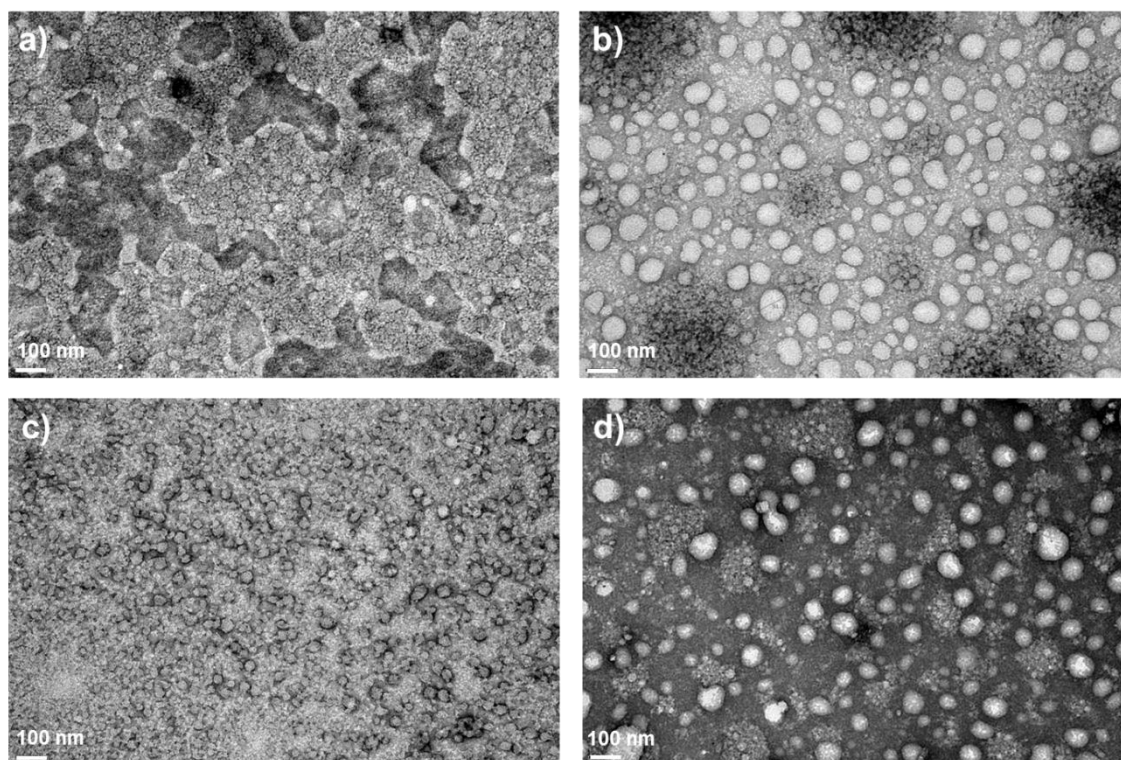


**Figure 7.12:** TEM micrographs of self-assembled block copolymers of (a) POEOMA<sub>16</sub>-*b*-PNVCL<sub>126</sub>, (b) POEOMA<sub>16</sub>-*b*-PNVCL<sub>198</sub>, (c) POEOMA<sub>16</sub>-*b*-PNVCL<sub>240</sub> and (d) POEOMA<sub>16</sub>-*b*-PNVCL<sub>390</sub>, taken at a Mag. x 100 000 (0.5 mg.mL<sup>-1</sup>).

The aggregation behavior of the block copolymer having the larger PNVCL segment (POEOMA<sub>16</sub>-*b*-PNVCL<sub>390</sub>) was monitored by DLS as a function of temperature. Each sample was left to equilibrate in a water bath inside the cuvette, equipped with a magnetic stirring, for 10 minutes and then analyzed. The dependence of the  $D_h$  with the solution temperature is shown in Figure 7.13, and the solution transmittance measurements as a function of temperature in the same range of temperatures as the DLS assay, for two distinct heating rates (1.0 and 0.1 °C.min<sup>-1</sup>) is plotted in Figure 7.14.



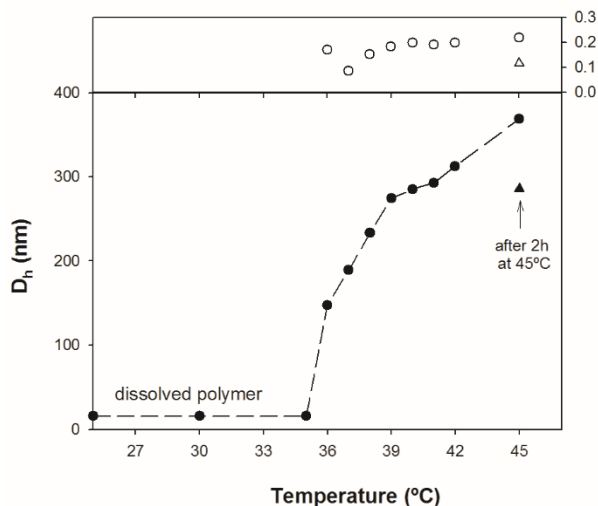


**Figure 7.13:** Dependence of the hydrodynamic diameter ( $D_h$ ) of aqueous solution of POEOMA<sub>16</sub>-*b*-PNVCL<sub>390</sub> in water ( $0.5 \text{ mg}\cdot\text{mL}^{-1}$ ) with temperature.

For temperatures below  $36 \text{ }^\circ\text{C}$ , the block copolymer ( $0.5 \text{ mg}\cdot\text{mL}^{-1}$ ) is completely soluble and no particles were formed. For these temperatures, the scattering intensity is very low and the DLS attenuation factor, a quality parameter in the DLS analysis, is very high (around 10). By increasing the solution temperature above the  $36 \text{ }^\circ\text{C}$ , the POEOMA-*b*-PNVCL copolymer becomes amphiphilic due to the phase separation of the PNVCL segment and aggregates with  $D_h$  in the range of 200 nm are formed. It is clear from Figure 7.13 that the unimer to aggregates transition occurs for temperatures above  $36 \text{ }^\circ\text{C}$ . However, the results show that a gradual and slow solution temperature increase, promotes the formation of particles with larger  $D_h$  (around 300 nm) and a moderate size distribution ( $\text{PDI} \sim 1.2$ ). These values increase along with the temperature ramp (Figure 7.13). These results highlight the possibility to form different structures using the same copolymers by only changing the self-assembly conditions. The DLS attenuation factor, also decreases in the course of the temperature ramp (from 7 at  $37 \text{ }^\circ\text{C}$  up to 5 at  $45 \text{ }^\circ\text{C}$ ), which confirms the formation of the aggregates. Moreover, at the end of the heating ramp, after 2h at  $45 \text{ }^\circ\text{C}$ , the  $D_h$  of the self-assemblies decreases, from 369 nm to 286 nm, as well as the PDI value, suggesting an improvement in the packing of the hydrophobic chains of the block copolymer. Interestingly, these results demonstrate that a fast heating cycle favors the formation of smaller self-assembly aggregates with narrow size distributions, as observed in Table 7.3, contrarily to what occurs when the block copolymer solution is gradually heated. The turbidimetry results

(Figure 7.14) corroborate these observations. A sharp drop in the solution transmittance was observed for temperatures around 36 °C followed by a recovery in the transmittance up to 50% and stabilizes for temperatures above 45 °C. Faster heating rates lead to faster block copolymer stabilization.

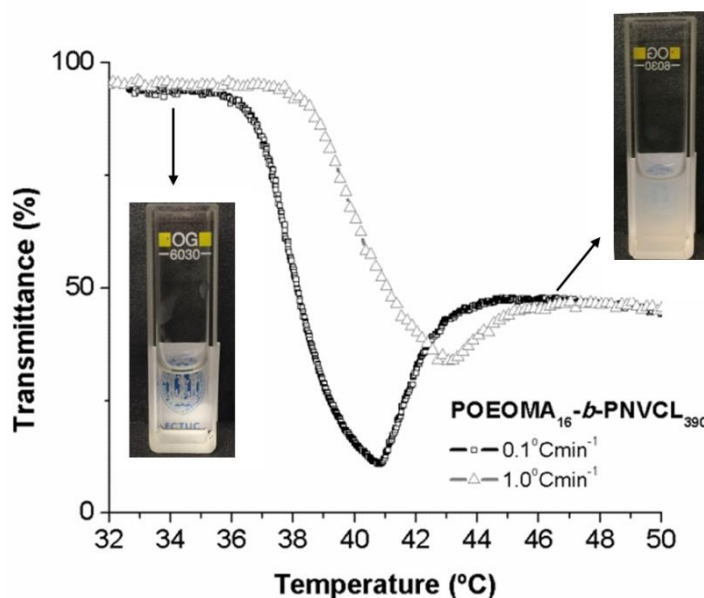


**Figure 7.14:** Transmittance measurements as a function of temperature for 0.5 mg.mL<sup>-1</sup> aqueous solution of the POEOMA<sub>16</sub>-*b*-PNVCL<sub>390</sub> copolymer at two different heating rates, 1.0 °C.min<sup>-1</sup> (triangle grey symbol) and 0.1 °C.min<sup>-1</sup> (square black symbol) with pictures of the sample taken at 30 °C and 45 °C.

Once the LCST of the PNVCL segment is affected by the presence of salts in the solution (Chapter 6), the DLS analysis of the block copolymers was performed in PBS (pH 7.4) and physiological saline solutions (NaCl 0.9%). It has been reported that the presence of additives in solution, such as salts, might influence the size and the final shape of the aggregates<sup>52</sup>. In our case, the DLS results confirm the presence of large aggregates in salted aqueous solutions at 45 °C for copolymer concentrations of 1.0 mg.mL<sup>-1</sup>, with  $D_h > 560$  nm. This observation could be related with the accentuated turbidimetry of the solution at this temperature. To avoid interferences with the light scattering, and reduce the interactions of the salts with the PNVCL segment, the solutions were diluted up to 0.1 mg.mL<sup>-1</sup> without compromising the quality of the measurements, i.e., the DLS attenuation factor was always above 8. The results of the  $D_h$  and PDI of the block copolymer self-assemblies are shown in Table 7.4.

**Table 7.4:** Characteristics of the self-assembled structures formed at 45 °C from the POEOMA-*b*-PNVCL copolymers in PBS (pH 7.4) or physiological saline (NaCl 0.9 %) solutions.

	Solvent	Conc. (mg.mL <sup>-1</sup> )	D <sub>h</sub> (nm) <sup>a</sup>	PDI	σ (nm) <sup>b</sup>
<b>POEOMA<sub>16</sub>-<i>b</i>-PNVCL<sub>126</sub></b>	NaCl 0.9%	1.0	642	0.050	144
		0.1	262	0.082	75
	PBS (pH 7.4)	1.0	697	0.144	264
		0.1	266	0.108	87
<b>POEOMA<sub>16</sub>-<i>b</i>-PNVCL<sub>198</sub></b>	NaCl 0.9%	1.0	582	0.225	276
		0.2	436	0.185	188
	PBS (pH 7.4)	0.1	264	0.061	65
		1.0	792	0.137	293
<b>POEOMA<sub>16</sub>-<i>b</i>-PNVCL<sub>240</sub></b>	NaCl 0.9%	1.0	726	0.147	278
		0.1	259	0.023	39
	PBS (pH 7.4)	1.0	915	0.340	534
		0.1	331	0.027	54
<b>POEOMA<sub>16</sub>-<i>b</i>-PNVCL<sub>390</sub></b>	NaCl 0.9%	1.0	726	0.147	278
		0.1	284	0.081	81
	PBS (pH 7.4)	1.0	562	0.085	164
		0.1	302	0.110	100

<sup>a</sup>mean value of the hydrodynamic diameter of the particle; <sup>b</sup>PDI width (σ) determined using the equation:  $PDI = (\sigma/D_h)^2$ .

Detailed plots with the DLS curves for the different block copolymer solutions are presented in Annex F (Figure F.14 and Figure F.15).

The transmittance measurements as a function of temperature for 0.1 mgmL<sup>-1</sup> of physiological saline solution of the POEOMA-*b*-PNVCL copolymers at a heating rate 1.0 °C.min<sup>-1</sup> suggest only a slight drop in the solution turbidimetry, 80% transmittance at 45 °C for the block copolymer with shorter PNVCL segment and 60% for the block copolymer with larger PNVCL segment (Annex F, Figure F.13). Moreover, the diluted nature of the solutions increases the T<sub>CP</sub> of the block copolymers and smooths the transition in the solution transmission. However, it should be noted that at 45 °C all the PNVCL chains are insoluble.

#### **7.4.6. Fluorescence assays - studies of guest loading and triggered release**

Nile red (NR) was used as a model hydrophobic drug. Fluorescence spectroscopy allows the study of the guest loading and triggered release of the NR from the nanostructures. NR has a very poor water solubility ( $< 1 \mu\text{g}\cdot\text{mL}^{-1}$  at  $25 \text{ }^\circ\text{C}$ )<sup>55</sup> and its fluorescence emission in aqueous solutions is negligible. However, its fluorescence increases substantially when NR is located in the hydrophobic domains of the self-assembled nanostructures.<sup>56</sup>

Solutions of block copolymer with NR were prepared as described. The NR solution in THF was added to the copolymer aqueous solution. Thereafter the block copolymer solution was stirred in the absence of light and heated ( $45^\circ\text{C}$ ) to allow the formation of the nanostructures and the evaporation of the organic solvent. Due to the reduced water solubility of the NR, this molecule is entrapped in the hydrophobic domain of the nanostructures. The non-encapsulated NR was removed by filtration. A light purple/pink dispersion of copolymer was observed, indicating the success of the NR encapsulation<sup>57</sup> (Annex F, Figure F.16). The presence of NR inside the hydrophobic domain of the block copolymer nanostructures was confirmed by the specific emission at ca. 622 nm. To ensure the formation of the nanostructures with encapsulated NR, the fluorescent assays were done at  $45 \text{ }^\circ\text{C}$ , in which the PNVCL segment is completely hydrophobic. Figure 7.15 (a) shows the intensity of NR emission as a function of the solution concentration of POEOMA-*b*-PNVCL copolymer. An abrupt increase in the fluorescence intensity was observed with increasing the block copolymer concentration, indicating the formation of the self-assemblies and the migration of the NR to the hydrophobic domains. The critical micelle concentration (CMC) values were determined by the interception of both linear fittings obtained from the plot of the maximum intensity versus the logarithm of copolymer concentration (Figure 7.15 (b)). The CMC values for all the block copolymer synthesized are lower than  $84 \text{ mg}\cdot\text{L}^{-1}$  (Table 7.3). By increasing the volume fraction of the PNVCL segment, the CMC values decrease, up to  $21 \text{ mg}\cdot\text{L}^{-1}$ , indicating that the POEOMA-*b*-PNVCL copolymers with larger NVCL segments form more stable particles at the temperature of the assays. One should note that it was very difficult to ensure the control of the temperature throughout the test, and a slight drop in the temperature could be sufficient to disrupt the self-assemblies and release the dye. Moreover, for the CMC assays, the concentration of the block copolymers started from  $0.25 \text{ mg}\cdot\text{mL}^{-1}$  due to the resolution of the fluorescence

spectrometer used. The temperature triggered release of the hydrophobic content is demonstrated by the decrease of the NR emission with the decrease of the temperature of the copolymer solution (Annex F, Figure F.17).

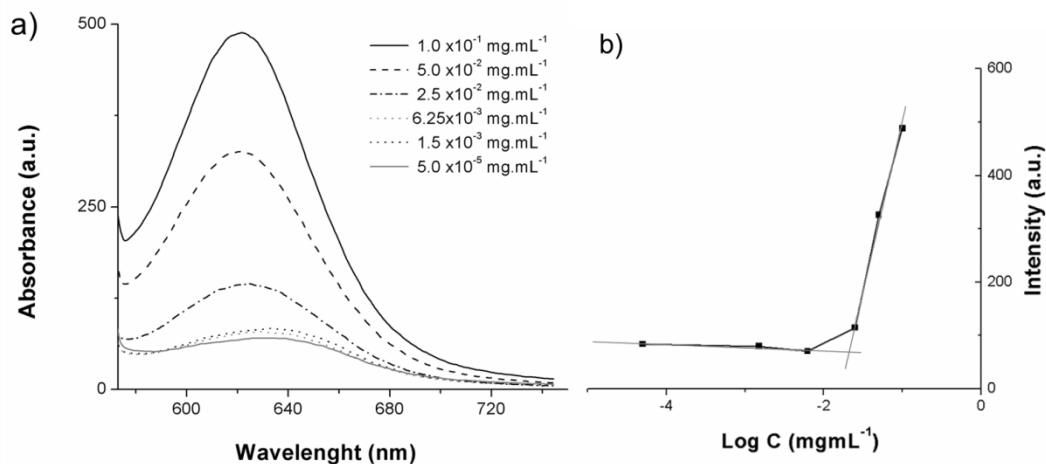


**Figure 7.15:** Fluorescence spectra of Nile Red in water at different concentrations of the POEOMA<sub>16</sub>-*b*-PNVCL<sub>390</sub> copolymer (left) and plot of intensity vs logarithm of concentration of POEOMA<sub>16</sub>-*b*-PNVCL<sub>390</sub> copolymer (right).

The drug loading capacity (DLC) and the drug loading efficiency (DLE) of the polymeric aggregates were also determined using NR as a model hydrophobic drug. In this case, the concentration of the NR solution was increased and a control experiment without the block copolymer was also performed, in order to evaluate the success of the removal of the non-encapsulated NR by filtration. In fact, similar studies reported in the literature<sup>6, 57-59</sup> do not present control experiments without the copolymer and assume that the untrapped NR is retained in the filter. In our case, it was observed that, despite the lack of solubility of NR in water, there are some NR particles, with diameter smaller than the pore filter that passed through the filter and remain in suspension. Those particles are more visible after the disruption of the self-assemblies with THF (Annex F, Figure F.18). For the present study, the DLC and DLE calculated values (Table 7.5) were corrected taking into account the absorbance of the control samples (samples without copolymer). For the block copolymer solutions, the results reveal that the increase in the hydrophobic domain in the block copolymers reduces the DLC and the DLE of the NR suggesting that higher PNVCL segments in the copolymers promote

a higher packing of the hydrophobic domain in the self-assemblies and reduces the available space to accommodate the hydrophobic guest molecules.

In fact, the NR is not the appropriate model compound to study the DLC and the DLE due the high concentrations required for the assays. Nevertheless, NR is a good model to prove the capacity of such structures to accommodate and release hydrophobic small molecules by fluorescent spectroscopy. However, in order to understand the relasing profiles and evaluate the DLC and DLE, doxorubicin or paclitaxel are more appropriate hydrophobic model drugs. Also, it would be interesting to test one hydrophilic model compound, such as the doxorubicin hydrochloride since the self-assemblies presented in this study may have an aqueous core compartment able to accommodate such molecules. Those tests would eventually demonstrate the capacity for encapsulation of both types of guest molecules (hydrophilic and hydrophobic).

**Table 7.5:** Results from the encapsulation assays with Nile red.

Copolymer	Drug loading capacity (%)		Drug loading efficiency (%)	
	(a)	(b)	(a)	(b)
<b>POEOMA<sub>16</sub>-<i>b</i>-PNVCL<sub>126</sub></b>	92	53	46	27
<b>POEOMA<sub>16</sub>-<i>b</i>-PNVCL<sub>198</sub></b>	85	46	42	23
<b>POEOMA<sub>16</sub>-<i>b</i>-PNVCL<sub>240</sub></b>	78	39	39	20
<b>POEOMA<sub>16</sub>-<i>b</i>-PNVCL<sub>390</sub></b>	69	30	34	15
<b>Control experiment</b>	36	---	18	---

(a) Values before correction with the values obtained from the control experiment, (b) values after the correction with the values obtained from the control experiment

## 7.5. Conclusions

Novel POEOMA-*b*-PNVCL copolymers were prepared by a simple CuAAC reaction between an azide terminated POEOMA synthesized by ATRP and an alkyne terminated PNVCL obtained by RAFT polymerization. In diluted solutions, those temperature-responsive block copolymers form very stable spherical aggregates with  $D_h > 150$  nm, for temperatures above the  $T_{CP}$  of the NVCL segment, which depend on copolymer concentration and solution conditions. The hydrophobic domain of the self-assembled structures allows the entrapment of a small hydrophobic molecule. Fluorescent studies demonstrate the temperature dependence of the assembly/disassembly of the POEOMA-*b*-PNVCL copolymers. The block copolymers reported here can be used as promising temperature-responsive nanocarriers, although the encapsulation of hydrophilic molecules to prove the solution vesicular structure should be performed. Moreover, after the “click” coupling reaction, both polymers possess  $\omega$  chain-end functionalities that can be used for targeting the particles, add fluorescence molecules or even form polymer-drug conjugates, and by that means extend the range of applications of these temperature-responsive structures.

## 7.6. References

1. Beija, M., J.-D. Marty, and M. Destarac (2011). Thermoresponsive poly(N-vinyl caprolactam)-coated gold nanoparticles: sharp reversible response and easy tunability. *Chemical Communications*, 47(10): 2826-2828.
2. Shao, L., M. Hu, L. Chen, L. Xu, and Y. Bi (2012). RAFT polymerization of N-vinylcaprolactam and effects of the end group on the thermal response of poly(N-vinylcaprolactam). *Reactive and Functional Polymers*, 72(6): 407-413.
3. Meeussen, F., E. Nies, H. Berghmans, S. Verbrugghe, E. Goethals, and F. Du Prez (2000). Phase behaviour of poly(N-vinyl caprolactam) in water. *Polymer*, 41(24): 8597-8602.
4. Ramos, J., A. Imaz, and J. Forcada (2012). Temperature-sensitive nanogels: poly(N-vinylcaprolactam) versus poly(N-isopropylacrylamide). *Polymer Chemistry*, 3(4): 852-856.

5. Thomassin, J.M., K. Mathieu, A. Kermagoret, C.A. Fustin, C. Jerome, and A. Debuigne (2015). Double thermo-responsive hydrogels from poly(vinylcaprolactam) containing diblock and triblock copolymers. *Polymer Chemistry*, 6(10): 1856-1864.
6. Liu, J., C. Detrembleur, A. Debuigne, M.-C. De Pauw-Gillet, S. Mornet, L. Vander Elst, S. Laurent, E. Duguet, and C. Jerome (2014). Glucose-, pH- and thermo-responsive nanogels crosslinked by functional superparamagnetic maghemite nanoparticles as innovative drug delivery systems. *Journal of Materials Chemistry B*, 2(8): 1009-1023.
7. Wan, D., Q. Zhou, H. Pu, and G. Yang (2008). Controlled radical polymerization of N-vinylcaprolactam mediated by xanthate or dithiocarbamate. *Journal of Polymer Science Part A: Polymer Chemistry*, 46(11): 3756-3765.
8. Devasia, R., R. Borsali, S. Lecommandoux, R.L. Bindu, N. Mougin, and Y. Gnanou (2005). Synthesis of poly(N-vinylcaprolactam)-block-poly(N-vinylpyrrolidone) diblock copolymer by RAFT and the formation of thermosensitive mesoglobules in water. *Abstracts of Papers of the American Chemical Society*, 230: 512-POLY.
9. Hurtgen, M., J. Liu, A. Debuigne, C. Jerome, and C. Detrembleur (2012). Synthesis of thermo-responsive poly(N-vinylcaprolactam)-containing block copolymers by cobalt-mediated radical polymerization. *Journal of Polymer Science Part A: Polymer Chemistry*, 50(2): 400-408.
10. Kermagoret, A., K. Mathieu, J.-M. Thomassin, C.-A. Fustin, R. Duchene, C. Jerome, C. Detrembleur, and A. Debuigne (2014). Double thermoresponsive di- and triblock copolymers based on N-vinylcaprolactam and N-vinylpyrrolidone: synthesis and comparative study of solution behaviour. *Polymer Chemistry*.
11. Kermagoret, A., C.-A. Fustin, M. Bourguignon, C. Detrembleur, C. Jerome, and A. Debuigne (2013). One-pot controlled synthesis of double thermoresponsive N-vinylcaprolactam-based copolymers with tunable LCSTs. *Polymer Chemistry*, 4(8): 2575-2583.
12. Yang, Y.Z., J. Li, M.Q. Hu, L. Chen, and Y.M. Bi (2014). Well-defined poly(DL-lactide)-*b*-poly(N-vinylcaprolactam) copolymers: synthesis, solution properties and in vitro degradation. *Journal of Polymer Research*, 21(9).
13. Singh, P., A. Srivastava, and R. Kumar (2012). Synthesis of amphiphilic poly(N-vinylcaprolactam) using ATRP protocol and antibacterial study of its silver nanocomposite. *Journal of Polymer Science Part A: Polymer Chemistry*, 50(8): 1503-1514.
14. Jiang, X., Y. Li, G. Lu, and X. Huang (2013). A novel poly(N-vinylcaprolactam)-



- based well-defined amphiphilic graft copolymer synthesized by successive RAFT and ATRP. *Polymer Chemistry*, 4(5): 1402-1411.
15. Chen, J., M. Liu, H. Gong, G. Cui, S. Lu, C. Gao, F. Huang, T. Chen, X. Zhang, and Z. Liu (2013). Synthesis of linear amphiphilic tetrablock quaterpolymers with dual stimulus response through the combination of ATRP and RAFT by a click chemistry site transformation approach. *Polymer Chemistry*, 4(6): 1815-1825.
  16. Liu, J., C. Detrembleur, M.C. De Pauw-Gillet, S. Mornet, E. Duguet, and C. Jerome (2014). Gold nanorods coated with a thermo-responsive poly(ethylene glycol)-b-poly(N-vinylcaprolactam) corona as drug delivery systems for remotely near infrared-triggered release. *Polymer Chemistry*, 5(3): 799-813.
  17. Bi, Y., C. Yan, L. Shao, Y. Wang, Y. Ma, and G. Tang (2013). Well-defined thermoresponsive dendritic polyamide/poly(N-vinylcaprolactam) block copolymers. *Journal of Polymer Science Part A: Polymer Chemistry*, 51(15): 3240-3250.
  18. Yu, Y., H. Kang, and J. Youk (2012). Synthesis and micellar characterization of thermosensitive amphiphilic poly( $\epsilon$ -caprolactone)-b-poly(N-vinylcaprolactam) block copolymers. *Colloid and Polymer Science*, 290(12): 1107-1113.
  19. Yu, Y.C., G. Li, J. Kim, and J.H. Youk (2013). One-pot synthesis of poly(N-vinylcaprolactam)-based biocompatible block copolymers using a dual initiator for ROP and RAFT polymerization. *Polymer*, 54(22): 6119-6124.
  20. Garcia-Olaiz, G.D., K.A. Montoya-Villegas, A. Licea-Claverie, and N.A. Cortez-Lemus (2015). Synthesis and characterization of four- and six-arm star-shaped poly(epsilon-caprolactone)-b-poly(N-vinylcaprolactam): Micellar and core degradation studies. *Reactive & Functional Polymers*, 88: 16-23.
  21. Wang, X.S. and S.P. Armes (2000). Facile Atom Transfer Radical Polymerization of Methoxy-Capped Oligo(ethylene glycol) Methacrylate in Aqueous Media at Ambient Temperature. *Macromolecules*, 33(18): 6640-6647.
  22. Pressly, E.D., R. Rossin, A. Hagooley, K.-i. Fukukawa, B.W. Messmore, M.J. Welch, K.L. Wooley, M.S. Lamm, R.A. Hule, D.J. Pochan, and C.J. Hawker (2007). Structural Effects on the Biodistribution and Positron Emission Tomography (PET) Imaging of Well-Defined  $^{64}\text{Cu}$ -Labeled Nanoparticles Comprised of Amphiphilic Block Graft Copolymers. *Biomacromolecules*, 8(10): 3126-3134.
  23. Oh, J.K., D.J. Siegwart, H.-i. Lee, G. Sherwood, L. Peteanu, J.O. Hollinger, K. Kataoka, and K. Matyjaszewski (2007). Biodegradable Nanogels Prepared by Atom Transfer Radical Polymerization as Potential Drug Delivery Carriers:

- Synthesis, Biodegradation, in Vitro Release, and Bioconjugation. *Journal of the American Chemical Society*, 129(18): 5939-5945.
24. Tao, L., G. Mantovani, F. Lecolley, and D.M. Haddleton (2004).  $\alpha$ -Aldehyde Terminally Functional Methacrylic Polymers from Living Radical Polymerization: Application in Protein Conjugation "Pegylation". *Journal of the American Chemical Society*, 126(41): 13220-13221.
  25. Reyes-Ortega, F., F.J. Parra-Ruiz, S.E. Averick, G. Rodriguez, M.R. Aguilar, K. Matyjaszewski, and J. San Roman (2013). Smart heparin-based bioconjugates synthesized by a combination of ATRP and click chemistry. *Polymer Chemistry*, 4(9): 2800-2814.
  26. Yao, Y., D.-F. Feng, Y.-P. Wu, Q.-J. Ye, L. Liu, X.-X. Li, S. Hou, Y.-L. Yang, C. Wang, L. Li, and X.-Z. Feng (2011). Influence of block sequences in polymer vectors for gene transfection in vitro and toxicity assessment of zebrafish embryos in vivo. *Journal of Materials Chemistry*, 21(12): 4538-4545.
  27. Üzgün, S., Ö. Akdemir, G. Hasenpusch, C. Maucksch, M.M. Golas, B. Sander, H. Stark, R. Imker, J.-F. Lutz, and C. Rudolph (2010). Characterization of Tailor-Made Copolymers of Oligo(ethylene glycol) Methyl Ether Methacrylate and N,N-Dimethylaminoethyl Methacrylate as Nonviral Gene Transfer Agents: Influence of Macromolecular Structure on Gene Vector Particle Properties and Transfection Efficiency. *Biomacromolecules*, 11(1): 39-50.
  28. Yang, Y.Q., W.J. Lin, B. Zhao, X.F. Wen, X.D. Guo, and L.J. Zhang (2012). Synthesis and Physicochemical Characterization of Amphiphilic Triblock Copolymer Brush Containing pH-Sensitive Linkage for Oral Drug Delivery. *Langmuir*, 28(21): 8251-8259.
  29. Kolb, H.C., M.G. Finn, and K.B. Sharpless (2001). Click chemistry: Diverse chemical function from a few good reactions. *Angewandte Chemie-International Edition*, 40(11): 2004-+.
  30. Xia, J., S.G. Gaynor, and K. Matyjaszewski (1998). Controlled/"Living" Radical Polymerization. Atom Transfer Radical Polymerization of Acrylates at Ambient Temperature. *Macromolecules*, 31(17): 5958-5959.
  31. Mespouille, L., M. Vachaudéz, F. Suriano, P. Gerbaux, O. Coulembier, P. Degee, R. Flammang, and P. Dubois (2007). One-pot synthesis of well-defined amphiphilic and adaptative block copolymers via versatile combination of "Click" chemistry and ATRP. *Macromolecular Rapid Communications*, 28: 2151-2158.
  32. Gois, J.R., D. Konkolewicz, A.V. Popov, T. Guliasvili, K. Matyjaszewski, A.C. Serra, and J.F.J. Coelho (2014). Improvement of the control over SARA ATRP

- of 2-(diisopropylamino)ethyl methacrylate by slow and continuous addition of sodium dithionite. *Polymer Chemistry*, 5(16): 4617-4626.
33. Gillies, E.R., T.B. Jonsson, and J.M.J. Frechet (2004). Stimuli-responsive supramolecular assemblies of linear-dendritic copolymers. *Journal of the American Chemical Society*, 126(38): 11936-11943.
  34. Giacomelli, C., V. Schmidt, and R. Borsali (2007). Specific Interactions Improve the Loading Capacity of Block Copolymer Micelles in Aqueous Media. *Langmuir*, 23(13): 6947-6955.
  35. Lutz, J.-F. (2008). Polymerization of oligo(ethylene glycol) (meth)acrylates: Toward new generations of smart biocompatible materials. *Journal of Polymer Science Part A: Polymer Chemistry*, 46(11): 3459-3470.
  36. Lutz, J.-F., J. Andrieu, S. Üzgün, C. Rudolph, and S. Agarwal (2007). Biocompatible, Thermoresponsive, and Biodegradable: Simple Preparation of "All-in-One" Biorelevant Polymers. *Macromolecules*, 40(24): 8540-8543.
  37. Knop, K., R. Hoogenboom, D. Fischer, and U.S. Schubert (2010). Poly(ethylene glycol) in Drug Delivery: Pros and Cons as Well as Potential Alternatives. *Angewandte Chemie International Edition*, 49(36): 6288-6308.
  38. Hussain, H., K.Y. Mya, and C. He (2008). Self-Assembly of Brush-Like Poly[poly(ethylene glycol) methyl ether methacrylate] Synthesized via Aqueous Atom Transfer Radical Polymerization. *Langmuir*, 24(23): 13279-13286.
  39. Bes, L., S. Angot, A. Limer, and D.M. Haddleton (2003). Sugar-Coated Amphiphilic Block Copolymer Micelles from Living Radical Polymerization: Recognition by Immobilized Lectins. *Macromolecules*, 36(7): 2493-2499.
  40. Cai, T., M. Li, B. Zhang, K.-G. Neoh, and E.-T. Kang (2014). Hyperbranched polycaprolactone-click-poly(N-vinylcaprolactam) amphiphilic copolymers and their applications as temperature-responsive membranes. *Journal of Materials Chemistry B*, 2(7): 814-825.
  41. Rostovtsev, V.V., L.G. Green, V.V. Fokin, and K.B. Sharpless (2002). A stepwise Huisgen cycloaddition process: Copper(I)-catalyzed regioselective "ligation" of azides and terminal alkynes. *Angewandte Chemie-International Edition*, 41(14): 2596-+.
  42. Medeiros, S.F., J.C.S. Barboza, M.I. Re, R. Giudici, and A.M. Santos (2010). Solution Polymerization of N-vinylcaprolactam in 1,4-dioxane. Kinetic Dependence on Temperature, Monomer, and Initiator Concentrations. *Journal of Applied Polymer Science*, 118(1): 229-240.

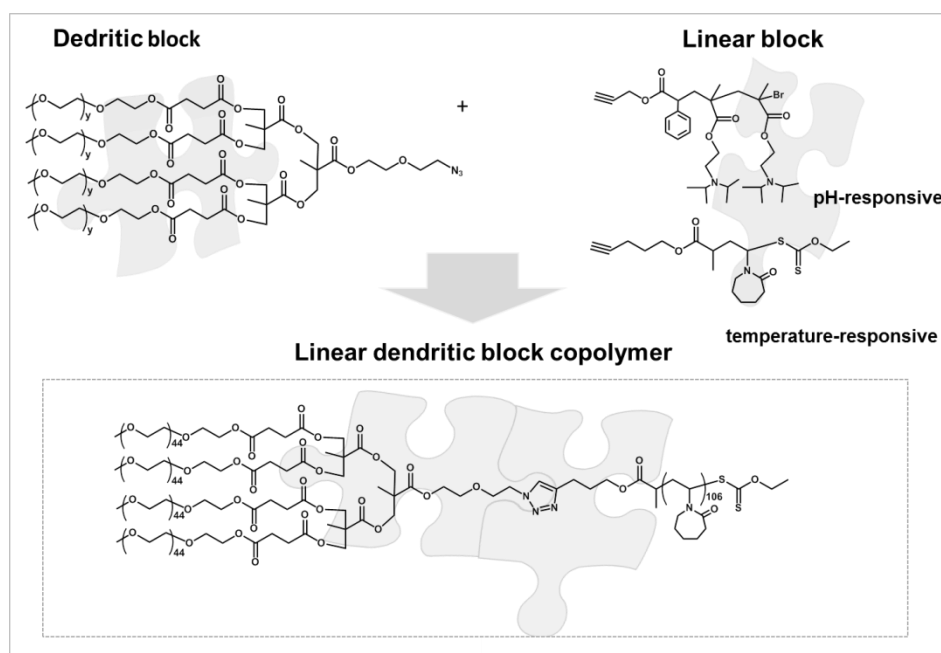
43. Onaca, O., R. Enea, D.W. Hughes, and W. Meier (2009). Stimuli-Responsive Polymersomes as Nanocarriers for Drug and Gene Delivery. *Macromolecular Bioscience*, 9(2): 129-139.
44. Israelachvili, J.N. (1992). Intermolecular and surface forces: London:Harcourt Brace and Company.
45. Giacomelli, C., L. Le Men, R. Borsali, J. Lai-Kee-Him, A. Brisson, S.P. Armes, and A.L. Lewis (2006). Phosphorylcholine-Based pH-Responsive Diblock Copolymer Micelles as Drug Delivery Vehicles: Light Scattering, Electron Microscopy, and Fluorescence Experiments. *Biomacromolecules*, 7(3): 817-828.
46. Lutz, J.-F. and A. Hoth (2006). Preparation of Ideal PEG Analogues with a Tunable Thermosensitivity by Controlled Radical Copolymerization of 2-(2-Methoxyethoxy)ethyl Methacrylate and Oligo(ethylene glycol) Methacrylate. *Macromolecules*, 39(2): 893-896.
47. Sun, G. and Z. Guan (2010). Synthesis and Investigation of Core-Shell Dendritic Nanoparticles with Tunable Thermosensitivity. *Macromolecules*, 43(23): 9668-9673.
48. Chan, N., H.W. Jung, S.M. Noh, and J.K. Oh (2014). Functional amphiphilic oligo(ethylene oxide) methacrylate-based block copolymers: synthesis by an activator regenerated by electron transfer process for atom transfer radical polymerization and aqueous micellization. *Polymer International*, 63(5): 858-867.
49. Tan, B.H., H. Hussain, Y. Liu, C.B. He, and T.P. Davis (2010). Synthesis and Self-Assembly of Brush-Type Poly[poly(ethylene glycol)methyl ether methacrylate]-block-poly(pentafluorostyrene) Amphiphilic Diblock Copolymers in Aqueous Solution. *Langmuir*, 26(4): 2361-2368.
50. Cheng, Zhu, E.T. Kang, and K.G. Neoh (2005). Brush-Type Amphiphilic Diblock Copolymers from "Living"/Controlled Radical Polymerizations and Their Aggregation Behavior. *Langmuir*, 21(16): 7180-7185.
51. Yang, Y.Q., L.S. Zheng, X.D. Guo, Y. Qian, and L.J. Zhang (2011). pH-Sensitive Micelles Self-Assembled from Amphiphilic Copolymer Brush for Delivery of Poorly Water-Soluble Drugs. *Biomacromolecules*, 12(1): 116-122.
52. Choucair, A. and A. Eisenberg (2003). Control of amphiphilic block copolymer morphologies using solution conditions. *Eur. Phys. J. E*, 10(1): 37-44.
53. Bates, F.S. and G.H. Fredrickson (1990). Block Copolymer Thermodynamics: Theory and Experiment. *Annual Review of Physical Chemistry*, 41(1): 525-557.

- 
54. Jain, S. and F.S. Bates (2003). On the Origins of Morphological Complexity in Block Copolymer Surfactants. *Science*, 300(5618): 460-464.
  55. Stuart, M.C.A., J.C. van de Pas, and J.B.F.N. Engberts (2005). The use of Nile Red to monitor the aggregation behavior in ternary surfactant–water–organic solvent systems. *Journal of Physical Organic Chemistry*, 18(9): 929-934.
  56. Zhou, X., S. Luo, R. Tang, R. Wang, and J. Wang (2015). Diblock Copolymers of Polyethylene Glycol and a Polymethacrylamide with Side-Chains Containing Twin Ortho Ester Rings: Synthesis, Characterization, and Evaluation as Potential pH-Responsive Micelles. *Macromolecular Bioscience*, 15(3): 385-394.
  57. Jin, N., E.A. Morin, D.M. Henn, Y. Cao, J.W. Woodcock, S. Tang, W. He, and B. Zhao (2013). Agarose Hydrogels Embedded with pH-Responsive Diblock Copolymer Micelles for Triggered Release of Substances. *Biomacromolecules*, 14(8): 2713-2723.
  58. Toughraï, S., V. Malinova, R. Masciadri, S. Menon, P. Tanner, C. Palivan, N. Bruns, and W. Meier (2015). Reduction-Sensitive Amphiphilic Triblock Copolymers Self-Assemble Into Stimuli-Responsive Micelles for Drug Delivery. *Macromolecular Bioscience*, 15(4): 481-489.
  59. Liu, J., C. Detrembleur, M. Hurtgen, A. Debuigne, M.-C. De Pauw-Gillet, S. Mornet, E. Duguet, and C. Jerome (2014). Reversibly crosslinked thermo- and redox-responsive nanogels for controlled drug release. *Polymer Chemistry*, 5(1): 77-88.



# Chapter 8

## Synthesis of stimuli-responsive linear dendritic block copolymers via “click” chemistry







## 8.1. Abstract

Responsive polymers with linear-dendritic architectures were developed using a “click” coupling strategy. Polyester dendrimers based on the monomer 2,2-bis(hydroxymethyl) propionic acid (bis-MPA) with either alkyne or azide focal point moieties were developed. The peripheral groups of the bis-MPA dendrom were functionalized with PEG segments to improve its water solubility. As linear segments, two distinct stimuli responsive polymers were synthesized: a temperature responsive based on the poly(*N*-vinyl caprolactam) (PNVCL) and pH-responsive based on the poly(2-(diisopropylamino)ethyl methacrylate) (PDPA). The linear dendritic block copolymers (LDBC) were synthesized by the “click” conjugation strategy between the linear and the dendritic segment. The success of the reaction was verified by  $^1\text{H}$  NMR spectroscopy.

## 8.2. Introduction

Linear dendritic block copolymers (LDBC) possess a unique polymer architecture consisting of a linear chain attached to a dendritic, branched building block. This hybrid structure takes advantage of the chain entanglement of the linear polymers and the high peripheral functionality of the dendrimers. LDBC have been reported as a potential strategy in the development of supramolecular nanocarriers for biomedical applications.<sup>1-8</sup> Depending on the chemical structure of the different blocks, and the size (and generation) of the amphiphilic LDBC, these structures can form very stable supramolecular aggregates in solution. In most of amphiphilic linear-dendrimer systems reported, the hydrophobic part is composed by the dendritic block, acting as the nano-encapsulating core of micelles.<sup>3</sup> In comparison to the traditional linear AB-type block copolymers, the LDBC can take advantage of its cone shaped molecular architecture<sup>9</sup> to develop very stable micellar aggregates with reduced critical micelle concentration (CMC) in the range of  $10^{-8}$  M.<sup>3, 10</sup> This special arrangement enables the further dendritic surface functionalization, which results in the improvement of the nanostructure performance. The majority of the published studies concerning self-assembly of LDBC deal with the formation of spherical micelles. A few reports are available dealing with other morphologies such as cylindrical micelles<sup>11</sup> or polymer vesicles.<sup>2, 11, 12</sup> Most of the LDBC reported were developed for drugs<sup>13, 14</sup> or genetic material encapsulation by

self-assembly into supramolecular structures<sup>15</sup>, or the formation polyplexes by direct complexation with genetic material.<sup>16, 17</sup> There are only a few reports in the literature concerning LDBC that have stimuli-responsive segments.<sup>2, 3, 18, 19</sup>

In this work, several pH and temperature LDBC are described for the first time. The copolymers were synthesized by a simple “click” coupling strategy between an azide functionalized poly(ester dendron) and alkyne terminated linear pH- and temperature-responsive polymers in view of understanding the influence of the length (and generation) of each block in the properties of the supramolecular aggregates formed by the self-assembly of the copolymers.

### **8.3. Experimental Section**

#### **8.3.1. Materials**

2,2-bis (hydroxymethyl)propionic acid (bis-MPA) (98%, Aldrich), 2,2-dimethoxypropane (98%, Sigma-Aldrich), triethylamine (Et<sub>3</sub>N) (≥ 99%, Sigma Aldrich), N,N'-dicyclohexylcarbodiimide (DCC) (99%, Aldrich), 2-(2-chloroethoxy)ethanol (99%, Sigma-Aldrich), sodium azide (≥99.5%, Sigma-Aldrich), hexadecyltrimethylammonium bromide (≥ 99%, Sigma), propargyl alcohol (PA) (99%, Aldrich), Dowex<sup>®</sup> 50W-X2 resin (hydrogen form, 100-200 mesh, Sigma Aldrich), 4-(dimethylamino)pyridine (DMAP) (≥ 99%, Aldrich), N,N'-diisopropylcarbodiimide (DIC) (99%, Aldrich), succinic anhydride (≥ 99%, Aldrich), thionyl chloride (≥ 99%, Sigma Aldrich),  $\alpha$ -bromophenylacetic acid (98%, Aldrich), sodium ascorbate (NaAsc) (≥ 98%, Sigma), copper(II) sulfate pentahydrate (CuSO<sub>4</sub>·5H<sub>2</sub>O) (≥98%, Aldrich), sodium dithionite (Na<sub>2</sub>S<sub>2</sub>O<sub>4</sub>), (85%, ACROS Organics), copper(II) bromide (CuBr<sub>2</sub>) (99.999%, Aldrich), anhydrous magnesium sulphate (MgSO<sub>4</sub>) (99%, Aldrich), anhydrous sodium sulfate (Na<sub>2</sub>SO<sub>4</sub>) (≥ 98 %, Fisher Chemical), deuterated chloroform (CDCl<sub>3</sub>) (99.8%, Cambridge Isotope Laboratories), water (HPLC grade, Fisher Scientific), isopropanol (IPA) (ACS grade, Fisher Scientific), acetone (HPLC grade, Fisher Scientific), dichloromethane (DCM) (99.99%, Fisher Scientific), ethyl acetate (99.98 %, Fisher Scientific), hexane (99.05%, Fisher Scientific), tetrahydrofuran (THF) (≥ 99.9%, Sigma-Aldrich), diethyl ether (99.85%, Fisher Scientific), dimethylformamide (DMF) (≥99.8%; Sigma-Aldrich) were used as received.

2-(Diisopropylamino)ethyl methacrylate (DPA) (97%, Scientific Polymer Products Inc.) was passed over a column of basic alumina to remove inhibitor prior to use. Poly(ethylene glycol) monomethyl ether (mPEG<sub>44</sub> (MW= 2000 Da, Aldrich) and mPEG<sub>113</sub> (MW= 5000 Da, Aldrich) and p-toluenesulfonic acid (TsOH) ( $\geq 98\%$ , Sigma-Aldrich) were dried by azeotropic distillation. Tris(2-(dimethylamino)ethyl)amine (Me<sub>6</sub>TREN)<sup>20</sup> and 4-(dimethylamino)pyridinium p-toluenesulfonate (DPTS)<sup>21</sup> were synthesized according to the procedures reported in the literature.

A series of alkyne-terminated poly(*N*-vinyl caprolactam) (PNVCL) with different molecular weights were synthesized according to the procedures described in Chapter 6.

### 8.3.2. Characterization

A KDS Scientific, Legato 101 syringe pump was used for continuous feeding polymerizations of DPA.

<sup>1</sup>H nuclear magnetic resonance (NMR) spectra were recorded on a Bruker Avance III 400 MHz (or Bruker Avance 500 MHz) spectrometer, at room temperature, with a 5 mm TXI triple resonance detection probe, in CDCl<sub>3</sub> with tetramethylsilane (TMS) as an internal standard. Conversion of monomers was determined by integration of monomer and polymer peaks using MestReNova software version: 6.0.2-5475.

The chromatographic parameters, the number-average MW ( $M_{n,GPC}$ ) and dispersity, ( $D$ ) of the synthesized polymers were determined by gel permeation chromatography (GPC) using different systems: For the PDPA samples, the GPC system used a Waters 515 HPLC pump and a Waters 2414 refractive index detector using PSS columns (Styrogel 10<sup>2</sup>, 10<sup>3</sup>, 10<sup>5</sup> Å) with THF containing 10 mM LiTf<sub>2</sub>N and 10 mM 1-butylimidazole as the eluent, at a flow rate of 1 mL.min<sup>-1</sup> at 35 °C.<sup>22</sup> The GPC samples were prepared in THF with diphenyl ether as the internal standard. For the PDPA LDBC, the GPC analysis was performed using a Viscotek (ViscotekTDAmx) with a differential viscometer (DV), right-angle laser-light scattering (RALLS, Viscotek), and refractive index (RI) detectors, using column set of a PL 10 µm guard column followed by one MIXED-E PLgel column and one MIXED-C PLgel column. Filtered THF was used as an eluent at a flow rate of 1 mL.min<sup>-1</sup> at 30 °C. The samples were filtered through a polytetrafluoroethylene membrane with 0.2 µm pore before injection and the system

was calibrated with narrow PS standards. For the GPC analysis of the PNVCL and PNVCL LDBC samples, the system was equipped with a refractive index (RI) (Knauer K-2301), a differential viscometer (DV) and a right angle light scattering (Viscotek 270 Dual Detector) detectors. The column set consisted of a PL 10- $\mu$ L guard column (50 x 7.5 mm<sup>2</sup>), followed by two MIXED-B PL columns (300 x 7.5 mm<sup>2</sup>, 10  $\mu$ L). The HPLC pump was set with a flow rate of 1 mL.min<sup>-1</sup> and the analyses were carried out at 60 °C using an Elder CH-150 heater. The eluent was DMF, containing 0.3% of LiBr. The samples were filtered through a polytetrafluoroethylene (PTFE) membrane with 0.2  $\mu$ m pore size before injection (100  $\mu$ L). The system was calibrated with narrow PMMA standards. The  $M_{n, GPC}$  and  $D$  of the synthesized polymers were determined by using a multidetector calibration system (OmniSEC software version: 4.6.1.354). Fourier-transform infrared spectroscopy (FTIR) was performed at 64 scans and with a 4 cm<sup>-1</sup> resolution between 500 and 4000 cm<sup>-1</sup>, using a JASCO 4200 FTIR spectrometer, operating in the ATR mode (MKII GoldenGate™ Single Reflexion ATR System).

Dynamic light scattering (DLS) measurements were performed on a Malvern Instrument Zetasizer Nano-ZS (Malvern Instruments Ltd., UK). The particle size distribution (in intensity), average hydrodynamic particle size average (z-average) and polydispersity index (PDI) were determined with Zetasizer 7.03 software. Measurements were made at 25 °C or 45 °C and using a backward scattering angle of 173°. The PDPA LDBC samples were filtered before measurements through a 0.45  $\mu$ m pore size PET filter (Chromafil® PET, Macherey-Nagel). At least three measurements were taken for each sample.

Transmission electron microscopy (TEM) was used to observe the size and morphology of the nanoaggregates prepared with the different copolymers. For the PDPA copolymers the aqueous dispersion (1.0 mg.mL<sup>-1</sup>) was deposited onto a formvar-carbon-coated copper grid. Due to the temperature dependence of the PNVCL nanostructures, 8  $\mu$ L of copolymer solution aqueous dispersion at 45 °C (0.2 mg.mL<sup>-1</sup>) was placed on 400 mesh copper grid, inside an oven (45 °C), and the excess of water was gently removed with a paper filter. The sample was cooled down in liquid nitrogen and freeze dried to remove the water traces. All the samples were negatively stained with uranyl acetate 1% wt aqueous solution and then examined using a Jeol JEM 1400 transmission electron microscope (Germany). Images were digitally recorded using a Gatan SC 1000 ORIUS CCD Camera (Warrendale, USA).

### 8.3.3. Procedures

#### Synthesis of isopropylidene-2,2-bis(methoxy) propionic Acid, (1).

The protection of the hydroxyl groups of the bis-MPA was performed according to the procedures reported in the literature<sup>23</sup>. Briefly, 10.00g (74.55 mmol) of bis-MPA, 13.75 mL (111.83 mmol) of 2,2-dimethoxypropane and 0.78 g (4.10 mmol) of dry TsOH were dissolved in 50 mL of acetone. The reaction was left for 2h at room temperature. 0.62 mL (0.47 mmol) of Et<sub>3</sub>N was added to neutralize the catalyst. The solvent was evaporated; the residue was dissolved in 250 mL of DCM and washed with water (2x 20 mL). The organic phase was dried with Na<sub>2</sub>SO<sub>4</sub>. The organic solvent was removed under reduced pressure and the pure product (1) was obtained as white crystals. <sup>1</sup>H NMR (400 MHz, CDCl<sub>3</sub>, δ (ppm)): 1.20 (s, 3H, -CH<sub>3</sub>), 1.42 (s, 3H, -CH<sub>3</sub>), 1.45 (s, 3H, -CH<sub>3</sub>), 3.69 (d, 2H, -CH<sub>2</sub>O), 4.18 (d, 2H, -CH<sub>2</sub>O).

#### Synthesis of bis-MPA anhydride (1.1).

The anhydride of the protected bis-MPA (1) was synthesized according to the literature procedures<sup>24</sup>. The compound (1) 10.00g (57.41 mmol) was dissolved in 50 mL of anhydrous DCM. DCC 5.92 g (28.70 mmol) was added to the mixture and the reaction proceeded at room temperature for 12h under nitrogen. The DCC-urea was filtered off and the DCM evaporated. The viscous residue was diluted in 500 mL of hexane, stirred until the formation of a white solid and the solution was cooled down in the freezer overnight. The product was filtered and dried under vacuum to obtain (1.1). <sup>1</sup>H NMR (400 MHz, CDCl<sub>3</sub>, δ (ppm)): 1.21 (s, 3H, -CH<sub>3</sub>), 1.25 (s, 3H, -CH<sub>3</sub>), 1.41 (s, 6H, -CH<sub>3</sub>), 1.43 (s, 6H, -CH<sub>3</sub>), 3.69 (d, 4H, -(CH<sub>2</sub>O)<sub>2</sub>), 4.20 (d, 4H, -(CH<sub>2</sub>O)<sub>2</sub>).

#### Synthesys of bis-MPA dendrons:

i) **Synthesis of azido ethoxy ethanol, (8) (adapted from<sup>25</sup>)**. 5.00 mL of 2-(2-chloroethoxy)ethanol (44.87 mmol), 11.67 g of sodium azide (179.50 mmol), 164 mg of hexadecyltrimethylammonium bromide (0.45 mmol) and 25 mL of water were mixed in reflux for 24h. After, the mixture was cooled down to room temperature and treated with HCl solution. The solution was saturated with NaCl and the product was extracted with ethyl acetate (3 times). The organic phase was dried over sodium sulphate anhydrous and the solvent evaporated to give 5.85 g of azido ethoxy ethanol (8) (yield 95%). <sup>1</sup>H NMR (400 MHz, CDCl<sub>3</sub>, δ (ppm)): 2.41 (m, 1H, -OH), 3.42 (t, 2H, -CH<sub>2</sub>-N<sub>3</sub>), 3.62 (t, 2H, -CH<sub>2</sub>-O), 3.70 (t, 2H, -CH<sub>2</sub>-O) 3.76 (m, 2H, -CH<sub>2</sub>-OH).

**ii) Synthesis of N<sub>3</sub>-G#1-Ac dendron, (9).** The acetonide-protected monomer (**1**), 8.77 g (50.33 mmol), and the azido ethoxy ethanol (**8**) 6.00 g (47.76 mmol) were dissolved in 100 mL DCM. The reaction flask was flushed with argon, and 0.56 g, (4.58 mmol) of DMAP, 1.35 g (4.58 mmol) of DPTS and 11.33 g (54.91 mmol) of DCC were added. The reaction proceeded under argon atmosphere, at room temperature for 24h. Once the reaction was complete the DCC-urea was filtered off. The product was purified by column chromatography eluting with hexanes and slowly increases the polarity with ethyl acetate. The product (**9**) was obtained as a yellow oil. <sup>1</sup>H NMR (400 MHz, CDCl<sub>3</sub>, δ (ppm)): 1.21 (s, 3H, -CH<sub>3</sub>), 1.38 (s, 3H, -CH<sub>3</sub>), 1.42 (s, 3H, -CH<sub>3</sub>), 3.37 (t, 2H -CH<sub>2</sub>-N<sub>3</sub>), 3.65 (d, 2H, -CH<sub>2</sub>O), 3.67 (t, 2H, -CH<sub>2</sub>O), 3.72 (t, 2H, -CH<sub>2</sub>O), 4.20 (d, 2H, -CH<sub>2</sub>O), 4.31 (t, 2H, -CH<sub>2</sub>O).

**iii) Synthesis of At-G#1-Ac dendron, (17).** Isopropylidene-2,2-bis(methoxy) propionic Acid (**1**), 6.511 g (37.38 mmol), and the propargyl alcohol 3,26 mL (55.97 mmol) were dissolved in 100 mL DCM and bubbled with argon. 0.46 g (3.75 mmol) of DMAP, 1.10 g (3.75 mmol) of DPTS and 9.27 g (44.92 mmol) of DCC were added and the reaction flask was flushed with Argon. The reaction proceeded at room temperature for 24h. Once the reaction was complete the DCC-urea was filtered off. The product was purified by column chromatography eluting with hexane and slowly increases the polarity with ethyl acetate (9:1). The At-G#1 Ac Dendron was obtained as transparent oil. Yield: 6.14 g (77.4%). The results are in accordance with the literature <sup>26</sup>. <sup>1</sup>H NMR (400 MHz, CDCl<sub>3</sub>, δ (ppm)): 1.21 (s, 3H, -CH<sub>3</sub>), 1.38 (s, 3H, -CH<sub>3</sub>), 1.42 (s, 3H, -CH<sub>3</sub>), 2.46 (t, 1H C≡CH), 3.65 (d, 2H, -CH<sub>2</sub>O), 4.20 (d, 2H, -CH<sub>2</sub>O), 4.74 (d, 2H, CH<sub>2</sub>C≡CH).

**iv) Typical procedure for dendron deprotection, N<sub>3</sub>-G#x-(OH)<sub>y</sub> and At- G#x-(OH)<sub>y</sub> dendrons.** The N<sub>3</sub>-G#x Ac dendron was dissolved in methanol and a tea spoon of Dowex<sup>®</sup> 50W-X2-200 resin was added. The reaction proceeded at room temperature overnight. The resin was filtrated off and the product concentrated to give the N<sub>3</sub>-G#x-(OH)<sub>y</sub>.

**N<sub>3</sub>-G#1-(OH)<sub>2</sub> (10):** <sup>1</sup>H NMR (400 MHz, CDCl<sub>3</sub>, δ (ppm)): 1.08 (s, 3H, -CH<sub>3</sub>), 2.90 (s, 2H, (-OH)<sub>2</sub>), 3.37 (t, 2H -CH<sub>2</sub>-N<sub>3</sub>), 3.65 (d, 2H, -CH<sub>2</sub>O), 3.67 (t, 2H, -CH<sub>2</sub>O), 3.71 (t, 2H, -CH<sub>2</sub>O), 3.84 (d, 2H, -CH<sub>2</sub>O), 4.32 (t, 2H, -CH<sub>2</sub>O).

**N<sub>3</sub>-G#2-(OH)<sub>4</sub> (12):** <sup>1</sup>H NMR (400 MHz, CDCl<sub>3</sub>, δ (ppm)): 1.06 (s, 6H, -(CH<sub>3</sub>)<sub>2</sub>), 1.32 (s, 3H, -CH<sub>3</sub>), 3.39 (t, 2H, -CH<sub>2</sub>-N<sub>3</sub>), 3.70 (m, 8H, -(CH<sub>2</sub>O)<sub>4</sub>), 3.83 (m, 4H, -(CH<sub>2</sub>O)<sub>2</sub>), 4.30 (d, 4H, -(CH<sub>2</sub>O)<sub>2</sub>), 4.46 (d, 2H, -CH<sub>2</sub>O).

**N<sub>3</sub>-G#3-(OH)<sub>8</sub> (14):** <sup>1</sup>H NMR (400 MHz, CDCl<sub>3</sub>, δ (ppm)): 1.07 (12H, -(CH<sub>3</sub>)<sub>4</sub>), 1.19 (6H, -(CH<sub>3</sub>)<sub>2</sub>), 1.30 (3H, -CH<sub>3</sub>), 3.38 (2H, -CH<sub>2</sub>-N<sub>3</sub>), 3.60 (4H, -(CH<sub>2</sub>O)<sub>2</sub>), 3.63 (4H, -(CH<sub>2</sub>O)<sub>2</sub>), 3.66 (2H, -CH<sub>2</sub>O), 3.70 (2H, -CH<sub>2</sub>O), 3.76 (2H, -CH<sub>2</sub>O), 4.13 (4H, -(CH<sub>2</sub>O)<sub>2</sub>), 4.16 (4H, -(CH<sub>2</sub>O)<sub>2</sub>), 4.28 (4H, -(CH<sub>2</sub>O)<sub>2</sub>), 4.30 (8H, -(CH<sub>2</sub>O)<sub>4</sub>).

**At-G#1-(OH)<sub>2</sub> (18):** <sup>1</sup>H NMR (400 MHz, CDCl<sub>3</sub>, δ (ppm)): 1.09 (s, 3H, -CH<sub>3</sub>), 2.50 (t, 1H C≡CH), 2.90 (s, 2H -(OH)<sub>2</sub>), 3.73 (d, 2H, -CH<sub>2</sub>O), 3.92 (d, 2H, -CH<sub>2</sub>O), 4.75 (d, 2H, CH<sub>2</sub>C≡CH).

**At-G#2-(OH)<sub>4</sub> (20):** <sup>1</sup>H NMR (400 MHz, CDCl<sub>3</sub>, δ (ppm)): 4.74 (d, 2H, CH<sub>2</sub>C≡H), 4.46 (d, 2H, -CH<sub>2</sub>O), 4.30 (d, 2H, -CH<sub>2</sub>O), 3.84 (m, 4H, -(CH<sub>2</sub>O)<sub>2</sub>), 3.71 (d, 4H, -(CH<sub>2</sub>O)<sub>2</sub>), 3.21 (s, 4H, -OH), 2.50 (t, 1H, C≡H), 1.33 (s, 6H, -CH<sub>3</sub>), 1.06 (s, 6H, -(CH<sub>3</sub>)<sub>2</sub>).

**v) Typical procedure for dendron synthesis, N<sub>3</sub>-G#x-Ac and At- G#x-Ac dendrons.**

The esterification was performed through anhydride coupling method described by Hult and co-workers<sup>27</sup>, using different ratios of reagents to hydroxyl group in order to afford the product with high yields (5 equiv of pyridine, 0.15 equiv of DMAP, and 1.3 equiv of anhydride of (1.1). The product was purified by column chromatography eluting with a solution 60:40 hexanes and ethyl acetate.

**N<sub>3</sub>-G#2-Ac dendron (11):** <sup>1</sup>H NMR (400 MHz, CDCl<sub>3</sub>, δ (ppm)): 1.15 (s, 6H, -(CH<sub>3</sub>)<sub>2</sub>), 1.30 (s, 3H, -CH<sub>3</sub>), 1.35 (s, 6H, -(CH<sub>3</sub>)<sub>2</sub>), 1.41 (s, 6H, -(CH<sub>3</sub>)<sub>2</sub>), 3.37 (t, 2H, -CH<sub>2</sub>-N<sub>3</sub>), 3.62 (d, 4H, -(CH<sub>2</sub>O)<sub>2</sub>), 3.66 (t, 2H, -CH<sub>2</sub>O), 3.70 (t, 2H, -CH<sub>2</sub>O), 4.15 (d, 4H, -(CH<sub>2</sub>O)<sub>2</sub>), 4.28 (t, 2H, -CH<sub>2</sub>O), 4.33 (s, 4H, -(CH<sub>2</sub>O)<sub>2</sub>).

**N<sub>3</sub>-G#3-Ac dendron (13):** <sup>1</sup>H NMR (400 MHz, CDCl<sub>3</sub>, δ (ppm)): 1.14 (9H, -(CH<sub>3</sub>)<sub>3</sub>), 1.25 (12H, -(CH<sub>3</sub>)<sub>4</sub>), 1.35 (12H, -(CH<sub>3</sub>)<sub>4</sub>), 1.41 (12H, -(CH<sub>3</sub>)<sub>4</sub>), 3.38 (2H, -CH<sub>2</sub>-N<sub>3</sub>), 3.60 (4H, -(CH<sub>2</sub>O)<sub>2</sub>), 3.63 (4H, -(CH<sub>2</sub>O)<sub>2</sub>), 3.66 (2H, -CH<sub>2</sub>O), 3.70 (2H, -CH<sub>2</sub>O), 3.76 (2H, -CH<sub>2</sub>O), 4.13 (4H, -(CH<sub>2</sub>O)<sub>2</sub>), 4.16 (4H, -(CH<sub>2</sub>O)<sub>2</sub>), 4.28 (4H, -(CH<sub>2</sub>O)<sub>2</sub>), 4.30 (8H, -(CH<sub>2</sub>O)<sub>4</sub>).

**At-G#2- Ac dendron (19):**  $^1\text{H}$  NMR (400 MHz,  $\text{CDCl}_3$ ,  $\delta$  (ppm)): 4.72 (d, 2H,  $\text{CH}_2\text{C}\equiv\text{H}$ ), 4.33 (d, 4H,  $-(\text{CH}_2\text{O})_2$ ), 4.15 (d, 4H,  $-(\text{CH}_2\text{O})_2$ ), 3.62 (d, 4H,  $-(\text{CH}_2\text{O})_2$ ), 2.47 (t, 1H,  $\text{C}\equiv\text{H}$ ), 1.41 (s, 6H,  $-(\text{CH}_3)_2$ ), 1.36 (s, 6H,  $-(\text{CH}_3)_2$ ), 1.31 (s, 3H,  $-\text{CH}_3$ ), 1.15 (s, 6H,  $-(\text{CH}_3)_2$ ).

#### **Typical procedures for the synthesis of mPEG-COOH.**

mPEG-COOH was synthesized according to the procedure reported in literature.<sup>28</sup> Briefly, 10 g of mPEG<sub>5000</sub> (2.0 mmol) previously dried through azeotropic distillation, 0.8 g of succinic anhydride (8.0 mmol) and 0.5 g of DMAP (4.0 mmol) were dissolved in 40 mL of DCM and the reaction proceeded at room temperature for 12 h. The solvent was removed under reduced pressure and then the residue was dissolved in 50 mL of water. The product was extracted 3 times with DCM (30 mL), and dried over  $\text{Na}_2\text{SO}_4$ . The solvent was evaporated and the mPEG<sub>5000</sub>-COOH was obtained as a white solid.  $^1\text{H}$  NMR (400 MHz,  $\text{CDCl}_3$ ,  $\delta$  (ppm)): 4.26 (t, 2H), 3.82–3.45 (m, 418H), 3.37 (s, 3H), 2.66 (m, 4H). GPC:  $M_{n,\text{GPC}}=5.05 \times 10^3$ ;  $D=1.03$ . The same synthesis strategy was adopted for the modification of mPEG<sub>2000</sub>.

#### **Typical procedure for dendron conjugation with mPEG-COOH.**

The conjugation of the mPEG-COOH with the dendron  $-\text{OH}$  groups was accessed following the reported procedures<sup>28</sup>. Briefly,  $\text{N}_3\text{-G}\#1\text{-(OH)}_2$  (70 mg, 0.28 mmol), mPEG<sub>5000</sub>-COOH (5.81 g, 1.13 mmol) and DMAP (17.0 mg, 0.14 mmol) were dissolved in DCM (30 mL) and the solution bubbled with nitrogen. DIC (0.21 mL, 1.36 mmol) were added to the previous solution and the reaction proceeded at room temperature overnight. The product was filtered, concentrated in the rotatory evaporator and then precipitated in a cold mixture of THF: diethyl ether (100:400 mL). The product was vacuum dried to obtain a mixture of the initial PEG and the product  $\text{N}_3\text{-G}\#1\text{-(mPEG}_{5000})_2$  as a white powder. The product was used in excess in the following experiments with no additional purification steps.

#### **Synthesis of propargyl bromophenyl acetate (PgEBPA):**

**i)  $\alpha$ -Bromophenyl acetyl chloride, (A).** 1.52 mL of thionyl chloride (20.84 mmol) was slowly added to 3.01 g of  $\alpha$ -bromophenylacetic acid (14.00 mmol). A little amount of DMF (10  $\mu\text{L}$ ) was added to catalyze the reaction. The mixture was heated to 85  $^\circ\text{C}$  and



stirred until the complete release of gaseous by-products of the reaction. The mixture was cooled at r.t. and the excess of thionyl chloride was removed under reduced pressure. The product was used without any further purification steps.

**ii) PgEBPA, (B).** A solution of propargyl alcohol (0.94 ml, 16.11 mmol) and Et<sub>3</sub>N (2.25 ml, 16.11 mmol) in 30 ml of DCM was prepared and cooled down. The  $\alpha$ -bromophenyl acetyl chloride was slowly added to the previous solution and the mixture was stirred for 1h at 0°C. The final product was washed three times with water and dried under Na<sub>2</sub>SO<sub>4</sub>. The solvent was removed on a rotary evaporator and the product was distilled under vacuum. <sup>1</sup>H NMR (500 MHz, CDCl<sub>3</sub>,  $\delta$  (ppm)): 7.5 (m, 2H, -ArH), 7.37 (m, 3H, -ArH), 5.47 (s, 1H, -CH), 4.88 (m, 2H, -OCH<sub>2</sub>), 2.73 (m, 1H, -C $\equiv$ CH).

#### **Typical procedure for the synthesis of alkyne terminated PDPA (AT-PDPA).**

The synthesis of AT-PDPA was done via supplemental activator and reducing agent (SARA) atom transfer radical polymerization (ATRP) using the PgEBPA as initiator and following a recently reported method that involves the slow and continuous feed of Na<sub>2</sub>S<sub>2</sub>O<sub>4</sub> (Chapter 3), in a mixture IPA/water at 40 °C. Reaction conditions: [PDPA]<sub>0</sub>/[PgEBPA]<sub>0</sub>/[Na<sub>2</sub>S<sub>2</sub>O<sub>4</sub>]<sub>0</sub>/[CuBr<sub>2</sub>]<sub>0</sub>/[Me<sub>6</sub>TREN]<sub>0</sub>=50/1/0.2/0.1/0.2 (molar). Briefly, a mixture of CuBr<sub>2</sub> (3.90 mg, 9.40  $\mu$ mol), Me<sub>6</sub>TREN (4.30 mg, 18.07  $\mu$ mol) and water (83 $\mu$ L) was placed in a Schlenk tube reactor that was sealed by using a rubber septa. Na<sub>2</sub>S<sub>2</sub>O<sub>4</sub> (3.90 mg, 22.40  $\mu$ mol) and a mixture of DPA (1.00 g, 4.70 mmol) and PgEBPA (23.80 mg, 94.00  $\mu$ mol) in IPA (3.17 mL) (previously bubbled with nitrogen for about 15 minutes) was added to the reactor and frozen in liquid nitrogen. The reaction mixture was deoxygenated by three freeze-pump-thaw cycles and purged with nitrogen. The Schlenk tube was placed in an oil bath at 40 °C with stirring (600 rpm). An aqueous solution of Na<sub>2</sub>S<sub>2</sub>O<sub>4</sub> (84  $\mu$ L, 335 mM) (previous purged with nitrogen) was slow feed into the reaction mixture using a syringe pump at a feed rate 58 nL.min<sup>-1</sup> (19.53 nmol.min<sup>-1</sup>). The polymerization proceeded for 24h at 40 °C (98% conversion,  $M_{n,th} = 10.75 \times 10^3$ ,  $M_{n,GP} = 11.31 \times 10^3$ ,  $D = 1.18$ ). The final polymer was purified by dialysis.

**Typical procedure for the “click” conjugation reaction between the dendron and the linear polymer.**

100 mg of the alkyne-terminated PNVCL ( $M_{n, GPC} = 16.13 \times 10^3$ ,  $D = 1.38$ ) (6.20  $\mu\text{mol}$ ) and 117 mg of  $\text{N}_3\text{-G\#1-(PEG}_{44}\text{)}_2$  (24.80  $\mu\text{mol}$ ) were dissolved into 10 mL of THF. The mixture was placed in a round-bottom flask equipped with a magnetic stir bar and sealed with a rubber septum. 6.1 mg of NaAsc (31.00  $\mu\text{mol}$ ) was added to the solution and the mixture was bubbled with nitrogen for 20 min to remove oxygen. Lastly, a degassed stock solution of  $\text{CuSO}_4 \cdot 5\text{H}_2\text{O}$  (61.5 mM; 250  $\mu\text{L}$ ) in deionized water was injected into the flask under nitrogen atmosphere. The reaction was allowed to proceed under stirring at 30 °C for 24 h. The final reaction mixture was dialyzed (MW cut-off 12 400 Da) against deionized water and the block copolymer was obtained after freeze drying. The product was analyzed by GPC in order to confirm the success of the “click” reaction. Analogous “click” reactions were used for the synthesis of both PDPA and PNVCL copolymers.

**Self-assembly of PDPA copolymers.**

The solution self-assembly of the PDPA copolymers was done following the solvent exchange method. The block copolymer was firstly dissolved in THF at a concentration of 10  $\text{mg}\cdot\text{mL}^{-1}$ . 500  $\mu\text{L}$  of the solution were then added drop-wise to 5 mL of Milli-Q water at alkaline pH (~8), under vigorous stirring. The sample was left overnight at room temperature, under stirring to evaporate the organic solvent and stabilize the nanostructures. This stock particle solution with concentration 1.0  $\text{mg}\cdot\text{mL}^{-1}$  was used in the subsequent studies for nanoparticles size and morphology, DLS and TEM.

**Self-assembly of NVCL copolymers.**

The PNVCL copolymers were dissolved in Milli Q water (0.2  $\text{mg mL}^{-1}$ ). The solutions were allowed to dissolve overnight and filtered through a 0.45  $\mu\text{m}$  PET filter (Chromafil® PET, Macherey-Nagel). The self-assembled structures were directly obtained by increasing the solution temperature up to 45 °C under magnetic stirring.

## 8.4. Results and Discussion

### 8.4.1. Dendron synthesis

The synthesis of the aliphatic polyester dendrons was initially accomplished by the double stage convergent approach proposed by Fréchet and colleagues<sup>23</sup>, based on the monomer 2,2-bis(hydroxymethyl) propionic acid (bis-MPA). The reactions involved in the synthesis are presented in Figure 8.1. After the protection of the hydroxyl groups of the bis-MPA (Figure 8.1,(1)) and the acid group protection using a benzyl ester group (Figure 8.1,(3)), the two protected molecules reacted with each other by an esterification reaction using *N,N*-dicyclohexylcarbodiimide (DCC) as the coupling agent and 4-(dimethylamino)pyridinium *p*-Toluenesulfonate (DPTS), resulting in the second generation dendron, [G#2]-CO<sub>2</sub>CH<sub>2</sub>C<sub>6</sub>H<sub>5</sub>, (3). The benzyl ester group of (3) was selectively removed by catalytic hydrogenolysis, under atmospheric pressure, using 10 wt% of palladium on carbon (Pd/C) as catalyst (Figure 8.1,(4)) and the acetonide groups are deprotected through Dowex-X2 resin (Figure 8.1(5)). The fourth generation dendron, [G#2]-CO<sub>2</sub>CH<sub>2</sub>C<sub>6</sub>H<sub>5</sub>,(6), results from the esterification reaction of the molecules (4) and (5). The dendron with a carboxylic acid moiety in the focal point (7), was easily obtained after removal of the benzyl ester protecting group. At this point, the carboxylic group at the core could be easily converted in another functional group for posterior coupling reactions. The dendron synthesis was completed after the removal of the peripheral acetonide protective groups of molecule through the use of a cationic resin. The resultant molecules were characterized by <sup>1</sup>H NMR spectroscopy (data not shown).

This strategy revealed to be extremely laborious and time consuming, essentially due to the esterification by-products (*N*-cyclourea) and the need of exhaustive purification steps. For high generations, the yields were low and important amounts of dendron molecules were lost during the synthesis. Moreover, this strategy only allows the synthesis of the second and fourth generation dendrons, with 4 or 16 peripheral hydroxyl groups respectively, with a carboxylic acid moiety in the focal point that is very difficult to modify due to the steric hindrance of the dendron tree.

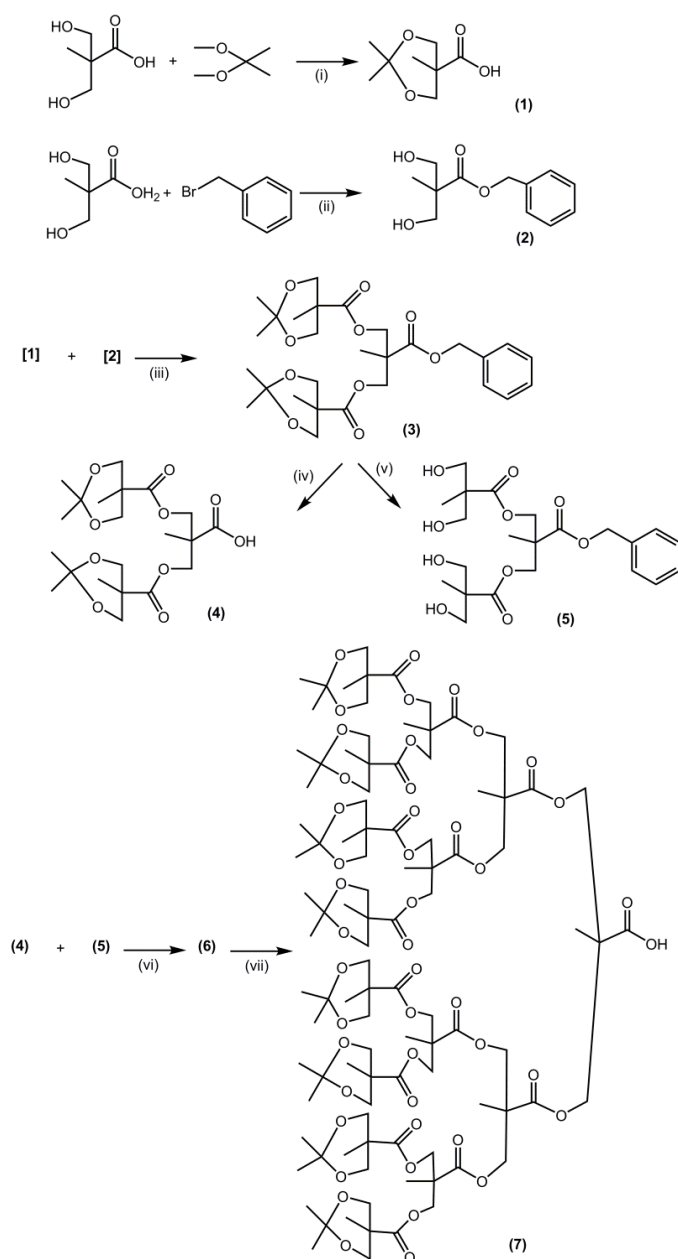


**Figure 8.1:** Schematic representation of the synthesis of the 4<sup>th</sup> generation polyester dendron by the double stage convergent approach<sup>23</sup>. (i) TsOH, acetone, r.t.; (ii) KOH, DMF, 100 °C; (iii) DCC, DPTS, DCM; r.t. (iv) Pd/C, H<sub>2</sub>, EtOAc, r.t.; (v) Dowex<sup>®</sup>, H<sup>+</sup>, EtOAc, r.t.; (vi) DCC, DPTS, DCM, r.t.; (vii) Pd/C, H<sub>2</sub>, EtOAc.

Therefore, a different approach for the dendron synthesis was adopted, the divergent growth based on anhydride coupling from bis-MPA. The anhydride coupling reported by Frechet and co-workers<sup>24</sup>, proved to be a more versatile and easier strategy for the synthesis of dendrons with different generations growing from a specific moiety in the focal point. It is a low temperature esterification, with short reaction times and high

yields, which avoids the exhaustive use of DCC in the consecutive steps and the resulting formation of the *N*-cyclourea by-product.<sup>27</sup> Also, it allows the dendron synthesis from a previous functionalized core, avoiding further modification reactions. The goal was to develop a library of dendrons with different generations, with two distinct functionalities that could be further used in “click” coupling reactions with different linear polymers. A schematic representation of anhydride synthesis and the dendron synthesis strategy from either an azide or alkyne core molecule using an acetonide protected monomer is presented in Figure 8.2, Figure 8.3 and Figure 8.4, respectively. The anhydride of the bis-MPA monomer (**1.1**), was obtained by the self-condensation of the protected bis-MPA (**1**), using *N,N'* dicyclohexylcarbodiimide (DCC) (Figure 8.2) and then used in the divergent synthesis of the dendrons.

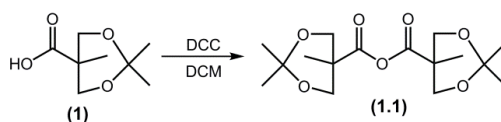


**Figure 8.2:** Schematic representation of the anhydride synthesis from the acetonide protected monomer.

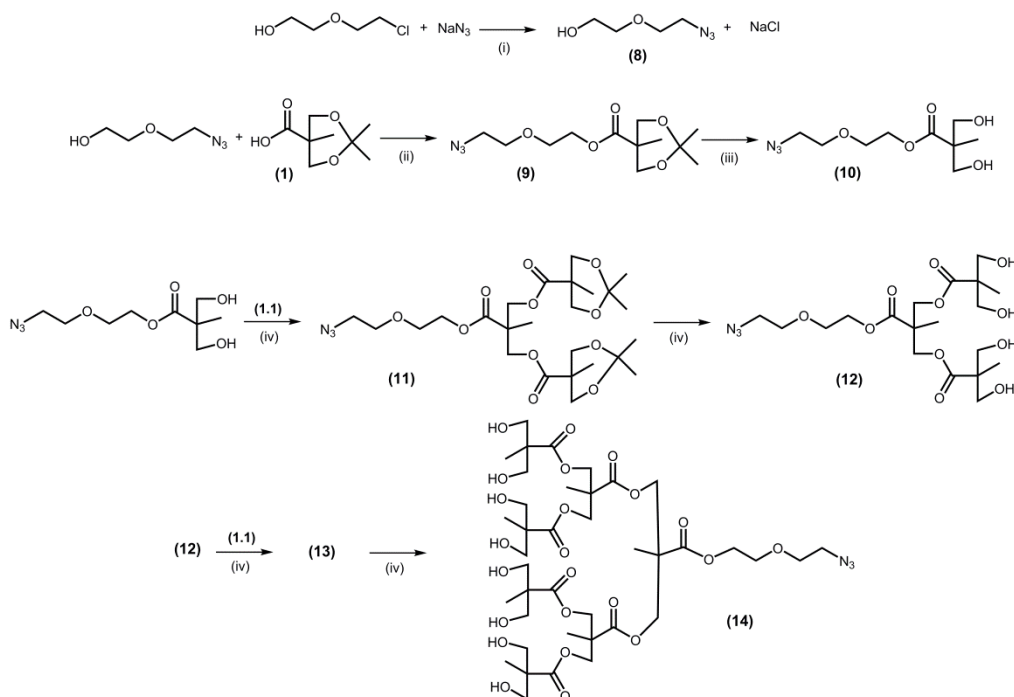


**Figure 8.3:** Schematic representation of the synthesis of different generation dendrons, by the divergent grow based on anhydride coupling from bis-MPA, with an azide group at the focal point. (i)  $\text{H}_2\text{O}$ , reflux; (ii) DMAP, DPTS, DCC, DCM, r.t.; (iii) Dowex<sup>®</sup>,  $\text{H}^+$ , MeOH, r.t.; (iv) DMAP, pyridine, DCM.

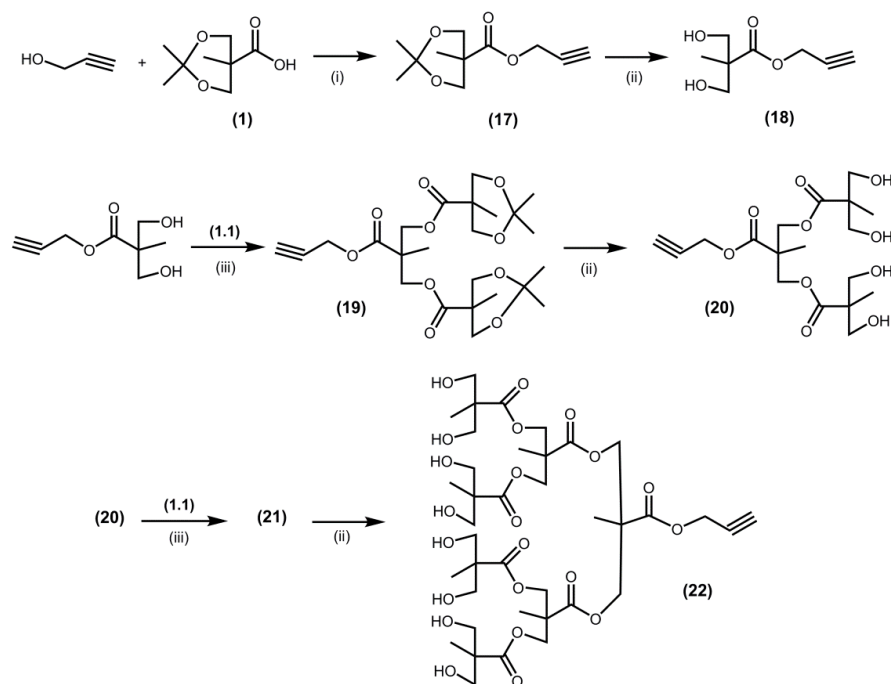


**Figure 8.4:** Schematic representation of the synthesis of different generation dendrons, by the divergent grow based on anhydride coupling from bis-MPA, with an alkyne group at the focal point. (i) DMAP, DPTS, DCC, DCM, r.t.; (ii) Dowex<sup>®</sup>, H<sup>+</sup>, MeOH, r.t.; (iii) DMAP, pyridine, DCM.

Several distinct dendrons, up to the 3<sup>rd</sup> generation, either with an azide or an alkyne core functionality were synthesized. Each molecule was characterized by <sup>1</sup>H NMR spectroscopy and FTIR-ATR. As an example, Figure 8.5 shows the <sup>1</sup>H NMR spectra of the protected 1<sup>st</sup> and 2<sup>nd</sup> generation N<sub>3</sub>-dendron as well as the 2<sup>nd</sup> generation N<sub>3</sub>-dendron after the deprotection of the –OH groups. The presence of the characteristic peak of the methylene protons close to the azide group at 3.39 ppm confirms the presence of the N<sub>3</sub> functionality in the focal point of the dendron (Figure 8.5). This result was obtained for all the azide-dendrons up to the 3<sup>rd</sup> generation. The success of the deprotection reaction was confirmed by the disappearance of the signals around 1.4 ppm, characteristic from the methyl protons of the acetonide moiety.

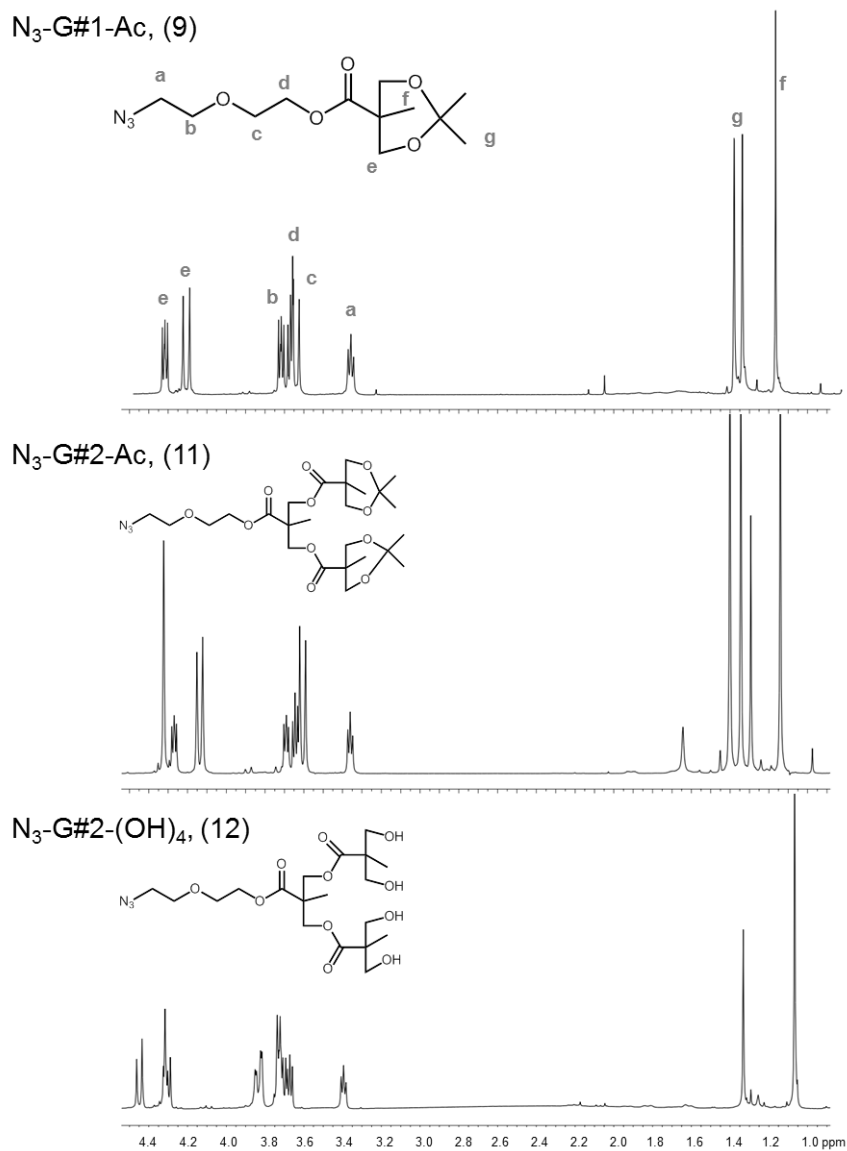


**Figure 8.5:** <sup>1</sup>H NMR spectra of N<sub>3</sub>-G#1-Ac ((9), N<sub>3</sub>-G#2-Ac (11), N<sub>3</sub>-G#1-(OH)<sub>4</sub> (12), in CDCl<sub>3</sub>.

The presence of the azide functionality was also proved by FTIR-ATR due to the presence of the characteristic N<sub>3</sub> signal at 2100 cm<sup>-1</sup> (Figure 8.6) in all of the dendrons synthesized.

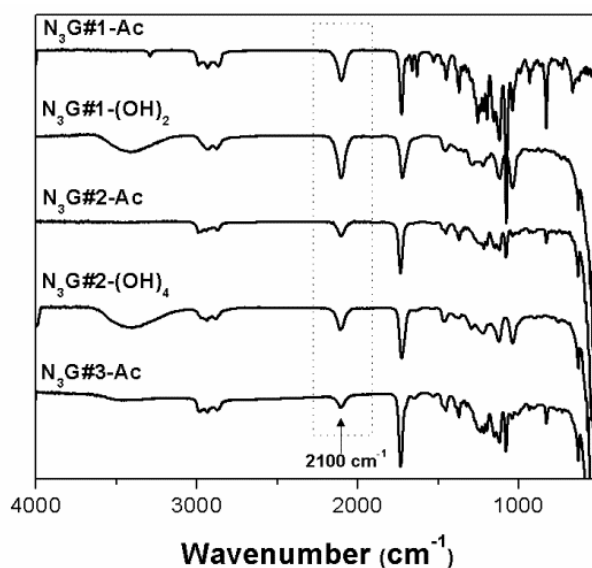


**Figure 8.6:** FTIR-ATR spectra of the azido functionalized dendrons.

The <sup>1</sup>H NMR analysis of the alkyne-functionalized dendron, especially for the 3<sup>rd</sup> generation dendron, reveals a decrease in the integral area of the characteristic peak of the proton from the alkyne functionality, at 2.50 ppm. This result suggests some loss of the dendron focal point functionality during the synthesis procedures and/or during the purification steps, namely in the column chromatography. A detailed MALDI-TOF analysis of the sample from the 3<sup>rd</sup> generation dendron with the alkyne core reveals that only part of the sample corresponds to the At-G#3-Ac (Figure G.1, Annexe G). The remaining contaminations in the sample correspond to the hydrolyzed dendrons, i.e., dendrons without the alkyne functionality, and also deprotected dendrons, i.e., dendrons that have their peripheral -OH groups. These results suggest that the dendrons with the azide moiety at the focal point are more stable to the synthesis conditions and purification steps. Thereafter, those dendrons were preferred to the following synthesis.



### 8.4.2. Dendron functionalization

After the deprotection of the –OH groups, the aliphatic hydroxyl-terminated dendron could be further functionalized with linear PEG segments in order to increase its water solubility and biocompatibility. The functionalization of LDBC with PEG linear segments is a very discussed strategy and was recently reviewed by Sousa-Herves *et al.*<sup>29</sup>

From the coupling strategies tested to conjugate the mPEG segments to the dendron –OH groups, the reaction with the chain-end modified carboxylic acid mPEG (mPEG-COOH) demonstrated to be the most efficient reaction. Other strategies for dendron functionalization, such as the mPEG CDI activation, that forms mPEG carbamate that would react directly with the –OH groups forming the carbonate bond, or even the conjugation of the mPEG acyl chlorides (mPEG-COCl resultant from the modification of mPEG-COOH) with the OH-groups have low reactivity, high sensibility and harsh reaction conditions, when compared to the adopted strategy.

In this work, two mPEG-COOH with MW 2000 and 5000 respectively were synthesized from the correspondent mPEG by anhydride coupling (Figure 8.7 (a)). The success of the modification reaction was confirmed by FTIR-ATR and <sup>1</sup>H NMR spectroscopy. The comparison of the FTIR-ATR spectra of mPEG-OH and the mPEG-COOH, presented in Figure 8.8 confirms the success of the reaction due to the appearance of a new bands at 1783 and 1735 cm<sup>-1</sup> characteristic of the C=O stretch of carbonyl compounds (C=O-O-H and C=O-O-R, respectively) (mPEG-COOH spectrum).

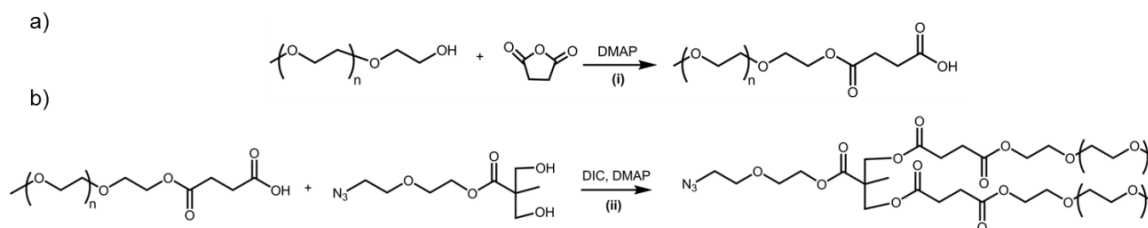


**Figure 8.7:** Schematic representation of the synthesis of mPEG-COOH (a) and the conjugation to the N<sub>3</sub>-G#1-(OH)<sub>2</sub> dendron. (i) and (ii) DCM, r.t..

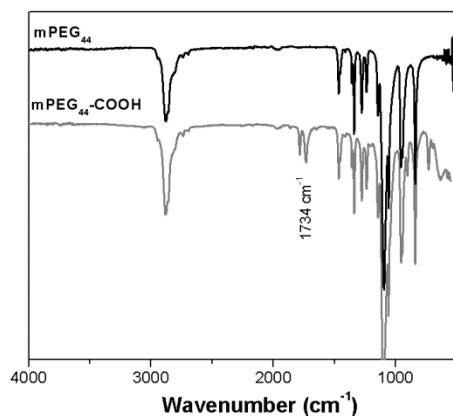


**Figure 8.8:** FTIR-ATR spectra of the mPEG and mPEG-COOH.

The presence of the characteristic protons from the dendron: the methyl group (f) around 1.1 ppm as well as the  $-\text{CH}_2$  groups (e) at 4.3 ppm in the  $^1\text{H}$  NMR spectrum of the compound  $\text{N}_3\text{-G\#1-(mPEG}_{44})_2$  (Figure 8.9) also proves the efficiency of the conjugation reaction.

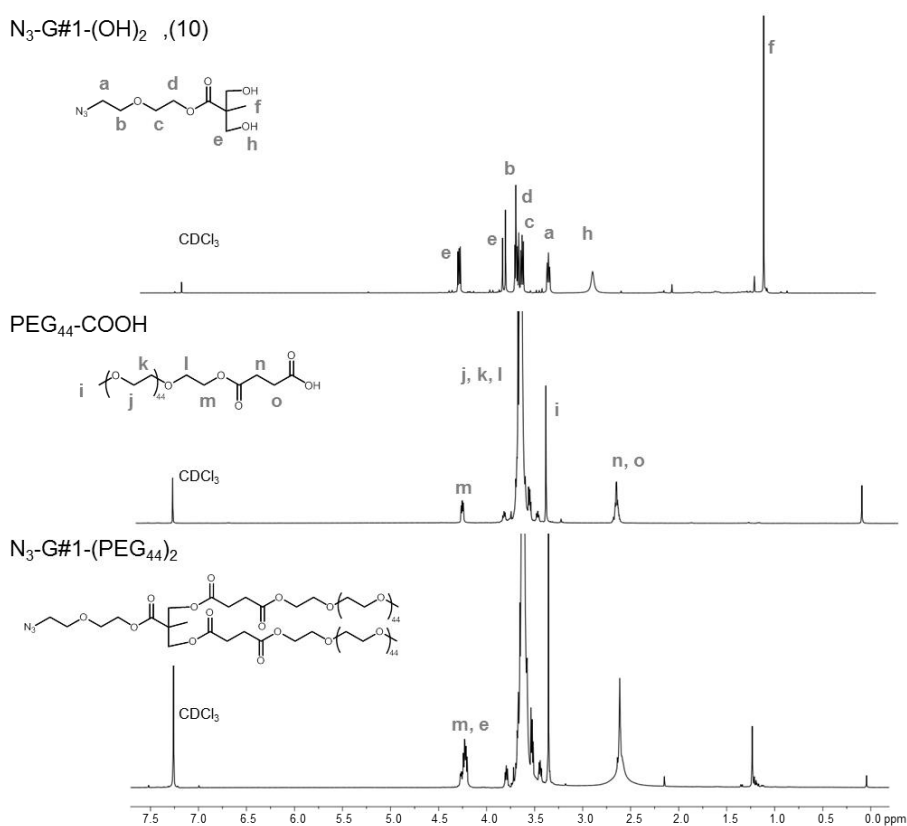


**Figure 8.9:**  $^1\text{H}$  NMR spectra of  $\text{N}_3\text{-G\#1-(OH)}_2$  (10),  $\text{mPEG}_{44}\text{-COOH}$  and  $\text{N}_3\text{-G\#1-(mPEG}_{44})_2$ , in  $\text{CDCl}_3$ .

After the modification of the mPEG end group, the conjugation of the dendron was achieved by a simply DIC mediated reaction between the peripheral –OH groups of the dendron and the –COOH group of the modified mPEG (Figure 8.7 (b))<sup>28</sup>. The success of the reaction was evaluated by FTIR-ATR, <sup>1</sup>H NMR and GPC analysis. The FTIR-ATR spectra of the azide dendron after the functionalization with mPEG-COOH (Figure 8.10) reveals the characteristic N<sub>3</sub> stretching vibration at 2100 cm<sup>-1</sup>. The large absorption band at 3400 cm<sup>-1</sup>, which corresponds to the peripheral –OH groups from the dendron, disappeared confirming the success of the dendron functionalization.

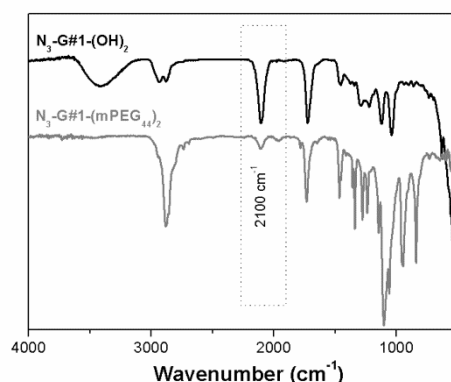


**Figure 8.10:** FTIR-ATR spectra of the initial 1<sup>st</sup> generation azide dendron (N<sub>3</sub>-G#1-(OH)<sub>2</sub>) and after functionalization with mPEG-COOH (N<sub>3</sub>-G#1-(mPEG<sub>44</sub>)<sub>2</sub>).

To guarantee the completion of the reaction mPEG-COOH was used in excess. After the synthesis, several purification procedures were performed to remove the unreacted mPEG-COOH. Even, after several days in dialysis (Mw cut-off 3500, 8000 or 12400 Da, dependent on the dendron molecular weight), the GPC of the product show two distinct distributions (Figure 8.11): one from the dendron functionalized with mPEG, and other one from the initial mPEG-COOH. However, despite the dendron contamination our expectation was that because the mPEG-COOH segments would not affect further reactions, this issue was not exhaustive considered.

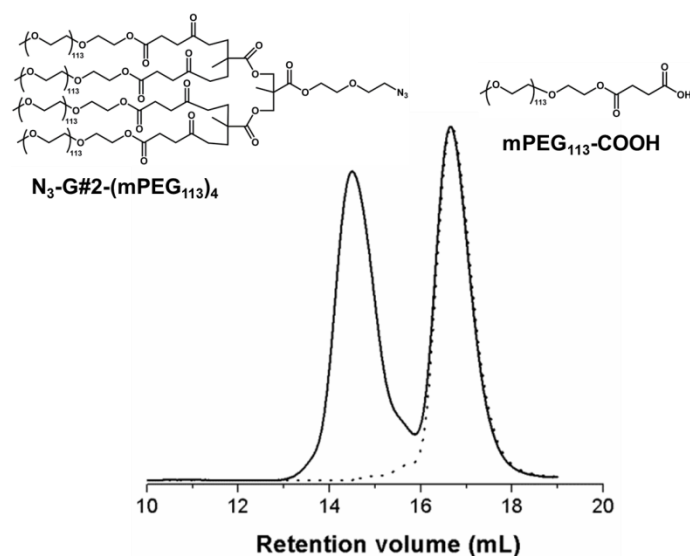


**Figure 8.11:** GPC traces of the mPEG<sub>113</sub>-COOH (dashed line) and the 2<sup>nd</sup> generation azide dendron functionalized with mPEG<sub>113</sub> (N<sub>3</sub>-G#2-(mPEG<sub>113</sub>)<sub>4</sub>) (solid line).

The characteristics of the PEG-modified synthesised dendrons are summarized in Table 8.1.

**Table 8.1:** N<sub>3</sub>-dendron-(OH)<sub>x</sub> functionalization with PEG segments.

Dendron before PEG functionalization	Dendron after PEG functionalization	
	nomenclature	MW (x 10 <sup>3</sup> )
N <sub>3</sub> -G#0-(OH)	N <sub>3</sub> -G#0-(mPEG <sub>113</sub> )	5.26
N <sub>3</sub> -G#1-(OH) <sub>2</sub>	N <sub>3</sub> -G#1-(mPEG <sub>44</sub> ) <sub>2</sub>	4.50
	N <sub>3</sub> -G#1-(mPEG <sub>113</sub> ) <sub>2</sub>	10.50
N <sub>3</sub> -G#2-(OH) <sub>4</sub>	N <sub>3</sub> -G#2-(mPEG <sub>44</sub> ) <sub>4</sub>	8.99
	N <sub>3</sub> -G#2-(mPEG <sub>113</sub> ) <sub>4</sub>	20.99

### 8.4.3. Synthesis of alkyne terminated linear polymers

The block copolymers were based on the dendritic molecules described in the previous section and a linear segment composed by a stimuli-responsive polymer. Two distinct responsive polymers with an alkyne  $\alpha$ -chain-end functionality were synthesized. Poly(2-diisopropylamino) ethyl methacrylate (PDPA) was chosen as a pH-responsive polymer, while poly(*n*-vinyl caprolactam) (PNVCL) was selected as a temperature-responsive one.

The linear pH-responsive PDPA was synthesized through the SARA ATRP using the slow and continuous feed of  $\text{Na}_2\text{S}_2\text{O}_4$  solution, as reported in Chapter 3<sup>30</sup>. This method allows the preparation of well-defined PDPA with controlled MW and narrow  $D$ . It is well known that the structure of the initiator has a major influence in the properties of the final polymer and polymerization kinetics<sup>31</sup>. Ethyl  $\alpha$ -bromophenyl acetate (EBPA) has been reported as a very active initiator, with promising results in the controlled polymerization of DPA, in comparison to the ethyl 2-bromoisobutyrate (EBiB).<sup>30</sup> Herein, the strategy was the synthesis of a new ATRP initiator based on EBPA with an alkyne moiety, the propargyl bromophenyl acetate (PgEBPA) that allows the straightforward synthesis of alkyne terminated PDPA (AT-PDPA).

The synthesis of PgEBPA was divided into two steps (Figure 8.12): the synthesis of the  $\alpha$ -bromophenyl acetyl chloride (Figure 8.12, **(A)**) from the  $\alpha$ -bromophenyl acetic acid followed by the acyl chloride reaction with propargyl alcohol. The choice of the acyl chloride reaction allowed the synthesis of the PgEBPA (Figure 8.12, **(B)**) with high yields using a cleaner method that avoids the secondary by-products and further purification steps. The success of the reaction was confirmed by  $^1\text{H}$  NMR spectroscopy (Figure 8.12).

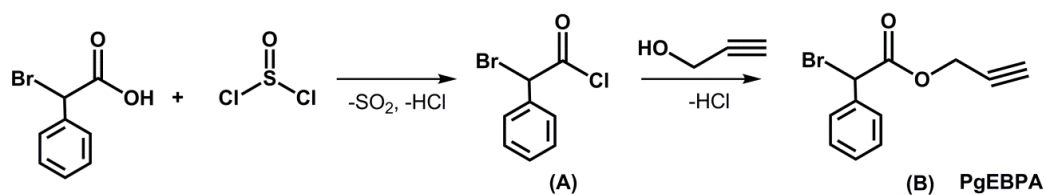


**Figure 8.12:** two-step synthesis of PgEBPA.

AT-PDPA was obtained through the SARA ATRP using the alkyne modified EBPA and a Cu(II)Br<sub>2</sub>/Me<sub>6</sub>TREN catalytic system, at 40 °C in IPA/water mixture and continuous feeding of Na<sub>2</sub>S<sub>2</sub>O<sub>4</sub>. The initial concentration of Na<sub>2</sub>S<sub>2</sub>O<sub>4</sub> in the reaction mixture was established to be 0.2 molar ratio (relatively to the initiator). The reaction started with 2.5% (v/v) of water in the reaction mixture. The feeding solution of 0.3 molar ratio (relatively to the initiator) prepared into the remainder 2.5 % (v/v) of water was continuous feed into the system, during 24h. The characteristics of the AT-PDPA synthesized are listed in Table 8.2. The slow feeding of Na<sub>2</sub>S<sub>2</sub>O<sub>4</sub> into the reaction mixture allows the synthesis of well-defined PDPA with controlled MW with very low  $\bar{D}$  (< 1.2) in high yields.

**Table 8.2:** Characteristics of the AT-PDPA synthesized by SARA ATRP with Na<sub>2</sub>S<sub>2</sub>O<sub>4</sub>, in IPA/water = 95/5 (v/v) at 40 °C. Reaction conditions: [DPA]<sub>0</sub>/[PgEBPA]<sub>0</sub>/[Na<sub>2</sub>S<sub>2</sub>O<sub>4</sub>]<sub>0</sub>/[CuBr<sub>2</sub>]<sub>0</sub>/[Me<sub>6</sub>TREN]<sub>0</sub>=DP/1/0.2/0.1/0.2 + feeding Na<sub>2</sub>S<sub>2</sub>O<sub>4</sub>.

Entry	DP	Conv, % <sup>a</sup>	$M_{n,th} \times 10^3$ <sup>a</sup>	$M_{n,GPC} \times 10^3$ <sup>b</sup>	$\bar{D}$ <sup>b</sup>
PDPA <sub>19</sub>	20	96	4.22	5.93	1.17
PDPA <sub>49</sub>	50	98	10.75	11.31	1.18
PDPA <sub>102</sub>	150	68	21.88	29.50	1.19

<sup>a</sup> determined by <sup>1</sup>H NMR, <sup>b</sup> data from THF GPC.

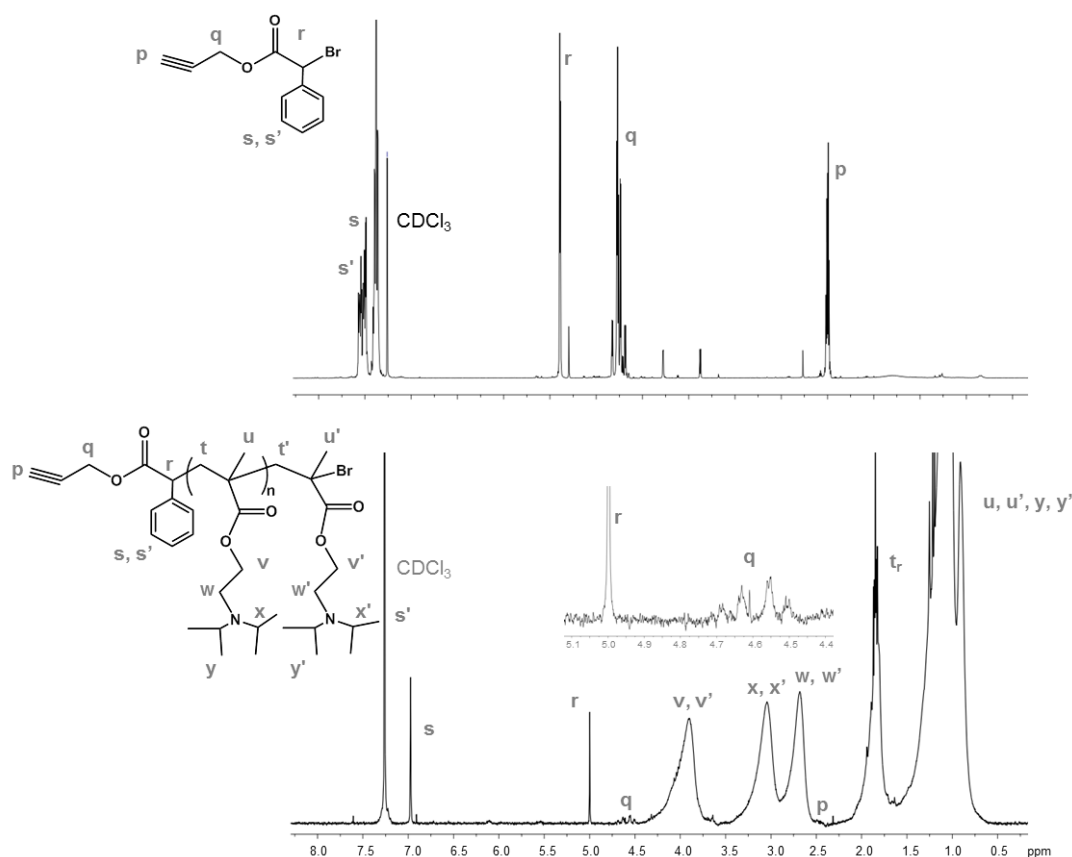


**Figure 8.13:** The  $^1\text{H}$  NMR spectra of PgEBPA initiator and AT-PDPA in  $\text{CDCl}_3$  ( $M_{n,\text{GPC}} = 11.31 \times 10^3$ ,  $D = 1.18$ ,  $M_{n,\text{NMR}} = 5.90 \times 10^3$ ).

The chemical structure of the PDPA obtained by SARA ATRP as well as the presence of the alkyne chain-end functionality was confirmed by  $^1\text{H}$  NMR spectroscopy. A  $^1\text{H}$  NMR spectrum of PDPA is shown in Figure 8.12. The peaks observed at 3.82 ppm ( $\mathbf{v}$ ,  $-\text{OCH}_2-$ ), 2.98 ppm ( $\mathbf{x}$ ,  $-(\text{CH}-\text{N})_2-$ ), 2.62 ppm ( $\mathbf{w}$ ,  $-\text{CH}_2\text{N}-$ ), 1.7-2.1 ppm ( $\mathbf{t}$ ,  $-\text{CH}_2-$  of the polymer backbone), resonances at 1 ppm ( $\mathbf{y}$  –  $(\text{CH}(\text{CH}_3)_2-$ ;  $\mathbf{u}$ , “methacrylic”  $\text{CH}_3$ ) are in agreement with the expected PDPA chemical structure<sup>32</sup>. The presence of the alkyne functionality in the PDPA chain is proved by the presence of the peak of the methylene group ( $\mathbf{q}$ ) of the initiator fragment ( $\text{CH}_2$ ) around 4.6 ppm. The signal of the alkyne proton ( $\mathbf{p}$ ) and the protons from the aromatic ring ( $\mathbf{s}$  and  $\mathbf{s}'$ ) are partially overlapped with the signals of the polymeric chain or from the deuterated solvent, respectively. The proton from the initiator fragment near the aromatic ring ( $\mathbf{r}$ ) allows estimating the number average MW,  $M_{n,\text{NMR}} = 5.90 \times 10^3$ , calculated using the equation  $M_{n,\text{NMR}} = [(I(\mathbf{v})/2)/(I(\mathbf{r}))] \times \text{MW}_{\text{DPA}} + \text{MW}_{\text{PgEBPA}}$ , where  $I(\mathbf{v})$  is the integral of the  $-\text{CH}_2$  of the PDPA unit ( $\mathbf{v}$ ) and  $I(\mathbf{r})$  is the integral of the proton ( $\mathbf{r}$ ) from the initiator fragment.

The linear temperature-responsive PNVCL was synthesized by RAFT according to the procedures described in Chapter 6, using the protected alkyne-terminated RAFT agent (PAT-X<sub>1</sub>). The characteristics of the PNVCL synthesized are summarized in Table 8.3. The alkyne terminated PNVCL was obtained after a simple deprotection reaction.

**Table 8.3:** Characteristics of the PNVCL synthesized by RAFT polymerization with PAT-X<sub>1</sub>, in 1,4-dioxane at 60 °C. Reaction conditions: [NVCL]<sub>0</sub>/[PAT-X<sub>1</sub>]<sub>0</sub>/[AIBN]<sub>0</sub>=600/1/0.5, (NVCL/solvent ratio: 1/1 (w/w)).

Entry	Time	Conv, % <sup>a</sup>	$M_{n,th} \times 10^3$ <sup>a</sup>	$M_{n,GPC} \times 10^3$ <sup>b</sup>	$\bar{D}$ <sup>b</sup>
PNVCL <sub>106</sub>	3h30	18	15.1	16.13	1.38
PNVCL <sub>131</sub>	4h00	21	17.8	22.88	1.38
PNVCL <sub>195</sub>	4h30	33	27.4	32.82	1.26
PNVCL <sub>225</sub>	5h00	38	31.6	35.90	1.24

<sup>a</sup> determined by <sup>1</sup>H NMR, <sup>b</sup> data from DMF GPC.

#### 8.4.4. Synthesis of linear-dendritic block copolymers

The combination of the dendritic segment (dendron) with linear polymer chain to form a hybrid linear-dendritic block copolymer (LDBC) was achieved through the coupling strategy, using the copper catalyzed azide–alkyne [3+2] dipolar cycloaddition reaction (CuAAC) between the azide moiety of the dendron focal point and the alkyne  $\alpha$ -chain-end functionality of the linear polymer. The CuAAC reaction has recently proved to be a very powerful synthetic tool in polymer science due to its high selectivity and complete conversion obtained under mild reaction conditions.<sup>33-35</sup> The use of “click” chemistry strategies have been reported has a simple and efficient route for the synthesis of LDBC<sup>19, 36-39</sup>. An important advantage of this strategy is the possibility to characterize both polymer and dendron structures before the linkage and the possibility of obtaining the LDBC in a single step from well-defined starting materials.

Several copolymers were synthesized from the CuAAC reaction between the alkyne terminated linear polymers (PDPA or PNVCL) and the diverse generations of the azide core dendrons functionalized with mPEG (mPEG<sub>44</sub> or mPEG<sub>113</sub>) (Figure 8.14 and



Figure 8.15). Table 8.4 and Table 8.5 summarize the characteristics of the temperature- and pH-responsive copolymers synthesized.

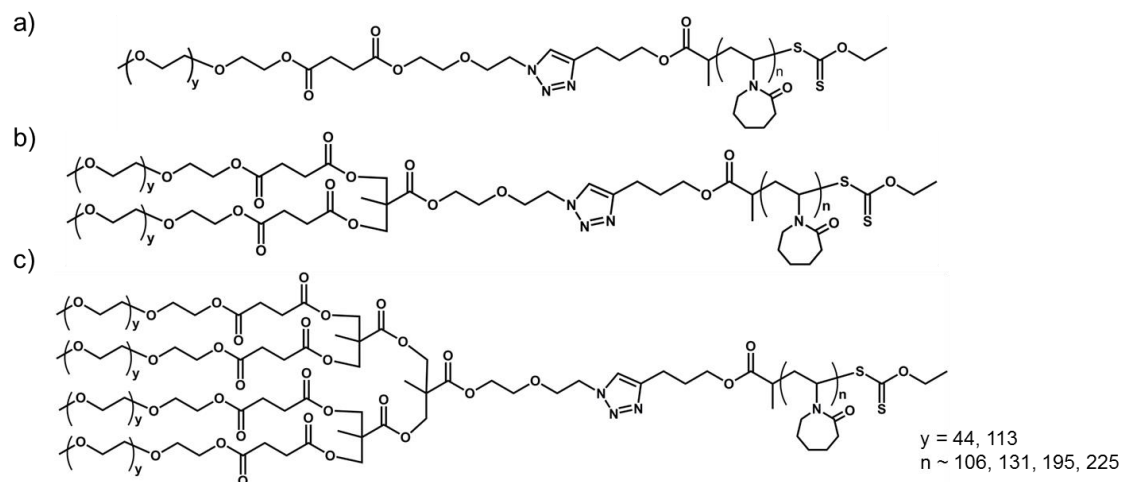


**Figure 8.14:** Schematic representation of (a)  $(\text{PNVCL})_n\text{-G\#0-mPEG}_y$ , (b)  $(\text{PNVCL})_n\text{-G\#1-(mPEG}_y)_2$  and (c)  $(\text{PNVCL})_n\text{-G\#2-(mPEG}_y)_4$ .

**Table 8.4:** Characteristics of the temperature-responsive LDBC synthesized by CuAAC.

	LDBC	Dendron			PNVCL $M_{n,\text{GPC}} (\times 10^3)$
		corona	nomenclature	MW ( $\text{g}\cdot\text{mol}^{-1}$ )	
Figure 8.14 (a)	$\text{PNVCL}_{106}\text{-G\#0-mPEG}_{113}$	mPEG <sub>113</sub>	$\text{N}_3\text{-G\#0-(mPEG}_{113})$	5260	16.13
	$\text{PNVCL}_{131}\text{-G\#0-mPEG}_{113}$				22.88
	$\text{PNVCL}_{195}\text{-G\#0-mPEG}_{113}$				32.82
Figure 8.14 (b)	$\text{PNVCL}_{106}\text{-G\#1-(mPEG}_{44})_2$	mPEG <sub>44</sub>	$\text{N}_3\text{-G\#1-(mPEG}_{44})_2$	4503	16.13
	$\text{PNVCL}_{225}\text{-G\#1-(mPEG}_{44})_2$				35.9
	$\text{PNVCL}_{106}\text{-G\#1-(mPEG}_{113})_2$	mPEG <sub>113</sub>	$\text{N}_3\text{-G\#1-(mPEG}_{113})_2$	10504	16.13
	$\text{PNVCL}_{131}\text{-G\#1-(mPEG}_{113})_2$				22.88
	$\text{PNVCL}_{225}\text{-G\#1-(mPEG}_{113})_2$				35.9
Figure 8.14 (c)	$\text{PNVCL}_{106}\text{-G\#2-(mPEG}_{44})_4$	mPEG <sub>44</sub>	$\text{N}_3\text{-G\#2-(mPEG}_{44})_4$	8992	16.13
	$\text{PNVCL}_{131}\text{-G\#2-(mPEG}_{44})_4$				22.88
	$\text{PNVCL}_{225}\text{-G\#2-(mPEG}_{44})_4$				35.9
	$\text{PNVCL}_{131}\text{-G\#2-(mPEG}_{113})_4$	mPEG <sub>113</sub>	$\text{N}_3\text{-G\#2-(mPEG}_{113})_4$	20992	22.88
	$\text{PNVCL}_{225}\text{-G\#2-(mPEG}_{113})_4$				35.9

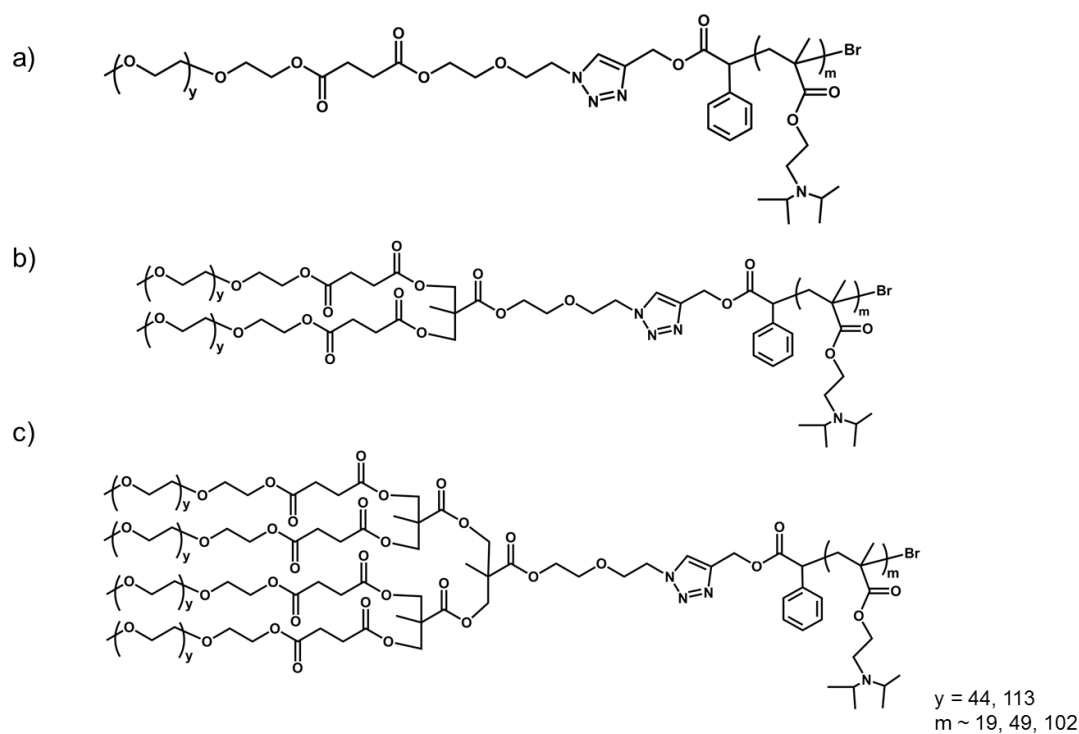
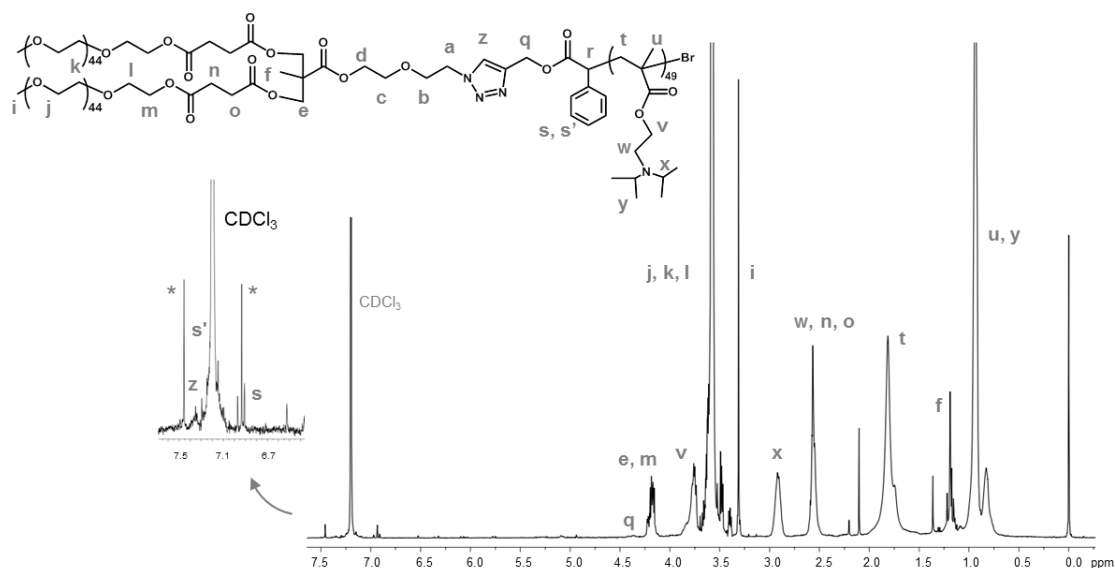


**Figure 8.15:** Schematic representation of (a)  $(PDPA)_n$ -G#0- $mPEG_y$ , (b)  $(PDPA)_n$ -G#1- $(mPEG_y)_2$  and (c)  $(PDPA)_n$ -G#2- $(mPEG_y)_4$ .

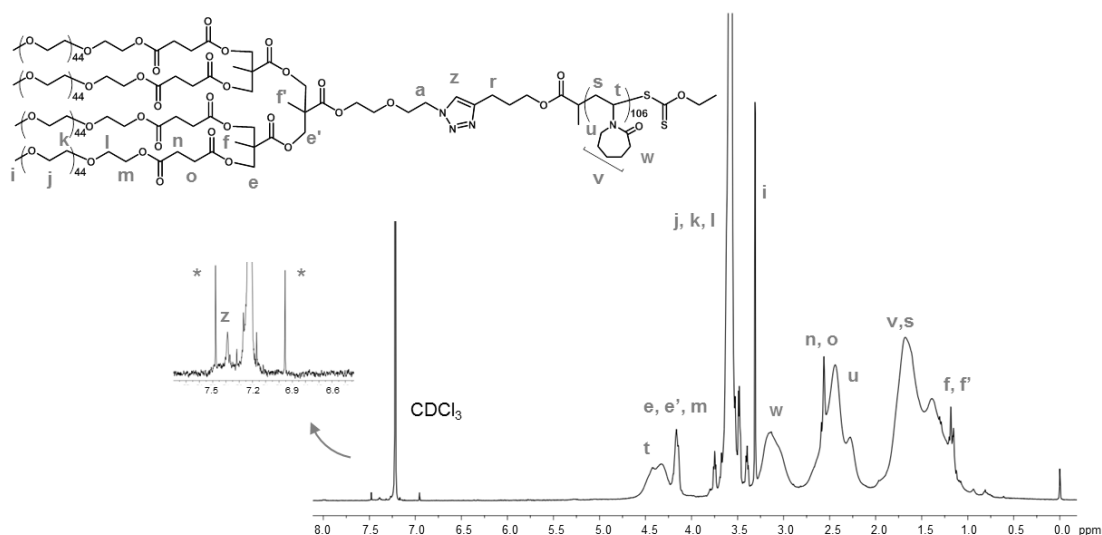
**Table 8.5:** Characteristics of the pH-responsive LDBC synthesized by CuAAC.

Figure 8.15	LDBC	Dendron			PDPA
		corona	nomenclature	MW ( $g \cdot mol^{-1}$ )	$M_{n,GPC}$ ( $\times 10^3$ )
(a)	$PDPA_{19}$ -G#0- $mPEG_{113}$	$mPEG_{113}$	$N_3$ -G#0- $(mPEG_{113})$	5.260	5.9
	$PDPA_{49}$ -G#0- $mPEG_{113}$				11.3
(b)	$PDPA_{19}$ -G#1- $(mPEG_{44})_2$	$mPEG_{44}$	$N_3$ -G#1- $(mPEG_{44})_2$	4503	5.9
	$PDPA_{49}$ -G#1- $(mPEG_{44})_2$				11.3
	$PDPA_{102}$ -G#1- $(mPEG_{44})_2$				22.0
	$PDPA_{49}$ -G#1- $(mPEG_{113})_2$	$mPEG_{113}$	$N_3$ -G#1- $(mPEG_{113})_2$	10504	11.3
	$PDPA_{102}$ -G#1- $(mPEG_{113})_2$				22.0
(c)	$PDPA_{49}$ -G#2- $(mPEG_{44})_4$	$mPEG_{44}$	$N_3$ -G#2- $(mPEG_{44})_4$	8992	11.3
	$PDPA_{102}$ -G#2- $(mPEG_{44})_4$				22.0
	$PDPA_{102}$ -G#2- $(mPEG_{113})_4$	$mPEG_{113}$	$N_3$ -G#2- $(mPEG_{113})_4$	20992	22.0

To evaluate the success of the “click” coupling reaction, the copolymers were analyzed by  $^1\text{H}$  NMR and GPC. Figure 8.16 and Figure 8.17 show the  $^1\text{H}$  NMR spectra of two distinct samples of both copolymers: the  $\text{PDPA}_{49}\text{-G}\#1\text{-(mPEG)}_{44}\text{)}_2$  and  $\text{N}_3\text{-G}\#2\text{-(mPEG)}_{44}\text{)}_4$  respectively. In both spectra, it is possible to observe the characteristic peaks of the protons from the dendron and the linear segments as well as the characteristic signal from the triazole ring proton (z) around 7.4 ppm.



**Figure 8.16:**  $^1\text{H}$  NMR spectrum of the  $\text{PDPA}_{49}\text{-G}\#1\text{-(mPEG)}_{44}\text{)}_2$  obtained after the “click” reaction between the  $\text{N}_3\text{-G}\#1\text{-(mPEG)}_{44}\text{)}_2$  and  $\text{AT-PDPA}_{49}$ , in  $\text{CDCl}_3$  (\*: rotational bands).



**Figure 8.17:**  $^1\text{H}$  NMR spectrum of the  $\text{PNVCL}_{106}\text{-G}\#2\text{-(mPEG)}_{44}\text{)}_4$  obtained after the “click” reaction between the  $\text{N}_3\text{-G}\#2\text{-(mPEG)}_{44}\text{)}_4$  and  $\text{AT-PNVCL}_{106}$ , in  $\text{CDCl}_3$  (\*: rotational bands).

The characterization of the copolymers by GPC was challenging. Figure 8.18 and Figure 8.19 show the RALS signals from the “click” coupled product (after dialysis) and the correspondent homopolymer for PDPA and PNVCL respectively. These curves reveal the movement of the GPC curve towards low retention volumes (i.e., high MW values) indicating the success of the coupling reaction. However, for the same samples, the signals from the other GPC detectors (i.e., RI and viscosity detector) did not present a perfect unimodal distribution. In most of the copolymer samples analyzed, the GPC traces were not unimodal or symmetric (indicating the presence of a low molecular weight shoulder) (see Annex G, Figure G.2 and Figure G.2).

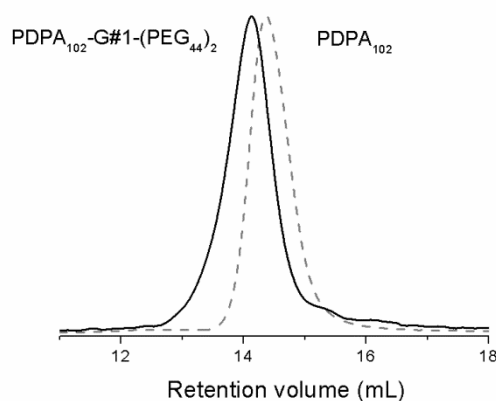


**Figure 8.18:** GPC traces of the RALS signal of the PDPA<sub>102</sub> and the LDBC, PDPA<sub>102</sub>-G#1-(mPEG<sub>44</sub>)<sub>2</sub> copolymer, after the “click” coupling reaction.

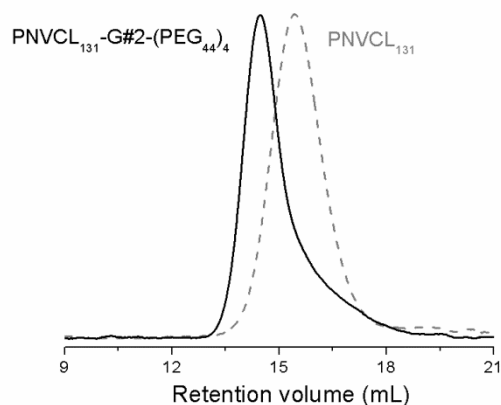


**Figure 8.19:** GPC traces of the RALS signal of the PNVCL<sub>131</sub> and the LDBC, PNVCL<sub>131</sub>-G#2-(mPEG<sub>44</sub>)<sub>4</sub> copolymer, after the “click” coupling reaction.

This result could be related with product contamination with PEG segments resultant either from the excess of PEG dendron used for the coupling reaction or the mPEG-COOH segments from the initial dendron functionalization. The set of GPC columns used in the equipment could also be insufficient to resolve the different signals. Another hypothesis that can explain the presence of the low molecular weight shoulder in the GPC curves of the copolymer is the lack efficiency of the “click” coupling reaction, resulting in the contamination of the “click” product with unreacted dendron and linear polymer. The GPC results also reveal that, despite using the exact same reaction conditions between assays, there was no reproducibility among the “click” reactions of the homopolymer (PNVCL or PDPA), suggesting that some coupling reactions were more effective than others (results not shown). Consequently, it was not possible to resolve the signals and consequently the chromatographic parameters such as  $M_{n, GPC}$  and  $D$  were not possible to determine accurately.

Even so, due to the presence of the responsive linear segments, the ability of such block copolymers to form particles in solution were evaluated, in a very preliminary approach, by dynamic light scattering (DLS) and electron microscopy (TEM). For the NVCL based copolymers, the increase of the solution temperature above the PNVCL low critical solution temperature (LCST) led to the self-assembly of the copolymer (Chapter 7). Taking in consideration the results obtained for the self-assembly of poly(oligo(ethylene oxide) methyl ether methacrylate-*b*-PNVCL copolymers (Chapter 7), in this work the analysis of PNVCL-PEG terminated dendrimers were performed at 45 °C with a concentration of 0.2 mg.mL<sup>-1</sup>. In the case of the PDPA based copolymers the self-assembled structures were obtained at physiological pH (pH ~ 7.4) by the solvent exchange method with a final copolymer concentration of 1.0 mg.mL<sup>-1</sup>. All the copolymers were able to form self-assembled aggregates in solution as seen from TEM images and DLS experiments. However, due to the assumptions presented above concerning the purity of the polymer, the DLS and TEM results were not representative and no relationship could be taken between the different architectures. For this reason, those results are only presented in supporting information (Annex G, Table G.1, Table G.2, Table G.3 and Table G.4).

## 8.5. Conclusions

Polyester dendrons with an azide focal point were successfully synthesized based on the anhydride coupling approach up to the 3<sup>rd</sup> generation and the peripherals –OH groups of the dendron were functionalized with PEG segments with different chain lengths. The CuAAC reaction between the azide dendron and two different linear responsive polymers was successfully accomplished in order to obtain a library of copolymers with different compositions. The present results correspond to a preliminary approach for the synthesis of LDBC. The improvement of the synthesis and purification methods should be considered in order to obtain products that allow the further reproducible preparation of self-assemble nanocaggregates.

## 8.6. References

1. Dong, C.M. and G. Liu (2013). Linear-dendritic biodegradable block copolymers: from synthesis to application in bionanotechnology. *Polymer Chemistry*, 4(1): 46-52.
2. Tian, L., P. Nguyen, and P.T. Hammond (2006). Vesicular self-assembly of comb-dendritic block copolymers. *Chemical Communications*, (33): 3489-3491.
3. Tian, L. and P.T. Hammond (2006). Comb-dendritic block copolymers as tree-shaped macromolecular amphiphiles for nanoparticle self-assembly. *Chemistry of Materials*, 18(17): 3976-3984.
4. Qiao, H., J. Li, Y. Wang, Q. Ping, G. Wang, and X. Gu (2013). Synthesis and characterization of multi-functional linear-dendritic block copolymer for intracellular delivery of antitumor drugs. *International Journal of Pharmaceutics*, 452(1–2): 363-373.
5. Poon, Z., J.A. Lee, S. Huang, R.J. Prevost, and P.T. Hammond (2011). Highly stable, ligand-clustered "patchy" micelle nanocarriers for systemic tumor targeting. *Nanomedicine-Nanotechnology Biology and Medicine*, 7(2): 201-209.
6. Poon, Z., S. Chen, A.C. Engler, H.-i. Lee, E. Atas, G. von Maltzahn, S.N. Bhatia, and P.T. Hammond (2010). Ligand-Clustered "Patchy" Nanoparticles for Modulated Cellular Uptake and In Vivo Tumor Targeting. *Angewandte Chemie International Edition*, 49(40): 7266-7270.

7. Luo, J., K. Xiao, Y. Li, J.S. Lee, L. Shi, Y.-H. Tan, L. Xing, R. Holland Cheng, G.-Y. Liu, and K.S. Lam (2010). Well-Defined, Size-Tunable, Multifunctional Micelles for Efficient Paclitaxel Delivery for Cancer Treatment. *Bioconjugate Chemistry*, 21(7): 1216-1224.
8. Bonner, D.K., C. Leung, J. Chen-Liang, L. Chingozha, R. Langer, and P.T. Hammond (2011). Intracellular Trafficking of Polyamidoamine-Poly(ethylene glycol) Block Copolymers in DNA Delivery. *Bioconjugate Chemistry*, 22(8): 1519-1525.
9. Israelachvili, J.N. (1992). Intermolecular and surface forces: London:Harcourt Brace and Company.
10. Rodriguez-Hernandez, J., F. Checot, Y. Gnanou, and S. Lecommandoux (2005). Toward 'smart' nano-objects by self-assembly of block copolymers in solution. *Progress in Polymer Science*, 30: 691-724.
11. del Barrio, J., L. Oriol, C. Sanchez, J.L. Serrano, A. Di Cicco, P. Keller, and M.H. Li (2010). Self-Assembly of Linear-Dendritic Diblock Copolymers: From Nanofibers to Polymersomes. *Journal of the American Chemical Society*, 132(11): 3762-3769.
12. Jang, C.J., J.H. Ryu, J.D. Lee, D. Sohn, and M. Lee (2004). Synthesis and supramolecular nanostructure of amphiphilic rigid aromatic-flexible dendritic block molecules. *Chemistry of Materials*, 16(22): 4226-4231.
13. Gillies, E.R. and J.M.J. Frechet (2005). pH-responsive copolymer assemblies for controlled release of doxorubicin. *Bioconjugate Chemistry*, 16(2): 361-368.
14. Gillies, E.R., T.B. Jonsson, and J.M.J. Frechet (2004). Stimuli-responsive supramolecular assemblies of linear-dendritic copolymers. *Journal of the American Chemical Society*, 126(38): 11936-11943.
15. Wood, K.C., S.R. Little, R. Langer, and P.T. Hammond (2005). A family of hierarchically self-assembling linear-dendritic hybrid polymers for highly efficient targeted gene delivery. *Angewandte Chemie-International Edition*, 44(41): 6704-6708.
16. Kim, T., H.J. Seo, J.S. Choi, H.S. Jang, J. Baek, K. Kim, and J.S. Park (2004). PAMAM-PEG-PAMAM: Novel triblock copolymer as a biocompatible and efficient gene delivery carrier. *Biomacromolecules*, 5(6): 2487-2492.
17. Wood, K.C., S.M. Azarin, W. Arap, R. Pasqualini, R. Langer, and P.T. Hammond (2008). Tumor-Targeted Gene Delivery Using Molecularly Engineered Hybrid Polymers Functionalized with a Tumor-Homing Peptide. *Bioconjugate Chemistry*, 19(2): 403-405.

18. Lee, H.I., J.A. Lee, Z.Y. Poon, and P.T. Hammond (2008). Temperature-triggered reversible micellar self-assembly of linear-dendritic block copolymers. *Chemical Communications*, (32): 3726-3728.
19. Kim, Y.S., E.S. Gil, and T.L. Lowe (2006). Synthesis and characterization of thermoresponsive-co-biodegradable linear-dendritic copolymers. *Macromolecules*, 39(23): 7805-7811.
20. Ciampolini, M. and N. Nardi (1966). Five-Coordinated High-Spin Complexes of Bivalent Cobalt, Nickel, and Copper with Tris(2-dimethylaminoethyl)amine. *Inorganic Chemistry*, 5(1): 41-44.
21. Moore, J.S. and S.I. Stupp (1990). Room temperature polyesterification. *Macromolecules*, 23(1): 65-70.
22. He, H., M. Zhong, B. Adzima, D. Luebke, H. Nulwala, and K. Matyjaszewski (2013). A Simple and Universal Gel Permeation Chromatography Technique for Precise Molecular Weight Characterization of Well-Defined Poly(ionic liquid)s. *Journal of the American Chemical Society*, 135(11): 4227-4230.
23. Ihre, H., A. Hult, J.M.J. Frechet, and I. Gitsov (1998). Double-stage convergent approach for the synthesis of functionalized dendritic aliphatic polyesters based on 2,2-bis(hydroxymethyl)propionic acid. *Macromolecules*, 31(13): 4061-4068.
24. Ihre, H., O.L.P. De Jesus, and J.M.J. Frechet (2001). Fast and convenient divergent synthesis of aliphatic ester dendrimers by anhydride coupling. *Journal of the American Chemical Society*, 123(25): 5908-5917.
25. Mespouille, L., M. Vachaudez, F. Suriano, P. Gerbaux, O. Coulembier, P. Degee, R. Flammang, and P. Dubois (2007). One-pot synthesis of well-defined amphiphilic and adaptative block copolymers via versatile combination of "Click" chemistry and ATRP. *Macromolecular Rapid Communications*, 28: 2151-2158.
26. Wu, P., M. Malkoch, J.N. Hunt, R. Vestberg, E. Kaltgrad, M.G. Finn, V.V. Fokin, K.B. Sharpless, and C.J. Hawker (2005). Multivalent, bifunctional dendrimers prepared by click chemistry. *Chemical Communications*, (46): 5775-5777.
27. Malkoch, M., E. Malmström, and A. Hult (2002). Rapid and Efficient Synthesis of Aliphatic Ester Dendrons and Dendrimers. *Macromolecules*, 35(22): 8307-8314.
28. Ma, X., Z. Zhou, E. Jin, Q. Sun, B. Zhang, J. Tang, and Y. Shen (2013). Facile Synthesis of Polyester Dendrimers as Drug Delivery Carriers. *Macromolecules*, 46(1): 37-42.
29. Sousa-Herves, A., R. Riguera, and E. Fernandez-Megia (2012). PEG-dendritic block copolymers for biomedical applications. *New Journal of Chemistry*, 36(2): 205-210.



30. Gois, J.R., D. Konkolewicz, A.V. Popov, T. Guliashvili, K. Matyjaszewski, A.C. Serra, and J.F.J. Coelho (2014). Improvement of the control over SARA ATRP of 2-(diisopropylamino)ethyl methacrylate by slow and continuous addition of sodium dithionite. *Polymer Chemistry*, 5(16): 4617-4626.
31. Tang, W., Y. Kwak, W. Braunecker, N.V. Tsarevsky, M.L. Coote, and K. Matyjaszewski (2008). Understanding Atom Transfer Radical Polymerization: Effect of Ligand and Initiator Structures on the Equilibrium Constants. *Journal of the American Chemical Society*, 130(32): 10702-10713.
32. Gois, J.R., N. Rocha, A.V. Popov, T. Guliashvili, K. Matyjaszewski, A.C. Serra, and J.F.J. Coelho (2014). Synthesis of well-defined functionalized poly(2-(diisopropylamino)ethyl methacrylate) using ATRP with sodium dithionite as a SARA agent. *Polymer Chemistry*.
33. Lutz, J.F. (2007). 1,3-dipolar cycloadditions of azides and alkynes: A universal ligation tool in polymer and materials science. *Angewandte Chemie-International Edition*, 46(7): 1018-1025.
34. Meldal, M. and C.W. Tornøe (2008). Cu-catalyzed azide-alkyne cycloaddition. *Chemical Reviews*, 108(8): 2952-3015.
35. Binder, W.H. and R. Sachsenhofer (2008). 'Click' chemistry in polymer and material science: An update. *Macromolecular Rapid Communications*, 29(12-13): 952-981.
36. Hua, C., S.M. Peng, and C.M. Dong (2008). Synthesis and characterization of linear-dendron-like poly(epsilon-caprolactone)-b-poly(ethylene oxide) copolymers via the combination of ring-opening polymerization and click chemistry. *Macromolecules*, 41(18): 6686-6695.
37. del Barrio, J., L. Oriol, R. Alcala, and C. Sanchez (2009). Azobenzene-Containing Linear-Dendritic Diblock Copolymers by Click Chemistry: Synthesis, Characterization, Morphological Study, and Photoinduction of Optical Anisotropy. *Macromolecules*, 42(15): 5752-5760.
38. Peng, S.M., Y. Chen, C. Hua, and C.M. Dong (2009). Dendron-like Polypeptide/Linear Poly(ethylene oxide) Biohybrids with Both Asymmetrical and Symmetrical Topologies Synthesized via the Combination of Click Chemistry and Ring-Opening Polymerization. *Macromolecules*, 42(1): 104-113.
39. Javakhishvili, I., W.H. Binder, S. Tanner, and S. Hvilsted (2010). Facile synthesis of linear-dendritic cholesteryl-poly(epsilon-caprolactone)-b-(L-lysine)(G2) by thiol-ene and azide-alkyne "click" reactions. *Polymer Chemistry*, 1(4): 506-513.



# Chapter 9

---

---

**Final remarks**



## 9.1. Overall conclusions

The conjugation of reversible deactivation radical polymerization (RDRP) methods with other organic chemistry approaches allows the synthesis of well-defined macromolecules with controlled properties that have a potential application in the biomedical field.

The use of inorganic sulfites as supplemental activators and reducing agents (SARA) in the atom transfer radical polymerization (ATRP) of a pH-responsive monomer, the 2-(diisopropylamino)ethyl methacrylate (DPA), was reported for the first time (Chapter 2). This method allows the synthesis of well-defined polymers with controlled molecular weight, and low dispersity, under eco-friendly, inexpensive and less toxic reaction conditions. The use of “click” functionalized ATRP initiators enables the inclusion of such functionalities in the polymer chain-end, without the need of any post-polymerization reaction and facilitates the polymer functionalization or the conjugation of distinct block, extending the range of possible applications. The slow and continuous feed of sodium dithionite to the reaction mixture improves the control over the polymerization and allows the reaction to proceed under reduced concentrations of copper catalyst, which is of extremely importance when producing polymers for biomedical applications (Chapter 3). The developed this SARA ATRP method was extended to the polymerization of other hydrophilic monomers, such as oligo(ethylene oxide) methyl ether methacrylate (OEOMA) and, by a straightforward strategy of sequential monomer addition, is possible to obtain block copolymers of poly(2-(diisopropylamino)ethyl methacrylate)-*b*- poly(oligo(ethylene oxide) methyl ether methacrylate) (POEOMA-*b*-PDPA) (Chapter 4). The amphiphilic nature of the POEOMA-*b*-PDPA copolymers for solution pH > 6.25 allows the development of stable pH-responsive nanoparticles. It was found that, the length of the PDPA segments as well as the method applied for the self-assembly of such block copolymers plays an important role in the final nanoparticle size and morphology.

The work described in Chapter 5 extended the use of RDRP methods to the polymerization of less-activated monomers through the reversible addition-fragmentation chain-transfer polymerization. New alkyne functionalized RAFT agents were developed and evaluated for the controlled polymerization of vinyl acetate (VAc) (Chapter 5). The protected alkyne containing xanthate RAFT agent (PAT-X<sub>1</sub>) is able to

efficiently control the polymerization of VAc, with a good control over the molecular weight and with low dispersity, which is frequently a challenging result for this class of monomers. The use of such RAFT agent was applied for the polymerization of the temperature-responsive *N*-vinyl caprolactam (NVCL) (Chapter 6). The xanthate mediated RAFT polymerization of NVCL allows the synthesis of well-defined polymers with tunable low critical solution temperature (LCST). By controlling the polymer molecular weight, solution characteristics or heating rate is possible to adjust the temperature response of the homopolymer. The use alkyne-terminated RAFT agents allows further “click” conjugation reactions to afford poly(*N*-vinyl caprolactam) block copolymers. This method enables the coupling of polymers synthesized by distinct RDRP methods, such as ATRP and RAFT to afford the conjugation of bocks with distinct chemical properties. Therefore, novel block copolymers composed by OEOMA and NVCL were developed (Chapter 7) and evaluated as temperature responsive nanocarriers. In diluted solutions, those bock copolymers form very stable self-assembly aggregates with dimeter  $> 150$  nm, for temperature above the cloud point temperature ( $T_{CP}$ ) of the PNVCL segment. At this temperature the PNVCL segment is completely hydrophobic and is able to accommodate small hydrophobic molecules such as nile red (NR) as observed by fluorescent studies. However, due to the responsive nature of the PNVCL block, the assembly process is reversible and therefore the decrease of solution temperature causes the disassembly of the copolymer aggregates and consequent release of NR.

Throughout the PhD research work, “click” functionalized ATRP initiators as well as alkyne-terminated RAFT agents, were developed in order to facilitate the conjugation of distinct polymeric segments, otherwise difficult to accomplish, or further block copolymer functionalization. In Chapter 8, one distinct block copolymer architecture was presented: the linear dendritic block copolymers (LBDC), based on the conjugation of a polyester dendritic segment with the linear responsive blocks described above. This type of block copolymers has been reported has a potential macromolecular architecture for the development of very stable self-assembled nanoparticles. However, the laborious synthetic procedures involved in the synthesis, the loss of the core reactivity throughout the synthesis, and the difficulty to purify completely the final copolymers, especially when the dendron peripheral groups were functionalized with PEG segments, hampered the complete characterization of the LBDC and limits its potential applications.

Overall, this research work has contributed for the development of the SARA ATRP system based on sodium dithionite as well as the improvement of RAFT polymerization of less-activated monomers through the use of functionalized xanthates. By using the “click” functionalities in both methods, novel tailor made responsive block copolymers were prepared according to the specificity of the final application.

## 9.2. Recommendations for future work

The development of polymeric materials to be applied in the biomedical field should rely in sustainable polymerization methods that allow the development of well-defined macromolecules. Due to the development of the SARA ATRP system based on the use of sodium dithionite (Food and Drug Administration (FDA) approved compound), the polymerization of PDPA and other biomedical relevant (co)polymers is now accessible through more “green” procedures. The work presented here opens the possibility of development of controlled polymers using very low concentration of the metal catalyst and more eco-friendly reaction conditions. Ultimately, a deeper study in the polymerization of PDPA using TPMA as ligand can contribute to the development of catalytic systems that used only a residual amount of copper catalyst (< 100 ppm). The use of an alkyne (or azide) terminated initiator for the SARA ATRP (following the strategy presented in chapters 2 to 4) allow the direct conjugation of functional molecules to the  $\alpha$ -chain-end of the (co)polymer and opens the possibility to develop functionalized nanocarriers based on PEOMA-*b*-PDPA. Specific moieties, such as folic acid, can be used to promote the active targeting and enhance the efficiency of the therapeutics. Following this strategy for the development of pH-responsive nanocarriers, the results obtained in a preliminary assay of biocompatibility performed for one of the block copolymers presented in Chapter 4 (MC3T3 cells) (data not shown) revealed that the reported POEOMA-*b*-PDPA is non-cytotoxic for concentrations up to 0.4 mg.mL<sup>-1</sup>. However, further biocompatibility assays should be carried out. Furthermore, for the POEOMA-*b*-PDPA copolymers, additional studies to optimize the self-assembly induced by the solvent exchange method should be performed in order to understand the role of the solvents and polymer concentration in the nanoparticle

morphology, size and distribution. This issue is of particular importance for the development of nanocarriers for hydrophobic drugs since this is the most used method for the encapsulation of drugs while the self-assembly aggregate is formed.

The developments in the polymerization of poly(*N*-vinyl caprolactam) (PNVCL) will open the possibility to develop new well-defined temperature-responsive systems. The results obtained contributed to the understanding of the solution behavior of the PNVCL (co)polymers. It is a very interesting polymer to apply in the biomedical field due to its sharp and reversible solution phase transition for temperatures around 37 °C. Concerning the self-assembly aggregates formed from the block copolymers described in Chapters 7, it is necessary to perform studies of encapsulation of different hydrophobic guest molecules, as well as hydrophilic ones, to understand the morphology of the resultant self-assembly aggregates and consolidate the observations reported. It would be interesting to evaluate the ability of the POEOMA-*b*-PNVCL copolymers to encapsulate both types of guest molecules. However, the impossibility to maintain the amphiphilic character of the PNVC based copolymers at room temperature, results in a fast disassembly behavior of POEOMA-*b*-PNVCL turns such block copolymers very unstable materials to use as nanocarriers. In fact, PNVCL and/or PNVCL based copolymers could be promising structures for coating applications and to develop temperature responsive surfaces.

Concerning the linear dendritic block copolymer architecture and its potential in the development of very stable nanocarriers for biomedical applications, a different type of synthesis strategy for the dendron should be followed. In recent years, the synthesis of dendritic molecules have been simplified through the use of accelerated approaches that avoids the use of the protection/deprotection steps and the need of the intermediate purification steps.<sup>1</sup> The simplification of the dendron synthesis and the easy conjugation with the linear responsive (co)polymers through the “click” coupling strategies presented here, may open the possibility to develop new nanocarriers with potential applications as DDS.



### 9.3. References

1. Walter, M.V. and M. Malkoch (2012). Simplifying the synthesis of dendrimers: accelerated approaches. *Chemical Society Reviews*, 41(13): 4593-4609.



# **Annexes**

---

---



# Annex A

**Supporting information for Chapter 2.** Synthesis of well-defined functionalized poly(2-(diisopropylamino)ethyl methacrylate)

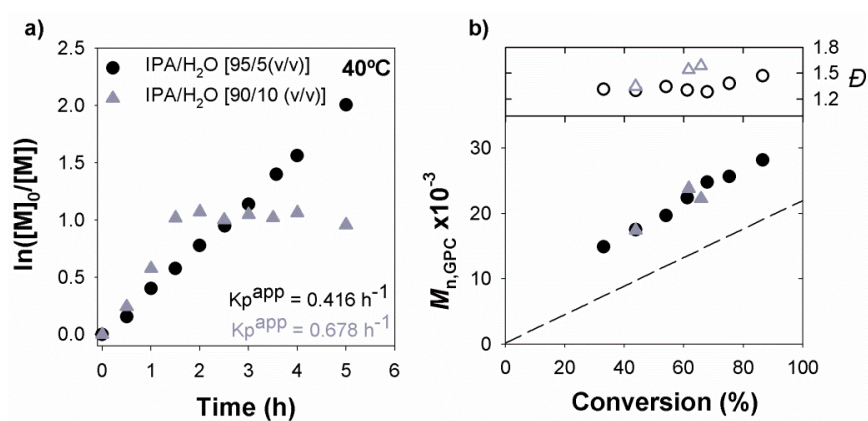


**Figure A.1:** a) Kinetic plot  $\ln([M]_0/[M])$  vs. time and (b) evolution of  $M_{n,GPC}$  and  $\bar{D}$  with conversion (the dashed line represents theoretical MW at a given conversion), for ATRP of DPA in the presence of CuBr<sub>2</sub>/Me<sub>6</sub>TREN with Na<sub>2</sub>S<sub>2</sub>O<sub>4</sub> in two different IPA/H<sub>2</sub>O mixtures. Conditions:  $[DPA]_0/\text{solvent} = 1/2$  (v/v),  $[IPA]/[H_2O] = 0.95/0.05$  (v/v) (circle symbols) or  $0.90/0.10$  (v/v) (triangle symbols);  $[DPA]_0/[EBiB]_0/[Na_2S_2O_4]_0/[CuBr_2]_0/[Me_6TREN]_0 = 100/1/1/0.1/0.1$  (molar); T= 40 °C.

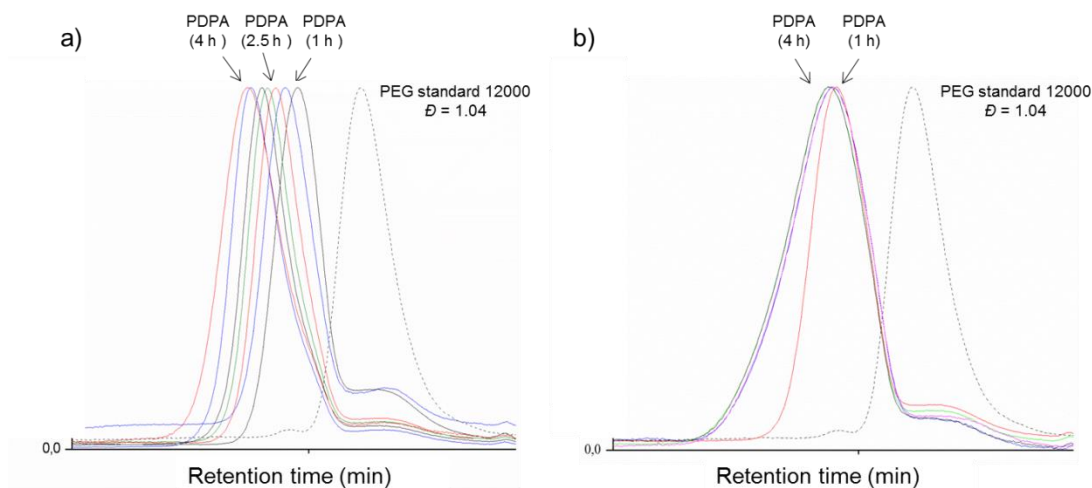


**Figure A.2:** SEC traces of PEG standard ( $M_p = 12\,000\text{ g}\cdot\text{mol}^{-1}$ ;  $\bar{D} = 1.04$ ) and PDPA samples. Conditions: (a)  $[\text{DPA}]_0/\text{solvent} = 1/2$  (v/v),  $[\text{IPA}]/[\text{H}_2\text{O}] = 0.95/0.05$  (v/v);  $[\text{DPA}]_0 / [\text{EBiB}]_0 / [\text{Na}_2\text{S}_2\text{O}_4]_0 / [\text{CuBr}_2]_0 / [\text{Me}_6\text{TREN}]_0 = 100/1/1/0.1/0.1$  (molar);  $T = 40\text{ }^\circ\text{C}$ ; (b)  $[\text{DPA}]_0/\text{solvent} = 1/2$  (v/v),  $[\text{IPA}]/[\text{H}_2\text{O}] = 0.90/0.10$  (v/v),  $[\text{DPA}]_0 / [\text{EBiB}]_0 / [\text{Na}_2\text{S}_2\text{O}_4]_0 / [\text{CuBr}_2]_0 / [\text{Me}_6\text{TREN}]_0 = 100/1/1 / 0.1/0.1$  (molar);  $T = 40\text{ }^\circ\text{C}$ .

**Table A.1:** Details for the various kinetic points in the polymerization of DPA. Conditions  $[\text{DPA}]_0/\text{solvent} = 1/2$  (v/v),  $[\text{IPA}]/[\text{H}_2\text{O}] = 0.95/0.05$  (v/v);  $[\text{DPA}]_0 / [\text{EBiB}]_0 / [\text{Na}_2\text{S}_2\text{O}_4]_0 / [\text{CuBr}_2]_0 / [\text{Me}_6\text{TREN}]_0 = 50/1/1/0.1/0.1$  (molar);  $T = 40\text{ }^\circ\text{C}$ .

Kinetic point (h)	Conv. (%)	$M_{n,\text{th}} \times 10^3$	$M_{n,\text{GPC}} \times 10^3$	$\bar{D}$	GPC main trace			GPC minor trace		
					$M_{n,\text{GPC}} \times 10^3$	$\bar{D}$	%	$M_{n,\text{GPC}} \times 10^3$	$\bar{D}$	%
1	29	3.31	10.12	1.99	16.91	1.03	58.2	8.01	1.09	41.8
2	47	5.15	12.27	1.23	19.72	1.05	82.9	8.06	1.08	17.1
2.5	58	6.38	15.48	1.19	19.77	1.05	87.6	7.73	1.07	12.4
3	67	7.35	16.61	1.18	20.97	1.04	89.5	8.08	1.09	10.5
4	78	8.48	17.99	1.19	22.43	1.04	91.9	8.19	1.10	8.1
5	88	9.57	20.16	1.14	23.60	1.04	93.4	8.84	1.08	6.6

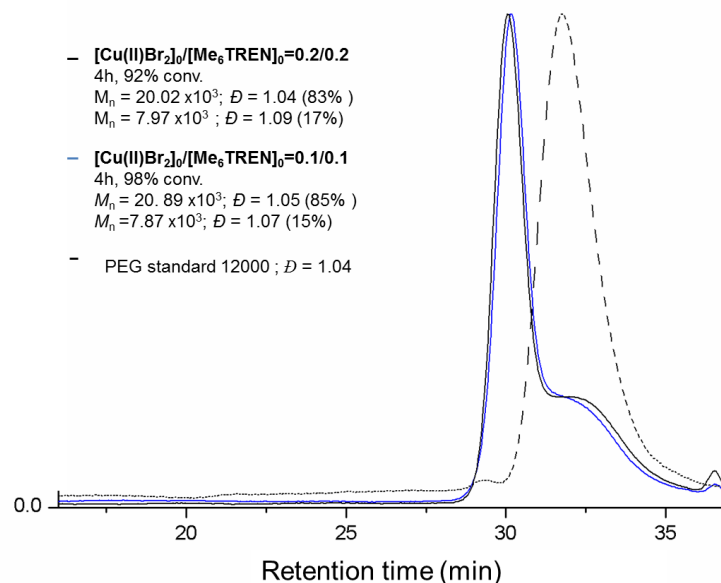


**Figure A.3:** SEC traces of PEG standard ( $M_p = 12\,000\text{ g}\cdot\text{mol}^{-1}$ ;  $D = 1.04$ ) and PDPA samples for two synthesized using two different concentrations of copper complex (0.1 and 0.2). Conditions:  $[\text{DPA}]_0/\text{solvent} = 1/2$  (v/v),  $[\text{IPA}]/[\text{H}_2\text{O}] = 0.95/0.05$  (v/v);  $[\text{DPA}]_0 / [\text{EBiB}]_0 / [\text{Na}_2\text{S}_2\text{O}_4]_0 / [\text{CuBr}_2]_0 / [\text{Me}_6\text{TREN}]_0 = 20/1/1/0.1/0.1$  (molar) and  $20/1/1/0.2/0.2$ ;  $T = 40\text{ }^\circ\text{C}$ .

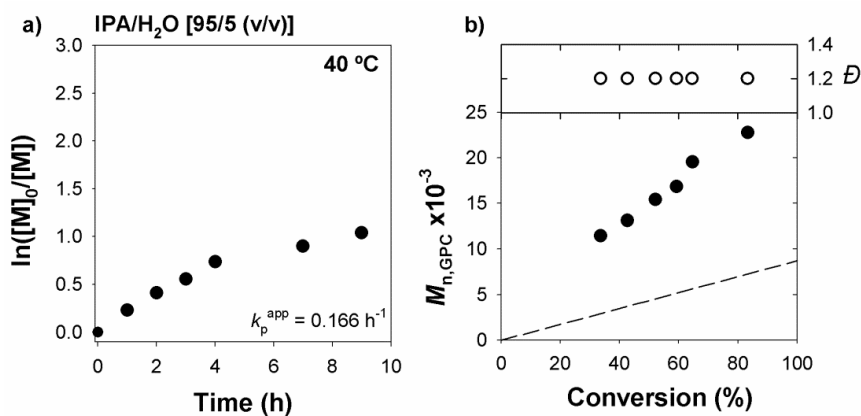


**Figure A.4:** (a) Kinetic plot  $\ln([M]_0/[M])$  vs. time and (b) evolution of  $M_{n,\text{GPC}}$  and  $D$  with conversion (the dashed line represents theoretical MW at a given conversion), for ATRP of DPA in the presence of  $\text{CuBr}_2/\text{Me}_6\text{TREN}$  with  $\text{Cu(I)Br}$ . Reaction conditions:  $[\text{DPA}]_0/\text{solvent} = 1/2$  (v/v),  $[\text{IPA}] / [\text{H}_2\text{O}] = 0.95/0.05$  (v/v);  $[\text{DPA}]_0 / [\text{PgBiB}]_0 / [\text{CuBr}]_0 / [\text{CuBr}_2]_0 / [\text{Me}_6\text{TREN}]_0 = 40/1/1/0.1/1.2$  (molar);  $T = 40\text{ }^\circ\text{C}$ .





## Annex B

**Supporting information for Chapter 3.** Improvement of the control over SARA ATRP of 2-(diisopropylamino)ethyl methacrylate by slow and continuous addition of sodium dithionite

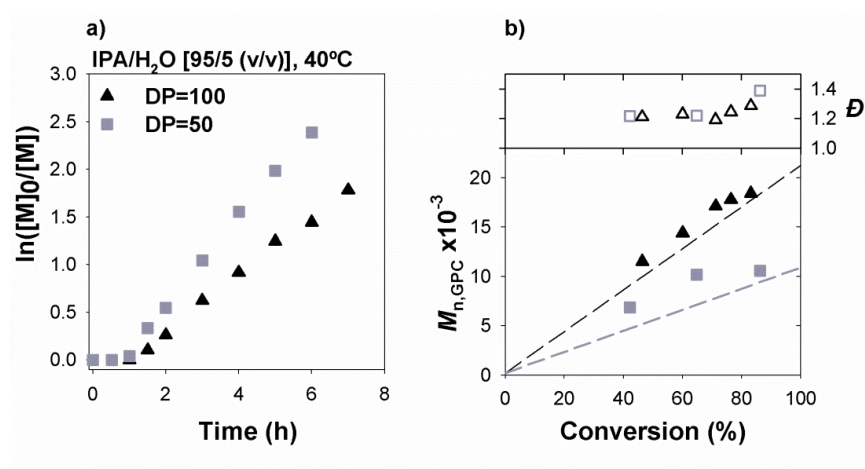


**Figure B.1:** Effect of target DP on the SARA ATRP of DPA in IPA/H<sub>2</sub>O = 0.95/ 0.05 (v/v) at 40 °C. (a) First-order kinetic plot, (b) evolution of MW and  $D$  with conversion (the dashed line represents theoretical MW at a given conversion). Reaction conditions:  $[DPA]_0/[EBPA]_0/[Na_2S_2O_4]_0/[CuBr_2]_0/[Me_6TREN]_0 = 100/1/0.5/0.1/0.1$  (molar) and  $[DPA]_0/[EBPA]_0/[Na_2S_2O_4]_0/[CuBr_2]_0/[Me_6TREN]_0 = 50/1/0.5/0.1/0.2$  (molar).

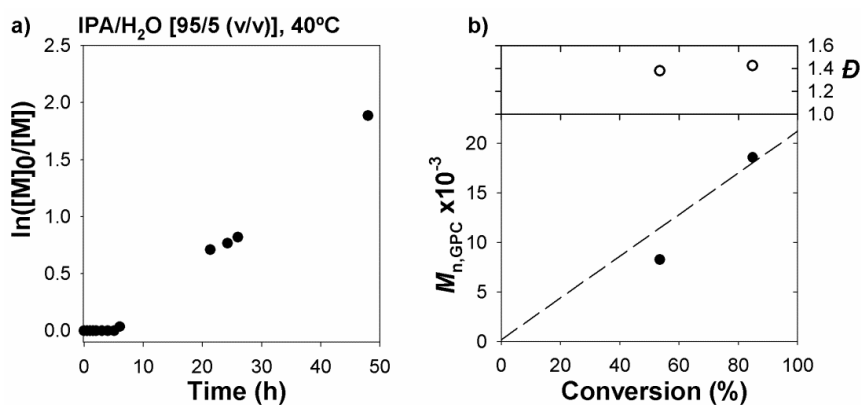


**Figure B.2:** SARA ATRP of DPA with  $\text{Na}_2\text{S}_2\text{O}_4$ , in IPA/ $\text{H}_2\text{O}$  = 0.95/0.05 (v/v) at 40 °C. (a) First-order kinetic plot, (b) evolution of MW and  $\bar{D}$  with conversion (the dashed line represents theoretical MW at a given conversion). Conditions:  $[\text{DPA}]_0/[\text{EBiB}]_0/[\text{Na}_2\text{S}_2\text{O}_4]_0/[\text{CuBr}_2]_0/[\text{Me}_6\text{TREN}]_0 = 100/1/0.3/0.1/0.1$  (molar).

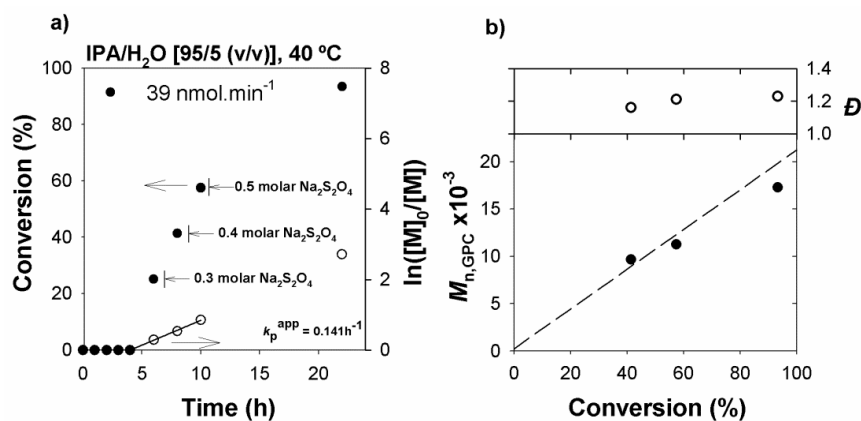


**Figure B.3:** SARA ATRP of DPA with feeding rate of aqueous solution of  $\text{Na}_2\text{S}_2\text{O}_4$ , 39.1  $\text{nmol}\cdot\text{min}^{-1}$ , in IPA/ $\text{H}_2\text{O}$  = 0.95/0.05 (v/v) at 40 °C. (a) First-order kinetic plot, (b) evolution of MW and  $\bar{D}$  with conversion (the dashed line represents theoretical MW at a given conversion). Conditions:  $[\text{DPA}]_0/[\text{EBPA}]_0/[\text{Na}_2\text{S}_2\text{O}_4]_0/[\text{CuBr}_2]_0/[\text{Me}_6\text{TREN}]_0 = 100/1/0/0.1/0.2$  (molar).

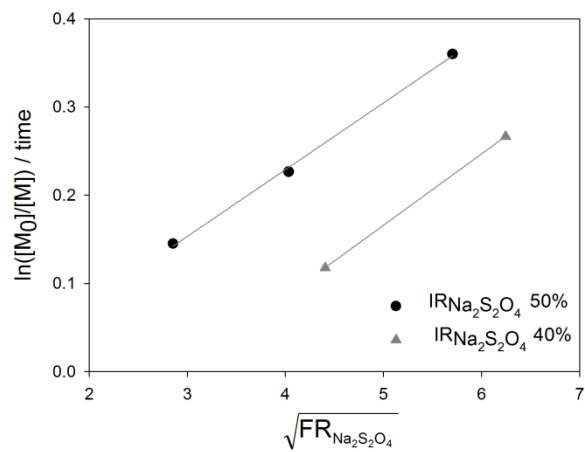


**Figure B.4:** Effect of the feeding rate ( $FR_{Na_2S_2O_4}$ ) on the polymerization rate;  $\ln([M_0]/[M])/time$  vs  $\sqrt{FR_{Na_2S_2O_4}}$



## Annex C

**Supporting information for Chapter 4.** Brush-type pH-responsive block copolymers and its self-assembly properties

**Table C.1:** Hydrodynamic volume and PDI of the POEOMA-*b*-PDPA copolymers, for different pH values during the titration experiment.

POEOMA <sub>17</sub> - <i>b</i> -PDPA <sub>45</sub>			POEOMA <sub>18</sub> - <i>b</i> -PDPA <sub>91</sub>		
pH	D <sub>h</sub> (nm)	PDI	pH	D <sub>h</sub> (nm)	PDI
2.1	10.2		2.2	10.8	
5.8	15.0		5.8	12.6	
6.35	35.3	0.40	6.25	89.3	0.16
7.4	33.3	0.36	7.4	86.6	0.16
8.2	32.2	0.33	8.2	85.7	0.16



## Annex D

**Supporting information for Chapter 5.** Synthesis of alkyne-terminated xanthates for the efficient RAFT polymerization of less-activated monomers

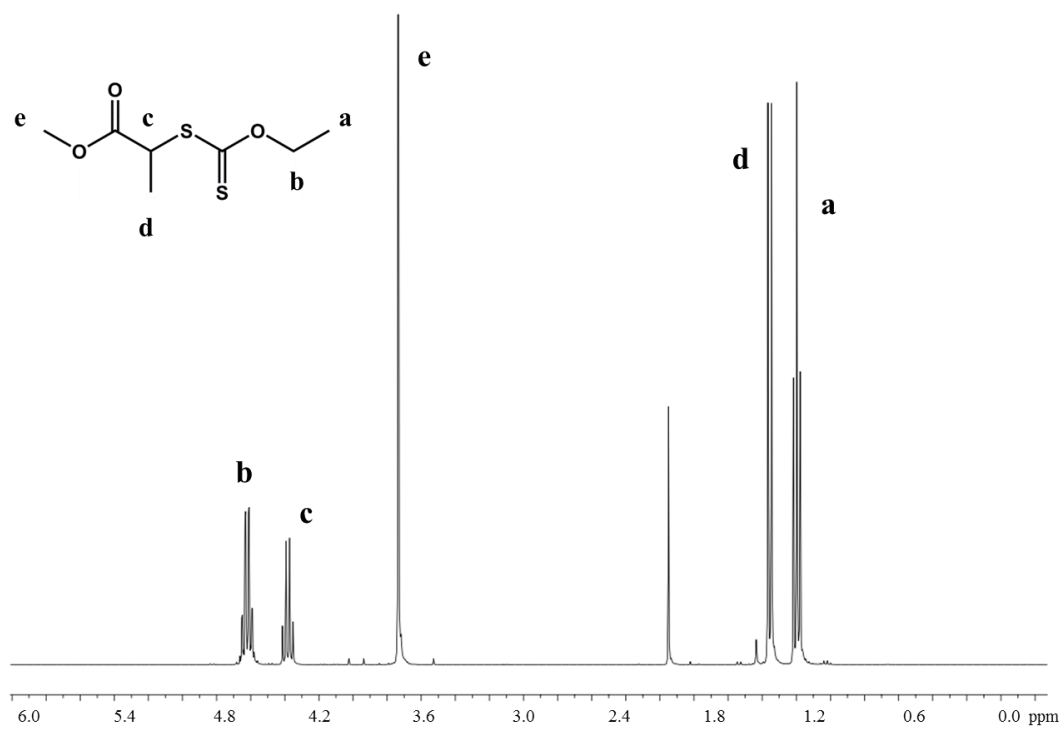


**Figure D.1:** <sup>1</sup>H NMR spectrum of X<sub>1</sub> in CDCl<sub>3</sub>.

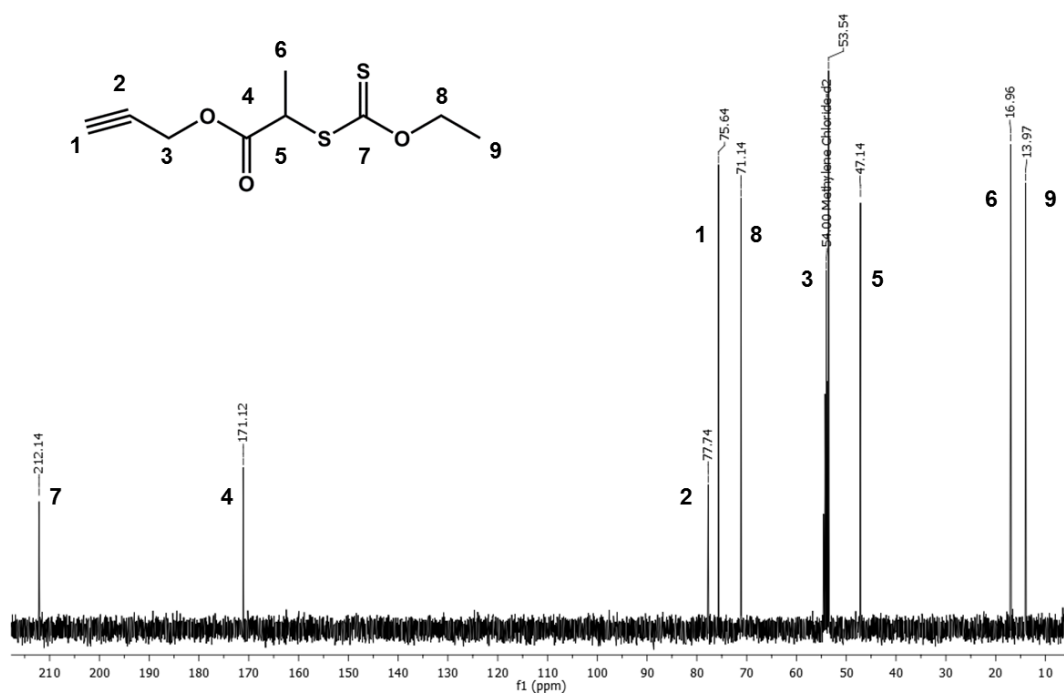


Figure D.2: <sup>13</sup>C NMR spectrum of AT-X<sub>1</sub> in CD<sub>2</sub>Cl<sub>2</sub>.

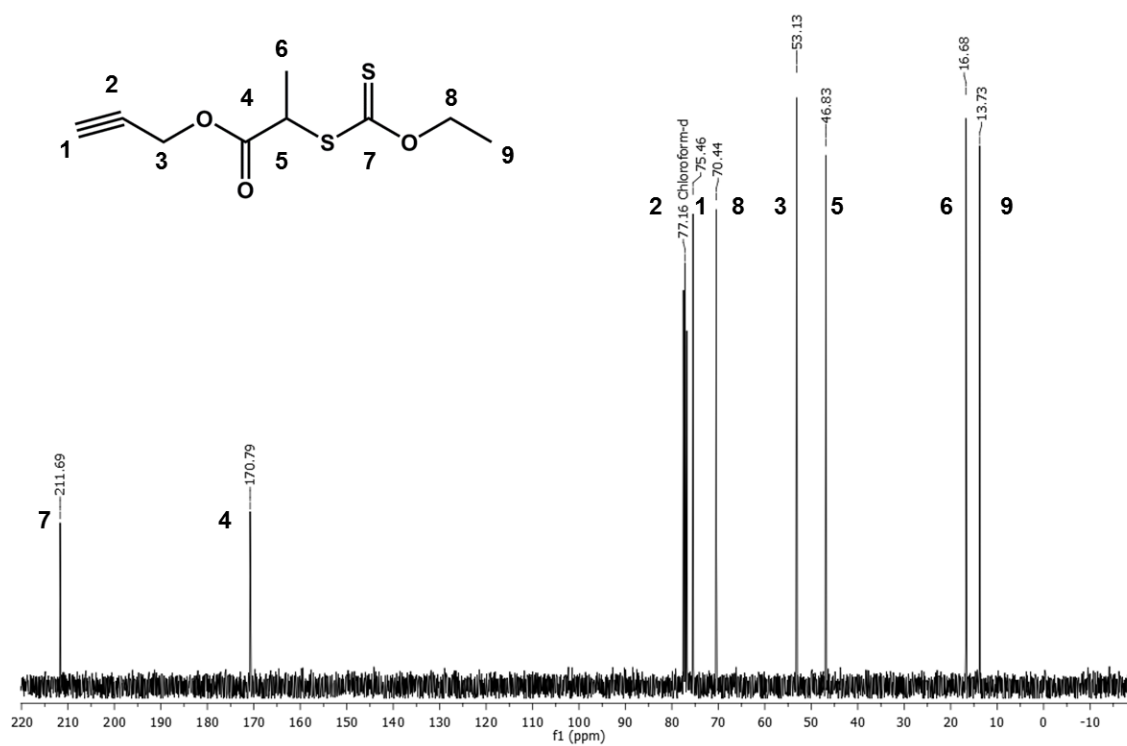


Figure D.3: <sup>13</sup>C NMR spectrum of AT-X<sub>1</sub> in CDCl<sub>3</sub>.



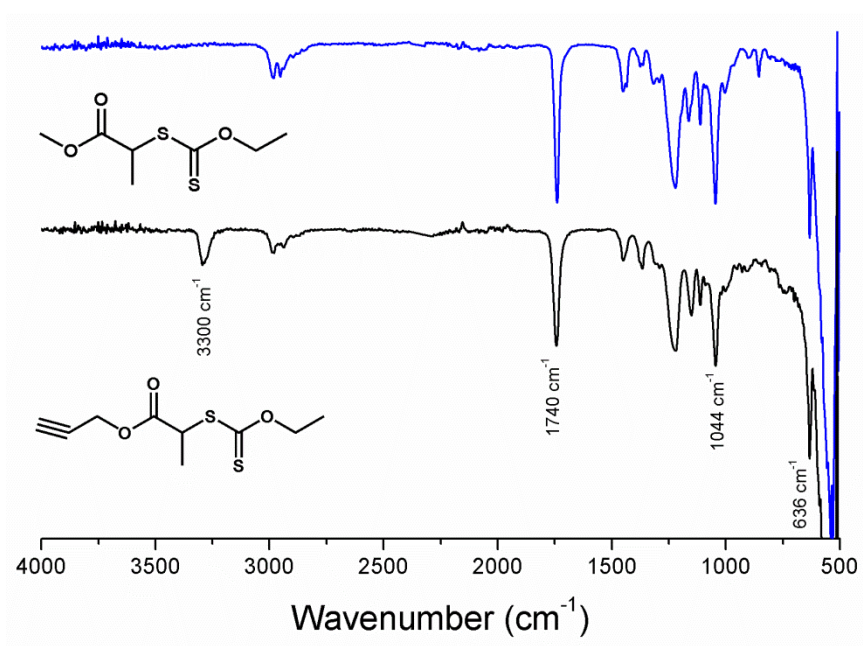
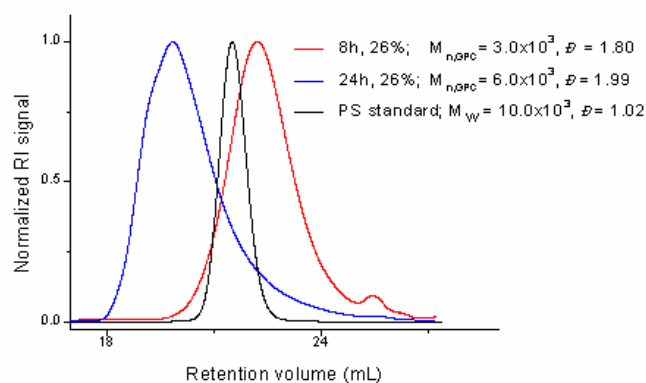


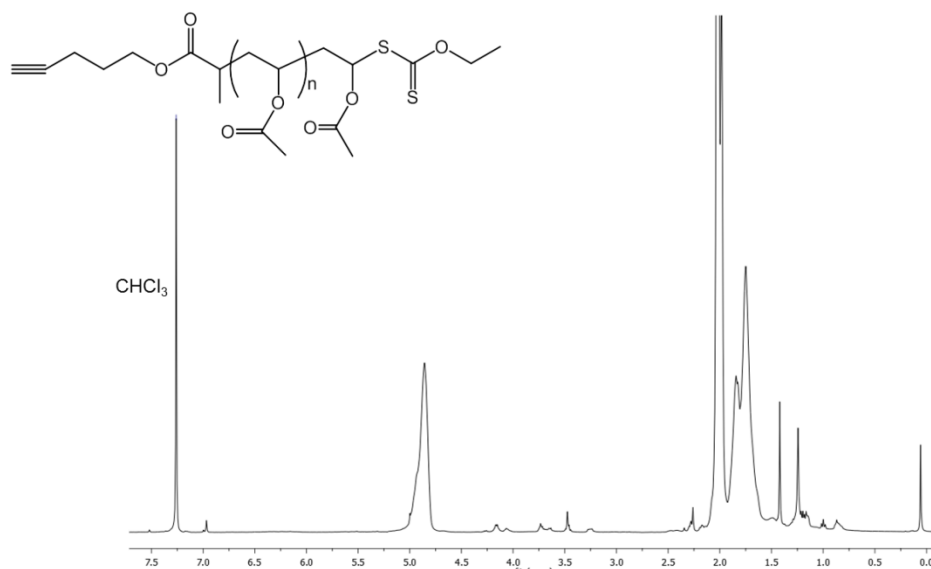
Figure D.4: FTIR-ATR spectra of the X<sub>1</sub> and AT-X<sub>1</sub>.



Figure D.5: <sup>13</sup>C NMR spectrum of PAT-X<sub>1</sub> in CDCl<sub>3</sub>.



**Figure D.6:** GPC traces of poly(styrene) (PS) standard ( $M_p = 10\ 050\ \text{g}\cdot\text{mol}^{-1}$ ;  $D = 1.02$ ) and PVAc samples taken at different times of reaction. Conditions:  $[\text{VAc}]_0/[\text{1,4-dioxane}]_0 = 1/1$  (m/m);  $[\text{VAc}]_0/[\text{AT-X}_1]_0/[\text{AIBN}]_0 = 100/1/0.2$ ,  $T = 60\ ^\circ\text{C}$ .



**Figure D.7:**  $^1\text{H}$  NMR spectrum of PVAc after the deprotection of the alkyne moiety in  $\text{CDCl}_3$ .

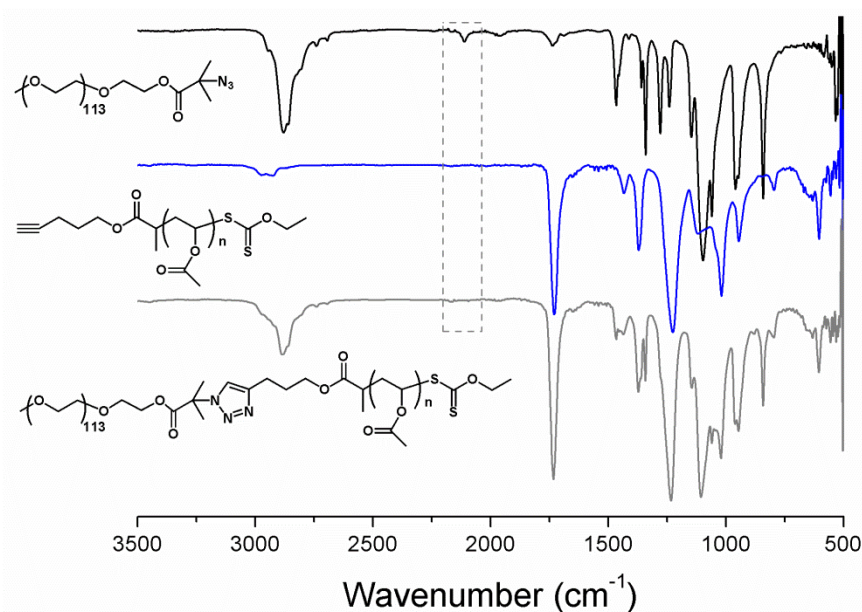


**Figure D.8:** FTIR-ATR spectra of the azido terminated-poly(ethylene glycol) (mPEG<sub>113</sub>-N<sub>3</sub>), alkyne terminated PVAc and the copolymer mPEG<sub>113</sub>-*b*-PVAc after the coupling reaction.

### Synthesis of azido terminated-poly(ethylene glycol) (mPEG<sub>113</sub>-N<sub>3</sub>)

mPEG<sub>113</sub>-N<sub>3</sub> was synthesized from poly(ethylene glycol) monomethyl ether bromoisobutyrate (mPEG<sub>113</sub>-BiB) by a nucleophilic substitution with sodium azide (NaN<sub>3</sub>). NaN<sub>3</sub> (2.04 g, 31.43 mmol) was added to a solution of mPEG<sub>113</sub>-BiB (4.00 g, 0.79 mmol) in DMF (60 mL) and the reaction proceeded for 24h at 85 °C. The final reaction mixture was dialyzed against deionized water, and the polymer was isolated after freeze drying. <sup>1</sup>H NMR (400 MHz, CDCl<sub>3</sub>) (Figure S9): δ (ppm) 4.32 (t, 2H, -O-CH<sub>2</sub>-), 3.4 (m, 454H, (-O-CH<sub>2</sub>-CH<sub>2</sub>-)<sub>113</sub>), 3.37 (s, 3H, -CH<sub>3</sub>), 1.48 (s, 6H, -(CH<sub>3</sub>)<sub>2</sub>N<sub>3</sub>).

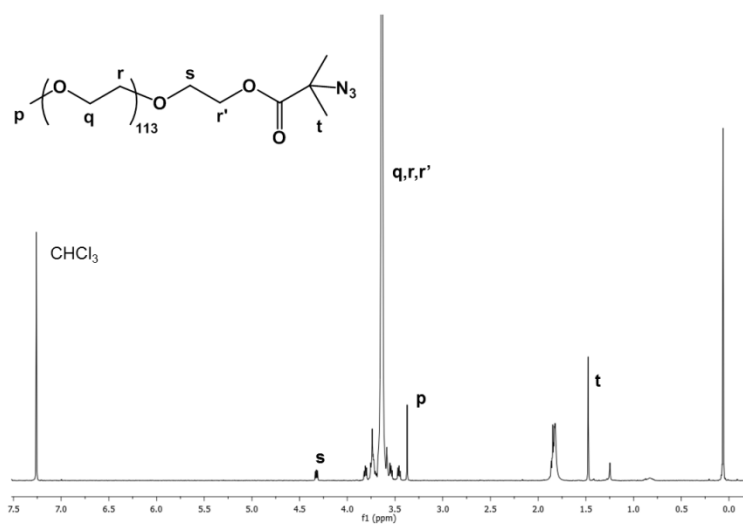


**Figure D.9:** <sup>1</sup>H NMR spectrum of azido terminated-poly(ethylene glycol) (mPEG<sub>113</sub>-N<sub>3</sub>) in CDCl<sub>3</sub>.

## Annex E

### Supporting information for Chapter 6. RAFT polymerization of alkyne terminated *N*-vinyl caprolactam: kinetic studies and polymer characterization

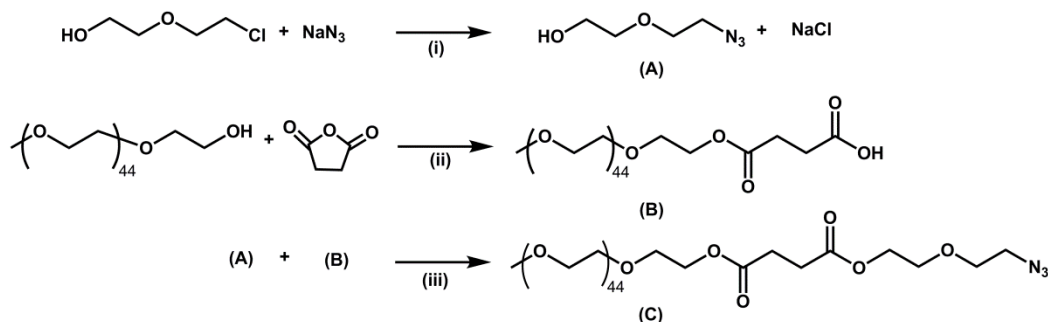


**Figure E.1:** Synthesis of azido-terminated mPEG (mPEG-N<sub>3</sub>) (C). (i) H<sub>2</sub>O, reflux; (ii) DMAP, DCM, r.t.; (iii) DMAP, DIC, DCM, r.t..

**Synthesis of azido ethoxy ethanol** (Figure E.1, (A)) (adapted from<sup>38</sup>): 5.00 mL of 2-(2-Chloroethoxy)ethanol (44.87 mmol), 11.67 g of sodium azide (179.50 mmol), 164 mg of hexadecyltrimethyl ammonium bromide (0.45 mmol) and 25 mL of water were mixed in reflux for 24h. After that the mixture were cooled down to room temperature and treated with HCl solution. The water solution was saturated with NaCl and the product was extracted with ethyl acetate (3 times). The organic phase was dried over anhydrous sodium sulfate and the solvent evaporated to give 5.85 g of azido ethoxy ethanol (yield 95%). <sup>1</sup>H NMR (CDCl<sub>3</sub>, 400 MHz),  $\delta$  (ppm): 2.41 (m, 1H, -OH), 3.42 (t, 2H, -CH<sub>2</sub>-N<sub>3</sub>), 3.62 (t, 2H, -CH<sub>2</sub>-O), 3.70 (t, 2H, -CH<sub>2</sub>-O) 3.76 (m, 2H, -CH<sub>2</sub>-OH). IR spectra (cm<sup>-1</sup>): 3400 ( $\nu_{\text{OH}}$ ), 2100 ( $\nu_{\text{N}_3}$ ).

**Synthesis of PEG-COOH** (Figure E.1, (B)) (adapted from<sup>39</sup>): 10.00 g of mPEG<sub>5000</sub> (2.00 mmol) ( $M_{n,\text{GPC}} = 5.059 \times 10^3$ ;  $D=1.03$ ) previous dried thought azeotropic distillation, 0.80g of succinic anhydride (8.00 mmol) and 0.50 g of DMAP (4.00 mmol) were dissolved in 40 mL of DCM and the reaction proceeded at room temperature for 12 h. The solvent was removed under reduced pressure and then the residue was dissolved in 50mL of water. The product was extracted 3 times with DCM (30 mL), and dried over anhydrous sodium sulfate. The solvent was evaporated and the mPEG-

COOH was obtained as a white solid.  $^1\text{H}$  NMR ( $\text{CDCl}_3$ , 400 MHz,  $\delta$  (ppm)): 4.22 (t, 2H,  $-\text{O}-\text{CH}_2-$ ), 3.79–3.42 (m, 454H,  $(-\text{O}-\text{CH}_2-\text{CH}_2-)_{113}$ ), 3.34 (s, 3H,  $-\text{CH}_3$ ), 2.60 (m, 4H,  $-(\text{CH}_2)_2-$ ). IR spectra ( $\text{cm}^{-1}$ ): 1734 ( $\nu_{\text{C=O}}$ ). GPC:  $M_{n,\text{GPC}} = 5.69 \times 10^3$ ;  $D=1.04$ .

**Synthesis of  $\text{N}_3$ -PEG** (Figure E.1, (C)) (adapted from <sup>39</sup>): 70 .0 mg of azido ethoxy ethanol (0.53 mmol), 2.75 g of PEG-COOH (0.53 mmol) and 7.83 mg of DMAP (0.06 mmol) were dissolved in 30 mL of DCM and the solution bubbled with  $\text{N}_2$ . 99  $\mu\text{L}$  of  $\text{N,N}'$ -diisopropylcarbodiimide (DIC) (0.64 mmol) was added to the previous solution and the reaction proceeded at room temperature overnight. The product was filtrate, concentrated in the rotatory evaporator and then precipitated in a cold mixture of THF:ether (100:400 mL). The product was vacuum dried to obtain the product  $\text{N}_3$ -PEG<sub>5000</sub> as a white powder.  $^1\text{H}$  NMR ( $\text{CDCl}_3$ , 400 MHz,  $\delta$ (ppm): 4.22 (4H,  $-\text{O}-\text{CH}_2-$ ), 4.00 (2H,  $-\text{O}-\text{CH}_2-$ ), 3.79–3.42 (456H,  $(-\text{O}-\text{CH}_2-\text{CH}_2-)_{113}$ ),  $-\text{O}-\text{CH}_2-$ ), 3.38 (2H,  $-\text{CH}_2-\text{N}_3$ ), 3.34 (3H,  $-\text{CH}_3$ ), 2.66 (4H,  $-(\text{CH}_2)_2-$ ). IR spectra ( $\text{cm}^{-1}$ ): 2100 ( $\nu_{\text{N}_3}$ ). GPC:  $M_{n,\text{GPC}} = 5.06 \times 10^3$ ;  $D=1.04$ .

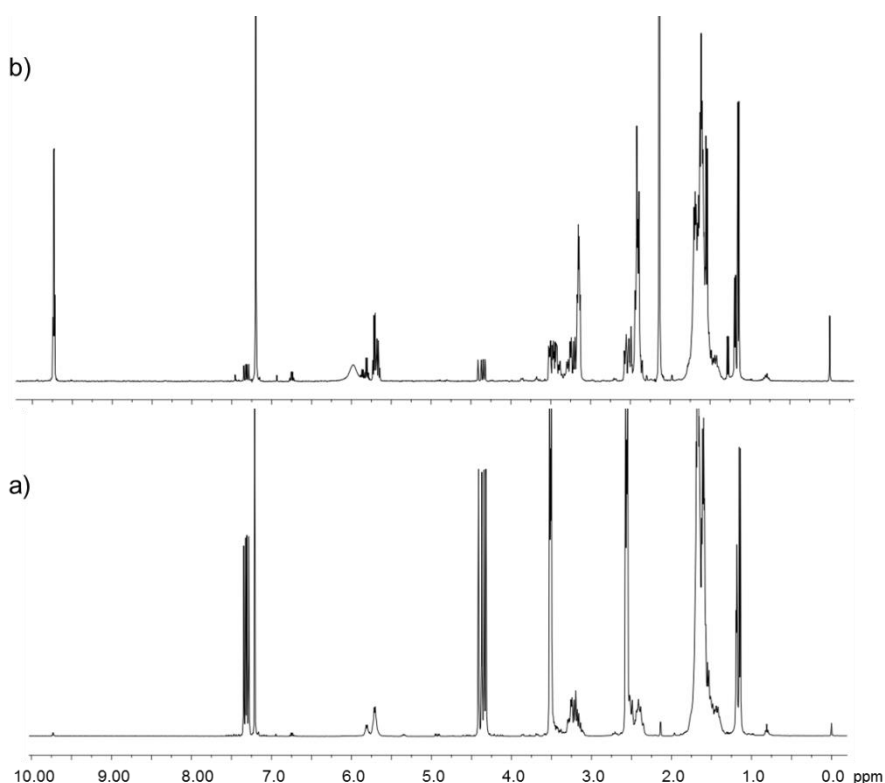


**Figure E.2:**  $^1\text{H}$  NMR spectrum of NVCL before the purification procedures (a) and the degraded monomer after the distillation (b), in  $\text{CDCl}_3$ .

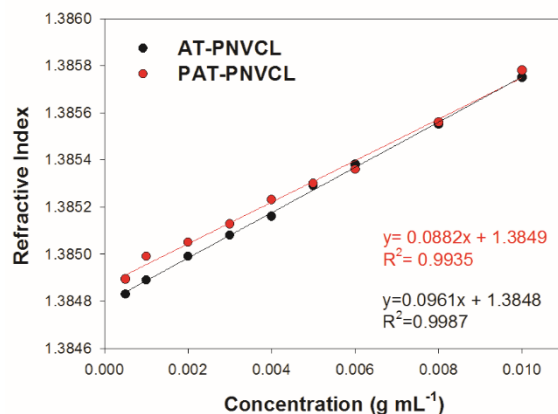


**Figure E.3:** Determination of  $dn/dc$  values of PNVL samples in DMF at 60°C. (PNVL samples prepared by RAFT polymerization using AT-CTA or PAT-CTA in 1,4-dioxane at 60°C. PAT-PNVCL:  $M_{n,th}=48.0 \times 10^3$ ;  $M_{n,GPC}=59.46 \times 10^3$ ,  $D=1.20$ ; AT-PNVCL:  $M_{n,th}=32.0 \times 10^3$ ;  $M_{n,GPC}=29.05 \times 10^3$ ,  $D=1.28$ ).

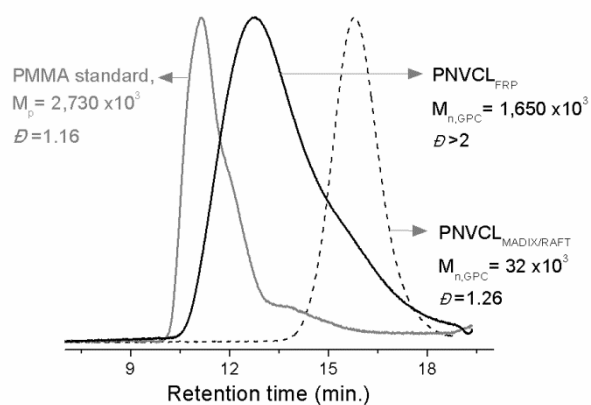


**Figure E.4:** GPC traces of PMMA standard (grey line) and PNVL samples synthesized through FRP (black straight line) and MADIX/RAFT polymerization (black dash line).

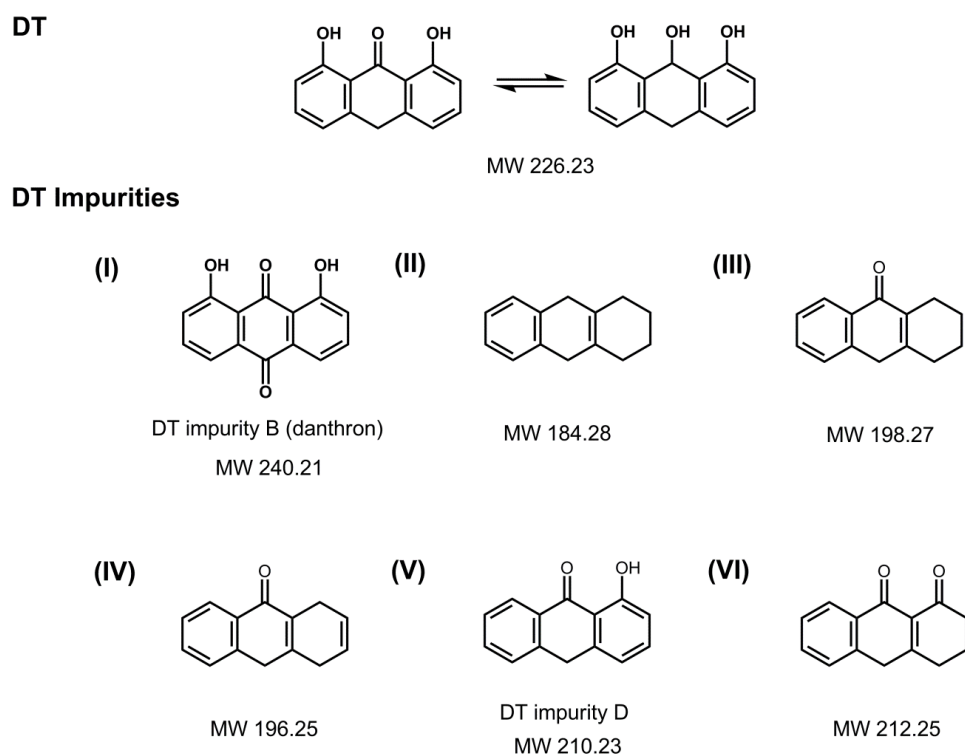


**Figure E.5:** Schematic representation of the dithranol (DT) and some DT impurities (found in the MALDI-TOF-MS spectrum of PNVCL) and the correspondent MW.

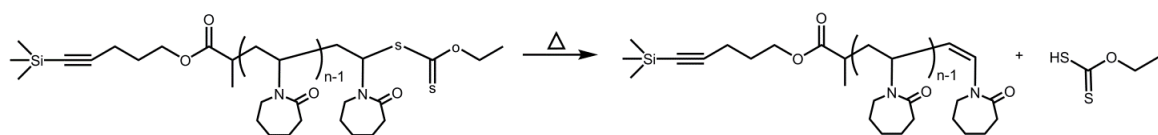


**Figure E.6:** Schematic representation of the mechanisms of thermolysis of PNVCL.



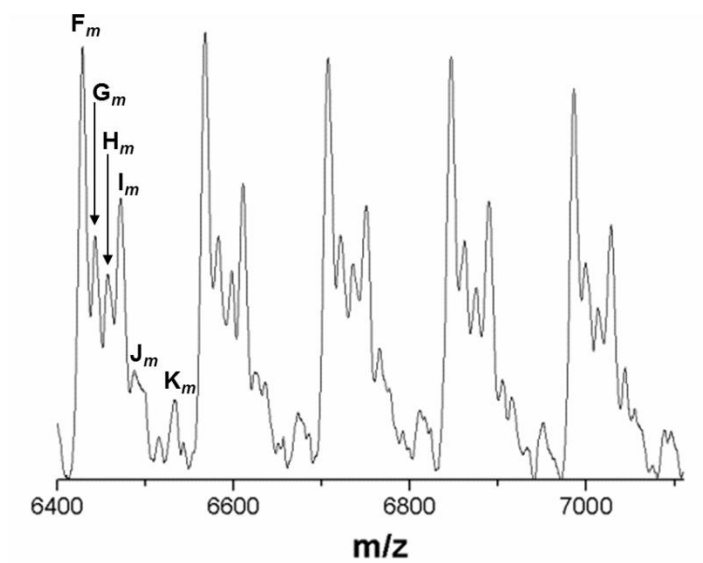


**Figure E.7:** MALDI-TOF-MS in the linear mode (using DT as a matrix) from  $m/z$  6400 to 7100 of alkyne-terminated PNVCL after the deprotection reaction ( $M_{n, \text{GPC}} = 18.92 \times 10^3$ , and  $\mathcal{D} = 1.33$ ).

**Table E.1:** MALDI-TOF-MS peak assignment for alkyne-terminated PNVCCL, after the deprotection reaction.

	F set		G set		H set		I set		J set		Kset	
<i>n</i>	MW <sub>cat</sub> <sup>a</sup>	MW <sub>exp</sub>	MW <sub>cat</sub> <sup>b</sup>	MW <sub>exp</sub>	MW <sub>cat</sub> <sup>c</sup>	MW <sub>exp</sub>	MW <sub>cat</sub> <sup>d</sup>	MW <sub>exp</sub>	MW <sub>cat</sub> <sup>e</sup>	MW <sub>exp</sub>	MW <sub>cat</sub> <sup>f</sup>	MW <sub>exp</sub>
43	F <sub>1</sub> 6430.2	6428.5	G <sub>1</sub> 6442.1 - 6444.2	6442.8	H <sub>1</sub> 6456.1-6458.1	6457.3	I <sub>1</sub> 6472.1	6471.8	J <sub>1</sub> 6486.1	6487.1		
44	F <sub>2</sub> 6569.4	6567.7	G <sub>2</sub> 6581.3 - 6583.3	6582.8	H <sub>2</sub> 6595.3-6597.3	6597.5	I <sub>2</sub> 6611.3	6610.7	J <sub>2</sub> 6625.3	6625.1		
45	F <sub>3</sub> 6708.6	6706.9	G <sub>3</sub> 6720.5 - 6722.5	6720.9	H <sub>3</sub> 6734.5-6736.5	6735.2	I <sub>3</sub> 6750.5	6750.5	J <sub>3</sub> 6764.5	6765.4		
46	F <sub>4</sub> 6847.8	6846.5	G <sub>4</sub> 6859.7 - 6861.7	6861.8	H <sub>4</sub> 6873.7-6875.7	6874.9	I <sub>4</sub> 6889.7	6889.5	J <sub>4</sub> 6903.7	6904.8	K <sub>1</sub> 6541.5	6536.9
47	F <sub>5</sub> 6987.0	6985.9	G <sub>5</sub> 6998.9 - 7000.9	6998.9	H <sub>5</sub> 7012.9-7014.9	7012.9	I <sub>5</sub> 7028.9	7028.1	J <sub>5</sub> 7042.9	7044.0	K <sub>2</sub> 6680.7	6679.3
48											K <sub>3</sub> 6819.9	6817.4
49											K <sub>4</sub> 6959.1	6956.7
50											K <sub>5</sub> 7098.3	7096.7

*n*-the number of repeat units (NVCL), where dep(PAT-X<sub>1</sub>) = 260.37 g·mol<sup>-1</sup>, NVCL = 139.20 g·mol<sup>-1</sup>, SHCSOCH<sub>2</sub>CH<sub>3</sub> = 122.21 g·mol<sup>-1</sup>; DT<sub>imp(0)</sub> = 240.21 g·mol<sup>-1</sup>; DT<sub>imp(1)</sub> = 184.28 g·mol<sup>-1</sup>; DT<sub>imp(2)</sub> = 198.27 g·mol<sup>-1</sup>; DT<sub>imp(3)</sub> = 196.25 g·mol<sup>-1</sup>; DT<sub>imp(4)</sub> = 210.23 g·mol<sup>-1</sup>; DT<sub>imp(5)</sub> = 212.25 g·mol<sup>-1</sup>.

<sup>a</sup> MW<sub>cat</sub> = [dep(PAT- X<sub>1</sub>)] + *n*PNVCL + DT<sub>imp(0)</sub>; <sup>b</sup> MW<sub>cat</sub> = [dep(PAT- X<sub>1</sub>) + *n*PNVCL] + DT<sub>imp(1)</sub>; or MW<sub>cat</sub> = [dep(PAT- X<sub>1</sub>) + *n*PNVCL] + DT<sub>imp(2)</sub>; <sup>c</sup> MW<sub>cat</sub> = [dep(PAT- X<sub>1</sub>) + *n*PNVCL] + DT<sub>imp(3)</sub>; or MW<sub>cat</sub> = [dep(PAT-CTA) + *n*PNVCL] + DT<sub>imp(4)</sub>; <sup>d</sup> MW<sub>cat</sub> = [dep(PAT-CTA) + *n*PNVCL] + DT<sub>imp(5)</sub>; <sup>e</sup> MW<sub>cat</sub> = [dep(PAT-CTA) + *n*PNVCL] + DT<sub>imp(0)</sub>; <sup>f</sup> MW<sub>cat</sub> = [dep(PAT- X<sub>1</sub>) + *n*PNVCL] - SHCSOCH<sub>2</sub>CH<sub>3</sub>.

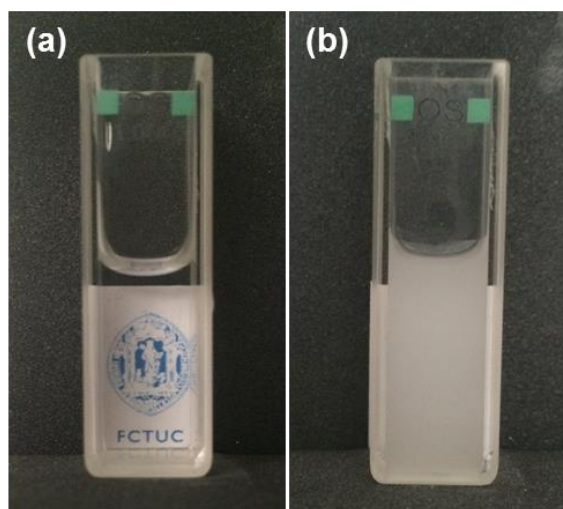


**Figure E.8:** Pictures of the PNVCL homopolymer solution ( $1.0 \text{ mgmL}^{-1}$ ) at room temperature (a) and above the  $T_{CP}$  (b).

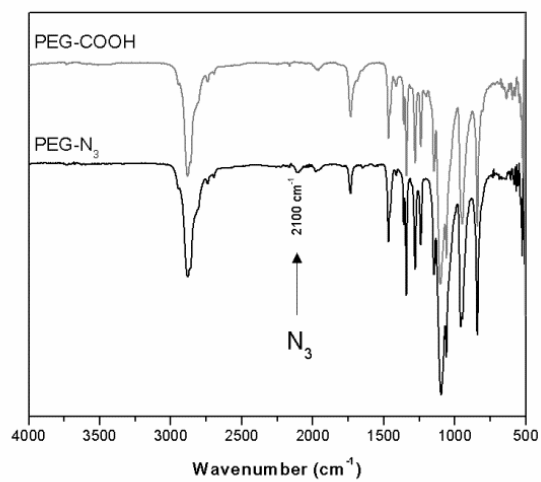


**Figure E.9:** FTIR-ATR spectra of the PEG-COOH and PEG- $N_3$ .



## Annex F

**Supporting information for Chapter 7.** Synthesis of new thermo-responsive nanocarriers based on POEOMA-*b*-PNVCL prepared using a combination of ATRP, RAFT and CuAAC

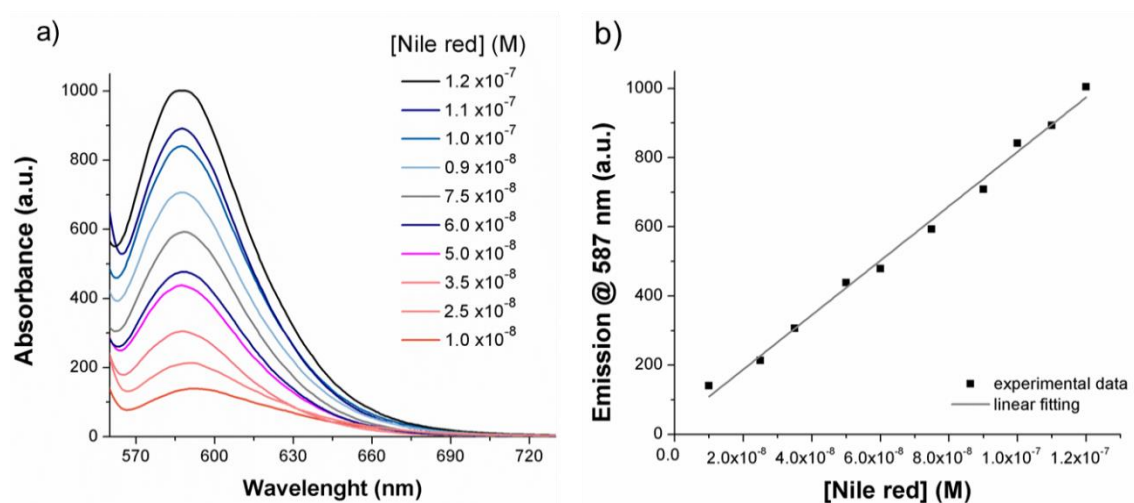


**Figure F.1:** UV-vis absorption spectra acquired as a function of Nile red concentration in THF (a), and the respective analytical curve (b).

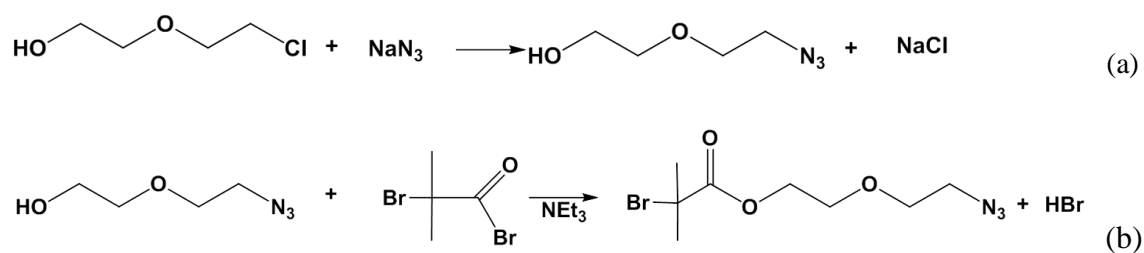


**Figure F.2:** Schematic representation of the 2-(2-azidoethoxy)ethyl bromoisobutyrate ( $\text{N}_3\text{E}^i\text{BBr}$ ) synthesis.

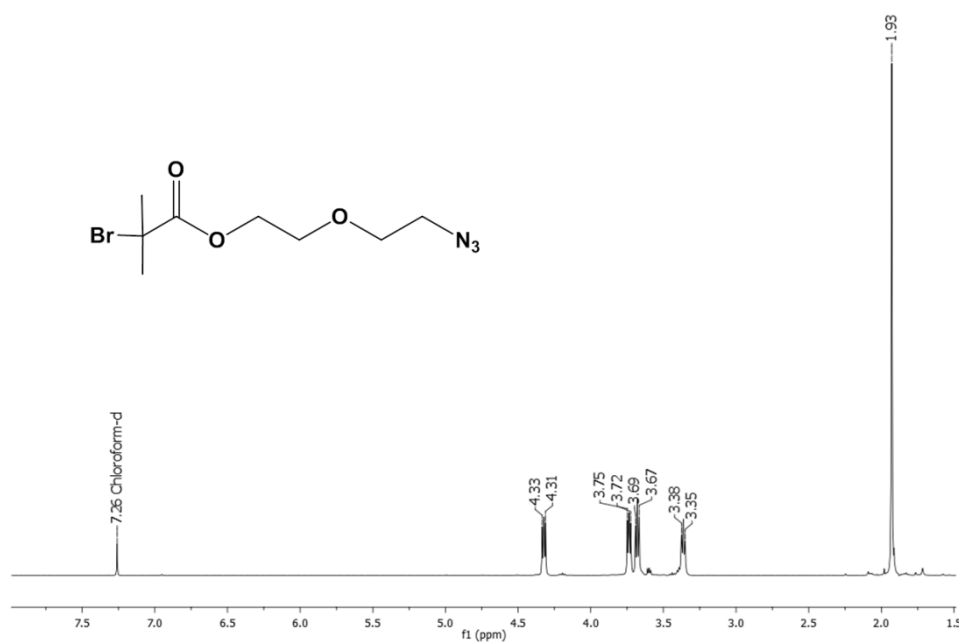


**Figure F.3:** The  $^1\text{H}$  NMR spectrum of  $\text{N}_3\text{EtBBBr}$  in  $\text{CDCl}_3$ .  $^1\text{H}$  NMR (400 MHz,  $\text{CDCl}_3$ ,  $\delta$  (ppm)): 1.95 (s, 6H,  $(\text{CH}_3)_2\text{C}$ ), 3.39 (t, 2H,  $\text{CH}_2\text{N}_3$ ), 3.70 (t, 2H,  $\text{N}_3\text{CH}_2\text{CH}_2\text{O}$ ), 3.76 (t, 2H,  $\text{COOCH}_2\text{CH}_2\text{O}$ ), 4.35 (t, 2H,  $\text{CH}_2\text{OCO}$ ).

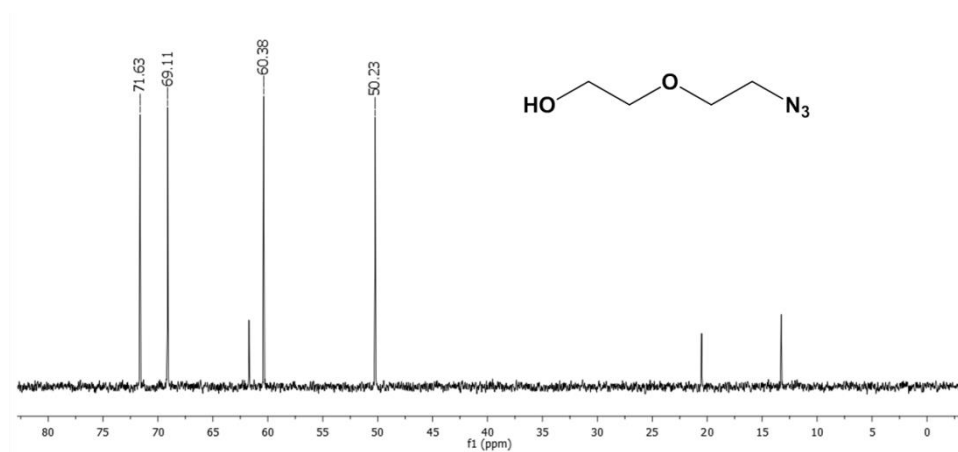


**Figure F.4:** The  $^{13}\text{C}$  NMR spectrum of 2-(2-azidoethoxy)ethanol in  $\text{D}_2\text{O}$ .  $^{13}\text{C}$  NMR (100 MHz,  $\text{D}_2\text{O}$ ,  $\delta$  (ppm)): 50.23 ( $\text{N}_3\text{-CH}_2\text{-}$ ), 60.38 ( $\text{-CH}_2\text{-OH}$ ), 69.12 ( $\text{N}_3\text{-CH}_2\text{-CH}_2\text{-O}$ ), 71.64 ( $\text{O-CH}_2\text{-CH}_2\text{-OH}$ ).

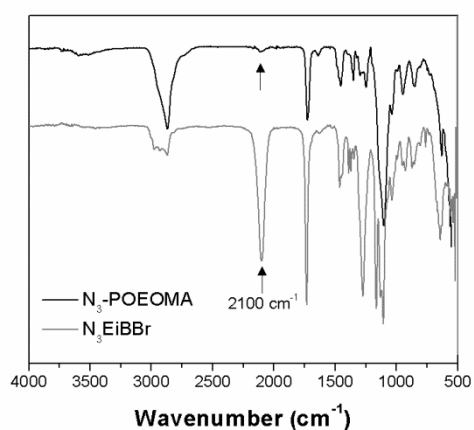


**Figure F.5:** FTIR ATR spectra of (2-azidoethoxy)ethyl bromoisobutyrate ( $N_3EiBBr$ ) and  $\alpha$ -azide terminated POEOMA ( $N_3$ -POEOMA).

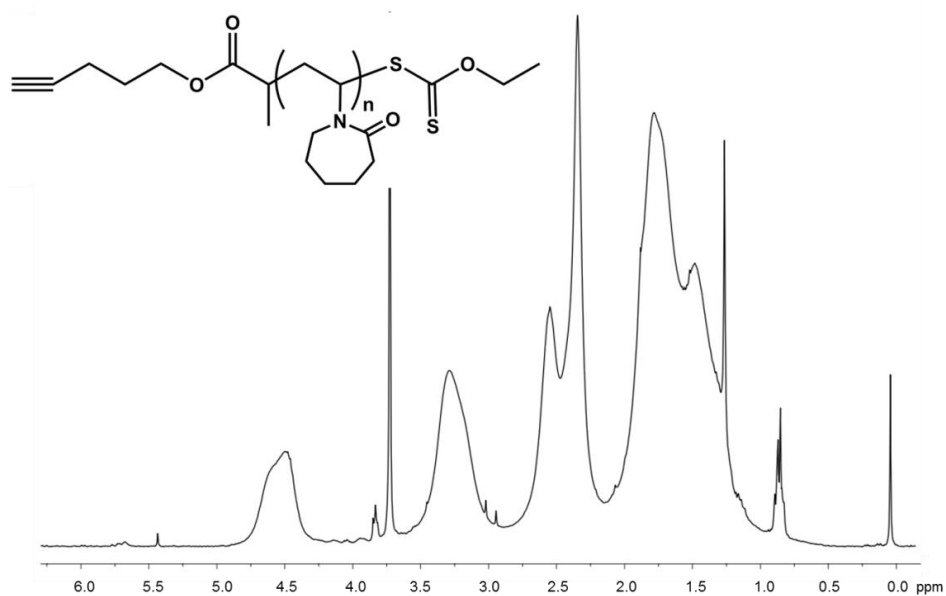


**Figure F.6:**  $^1H$  NMR spectra in  $CDCl_3$  of alkyne-terminated PNVCN obtained by RAFT, after the deprotection reaction. Reaction conditions:  $[NVCL]_0/[PAT-X_1]_0/[AIBN]_0 = 600/1/0.5$  (molar) in 1,4-dioxane at  $60\text{ }^\circ C$ ,  $[NVCL]_0 = 3.71\text{ M}$  ( $M_{n,NMR} = 36.63 \times 10^3$ ,  $M_{n,GPC} = 38.40 \times 10^3$ ;  $D = 1.28$ ).

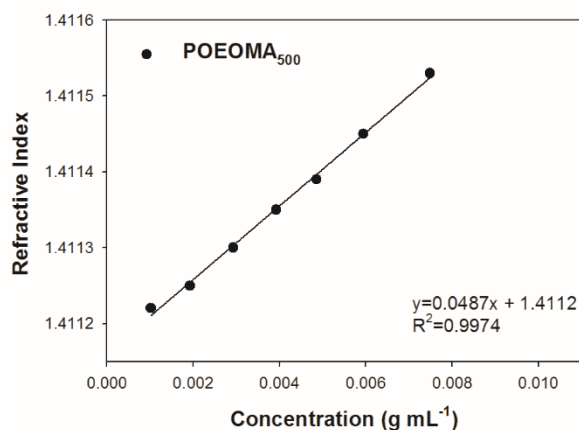


**Figure F.7:** Determination of  $dn/dc$  values of POEOMA samples in DMF at 60 °C.

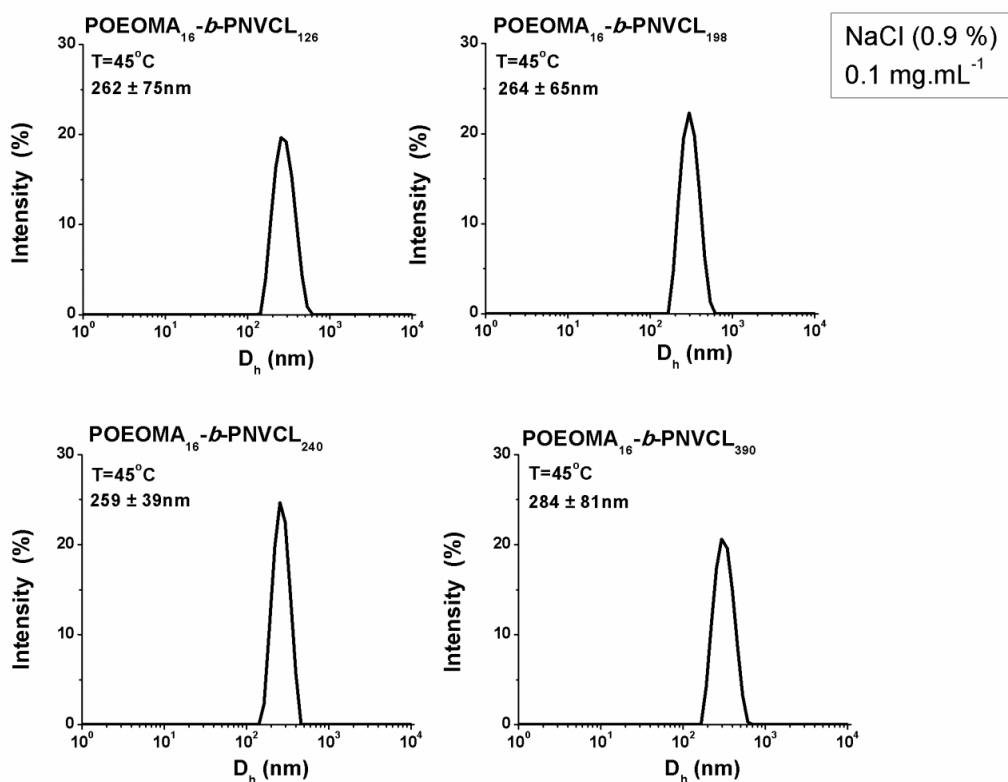


**Figure F.8:** Size distribution (by intensity) of POEOMA-*b*-PNVCL copolymers in physiological saline solution (NaCl 0.9 %) (0.1 mgmL<sup>-1</sup>), T = 45 °C.



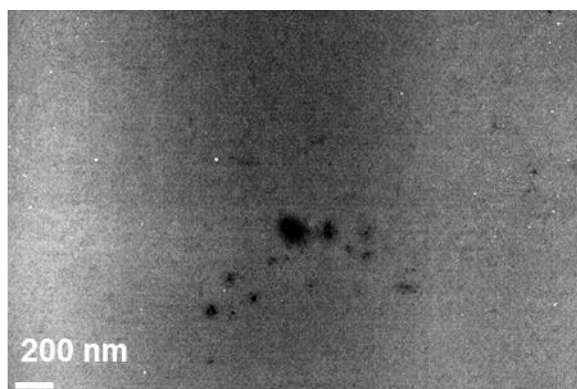


**Figure F.9:** TEM micrographs, negatively stained with uranyl acetate, of the control sample (without polymer) taken at a Mag x 50 000.

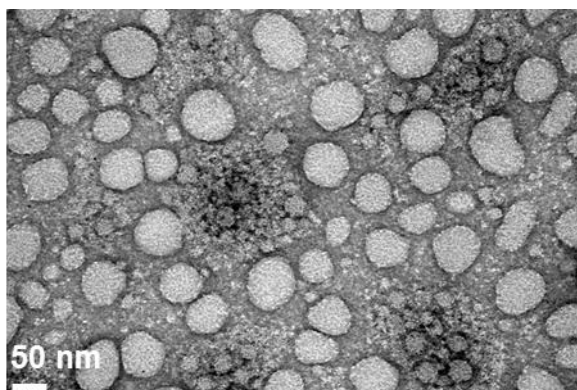


**Figure F.10:** TEM micrographs, negatively stained with uranyl acetate, of self-assembled block copolymers of POEOMA<sub>16</sub>-*b*-PNVCL<sub>198</sub> taken at a Mag. x 200 000 (0.5 mg.mL<sup>-1</sup>).

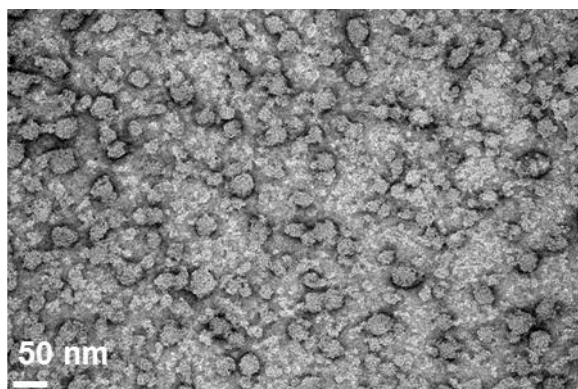


**Figure F.11:** TEM micrographs, negatively stained with uranyl acetate, of self-assembled block copolymers of POEOMA<sub>16</sub>-*b*-PNVCL<sub>240</sub> taken at a Mag. x 200 000 (0.5 mg.mL<sup>-1</sup>).

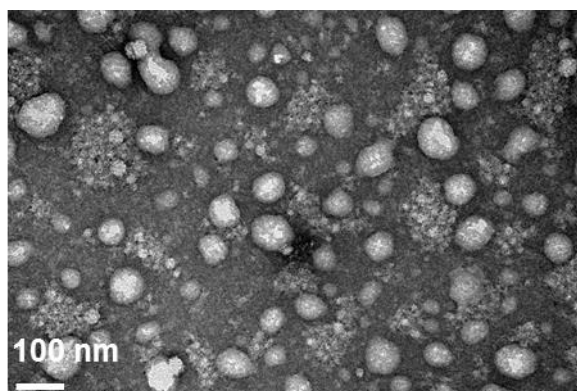


**Figure F.12:** TEM micrographs, negatively stained with uranyl acetate, of self-assembled block copolymers of POEOMA<sub>16</sub>-*b*-PNVCL<sub>390</sub> taken at a Mag. x 200 000 (0.5 mg.mL<sup>-1</sup>).

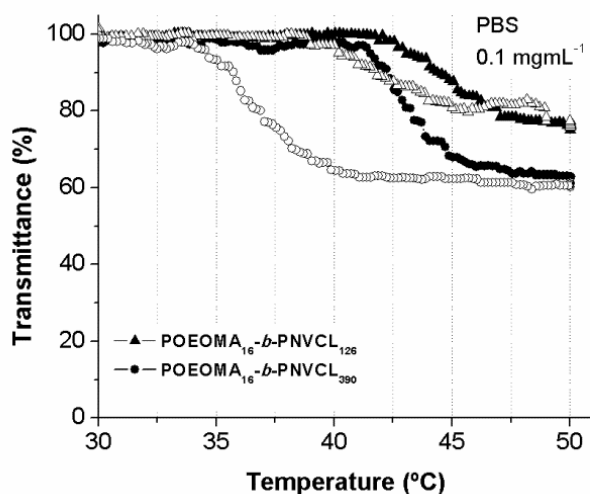


**Figure F.13:** Transmittance measurements as a function of temperature for 0.1 mg.mL<sup>-1</sup> of physiological saline solution for copolymer POEOMA<sub>16</sub>-*b*-PNVCL<sub>126</sub> (triangle symbols) and POEOMA<sub>16</sub>-*b*-PNVCL<sub>390</sub> (square symbols) (heating/cooling rate 1.0 °C.min<sup>-1</sup>). The full symbols correspond to the heating cycle and the unfilled symbols represent the cooling cycle.

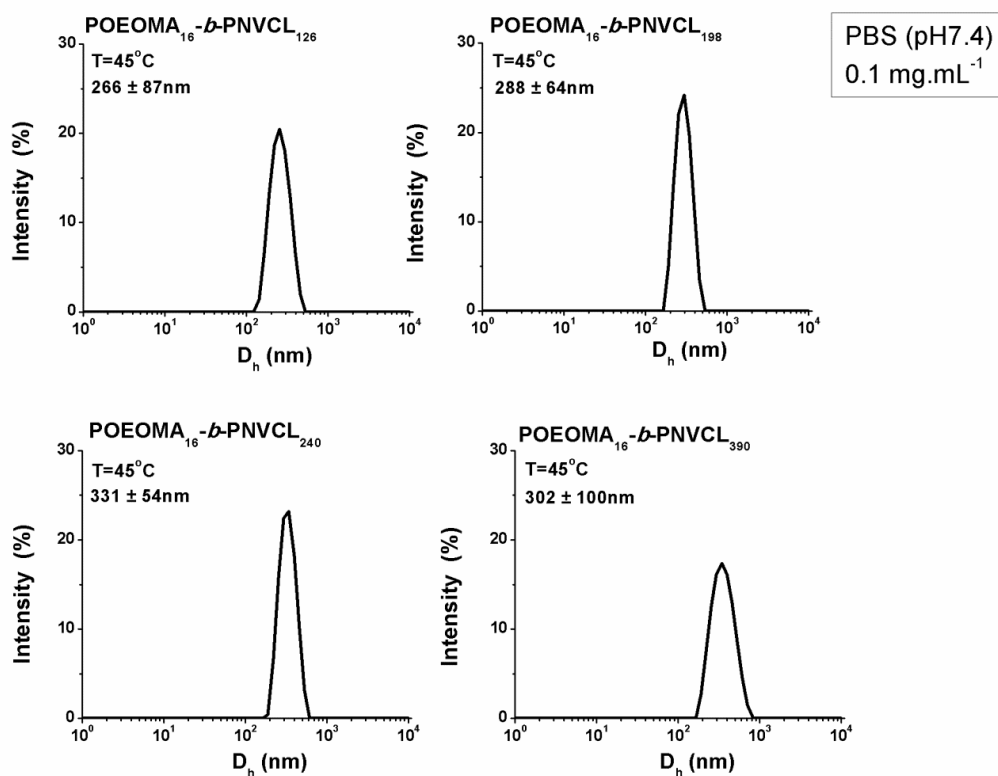


**Figure F.14:** Size distribution (by intensity) of POEOMA-*b*-PNVCL copolymers in PBS (7.4) solution ( $0.1 \text{ mgmL}^{-1}$ ),  $T= 45 \text{ }^\circ\text{C}$ .

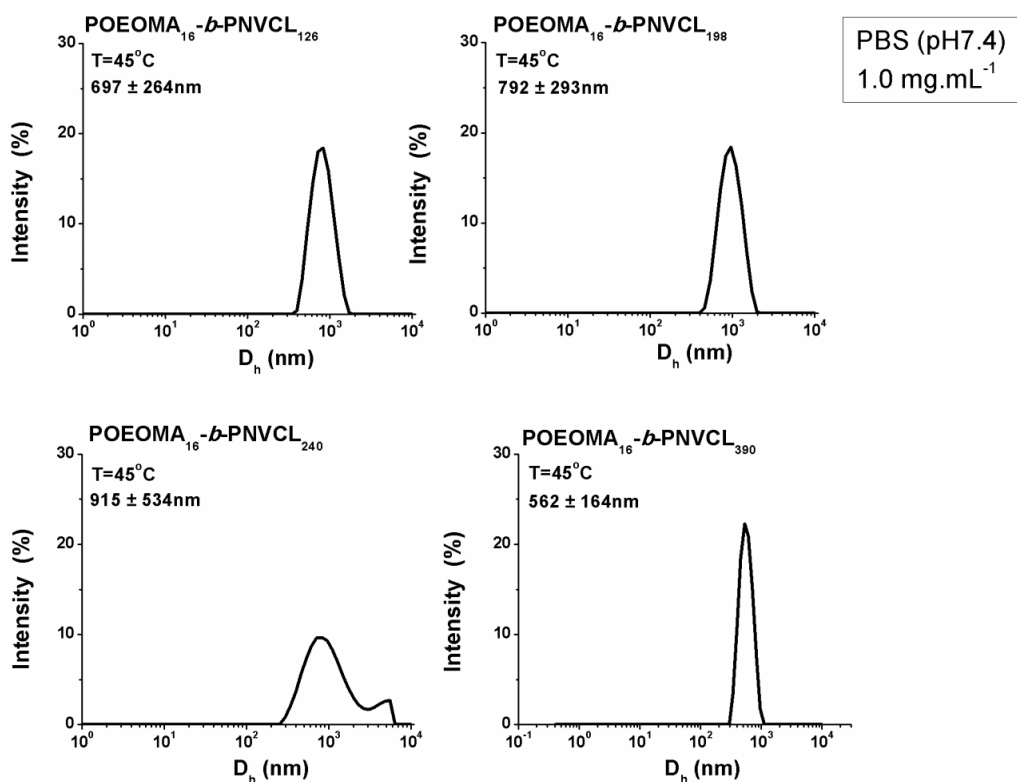


**Figure F.15:** Size distribution (by intensity) of POEOMA-*b*-PNVCL copolymers in PBS (7.4) solution ( $1.0 \text{ mg.mL}^{-1}$ ),  $T= 45 \text{ }^\circ\text{C}$ .

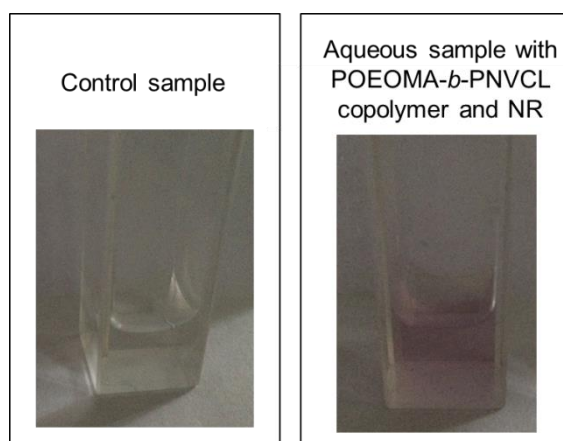


**Figure F.16:** Pictures of the NR aqueous solutions in the presence (right) and absence (left) of the block copolymer after the filtration ( $[NR]_{\text{initial}} = 1 \times 10^{-5} \text{ mg.mL}^{-1}$ ;  $[POEOMA-b-PNVCL] = 0.5 \text{ mg.mL}^{-1}$ ).

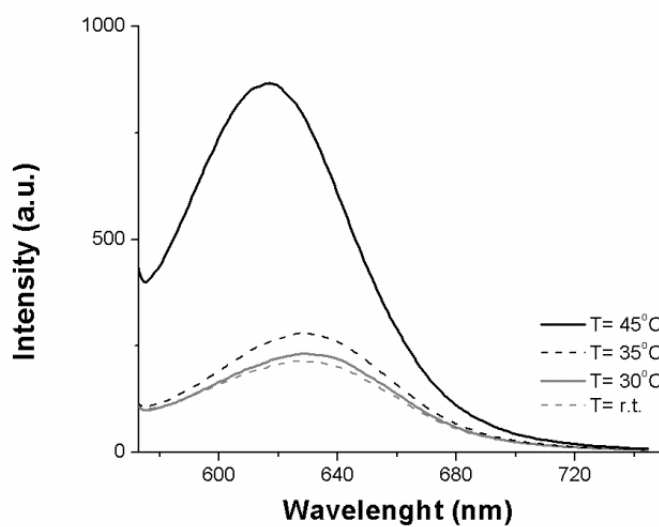


**Figure F.17:** Fluorescence spectra of Nile Red in aqueous solutions of POEOMA-*b*-PNVCL copolymer ( $0.5 \text{ mg.mL}^{-1}$ ) as a function of temperature.

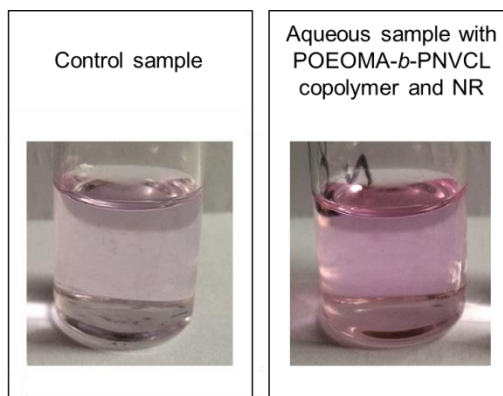


**Figure F.18:** Pictures of the NR encapsulation assays after filtration and dissolution with THF. Both samples were prepared by the same method, but the sample on the right had  $1.0 \text{ mg.mL}^{-1}$  of the copolymer POEOMA-*b*-PNVCL.



## Annex G

**Supporting information for Chapter 8.** Synthesis of stimuli-responsive linear dendritic block copolymers via “click” chemistry

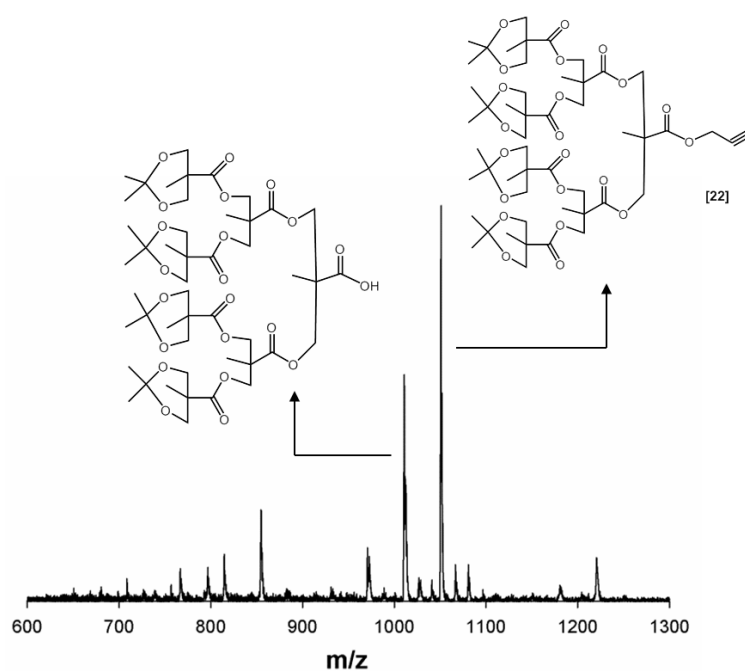


**Figure G.1:** MALDI-TOF in the linear mode (using DHB as matrix) from m/z 600 to 1300 of the alkyne functionalized 3<sup>rd</sup> generation Dendron.

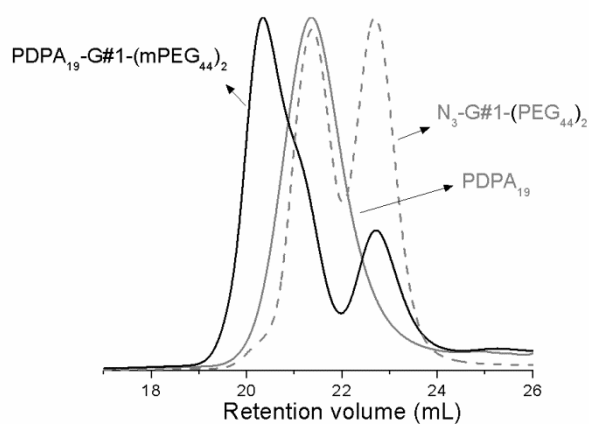


**Figure G.2:** GPC traces of the RI signal of the PDPA<sub>19</sub>, the N<sub>3</sub>-G#1-(PEG<sub>44</sub>)<sub>2</sub> and the LDBC, PDPA<sub>19</sub>-G#1-(mPEG<sub>44</sub>)<sub>2</sub> copolymer, after the “click” coupling reaction.

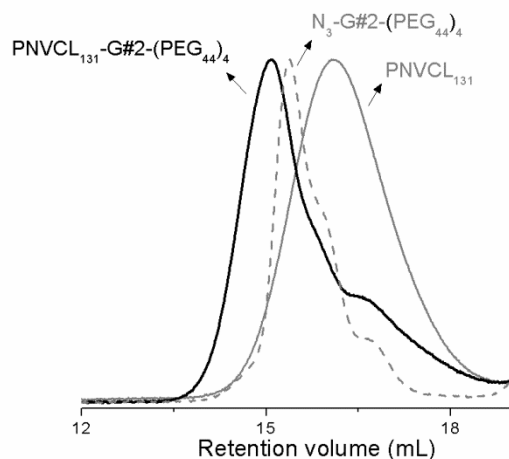


**Figure G.3:** GPC traces of the RI signal of the  $\text{PNVCL}_{131}$ , the  $\text{N}_3\text{-G\#2-(PEG}_{44}\text{)}_4$  and the LDBC,  $\text{PNVCL}_{131}\text{-G\#2-(mPEG}_{44}\text{)}_4$  copolymer, after the “click” coupling reaction

**Table G.1:** Characteristics of the aggregates formed by the solution self-assembly of the temperature-responsive LDBC at 45 °C ( $0.2 \text{ mg}\cdot\text{mL}^{-1}$ ).

	Copolymer	$D_h$ (nm) <sup>a</sup>	PDI
<b>G#0-PEG<sub>113</sub></b>	$\text{PNVCL}_{106}\text{-G\#0-PEG}_{113}$	208	0.149
	$\text{PNVCL}_{131}\text{-G\#0-PEG}_{113}$	294	0.127
	$\text{PNVCL}_{195}\text{-G\#0-PEG}_{113}$	204	0.049
<b>G#1-(PEG<sub>44</sub>)<sub>2</sub></b>	$\text{PNVCL}_{106}\text{-G\#1-(PEG}_{44}\text{)}_2$	169	0.167
	$\text{PNVCL}_{225}\text{-G\#1-(PEG}_{44}\text{)}_2$	227	0.015
<b>G#1-(PEG<sub>113</sub>)<sub>2</sub></b>	$\text{PNVCL}_{106}\text{-G\#1-(PEG}_{113}\text{)}_2$	214	0.276
	$\text{PNVCL}_{131}\text{-G\#1-(PEG}_{113}\text{)}_2$	392	0.206
	$\text{PNVCL}_{225}\text{-G\#1-(PEG}_{113}\text{)}_2$	412	0.167
<b>G#2-(PEG<sub>44</sub>)<sub>4</sub></b>	$\text{PNVCL}_{106}\text{-G\#2-(PEG}_{44}\text{)}_4$	200	0.205
	$\text{PNVCL}_{131}\text{-G\#2-(PEG}_{44}\text{)}_4$	183	0.132
	$\text{PNVCL}_{225}\text{-G\#2-(PEG}_{44}\text{)}_4$	186	0.100
<b>G#2-(PEG<sub>113</sub>)<sub>4</sub></b>	$\text{PNVCL}_{131}\text{-G\#2-(PEG}_{113}\text{)}_4$	346	0.186
	$\text{PNVCL}_{225}\text{-G\#2-(PEG}_{113}\text{)}_4$	271	0.145

<sup>a</sup>mean value of the hydrodynamic diameter of the particle

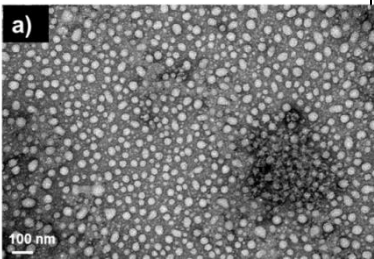
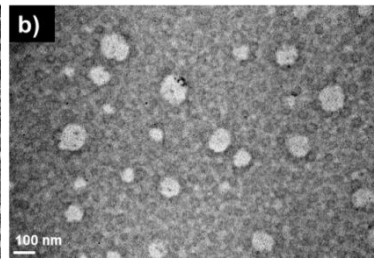
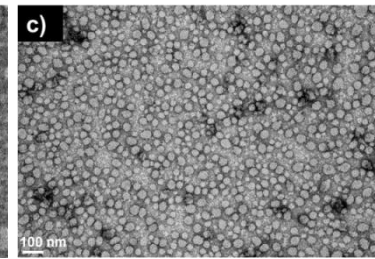
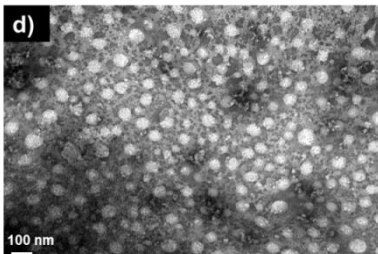
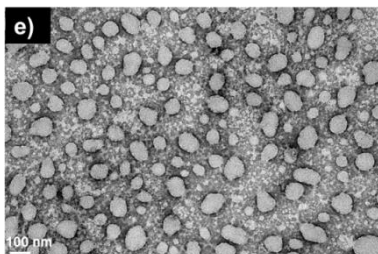
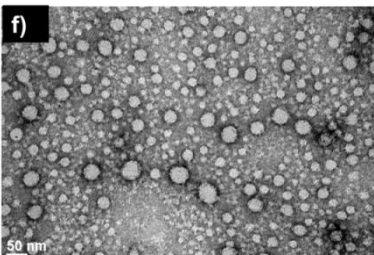
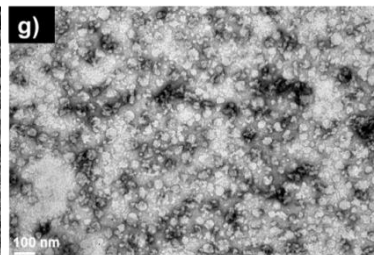
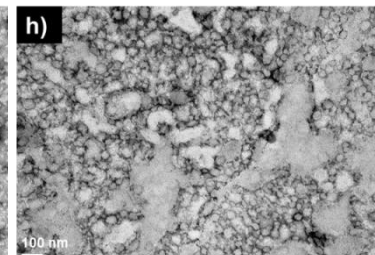


**Table G.2:** Characteristics of the aggregates formed by the solution self-assembly of the pH-responsive LDBC at 25 °C and pH 7.4 (1.0 mg.mL<sup>-1</sup>).

	<b>Copolymer</b>	<b>D<sub>h</sub> (nm)<sup>a</sup></b>	<b>PDI</b>
<b>G#0-PEG<sub>113</sub></b>	PDPA <sub>19</sub> -G#0-PEG <sub>113</sub>	178.6	0.438
	PDPA <sub>49</sub> -G#0-PEG <sub>113</sub>	114.3	0.333
<b>G#1-(PEG<sub>44</sub>)<sub>2</sub></b>	PDPA <sub>19</sub> -G#1-(PEG <sub>44</sub> ) <sub>2</sub>	144.7	0.454
	PDPA <sub>49</sub> -G#1-(PEG <sub>44</sub> ) <sub>2</sub>	188.4	0.351
	PDPA <sub>102</sub> -G#1-(PEG <sub>44</sub> ) <sub>2</sub>	179.7	0.096
<b>G#1-(PEG<sub>113</sub>)<sub>2</sub></b>	PDPA <sub>49</sub> -G#1-(PEG <sub>113</sub> ) <sub>2</sub>	150.9	0.235
	PDPA <sub>102</sub> -G#1-(PEG <sub>113</sub> ) <sub>2</sub>	125.4	0.11
<b>G#1-(PEG<sub>44</sub>)<sub>4</sub></b>	PDPA <sub>49</sub> -G#1-(PEG <sub>44</sub> ) <sub>4</sub>	130.2	0.187
	PDPA <sub>102</sub> -G#1-(PEG <sub>44</sub> ) <sub>4</sub>	205.5	0.132

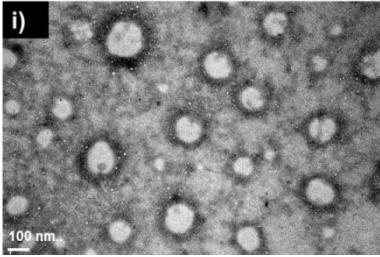
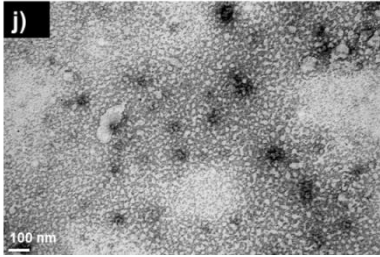
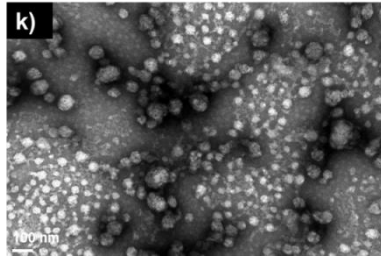
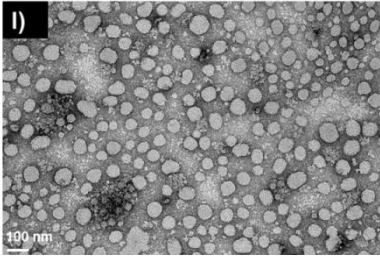
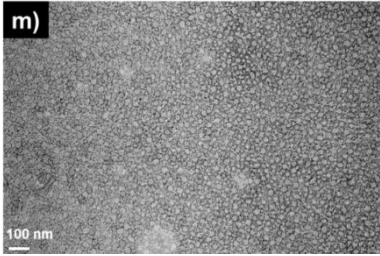
<sup>a</sup>mean value of the hydrodynamic diameter of the particle

**Table G.3:** Characteristics of the aggregates formed by the solution self-assembly of the temperature-responsive LDBC at 45 °C (0.2 mg.mL<sup>-1</sup>). TEM micrographs taken at Mag. x 100 000 and DLS results (D<sub>h</sub> and PDI).

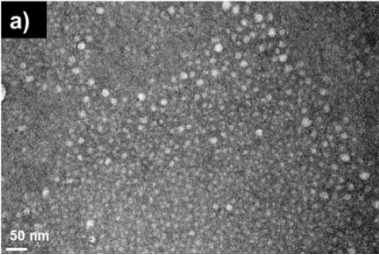
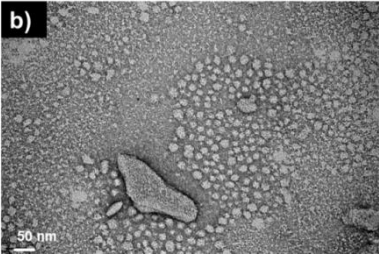
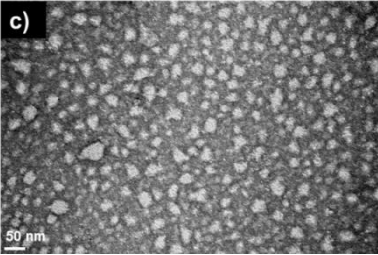
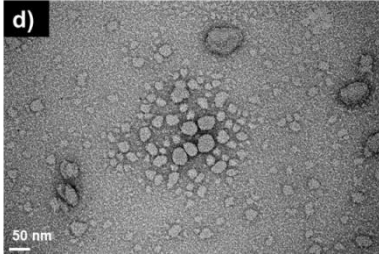
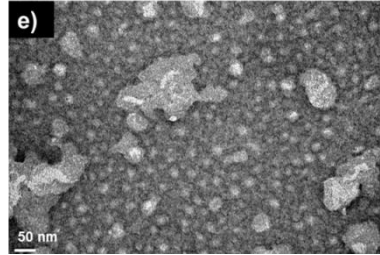
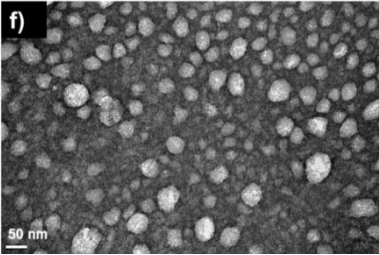
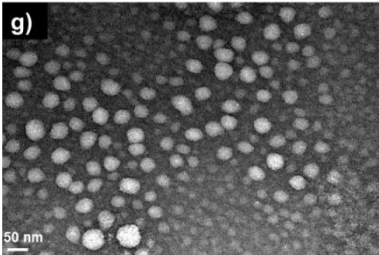
<b>G#0-PEG<sub>113</sub></b>		
PNVCL <sub>106</sub> -G#0-PEG <sub>113</sub>	PNVCL <sub>131</sub> -G#0-PEG <sub>113</sub>	PNVCL <sub>195</sub> -G#0-PEG <sub>113</sub>
		
<b>G#1-(PEG<sub>44</sub>)<sub>2</sub></b>		
PNVCL <sub>106</sub> -G#1-(PEG <sub>44</sub> ) <sub>2</sub>	PNVCL <sub>225</sub> -G#1-(PEG <sub>44</sub> ) <sub>2</sub>	
		
<b>G#1-(PEG<sub>113</sub>)<sub>2</sub></b>		
PNVCL <sub>106</sub> -G#1-(PEG <sub>113</sub> ) <sub>2</sub>	PNVCL <sub>131</sub> -G#1-(PEG <sub>113</sub> ) <sub>2</sub>	PNVCL <sub>225</sub> -G#1-(PEG <sub>113</sub> ) <sub>2</sub>
		

(Continue in the next page)

**Table G.3 (cont.):** Characteristics of the aggregates formed by the solution self-assembly of the temperature-responsive LDBC at 45 °C (0.2 mg.mL<sup>-1</sup>). TEM micrographs taken at Mag. x 100 000 and DLS results ( $D_h$  and PDI).

<b>G#2-(PEG<sub>44</sub>)<sub>4</sub></b>		
<b>PNVCL<sub>106</sub>-G#2-(PEG<sub>44</sub>)<sub>4</sub></b>	<b>PNVCL<sub>131</sub>-G#2-(PEG<sub>44</sub>)<sub>4</sub></b>	<b>PNVCL<sub>225</sub>-G#2-(PEG<sub>44</sub>)<sub>4</sub></b>
		
<b>G#2-(PEG<sub>113</sub>)<sub>4</sub></b>		
<b>PNVCL<sub>131</sub>-G#2-(PEG<sub>113</sub>)<sub>4</sub></b>	<b>PNVCL<sub>225</sub>-G#2-(PEG<sub>113</sub>)<sub>4</sub></b>	
		

**Table G.4:** Characteristics of the aggregates formed by the solution self-assembly of the pH-responsive LDBC at 25 °C and pH 7.4 (1.0 mg.mL<sup>-1</sup>). TEM micrographs taken at Mag. x 200 000 and DLS results (D<sub>h</sub> and PDI).

<b>G#0-PEG<sub>113</sub></b>		
PDPA <sub>19</sub> -G#0-PEG <sub>113</sub>	PDPA <sub>49</sub> -G#0-PEG <sub>113</sub>	
		
<b>G#1-(PEG<sub>44</sub>)<sub>2</sub></b>		
PDPA <sub>19</sub> -G#1-(PEG <sub>44</sub> ) <sub>2</sub>	PDPA <sub>49</sub> -G#1-(PEG <sub>44</sub> ) <sub>2</sub>	PDPA <sub>102</sub> -G#1-(PEG <sub>44</sub> ) <sub>2</sub>
		
<b>G#1-(PEG<sub>113</sub>)<sub>2</sub></b>		
PDPA <sub>49</sub> -G#1-(PEG <sub>113</sub> ) <sub>2</sub>	PDPA <sub>102</sub> -G#1-(PEG <sub>113</sub> ) <sub>2</sub>	
		
<b>G#1-(PEG<sub>44</sub>)<sub>4</sub></b>		
PDPA <sub>49</sub> -G#1-(PEG <sub>44</sub> ) <sub>4</sub>	PDPA <sub>102</sub> -G#1-(PEG <sub>44</sub> ) <sub>4</sub>	
